Medicinal Chemistry and Pharmacology of Ectonucleotidases: Assay Development and Characterisation of Inhibitors

Dissertation

zur Erlangung des Doktorgrades (Dr. rer. nat.)
der
Mathematisch-Naturwissenschaftlichen Fakultät
der
Rheinischen Friedrich-Wilhelms-Universität Bonn

vorgelegt von

Salahuddin Mirza

aus Dera Ismail Khan (Pakistan)

Bonn im Januar 2025

Angefertigt mit Genehmigung der Mathematisch-Naturwissenschaftlichen Fakultät
der Rheinischen Friedrich-Wilhelms-Universität Bonn

Gutachterin/Betreuerin: Prof. Dr. Christa E. Müller
Gutachter: Prof. Dr. Gerd Bendas

Tag der Promotion: 21.01.2025
Erscheinungsjahr: 2025

Dedicated to my family, supervisors, and friends…

In all chaos, there is a cosmos and, in all disorders, a secret order.

~Carl Jung

Diese Dissertation ist eine Zusammenfassung der Arbeiten, die vom 4. April 2016 – 20. März 2023 am Pharmazeutischen Institut der Rheinischen Friedrich-Wilhelms-Universität Bonn unter der Betreuung von Prof. Dr. Christa E. Müller durchgeführt wurden

Contents

List of Figures

Chapter 3

Chapter 4

Chapter 5

List of Tables

Chapter 1

Chapter 2

Chapter 3

Chapter 4

Abbreviations:

8-BuS-ADP	8-Thiobutyladenosine-5′-diphosphate
8-BuS-AMP	8-Thiobutyladenosine-5′-monophosphate
8-BuS-ATP	8-Thiobutyladenosine-5´-triphosphate
α value	Inhibition mechanism determinant
aa	amino acid
ACR	apyrase-conserved region
ADA	adenosine- deaminase
ADK	adenylate kinase
ADP	adenosine diphosphate
AK	arbeitskreis (en:working group)
AMP	adenosine monophosphate
AP	alkaline phosphatase
APS	ammonium persulfate
ARL67156	N^6-Diethyl-β-γ-dibromo-methylene-ATP
ATP	adenosine triphosphate
AUC	area under the curve
bp	base pair
CD39	cluster of differentiation 39
CD39L1	CD39-like Protein (cluster of differentiation 39-like 1)
CD39L3	CD39-like Protein (cluster of differentiation 39-like 3)
CD73	cluster of differentiation 73

CE	capillary electrophoresis
DMSO	dimethyl sulfoxide
dNTP	deoxynucleotide
EDTA	Ethylenediaminetetraacetic acid
GMP	Guanosine monophosphate
h	hour
HEPES	2-[4-(2-hydroxyethyl)piperazin-1-yl]ethanesulfonic acid
HPLC	High-performance liquid chromatography
HTS	high-throughput screening
IC_{50}	half maximum inhibitory concentration
k_{cat}	turnover number
K_i	inhibitory constant
K_m	michaelis-menten constant
kDa	kilodalton
LB	lysogeny broth
min	minute
n.d.	not determined
NAD	nicotinamide adenine dinucleotide
NTPDases	ecto-nucleoside triphosphate diphosphohydrolases
***p*-Nph-5'-TMP**	*p*-nitrophenyl-5' thymidine monophosphate
NPP1	nucleotide pyrophosphatase/phosphodiesterase 1
NPP3	nucleotide pyrophosphatase/phosphodiesterase 3
NPPs	nucleotide pyrophosphatases/phosphodiesterases

NT5E	ecto-5'-nucleotidase
OD	optical Density
Pi	inorganic Phosphate
PLP	pyridoxal-5´-Phosphate
PLAP	placental Alkaline Phosphatase
***p*-NPP**	*para*-Nitrophenylphosphate
POM	polyoxometalate
PPi	diphosphate (or pyrophosphate)
RT	room temperature
SDS	sodium dodecyl sulfate
SEM	standard error of the mean
Sf9	Spodoptera frugiperda *9*
T_m	melting temperature
TAE	tris-acetate-EDTA
TEMED	tetramethylethylenediamine
TMD	transmembrane domain
TNAP	Tissue-nonspecific alkaline phosphatase
Tris	tris(hydroxymethyl)aminomethane
UDP	uridine diphosphates
UTP	uridine triphosphate
v	velocity
vs	versus

Chapter 1

Modulatory role of purinergic signalling in cancer

Summary

Tumours and microenvironments are characterised by signalling mechanisms connecting cellular and sub-cellular components that assist tumour cells in growth and evading immune surveillance. Genetic mutations of these pathways are linked to cancer. There is a plethora of new treatments specifically targeting cancer cells, including solid tumours. Therapies towards cancer signalling pathways are already under clinical trials. However, what truly inspires us is the potential of purinergic signalling in cancer treatment. Undeniably, purinergic signalling is crucial in immune evasion, angiogenesis, and metastasis of tumours. This involves a highly connected system of nucleotide transporters (connexin-43 hemichannels, pannexin-1, and ABC transporters), extracellular nucleotides (ATP, NAD^+, UTP, and dinucleotide polyphosphates), purinergic receptors (P1 and P2), and ectonucleotidases (NTPDases, NADases, NPPs, and ecto-5'-nucleotidases). Tumours are associated with modifying the typical physiological environment to a hypoxic and more acidic extracellular environment. A hypoxic or inflamed tissue environment causes the activation of transmembrane-bound nucleotide transporters and channels intracellular nucleotides to the extracellular side. Besides this systematic transport, cellular necrosis and vesicular transport add to this nucleotide burden. This leads to a significant increase in extracellular nucleotide concentration ranging from low nanomolar to millimolar levels. High nucleotide concentrations, most importantly of ATP and NAD^+, act as a pro-inflammatory trigger for the recruitment of immune cells to target inflamed tissues or cancer cells. Nucleotides act as ligands for membrane-bound G protein-coupled receptors and ion channels (P2Y and P2X receptors).

Cancer cells abundantly express surface-located enzymes, ectonucleotidases that hydrolyse extracellular nucleotides to limit their pro-inflammatory effects. NTPDases (1 – 8) hydrolyse ATP and UTP to their monophosphate analogue AMP and UMP, respectively. On the other hand, NADases (CD38, CD157) potently hydrolyse NAD^+ to cyclic-ADPR or ADPR. CD157 mainly produces the cyclic product; however, ADPR is the main product of CD38 activity. NPPs (1 – 7) represent a class of ecto-enzymes having

ATPase and NADase activity by hydrolysing them to AMP. NPPs can also hydrolyse numerous other substrates, such as ADPR, Ap_nA, UTP, and UDP-glucose, to the nucleoside monophosphate. A net outcome of these enzyme reactions is the neutralisation of pro-inflammatory signals. The GPI-anchored ecto-5'-NT hydrolyses monophosphates, in particular, AMP to adenosine. This represents an anti-inflammatory feedback response by tumour cells to limit immune cell recruitment by activating G protein-coupled adenosine receptor subtypes (A_1, A_{2A}, A_{2B}, and A_3). This inhibition of immune cell recruitment helps tumour cells to propagate silently. Numerous drug candidates targeting different purinergic signalling components are under investigation, and some are undergoing clinical trials.

Ectonucleotidases are widely expressed in different tumours, including the most virulent and non-responsive types, such as triple-negative breast cancer, lung, brain, colorectal, ovarian, hepatic, prostate, leukaemia, and skin cancer. Wide-spread expression of these enzymes reflects that tumour cells use multiple paths to avoid immune surveillance. An interesting fact is that these enzymes are co-expressed and work nearby. If one set of enzymes is inhibited, there is always an alternative arrangement to hydrolyse nucleotides. Some of these enzymes are released in exosomal vesicles, which are mobile and can hydrolyse distant nucleotide molecules. We briefly summarise the involvement of purinergic signalling components in tumour metastasis in connection to major tumour types. Inhibition of their enzymatic activity is considered a potential immunotherapy.

1.0 Introduction

1.1 Tumour microenvironment

Tumour cells are engaged in highly complex physiological processes to maintain proliferative signalling, leading to angiogenesis and metastasis. Surrounding immune cells can help tumours achieve this uncontrolled growth (Hanahan & Weinberg, 2011). The tumour microenvironment (TME) is altered so that proliferation is supported. Tumour-induced interactions in the TME are critical for metastasis and for escaping immune surveillance by leukocytes, such as T- and B- lymphocytes, dendritic cells (DC), macrophages, myeloid suppressor cells, tumour-associated fibroblasts, adipocytes, vascular endothelial and natural killer (NK) cells (Balkwill et al., 2012; Whiteside, 2008). The concerted action of different components of the TME maintains an immunosuppressive surrounding that is required for the tumour cells' growth (Lang et al., 2006).

1.1.1 The human immune system

The immune system is designed to protect the body from infections, such as bacteria, viruses, fungi, parasites, and cancer. It can discriminate between "self" (the body's cells) and "non-self" (external agents and infections) to get rid of or neutralise any potential health risks (Marshall et al., 2018). The immune system is divided into the innate immune system (which has no previous memory of infection and is non-specific) and the adaptive or acquired immune system (which has a highly specific memory).

a. Organs of the immune system

The major organs of the immune system include the primary lymphoid organs, the thymus, and the bone marrow. The thymus is located in the upper chest, where lymphocytes are converted to mature T-cells, and the bone marrow is where immune cells originate. Secondary lymphoid organs include:

- The liver that produces phagocytes to capture foreign pathogens
- Tonsils that harbour lymphocytes in the throat
- Lymph nodes that contain B- and T-cells

- Spleen that purifies blood and is the place where immune cells interact with foreign substances
- Blood is the principal mode of transportation of physiological materials.

b. The innate immune response

The innate immune system is the body's first line of defence that offers immediate antigen-independent protection (Turvey et al. 2010). Physical and physiological barriers, lysosomes, and phagocytes are major innate immune system components. Figure 1.1 depicts the details of the immune defence.

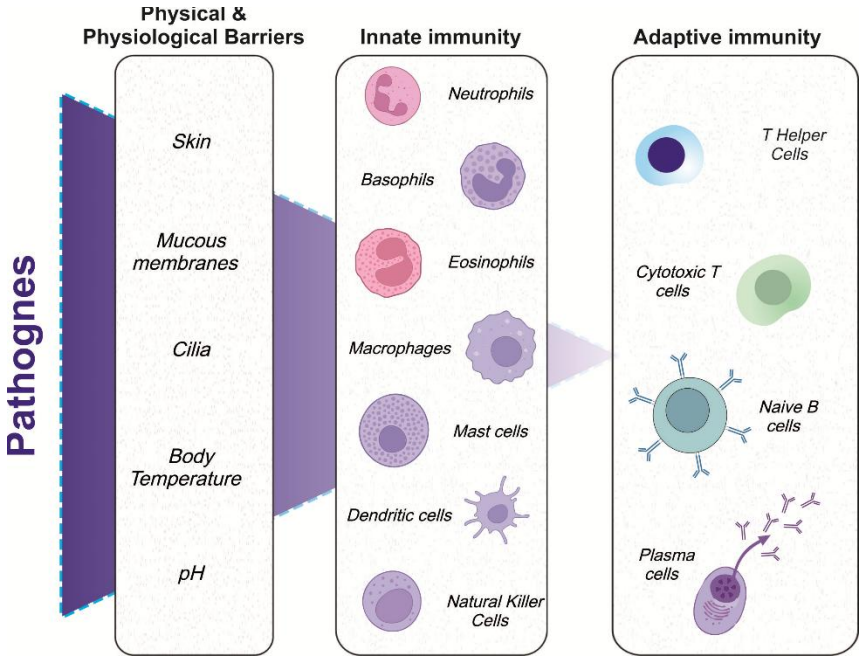

Figure 1.1: Overview of human defence components against foreign invaders. The figure is adapted from https://www.enzolifesciences.com and produced using Corel Draw 16 and https://www.biorender.com.

c. Acquired immune response

This is a type of immunity that arises after a person acquires antibodies or when their immune system reacts to a foreign substance or bacterium (Marshall et al., 2018). The acquired immune response is more specific. It involves two primary lymphocyte types:

i. B-Lymphocytes

B-lymphocytes (B-cells) mature in the bone marrow and recognise foreign elements through antigen-specific B-cell receptors (BCR). BCR identify their specific antigen that is

then engulfed (Pierce 2009), (Akkaya et al. 2020). Specialised glycoproteins, the major histocompatibility complex II (MHC II), help B-cells present antigen fragments on their surface and boost immune response. B-cells need Helper T-cells to be activated completely. Activated Helper T-cells release cytokines that further boost B-cells. B-cells divide rapidly after the first antigen exposure to produce identical daughter cells. Some daughter cells become plasma cells, which release antibodies against the antigen (IgA, IgD, IgE, IgG, and IgM) that circulate in the blood and lymph to identify and neutralise unique antigens and foreign pathogenic materials (Forthal, 2014). Other daughter cells become memory B-cells that detect the same antigen quickly and create a more robust initial immune response. The details of B-cell activation and neutralisation are summarised in Figure 1.2.

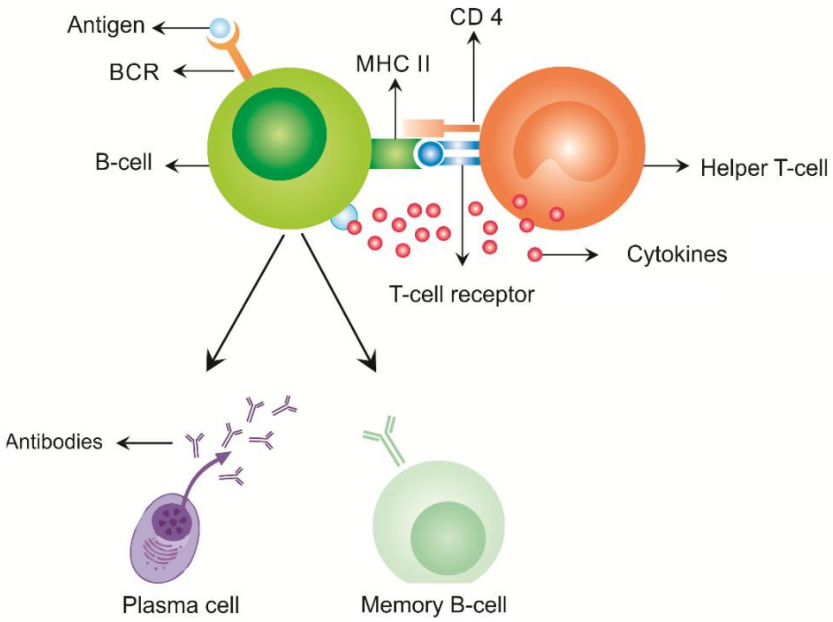

Figure 1.2: Schematic presentation of B-cell-originated immune response. The figure is produced using Coral Draw 16 and biorender software.

ii. T-Lymphocytes

T-lymphocytes are initially produced in hematopoietic stem cells and mature in the thymus. They express T-cell receptors (TCR) at their surface to interact with MHCs containing antigen fragments (Hwang et al., 2020). During the maturation process in the thymus, T-cells are differentiated into distinct subtypes with variable functions, such as Helper $CD4^+$, cytotoxic $CD8^+$, regulatory $CD4^+$, and memory T-cells.

a. Helper $CD4^+$ T-cells

These cells express CD4 glycoprotein on their surface and help other cells in maturation and activation, e.g. differentiation of B-cells into plasma or memory cells and activation of cytotoxic T-cells and macrophages. Antigen encounter activates Helper T cells that secrete cytokines to generate an immune response.

b. Cytotoxic $CD8^+$ T-cells

Cytotoxic $CD8^+$ T-cells express CD8 glycoprotein on their surface. These cells specialise in killing pathogens and cancer cells after binding with specific peptides. $CD8^+$ T-cells release IL-2 and IFN-γ.

c. Regulatory $CD4^+$ T-cells (Treg)

Tregs maintain immunological tolerance and prevent overreactions that could damage tissues. These cells develop in the thymus or the peripheral system and are named accordingly. Treg is further classified into Forkhead Box 3 ($FOXP3^+$ and $FOXP3^-$), which controls the regulatory pathway.

d. Memory T-cells

After an encounter with antigens, T-cells are differentiated into memory T-cells for future combat. Different subtypes of memory T-cells have been described, including central memory T-cells (lymph node), effector memory T-cells (peripheral circulation), tissue-resident memory T-cells (skin and lungs), and virtual memory T-cells (peripheral circulation).

e. Activation of T-cells

An extracellular signal is required to activate T-cells, starting with binding antigens and antigen-presenting cells (APCs) to T-cell receptors (TCR). Peptide antigens are processed by either MHC complexes I or II. All nucleated cells display MHC class I; however, antigen-presenting cells, including macrophages, dendritic cells, and B cells, express MHC class II. MHC I usually work with intracellular antigens and activates cytotoxic T-cells, while MHC II works more extracellularly and with Helper T-cells. TCR-antigen complex initiates several intracellular signalling pathways involving various molecules (Hwang et al., 2020). Large amounts of cytokines are released due to Helper

T-cell activation, which activates cytotoxic T-cells and, in turn, attacks the infected cells via MHC class 1. This interaction leads to the secretion of granzyme and perforins. Perforins make pores in cellular membranes from which granzyme enters the cells, leading to the death of infected cells. The details of T-cell activation are described in Figure 1.3.

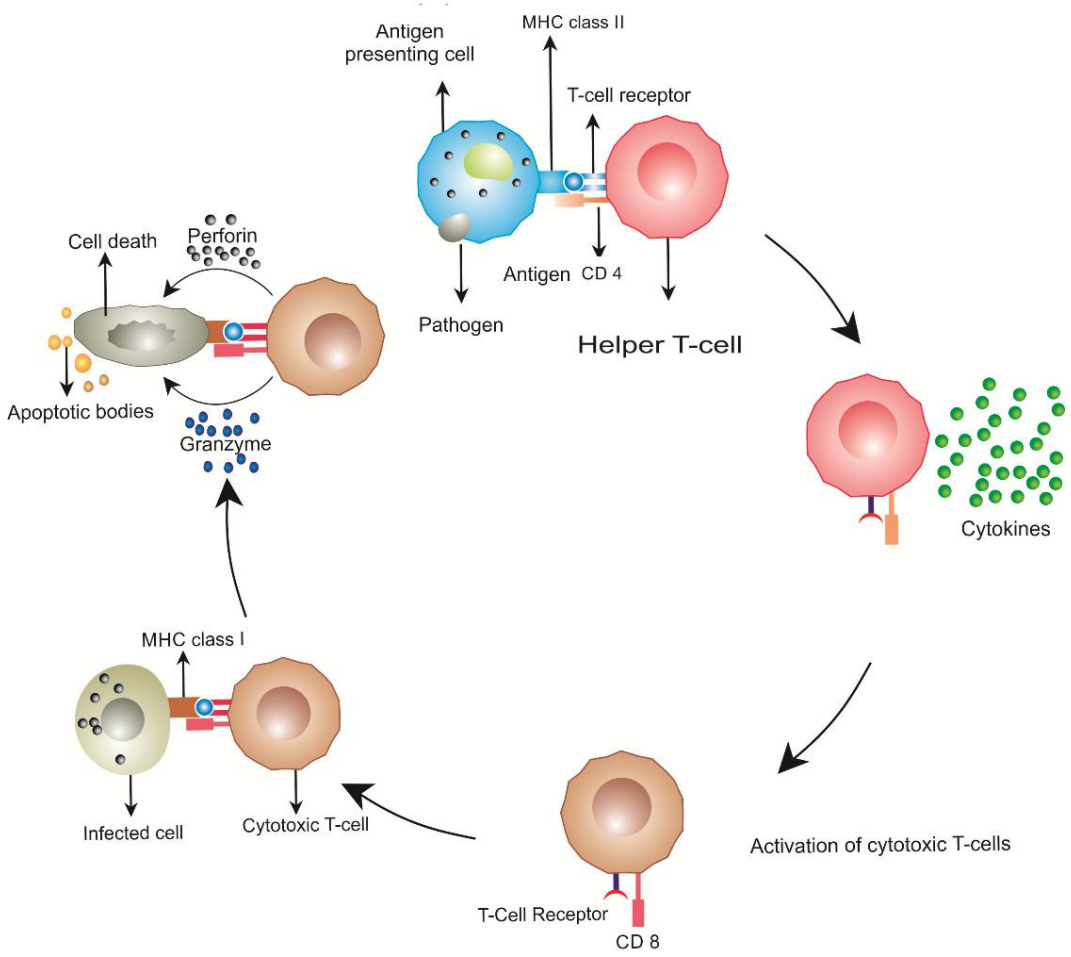

Figure 1.3: Schematic presentation of T-cell-based immune response. The figure is produced using Coral Draw 16 and biorender software.

1.2 Signaling pathways in cancer

Complex interactions significantly influence the emergence and spread of cancer via signalling pathways that control critical cellular functions (differentiation, growth, survival, and apoptosis). Dysregulations (mutations and overactivation) of these pathways result in the development and spread of cancer (Sanchez-Vega et al., 2018).

1. PI_3K/AKT/mTOR Pathway

Phosphatidylinositol-3-kinase/Protein kinase B/mammalian target of rapamycin (PI_3K/AKT/ mTOR) is a crucial signalling system that controls critical cellular processes related to cell growth, survival, metabolism, and proliferation (Peng et al., 2022).

a. Activation of the pathway

The activation of PI_3K is initiated by growth factors, including insulin-like growth factor 1 (IGF-1) or epidermal growth factor (EGF). Receptor tyrosine kinases (RTKs) are triggered by this interaction that in turn activates PI_3K (Hemmings & Restuccia, 2012; J. Yang et al., 2019). Phosphatidylinositol-3,4,5-trisphosphate (PIP_3) is formed when PI_3K phosphorylates phosphatidylinositol lipids of the cell membrane. AKT is then attracted to the cell membrane by PIP_3 and phosphoinositide-dependent kinase 1 (PDK1), where it is phosphorylated and activated by mTORC2 (mammalian target of rapamycin complex 2). mTOR is made up of the mTORC1 and mTORC2 complexes. AKT directly controls mTORC1, which is essential for regulating cell growth, protein synthesis, and autophagy. mTORC2 controls cytoskeletal structure and cell viability. Enhanced activation of PI_3K/AKT is controlled through negative regulators, protein phosphatase 2 (PP2A), phosphatase, and tensin homolog (PTEN). PI_3K/AKT/mTOR pathway activation leads to essential downstream cellular functions. AKT protein suppresses pro-apoptotic factors and stimulates anti-apoptotic pathways to further aid in the tumour cells' resistance towards programmed cell death (Porta et al. 2014). Moreover, mTORC1 is associated with cell growth and proliferation.

b. Cancer

Many cancers exhibit a dysregulation of the PI_3K/AKT/mTOR pathway due to genetic mutations or changes in essential elements. For instance, malignancies, including breast, ovarian, and colorectal cancers, typically contain mutations in the PIK_3CA gene (which codes for the catalytic subunit of PI_3K). Moreover, mutations in the PTEN gene are reported, which alter its cancer-suppressing ability. A frequent alteration of this pathway is reported in solid tumours (Myers et al., 1998), (LoRusso, 2016).

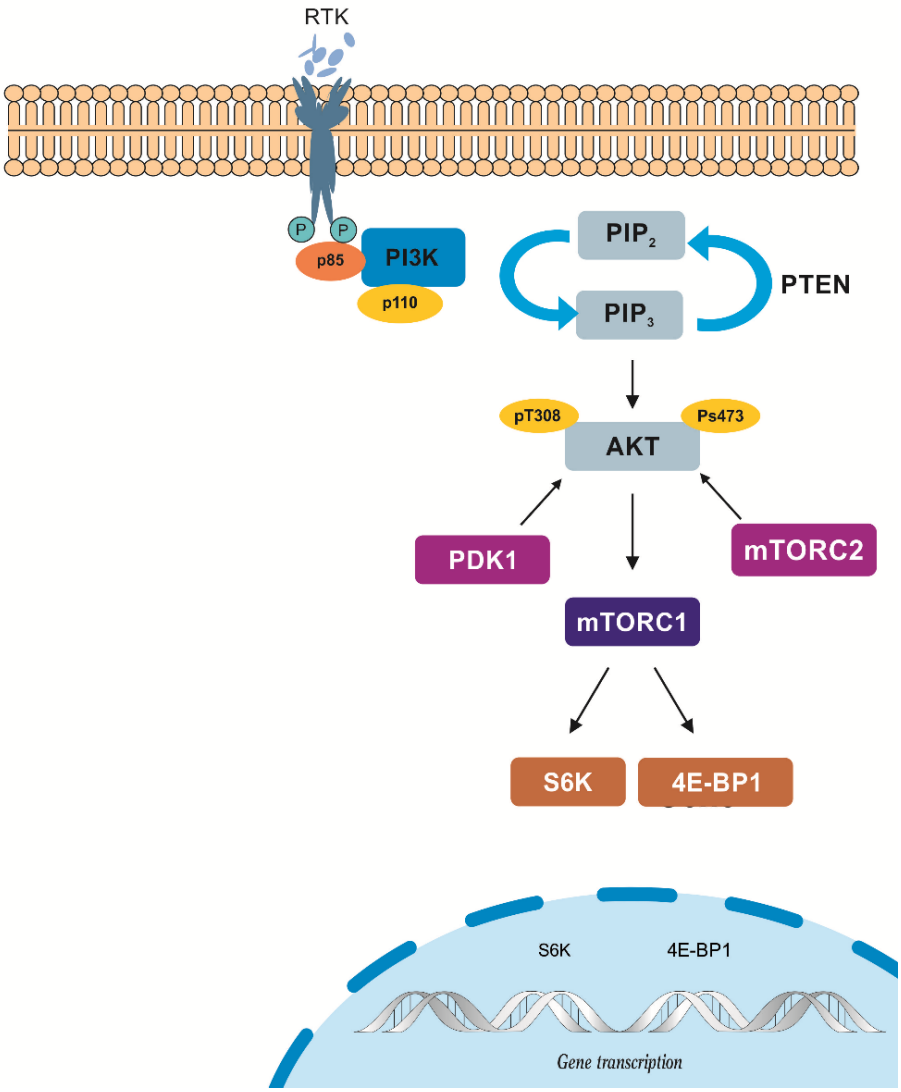

Figure 1.4: Schematic diagram of PI_3K/AKT/mTOR signalling pathway. The figure is modified from (Porta et al. 2014), and is produced using Coral Draw 16.

c. Therapeutic approaches

Considering their devastating role in cancer, therapeutic strategies targeting these pathways are essential. Currently, numerous inhibitors of different components of this pathway are under clinical trials, including inhibitors of PI_3K (Pan-PI_3K, isoform-selective PI_3K, and dual PI_3K-mTOR inhibitors), AKT inhibitors (GSK-2141795, GSK-2110183) and mTOR inhibitors RAD001, MLN0128, and AZD014 (Y. He et al., 2021). Despite massive efforts, the pathway's signalling network's complexity and redundancy pose considerable challenges in achieving effective and specific therapeutic outcomes.

2. MAPK pathway

Mitogen-activated protein kinase (MAPK) is a serine-threonine-specific protein involved in a pathway that utilises the Ras/Raf/MEK/ERK signalling route to modulate certain biological functions of cell growth, proliferation, and death (Hilger et al. 2002). The MAPK pathway transcribes extracellular signals via membrane-bound receptor tyrosine kinases (RTKs) and rat sarcoma (Ras) protein via rapidly accelerated fibrosarcoma (Raf), MAP kinase (MEK), and extracellular-signal-related kinase (ERK) into the nucleus.

a. Activation of the pathway

The pathway is triggered by extracellular signals, such as epidermal growth factor (EGF) binding to cell surface RTKs. Activated RTKs then phosphorylate and activate the RAS protein, which is subsequently dimerised. It uses its GTPase function to start a series of events, including activating Raf kinases through phosphorylation (Raf-1, B-Raf). MEK (Mitogen-Activated Protein Kinase kinase) is phosphorylated by activated Raf. Erk is phosphorylated and activated by MEK, which then moves to the nucleus and phosphorylates several transcription factors for targeted gene expression (Dillon et al., 2021; Knight et al., 2014)**.**

b. Cancer implications

Dysregulation due to mutations is linked to the development of cancers in different organs (Campbell et al., 2021)**.** Many human malignancies, including colorectal, lung, and pancreatic cancers, include Ras genes (H-Ras, K-Ras, and N-Ras) mutations. These mutations cause Ras to be constantly activated, which promotes uncontrolled cell proliferation. Melanoma and particular kinds of thyroid and colorectal malignancies frequently harbour B-Raf gene mutations. A well-known example is the V600E mutation, which results in constitutively active BRAF and abnormal signalling (Burotto et al., 2014; Loo et al., 2018).

c. Therapeutic approaches

The MAPK pathway is targeted through inhibitors of multiple signalling steps, including small-molecule inhibitors of B-Raf, MEK, and Erk1/2 (English et al. 2002)**.** Different Raf inhibitors are reported at an IC_{50} value in the low nM range. Numerous clinical trials and

in-vitro/in-vivo analyses of the inhibitory potential of these small molecules are currently under investigation.

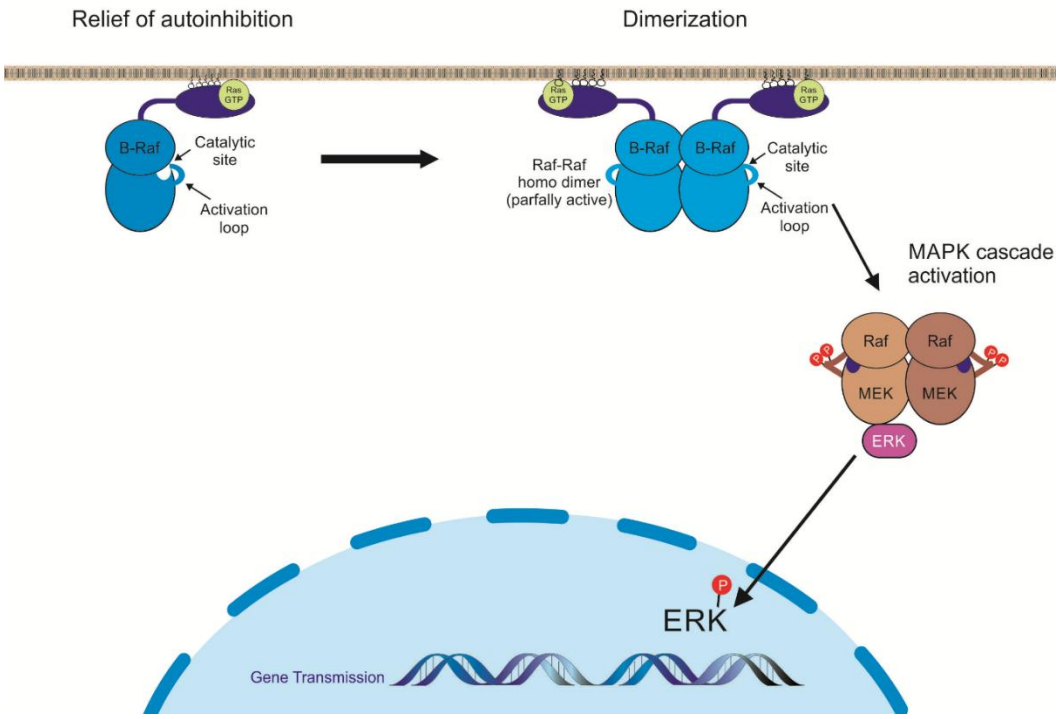

Figure 1.5: Schematic presentation of MAPK signalling system. The figure is produced using Coral Draw 16.

3. NF-*k*B signalling pathway

The Nuclear Factor-kappa B (NF-*k*B) pathway comprises different components that control immunological responses through DNA transcription, cytokine production, and cell survival (Ghosh et al. 2021). The five major interacting components of this pathway consist of NF-*k*B1 (p50), NF-KB2 (p52), and the reticuloendotheliosis viral homolog (RelA, RelB, and cRel). Two sub-pathways are reported: canonical NF-*k*B and non-canonical NF-*k*B pathways. Both rely on different initiator signals as well as effector components.

a. Activation of the pathway

i. Canonical pathway

Pro-inflammatory cytokines (including TNF-α, IL-1β, and LPS), microorganisms, stress signals, and growth factors trigger the NF-*k*B pathway activation (Hayden et al. 2004). This interaction starts downstream phosphorylation of I*k*B kinases (I*k*K) comprising I*k*Kα, I*k*Kβ, and I*k*Kγ. Phosphorylated I*k*Kα and β then ubiquitinate the phosphorylated-I*k*Bα to

induce its degradation by the proteasome. This relieves the NF-*k*B complex p50/RelA dimer translocates to the nucleus. NF-*k*B regulates the transcription of target genes involved in immunological responses, inflammation, cell survival, and proliferation by binding to specific DNA sequences.

ii. Non-canonical pathway

Apart from the classical or canonical NF-*k*B pathway, an alternative or non-canonical pathway exists that regulates sophisticated biological functions such as osteoclastogenesis, lymphoid organ development, and survival (Dejardin, 2006). Pathway activation starts with extracellular stimuli such as B-cell activation factor belonging to the TNF family receptors (BAF-R), receptor activator of NF-kB (RANK), lymphotoxin LTα1β2, and CD40L. NF-kB-inducing kinase (NIK) is stabilised and activated due to this interaction. Activated NIK then recruits the IKKα/p100 complex, causing phosphorylation of p100 and ubiquitination. The processing product p100 activates the p52/RelB complex that gets internalised into the nucleus to perform gene transcription.

b. Cancer

Genetic alteration (point mutations or base pair deletions) of different components of the pathway can lead to pathological consequences, including cancer (Courtois et al. 2006). Several studies relate such mutations with the worsening of cancers of the liver, colorectal, prostate, head, and neck and in haematological malignancies (leukaemia and multiple myeloma) (F. Li et al., 2015). Similar to canonical pathways, the excessive activation of non-canonical pathways is associated with a large number of pathologies related to bone and joints, GIT, and haematological origin (Choi et al., 2019).

c. Therapeutic approaches

Different strategies have been adopted for blocking the NF-kB pathways due to their relevance in difficult-to-treat cancers (Ramadass et al. 2020). Many macromolecules, biologicals, and small-molecule inhibitors are in different phases of clinical trials targeting receptor-ligand binding interface, proteasome inhibitors, I*k*Kα inhibitors, NIK inhibitors, REL-A and B activation, and binding inhibitors. Apart from synthetic molecules, several compounds extracted from plant origin showed promising results for NF-*k*B pathway inhibition (Nam, 2006).

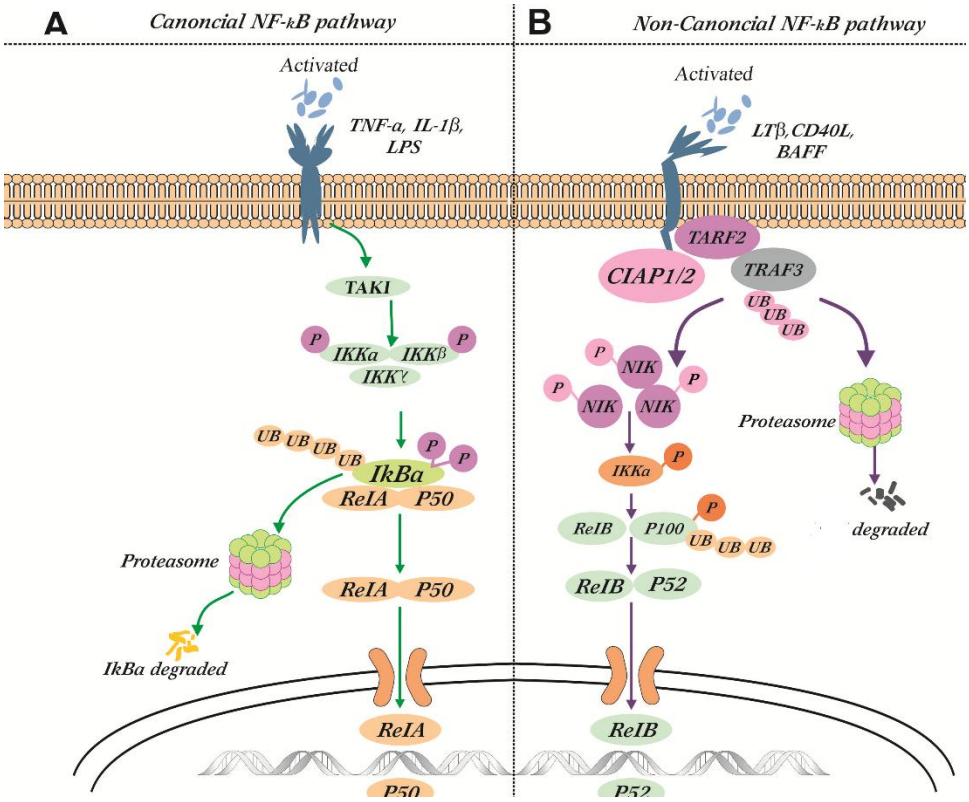

Figure 1.6: **Schematic representation of NF-*k*B pathway**. The figure is modified from (Chen et al., 2021), and is produced using Corel Draw 16.

1.3 Purinergic signalling

Purinergic signalling (PS) is a complex and vital inter- and intracellular signalling system involving cell membrane receptors/transporters, extracellular substrates, and ecto-enzymes. The components of (PS) are coordinated in a highly sophisticated manner to initiate an immune response (Zimmermann, 2020; Zimmermann et al., 2012). Interest in these mechanisms has been growing for decades owing to their involvement in numerous cellular processes under normal and pathological conditions. The term “purinergic signalling” was first coined by *Geoffrey Burnstock* when he found that the purine nucleotide ATP is responsible for inhibitory neurotransmission in the gut and excitatory neurotransmission in the gall bladder (Burnstock, 1972). During those times, ATP was comprehensively perceived as an intracellular energy source and was unlikely to be involved in extracellular signalling. Decades after the initial “purinergic hypothesis” was proposed, Burnstock reported ATP co-transmission with nor-adrenaline (NA) from

sympathetic nerves (Burnstock et al., 1990), and with γ-aminobutyric acid (GABA), acetylcholine (Ach), glutamate, and nitric oxide (NO) in the peripheral and central nervous system (Burnstock, 2012). It is now well known that purinergic signalling plays a crucial role in several physiological processes, such as neurotransmission, cardiovascular control, immunological responses, and inflammation. It modulates immune cell behaviour and influences innate and adaptive immune responses, including immune cell migration, cytokine release, and antigen presentation. Understanding purinergic signalling mechanisms offers potential therapeutic avenues for managing inflammatory conditions, and therapeutic modalities are developed that modify these pathways. Enhanced purinergic signalling is observed under hypoxic and inflammatory conditions associated with melanomas, gliomas, lung, colorectal, ovarian, breast, prostate, and cervical cancers (Burnstock & Di Virgilio, 2013; Coddou, 2019; Diezmos et al., 2016; Schmid et al., 2015; Schneider et al., 2015; Virgilio et al., 2016). Besides cancer, a well-documented role of purinergic signalling is evident in Alzheimer's and Parkinson's diseases (Navarro et al., 2015), epilepsy (Audinat, 2016), and neuropathic pain (Tsuda et al.,2015).

1.3.1 Purinergic receptors

Different subtypes of purinergic receptors were cloned and characterised, making the breakthrough in purinergic signalling possible. These receptors control critical subcellular biological functions involved in cell division, maturation, migration, and cell death. They are classified as P1 and P2 receptors expressed on the cell membrane of almost all eukaryotes.

a. P1 receptors (adenosine receptors)

P1 receptors are seven transmembrane (7-TM) receptors, also referred to as adenosine receptors (ARs) because they are activated by adenosine (Jacobson et al., 2016). These G protein-coupled receptors (GPCRs) activate or inhibit specific intracellular signalling pathways. G proteins have three subunits: α, β, and γ. The binding of adenosine with its receptors can induce an exchange of GDP for GTP on the α-subunit of the G protein, resulting in conformational changes. The α-subunit subsequently separates from the β-γ complex and interacts with diverse effector molecules to control their function, including

enzymes and ion channels (Borea et al., 2018). The main signalling pathways that are regulated by adenosine receptors are:

- *Adenylate cyclase (AC)*: The enzyme AC produces the second messenger cyclic AMP (cAMP) by hydrolysing intracellular ATP. cAMP, in turn, activates protein kinase A (PKA). Depending on their subtype and the type of G protein they pair with, adenosine receptors can either promote or inhibit AC activity. A_{2A} and A_{2B} receptors activate AC by coupling with Gs proteins, while A_1 and A_3 receptors typically inhibit AC by interacting with G_i proteins.

- *Phospholipase C (PLC)*: PLC hydrolyses the second messenger, phosphatidylinositol 4,5-bisphosphate (PIP_2), to create IP_3 and DAG, which control intracellular calcium levels and protein kinase C (PKC) activity, respectively. Adenosine receptors can activate PLC by connecting with Gq/11 proteins or interfacing with beta-gamma complexes of Gi/o proteins. It has been demonstrated that A_1, A_{2B}, and A_3 receptors can activate PLC.

- *Phosphatidylinositol 3-kinase (PI_3K)*: Phosphorylation of phosphatidylinositol 4,5-bisphosphate (PIP_2) by the enzyme PI_3K results in the production of phosphatidylinositol 3,4,5-trisphosphate (PIP_3), a second messenger that stimulates Akt and other downstream targets involved in cell growth, metabolism, and survival. By interacting with Gi/o proteins (A_1 and A_3), adenosine receptors can activate PI_3K.

- *Mitogen-activated protein kinase (MAPK) pathway*: Serine/threonine kinases called MAPKs control proliferation, differentiation, death, and inflammation of cells. Extracellular signal-regulated kinases (ERKs), c-Jun N-terminal kinases (JNKs), and p38 MAPKs are the three primary subfamilies of MAPKs. By connecting with other receptors like growth factor receptors or integrins or by partnering with various G proteins, adenosine receptors can activate MAPKs. The pathway is activated by all four receptor subtypes (A_1, A_{2A}, A_{2B}, and A_3).

Under hypoxic conditions, a rapid overexpression of receptors occurs due to the increased extracellular concentration of adenosine either because of enzymatic hydrolysis of extracellular nucleotides by ectonucleotidases or intra-to-extracellular transport.

Nucleoside transporters belong to the equilibrative or the concentrative nucleoside transporter family (ENTs and CNTs) (Anglada et al., 2018). Mainly, ENT1 is involved in the transport of adenosine. The physiological functions of the other subtypes have not yet been explored well. The adenosine transport is bi-directional, and adenosine kinase (ADKs) and adenosine deaminases (ADAs) control intracellular adenosine concentrations (Xu et al., 2017). Adenosine signalling plays a role in different pathological conditions, including cancer, nervous system abnormalities, and cardiovascular complications (Jacobson et al., 2006). These signalling pathways can impact numerous transcription factors that control gene expression and physiological processes. The following transcription factors influence adenosine receptors, leading to their pathological functions (Hilaire et al., 2009):

- Hypoxia-inducible factor 1 (HIF-1): A transcription factor HIF-1 controls the expression of genes related to oxygen homeostasis, angiogenesis, glycolysis, and cell survival in hypoxic environments. HIF-1α increases A_{2B} receptor expression. Adenosine receptors (A_{2A}, A_{2B}, and A_3) can stimulate the PI_3K/Akt pathway or elevate intracellular cAMP levels to activate HIF-1α.
- Cyclic AMP-responsive element-binding protein (CRE): CRE controls the expression of genes related to neural plasticity, memory, learning, and stress response. Adenosine receptors (A1, A_{2A}, and A_3) can activate CRE by raising intracellular cAMP levels or engaging the MAPK pathway.
- Nuclear factor-kappa B (NF-*k*B): NF-*k*B controls the expression of genes related to immunology, oncogenesis, inflammation, and cell survival. Adenosine receptors can either activate or inhibit NF-*k*B. A_{2A} and A_{2B} receptors typically activate NF-*k*B by activating the PLC/IP_3/Ca^{2+} pathway. A_1 and A_3 receptors usually inhibit NF-*k*B by increasing intracellular cAMP levels or activating the PI_3K/Akt pathway.

- Numerous clinical trials are currently in progress to investigate adenosine receptor signalling. The complex signalling mechanisms, the extensive distribution of these receptors, and the potential adverse effects of receptor activation or inhibition present challenges in developing adenosine receptor ligands for particular clinical applications.

Table 1.1: Adenosine receptor subtypes, signalling, and selected agonists and antagonists (Borea et al. 2018; Jacobson et al. 2016)

Name	A_1	A_{2A}	A_{2B}	A_3
G protein coupling	Gi/o	Gs	Gs, Gq/11	Gi, Gq/11
Effector system	⇩ Adenylyl cyclase ⇧ Phospholipase C ⇧ MAP kinase ⇧ PI 3-kinase	⇧ Adenylyl cyclase ⇧ MAP kinase	⇧ Adenylyl cyclase ⇧ Phospholipase C ⇧ MAP kinase	⇩Adenylyl cyclase ⇧ Phospholipase C ⇧ MAP kinase ⇧ PI 3-kinase
Adenosine affinity (nM)	10	30	1000	100
Agonists	CCPA, R-PIA, CPA, IB-MECA, NECA	CGS21680, HE-NECA,	NECA, BAY60–6583, IB-MECA	IB-MECA, MRS5698, NECA
Antagonists	PSB-36, caffeine, theophylline	SCH442416, caffeine, theophylline	PSB-603, caffeine, theophylline	MRE3008F20, caffeine, theophylline
PAM	T62			LUF6000

BAY60–6583, 2-[[6-amino-3,5-dicyano-4-[4-(cyclopropylmethoxy)phenyl]-2-pyridinyl]thio]-acetamide; CCPA, 2-chloro-*N*-cyclopentyladenosine; MRS5698, (1S,2R,3S,4R,5S)-4-[6-[[(3-chlorophenyl)methyl]amino]-2-[2-(3,4-difluorophenyl)-ethynyl]-9H-purin-9-yl]-2,3-dihydroxy-*N*-methylbicyclo[3.1.0]hexane-1-carboxamide; LUF6000, *N*-(3,4-dichloro-phenyl)-2-cyclohexyl-1H-imidazo[4,5-c]quinolin-4-amine; MRE 3008F20, *N*-[2-(2-furanyl)-8-propyl-8H-pyrazolo[4,3-e][1,2,4]triazolo[1,5-c]pyrimidin-5-yl]-*N*'-(4-methoxyphenyl)urea; PAM, positive allosteric modulators;PSB36, 1-butyl-8-(hexahydro-2,5-methanopentalen-3a(1H)-yl)-3,7-dihydro-3-(3-hydroxypropyl)-1H-purine-2,6-dione; PSB-603, 8-[4-[4-(4-chlorophenzyl)piperazide-1-sulfonyl)phenyl]]-1-propylxanthine; SCH 58261, 2-(2-furanyl)-7-(2-phenylethyl)-7H-pyrazolo[4,3-e][1,2,4]triazolo[1,5-c]pyrimidin-5-amine; T62, 2-amino-4,5,6,7-tetrahydrobenzo [b]thiophen-3-yl)-(4-chlorophenyl)-methanone;

b. P2Y receptors

P2Y receptors belong to the δ-branch of rhodopsin-like 7-transmembrane GPCRs that are activated by adenine and uracil nucleotides; ATP, ADP, UTP, UDP, UDP-glucose, and dinucleotide polyphosphates (Jacobson et al., 2016). Further classification of P2Y receptors is based on the type of G proteins linked to the receptors. The subtypes are either $P2Y_1$-like that include $P2Y_1$, $P2Y_2$, $P2Y_4$, $P2Y_6$ and $P2Y_{11}$ (Gq coupling, $P2Y_{11}$, also Gs-coupled). $P2Y_{12}$-like, including $P2Y_{12}$, $P2Y_{13}$, and $P2Y_{14}$ (Gi-coupling). Gq proteins, upon activation, stimulate the phospholipase C/inosine triphosphate (PLC)/IP_3 and Ca^{2+} signalling pathways. $P2Y_{12}$, $P2Y_{13}$, and $P2Y_{14}$ receptor activation leads to adenylyl cyclase (AC) inhibition. Considering the important role of these receptors under physiological and pathological conditions, numerous synthetic derivatives are reported that could modulate the receptor functions (Müller et al., 2021). Representative compounds are enlisted in Table 1.2.

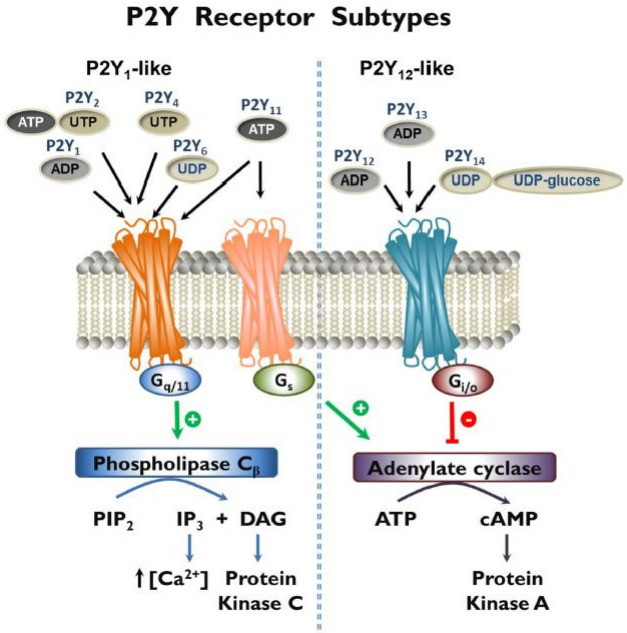

Figure 1.7: Schematic presentation of P2Y receptor subtypes activation by their physiological agonists leading to the modulation of the second messenger system [modified from (Müller et al., 2021)]

Table 1.2: Characteristics of P2Y receptor (Müller et al., 2021)

	Agonist (EC_{50} μM)	**G protein**	**Synthetic Antagonist (EC_{50} in μM)**	**Pathological function**	**Literature**
$P2Y_1$	ADP (10), Ap4U (1)	Gq	MRS2500 (0.00078–0.0084)	Venous thrombosis, Pain sensation, Glial signalling, proliferation of retinal progenitor cells	(Bird et al., 2012) (Franke et al. 2014), (Pereira et al., 2017), (Jacob et al., 2014)
$P2Y_2$	ATP (0.1), UTP (0.01)	Gq	AR-C118925 (0.0574–0.716)	Vascular calcification, proliferation of cardiac progenitor cells, metastatic breast cancer	(Qian et al., 2017), (Khalafalla, Greene, et al., 2017), (Eun et al., 2015),
$P2Y_4$	UTP (~ 1)	Gq	PSB-16133 (0.233)	Myocardial infarction, myocardial hypertrophy	(Horckmans et al., 2015),
$P2Y_6$	UDP (~ 0.3)	Gq	MRS2578 (0.037)	Cardiac hypertrophy, Parkinson's disease, Pulmonary fibrosis	(Clouet et al., 2016), (X. Yang et al., 2017), (T. Müller et al., 2017)
$P2Y_{11}$	ATP (~ 10)	Gq, Gs	NF340 (0.0724–0.372)	Nociceptive function, hepatocellular carcinoma,	(Barragán et al., 2015), (Khalid et al., 2017)
$P2Y_{12}$	ADP (~ 0.1)	Gi	PSB-0739 (0.0004–0.0249)	Platelet aggregation, cancer, vascular smooth muscle inflammation	(Gündüz et al., 2017), (Ballerini et al., 2018)
$P2Y_{13}$	ADP (~ 0.01)	Gi	MRS2211 (0.501–1.07)	Cardiovascular complications, hippocampal neurogenesis	(Verdier et al., 2019), (Stefani et al., 2018)
$P2Y_{14}$	UDP (~ 0.1), UDP-glucose	Gi	PPTN (0.000434)	Vasoconstriction, heart failure, gliomas	(Khalafalla et al., 2017), (Curet et al., 2018)

c. P2X receptors

P2X receptors are trimeric ion channel receptors further classified into seven subtypes (P2X1-7). The classification of P2X receptors is based on their pharmacology. These receptors are activated within milliseconds after binding of ATP (Jacobson et al., 2016). The P2X1 subtype is the most sensitive and requires only a nanomolar ATP concentration to be activated, while the P2X7 is the least sensitive and requires up to a millimolar concentration. This is interesting since, under inflammatory and hypoxic conditions, the extracellular concentration of ATP significantly increases from low nanomolar up to the millimolar range (Idzko et al., 2015). The receptor's activation leads to Na^+, K^+, and Ca^{2+} influx into the cytosol. Intracellular Ca^{2+} is further increased by activating voltage-gated Ca^{2+} channels and activating intracellular Ca^{2+}-dependent release and signalling pathways (Roger et al., 2015). These receptors are widely expressed throughout the body, including smooth muscle cells and the central nervous system. Increased intracellular concentrations of the cations have variable pathological outcomes related, e.g., to the heart, muscle contractions, synaptic transmission, and metabolism (Baker et al., 2013). Selective blocking of P2X receptor subtypes may become an effective therapeutic option for managing cough, pain, inflammation, and neurodegenerative diseases (North, 2016). Different synthetic approaches were adopted to discover the potent P2X subtype-selective inhibitors. An excellent review was previously published by our group that summarises the small molecule inhibitors for P2Y and P2X receptors (Müller et al., 2021). The most potent inhibitors of human P2X receptor subtypes are depicted in Table 1.3. The P2X1-selective small molecules (PSB-2001, NF023) inhibit receptor function by low nanomolar EC. Numerous small molecules are reported for the rat variant of P2X2, and very few compounds, such as ambroxol, inhibit the human P2X2 receptors with moderate potency. Similarly, AF-906 and BLU-5937 are P2X3-selective antagonists, whereas PSB-15417 and related structures are reported to inhibit P2X4 receptor activation. The P2X7 receptor is involved in many immune-modulatory mechanisms related to pathological outcomes. AZ10606120 is reported as the most potent and selective P2X7 receptor inhibitor with picomolar potency (Kan et al., 2023). P2X7 inhibitors are essential therapeutic candidates as the receptor is active under pathological conditions.

Table 1.3: Characteristics of P2X receptors (Müller et al., 2021)

	ATP binding affinity (μM)	Antagonist [(EC_{50} μM), (human variant)]	Therapeutic target	Literature
P2X1	0.1 – 0.7	PSB-2001 (0.0192) NF023 (0.210)	Thrombosis, Liver regeneration, asthma	(Oury et al., 2015), (Kudira et al., 2016), (Wright et al., 2016)
P2X2	2 – 8	Ambroxol (5.70)	Diabetic retinopathy Muscle atrophy	(Mancini et al., 2018) (Ryten et al., 2007)
P2X3	1	AF-906 (0.005) BLU-5937 (0.008)	Musculoskeletal pain Hepatocellular carcinoma Articular hyperalgesia	(de Melo Aquino et al., 2019), (Maynard et al., 2015), (Teixeira et al., 2017)
P2X4	1 – 10	PSB-15417 (0.0219) PSB-12054 (0.19)	Liver fibrosis, neuropathic pain, neuroinflammation, Lung injury	(Guilcher et al., 2018), (Stokes et al., 2017), (Hasan et al., 2018)
P2X5	0.5	-	Periodontitis, bone loss-related inflammatory conditions (osteoporosis)	(Kim et al., 2018), (Kim et al., 2017),
P2X6	-	-	Human bladder cancer, renal cell cancer	(Dietrich et al., 2022), (Gong et al., 2019)
P2X7	2 – 4	AZ10606120 (0.0014)	Diabetes mellites, osteoporosis, solid tumours, neuropathic pain, smoke-induced lung inflammation, emphysema, inflammation	(Sathanoori et al., 2015), (Jorgensen, 2019), (Roger et al., 2015), (Guo et al., 2007), (Lucattelli et al., 2011), (Virgilio et al., 2017)

1.3.2 Extracellular nucleotides

Nucleotides such as ATP, UTP, NAD^+, ADPR, and Ap_nA are released to the extracellular environment during inflammation and disease states. The concentrations of these extracellular components increase by many-fold (nanomolar–millimolar range) to activate signalling mechanisms, binding to various purinergic receptors based on their affinity (Idzko et al., 2015). Nucleotide release can be facilitated by transmembrane channels, connexin-43 hemichannels, or pannexin-1 (Dosch et al., 2018). These channels are usually closed under physiological conditions, and a pathological trigger is required for their opening. Nucleotide bursts are also observed upon cellular death/necrosis. Moreover, nucleotides are further released to the extracellular environment through secretory vesicles.

a. ATP

ATP is the primary signalling nucleotide in the extracellular TME, quickly cleaved by ecto ATPases. It also acts as a ligand for P2 (P2X and P2Y) receptors (Di Virgilio et al., 2018). Increased ATP secretion was observed following exposure to low O_2 levels, as evident

during hypoxic conditions in the TME (Orriss et al., 2009). Seizure-induced ATP release has also been observed (Beamer et al., 2019). This outward flow of ATP contributes to the proinflammatory environment around tumour cells, favouring immune cell recruitment and cell death. However, tumour cells express surface-located enzymes known as ectonucleotidases that hydrolyse ATP to neutralise this pro-inflammatory environment. Amongst these, Ecto-ATPases include nucleoside triphosphate diphosphohydrolase (NTPDases), and nucleotide pyrophosphatase/ phosphodiesterases (NPPs) that hydrolyse ATP to AMP, which is further hydrolysed to adenosine by other enzymes, e.g., ecto-5'-nucleotidases (CD73). Adenosine build-up around the tumour is anti-inflammatory, prevents immune cell recruitment, and allows cancer to escape from defence surveillance. Homeostasis of extracellular ATP (eATP) and intracellular ATP (iATP) is essential to the functioning of biosynthetic machinery and to alleviate stress (Aghdam et al., 2018). However, this tight balance of eATP/iATP deviates significantly from normal in the case of cancers. This imbalance promotes tumour via activation or inhibition of variable signalling pathways, including P1 and P2 receptors (Alvarez, 2021). Targeting ATP/adenosine signalling constitutes a novel strategy for the immunotherapy of different tumours either by inhibiting the hydrolysis of ATP/ADP/AMP by ectoenzymes or by hindering the binding of adenosine to its receptors.

b. Nicotinamide adenine dinucleotide NAD^+/adenosine di-phosphate ribose (ADPR)

NAD^+ and its reduced form NADH are essential for regulating critical cellular mechanisms of energy production and DNA repair (Mattson et al., 2018). It is now acknowledged that maintaining homeostasis of NAD^+ concentrations in the cellular compartment is critical for avoiding pathologies like cancer, diabetes, neurodegenerative diseases, ageing, and others (Schultz et al., 2016). Connexin-43 hemichannels systematically control Intra/extracellular concentrations of NAD^+ and can be altered through cellular necrosis (Bruzzone et al., 2000). In the extracellular compartment, NAD^+ activates not only P2X7 receptors but also the ectoenzymes that hydrolyse it (Seman et al., 2003). Age-related decrease in NAD^+ levels is observed with a proportional increase in NAD^+ hydrolases; [NAD^+ glycohydrolases (CD38/157), ADP-ribosyltransferases (ARTs), poly-ADP-ribose polymerases (PARPs), sirtuins, and NPPs] (Aman et al., 2018; Goody & Henry, 2018). The main hydrolyser of NAD^+ in the extracellular milieu is CD38/157, which breaks the

glycosidic bond between nicotinamide and ADP ribose (ADPR) thereby releasing ADPR. NPPs hydrolyse α,β-phosphodiester bonds and release AMP as the main product. NPPs can potently hydrolyse ADPR to AMP, leaving an abundance of AMP in the extracellular environment, ultimately leading to adenosine overburden and immunosuppression (Haag et al., 2007). These two hydrolysing pathways of eATP and eNAD+ constitute the canonical (CD39/73) and the noncanonical (CD38/NPPs/CD73) adenosinergic pathways, respectively (Horenstein et al., 2013). ADPR can be transported to the intracellular compartment in exchange for NAD^+ utilising the same connexin-43 hemichannels. Intracellularly, ADPR acts as a second messenger that initiates intracellular Ca^{+2} release through ryanodine receptors on the endoplasmic reticulum (Song et al., 2011). Enhanced intracellular concentrations of Ca^{2+} lead to the modulation of cellular responses.

c. Dinucleoside polyphosphate (Np_nN)

Dinucleoside polyphosphates (Np_nN, N = adenosine, uridine, p = phosphate, n = 2 – 6) have emerged as essential signalling molecules in purinergic signalling by modulating P2 receptor function. Yegutkin et al., 2008, reported a comparative analysis of these polyphosphates, which can modulate purinergic response by inhibiting adenylate kinase. Binding sites for these nucleotides are reported in the membranes of different tissues, including lung membranes (Laubinger et al., 1999). A significant increase in the concentration of diadenosine tetraphosphate (Ap_4A) and ectonucleotidase function (mainly NPP1) is observed in glaucomatous retinas (Pérez de Lara et al., 2018). A many-fold increase in the concentration of Ap_4A and Ap_5A is recorded from corneal epithelial cells due to mechanical stress (Carracedo et al., 2013). The overexpression of P2X and P2Y receptors in the eye has been reviewed (Sanderson et al., 2014). Ap_4A acts at P2 receptors and modulates the immune response. Ap_3A and Ap_4A have long been reported to be present in a micromolar concentration in platelets, and their hydrolysis by ectonucleotidases yields P2 receptor agonists, leading to a cascade of purinergic signalling (Hoyle et al., 2001; Lüthje et al., 1983; Lüthje et al., 1988). Ap_4A is concomitantly released from platelets along with Ap_3A. Dinucleotide receptors are overexpressed in the central nervous system (CNS) and myocardial tissues, adrenal glands, and endothelial cells (Jankowski et al., 2003; Luo et al., 2004; Pintor et al., 1995; Zhou et al., 2019).

Secretory mechanisms release these polyphosphates from the cytosol to act as extracellular nucleotides. Potent hydrolysis of these substrates was observed by ectonucleotidases, mainly NPP1, -3, and -4 (Vollmayer et al., 2003). NPP1 favours Ap4A as a substrate. The resulting hydrolysis product ATP is hydrolysed to AMP by either NPPs or NTPDases. Nucleotide polyphosphate hydrolysis forms AMP, then hydrolysed by ecto-5'-NT to adenosine.

d. Uridine nucleotides and nucleotide sugars

The uridine nucleotide UTP is transported to the extracellular sites either by pannexin-1 hemichannels or in secretory vesicles, where it interacts potently with P2Y receptor subtypes $P2Y_2$ and $P2Y_6$ promoting, e.g., fibrosis (Ferrari et al., 2016; Lazarowski et al., 1997; Lazarowski & Boucher, 2001; Vinken, 2015). Targeting purinergic signalling in viral infections could be an effective therapeutic strategy since the abundant release of both ATP and UTP is reported in the extracellular environment (Ferrari et al., 2018). Ectoenzymes e.g., NTPDases, and NPPs, in concert with ecto-5'-NT (CD73), hydrolyse UTP and UDP to UMP and ultimately to uridine that have critical intracellular functions (Ipata et al., 2010). Uridine nucleotide signalling regulates hepatic functions and induces hematopoietic stem cell migration, bicarbonate secretion in gallbladder epithelium, the proliferation of renal mesangial cells, human keratinocytes, and affects systolic heart failure. Uridine-based nucleotide sugars uridine 5'-diphosphate-α-D-glucose (UDP-GLc), uridine 5'-diphosphate-α-D-galactose (UDP-Gal), uridine 5'-diphosphate-N-acetyl-α-D-glucosamine/ galactosamine (UDP-GlcNAc) / (UDP-Gal-NAc) perform critical cellular functions including post-translational glycosylation (Adeva-Andany et al., 2016; Hirschberg, 2018; Orellana et al., 2016). Besides their intracellular role, UDP sugars are potent natural agonists for $P2Y_{14}$ receptors, modulating immune cells, hematopoietic stem cells, and astrocytes, as well as promoting neutrophils in lung inflammation (Lazarowski & Harden, 2015; Sesma et al., 2009). A transport pathway was proposed for UDP-sugars from the lumen of the endoplasmic reticulum and Golgi bodies (EPR/GB) as secretary vesicles shipped to the extracellular space. These ectonucleotides are essential for cancer and immune cell signalling, and their abundance in the extracellular spaces highlights inflammatory conditions.

1.3.3 Ectonucleotidases

Cell surface-located ectonucleotidases hydrolyse pro-inflammatory nucleotides (ATP, NAD^+, UTP, and polyphosphates) to anti-inflammatory adenosine (Zimmermann et al., 2012). Five major types of ectonucleotidases are ecto-nucleoside triphosphate diphosphohydrolases (E-NTPDases 1 – 8, CD39, EC 3.6.1.5), ecto-5′-nucleotidase (CD73, EC 3.1.3.5), NAD^+ glycohydrolases (CD38/CD157, EC 3.2.2.5), ecto-nucleotide pyrophosphatase /phosphodiesterases (E-NPPs 1 – 7, EC 3.6.1.9, EC 3.1.4.1), and alkaline phosphatases (APs, EC 3.1.3.1). These enzymes can hydrolyse a variety of significant nucleotides. Numerous reports suggest these enzymes work in pairs and are co-expressed in close localities. One such enzyme pair is the CD39/CD73 pair, which comprises canonical or the classical pathway of extracellular adenosine production. This pair can potently hydrolyse ATP and UTP to adenosine and uridine, respectively (Ferrero et al., 2018). CD38 and CD157 prefer NAD^+ and potently hydrolyse it to ADPR; however, for CD157, cyclic ADPR is the primary product. E-NPPs possess less substrate-specificity, and they are capable of hydrolysing ATP, nicotinamide-adenine-dinucleotide or NAD^+, and nucleotide sugars ADP-ribose, UDP-glucose UDP-galactose along with guanosine, uridine, and cytidine triphosphates. Major hydrolysis products of E-NPP hydrolysis are monophosphates of the respective nucleosides. Together with CD73 and CD38, NPPs constitute the non-canonical pathway of extracellular adenosine production. The path is highly expressed in various pathological conditions and certain cancer types. APs can hydrolyse ATP directly to adenosine and, therefore, don’t need CD73 and can initiate anti-inflammatory responses independently. mRNA analysis of cancer cell lines showed that different ectonucleotidases are co-expressed and work nearby. The primary outcome of this coordinated hydrolysis cascade is the production of immunosuppressive adenosine.

For more in-depth information on each subtype of ectonucleotidases, refer to the specific chapter dedicated to each subtype. These chapters will cover topics such as preferred substrates, monitoring assays, kinetic analysis for different substrates compared to other enzymes, and small-molecule inhibitors for these enzymes. The primary focus, however, is on nucleotide hydrolysing enzymes such as NPP1, NPP3, CD39, CD38, and CD73.

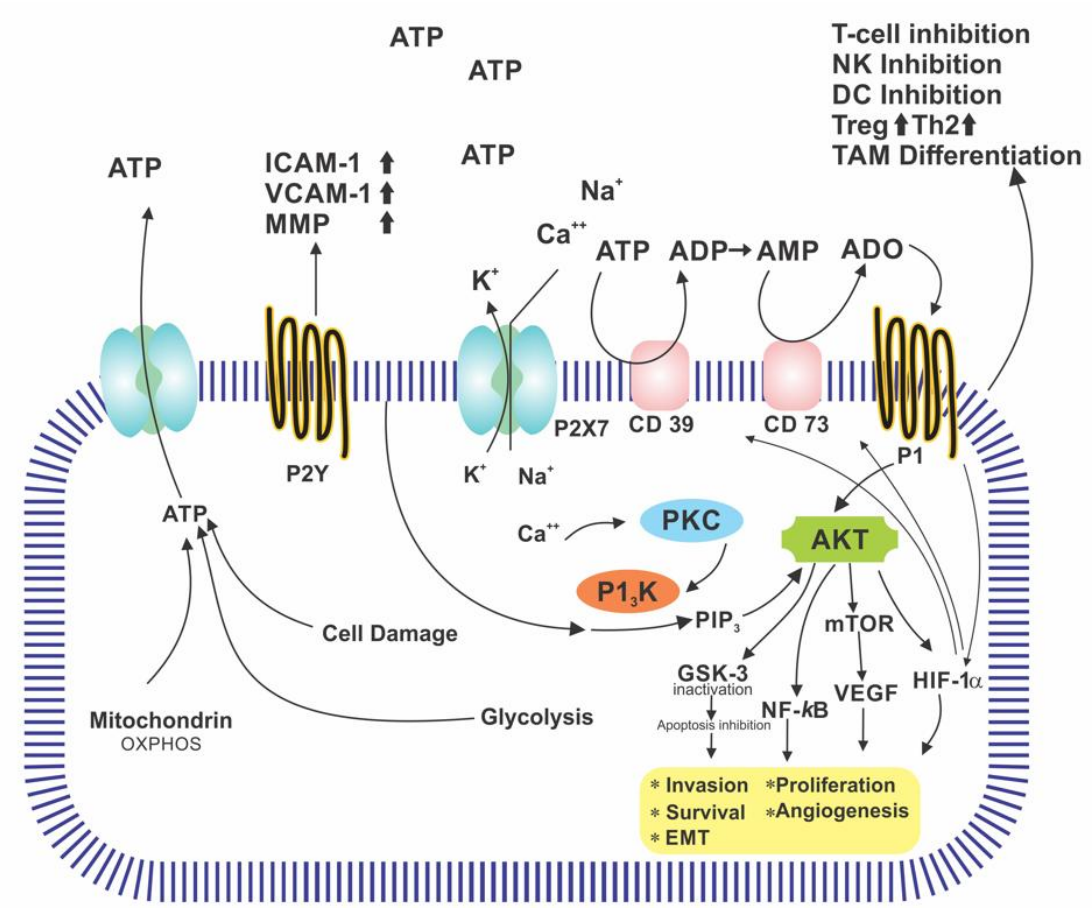

Figure 1.8: Purinergic signalling under hypoxic and inflammatory conditions. The figure is modified from (Aria et al., 2022). DC, dendritic cell; EMT, epithelial-mesenchymal transition; GSK-3, glycogen synthase kinase-3; HIF-1a, hypoxia-inducible factor 1-alpha; ICAM-1, intercellular Adhesion Molecule 1; MMP, matrix metallopeptidase; mTOR, mammalian target of rapamycin; NF-kb, nuclear factor kappa B; NK cell, natural killer cell; OXPHOS, oxidative phosphorylation; PANX, pannexin; PI_3K, phosphoinositide 3-kinases; PIP2, phosphatidylinositol-4, 5-bisphosphate; PIP3, phosphatidylinositol-3, 4, 5-triphosphate; PKC, protein kinase C; TAM, tumor-associated macrophage; Th2, T helper type 2; Treg, regulatory T cell; VCAM-1, vascular cell adhesion molecule 1; VEGF, vascular endothelial growth factor.

1.4 Purinergic signalling in cancer

Purinergic signalling has a role in the pathogenesis of several tumours and the interaction of the immune cells with the tumour. Overexpression of purinergic signaling components such as P2 receptors P2X, P2Y, P1 receptors (A_1, A_{2A}, A_{2B}, A_3), and ectonucleotidases (CD39, CD38, NPP1, NPP3, and CD73) are reported in cancer. It constitutes a highly active signalling pathway in the TME, causing potent hydrolysis of the nucleotides ATP, NAD^+, ADPR, Ap_nA, and AMP into adenosine that initiates intracellular signalling via

adenosine receptors (Zanoni et al., 2022). Tumor-associated molecules are essential targets for the development of immunotherapeutics, which is established as an important therapeutic modality alongside chemotherapeutics, radiotherapeutics, and targeted therapies such as kinase inhibitors (Ge et al., 2020). Novel therapeutic approaches that could selectively target cancer cells by activating the immune system are investigated. In the subsequent paragraphs, we will briefly discuss purinergic signalling components overexpressed in cancers.

1. *Triple-negative breast cancer (TNBCs)*

Associated with a low-grade prognosis, TNBC is a subtype of breast cancer that shows no expression of estrogen/progesterone receptors (ER/PR) and human epidermal growth factor receptor 2 (HER2). This is associated with an enhanced risk of visceral metastasis (C. Anders & Carey, 2008; Dent et al., 2009; Yin et al., 2020). TNBC differs from other breast cancers by its rapid spread and limited therapeutic options. Complex signalling mechanisms are evident in TNBCs that could be promising targets for drug discovery (Hossain et al., 2018; Nedeljkovi´c & Damjanovi´cdamjanovi´c, 2019; Pohl et al., 2017; Qin et al., 2019). Purinergic signalling has emerged as a significant contributor to the metastasis of these cancers. Adenosine receptors A_1, A_{2A}, A_{2B}, P2X2, P2X6 and P2X7 are involved in proliferation (Aria et al., 2022). Overexpression of nucleoside diphosphate kinases (NDPK), CD39, CD73, adenosine deaminases (ADA), adenylate kinases (AK), and the development of chemoresistance (Duan et al., 2021; Ruiz-rodríguez et al., 2020). An increased level of CD73 mRNA was recorded in TNBC cell lines MDA-MB-231 following incubation with adenosine (Sandoval et al., 2016). Overexpression of ARs is observed to contribute to cancer development and metastasis (Feng et al., 2017). In preliminary data from our lab, a high ATPase and NADase activity was observed in MDA-MB-231 cell lines linked with appreciable hydrolysis of *para*-nitrophenol-5'-thymidine monophosphate (*p*-NPh-5'-TMP), suggesting a high NPPs activity alongside CD39 and CD73. Treating MDA-MB-231 cell lines with the ATP analogue adenosine-5'-[γ-thio] triphosphate (ATPγ S) significantly reduced the growth of breast cancer cells in an in-vivo mice model (Liu et al., 2021)The inhibitory effect of ATPγ S might be due to the downregulation of P2Y11 receptors on breast cancer cells, which suppresses cell migration and growth.

2. Lungs cancer (LnC)

LnCs are associated with a high disease incidence/mortality ratio and a low 5-year survival rate. They are subdivided into small cell lung cancer (SCLC) and non-small cell lung cancer (NSCLC) types. Tobacco smoking is considered a causative agent in approximately 80 – 90 % of the incidences (Spiro et al., 2005). Cancer cell-specific signalling is reported for LnCs (Galluzzo & Bocchetta, 2011; H. Guo et al., 2014; Hassan et al., 2016; K. Park et al., 2011; Rapp et al., 2017; Scoyk et al., 2008; Shigematsu & Gazdar, 2006; Stewart et al., 2014; Velcheti & Govindan, 2007; L. Wang et al., 2017; Xi & Chen, 2014). Expression of purinergic signalling components was previously reported on lung alveoli, and their altered functions are involved in the pathological conditions relating to both NSCLC and SCLC. High levels of adenosine reflect the activation of the adenosinergic pathway (Schneider et al., 2015), (Le et al., 2019). Overexpression of CD39 and CD73 is observed on NSCLCs under hypoxic conditions (T. Anders et al., 2020; Giatromanolaki et al., 2020). Upregulation of CD39 and CD73 indicates these enzymes' concerted action in hydrolysing ATP and ADP to adenosine.

3. Colorectal cancer (CRC)

Due to its heterogeneity, CRC is associated with a higher mortality rate and presents a challenge for developing immunotherapies (Ciardiello et al., 2019). Several treatments that target various tumour pathways are in different phases of clinical trials (Xie et al., 2020). These candidates include EGF/EGFR (epidermal growth factor/EGF receptor), VEGF/VEGFR (vascular endothelial growth factor/VEGF receptor), and HGF (hepatocyte growth factor). The activation of several mechanisms induces tumour immune escape. (Grasso et al., 2018; Tacconi et al., 2019). Due to nucleotide hydrolysis catalysed by the ectonucleotidases CD39/CD73 tandem pair and the upregulation of P2Y, P2X, and AR signalling has been recognised as a crucial mechanism (Madariaga et al., 2021). According to reports, patients with metastatic CRC who carried a CD39 variant allele had higher tumour responses to treatment (Gal et al., 2021). However, no information on whether non-canonical purinergic pathways (CD38/NPP1/CD73) are present in these cell lines requires additional study in the presence selective substrates of these enzymes and their inhibitors

4. Brain cancer

Highly aggressive brain tumour cells generally resist conventional chemotherapies (Huang et al., 2010). Signaling mechanisms could be possible drug targets for therapy. The TME of GBMs is highly immunosuppressive, with mounting evidence for tumor-associated macrophages, dendritic, and regulatory T cells (K. K. Jain, 2018; Rita et al., 2020). The observed activation of the adenosinergic pathway on GBMs gave high hopes for discovering immunotherapies (Jin et al., 2021). Activation of the CD39/73 tandem pair along with ARs is reported as a highly active pathway for the hydrolysis of extracellular ATP to adenosine; however, the presence of NPP1 enzymes is also observed (Lopez et al., 2021). NPP overexpression reflects the availability of both canonical (CD39/73) and non-canonical (NPPs/CD73) adenosinergic pathways. Both these pathways operate under somewhat different mechanisms to produce adenosine. CD39/73 enzymes hydrolyse ATP and ADP while (NPPs/CD73) nexus hydrolyse various substrates to adenosine. In tumour microenvironments where both pathways are active, inhibiting one pathway is insufficient to limit adenosine production. Therefore, combination therapy is advised to counter these highly virulent cancers (Ferrero et al., 2018). CD73 downregulation and adenosine depletion are linked with reduced glioblastoma growth and aggressiveness in both in-vitro and in-vivo settings (Azambuja, Ludwig, et al., 2019; Niechi et al., 2019).

5. Urinary tract cancer

Purinergic signalling is exceedingly functional during physiological and pathophysiological mechanisms involving the lower urinary tract. In this regard, an excellent review was previously published highlighting the critical role of purinergic receptors P2X1-3, 5, and 7 in the inflammation of the lower urinary tract (Burnstock, 2014), including cancer (bladder, prostate, and ovarian). A significant upregulation of purinergic signalling components is reported during urinary tract pathology. An enhanced extracellular concentration of nucleotides and their role in initiating immune response is well documented throughout this tract (Burnstock, 2013; Fry et al., 2021; Maynard et al., 2022). High adenosine concentrations are measured in the extracellular compartment, pointing to ectonucleotidase expression in these tissues. Ectonucleotidases may play an essential role in cancer propagation and metastasis. Primary urinary tract tumours include;

a. Bladder cancer

Bladder cancer has a higher prevalence in the urinary tract and is associated with a high recurrence rate. It is characterised by abnormal DNA methylation. Further analysis revealed a loss of heterozygosity at chromosomes 4p, 9p, 8p, 11p, and 13q significantly linked with a high-grade tumour (Besaratinia et al., 2013; Idlowles et al., 1994). An excellent review article on genetic mutations in bladder cancer has previously been published (Tran et al., 2021). The mRNA analysis of human bladder cancer cell lines HTB-9, HT1376, RT4, 5637, and T24 revealed that the overexpression of estrogen receptor-β was directly linked to the growth of bladder tumours offering an opportunity to target these virulent cancers (Ide et al., 2021; Ramos et al., 2014; Shen et al., 2006). Besides androgen receptors, expression of P2X1, 4, and 7 receptors are widely reported, pointing to the role of extracellular ATP (Ledderose et al., 2023). Moreover, the expression of ectonucleotidases is well documented. mRNA analysis revealed NTPDase 1-3 and 8 and CD73 expression. Whereas NTPDase-1 is localised in the endothelium, NTPDase-2 is close to the detrusor in the region of the lamina propria, NTPDase-3 is expressed in basal epithelial cells, NTPDase-8 in the urothelium and CD73 is localised in the detrusor smooth muscles (Yu et al., 2011). In another report analysing mRNA expression of significant ectonucleotidases in grade 1 (RT4) and grade 3 (T24) bladder cancer cell lines, overexpression of NPP1 mRNA was recorded alongside NTPDase-5, CD73, NPP2, and NPP3. A potent hydrolysis of the NPP-specific substrate *para*-nitrophenol-5'-thymidine monophosphate (*p*-NPh-5'-TMP) was observed, providing evidence for the functional role of NPPs in these cell lines (Stella et al., 2010). A study conducted in bladder cancer patients on ectonucleotidases CD39 and CD73 resulted in the upregulation of both enzymes that can contribute to the development and metastasis of bladder cancer (Ferreira et al., 2021).

b. Prostate cancer

Androgen receptors, testosterone, and 5α-dihydrotestosterone (DHT) are essential signalling molecules in the development and growth of prostate cancers. Reducing serum androgen levels and inhibiting its receptor is the cornerstone therapy for initial prostate cancer cases, and several therapeutic approaches have already been established targeting AR signalling (Aurilio et al., 2020). Immunotherapy has yet to produce results

against prostate cancer as it did against other solid tumours such as breast, renal, and lung cancer. A possible reason for its low impact is the highly immunosuppressive TME around prostate tumours, often highlighted as “cold tumours” (Kantoff et al., 2010; Amsberg et al., 2022). The immunosuppressive surrounding is maintained by prostate inherent factors such as regulatory T cells, tumour associated-macrophages-fibroblast-cytokines, myeloid-derived suppressor cells (MDSCs), cytotoxic T lymphocyte-associated protein-4, programmed cell death-1/ligand-1 (PD-1/-L1), and adenosine production (Stultz et al., 2021). Several reports suggest an overexpression of purinergic signalling components (receptors and enzymes) in the TME of prostate cancer that may contribute to its growth. Hypoxia-inducible factor-1α (HIF-1α) and vascular endothelial growth factor (VEGF) activate ATP binding to the P2X receptor subtypes P2X4 and P2X7. This activation stimulates prostate cancer growth via mitogen-associated protein kinases (MAPKs), p38, ERK1/2, and PTEN, PI_3K, and AKT pathways. $P2Y_2$ utilises Src/p38/CoX-2 pathway to stimulate tumour growth (L. Chen et al., 2004; Z. Wang et al., 2023). Adenosine production pathways in prostate cancer are primarily comprised of prostatic acid phosphatase (PAP). PAP is reported to hydrolyse AMP to adenosine, like CD73 potently, and is expressed as a membrane-bound and soluble variant showing optimum enzymatic activity under acidic pH conditions (Zimmermann, 2009).

c. Ovarian cancer

Ovarian cancers (OC) are subdivided into epithelial OC and non-epithelial OC, with the former comprising more than 90 % of the cases. EOCs are further subdivided into endometrioid carcinoma (EC), clear cell carcinoma (CCC), mucinous carcinoma (MC), low-grade serous carcinoma (LGSC), and high-grade serous carcinoma (HGSC). HGSC is the most lethal and abundant tumour, accounting for more than 70% of cases. It is associated with a high proliferation rate representing the advanced stages III and IV (Rosen et al., 2009). OC has shown limited response to immunotherapy [anti-programmed cell death-1/-L1 (anti-PD-1/PD-L1)]. A growing body of research indicates that OC cells release a lot of extracellular vesicles (EVs), which are crucial for tumour growth and recurrence. In OCs TME, stromal and immune cells communicate to evade the immune system, resulting in metastasis (Tian et al., 2022). Several immune escape signalling pathways are reported (Krockenberger et al., 2008), (Gao et al., 2021; Wolf et al., 2020).

Wide-spread expression of ectonucleotidases, particularly CD39 and CD73, is reported in HGSC, representing a pathway for escaping immune surveillance. The concerted action of these enzymes hydrolyses ATP to adenosine (Bareche et al., 2021). GPI-anchored CD73 is overexpressed on OC-initiating cells with a primary role in cancer development and progression (Lupia et al., 2018). Down-regulation of CD39/73 expression or inhibition of enzymatic activity could be an effective treatment option to suppress myeloid-derived suppressor cell (MDSC) function (L. Li et al., 2018). Anti-CD39 and anti-CD73 antibodies improve targeted therapy of OC cases (Fm Häusler et al., 2014). In preliminary experiments conducted in our lab at AK Muller, a higher expression of NPP enzymes was observed in OC cell lines. Potent hydrolysis of the artificial substrate *p*-NPh-5'-TMP was observed. The NPP activity was inhibited using recently developed inhibitors from our lab.

6. Leukaemia

Abnormal production of white blood cells (WBC) is characterised by bone marrow malfunctioning. Leukaemia is subdivided into four subtypes; acute lymphoblastic leukaemia (ALL) is most frequent in children. However, it can also affect adults. The most prevalent form of acute leukaemia in adults is acute myeloid leukaemia (AML); in elderly patients (> 60), chronic lymphocytic leukaemia (CLL) and more uncommon chronic myeloid leukaemia (CML). Numerous critical signalling components that control different cellular functions are dysregulated in leukaemia, possibly due to overexpression of signalling components, a functional mutation, or indirectly via molecular binding on the extracellular sides (Bongiovanni et al., 2017). Signalling components that regulate cellular functions are well explored (Park et al., 2010; Scholl et al., 2008). Multiple mechanisms are active in leukaemia, which is linked to immune escape (Vago et al., 2020).

Immunotherapy is the mainstay of leukaemia treatment, and several ongoing clinical trials target different immune system components, including monoclonal antibodies, T-cell therapy, adoptive-NK therapy, immune checkpoint blockade via PD-1/PD-L1, CTLA4, TIM3, and leukaemia vaccines (Isidori et al., 2021). Purinergic signalling is another vital pathway functional in leukaemia, and several reports highlight its critical role in the disease process. Expression of P2R is reported on AML, particularly P2X7, P2Y2, and P2Y4 receptors (Salvestrini et al., 2012). Numerous reports suggest widespread expression of ectonucleotidases belonging to two connected adenosinergic pathways:

canonical and non-canonical. The canonical path comprises CD39 and CD73, hydrolyse extracellular ATP into adenosine. The non-canonical pathway is more diversified, consisting of CD38/NPP1/CD73 that hydrolyses both ATP and NAD^+ to immunosuppressive adenosine (Abousamra et al., 2015; Ferrero et al., 2019; Horenstein et al., 2013; Perry et al., 2012; Vaisitti et al., 2019). The adenosine burden initiates a sequence of events, leading tumour cells to bypass immune defence.

7. Pancreatic cancers (PC)

These cancers can either be endocrine or exocrine, where the latter type is more abundant, with >90% of the cases belonging to the exocrine origin. In exocrine tumours, approximately 85% of the cases are pancreatic ductal adenocarcinoma (PDAC), which affects the cell lining and is characterised by the worst prognosis (Kleeff et al., 2016). It was considered difficult to treat cancer in the past because of the involvement of multiple signalling pathways; however, during the last few years, significant progress has been made in understanding these mechanisms for specific tumour targeting. The abnormality of signalling components of pancreatic cancer leads to tumour growth and metastasis (Ishiwata et al., 2012; Kleeff et al., 2016). Purinergic signalling is abundantly reported in pancreatic tumours, and numerous pieces of evidence suggest the expression of P1 and P2 receptors (Burnstock, 2014). It is further observed that voltage-dependent Ca^{2+} influx causes the release of ATP/ADP, which in turn activates purinergic receptors of the Gq/11-coupled $P2Y_1$ receptor and induces activation of subsequent intracellular signalling mechanisms (Khan et al., 2014). The highly immunosuppressive environment of pancreatic tumours is due to the overexpression of Ars, particularly A_{2B} causing tumour invasiveness and metastasis (Strickland et al., 2023). Overexpression of purinergic receptors is coupled with the enhanced expression of ectonucleotidases, mainly NTPDases and CD73 (Jacoberger-Foissac et al., 2023; Syed et al., 2013). The concerted action of CD39 and CD73 further enhances the immunosuppressive nature of TME in PCs. Moreover, a soluble form of CD73 (GP1 anchor detached) further increases this adenosine burden. Less research is reported on the overexpression of NPP1 and CD38 on pancreatic cancer cells.

8. Hepatocellular carcinoma (HCC)

Hepatocellular carcinoma (HCC) is the primary liver cancer characterised by a poor prognosis and often leads to cirrhosis (80–90% of patients). HBV and HCV lead to approximately 80 –90% of all HCCs, where HCV has been the most common viral cause (Nordenstedt et al., 2010). Obesity, diabetes, and linked non-alcoholic fatty liver disease are the major risk factors (Mittal et al., 2013). Tumour-specific signalling pathways have previously been reported for HCC (Fabregat et al., 2016; He et al., 2020; Ro et al., 2021; Xue et al., 2021). Purinergic signalling has a role in liver pathologies where reports suggest overexpression of purinergic receptors P1 and P2 (Jain et al., 2021). P2X and P2Y receptors are involved in pathological cases such as non-alcoholic fatty liver disease, fibrosis, and HCC. Upregulation of ectonucleotidases, mainly NTPDases (CD39 and NTPDase 2) and CD73, is observed in HCC, further emphasising the involvement of these enzymes in the breakdown of nucleotides to nucleosides resulting in immunosuppression (Wang et al., 2020).

During this research period, some cancer cell lines were evaluated based on their ability to hydrolyse ATP and NAD^+. The findings are presented in chapters 2 and 3 of this thesis.

Table 1.4: Purinergic signalling in primary cancers

Cancer type	Purinergic receptors	Enzymes	References
Triple-negative breast cancer	A_1, A_{2A}, A_{2B} P2X2, P2X6 and P2X7	Nucleoside diphosphate kinases (NDPK), CD39, CD73, adenosine deaminases (ADA), adenylate kinases (AK) NPP1 (AK Muller)	(Aria et al., 2022) (Duan et al., 2021; Ruiz-rodríguez et al., 2020) In this study
Lung cancer		CD39, CD73	(T. Anders et al., 2020; Giatromanolaki et al., 2020)
Colorectal cancer	P2Y, P2X, and AR	CD39, CD73	(Madariaga et al., 2021) (Gal et al., 2021)
Brain cancer		CD39, CD73, NPP1	(Azambuja, Ludwig, et al., 2019; Niechi et al., 2019). (Lopez et al., 2021)
Bladder cancer	P2X1, 4, and 7	NTPDase 1-3 and 8 and CD73 NPP1, NPP2 and NPP3	(Ledderose et al., 2023) (Ferreira et al., 2021) (Yu et al., 2011) (Stella et al., 2010)

Prostate cancer	P2X4 and P2X7 P2Y2	prostatic acid phosphatase (PAP)	(L. Chen et al., 2004; Z. Wang et al., 2023) (Zimmermann, 2009)
Ovarian cancer		CD39, CD73 NPP1	(L. Li et al., 2018) AK Muller
Leukeamia	P2X7, P2Y2, and P2Y4	CD38, NPP1, CD73	(Salvestrini et al., 2012) (Abousamra et al., 2015; Ferrero et al., 2019; Horenstein et al., 2013; Perry et al., 2012; Vaisitti et al., 2019)
Pancreatic cancer		CD39, CD73	(Jacoberger-Foissac et al., 2023; Syed et al., 2013)
Hepatocellular carcinoma	AR, P2X and P2Y	CD39, CD73	(Jain et al., 2021) (Wang et al., 2020)

1.5 Conclusion

Cancer cells and tissues are not a singular entity but a combination of numerous concerted components that work in tandem and nearby. The role of purinergic signalling in tumours is well-documented and highlighted. An upregulation of purinergic receptors and ectonucleotidases is linked with most difficult-to-treat cancers and could expedite the resistance towards immune surveillance. Extracellular nucleotides such as ATP and NAD^+ are significant triggers in the purinergic signalling process where an uplift in their concentrations is reported. Multiple mechanisms, such as ATP transporters, connexion-43 hemichannel, pannexin-1, cellular necrosis, and vesicular transport, contribute to this increase. High extracellular nucleotide concentration creates a pro-inflammatory environment that invites immune cells to attack the pathogen, foreign particles, dead cells, and tumours. In turn, an upregulation of ectonucleotidases is reported in many tumours. These enzymes hydrolyse nucleotides to adenosine, transforming the pro-inflammatory milieu into an anti-inflammatory, helping tumours bypass immune surveillance and silently propagate. Inhibition of these ectoenzymes (ectonucleotidases) by different therapeutic modalities, such as antibodies and small-molecule inhibitors, can potentially target this escape route. Moreover, two adenosine-producing pathways have been recognised. The canonical CD39/73 and non-canonical CD38/NPP/CD73. The inhibition of one pathway is only sometimes sufficient to seize adenosine production.

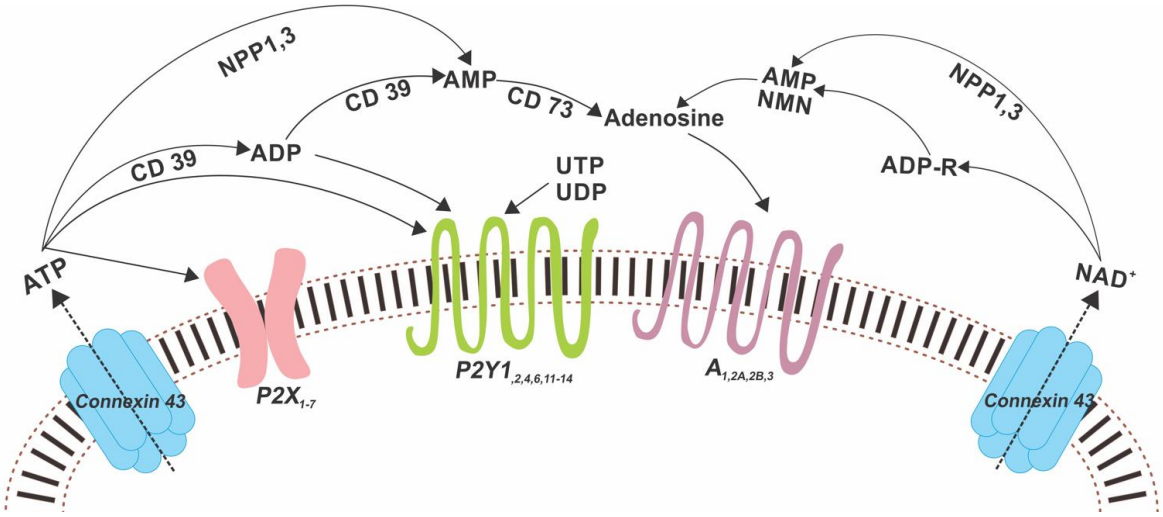

Figure 1.9: Overview of purinergic signalling representing nucleotide transporters, purinergic receptors, and ectonucleotidases.

Acknowledgement

The author thanks Mr Tahir (ColourGraphics D. I. Khan) for helping with figures using Corel Draw 16 during a two-month training course.

References

Abousamra, N. K., Salah El-Din, M., Hamza Elzahaf, E., & Esmael, M. E. (2015). Ectonucleoside triphosphate diphosphohydrolase-1 (E-NTPDase1/CD39) as a new prognostic marker in chronic lymphocytic leukemia. *Leuk. Lymphoma*, *56*, 113–119. https://doi.org/10.3109/10428194.2014.907893

Adeva-Andany, M. M., González-Lucán, M., Donapetry-García, C., Fernández-Fernández, C., & Ameneiros-Rodríguez, E. (2016). Glycogen metabolism in humans. *BBA Clin.*, *5*, 85–100. https://doi.org/10.1016/j.bbacli.2016.02.001

Aghdam, M. S., Jannatizadeh, A., Luo, Z., & Paliyath, G. (2018). Ensuring sufficient intracellular ATP supplying and friendly extracellular ATP signaling attenuates stresses, delays senescence and maintains quality in horticultural crops during postharvest life. *Trends Food Sci. Technol.*, *76*, 67–81. https://doi.org/10.1016/j.tifs.2018.04.003

Akkaya, M., Kwak, K., & Pierce, S. K. (2020). B cell memory: building two walls of protection against pathogens. In *Nat. Rev. Immunol.* (Vol. 20, pp. 229–238). Nature Research. https://doi.org/10.1038/s41577-019-0244-2

Alvarez, C. L. (2021). Extracellular ATP and adenosine in tumor microenvironment : Roles in epithelial – mesenchymal transition , cell migration , and invasion. *J. Cell. Physiol.*, *236*, 1–12. https://doi.org/10.1002/jcp.30580

Aman, Y., Qiu, Y., Tao, J., & Fang, E. F. (2018). Translational Medicine of Aging Therapeutic potential of boosting NAD+ in aging and age-related diseases. *Transl. Med. Aging*, *2*, 30–37. https://doi.org/10.1016/j.tma.2018.08.003

Anders, C., & Carey, L. A. (2008). Understanding and Treating Triple-Negative Breast Cancer. *Oncology*, *22*, 1233–1243.

Anders, T., Gyrid, S., & Wahl, F. (2020). Ectonucleotidase CD39 and Checkpoint Signalling Receptor Programmed Death 1 are Highly Elevated in Intratumoral Immune Cells in Non e small-cell Lung Cancer. *Transl. Oncol.*, *13*, 17–24. https://doi.org/10.1016/j.tranon.2019.09.003

Aria, H., Rezaei, M., Nazem, S., Daraei, A., Nikfar, G., Mansoori, B., Bahmanyar, M., Tavassoli, A., Vakil, M. K., & Mansoori, Y. (2022). Purinergic receptors are a key bottleneck in tumor metabolic reprogramming: The prime suspect in cancer therapeutic resistance. *Front. Immunol.*, *13*. https://doi.org/10.3389/fimmu.2022.947885

Aurilio, G., Cimadamore, A., Mazzucchelli, R., Lopez-Beltran, A., Verri, E., Scarpelli, M., Massari, F., Cheng, L., Santoni, M., & Montironi, R. (2020). Androgen Receptor Signaling Pathway in Prostate Cancer: From Genetics to Clinical Applications. In *Cells* (Vol. 9, pp. 1–14). NLM (Medline). https://doi.org/10.3390/cells9122653

Azambuja, J. H., Ludwig, N., Braganhol, E., & Whiteside, T. L. (2019). Inhibition of the Adenosinergic Pathway in Cancer Rejuvenates Innate and Adaptive Immunity. *Int. J. Mol. Sci*, *20*, 1–23.

Baker, K. D., Edwards, T. M., & Rickard, N. S. (2013). The role of intracellular calcium stores in synaptic plasticity and memory consolidation. *Neurosci. Biobehav. Rev.*, *37*, 1211–1239. https://doi.org/10.1016/j.neubiorev.2013.04.011

Balkwill, F. R., Capasso, M., & Hagemann, T. (2012). The tumor microenvironment at a glance. *J. Cell Sci.*, *125*, 5591–5596. https://doi.org/10.1242/jcs.116392

Ballerini, P., Dovizio, M., Bruno, A., Tacconelli, S., & Patrignani, P. (2018). P2Y12 receptors in tumorigenesis and metastasis. In *Front. Pharmacol.* (Vol. 9, pp. 1–9). Frontiers Media S.A. https://doi.org/10.3389/fphar.2018.00066

Bareche, Y., Pommey, S., Carneiro, M., Buisseret, L., Cousineau, I., Thebault, P., Chrobak, P., Communal, L., Allard, D., Robson, S. C., Mes-Masson, A. M., Provencher, D., Lapointe, R., & Stagg, J. (2021). High-dimensional analysis of the adenosine pathway in high-grade serous ovarian cancer. *J Immunother. Cancer*, *9*, 1–10. https://doi.org/10.1136/jitc-2020-001965

Barragán-Iglesias, P., Mendoza-Garcés, L., Pineda-Farias, J. B., Solano-Olivares, V., Rodríguez-Silverio, J., Flores-Murrieta, F. J., Granados-Soto, V., & Rocha-González, H. I. (2015). Participation of peripheral P2Y1, P2Y6 and P2Y11 receptors in formalin-induced inflammatory pain in rats. *Pharmacol. Biochem. Behav.*, *128*, 23–32. https://doi.org/10.1016/j.pbb.2014.11.001

Beamer, E., Conte, G., & Engel, T. (2019). ATP release during seizures – A critical evaluation of the evidence. *Brain Res. Bull.*, *151*, 65–73. https://doi.org/10.1016/j.brainresbull.2018.12.021

Besaratinia, A., Cockburn, M., & Tommasi, S. (2013). Alterations of DNA methylome in human bladder cancer. *Epigenetics*, *8*, 1013–1022. https://doi.org/10.4161/epi.25927

Bird, J. E., Wang, X., Smith, P. L., Barbera, F., Huang, C., & Schumacher, W. A. (2012). A platelet target for venous thrombosis? P2Y1 deletion or antagonism protects mice from vena cava thrombosis. *J. Thromb. Thrombolysis*, *34*, 199–207. https://doi.org/10.1007/s11239-012-0745-3

Bongiovanni, D., Saccomani, V., & Piovan, E. (2017). Aberrant signaling pathways in t-cell acute lymphoblastic leukemia. In *Int. J. Mol. Sci.* (Vol. 18, pp. 1–29). MDPI AG. https://doi.org/10.3390/ijms18091904

Borea, P. A., Gessi, S., Merighi, S., Vincenzi, F., & Varani, K. (2018a). Pharmacology of Adenosine receptors: The state of the art. *Physiol Rev .*, *98*, 1591–1625. https://doi.org/10.1152/physrev.00049.2017

Borea, P. A., Gessi, S., Merighi, S., Vincenzi, F., & Varani, K. (2018b). Pharmacology of Adenosine Receptors: The State of the Art. *Physiol Rev*, *98*, 1591–1625. https://doi.org/10.1152/physrev.00049.2017.-Adenosine

Bruzzone, S., Guida, L., Zocchi, E., Franco, L., Flora, A. De, & Mezzocannone, V. (2000). Connexin 43 hemichannels mediate Ca 2+ -regulated transmembrane NAD + fluxes in intact cells. *FASEB j.*, *15*, 1–17.

Burnstock, G. (1972). Purinergic nerves. *Pharmacol. Rev.*, *24*, 510–581.

Burnstock, G. (2012). Discovery of purinergic signalling , the initial resistance and current explosion of interest. *Br. J. Pharmacol.*, *167*, 238–255. https://doi.org/10.1111/j.1476-5381.2012.02008.x

Burnstock, G. (2013). Purinergic signalling in the lower urinary tract. In *Acta Physiologica* (Vol. 207, pp. 40–52). https://doi.org/10.1111/apha.12012

Burnstock, G. (2014a). Purinergic signalling in endocrine organs. *Purinergic Signalling*, *10*, 189–231. https://doi.org/10.1007/s11302-013-9396-x

Burnstock, G. (2014b). Purinergic signalling in the urinary tract in health and disease. *Purinergic Signalling*, *10*, 103–155. https://doi.org/10.1007/s11302-013-9395-y

Burnstock, G., & Di Virgilio, F. (2013). Purinergic signalling and cancer. *Purinergic Signalling*, *9*, 491–540. https://doi.org/10.1007/s11302-013-9372-5

Burnstock, G., & Street, G. (1990). Noradrenaline and ATP as cotransmitters in sympathetic nerves. *Neurchem. Int.*, *17*, 357–368. https://doi.org/10.1016/0197-0186(90)90158-p.

Burotto, M., Chiou, V. L., Lee, J. M., & Kohn, E. C. (2014). The MAPK pathway across different malignancies: A new perspective. In *Cancer* (Vol. 120, pp. 3446–3456). John Wiley and Sons Inc. https://doi.org/10.1002/cncr.28864

Campbell, B. B., Galati, M. A., Stone, S. C., Riemenschneider, A. N., Edwards, M., Sudhaman, S., Siddaway, R., Komosa, M., Nunes, N. M., Nobre, L., Morrissy, A. S., Zatzman, M., Zapotocky, M., Joksimovic, L., Kalimuthu, S. N., Samuel, D., Mason, G., Bouffet, E., Morgenstern, D. A., … Tabori, U. (2021). Mutations in the RAS/MAPK pathway drive replication repair-deficient hypermutated tumors and confer sensitivity to mek inhibition. *Cancer Discovery*, *11*, 1454–1467. https://doi.org/10.1158/2159-8290.CD-20-1050

Carracedo, G., Guzman-Aranguez, A., Loma, P., & Pintor, J. (2013). Diadenosine polyphosphates release by human corneal epithelium. *Exp. Eye Res.*, *113*, 156–161. https://doi.org/10.1016/j.exer.2013.05.022

Chen, L., He, H. Y., Li, H. M., Zheng, J., Heng, W. J., You, J. F., & Fang, W. G. (2004). ERK1/2 and p38 pathways are required for P2Y receptor-mediated prostate cancer invasion. *Cancer Letters*, *215*, 239–247. https://doi.org/10.1016/j.canlet.2004.05.023

Chen, Q., Lu, X., & Zhang, X. (2021). Noncanonical nf-κb signaling pathway in liver diseases. In *J. Clin. Transl. Hepatol.* (Vol. 9, pp. 81–89). Xia and He Publishing Inc. https://doi.org/10.14218/JCTH.2020.00063

Choi, M. C., Jo, J., Park, J., Kang, H. K., & Park, Y. (2019). NF-κb signaling pathways in osteoarthritic cartilage destruction. *Cells*, *8*, 1–21. https://doi.org/10.3390/cells8070734

Ciardiello, D., Vitiello, P. P., Cardone, C., Martini, G., Troiani, T., Martinelli, E., & Ciardiello, F. (2019). Immunotherapy of colorectal cancer : Challenges for therapeutic e ffi cacy. *Cancer Treat. Rev.*, *76*, 22–32. https://doi.org/10.1016/j.ctrv.2019.04.003

Clouet, S., Di Pietrantonio, L., Daskalopoulos, E. P., Esfahani, H., Horckmans, M., Vanorlé, M., Lemaire, A., Balligand, J. L., Beauloye, C., Boeynaems, J. M., & Communi, D. (2016). Loss of mouse P2Y6 nucleotide receptor is associated with physiological macrocardia and amplified pathological cardiac hypertrophy. *J. Bio. Chem.*, *291*, 15841–15852. https://doi.org/10.1074/jbc.M115.684118

Coddou, C. (2019). Differential Effects of Purinergic Signaling in Gastric Cancer-Derived Cells Through P2Y and P2X Receptors. *Front. Pharmacol.*, *10*, 1–15. https://doi.org/10.3389/fphar.2019.00612

Courtois, G., & Gilmore, T. D. (2006). Mutations in the NF-κB signaling pathway: Implications for human disease. In *Oncogene* (Vol. 25, pp. 6831–6843). https://doi.org/10.1038/sj.onc.1209939

Curet, M. A., & Watters, J. J. (2018). P2Y14 receptor activation decreases interleukin-6 production and glioma GL261 cell proliferation in microglial transwell cultures. *J. Neuro-Oncol.*, *137*, 23–31. https://doi.org/10.1007/s11060-017-2700-9

de Almeida-Pereira, L., Magalhães, C. F., Repossi, M. G., Thorstenberg, M. L. P., Sholl-Franco, A., Coutinho-Silva, R., Ventura, A. L. M., & Fragel-Madeira, L. (2017). Adenine Nucleotides Control Proliferation In Vivo of Rat Retinal Progenitors by P2Y1 Receptor. *Mol. Neurobiol.*, *54*, 5142–5155. https://doi.org/10.1007/s12035-016-0059-0

Dejardin, E. (2006). The alternative NF-κB pathway from biochemistry to biology: Pitfalls and promises for future drug development. *Biochem. Pharmacol.*, *72*, 1161–1179. https://doi.org/10.1016/j.bcp.2006.08.007

de Melo Aquino, B., da Silva dos Santos, D. F., Jorge, C. O., Marques, A. C. S., Teixeira, J. M., Parada, C. A., & Oliveira-Fusaro, M. C. G. (2019). P2X3 receptors contribute to muscle pain induced by static contraction by a mechanism dependent on neutrophil migration. *Purinergic Signalling*, *15*, 167–175. https://doi.org/10.1007/s11302-019-09659-0

Dent, R., Hanna, Æ. W. M., Sun, P., & Narod, Æ. S. A. (2009). Pattern of metastatic spread in triple-negative breast cancer. *Breast Cancer Res. Treat.*, *115*, 423–428. https://doi.org/10.1007/s10549-008-0086-2

Dietrich, F., Cappellari, A. R., Filippi-Chiela, E. C., de Paula, P. B., de Souza, J. B., Agatti, S. W., Andrejew, R., Roesler, R., Morrone, F. B., & Battastini, A. M. O. (2022). High P2X6 receptor expression in human bladder cancer predicts good survival prognosis. *Mol. Cell. Biochem.*, *477*, 2047–2057. https://doi.org/10.1007/s11010-022-04425-0

Diezmos, E. F., Bertrand, P. P., Liu, L., Poole, D. P., & Liu, L. (2016). Purinergic Signaling in Gut Inflammation : The Role of Connexins and Pannexins. *Front. Neurosci.*, *10*, 1–11. https://doi.org/10.3389/fnins.2016.00311

Dillon, M., Lopez, A., Lin, E., Sales, D., Perets, R., & Jain, P. (2021). cancers Progress on Ras/MAPK Signaling Research and Targeting in Blood and Solid Cancers. *Cancers*, *13*, 1–35. https://doi.org/10.3390/cancers

Di Virgilio, F., Dal Ben, D., Sarti, A. C., Giuliani, A. L., & Falzoni, S. (2017). The P2X7 Receptor in Infection and Inflammation. In *Immunity* (Vol. 47, pp. 15–31). Cell Press. https://doi.org/10.1016/j.immuni.2017.06.020

Di Virgilio, F., Sarti, A. C., Falzoni, S., De Marchi, E., & Adinolfi, E. (2018). Extracellular ATP and P2 purinergic signalling in the tumour microenvironment. *Nat. Rev. Cancer*, *18*, 601–618.

Dosch, Michel, Joël Gerber, F. J. and G. B. (2018). Mechanisms of ATP Release by Inflammatory Cells. *Int. J. Mol. Sci*, *19*, 1–16.

Duan, S., Nordmeier, S., Byrnes, A. E., & Buxton, I. L. O. (2021). Extracellular Vesicle-Mediated Purinergic Signaling Contributes to Host Microenvironment Plasticity and Metastasis in Triple Negative Breast Cancer. *Int. J. Mol. Sci*, *22*, 1–21.

English, J. M., & Cobb, M. H. (2002). Pharmacological inhibitors of MAPK pathways. *Trends Pharmacol. Sci.*, *23*, 40–45. https://doi.org/https://doi.org/10.1016/S0165-6147(00)01865-4

Eun, S. Y., Ko, Y. S., Park, S. W., Chang, K. C., & Kim, H. J. (2015). P2Y2 nucleotide receptor-mediated extracellular signal-regulated kinases and protein kinase C activation induces the invasion of highly metastatic breast cancer cells. *Oncol. Rep.*, *34*, 195–202. https://doi.org/10.3892/or.2015.3972

Fabregat, I., Moreno-Càceres, J., Sánchez, A., Dooley, S., Dewidar, B., Giannelli, G., & ten Dijke, P. (2016). TGF-β signalling and liver disease. *FEBS Journal*, *283*, 2219–2232. https://doi.org/10.1111/febs.13665

Feng, J., Li, L., Zhang, N., Liu, J., Zhang, L., Gao, H., Wang, G., Li, Y., Zhang, Y., Li, X., Liu, D., Lu, J., & Huang, B. (2017). Androgen and AR contribute to breast cancer development and metastasis : an insight of mechanisms. *Oncogene*, *36*, 2775–2790. https://doi.org/10.1038/onc.2016.432

Ferrari, D., Gambari, R., Idzko, M., Tobias, M., & Albanesi, C. (2016). Purinergic signaling in scarring. *FASEB j.*, *30*, 3–12. https://doi.org/10.1096/fj.15-274563

Ferrari, D., Idzko, M., Müller, T., Manservigi, R., & Marconi, P. (2018). Purinergic Signaling : A New Pharmacological Target Against Viruses ? *Trends Pharmacol. Sci.*, *39*, 926–936. https://doi.org/10.1016/j.tips.2018.09.004

Ferrero, E., Faini, A. C., & Malavasi, F. (2018). A phylogenetic view of the leukocyte ectonucleotidases. *Immunol. Lett.*, *205*, 51–58. https://doi.org/10.1016/j.imlet.2018.06.008

Ferrero, E., Faini, A. C., & Malavasi, F. (2019). A phylogenetic view of the leukocyte ectonucleotidases. In *Immunol. Lett.* (Vol. 205, pp. 51–58). Elsevier B.V. https://doi.org/10.1016/j.imlet.2018.06.008

Fm Häusler, S., Montalbán Del Barrio, I., Diessner, J., Stein, R. G., Strohschein, J., Hönig, A., Dietl, J., & Wischhusen, J. (2014). Anti-CD39 and anti-CD73 antibodies A1 and 7G2 improve targeted therapy in ovarian cancer by blocking adenosine-dependent immune evasion. *Am J Transl Res*, *6*, 129–139. www.ajtr.org

Forthal, D. N. (2014). Functions of Antibodies. *Microbiol Spectr.*, *2*, 1–17.

Franke, H., & Illes, P. (2014). Nucleotide signaling in astrogliosis. In *Neurosci. Lett.* (Vol. 565, pp. 14–22). Elsevier Ireland Ltd. https://doi.org/10.1016/j.neulet.2013.09.056

Fry, C. H., & McCloskey, K. D. (2021). Purinergic signalling in the urinary bladder – When function becomes dysfunction. *Auton Neurosci*, *235*, 1–24. https://doi.org/10.1016/j.autneu.2021.102852

Galluzzo, P., & Bocchetta, M. (2011). Notch signaling in lung cancer. *Expert Rev. Anticancer Ther*, *11*, 533–540.

Gal, M., Romero-lorca, A., Ant, B., Mal, D., Moreno, A., Fern, A., & Novillo, A. (2021). Genetic Variants of ANGPT1 , CD39 , FGF2 and MMP9 Linked to Clinical Outcome of Bevacizumab Plus Chemotherapy for Metastatic Colorectal Cancer. *Int. J. Mol. Sci*, *22*, 1–16.

Gao, Y., Xu, Y., Zhao, S., Qian, L., Song, T., Zheng, J., Zhang, J., & Chen, B. (2021). Growth differentiation factor-15 promotes immune escape of ovarian cancer via targeting CD44 in dendritic cells. *Exp. Cell Res.*, *402*, 1–10. https://doi.org/10.1016/j.yexcr.2021.112522

Ge, Z., Wu, S., Zhang, Z., & Ding, S. (2020). Mechanism of tumor cells escaping from immune surveillance of NK cells. In *Immunopharmacol. Immunotoxicol.* (Vol. 42, pp. 187–198). Taylor and Francis Ltd. https://doi.org/10.1080/08923973.2020.1742733

Ghosh, G., & Wang, V. Y. F. (2021). Origin of the Functional Distinctiveness of NF-κB/p52. In *Frontiers in Cell and Developmental Biology* (Vol. 9). Frontiers Media S.A. https://doi.org/10.3389/fcell.2021.764164

Giatromanolaki, A., Kouroupi, M., Pouliliou, S., Mitrakas, A., Hasan, F., Pappa, A., & Koukourakis, M. I. (2020). Ectonucleotidase CD73 and CD39 expression in non-small cell lung cancer relates to hypoxia and immunosuppressive pathways. *Life Sciences*, *259*, 1–9. https://doi.org/10.1016/j.lfs.2020.118389

Gong, D., Zhang, J., Chen, Y., Xu, Y., Ma, J., Hu, G., Huang, Y., Zheng, J., Zhai, W., & Xue, W. (2019). The m6A-suppressed P2RX6 activation promotes renal cancer cells migration and invasion through ATP-

induced Ca2+ influx modulating ERK1/2 phosphorylation and MMP9 signaling pathway. *J. Exp. Clin. Cancer Res.*, *38*, 1–16. https://doi.org/10.1186/s13046-019-1223-y

Goody, M. F., & Henry, C. A. (2018). A need for NAD+ in muscle development, homeostasis, and aging. *Skeletal Muscle*, *8*, 1–14. https://doi.org/10.1186/s13395-018-0154-1

Grasso, C. S., Giannakis, M., Wells, D. K., Hamada, T., Mu, X. J., Quist, M., Nowak, J. A., Nishihara, R., Qian, Z. R., Inamura, K., Morikawa, T., Nosho, K., Abril-rodriguez, G., Connolly, C., Escuin-ordinas, H., Geybels, M. S., Grady, W. M., Hsu, L., Hu-lieskovan, S., … Hudson, T. J. (2018). Genetic Mechanisms of Immune Evasion in Colorectal Cancer. *Cancer Discovery*, *8*, 730–749. https://doi.org/10.1158/2159-8290.CD-17-1327

Gündüz, D., Tanislav, C., Sedding, D., Parahuleva, M., Santoso, S., Troidl, C., Hamm, C. W., & Aslam, M. (2017). Uridine triphosphate thio analogues inhibit platelet P2Y12 receptor and aggregation. *Int. J. Mol. Sci.*, *18*, 1–12. https://doi.org/10.3390/ijms18020269

Guo, C., Masin, M., Qureshi, O. S., & Murrell-Lagnado, R. D. (2007). Evidence for functional P2X4/P2X7 heteromeric receptors. *Mol. Pharmacol.*, *72*, 1447–1456. https://doi.org/10.1124/mol.107.035980

Guo, H., Lu, Y., Wang, J., Liu, X., Keller, E. T., Liu, Q., Zhou, Q., Zhang, J., & Jian Zhang or Qinghua Zhou, C. (2014). Targeting the Notch signaling pathway in cancer therapeutics. *Thorac. Cancer*, *5*, 473–486. https://doi.org/10.1111/1759-7714.12143

Haag, F., Adriouch, S., Braß, A., Jung, C., Möller, S., Scheuplein, F., Bannas, P., Seman, M., & Koch-Nolte, F. (2007). Extracellular NAD and ATP: Partners in immune cell modulation. *Purinergic Signalling*, *3*, 71–81. https://doi.org/10.1007/s11302-006-9038-7

Hanahan, D., & Weinberg, R. A. (2011). Hallmarks of Cancer : The Next Generation. *Cell*, *144*, 646–674. https://doi.org/10.1016/j.cell.2011.02.013

Hasan, D., Satalin, J., van der Zee, P., Kollisch-Singule, M., Blankman, P., Shono, A., Somhorst, P., den Uil, C., Meeder, H., Kotani, T., & Nieman, G. F. (2018). Excessive extracellular ATP desensitizes P2Y2 and P2X4 ATP receptors provoking surfactant impairment ending in ventilation-induced lung injury. In *Int. J. Mol. Sci.* (Vol. 19, pp. 1–19). MDPI AG. https://doi.org/10.3390/ijms19041185

Hassan, W. A., Yoshida, R., Kudoh, S., & Motooka, Y. (2016). Evaluation of role of Notch3 signaling pathway in human lung cancer cells. *J. Cancer Res. Clin. Oncol.*, *142*, 981–993. https://doi.org/10.1007/s00432-016-2117-4

Hayden, M. S., & Ghosh, S. (2004). Signaling to NF-κB. In *Genes Dev.* (Vol. 18, pp. 2195–2224). https://doi.org/10.1101/gad.1228704

Hemmings, B. A., & Restuccia, D. F. (2012). PI3K-PKB/Akt pathway. *Cold Spring Harbor Perspect. Biol.*, *4*, 1–3. https://doi.org/10.1101/cshperspect.a011189

He, S., & Tang, S. (2020). WNT/β-catenin signaling in the development of liver cancers. *Biomed. Pharmacother.*, *132*, 1–8. https://doi.org/10.1016/j.biopha.2020.110851

He, Y., Sun, M. M., Zhang, G. G., Yang, J., Chen, K. S., Xu, W. W., & Li, B. (2021). Targeting PI3K/Akt signal transduction for cancer therapy. In *Signal Transduction Targeted Ther.* (Vol. 6, pp. 1–17). Springer Nature. https://doi.org/10.1038/s41392-021-00828-5

Hilaire, C. S. T., Carroll, S. H., Chen, H., & Ravid, K. (2009). Mechanisms of induction of adenosine receptor genes and its functional significance. In *J. Cell. Physiol.* (Vol. 218, pp. 35–44). https://doi.org/10.1002/jcp.21579

Hirschberg, C. B. (2018). My journey in the discovery of nucleotide sugar transporters of the Golgi apparatus. *J. Biol. Chem.*, *293*, 12653–12662. https://doi.org/10.1074/jbc.X118.004819

Horckmans, M., Esfahani, H., Beauloye, C., Clouet, S., di Pietrantonio, L., Robaye, B., Balligand, J.-L., Boeynaems, J.-M., Dessy, C., & Communi, D. (2015). Loss of Mouse P2Y4 Nucleotide Receptor Protects against Myocardial Infarction through Endothelin-1 Downregulation. *J. Immunol.*, *194*, 1874–1881. https://doi.org/10.4049/jimmunol.1401364

Horenstein, A. L., Chillemi, A., Zaccarello, G., Bruzzone, S., Quarona, V., Zito, A., Serra, S., & Malavasi, F. (2013a). A CD38/CD203A/CD73 ectoenzymatic pathway independent of CD39 drives a novel adenosinergic loop in human T lymphocytes. *OncoImmunology*, *2*, 1–14. https://doi.org/10.4161/onci.26246

Horenstein, A. L., Chillemi, A., Zaccarello, G., Bruzzone, S., Quarona, V., Zito, A., Serra, S., & Malavasi, F. (2013b). A CD38/CD203A/CD73 ectoenzymatic pathway independent of CD39 drives a novel adenosinergic loop in human T lymphocytes. *OncoImmunology*, *2*, 1–15. https://doi.org/10.4161/onci.26246

Hossain, F., Sorrentino, C., Ucar, D. A., Peng, Y., Matossian, M., Wyczechowska, D., Crabtree, J., Zabaleta, J., Morello, S., Valle, L. Del, Burow, M., Collins-burow, B., Pannuti, A., Minter, L. M., Golde, T. E., Osborne, B. A., & Miele, L. (2018). Notch Signaling Regulates Mitochondrial Metabolism and NF- κ B Activity in Triple-Negative Breast Cancer Cells via IKK α -Dependent Non-canonical Pathways. *Front. Oncol.*, *8*, 1–16. https://doi.org/10.3389/fonc.2018.00575

Hoyle, C. H. V., Hilderman, R. H., Pintor, J. J., Schlüter, H., & King, B. F. (2001). Diadenosine polyphosphates as extracellular signal molecules. *Drug Dev. Res.*, *52*, 260–273. https://doi.org/10.1002/ddr.1123

Huang, Z., Cheng, L., Guryanova, O. A., Wu, Q., & Bao, S. (2010). Cancer stem cells in glioblastoma — molecular signaling and therapeutic targeting. *Protein Cell*, *1*, 638–655. https://doi.org/10.1007/s13238-010-0078-y

Hwang, J. R., Byeon, Y., Kim, D., & Park, S. G. (2020). Recent insights of T cell receptor-mediated signaling pathways for T cell activation and development. In *Exp. Mol. Med.* (Vol. 52, pp. 750–761). Springer Nature. https://doi.org/10.1038/s12276-020-0435-8

Ide, H., & Miyamoto, H. (2021). Sex hormone receptor signaling in bladder cancer: A potential target for enhancing the efficacy of conventional non-surgical therapy. In *Cells* (Vol. 10, pp. 1–15). MDPI. https://doi.org/10.3390/cells10051169

Idlowles, M. A., Elder, P. A., Williamson, M., Paul Cairns, J., Shaw, M. E., & Law, M. G. (1994). Allelotype of Human Bladder Cancer. *Cancer Res.*, *54*, 531–538. http://aacrjournals.org/cancerres/article-pdf/54/2/531/2455689/crs0540020531.pdf

Ipata, P. L., Barsotti, C., Tozzi, M. G., Camici, M., & Balestri, F. (2010). Metabolic interplay between intra- and extra-cellular uridine metabolism via an ATP driven uridine-UTP cycle in brain. *Int. J. Biochem. Cell Biol.*, *42*, 932–937. https://doi.org/10.1016/j.biocel.2010.01.026

Ishiwata, T., Matsuda, Y., Yamamoto, T., Uchida, E., Korc, M., & Naito, Z. (2012). Enhanced expression of fibroblast growth factor receptor 2 IIIc promotes human pancreatic cancer cell proliferation. *Am. J. Pathol.*, *180*, 1928–1941. https://doi.org/10.1016/j.ajpath.2012.01.020

Isidori, A., Cerchione, C., Daver, N., DiNardo, C., Garcia-Manero, G., Konopleva, M., Jabbour, E., Ravandi, F., Kadia, T., Burguera, A. de la F., Romano, A., Loscocco, F., Visani, G., Martinelli, G., Kantarjian, H., & Curti, A. (2021). Immunotherapy in Acute Myeloid Leukemia: Where We Stand. In *Front. Oncol.* (Vol. 11, pp. 1–20). Frontiers Media S.A. https://doi.org/10.3389/fonc.2021.656218

Jacoberger-Foissac, C., Cousineau, I., Bareche, Y., Allard, D., Chrobak, P., Allard, B., Pommey, S., Messaoudi, N., McNicoll, Y., Soucy, G., Koseoglu, S., Masia, R., Lake, A. C., Seo, H., Eeles, C. B., Rohatgi, N., Robson, S. C., Turcotte, S., Haibe-Kains, B., & Stagg, J. (2023). CD73 Inhibits cGAS-STING

and Cooperates with CD39 to Promote Pancreatic Cancer. *Cancer Immunol. Res.*, *11*, 56–71. https://doi.org/10.1158/2326-6066.CIR-22-0260

Jacob, P. F., Vaz, S. H., Ribeiro, J. A., & Sebastião, A. M. (2014). P2Y1 receptor inhibits GABA transport through a calcium signalling-dependent mechanism in rat cortical astrocytes. *GLIA*, *62*, 1211–1226. https://doi.org/10.1002/glia.22673

Jacobson, et. al. (2006). Adenosine receptors as therapeutic targets. *Nat Rev Drug Discov*, *5*, 247–264. https://doi.org/10.1038/nrd1983.Adenosine

Jacobson, K. A., & Müller, C. E. (2016a). Medicinal chemistry of adenosine, P2Y and P2X receptors. *Neuropharmacology*, *104*, 31–49. https://doi.org/10.1016/j.neuropharm.2015.12.001

Jacobson, K. A., & Müller, C. E. (2016b). Medicinal chemistry of adenosine, P2Y and P2X receptors. In *Neuropharmacology* (Vol. 104, pp. 31–49). Elsevier Ltd. https://doi.org/10.1016/j.neuropharm.2015.12.001

Jain, K. K. (2018). A Critical Overview of Targeted Therapies for Glioblastoma. *Front Oncol*, *8*, 1–19. https://doi.org/10.3389/fonc.2018.00419

Jain, S., & Jacobson, K. A. (2021). Purinergic Signaling in Liver Pathophysiology. *Front. Endocrinol.*, *12*, 1–9. https://doi.org/10.3389/fendo.2021.718429

Jankowski, J., Jankowski, V., Seibt, B., Henning, L., Zidek, W., & Schlüter, H. (2003). Identification of dinucleoside polyphosphates in adrenal glands. *Biochem. Biophys. Res. Commun.*, *304*, 365–370. https://doi.org/10.1016/S0006-291X(03)00596-5

Jin, K., Mao, C., Chen, L., Wang, L., Liu, Y., & Yuan, J. (2021). Adenosinergic Pathway : A Hope in the Immunotherapy of Glioblastoma. *Cancers*, *13*, 1–21.

Jørgensen, N. R. (2019). Role of the purinergic P2X receptors in osteoclast pathophysiology. In *Curr. Opin. Pharmacol.* (Vol. 47, pp. 97–101). Elsevier Ltd. https://doi.org/10.1016/j.coph.2019.02.013

Kan, L. K., Drill, M., Jayakrishnan, P. C., Sequeira, R. P., Galea, E., Todaro, M., Sanfilippo, P. G., Hunn, M., Williams, D. A., O'Brien, T. J., Drummond, K. J., & Monif, M. (2023). P2X7 receptor antagonism by AZ10606120 significantly reduced in vitro tumour growth in human glioblastoma. *Scientific Reports*, *13*, 1–12. https://doi.org/10.1038/s41598-023-35712-5

Kantoff, P. W., Higano, C. S., Shore, N. D., Berger, E. R., Small, E. J., Penson, D. F., Redfern, C. H., Ferrari, A. C., Dreicer, R., Sims, R. B., Xu, Y., Frohlich, M. W., & Schellhammer, P. F. (2010). Sipuleucel-T Immunotherapy for Castration-Resistant Prostate Cancer. *N. Engl. J. Med.*, *363*, 411–422. https://doi.org/10.1056/nejmoa1001294

Khalafalla, F. G., Greene, S., Khan, H., Ilves, K., Monsanto, M. M., Alvarez, R., Chavarria, M., Nguyen, J., Norman, B., Dembitsky, W. P., & Sussman, M. A. (2017). P2Y2 nucleotide receptor prompts human cardiac progenitor cell activation by modulating hippo signaling. *Circ. Res.*, *121*, 1224–1236. https://doi.org/10.1161/CIRCRESAHA.117.310812

Khalafalla, F. G., Kayani, W., Kassab, A., Ilves, K., Monsanto, M. M., Alvarez, R., Chavarria, M., Norman, B., Dembitsky, W. P., & Sussman, M. A. (2017). Empowering human cardiac progenitor cells by P2Y14 nucleotide receptor overexpression. *J. Physiol.*, *595*, 7135–7148. https://doi.org/10.1113/JP274980

Khalid, M., Brisson, L., Tariq, M., Hao, Y., Guibon, R., Fromont, G., Alawieyah, S., Mortadza, S., Mousawi, F., Manzoor, S., Roger, S., & Jiang, L.-H. (2017). Carcinoma-specific expression of P2Y 11 receptor and its contribution in ATP-induced purinergic signalling and cell migration in human hepatocellular carcinoma cells. *Oncotarget*, *8*, 37278–37290. https://doi.org/10.18632/oncotarget.16191

Khan, S., Yan-Do, R., Duong, E., Wu, X., Bautista, A., Cheley, S., Macdonald, P. E., & Braun, M. (2014). Autocrine activation of P2Y1 receptors couples Ca2+ influx to Ca2+ release in human pancreatic beta cells. *Diabetologia*, *57*, 2535–2545. https://doi.org/10.1007/s00125-014-3368-8

Kim, H., Kajikawa, T., Walsh, M. C., Takegahara, N., Jeong, Y. H., Hajishengallis, G., & Choi, Y. (2018). The purinergic receptor P2X5 contributes to bone loss in experimental periodontitis. *BMB Reports*, *51*, 468–473. https://doi.org/10.5483/BMBRep.2018.51.9.126

Kim, H., Walsh, M. C., Takegahara, N., Middleton, S. A., Shin, H. I., Kim, J., & Choi, Y. (2017). The purinergic receptor P2X5 regulates inflammasome activity and hyper-multinucleation of murine osteoclasts. *Sci. Rep.*, *7*, 1–11. https://doi.org/10.1038/s41598-017-00139-2

Kleeff, J., Korc, M., Apte, M., La Vecchia, C., Johnson, C. D., Biankin, A. V., Neale, R. E., Tempero, M., Tuveson, D. A., Hruban, R. H., & Neoptolemos, J. P. (2016). Pancreatic cancer. *Nat. Rev. Dis. Primers*, *2*, 1–22. https://doi.org/10.1038/nrdp.2016.22

Knight, T., & Irving, J. A. E. (2014). Ras/Raf/MEK/ERK pathway activation in childhood acute lymphoblastic leukemia and its therapeutic targeting. In *Front. oncol.* (Vol. 4, pp. 1–12). Frontiers Research Foundation. https://doi.org/10.3389/fonc.2014.00160

Krockenberger, M., Dombrowski, Y., Weidler, C., Ossadnik, M., Hönig, A., Häusler, S., Voigt, H., Rgen, J., Becker, C., Leng, L., Steinle, A., Weller, M., Bucala, R., Dietl, J., & Wischhusen, J. (2008). Macrophage Migration Inhibitory Factor Contributes to the Immune Escape of Ovarian Cancer by Down-Regulating NKG2D 1. *J. Immunol.*, *180*, 7338–7348. https://doi.org/https://doi.org/10.4049/jimmunol.180.11.7338

Kudira, R., Malinka, T., Kohler, A., Dosch, M., Gomez De Ag€, M., Melin, N., Haegele, S., Starlinger, P., Maharjan, N., Saxena, S., Keogh, A., Stroka, D., Candinas, D., & Beldi, G. (2016). P2X1-Regulated IL-22 Secretion by Innate Lymphoid Cells Is Required for Efficient Liver Regeneration. *HEPATOLOGY*, *63*, 2004–2017. https://doi.org/10.1002/hep.28492/suppinfo

Lang, K., Entschladen, Æ. F., Weidt, Æ. C., & Zaenker, K. S. (2006). Tumor immune escape mechanisms : impact of the neuroendocrine system. *Cancer Immunol. Immunother.*, *55*, 749–760. https://doi.org/10.1007/s00262-006-0126-x

Laubinger, W., & Reiser, G. (1999). Evidence for a G protein-coupled diadenosine-5',5'-P, P-tetraphosphate Ap4A receptor binding site in lung membranes from rat. *Eur. J. Pharmacol*, *366*, 93–100. https://doi.org/https://doi.org/10.1016/S0014-2999(98)00902-9

Lazarowski, E. R., & Boucher, R. C. (2001). UTP as an Extracellular Signaling Molecule. *News Physiol. Sci.*, *16*, 1–5.

Lazarowski, E. R., Boucher, R. C., & Harden, T. K. (1997). Direct Demonstration of Mechanically Induced Release of Cellular UTP and Its Implication for Uridine Nucleotide Receptor Activation *. *J. Biol. Chem.*, *272*, 24348–24354.

Lazarowski, E. R., & Harden, T. K. (2015). UDP-Sugars as Extracellular Signaling Molecules : Cellular and Physiologic Consequences of P2Y 14 Receptor Activation. *Mol Pharmacol*, *88*, 151–160.

Ledderose, S., Rodler, S., Eismann, L., Ledderose, G., Rudelius, M., Junger, W. G., & Ledderose, C. (2023). P2X1 and P2X7 Receptor Overexpression Is a Negative Predictor of Survival in Muscle-Invasive Bladder Cancer. *Cancers*, *15*, 1–17. https://doi.org/10.3390/cancers15082321

Le Guilcher, C., Garcin, I., Dellis, O., Cauchois, F., Tebbi, A., Doignon, I., Guettier, C., Julien, B., & Tordjmann, T. (2018). The P2X4 purinergic receptor regulates hepatic myofibroblast activation during liver fibrogenesis. *J. Hepatol.*, *69*, 644–653. https://doi.org/10.1016/j.jhep.2018.05.020

Le, T. T., Berg, N. K., Harting, M. T., Li, X., Eltzschig, H. K., & Yuan, X. (2019). Purinergic Signaling in Pulmonary Inflammation. *Front. Immunol.*, *10*, 1–14. https://doi.org/10.3389/fimmu.2019.01633

Li, F., Zhang, J., Arfuso, F., Chinnathambi, A., Zayed, M. E., Alharbi, S. A., Kumar, A. P., Ahn, K. S., & Sethi, G. (2015). NF-κB in cancer therapy. In *Arch. Toxicol.* (Vol. 89, pp. 711–731). Springer Verlag. https://doi.org/10.1007/s00204-015-1470-4

Li, L., Wang, L., Li, J., Fan, Z., Yang, L., Zhang, Z., Zhang, C., Yue, D., Qin, G., Zhang, T., Li, F., Chen, X., Ping, Y., Wang, D., Gao, Q., He, Q., Huang, L., Li, H., Huang, J., … Zhang, Y. (2018). Metformin-induced reduction of CD39 and CD73 blocks myeloid-derived suppressor cell activity in patients with ovarian cancer. *Cancer Res.*, *78*, 1779–1791. https://doi.org/10.1158/0008-5472.CAN-17-2460

Liu, X., Riquelme, M. A., Tian, Y., Zhao, D., Acosta, F. M., Gu, S., & Jiang, J. X. (2021). ATP Inhibits Breast Cancer Migration and Bone Metastasis through Down-Regulation of CXCR4 and Purinergic Receptor P2Y11. *Cancers*, *13*, 1–16. https://doi.org/10.3390/cancers13174293

Loo, E., Khalili, P., Beuhler, K., Siddiqi, I., & Vasef, M. A. (2018). BRAF V600E Mutation Across Multiple Tumor Types: Correlation Between DNA-based Sequencing and Mutation-specific Immunohistochemistry. *Appl Immunohistochem Mol Morphol*, *10*, 709–713. https://doi.org/10.1097/PAI.0000000000000516

Lopez, V., Schäkel, L., Schuh, H. J. M., Schmidt, M. S., Mirza, S., Renn, C., Pelletier, J., Lee, S. Y., Sévigny, J., Alban, S., Bendas, G., & Müller, C. E. (2021). Sulfated Polysaccharides from Macroalgae Are Potent Dual Inhibitors of Human ATP-Hydrolyzing Ectonucleotidases NPP1 and CD39. *Mar. Drugs*, *19*, 1–13. https://doi.org/10.3390/md19020051

LoRusso, P. M. (2016). Inhibition of the PI3K/AKT/mTOR pathway in solid tumors. *J. Clin. Oncol.*, *34*, 3803–3815. https://doi.org/10.1200/JCO.2014.59.0018

Lucattelli, M., Cicko, S., Müller, T., Lommatzsch, M., De Cunto, G., Cardini, S., Sundas, W., Grimm, M., Zeiser, R., Dürk, T., Zissel, G., Sorichter, S., Ferrari, D., Di Virgilio, F., Virchow, J. C., Lungarella, G., & Idzko, M. (2011). P2X7 receptor signaling in the pathogenesis of smoke-induced lung inflammation and emphysema. *Am. J. Respir. Cell Mol. Biol.*, *44*, 423–429. https://doi.org/10.1165/rcmb.2010-0038OC

Lu, D., Zhao, Y., Tawatao, R., Cottam, H. B., Sen, M., Leoni, L. M., Kipps, T. J., Corr, M., & Carson, D. A. (2004). Activation of the Wnt signaling pathway in chronic lymphocytic leukemia. *PNAS*, *101*, 3118–3123. https://doi.org/10.1073/pnas.0308648100

Luo, J., Jankowski, V., Güngär, N., Neumann, J., Schmitz, W., Zidek, W., Schlüter, H., & Jankowski, J. (2004). Endogenous Diadenosine Tetraphosphate, Diadenosine Pentaphosphate, and Diadenosine Hexaphosphate in Human Myocardial Tissue. *Hypertension*, *43*(5), 1055–1059. https://doi.org/10.1161/01.hyp.0000126110.46402.dd

Lupia, M., Angiolini, F., Bertalot, G., Freddi, S., Sachsenmeier, K. F., Chisci, E., Kutryb-Zajac, B., Confalonieri, S., Smolenski, R. T., Giovannoni, R., Colombo, N., Bianchi, F., & Cavallaro, U. (2018). CD73 Regulates Stemness and Epithelial-Mesenchymal Transition in Ovarian Cancer-Initiating Cells. *Stem Cell Rep.*, *10*, 1412–1425. https://doi.org/10.1016/j.stemcr.2018.02.009

Lüthje, J., & Ogilvie, A. (1983). The presence of diadenosine 5′,5‴-P1,P3-triphosphate (Ap3A) in human platelets. *Biochem. Biophys. Res. Commun.*, *115*, 253–260. https://doi.org/10.1016/0006-291X(83)90997-X

Luthje, J., & Ogilvie, A. (1988). Catabolism of Ap4A and Ap3A in whole blood The dinucleotides are long-lived signal molecules in the blood ending up as intracellular ATP in the erythrocytes. *Eur. J. Biochem*, *173*, 241–245. https://doi.org/10.1111/j.1432-1033.1988.tb13990.x.

Madariaga, J. A., & Coddou, C. (2021). Autocrine and paracrine purinergic signaling in the most lethal types of cancer. *Purinergic Signal.*, *17*, 345–370.

Mancini, J. E., Ortiz, G., Potilinstki, C., Salica, J. P., Lopez, E. S., Croxatto, J. O., & Gallo, J. E. (2018). Possible neuroprotective role of P2X2 in the retina of diabetic rats. *Diabetol. Metab. Syndr.*, *10*, 1–12. https://doi.org/10.1186/s13098-018-0332-7

Marco Idzko1, Davide Ferrari2, and H. K. E. (2015). Nucleotide signalling during inflammation. *Nature*, *509*, 310–317.

Marshall, J. S., Warrington, R., Watson, W., & Kim, H. L. (2018). An introduction to immunology and immunopathology. In *Allergy, Asthma, Clin. Immunol.* (Vol. 14, pp. 5–14). BioMed Central Ltd. https://doi.org/10.1186/s13223-018-0278-1

Mattson, M. P., Croteau, D. L., Dan, X., Demarest, T. G., Okur, M. N., Bohr, V. A., Fakouri, N. B., & Babbar, M. (2018). NAD + Metabolism in Aging and Cancer. *Annu.Rev.Cancer Biol.*, *3*, 105–130. https://doi.org/10.1146/annurev-cancerbio-030518-055905

Maynard, J. P., Lee, J.-S., Sohn, B. H., Yu, X., Lopez-Terrada, D., Finegold, M. J., Goss, J. A., & Thevananther, S. (2015). P2X3 purinergic receptor overexpression is associated with poor recurrence-free survival in hepatocellular carcinoma patients. *Oncotarget*, *6*, 41162–41179. https://doi.org/10.18632/oncotarget.6240.

Maynard, J. P., & Sfanos, K. S. (2022). P2 purinergic receptor dysregulation in urologic disease. In *Purinergic Signalling* (Vol. 18, pp. 267–287). Springer Science and Business Media B.V. https://doi.org/10.1007/s11302-022-09875-1

Mendes Ferreira, J., Henrique Gomes Matheus, L., Vasconcelos Souza de Almeida, R., Augusto de Souza Melo, P., Ramos Moreira Leite, K., Bovolenta Murta, C., Francisco de Almeida Claro, J., Pinto Camacho, C., Pontes-Júnior, J., & Dellê, H. (2021). High CD39 expression is associated with the non-muscle-invasive phenotype of human bladder cancer. *Oncotarget*, *12*, 1580–1586. https://doi.org/https://doi.org/10.18632/oncotarget.28029

Mittal sahil, & El-Serag Hashem. (2013). Epidemiology of hepatocellular carcinoma: consider the population. *J. Clin. Gastroenterol.*, *47*, 1–10. https://doi.org/10.1097/mcg.0b013e3182872f29

Moon, H., & Ro, S. W. (2021). Mapk/erk signaling pathway in hepatocellular carcinoma. *Cancers*, *13*, 1–19. https://doi.org/10.3390/cancers13123026

Müller, C. E., & Namasivayam, V. (2021). Recommended tool compounds and drugs for blocking P2X and P2Y receptors. *Purinergic Signalling*, *17*, 633–648. https://doi.org/10.1007/s11302-021-09813-7

Müller, T., Fay, S., Vieira, R. P., Karmouty-Quintana, H., Cicko, S., Ayata, C. K., Zissel, G., Goldmann, T., Lungarella, G., Ferrari, D., Di Virgilio, F., Robaye, B., Boeynaems, J. M., Lazarowski, E. R., Blackburn, M. R., & Idzko, M. (2017). P2Y6 receptor activation promotes inflammation and tissue remodeling in pulmonary fibrosis. *Front. Immunol.*, *8*, 1–8. https://doi.org/10.3389/fimmu.2017.01028

Myers, M. P., Pass, I., Batty, I. H., Van Der Kaay, J., Stolarov, J. P., Hemmings, B. A., Wigler, M. H., Downes, C. P., & Tonks, N. K. (1998). The lipid phosphatase activity of PTEN is critical for its tumor supressor function. *Proc. Natl. Acad. Sci. USA*, *95*, 13513–13518. https://doi.org/10.1073/pnas.95.23.13513

Nam, N.-H. (2006). Naturally Occurring NF-B Inhibitors. *Mini-Rev. Med. Chem.*, *6*, 945–951. https://doi.org/https://doi.org/10.2174/138955706777934937

Nedeljkovi´c, M. N., & Damjanovi´cdamjanovi´c, A. (2019). Mechanisms of Chemotherapy Resistance in Triple-Negative Breast Cancer-How We Can Rise to the Challenge. *Cells*, *8*, 1–32. https://doi.org/10.3390/cells8090957

Niechi, I., Uribe-ojeda, A., Erices, I., Torres, Á., Uribe, D., Rocha, D., Silva, P., Richter, H. G., San, R., & Quezada, C. (2019). Adenosine Depletion as A New Strategy to Decrease Glioblastoma Stem-Like Cells Aggressiveness. *Cells*, *8*, 1–15.

Nordenstedt, H., White, D. L., & El-Serag, H. B. (2010). The changing pattern of epidemiology in hepatocellular carcinoma. *Dig. Liver Dis.*, *42*, 206–214. https://doi.org/10.1016/S1590-8658(10)60507-5

North, R. A. (2016). P2X receptors. *Phil. Trans. R. Soc. B* , *371*, 1–7. https://doi.org/10.1098/rstb.2015.0427

Orellana, A., Moraga, C., Araya, M., & Moreno, A. (2016). Overview of Nucleotide Sugar Transporter Gene Family Functions Across Multiple Species. *J.Mol.Biol*, *428*, 3150–3165. https://doi.org/10.1016/j.jmb.2016.05.021

Orriss, I. R., Knight, G. E., Utting, J. C., Taylor, S. E. B., Burnstock, G., & Arnett, T. R. (2009). Hypoxia stimulates vesicular ATP release from rat osteoblasts. *J. Cell. Physiol.*, *220*, 155–162. https://doi.org/10.1002/jcp.21745

Oury, C., Lecut, C., Hego, A., Wéra, O., & Delierneux, C. (2015). Purinergic control of inflammation and thrombosis: Role of P2X1 receptors. In *Comput. Struct. Biotechnol. J.* (Vol. 13, pp. 106–110). Elsevier B.V. https://doi.org/10.1016/j.csbj.2014.11.008

Park, K., Martelotto, L. G., Peifer, M., Sos, M. L., Karnezis, A. N., Mahjoub, M. R., Bernard, K., Conklin, J. F., Szczepny, A., Yuan, J., Guo, R., Ospina, B., Falzon, J., Bennett, S., Brown, T. J., Markovic, A., Devereux, W. L., Ocasio, C. A., Chen, J. K., … Sage, J. (2011). A crucial requirement for Hedgehog signaling in small cell lung cancer. *Nat. Med.*, *17*, 1504–1508. https://doi.org/10.1038/nm.2473

Park, S., Chapuis, N., Tamburini, J., Bardet, V., Cornillet-Lefebvre, P., Willems, L., Green, A., Mayeux, P., Lacombe, C., & Bouscary, D. (2010). Role of the PI3K/AKT and mTOR signaling pathways in acute myeloid leukemia. *Haematologica*, *95*, 819–828. https://doi.org/10.3324/haematol.2009.013797

Pastor-anglada et.al. (2018). Who Is Who in Adenosine Transport. *Front. Pharmacol.*, *9*, 1–10. https://doi.org/10.3389/fphar.2018.00627

Peng, Y., Wang, Y., Zhou, C., Mei, W., & Zeng, C. (2022). PI3K/Akt/mTOR Pathway and Its Role in Cancer Therapeutics: Are We Making Headway? In *Front. Oncol.* (Vol. 12, pp. 1–17). Frontiers Media S.A. https://doi.org/10.3389/fonc.2022.819128

Pérez de Lara, M. J., Guzmán-Aranguez, A., Gómez-Villafuertes, R., Gualix, J., Miras-Portugal, M. T., & Pintor, J. (2018). Increased Ap4A levels and ecto-nucleotidase activity in glaucomatous mice retina. *Purinergic Signalling*, *14*, 259–270. https://doi.org/10.1007/s11302-018-9612-9

Perry, C., Hazan-Halevy, I., Kay, S., Cipok, M., Grisaru, D., Deutsch, V., Polliack, A., Naparstek, E., & Herishanu, Y. (2012). Increased CD39 expression on CD4 + T lymphocytes has clinical and prognostic significance in chronic lymphocytic leukemia. *Ann. Hematol.*, *91*, 1271–1279. https://doi.org/10.1007/s00277-012-1425-2

Pierce, S. K. (2009). Understanding B cell activation: From single molecule tracking, through Tolls, to stalking memory in malaria. In *Immunol. Res.* (Vol. 43, pp. 85–97). https://doi.org/10.1007/s12026-008-8052-y

Pintor, J., & Teresa Miras-Portugal, M. (1995). P2 Purinergic Receptors for Diadenosine Polyphosphates in the Nervous System. *Gen. Pharmac*, *26*, 229–235. https://doi.org/https://doi.org/10.1002/(SICI)1520-6769(199703)20:2<69::AID-NRC187>3.0.CO;2-Y

Pohl, S., Brook, N., Agostino, M., Arfuso, F., Kumar, A. P., & Dharmarajan, A. (2017). Wnt signaling in triple-negative breast cancer. *Oncogenesis*, *6*, 1–12. https://doi.org/10.1038/oncsis.2017.14

Porta, C., Paglino, C., & Mosca, A. (2014). Targeting PI3K/Akt/mTOR signaling in cancer. In *Front. Oncol.* (Vol. 4, pp. 1–11). Frontiers Research Foundation. https://doi.org/10.3389/fonc.2014.00064

Qian, S., Regan, J. N., Shelton, M. T., Hoggatt, A., Mohammad, K. S., Herring, P. B., & Seye, C. I. (2017). The P2Y2 nucleotide receptor is an inhibitor of vascular calcification. *Atherosclerosis*, *257*, 38–46. https://doi.org/10.1016/j.atherosclerosis.2016.12.014

Qin, J., Yan, L., Zhang, J., & Zhang, W. (2019). STAT3 as a potential therapeutic target in triple negative breast cancer : a systematic review. *J. Exp. Clin. Cancer Res.*, *38*, 1–16.

R. A. Hilger M. E. Scheulen D. Strumberg. (2002). The Ras-Raf-MEK-ERK Pathway in the Treatment of Cancer. *Oncology*, *25*, 511518. https://doi.org/https://doi.org/10.1159/000068621

Ramadass, V., Vaiyapuri, T., & Tergaonkar, V. (2020). Small molecule nf-kb pathway inhibitors in clinic. In *Int. J. Mol. Sci.* (Vol. 21, pp. 1–43). MDPI AG. https://doi.org/10.3390/ijms21145164

Ramos, J. R., Pabijan, J., Garcia, R., & Lekka, M. (2014). The softening of human bladder cancer cells happens at an early stage of the malignancy process. *Beilstein J. Nanotechnol.*, *5*, 447–457. https://doi.org/10.3762/bjnano.5.52

Rapp, J., Jaromi, L., Kvell, K., Miskei, G., & Pongracz, J. E. (2017). WNT signaling – lung cancer is no exception. *Respir. Res.*, *18*, 1–16. https://doi.org/10.1186/s12931-017-0650-6

Rita, A., Antunes, P., Scheyltjens, I., Duerinck, J., Neyns, B., Movahedi, K., & Ginderachter, J. A. Van. (2020). Understanding the glioblastoma immune microenvironment as basis for the development of new immunotherapeutic strategies. *ELIFE*, *9*, 1–16.

Roger, S., Jelassi, B., Couillin, I., Pelegrin, P., Besson, P., & Jiang, L. (2015a). Understanding the roles of the P2X7 receptor in solid tumour progression and therapeutic perspectives. *Biochim. Biophys. Acta, Biomembr.*, *1848*, 2584–2602. https://doi.org/10.1016/j.bbamem.2014.10.029

Roger, S., Jelassi, B., Couillin, I., Pelegrin, P., Besson, P., & Jiang, L. H. (2015b). Understanding the roles of the P2X7 receptor in solid tumour progression and therapeutic perspectives. *Biochim. Biophys. Acta, Biomembr.*, *1848*, 2584–2602. https://doi.org/10.1016/j.bbamem.2014.10.029

Rosen, D. G., Yang, G., Liu, G., Mercado-Uribe, I., Chang, B., Xiao, X., Zheng, J., Xue, F.-X., & Liu, J. (2009). Ovarian cancer: pathology, biology, and disease models. *Front. Biosci.*, *14*, 2089–2102. https://doi.org/10.2741/3364

Ruiz-rodríguez, V. M., Turiján-espinoza, E., Guel-pañola, J. A., García-hernández, M. H., Zermeño-nava, J. D. J., & López-lópez, N. (2020). Chemoresistance in Breast Cancer Patients Associated With Changes in P2X7 and A2A Purinergic Receptors in CD8 + T Lymphocytes. *Front. Pharmacol.*, *11*, 1–13. https://doi.org/10.3389/fphar.2020.576955

Ryten, M., Koshi, R., Knight, G. E., Turmaine, M., Dunn, P., Cockayne, D. A., Ford, A. P. W., & Burnstock, G. (2007). Abnormalities in neuromuscular junction structure and skeletal muscle function in mice lacking the P2X2 nucleotide receptor. *Neuroscience*, *148*, 700–711. https://doi.org/10.1016/j.neuroscience.2007.06.050

Salvestrini, V., Zini, R., Rossi, L., Gulinelli, S., Manfredini, R., Bianchi, E., Piacibello, W., Caione, L., Migliardi, G., Ricciardi, M. R., Tafuri, A., Romano, M., Salati, S., Di Virgilio, F., Ferrari, S., Baccarani, M., Ferrari, D., & Lemoli, R. M. (2012). Purinergic signaling inhibits human acute myeloblastic leukemia cell proliferation, migration, and engraftment in immunodeficient mice. *Blood*, *119*, 217–226. https://doi.org/10.1182/blood-2011-07-370775

Sanchez-Vega, F., Mina, M., Armenia, J., Chatila, W. K., Luna, A., La, K. C., Dimitriadoy, S., Liu, D. L., Kantheti, H. S., Saghafinia, S., Chakravarty, D., Daian, F., Gao, Q., Bailey, M. H., Liang, W. W., Foltz, S. M., Shmulevich, I., Ding, L., Heins, Z., … Schultz, N. (2018). Oncogenic Signaling Pathways in The Cancer Genome Atlas. *Cell*, *173*, 321–337. https://doi.org/10.1016/j.cell.2018.03.035

Sanderson, J., Dartt, D. A., Trinkaus-Randall, V., Pintor, J., Civan, M. M., Delamere, N. A., Fletcher, E. L., Salt, T. E., Grosche, A., & Mitchell, C. H. (2014). Purines in the eye: Recent evidence for the physiological and pathological role of purines in the RPE, retinal neurons, astrocytes, Müller cells, lens, trabecular meshwork, cornea and lacrimal gland. *Exp. Eye Res.*, *127*, 270–279. https://doi.org/10.1016/j.exer.2014.08.009

Sandoval, A., Fernandez-gallardo, M., Gonza, R., Felix, R., & Monjaraz, E. (2016). Adenosine Stimulate Proliferation and Migration in Triple Negative Breast Cancer Cells. *PLoS ONE*, *11*, 1–14. https://doi.org/10.1371/journal.pone.0167445

Sathanoori, R., Swärd, K., Olde, B., & Erlinge, D. (2015). The ATP receptors P2X7 and P2X4 modulate high glucose and palmitate-induced inflammatory responses in endothelial cells. *PLoS ONE*, *10*, 1–24. https://doi.org/10.1371/journal.pone.0125111

Schmid, S., Kübler, M., Ayata, C. K., Lazar, Z., Haager, B., Hoßfeld, M., Meyer, A., Cicko, S., Elze, M., Wiesemann, S., Zissel, G., Passlick, B., & Idzko, M. (2015). microenvironment in metastasized non-small-cell lung cancer. *Lung Cancer*, *90*, 516–521. https://doi.org/10.1016/j.lungcan.2015.10.005

Schneider, G., Glaser, T., Lameu, C., Abdelbaset-ismail, A., Sellers, Z. P., Moniuszko, M., Ulrich, H., & Ratajczak, M. Z. (2015). Extracellular nucleotides as novel , underappreciated pro-metastatic factors that stimulate purinergic signaling in human lung cancer cells. *Mol. Cancer*, *14*, 1–15. https://doi.org/10.1186/s12943-015-0469-z

Scholl, C., Gilliland, D. G., & Fröhling, S. (2008). Deregulation of Signaling Pathways in Acute Myeloid Leukemia. *Semin. Oncol.*, *35*, 336–345. https://doi.org/10.1053/j.seminoncol.2008.04.004

Schultz, M. B., & Sinclair, D. A. (2016). Why NAD + Declines during Aging : It ' s Destroyed. *Cell Metab.*, *23*, 965–966. https://doi.org/10.1016/j.cmet.2016.05.022

Scoyk, M. V. A. N., Randall, J., Sergew, A., & Williams, L. M. (2008). Wnt signaling pathway and lung disease. *Transl. Res.*, *151*, 175–180. https://doi.org/10.1016/j.trsl.2007.12.011

Seman, M., Adriouch, S., Scheuplein, F., Krebs, C., Freese, D., Glowacki, G., Deterre, P., Haag, F., Koch-nolte, F., Diderot, D., & Paris, F.-. (2003). NAD-Induced T Cell Death : ADP-Ribosylation of Cell Surface Proteins by ART2 Activates the Cytolytic P2X7 Purinoceptor. *Immunity*, *19*, 571–582.

Sesma, J. I., Esther, C. R., Kreda, S. M., Jones, L., O'Neal, W., Nishihara, S., Nicholas, R. A., & Lazarowski, E. R. (2009). Endoplasmic reticulum/golgi nucleotide sugar transporters contribute to the cellular release of UDP-sugar signaling molecules. *J. Biol. Chem.*, *284*, 12572–12583. https://doi.org/10.1074/jbc.M806759200

Shen, S. S., Smith, C. L., Hsieh, J. T., Yu, J., Kim, I. Y., Jian, W., Sonpavde, G., Ayala, G. E., Younes, M., & Lerner, S. P. (2006). Expression of estrogen receptors-α and -β in bladder cancer cell lines and human bladder tumor tissue. *Cancer*, *106*, 2610–2616. https://doi.org/10.1002/cncr.21945

Shigematsu, H., & Gazdar, A. F. (2006). Somatic mutations of epidermal growth factor receptor signaling pathway in lung cancers. *Int. J. Cancer*, *262*, 257–262. https://doi.org/10.1002/ijc.21496

Song, E., Rah, S., Lee, Y., Yoo, C., Kim, Y., Yeom, J., Park, K., Kim, J., Kim, U., & Han, M. (2011). Connexin-43 Hemichannels Mediate Cyclic ADP-ribose Generation and Its Ca 2 ⁺-mobilizing Activity by NAD ⁺/ Cyclic. *J. Biol. Chem.*, *286*, 44480–44490. https://doi.org/10.1074/jbc.M111.307645

Spiro, S. G., & Silvestri, G. A. (2005). Centennial Review One Hundred Years of Lung Cancer. *Am. J. Respir. Crit. Care Med.*, *172*, 523–529. https://doi.org/10.1164/rccm.200504-531OE

Stefani, J., Tschesnokowa, O., Parrilla, M., Robaye, B., Boeynaems, J. M., Acker-Palmer, A., Zimmermann, H., & Gampe, K. (2018). Disruption of the microglial ADP receptor P2Y13 enhances adult hippocampal neurogenesis. *Front. Cell. Neurosci.*, *12*, 1–19. https://doi.org/10.3389/fncel.2018.00134

Stella, J., Bavaresco, L., Braganhol, E., Rockenbach, L., Farias, P. F., Wink, M. R., Azambuja, A. A., Barrios, C. H., Morrone, F. B., & Oliveira Battastini, A. M. (2010). Differential ectonucleotidase expression in human bladder cancer cell lines. *Urol. Oncol.: Semin. Orig. Invest.*, *28*, 260–267. https://doi.org/10.1016/j.urolonc.2009.01.035

Stewart, D. J., Chang, D. W., Ye, Y., Spitz, M., Lu, C., Shu, X., Wampfler, J. A., Marks, R. S., Garces, Y. I., Yang, P., & Wu, X. (2014). Wnt signaling pathway pharmacogenetics in non-small cell lung cancer. *Pharmacogenomics J*, *14*, 509–522. https://doi.org/10.1038/tpj.2014.21

Stokes, L., Layhadi, J. A., Bibic, L., Dhuna, K., & Fountain, S. J. (2017). P2X4 receptor function in the nervous system and current breakthroughs in pharmacology. *Front. Pharmacol.*, *8*, 1–15. https://doi.org/10.3389/fphar.2017.00291

Strickland, L. N., Faraoni, E. Y., Ruan, W., Yuan, X., Eltzschig, H. K., & Bailey-Lundberg, J. M. (2023). The resurgence of the Adora2b receptor as an immunotherapeutic target in pancreatic cancer. *Front. Immunol.*, *14*, 01–15. https://doi.org/10.3389/fimmu.2023.1163585

Stultz, J., & Fong, L. (2021). How to turn up the heat on the cold immune microenvironment of metastatic prostate cancer. In *Prostate Cancer Prostatic Dis.* (Vol. 24, pp. 697–717). Springer Nature. https://doi.org/10.1038/s41391-021-00340-5

Syed, S. K., Kauffman, A. L., Beavers, L. S., Alston, J. T., Farb, T. B., Ficorilli, J., Marcelo, M. C., Brenner, M. B., Bokvist, K., Barrett, D. G., & Efanov, A. M. (2013). Ectonucleotidase NTPDase3 is abundant in pancreatic-cells and regulates glucose-induced insulin secretion. *Am. J. Physiol. Endocrinol.Metab.*, *305*, 1319–1326. https://doi.org/10.1152/ajpendo.00328.2013.-Extracellular

Tacconi, C., Ungaro, F., Correale, C., Arena, V., Massimino, L., Detmar, M., Spinelli, A., Carvello, M., Mazzone, M., Oliveira, A. I., Rubbino, F., & Garlatti, V. (2019). Activation of the VEGFC / VEGFR3 Pathway Induces Tumor Immune Escape in Colorectal Cancer. *Cancer Res.*, *1*, 4196–4211. https://doi.org/10.1158/0008-5472.CAN-18-3657

Teixeira, J. M., Bobinski, F., Parada, C. A., Sluka, K. A., & Tambeli, C. H. (2017). P2X3 and P2X2/3 Receptors Play a Crucial Role in Articular Hyperalgesia Development Through Inflammatory Mechanisms in the Knee Joint Experimental Synovitis. *Mol Neurobiol*, *54*, 6174–6186. https://doi.org/10.1007/s12035-016-0146-2

Tian, W., Lei, N., Zhou, J., Chen, M., Guo, R., Qin, B., Li, Y., & Chang, L. (2022). Extracellular vesicles in ovarian cancer chemoresistance, metastasis, and immune evasion. *Cell Death and Disease*, *13*, 1–12. https://doi.org/10.1038/s41419-022-04510-8

Tran, L., Xiao, J. F., Agarwal, N., Duex, J. E., & Theodorescu, D. (2021). Advances in bladder cancer biology and therapy. In *Nat. Rev. Cancer* (Vol. 21, pp. 104–121). Nature Research. https://doi.org/10.1038/s41568-020-00313-1

Tsuda, M., Ph, D., & Inoue, K. (2015). Neuron-microglia interaction by purinergic signaling in neuropathic pain following neurodegeneration. *Neuropharmacology*, *104*, 76–81. https://doi.org/10.1016/j.neuropharm.2015.08.042

Turvey, S. E., & Broide, D. H. (2010). Innate immunity. *J. Allergy Clin. Immunol.*, *125*(2 SUPPL. 2), 1–17. https://doi.org/10.1016/j.jaci.2009.07.016

Vago, L., & Gojo, I. (2020). Immune escape and immunotherapy of acute myeloid leukemia. *J. Clin. Invest.*, *130*, 1552–1564. https://doi.org/10.1172/JCI129204

Vaisitti, T., Arruga, F., Guerra, G., & Deaglio, S. (2019). Ectonucleotidases in Blood Malignancies: A Tale of Surface Markers and Therapeutic Targets. In *Front. Immunol.* (Vol. 10, pp. 1–17). Frontiers Media S.A. https://doi.org/10.3389/fimmu.2019.02301

Velcheti, V., & Govindan, R. (2007). Hedgehog Signaling Pathway and Lung Cancer. *J. Thorac. Oncol.*, *2*, 7–10. https://doi.org/10.1097/JTO.0b013e31802c0276

Verdier, C., Ruidavets, J. B., Genoux, A., Combes, G., Bongard, V., Taraszkiewicz, D., Galinier, M., Elbaz, M., Ferrières, J., Martinez, L. O., & Perret, B. (2019). Common p2y13 polymorphisms are

associated with plasma inhibitory factor 1 and lipoprotein(a) concentrations, heart rate, and body fat mass: The GENES study. *Arch Cardiovasc Dis .*, *112*, 124–134. https://doi.org/10.1016/j.acvd.2018.09.003

Vinken, M. (2015). connexins , pannexins and their channels as gatekeepers of organ physiology. *Cell. Mol. Life Sci*, *72*, 2775–2778. https://doi.org/10.1007/s00018-015-1958-3

Virgilio, F. Di, Falzoni, S., Giuliani, A. L., & Adinolfi, E. (2016). P2 receptors in cancer progression and metastatic spreading. *Curr. Opin. Pharmacol.*, *29*, 17–25. https://doi.org/10.1016/j.coph.2016.05.001

Vollmayer, P., Clair, T., Goding, J. W., Sano, K., Servos, J., & Zimmermann, H. (2003). Hydrolysis of diadenosine polyphosphates by nucleotide pyrophosphatases/phosphodiesterases. *Eur. J. Biochem.*, *270*, 2971–2978. https://doi.org/10.1046/j.1432-1033.2003.03674.x

von Amsberg, G., Alsdorf, W., Karagiannis, P., Coym, A., Kaune, M., Werner, S., Graefen, M., Bokemeyer, C., Merkens, L., & Dyshlovoy, S. A. (2022). Immunotherapy in Advanced Prostate Cancer—Light at the End of the Tunnel? *Int. J. Mol. Sci.*, *23*, 1–30. https://doi.org/10.3390/ijms23052569

Wang, L., Cao, L., Wang, H., Liu, B., & Zhang, Q. (2017). Cancer-associated fibroblasts enhance metastatic potential of lung cancer cells through IL-6 / STAT3 signaling pathway. *Oncotarget*, *8*, 76116–76128.

Wang, P., Jia, J., & Zhang, D. (2020). Purinergic signalling in liver diseases: Pathological functions and therapeutic opportunities. *JHEP Reports*, *2*, 1–15. https://doi.org/10.1016/j.jhepr.2020.100165

Wang, Z., Zhu, S., Tan, S., Zeng, Y., & Zeng, H. (2023). The P2 purinoceptors in prostate cancer. *Purinergic Signalling*, *19*, 255–263. https://doi.org/10.1007/s11302-022-09874-2

Whiteside, T. L. (2008). The tumor microenvironment and its role in promoting tumor growth. *Oncogene*, *27*, 5904–5912. https://doi.org/10.1038/onc.2008.271

Wolf, D., Fiegl, H., Zeimet, A. G., Wieser, V., Marth, C., Sprung, S., Sopper, S., Hartmann, G., Reimer, D., & Boesch, M. (2020). High RIG-I expression in ovarian cancer associates with an immune-escape signature and poor clinical outcome. *Int. J. Cancer*, *146*, 2007–2018. https://doi.org/10.1002/ijc.32818

Wright, A., Mahaut-Smith, M., Symon, F., Sylvius, N., Ran, S., Bafadhel, M., Muessel, M., Bradding, P., Wardlaw, A., & Vial, C. (2016). Impaired P2X1 Receptor–Mediated Adhesion in Eosinophils from Asthmatic Patients. *J. Immunol*, *196*, 4877–4884. https://doi.org/10.4049/jimmunol.1501585

Xie, Y., Chen, Y., & Fang, J. (2020). Comprehensive review of targeted therapy for colorectal cancer. *Signal Transduction Targeted Ther.*, 1–68. https://doi.org/10.1038/s41392-020-0116-z

Xi, Y., & Chen, Y. (2014). Wnt signaling pathway : Implications for therapy in lung cancer and bone metastasis. *Cancer Letters*, *353*, 8–16. https://doi.org/10.1016/j.canlet.2014.07.010

Xue, C., Li, G., Lu, J., & Li, L. (2021). Crosstalk between circRNAs and the PI3K/AKT signaling pathway in cancer progression. *Signal Transduction Targeted Ther.*, *6*, 1–17. https://doi.org/10.1038/s41392-021-00788-w

Xu, Y., Wang, Y., Yan, S., Yang, Q., Zhou, Y., Zeng, X., Liu, Z., An, X., Toque, H. A., Dong, Z., Jiang, X., Fulton, D. J., Weintraub, N. L., Li, Q., Bagi, Z., Hong, M., Boison, D., Wu, C., & Huo, Y. (2017). adenosine kinase epigenetically modulates vascular in fl ammation. *Nat. Commun.*, *8*, 1–16. https://doi.org/10.1038/s41467-017-00986-7

Yang, J., Nie, J., Ma, X., Wei, Y., Peng, Y., & Wei, X. (2019). Targeting PI3K in cancer: Mechanisms and advances in clinical trials. In *Mol. Cancer* (Vol. 18, pp. 1–28). BioMed Central Ltd. https://doi.org/10.1186/s12943-019-0954-x

Yang, X., Lou, Y., Liu, G., Wang, X., Qian, Y., Ding, J., Chen, S., & Xiao, Q. (2017). Microglia P2Y6 receptor is related to Parkinson's disease through neuroinflammatory process. *J. Neuroinflammation*, *14*, 1–12. https://doi.org/10.1186/s12974-017-0795-8

Yin, L., Duan, J., Bian, X., & Yu, S. (2020). Triple-negative breast cancer molecular subtyping and treatment progress. *Cancer Res.*, *22*, 1–13.

Yu, W., Robson, S. C., & Hill, W. G. (2011). Expression and distribution of ectonucleotidases in mouse urinary bladder. *PLoS ONE*, *6*. https://doi.org/10.1371/journal.pone.0018704

Zanoni, M., Pegoraro, A., Adinolfi, E., & De Marchi, E. (2022). Emerging roles of purinergic signaling in anti-cancer therapy resistance. *Front. Cell Dev. Biol.*, *10*, 1–9. https://doi.org/10.3389/fcell.2022.1006384

Zhou, Z., Matsumoto, T., Jankowski, V., Pernow, J., Mustafa, S. J., Duncker, D. J., & Merkus, D. (2019). Uridine adenosine tetraphosphate and purinergic signaling in cardiovascular system: An update. In *Pharmacol. Res.* (Vol. 141, pp. 32–45). Academic Press. https://doi.org/10.1016/j.phrs.2018.12.009

Zimmermann, H. (2009). Prostatic acid phosphatase, a neglected ectonucleotidase. *Purinergic Signalling*, *5*, 273–275. https://doi.org/10.1007/s11302-009-9157-z

Zimmermann, H. (2020). History of ectonucleotidases and their role in purinergic signaling. *Biochem. Pharmacol.*, 114322. https://doi.org/10.1016/j.bcp.2020.114322

Zimmermann, H., Zebisch, M., & Sträter, N. (2012). Cellular function and molecular structure of ecto-nucleotidases. *Purinergic Signal.*, *8*, 437–502.

Chapter 2

Sensitive Fluorescence-based High-Throughput Assays for Monitoring Ectonucleotidase Activity in Cancer Cell Lines

Salahuddin Mirza, Tobias Claff, Christian Renn, Sangyong Lee**,** Anke Schiedel, Christa E. Müller*****

Pharma Center Bonn, Pharmaceutical Institute, Pharmaceutical & Medicinal Chemistry I, University of Bonn, An der Immenburg 4, D-53121 Bonn, Germany
Dedicated to Prof. Miras Portugal

Keywords: Ectonucleotidase, CD73, CD39, NPP1, N^6-etheno-nucleotides, cancer cell lines, high-throughput screening

Summary

Tumour cells consistently demonstrate overexpression of surface enzymes that hydrolyse extracellular nucleotides, such as ATP, ADP, AMP, NAD^+, ADPR, and nucleotide polyphosphates, leading to the production of adenosine. This process effectively alters the tumour microenvironment from a pro-inflammatory state to an anti-inflammatory/immunosuppressive one. The escalated adenosine levels subsequently activate adenosine receptors A_{2A} and A_{2B}, resulting in heightened cell proliferation, angiogenesis, and metastasis. The adenosinergic pathways involve two critical steps. Initially, nucleotides are converted to their mono-phosphate analogue, which is then transformed into the nucleoside. Several surface-located enzymes known as ectonucleotidases participate in this hydrolytic pathway. Extensive research has been undertaken on the localisation and properties of these enzymes. Various therapeutic strategies have been implemented to curb their enzymatic activity and uphold a pro-inflammatory milieu. The ATP–adenosine hydrolysis cascades are proposed as groundbreaking therapeutics for cancer (Immuno)therapy. Small-molecule inhibitors targeting different components of this adenosinergic pathway have already been identified, with some progressing through various phases of clinical trials. However, it has been noted that these ectonucleotidases function in concert, and inhibiting a single enzyme may not suffice to curtail adenosine production. Furthermore, existing biological assays present advantages and disadvantages when analysing cancer cell lines with concurrent activity of multiple enzymes.

Here, we report on the development of a fluorescence-based high-throughput screening (HTS) assay for identifying and characterising inhibitors of ectonucleotidases by using the etheno Ɛ-ATP, Ɛ-ADP, and Ɛ-AMP as substrates. This assay involves the precipitation of the remaining substrates and quantification of the enzymatic product Ɛ-adenosine by measuring the fluorescence of the supernatant using a plate reader. The assay is optimised for monitoring the AMPase activity of CD73 and the ATPase/ADPase activity of CD39 and NPP1 in cancer cell lines such as glioblastoma U87, astrocytoma, and triple-negative breast cancer (TNBC). The assay is highly sensitive with a limit of detection (LOD) as low as 18.2 ± 0.1 nM of the fluorescence Ɛ-adenosine. The low LOD value is favourable for analysing these reactions, considering the low K_m values of most of the enzymes of this pathway. This high-throughput screening (HTS) assay detects a 96-well plate in less than 20 min, which makes it suitable for screening large compound libraries. The assay is superior to previously reported methods concerning the straightforward application, cost-effectiveness, robustness, and utility.

1.0 Introduction

Overexpression of ectonucleotidases, including nucleoside triphosphate diphosphohydrolases (NTPDases), nucleotide pyrophosphatase/phosphodiesterases (NPPs), alkaline phosphatases (AP), and Ecto-5′-nucleotidase (CD73) has previously been reported on cancer cell lines (Aerts et al., 2011; Bageritz et al., 2014; Xu et al., 2013; Zimmermann et al., 2012). These are membrane-bound enzymes whose catalytic domain is located extracellularly, where they hydrolyse pro-inflammatory nucleotides (e.g., ATP) to anti-inflammatory and immunosuppressive nucleoside adenosine. Tissue inflammation and hypoxia activate transmembrane channel protein pannexin-1 or connexin-43 to transport nucleotides out of the cells (Dosch et al., 2018; Idzko et al., 2015). Besides this, uncontrolled transport exists due to cellular necrosis and vesicular transport. Extracellular ATP is gradually hydrolysed by cell-surface enzymes, including NTPDases, NPP, and AP, to AMP, further hydrolysed by CD73 to adenosine. These enzymes work in tandem and constitute a critical pathway of adenosine production (Ferrero et al. 2019). Adenosine can accumulate in the tumour microenvironment (TME), activating adenosine A_{2A} and A_{2B} receptors on immune cells and tumour cells with subsequent immunosuppression, cell proliferation, angiogenesis, and metastasis. Targeting these enzymes or the downstream adenosine receptors is an attractive therapeutic option for developing cancer Immunotherapy (Allard et al., 2014; Monteiro et al., 2018; Sek et al., 2018; Zhang et al., 2017).

1.1 Human CD73

Metalloenzyme CD73 (EC 3.1.3.5) is the final rate-limiting enzyme in the purinergic pathway that requires Zn^{2+} as a cofactor for catalytic activity. CD73 is a GPI-anchored enzyme with its catalytic domain in the extracellular environment and mainly hydrolyses AMP to adenosine and inorganic phosphate; however, comparatively low hydrolysis of CMP, IMP, GMP, and UMP is also reported (Zimmermann et al. 2012). The enzyme can hydrolyse nicotinamide-mononucleotide to nicotinamide riboside and NAD^+ to adenosine and nicotinamide ribosides (Garavaglia et al., 2012). Adenosine then either acts on adenosine receptors to produce an anti-inflammatory response or is converted to inosine

by the enzymatic function of adenosine deaminases. Adenosine transport is bi-directional; extracellular adenosine gets internalised and phosphorylated by intracellular kinases.

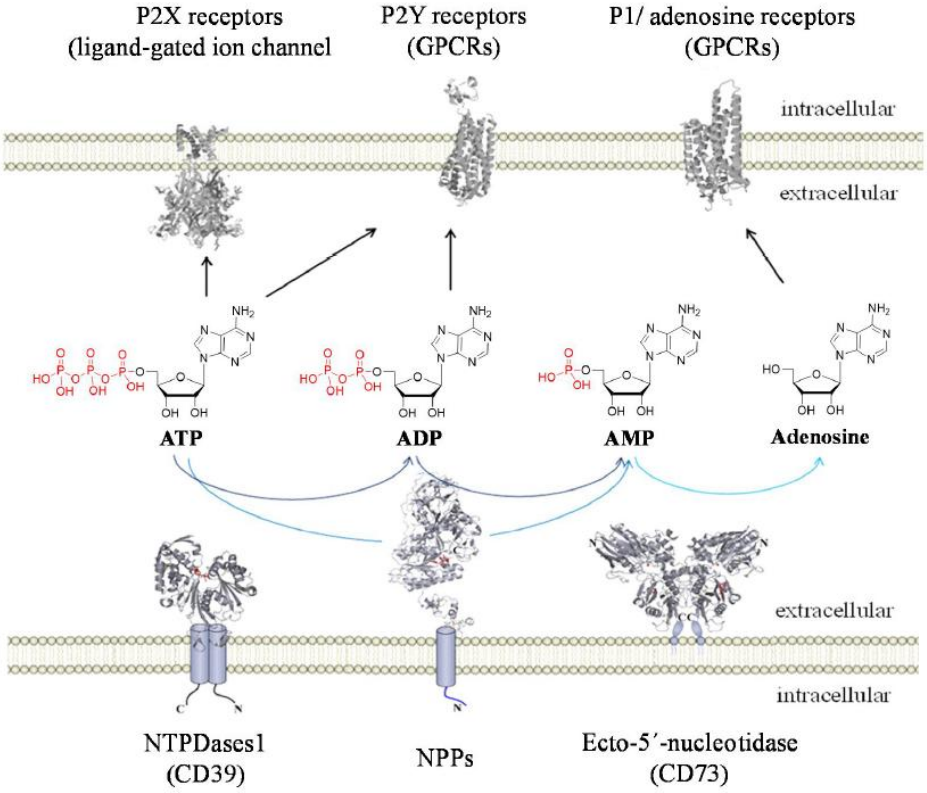

Figure 2.1: Purinergic signalling in the extracellular environment. ATP is sequentially hydrolysed to ADP, AMP, and finally adenosine.

1.2 Tissue localisation

CD73 is expressed in different tissues. The enzyme is detected in immune cells, including T cells, B cells, natural killer cells (NK), dendritic cells, and regulatory T cells (Tregs), which are linked to the suppression of immune response. Moreover, the enzyme is also located in endothelial cells lining blood vessels (regulation of vascular tone), brain and spinal cord (neurotransmission, neuroinflammation), renal vasculature and tubular cells, the epithelial lining of the intestine, and keratinocytes(Su et al., 2004; Zimmermann et al., 2012).

1.3 Assays for estimating ectonucleotidase activity

Ectonucleotidase activity is monitored by different in vitro assays utilising both natural and artificial substrates in high-throughput screening (HTS) and non-HTS assays. The substrates used in these assays are mostly phosphates of adenine and their fluorescence

and radioactive analogues. Each assay reported so far possesses some limitations alongside the benefits it offers.

Tritium-labeled AMP ([^{3}H]AMP) is used as a substrate for CD73-based reactions with a limit of detection (LOD) of ~ 30 nM. However, this assay involves a multi-step procedure and consists of working with radioactivity (Freundlieb et al., 2014). A highly efficient and sensitive HTS assay is reported for CD73 using rapid fire-tandem mass spectrometry (RF-MS/MS) employing four isotopically labelled AMP molecules (McManus et al., 2018). This assay involves high initial equipment costs. A few assays offer higher utility and can be used for monitoring both AMPase and ATPase activity. One such assay includes the malachite green assay. It is widely used to detect free phosphate P_i or PP_i produced during the enzymatic hydrolysis of the substrates (ATP, ADP, AMP, and phosphates of uridine, cytosine, and guanine) to their corresponding nucleosides (Baykov et al.1988). Despite being efficient and economical, the assay is unsuitable for coloured compounds and testing on intact cells. Nucleotidase activity can be monitored using capillary electrophoresis (CE) coupled DAD-detector with micromolar sensitivity, the antibody/tracer-based HTS (nanomolar sensitivity) to fluorescein coupled ATP-based CE assay (picomolar sensitivity), thin-layer chromatography using radiolabeled nucleotides (Fiene et al., 2015; Iqbal, Lévesque, et al., 2008; Lee et al., 2018; Yegutkin et al., 2012). However, besides their advantages, these assays involve either an expensive substrate or are not efficient by being time-consuming for screening campaigns. A sensitive HTS luciferase-based luminescence assay is based on ATP depletion from the reaction mixture, followed by converting AMP to ATP using an AMP–Glo^{TM} kit (Goueli & Hsiao, 2019). However, while analysing cancer cell lines having multiple enzymes co-expressed and working in tandem, the product AMP could further be hydrolysed to adenosine, which is prone to deamination or intracellular transport (Moreno et al., 2018). An HTS amplex red assay can monitor adenosine produced by nucleotide-hydrolyzing enzymes. A series of enzyme reactions lead to resorufin (AMP – adenosine – inosine – hypoxanthine – uric acid – H_2O_2 – resorufin – fluorescence detection λex/em 545/590 nm) (Helenius et al., 2012; Sachsenmeier et al., 2012). Considering the importance of ectonucleotidases in cancer propagation, an HTS assay with minimum background interference and high efficiency is essential for screening drug candidates.

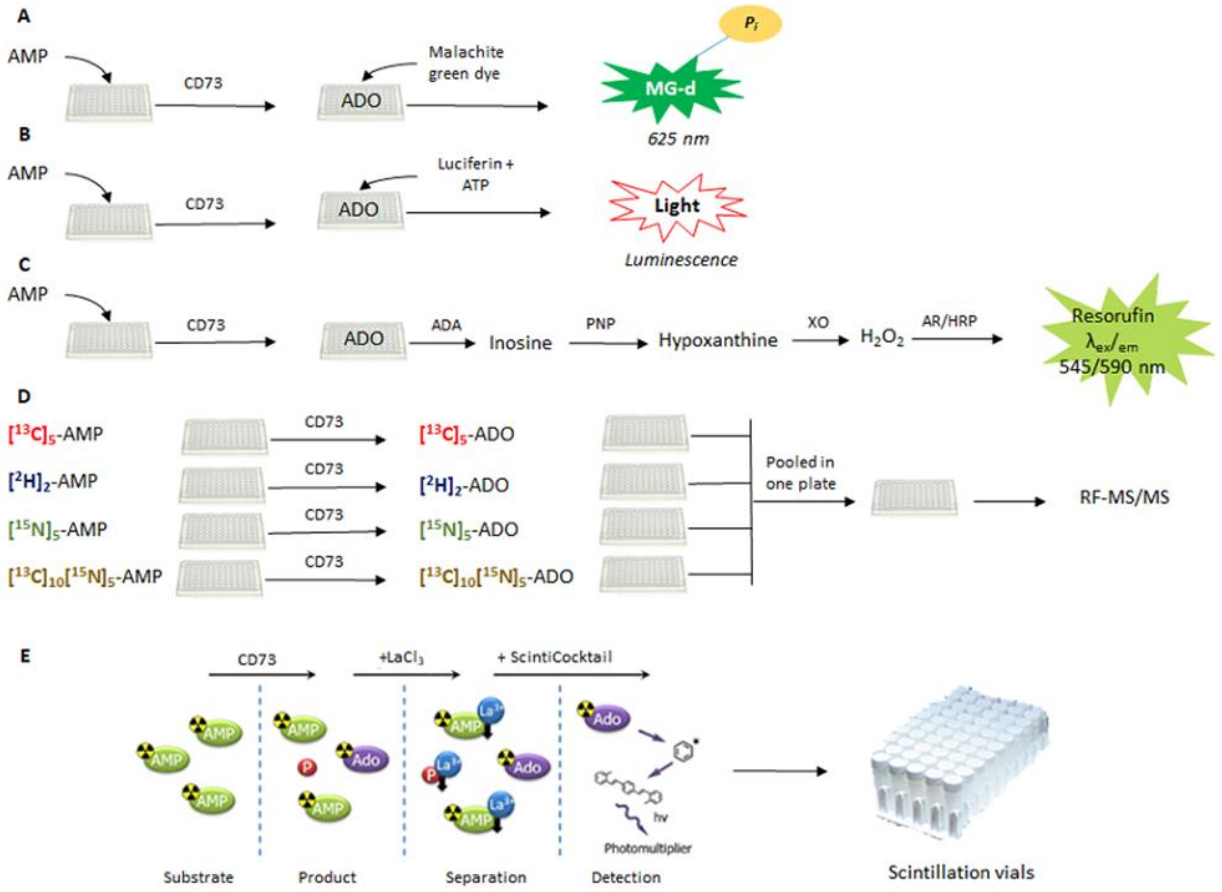

Figure 2.2: Assay mechanism for reported HTS and non-HTS assay for CD73. A. Malachite green assay is based on complex formation between free phosphate and molybdate to form phosphomolybdate (Ph-M) complex recognised by malachite green dye (MG-d), pH 2.0 to form MG-Ph-M being detected at 625 nm. B. Luciferase assay measures the reduction of AMP through inhibition of luminescence signals by inhibiting ATP-luciferin reaction. C. Amplex Red assay is based on the conversion of adenosine to inosine by adenosine deaminase (ADA), to hypoxanthine by bacterial purine nucleoside phosphorylase (PNP), to H_2O_2 by microbial xanthine oxidase (XO) and finally Amplex Red reagent with horseradish peroxidase (AR/HRP) form resorufin being detected at $\lambda_{ex/em}$ 545/590 nm. D. Rapid-flow mass spectrometry assay involved reacting four isotopic AMP with enzyme on separate assay plate (384 wells) followed by pooling of plates in one and detected 1536 reactions at one time using Rapid-fire MS/MS. E. Radioactive AMP is treated with CD73, followed by AMP depletion with lanthanum chloride and scintillation counting.

1.4 Small-molecule inhibitors of CD73

Different approaches have been adopted to potently inhibit nucleotide hydrolysis to adenosine by inhibiting ectonucleotidases. Several small molecule inhibitors of CD73 are reported with picomolar potency (Bhattarai et al., 2019; Lawson et al., 2020). Some of these drug candidates are currently under clinical trials. Moreover, specific CD73 antibodies and mRNA-based vaccines for ectonucleotidases have promised great potential (Hay et al., 2016; Stagg & Smyth, 2010). Some reported small molecule inhibitors are summarised below and divided into nucleotidic and non-nucleotidic scaffolds.

a. Nucleotidic scaffold

Both ATP and ADP are endogenous inhibitors of CD73 exhibiting micromolar IC_{50} values, and the structures that mimic both nucleotidic scaffolds have achieved great success towards CD73 (Freundlieb et al., 2014). Like in the case of α,β-methylene-ADP (AOPCP, AMPCP), the α,β-phosphate is replaced by methylene (-CH_2-), where the resulting non-hydrolysable molecule has achieved an inhibitory potency of 88.4 nM against rat CD73 (Bhattarai et al., 2015). Further modification of the AOPCP molecule led to the discovery of PSB-12379 and PSB-12489; notably, the latter molecule showed high potency towards human CD73 (~300 pM), (Bhattarai et al., 2019, 2020). However, the most potent molecule reported (AB680) has an inhibitory potency of 5 pM (Lawson et al., 2020). Despite having great therapeutic potential, the nucleotidic scaffolds possess metabolic stability issues and are targeted for NTPDases, NPPs, and APs, making them unavailable for interaction. Moreover, the possible hydrolysis products AMP and adenosine can further act on the adenosine receptors, further increasing immunosuppression. The compounds are further targeted by liver microsomal enzymes, which can quickly remove the inhibitors from the bloodstream. The strong negative charge on the molecule due to multiple phosphates can further hinder their absorption from the intestine. These limitations linked with nucleotide-based scaffolds limit their effectiveness as targeted inhibition of CD73 and, in fact, further worsen the adenosine burden, which needs further research.

b. Non-nucleotidic scaffold

Research for discovering potent and selective non-nucleotidic scaffolds revolves around xanthine, anthraquinone, benzonitrile, and isonicotinohydrazone. Xanthine scaffolds, as in caffeine and theophylline, were found to inhibit CD73 activity up to low micromolar IC50 values competitively. Further derivatisation of this scaffold yielded compounds PZB08511001A and PZB08511180A with a moderate IC_{50} value of 5.77 and 4.90 μM, respectively (Freundlieb, 2016). Anthraquinone scaffolds have found better placement in the active site, and the inhibitory potency of the most potent inhibitors has reached a low nanomolar level (Baqi et al., 2010). Moreover, benzonitrile derivatives have further improved inhibitory potency (Beatty et al., 2020). Apart from these scaffolds, sulfonamide and sulfonic acid derivatives were also evaluated, resulting in micromolar IC_{50} values (Iqbal et al., 2013). The isonicotinohydrazone derivatives have been reported to inhibit

human CD73 with an IC_{50} value of 190 nM (Channar et al., 2017). Non-nucleotidic scaffolds have shown less solubility of the compounds in the reaction settings, where the compounds at higher dilution precipitate with the reaction samples, leading to inaccurate assessment of the inhibitory potency. Figure 2.3 summarises the details of the most potent compounds in both scaffold types.

1.5 N^6-etheno nucleotides

N^6-etheno-bridged derivatives of adenine nucleotides (ε-ATP, ε-ADP, ε-AMP) and ε-adenosine were previously reported to have a similar hydrolytic profile as their respective natural analogues (Jackson et al., 2020). The presence of an etheno-bridge at the N^6-position blocks potential deamination and limits intracellular uptake. ε-AMP was previously reported for monitoring CD73-based hydrolysis to ε-adenosine using an HPLC system with a fluorescence detector (Bhatt et al., 2013; Evans et al., 2006; Gordon-Smith et al., 2015; Narravula et al., 2000; Zhou et al., 2007). A partial HTS assay was reported for ε-AMP using a plate reader. However, the samples were prepared in single vials using a large sample volume of 500 µL, consuming high amounts of the enzyme. Substrate precipitation was carried out by $ZnSO_4/Ba(OH)_2$ through centrifugation, followed by pipetting the supernatant to 96-well plates for measuring fluorescence. The assay is faster than the corresponding HPLC assay. However, sample preparation in single vials takes time and is unsuitable for screening large compound libraries (Newby et al., 1975). The enzymatic composition of the tumour microenvironment leads to high adenosine production because of the overexpression of ectonucleotidases CD39, NPP1, and CD73. This research aims to develop a sensitive, efficient, and robust HTS-compatible fluorescence assay for monitoring adenosine production by intact cancer cells. The HTS application of the assay is suitable for screening compound libraries that could inhibit multiple targets within one cancer cell line to yield a collective and intense inhibition of ATPase and AMPase activities. The inhibition of these activities could help to maintain a pro-inflammatory environment and increase the vulnerability of the tumour cells toward immune attack. The assay requires only minimal laboratory equipment, is straightforward, and is suitable for HTS applications.

CD73inhibitors

Nucleotidic

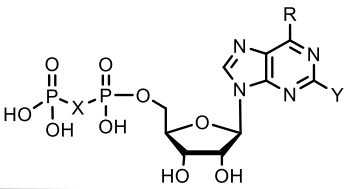

	R	X	Y	K_i (nM)
ADP[a]	—NH_2	—O—	—H	3380
AOPCP[b]	—NH_2	—CH_2—	—H	88.4
PSB12379[c]	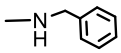	—CH_2—	—H	2.21
PSB12489[d]	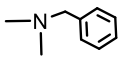	—CH_2—	—H	0.318
AB680[e]	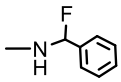	—CH_2—	—Cl	0.005

Non-nucleotidic

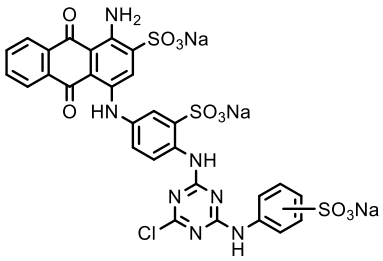

RB 2 K_i 3071 nM[f]

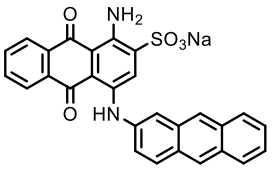

PSB-0963 K_i 150 nM[g]

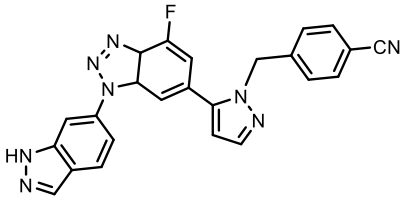

K_i 12 nM[h]

Figure 2.3: Structures of selected ectonucleotidase inhibitors. a. (Freundlieb et al., 2014), b. (Bhattarai et al., 2015), c. (Bhattarai et al., 2019), d. (Bhattarai et al., 2020), e. (Lawson et al., 2020), f. (Baqi et al., 2010), g. (Baqi & Müller, 2010), h. (Beatty et al., 2020).

2.0 Experimental

2.1 Materials and Methods

a. *Chemicals and reagents*

Ɛ-ATP, Ɛ-ADP, Ɛ-AMP, Ɛ-adenosine, and adenosine 5'- (α, β-methylene) diphosphate (AOPCP) were purchased from BIOLOG Life Science Institute (Bremen, Germany). The cDNA for the soluble human CD73 (Genbank accession no. NM_002526) was provided by Prof. Dr. Norbert Sträter (University of Leipzig, Germany) and NPP1 (NM_006208) from Origene Technologies, USA. Recombinant enzymes were expressed in-house. ATP, ADP, calcium chloride dihydrate, magnesium chloride, 4-(2-hydroxyethyl) piperazine-1-ethane-sulfonic acid (HEPES), and lanthanum chloride heptahydrate *N*-cyclohexyl-2-aminoethane-sulfonic acid (CHES) were purchased from Sigma–Aldrich (Steinheim, Germany). Dimethyl sulfoxide (DMSO), sodium dihydrogen phosphate (NaH_2PO_4), and sodium acetate (NaOAc) were obtained from Carl Roth (Karlsruhe, Germany). Corning® flat-bottom 96-well half-area microplates, black polystyrene, were purchased from Sigma–Aldrich (Steinheim, Germany). Cellfectin™ II Reagent (Thermo Fisher Scientific, MA, USA), baculovirus genomic ProEasy™ vector DNA (AB vector, CA, USA). Insect-XPRESS™ media (#: BE12-730Q, Lonza, Switzerland) and HisPur™ Ni^{2+}-NTA spin columns (#: 88226, Thermo Fisher Scientific, MA, USA) were used as protein expression and purification tools. EDTA free Protease inhibitors cocktail tablets (Roach Diagnostic GmbH, Germany).

b. Instrumentation

Fluorescence units were measured using a FlexStation® 3 Multi-Mode Microplate Reader (Medical Devices LLC. USA) using *Softmax Pro* 3.0 software for data collection. Nucleotides were precipitated in a 96-well plate using a SpeedVac plate centrifuge using precipitation buffer (LaboGene ApS, Denmark). Tests with natural substrates were performed by using the p/ACE™ MDQ plus capillary electrophoresis system (AB Sciex LLC, Framingham, USA). Data collection and peak area analysis were performed using 32 KARAT software from Beckman Coulter (Fullerton, CA, USA). Mithras LB 940 (Berthold Technology, France) is used for testing the *p*-Nph-5'-TMP assay.

2.2 Cell culture and membrane preparation

Triple-negative breast cancer (TNBC) and astrocytoma (AST) cell lines were cultured in Dulbecco's modified Eagle's medium (DMEM; GibcoBRL, Gaithersburg, MD., USA) supplemented with 10% fetal bovine serum (FBS; GibcoBRL), 1% Pen-strep at 37 °C in humidified 95% air and 10% CO_2. For U87 cell lines, 1% glutamine was added to the culture medium and incubated with 5% CO_2. Cells were harvested using trypsin reagent after rinsing with 1 x PBS and regularly split to 0.3 million cells/ml every 4th day. After the cells had grown into a monolayer of ~ 90% confluency again, the medium was decanted, and dishes were rinsed with 5 ml of phosphate-buffered saline (PBS) and frozen at -20˚C. Frozen cells were scraped off the dishes with 1 mL of an ice-cold buffer consisting of 25 mM Tris-HCl, 1 mM EDTA, 0.32 M saccharose, and 100 µM phenyl methyl sulfonyl fluoride (protease inhibitor) at pH 7.4 with a cell scraper. Cells were transferred to a sterile falcon tube and lysed with an Ultraturrax (6 cycles with 10 s each at high speed). Cell debris was removed by centrifuging samples at 1000 g for 10 min (4 °C). The supernatant was centrifuged at 48,000 g for 1 h (4 °C). The obtained pellets were resuspended in a washing buffer and centrifuged using the same conditions. After two more washing steps, the pellets were resuspended in (10 mM HEPES, 10 mM $MgCl_2$, 20 mM KCl, 30% glycerol, pH 7.4) and stored at -80 °C until use.

2.3 Expression and purification of recombinant enzymes

Soluble enzymes CD73 and NPP1 were produced by a former PhD colleague (Renn, 2019). Briefly, the extracellular catalytic domains of both enzymes were subcloned in the expression vector [For CD73; amino acids (AA) 28 – 550 excluding N-terminal signal peptides 1-27 and C-terminal GPI-anchor: AA 550-574, for NPP1; 98 – 925 (*p*-ACGP67-B)]. The plasmids were transfected into *Spodoptera frugiperda* (*sf9*) insect cells using Cellfectin™ II reagent and ProEasy™ baculovirus linearised DNA (*manufacturer specs.*). Protein expression was performed for 48h at 27°C. The signal peptide sequence of the expression vector helped proteins accumulate in the medium from where they are concentrated using an Amikon concentrator with a 30 kDa cut-off. The filtrate (CD73) was then purified using the manufacturer's protocols using HisPurTM Ni^{2+}-NTA spin columns. Protein concentration was measured by the Lowry method (Randall & Lewis, 1951).

2.4 Capillary electrophoresis assay for NPP1

The CE assay was performed as previously reported (Nassir et al., 2019). Briefly, a polyacrylamide-coated capillary [30 cm (20 cm effective length) × 50 µm (id), × 360 µm (od) purchased from Chromatographie Service GmbH (Langerwehe, Germany)] was used. Soluble NPP1 0.7 µg was reacted with 100 µM ATP for 30 min at 37 °C either with or without inhibitors, followed by boiling samples at 95 °C for 10 min. After cooling the plate briefly on ice for 5 min, samples were injected electrokinetically with a voltage of – 6 kV for 30 s. Finally, analytes were separated by applying a separation voltage of – 15 kV. Nucleotides were detected at an absorbance of 254 nm.

2.5 *p*-NPh-5'-TMP assay for analysing NPP activity

The artificial substrate *p*-nitrophenyl-5'-thymidine-monophosphate (*p*-Nph-5'-TMP) is a standard substrate for colourimetric determination of NPPs activity. The produced *p*-nitrophenolate has an intense yellow colour and an absorbance maximum of 405 nm (Cimpean et al., 2004). U87/ TNBC 50,000 cells/well, and astrocytoma 100,000 cells/well were treated with 400 µM of *p*-Nph-5'-TMP in reaction buffer; 50 mM Tris (pH 9.2), 2 mM $CaCl_2$, 0.2 mM $ZnCl_2$ for 60 min at 37 °C. The reaction was terminated by adding 20 µL of 0.1M NaOH, and the absorbance of *p*-nitrophenolate was measured at 405 nm using a Mithras LB 940 continuous plate reader equipped with MikroWin software for data acquisition.

2.6 Precipitation assay

This assay is based on the previously developed radioactive assay using [^{3}H]AMP (Freundlieb et al., 2014), and the partial HTS fluorescent assay using ε-AMP (Jamal et al., 1988), by combining both methods and developing a new HTS-compatible procedure. In the presence of sodium hydrogen phosphate, Lanthanum chloride could effectively precipitate nucleotide phosphates from a reaction mixture. Briefly, for estimating AMP hydrolysis, 90 ng of human soluble CD73, 1.5 x 10^3 cells of U87, TNBC, and astrocytoma were incubated with 10 µM ε-AMP for 30 min at 37 ºC in a 96-well plate in reaction buffer HEPES 10 mM (pH 7.4), 2 mM $CaCl_2$, and 1 mM $MgCl_2$ (HEPES buffer). In the inhibitor control sample, 10 µM of PSB-12489 was added. A precipitation control sample containing 10 µM ε-AMP was analysed without cells or enzymes to estimate the background signal-

to-noise ratio (S/N), if any. The reaction was terminated by adding a precipitation buffer containing 14.2 mM NaH_2PO_4 and 71.7 mM $LaCl_3$/NaOAc at pH 3.2. Nucleotides were precipitated upon cooling the samples for 10 min on ice, followed by centrifugation of the plates at 1200 rpm for 10 min. The precipitation step left Ɛ-adenosine in the supernatant. 100 µL of supernatant was then transferred to a fresh half-area 96-well fluorescence plate using multichannel pipettes. A fluorescence microplate reader measured the samples' relative fluorescence units (RFU at λ270/420 nm) (Flex station, Medical Devices LLC. USA). The assay procedure is illustrated in Figure 2. For the cell-based assay using Ɛ-ATP as the substrate, 5 x 10^4 cells of U87 or TNBC and 1 x 10^6 cells of astrocytoma previously washed with phosphate-free buffer were incubated with 10 µM Ɛ-(ATP/ADP) at 37 ºC for 60 min. The substrate precipitation steps were the same as described for Ɛ-AMP.

2.7 Assay validation and robustness

The assay procedure was validated both for Ɛ-AMP and Ɛ-ATP. Calibration curves were performed for Ɛ-adenosine using different concentrations ranging from 0.005 to 5 µM to investigate linearity and to measure the limit of detection (LOD) and the limit of quantification (LOQ). Briefly, a simulation of enzyme reaction was made by mixing an equal concentration of Ɛ-AMP/adenosine (for AMP hydrolysers) and Ɛ-ATP/ADP/adenosine (for ATP hydrolysers). The samples were then subjected to precipitation conditions discussed in section 2.6. Three independent tests were performed, each in triplicate. Data were analysed using GraphPad Prism 7 (GraphPad Software, La Jolla, CA, USA). LOD and LOQ were calculated by equation I and II:

$$\text{(I)} \qquad \mathrm{LOD} = \frac{3.3\times\sigma}{S} \qquad\qquad \text{(II)} \qquad \mathrm{LOQ} = \frac{10\times\sigma}{S}$$

σ = Standard deviation

S = Slope of the calibration curve

For precision and % accuracy, four concentrations of Ɛ-adenosine (50 to 750 nM) + Ɛ-ATP/AMP (50 to 750 nM) were subjected to $LaCl_3$/phosphate co-precipitation. The relative standard deviation (RSD) was calculated for six experiments, and % the accuracy was determined in three replicates. The effects of different pH values of the precipitation buffer (2 - 5.5) were checked. Precipitation buffers of 14.2 mM NaH_2PO_4 and 71.7 mM

$LaCl_3$/NaOAc at the respective pH were added to 10 µM of substrate Ɛ-AMP or the product Ɛ-adenosine. Moreover, the incubation time for the samples on ice and centrifugation of the plates were optimised for different periods (0 – 30min). The centrifugation speed of 1200 rpm was kept constant throughout the experiments. The suitability of the assay for HTS was investigated for a total of 48 positive reactions (with enzyme) and 48 negative reactions (without enzyme). Z'-factor was measured as previously described (Zhang et al., 1999).

2.8 Kinetic parameters

Kinetic parameters such as Michaelis-Menten constant (K_m) and maximum velocity (Vmax) were determined for different Ɛ-AMP concentrations ranging from 0.1 to 200 µM. The reaction was started by adding a specified amount of enzymes (90 ng of CD73) to 200 µl of the final reaction volume. Assay conditions were the same as reported in section 2.6. For cell lines, the whole cells of U87, TNBC, and AST were treated with either Ɛ-ATP/ Ɛ-ADP/ Ɛ-AMP (0.1 to 200 µM). Tests were performed as three independent experiments (each in triplicate). Vmax was calculated using the Michaelis-Menten equation implemented in GraphPad Prism 7.0 (GraphPad Software, San Diego, CA, USA).

2.9 Screening of compound libraries and concentration-dependent inhibition (IC_{50} values)

a. For soluble CD73

A library comprising 168 compounds distributed into two 96-well plates was screened vs. 10 µM Ɛ-AMP and recombinant CD73 to estimate assay efficiency in a high-throughput screening mode. Standard inhibitors of CD73, AOPCP, PSB-12489, and RB-2 were used as positive controls. The time required to analyse a single plate was estimated after adding the precipitation buffer. Assay conditions were the same as previously described in section 2.6. Standard inhibitors of human CD73; AOPCP (0.001 –5µM), PSB-12489 (0.0001 – 1 µM), and RB-2 (0.1 to 500 µM) were tested using human soluble CD73 and 10 µM of Ɛ-AMP at 37 °C for 30 min. IC_{50} values of the inhibitors were determined by nonlinear fitting of the experimental data using GraphPad Prism 7.0. Three independent experiments with triplicate observations were performed. K_i values were calculated from

IC_{50} values using the Cheng-Prusoff equation for competitive inhibitors (Cheng & Prusoff, 1973). For non-competitive inhibitors like RB-2, the IC_{50} value is considered the K_i value.

b. For cancer cell lines

A library of 200 diverse anthraquinone molecules was tested against U87 cell lines using 10 µM ε-ATP as a substrate under similar reaction conditions described above [the compound's structures will be revealed in a detailed structure-activity relationship (SAR) studies, which will be published elsewhere]. Two independent tests were performed with single-point observation. Hit compounds from the screening campaign of anthraquinone library vs. cell lines were further tested for IC_{50} calculations. For IC_{50} curves, a single compound PSB-1699 was investigated for 13 concentrations (0.001 – 150 µM) using ε-ATP as a substrate (see section 3.5). The results were further verified using CE assay with recombinant NPP1 and natural substrate ATP.

3.0 Results and Discussion

To develop a straightforward HTS-compatible assay, we initially employed soluble CD73 expressed in insect cells with readily available fluorescent nucleotide ε-AMP. To circumvent chromatographic separation, which would hardly be compatible with HTS, we explored the possibility of removing the remaining substrate from the fluorescent reaction product etheno-adenosine (ε-adenosine) by precipitation of the nucleotide with lanthanum chloride. This method had been successfully used for radioactive CD73 assays to separate [^{3}H]AMP from [^{3}H]adenosine. The precipitation buffer successfully removed ε-AMP from the reaction mixture by more than 99%, and the supernatant contained exclusively the product ε-adenosine. The period required for the operation is short, and radioactivity hazards have been successfully avoided. This fact made this assay compatible for high high-throughput screening of compound libraries.

To further optimise the assay system towards intact cells of U87, TNBC, and astrocytoma, we treated the cells with 10 µM ε-ATP. Before the reaction, cells were washed three times with phosphate buffer, and viable cells were counted. These cell lines contained multiple ectonucleotidases co-expressed on their surface, particularly NPP1, CD39, and CD73. These enzymes hydrolyse extracellular nucleotides to adenosine. Since our assay setting allows the detection of the final product ε-adenosine, we were more interested in the outcome of the reaction. Once the ε-ATP was added to the response, it was efficiently converted to ε-AMP by either NPPs or NTPDases. The resulting product ε-AMP is hydrolysed to adenosine by CD73, abundantly expressed on these cell lines. The precipitation procedure is depicted in Figure 2.4.

3.1 Assay linearity and validation

a. Method validation

The limit of detection (LOD) and the limit of quantification (LOQ) were determined to assess the sensitivity of the assay method. A calibration curve was drawn for ε-adenosine (0.005 - 5 µM, 11 concentrations) without treatment with precipitation buffer and ε-adenosine = ε-ATP + ε-ADP (0.001 – 10 µM, 12 concentrations) after treating the mixture with precipitation buffer. Method validation results are summarised in Table 1.1. A linear correlation was observed between ε-adenosine concentrations and relative fluorescence

units (RFU) with a correlation coefficient of R^2 = 0.9994 after ε-AMP precipitation (n = 3, each in triplicate) and R^2 = 0.9984 for ε-ATP/ε-ADP precipitation (n = 3, each in triplicate), (Figure 2.5) demonstrating excellent linearity of the assay over the tested concentrations. LOD/LOQ in the low nanomolar range allows testing reactions under low substrate concentrations close to the reported K_m for ectonucleotidases. This new assay is more sensitive than the frequently used malachite green assay for monitoring ATP hydrolysis and *p*-NPh-5'-TMP assay for NPPs. Complete precipitation of the substrates (> 99%) was observed over a pH range of 3.0 - 5.5 and a centrifugation speed of 1200 rpm. Ice Incubation of the post-reaction samples was not critical since the complete separation of substrate and the product was observed; however, after adding precipitation buffer, it is better to incubate samples for 10 min on ice to allow smooth precipitation. The assay showed high precision and % accuracy up to the low nanomolar range (nucleotides/ε-adenosine 50 –750 nM). The precision of the assay (5.2 – 9.1) and % accuracy (91 – 97 %) values are well within the accepted range as per ICH (International Council for Harmonization) guidelines (Taverniers et al., 2004). Significantly higher Z'-factor values of 0.87 (ε-AMP) and 0.84 (ε-ATP) confirmed the excellent suitability of the assay for HTS with a higher detection window (Figure 2.6).

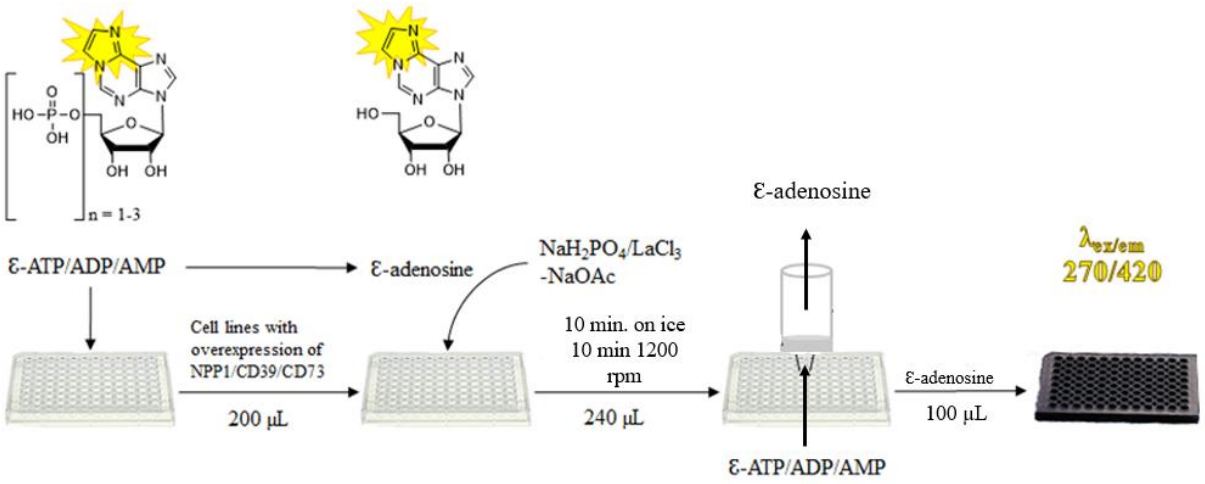

Figure 2.4: Assay procedure of fluorescence-based HTS assay for monitoring ectonucleotidase reactions. The fluorescent nucleotides ε-ATP, ADP, and AMP are converted to the product ε-adenosine by ectonucleotidases. The enzymatic reaction is terminated by adding precipitation buffer A up to the final concentration of (14.2 mM NaH_2PO_4) and B (71.7 mM $LaCl_3$/NaOAc, pH 3.2). Samples were incubated on ice for 10 min, followed by centrifugation of the plate at 1200 rpm for 10 min. 100 µL of the supernatant

containing the product Ɛ-adenosine exclusively is transferred to a black half-area plate, and fluorescence is measured at $\lambda_{ex/em}$ of 270/420 nm using a microplate reader.

Table 2.1. Assay validation for fluorescence substrates

Parameter	Observations		Acceptable range [a, b]
	Ɛ-Adenosine	Ɛ-ATP/ADP/Adenosine	
Regression equation	Y = 585.4*X + 47.7	Y = 1103*X + 87.4	
Linearity R^2 (n=3)	0.9994	0.9986	
LOD (Mean ± SD, nM) n =3	18.1 ± 0.1	69.2 ± 0.3	
LOQ (Mean ± SD, nM) n =3	55.6 ± 0.2	192 ± 1	
Accuracy (Recovery %), nM, n =3			
750	97.5	99.8	80 – 110[a]
500	91.1	107.8	80 – 110 [a]
250	90.9	109.2	80 – 110 [a]
50	93.7	104.3	80 – 120 [a]
Precision (RSD %), nM, n =6			
750	5.29	2.41	8 [a]
500	6.34	2.57	16 [a]
250	5.71	1.23	16 [a]
50	9.10	5.71	22.6 [a]
Z'-factor (n = 48)	0.87	0.84	0.5-1.0[b]
Detection time/plate (in min)	20	20	

[a.] acceptable range according to literature referencing (Taverniers et al., 2004) [b.] Z'-factor test (Zhang et al., 1999)

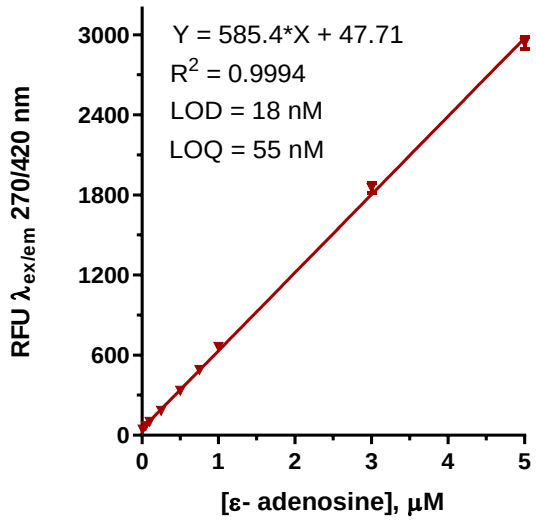

Figure 2.5: Assay validation for the fluorescent substrate. A calibration curve for eleven concentrations of Ɛ- adenosine from 0.005 - 5 µM. A total of 3 independent tests were recorded in triplicate observations by equation Y = 585.4*X + 47.71. Each point represents mean ± SD.

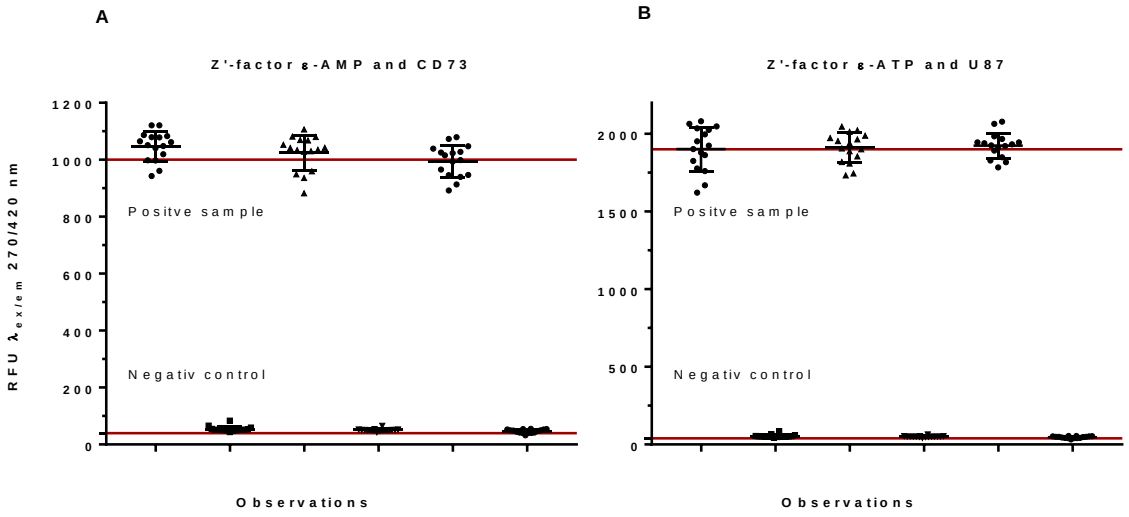

Figure 2.6: Determination of Z'-factor. Three independent reactions of either soluble CD73 or U87 whole cells were performed. Each reaction consisted of sixteen observations of either positive (with enzyme) or negative (without enzyme) samples. A. Substrate ε-AMP (10 µM) was treated with 90 ng of the CD73 diluted in HEPES reaction buffer. B. Substrate ε-ATP was treated first with 50,000 cells/well of U87 for 60 min in the HEPES reaction buffer. Reaction substrates were removed from the mixture under intense precipitation conditions offered by Na_2HPO_4/$LaCl_3$-NaOAc. Each data point represents a single observation. A large detection window and a Z'-factor of > 0.80 were observed for both substrates.

3.2 Maximum velocity and Michaelis-Menten constant (K_m)

The K_m value was determined for human CD73 under the optimised assay conditions using twelve different substrate concentrations (see Figure 2.7A). The determined kinetics parameters were: K_m 1.86 ± 0.11 µM, K_{cat} approx. 0.80 ± 0.02 s^{-1}, K_{cat}/K_m 0.430 ± 0.014 s^{-1} *μM^{-1}. The reported K_m for crude CD73 using ε-AMP was 25 µM (Jamal et al., 1988). Negative enzyme samples for each substrate concentration were processed equally as the enzyme samples to confirm no background interference. A complete precipitation of the substrates was observed up to the maximum concentration of 250 µM. The kinetic parameters obtained by using precipitation assay were consistent with the published data for the CD73, i.e. 2.53 – 59.1 µM (Freundlieb et al., 2014; Goueli & Hsiao, 2019; Iqbal, Jirovsky, et al., 2008; Jackson et al., 2020; McManus et al., 2018). The kinetic parameters of human CD73 using precipitation assay were variable compared to malachite green assay. The enzyme showed K_m of 17.0 ± 2.1 µM and *Vmax* of 2.51 ± 0.21 µmol/min/mg-protein while, with precipitation assay, a *Vmax* of 0.75 µmol/min/mg-protein was achieved (Renn, 2019). This low product turnover for etheno-linked substrate, as compared to the

natural substrate, needs further investigation by comparing both assays in a parallel setting.

Potent hydrolysis of ε-ATP was observed for the cell lines where the end product ε-adenosine was recovered due to simultaneous ATPase and AMPase activity. The ATPase activity could be due to CD39 and NPP1-based reactions. However, currently, we cannot exclude the presence of other ATP-hydrolyzing enzymes like AP. The NPP1-based activity was independently observed through its specific substrate *p*-NPh-5'-TMP. These results showed that all three enzymes, CD39, NPP1, and CD73, are active. However, U87 cell lines have a more dominant NPP1 activity than CD39. A much faster hydrolysis of AMP was observed than ATP and ADP, indicating a significantly high AMPase activity.

3.3 Screening of selected compound libraries

a. CD73

A library of 168 compounds was tested to measure the assay suitability for inhibition screening of CD73 reactions. Each plate contained standard CD73 inhibitors (AOPCP, PSB-12489, and RB-2) as positive controls. 70% inhibition was considered a hit. The assay conditions suit high-throughput screenings of CD73-based reactions. AOPCP derivatives showed approximately 90 % inhibition; however, RB-2 showed 65% inhibition. Full-scale inhibition testing was further performed for AOPCP, PSB-12489, and RB-2.

b. U87 whole cells

A selected library comprising 200 derivatives belonging to a common core structure was tested for inhibiting adenosine production in U87 cell lines. The hit rate was higher since the core scaffold is a promising NPP1 inhibitor, and we found 25 compounds that showed more than 70% inhibition. Structure-activity relationship (SAR) studies of these derivatives will be reported elsewhere.

3.4 Concentration-dependent inhibition of AMP hydrolysing CD73

Standard inhibitors of CD73 were further subjected to full-scale IC_{50} curve determination using the newly developed assay. The compounds showed IC_{50} values in a similar range as previously reported with radio-assay. This showed that the new assay can be a safer alternative to the radioactivity-based assay (Figure 2.9). The most potent inhibitor (PSB-

12489) was further investigated for blocking ε-AMP hydrolysis in TNBCs and AST cells. The results showed that the inhibitors blocked hydrolysis with similar IC_{50} values for TNBCs and AST cells; however, relatively higher IC_{50} values were observed for U87 cells (Table 2.2). The higher IC_{50} values in U87 cell lines reflect the possibility of some AMP hydrolysing enzymes other than CD73; however, this aspect was not analysed in the current report.

3.5 Determination of concentration-inhibition curves for cell lines

Hit compound from the screening campaigns towards the U87 cell line was further evaluated for a full-range IC_{50} and K_i determination. (Figure 2.10). First, we confirmed that the anthraquinone scaffold inhibited the particular enzyme (NPP1 or CD73) in the cell line. The selected hits were further tested for inhibition of U87 cell ability to produce adenosine when reacted with ε-AMP as a substrate. No significant inhibition of the enzyme activity was observed, and a high ε-AMP to ε-adenosine conversion was recorded. Compounds PSB-1699 were selected for thirteen concentration point detection. The IC_{50} value was in the low µM range vs. U87 cells. To further confirm the tested compounds as NPP1 inhibitors and not CD39, we tested PSB-1699 vs. recombinant NPP1 and its natural substrate ATP using a CE-UV detection system. The compound was equally potent towards human recombinant NPP1 as it was towards U87 whole cells (Figure 2.10).

U87, TNBC, and astrocytoma cell lines hydrolysed fluorescent nucleotides (ε-ATP/ADP/AMP) very efficiently, and a high product turnover was observed. N^6 etheno bridge blocks the further hydrolysis of an adenine ring and allows efficient analysis and screening of the inhibitors vs adenosine-producing cascade active on these cancer cells. NPPs, mostly NPP1, are the prominent enzymes in these cells, along with CD73. The activity of NPP1 was apparent owing to the hydrolysis of the NPP's specific artificial substrate, *p*-NPh-5'-TMP, which is currently the primary HTS screening substrate. Since the assay depends on the calorimetric detection of yellow-coloured p-nitrophenolate, it would be less applicable to investigating coloured compounds and plant pigments. The ε-ATP as substrates of NPP1 and CD39 allow investigation of these cell lines compared to the natural substrate. ε-AMP, on the other hand, allows further validation of CD73 reactions.

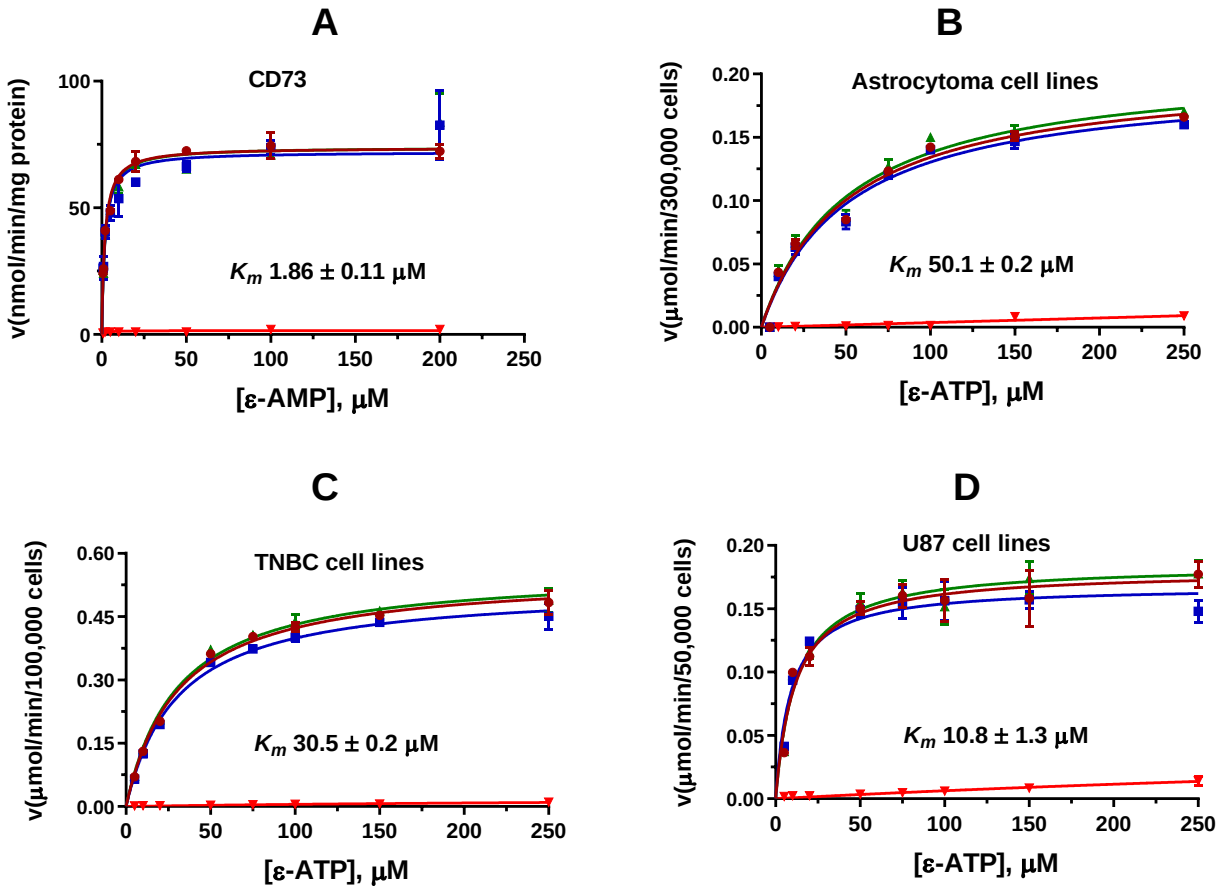

Figure 2.7: Michaelis-Menten constant and maximum velocity A) Kinetics testing was performed for CD73 with Ɛ-AMP concentrations (0.25 – 250 µM). Maximum velocity was checked for each cell line, B) U87, C) TNBC, and D) astrocytoma vs Ɛ-ATP (5 – 250 µM). K_m for Ɛ-AMP was recorded at 1.86 ± 0.11 µM. For U87 cell lines 10.8 ± 1.3 µM, TNBC 30.5 ± 0.2 µM, astrocytoma 51.1 ± 0.2 µM. Three independent tests with triplicate observations were performed individually in the Michaelis-Menten curves. Negative control for each substrate concentration without adding enzymes or cells is processed separately. Data is presented and mean ± SEM.

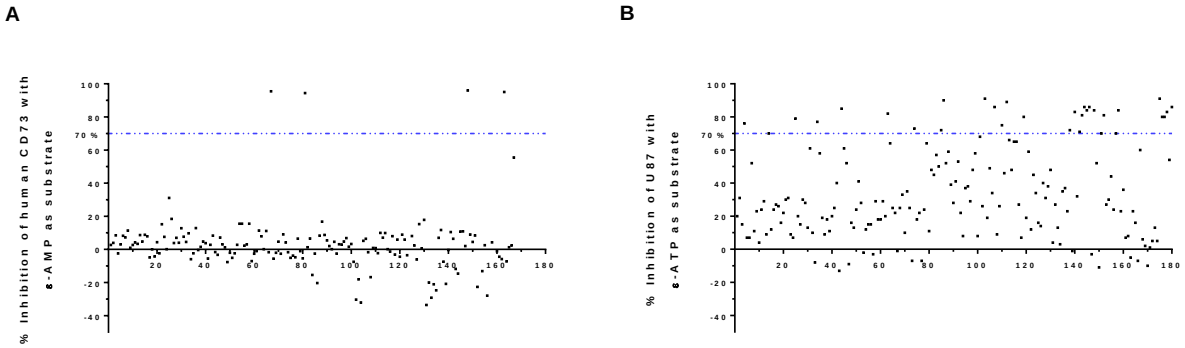

Figure 2.8: High throughput screening. A) 168 structures (10 µM) were treated with CD73 and 10 µM of Ɛ-AMP to calculate the screening efficiency of the newly developed assay. Positive control samples showed

expected % inhibition. B) 200 selected derivatives of a standard series of compounds at 10 µM concentration were mixed with U87 whole cells (50,000 cells/well) in the presence of 10 µM of ε-ATP for 60 min. 70 % inhibition was set as the cut-off value. The hit rate was calculated at 6.41.

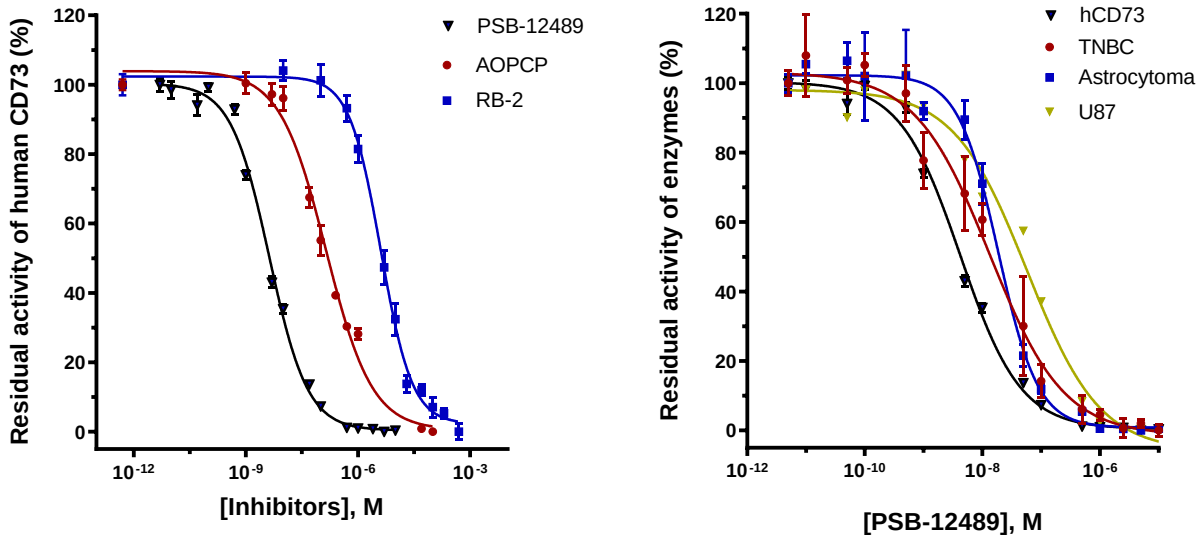

Figure 2.9: Concentration-dependent enzyme inhibition *IC₅₀*. A: Concentration-inhibition curves for standard CD73 inhibitors AOPCP, PSB-12489, and RB-2 were determined with the new assay by reacting 90 ng of the enzyme with 10 µM of substrate ε-AMP B: A direct comparison of IC_{50} values for the most potent inhibitor of CD73, PSB-12489 has been performed vs. hCD73, TNBC, U87, and AST cells. Samples were treated with strictly similar conditions. Three to five independent experiments were performed, each with duplicate observations. Each data point represents mean ± SEM.

Table 2.2: Concentration-dependent inhibition of CD73 and cancer cell lines

Compounds	Enzyme source	ε-AMP 10 µM		
		IC_{50} nM, (mean ± SEM)[a]	K_i nM, (mean ± SEM)[b]	Reported K_i values
AOPCP	Human CD73	208 ± 1	32.7 ± 1.9	88.4
RB-2	"	15100 ± 528	15100 ± 528	3070
PSB-12489	CD73[c]	4.23 ± 0.21	0.651 ± 0.003	0.318
"	TNBC	13.2 ± 3.6	ND[d]	ND[d]
"	Astrocytoma	18.6 ± 1.2	ND[d]	ND[d]
"	U87	57.5 ± 2.66	ND[d]	ND[d]

a. Values determined with fluorescence precipitation assay.
b. K_i values are calculated using the Cheng-Prusoff equation.
c. Recombinant CD73 expressed in *p*ACGP67-B expression system with K_m 1.86 ± 0.11 µM.
d. Not Determined

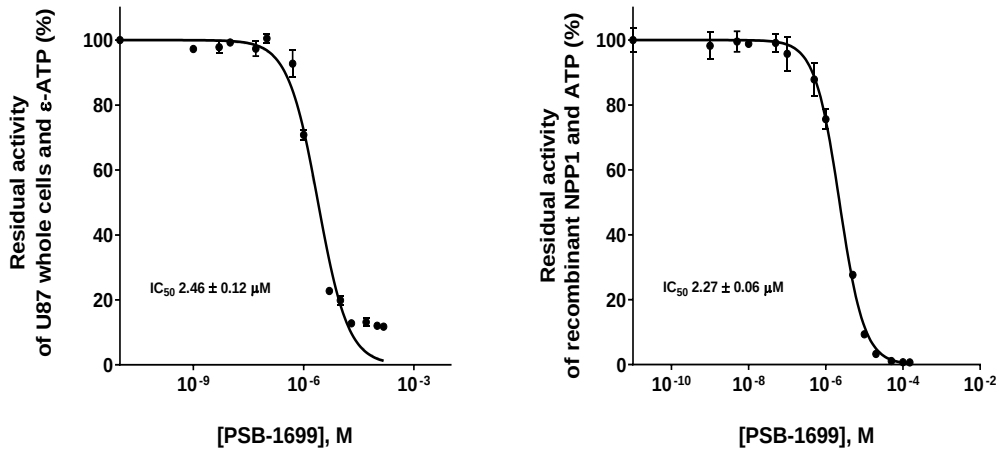

Figure 2.10: Concentration-dependent inhibition for potent anthraquinone derivative towards U87 cancer cell line. Hit compounds from the screening campaign were further tested for IC_{50} curve vs. U87 whole cells using either Ɛ-ATP or recombinant NPP1 and ATP. The structure of selected hit compounds is mentioned. Three independent tests were performed, and data are presented as mean ± SEM.

4.0 Conclusions

Ectonucleotidases are known to be overexpressed in many cancers, leading to increased production of immunosuppressive adenosine and metastasis. These enzymes work together, with the product of one enzyme's reaction becoming a substrate for the other (Zimmermann, 2020). The accumulation of adenosine in the tumour microenvironment converts the pro-inflammatory response of ATP to an anti-inflammatory one. This study created and validated a sensitive high-throughput screening (HTS) assay for monitoring ATPase/AMPases expressed on aggressive tumour cell lines U87, TNBC, and AST. We observed efficient ATPase activity due to the NPP1 enzyme, which was further confirmed by the hydrolysis of p-NPh-5'-TMP by these cell lines. Our goal was to observe the net production of adenosine by the cascade of enzymes expressed on these cell lines and to investigate inhibitors versus intact live cells. Previous reports have shown different enzymes' behaviour towards competitive inhibitors when treated with natural (ATP) and artificial substrate *p*-NPh-TMP (Lee et al., 2017). Therefore, this new HTS fluorescence assay is suitable for investigating cancer cell lines and their inhibition in the presence of ATP or a more natural alternative. The substrate was successfully precipitated from the reaction mix (up to 100%), and the ε-adenosine was quantified with a low signal-to-noise ratio. The assay can be established and performed in any laboratory without requiring expensive equipment or (bio)chemicals. It allows using substrates with low nanomolar

concentrations, making it a good choice for experimental designs that work at low substrate concentrations. Validation experiments showed robust results with precision and accuracy values within acceptable limits. The pH of the precipitation buffer and the centrifugation steps are the most critical parameters for complete substrate removal. The kinetics and IC_{50} experiments using the ε-AMP fluorescence assay replicate the findings with natural substrate AMP and [^{3}H]AMP, making this assay a safer, more efficient, and robust alternative to radio assays.

Conflict of Interest

The authors declare that the research was conducted without commercial or financial relationships that could create a conflict of interest.

1 Author Contributions

SM performed the experimental work and helped CEM write the manuscript. CR and TC expressed recombinant CD73. AS and SL contributed to data analysis. CEM designed the study and supervised the project overall. All authors contributed to the manuscript and approved the final version.

2 Funding

SM is thankful to the Higher Education Commission of Pakistan for funding his PhD studies and to the Bonn Graduate School of Drug Sciences (BIGS DrugS) for continuous academic support.

References

Aerts, Indra, Jean Jacques Martin, Peter Paul De Deyn, Chris Van Ginniken, Xaveer Van Ostade, MarkKockx, Guido Dua, and Herman Slegers. 2011. “The Expression of Ecto-Nucleotide Pyrophosphatase/Phosphodiesterase 1 (E-NPP1) Is Correlated with Astrocytic Tumor Grade.” *Clinical Neurology and Neurosurgery* 113: 224–29. https://doi.org/10.1016/j.clineuro.2010.11.018.

Allard, Bertrand, Martin Turcotte, and John Stagg. 2014. “Targeting CD73 and Downstream Adenosine Receptor Signaling in Triple-Negative Breast Cancer.” *Expert Opin. Ther. Targets* 18: 863–81.

Bageritz, J., L. Puccio, R. M. Piro, V. Hovestadt, E. Phillips, T. Pankert, J. Lohr, C. Herold-Mende, P. Lichter, and V. Goidts. 2014. “Stem Cell Characteristics in Glioblastoma Are Maintained by the Ecto-Nucleotidase E-NPP1.” *Cell Death Differ.* 21: 929–40. http://dx.doi.org/10.1038/cdd.2014.12.

Baqi, Younis, Sang Yong Lee, Jamshed Iqbal, Peter Ripphausen, Anne Lehr, Anja B. Scheiff, Herbert

Zimmennann, Jürgen Bajorath, and Christa E. Müller. 2010. “Development of Potent and Selective Inhibitors of Ecto-5′- Nucleotidase Based on an Anthraquinone Scaffold.” *J. Med. Chem.* 53: 2076–86.

Baqi, Younis, Mahmoud Rashed, Laura Schäkel, Enas M. Malik, Julie Pelletier, Jean Sévigny, Amelie Fiene, and Christa E. Müller. 2020. “Development of Anthraquinone Derivatives as Ectonucleoside Triphosphate Diphosphohydrolase (NTPDase) Inhibitors With Selectivity for NTPDase2 and NTPDase3.” *Front. Pharmacol.* 11: 1–15. https://doi.org/10.3389/fphar.2020.01282.

Baykov, A. A., O. A. Evtushenko, and S. M. Avaeva. 1988. “A Malachite Green Procedure for Orthophosphate Determination and Its Use in Alkaline Phosphatase-Based Enzyme Immunoassay.” *Anal. Biochem.* 171: 266–70.

Beatty, Joel W., Erick A. Lindsey, Rhiannon Thomas-Tran, Laurent Debien, Debashis Mandal, Jenna L. Jeffrey, Anh T. Tran, et al. 2020. “Discovery of Potent and Selective Non-Nucleotide Small Molecule Inhibitors of CD73.” *J.Med.Chem* 63: 3935–55. https://doi.org/10.1021/acs.jmedchem.9b01713.

Bhattarai, Sanjay, Marianne Freundlieb, Jan Pippel, Anne Meyer, Aliaa Abdelrahman, Amelie Fiene, Sang Yong Lee, et al. 2015. “α,β-Methylene-ADP (AOPCP) Derivatives and Analogues: Development of Potent and Selective Ecto-5′-Nucleotidase (CD73) Inhibitors.” *J. Med. Chem.* 58: 6248–63.

Bhattarai, Sanjay, Jan Pippel, Anne Meyer, Marianne Freundlieb, Constanze Schmies, Aliaa Abdelrahman, Amelie Fiene, et al. 2019. “X-Ray Co-Crystal Structure Guides the Way to Subnanomolar Competitive Ecto-5′-Nucleotidase (CD73) Inhibitors for Cancer Immunotherapy.” *Adv. Ther.* 2: 1–8.

Bhattarai, Sanjay, Jan Pippel, Emma Rose Scaletti, Riham Idris, Marianne Freundlieb, Georg Rolshoven, Christian Renn, et al. 2020. “2-Substituted α,β Methylene-ADP Derivatives: Potent Competitive Ecto-5′-Nucleotidase (CD73) Inhibitors with Variable Binding Modes.” *J. Med. Chem.* 63: 2941–57.

Cimpean, Anisoara, Cristiana Stefan, Rik Gijsbers, Willy Stalmans, and Mathieu Bollen. 2004. “Substrate-Specifying Determinants of the Nucleotide Pyrophosphatases/ Phosphodiesterases NPP1 and NPP2.” *Biochem. J.* 381: 71–77.

Dhaval P. Bhatt, Xuesong Chen, Jonathan D. Geiger, and Thad A. Rosenberger. 2013. “A Sensitive HPLC-Based Method to Quantify Adenine Nucleotides in Primary Astrocyte Cell Cultures.” *J. Chromatogr. B* 15: 889–99.

Dosch, Michel, Joël Gerber, Fadi Jebbawi and Guido Beldi. 2018. “Mechanisms of ATP Release by Inflammatory Cells.” *Int. J. Mol. Sci* 19: 1–16.

Evans, Bronwen A.J., Carole Elford, Annette Pexa, Karen Francis, Alis C. Hughes, Andreas Deussen, and Jack Ham. 2006. “Human Osteoblast Precursors Produce Extracellular Adenosine, Which Modulates Their Secretion of IL-6 and Osteoprotegerin.” *J. Bone Miner. Res.* 21: 228–36.

Fiene, Amelie, Younis Baqi, Joanna Lecka, Jean Sévigny, and Christa E. Müller. 2015. “Fluorescence Polarization Immunoassays for Monitoring Nucleoside Triphosphate Diphosphohydrolase (NTPDase) Activity.” *Analyst* 140: 140–48.

Freundlieb, Marianne, Herbert Zimmermann, and Christa E. Müller. 2014. “A New, Sensitive Ecto-5’-Nucleotidase Assay for Compound Screening.” *Analy. Biochem.* 446: 53–58.

Gordon-Smith, Sophie Botta, Simona Ursu, Simon Eaton, Halima Moncrieffe, and Lucy R. Wedderburn. 2015. “Correlation of Low CD73 Expression on Synovial Lymphocytes with Reduced Adenosine Generation and Higher Disease Severity in Juvenile Idiopathic Arthritis.” *Arthritis Rheumatol.* 67: 545–54.

Hay, Carl M., Erin Sult, Qihui Huang, Kathy Mulgrew, Stacy R. Fuhrmann, Kelly A. McGlinchey, Scott A.

Hammond, et al. 2016. “Targeting CD73 in the Tumor Microenvironment with MEDI9447.” *OncoImmunology* 5: 1–10.

Helenius, Mikko, Sirpa Jalkanen, and Gennady G. Yegutkin. 2012. “Enzyme-Coupled Assays for Simultaneous Detection of Nanomolar ATP, ADP, AMP, Adenosine, Inosine and Pyrophosphate Concentrations in Extracellular Fluids.” *Biochim. Biophys. Acta, Mol. Cell Res.* 1823: 1967–75.

Id, Said A Goueli, and Kevin Hsiao. 2019. “Monitoring and Characterizing Soluble and CD39.” *PLoS ONE* 14: 1–19.

Iqbal, Jamshed, David Jirovsky, Sang Yong Lee, Herbert Zimmermann, and Christa E. Müller. 2008a. “Capillary Electrophoresis-Based Nanoscale Assays for Monitoring Ecto-5′-Nucleotidase Activity and Inhibition in Preparations of Recombinant Enzyme and Melanoma Cell Membranes.” *Anal. Biochem.* 373: 129–40.

Iqbal, Jamshed, Aileen F. Knowles, and Christa E. Müller. 2010. “Development of a Microbioreactor with Ecto-Nucleoside Triphosphate Diphosphohydrolase 2 (NTPDase2) Immobilized on a Polyacrylamide-Coated Capillary at the Outlet.” *J. Chromatogr. A* 1217: 600–604.

Jackson, Edwin K., Delbert G. Gillespie, Dongmei Cheng, Zaichuan Mi, and Elizabeth V. Menshikova. 2020. “Characterization of the N6-Etheno-Bridge Method to Assess Extracellular Metabolism of Adenine Nucleotides: Detection of a Possible Role for Purine Nucleoside Phosphorylase in Adenosine Metabolism.” *Purinergic Signalling* 16: 187–211. https://doi.org/https://doi.org/10.1007/s11302-020-09699-x.

Jamal et. al. 1988. “A Novel Assay for 5’-Nucleotidase Using 1,N6-Etheno-AMP as Substrate, and Comments on the Properties of the Reaction Product, Ethenoadenosine.” *The Biochem. J.* 250: 369–73.

JI-HU-Zhang, Thomas D.Y. Chung, kevin R.Oldenburg. 1999. “A Simple Statistical Parameter for Use in Evaluation and Validation of High Throughput Screening Assays.” *J. Biomol. Screening* 4: 67–72.

Junker, Anna, Christian Renn, Clemens Dobelmann, Vigneshwaran Namasivayam, Shanu Jain, Karolina Losenkova, Heikki Irjala, et al. 2019. “Structure-Activity Relationship of Purine and Pyrimidine Nucleotides as Ecto-5′-Nucleotidase (CD73) Inhibitors.” *J. Med. Chem.* 62: 3677–95.

Lawson, Kenneth V., Jaroslaw Kalisiak, Erick A. Lindsey, Eric T. Newcomb, Manmohan Reddy Leleti, Laurent Debien, Brandon R. Rosen, et al. 2020. “Discovery of AB680: A Potent and Selective Inhibitor of CD73.” *J.Med.Chem* 63: 11448–68. https://doi.org/10.1021/acs.jmedchem.0c00525.

Lee Sang-Yong, Vigneshwaran Namasivayam et. al. 2017. “Substrate-Dependence of Competitive Nucleotide Pyrophosphatase/Phosphodiesterase1 (NPP1) Inhibitors.” *Front. Pharmacol.* 1: 1–15. https://doi.org/10.3389/fphar.2017.00054.

Lee, Sang Yong, Amelie Fiene, Wenjin Li, Theodor Hanck, Konstantin A. Brylev, Vladimir E. Fedorov, Joanna Lecka, et al. 2015. “Polyoxometalates - Potent and Selective Ecto-Nucleotidase Inhibitors.” *Biochem. Pharmacol.* 93: 171–81.

Lee, Sang Yong, Xihuan Luo, Vigneshwaran Namasivayam, Jennifer Geiss, Salahuddin Mirza, Julie Pelletier, Holger Stephan, Jean Sévigny, and Christa E. Müller. 2018. “Development of a Selective and Highly Sensitive Fluorescence Assay for Nucleoside Triphosphate Diphosphohydrolase1 (NTPDase1, CD39).” *Analyst* 143: 5417–30.

Malacrida, Alessio, Mirko Rivara, Alessandro Di Domizio, Giacomo Cislaghi, Mariarosaria Miloso, Valentina Zuliani, and Gabriella Nicolini. 2020. “3D Proteome-Wide Scale Screening and Activity Evaluation of a New ALKBH5 Inhibitor in U87 Glioblastoma Cell Line.” *Bioorg. Med. Chem.* 28: 115300. https://doi.org/10.1016/j.bmc.2019.115300.

Marco Idzko1, Davide Ferrari2, and Holger K. Eltzschig. 2015. “Nucleotide Signalling during Inflammation.” *Nature* 509: 310–17.

McManus, Jessica, Timothy He, Julie Ann Gavigan, Ghislaine Marchand, Stephanie Vougier, Olivier Bedel, Paul Ferrari, et al. 2018. “A Robust Multiplex Mass Spectrometric Assay for Screening Small-Molecule Inhibitors of CD73 with Diverse Inhibition Modalities.” *SLAS Discovery* 23: 264–73.

Monteiro, Inês, Selena Vigano, Mohamed Faouzi, Isabelle Treilleux, Olivier Michielin, Christine Ménétrier-Caux, Christophe Caux, Pedro Romero, and Laurence de Leval. 2018. “CD73 Expression and Clinical Significance in Human Metastatic Melanoma.” *Oncotarget* 9: 26659–69.

Moreno, Estefanía, Júlia Canet, Eduard Gracia, Carme Lluís, Josefa Mallol, Enric I. Canela, Antoni Cortés, and Vicent Casadó. 2018. “Molecular Evidence of Adenosine Deaminase Linking Adenosine A2A Receptor and CD26 Proteins.” *Front. Pharmacol.* 9: 1–18.

Nadel, Yael, Joanna Lecka, Yocheved Gilad, Gal Ben-David, Daniel Förster, Georg Reiser, Sarah Kenigsberg, et al. 2014. “Highly Potent and Selective Ectonucleotide Pyrophosphatase/ Phosphodiesterase i Inhibitors Based on an Adenosine 5′-(α or γ)-Thio-(α,β- or β,γ)-Methylenetriphosphate Scaffold.” *J.Med.Chem* 57: 4677–91. https://doi.org/10.1021/jm500196c.

Narravula, S, P F Lennon, B U Mueller, and S P Colgan. 2000. “Regulation of Endothelial CD73 by Adenosine: Paracrine Pathway for Enhanced Endothelial Barrier Function.” *J Immunol* 165: 5262–68.

Nassir, Molhm, Salahuddin Mirza, Uri Arad, Sangyong Lee, Muhammad Rafehi, Isaac Yaw Attah, Christian Renn, et al. 2019. “Adenine-(Methoxy)-Ethoxy-Pα,α-Dithio-Triphosphate Inhibits Pathologic Calcium Pyrophosphate Deposition in Osteoarthritic Human Chondrocytes.” *Org. Biomol. Chem.* 17: 9913–23.

Newby, A. C., J. P. Luzio, and C. N. Hales. 1975. “The Properties and Extracellular Location of 5’ Nucleotidase of the Rat Fat Cell Plasma Membrane.” *Biochem. J.* 146: 625–33.

Randall, Rose J, and A Lewis. 1951. “Protein Measurement with the Folin Phenol Reagent.” *J. Biol. Chem.* 193: 265–75.

Sachsenmeier, Kris F., Carl Hay, Erin Brand, Lori Clarke, Kim Rosenthal, Sandrine Guillard, Steven Rust, Ralph Minter, and Robert Hollingsworth. 2012. “Development of a Novel Ectonucleotidase Assay Suitable for High-Throughput Screening.” *J. Biomol. Screening* 17: 993–98.

Sek, Kevin, Christina Mølck, Gregory D. Stewart, Lev Kats, Phillip K. Darcy, and Paul A. Beavis. 2018. “Targeting Adenosine Receptor Signaling in Cancer Immunotherapy.” *Int. J. Mol. Sci.* 19: 1–29.

Stagg, J., U. Divisekera, N. McLaughlin, J. Sharkey, S. Pommey, D. Denoyer, K. M. Dwyer, and M. J. Smyth. 2010. “Anti-CD73 Antibody Therapy Inhibits Breast Tumor Growth and Metastasis.” *Proc. Natl. Acad. Sci.* 107: 1547–52.

Synnestvedt, Kristin, Glenn T. Furuta, Katrina M. Comerford, Nancy Louis, Jorn Karhausen, Holger K. Eltzschig, Karl R. Hansen, Linda F. Thompson, and Sean P. Colgan. 2002. “Ecto-5′-Nucleotidase (CD73) Regulation by Hypoxia-Inducible Factor-1 Mediates Permeability Changes in Intestinal Epithelia.” *J Clin Invest.* 110: 993–1002.

Taverniers, Isabel, Marc De Loose, and Erik Van Bockstaele. 2004. “Trends in Quality in the Analytical Laboratory. II. Analytical Method Validation and Quality Assurance.” *TrAC, Trends Anal. Chem.* 23: 535–52.

Xu, Shuo, Qian Qian Shao, Jin Tang Sun, Ning Yang, Qi Xie, Dong Hai Wang, Qi Bing Huang, et al. 2013. “Synergy between the Ectoenzymes CD39 and CD73 Contributes to Adenosinergic Immunosuppression in Human Malignant Gliomas.” *Neurooncology* 15: 1160–72.

Yegutkin, Gennady G., Bé Wieringa, Simon C. Robson, and Sirpa Jalkanen. 2012. “Metabolism of Circulating ADP in the Bloodstream Is Mediated via Integrated Actions of Soluble Adenylate Kinase-1 and NTPDase1/CD39 Activities.” *FASEB J.* 26: 3875–83.

Yung-Chi, Cheng, and William H. Prusoff. 1973. “Relationship between the Inhibition Constant (KI) and the Concentration of Inhibitor Which Causes 50 per Cent Inhibition (I50) of an Enzymatic Reaction.” *Biochem. Pharmacol.* 22: 3099–3108.

Zelikman, Vadim, Julie Pelletier, Luba Simhaev, Aviad Sela, Fernand Pierre Gendron, Guillaume Arguin, Hanoch Senderowitz, Jean Sévigny, and Bilha Fischer. 2018. “Highly Selective and Potent Ectonucleotide Pyrophosphatase-1 (NPP1) Inhibitors Based on Uridine 5′-P α,α -Dithiophosphate Analogues.” *J. Med. Chem.* 61: 3939–51. https://doi.org/10.1021/acs.jmedchem.7b01906.

Zhang, Chung, and Oldenburg. 1999. “A Simple Statistical Parameter for Use in Evaluation and Validation of High Throughput Screening Assays.” *J. Biomol. Screening*.

Zhang, Jiajia, Jiajia Dai, Qingxuan Zheng, Shuju Guo, Yanyan Yu, Wenpeng Hu, Yanan Gao, and Dayong Shi. 2020. “The Fluoro-Thiazolylhydrazone Compound TSC-3C Inhibits Triple Negative Breast Cancer (TNBC) Cell Line Activity by Promoting Apoptosis, Regulating the Mapk Pathway and Inducing Mitochondrial Dysfunction.” *Int. J. Mol. Sci.* 21: 1–15.

Zhang, Jin, Carmen Corciulo, Hailing Liu, Tuere Wilder, Mayumi Ito, and Bruce Cronstein. 2017. “Adenosine A2a Receptor Blockade Diminishes Wnt/β-Catenin Signaling in a Murine Model of Bleomycin-Induced Dermal Fibrosis.” *Am. J. Pathol.* 187: 1935–44. http://dx.doi.org/10.1016/j.ajpath.2017.05.005.

Zhou, Ping, Xiuling Zhi, Tingting Zhou, Sifeng Chen, Xiaobo Li, Li Wang, Lianhua Yin, Zhimin Shao, and Zhouluo Ou. 2007. “Overexpression of Ecto-5′-Nucleotidase (CD73) Promotes T-47D Human Breast Cancer Cells Invasion and Adhesion to Extracellular Matrix.” *Cancer Biol. Ther.* 6: 426–31.

Zimmermann, Herbert. 2020. “History of Ectonucleotidases and Their Role in Purinergic Signaling.” *Biochem. Pharmacol.*, 114322. https://doi.org/10.1016/j.bcp.2020.114322.

Zimmermann, Herbert, Matthias Zebisch, and Norbert Sträter. 2012. “Cellular Function and Molecular Structure of Ecto-Nucleotidases.” *Purinergic Signal.* 8: 437–502.

pAcGP67B-sCD73

MLLVNQSHQGFNKEHTSKMVSAIVLYVLLAAAAHSAF**AADLGS**WELTILHTNDVHSRLEQTSED
SSKCVNASRCMGGVARLFTKVQQIRRAEPNVLLLDAGDQYQGTIWFTVYKGAEVAHFMNALRY
DAMALGNHEFDNGVEGLIEPLLKEAKFPILSANIKAKGPLASQISGLYLPYKVLPVGDEVVGIVGY
TSKETPFLSNPGTNLVFEDEITALQPEVDKLKTLNVNKIIALGHSGFEMDKLIAQKVRGVDVVVG
GHSNTFLYTGNPPSKEVPAGKYPFIVTSDDGRKVPVVQAYAFGKYLGYLKIEFDERGNVISSHG
NPILLNSSIPEDPSIKADINKWRIKLDNYSTQELGKTIVYLDGSSQSCRFRECNMGNLICDAMINN
NLRHADEMFWNHVSMCILNGGGIRSPIDERNNGTITWENLAAVLPFGGTFDLVQLKGSTLKKAF
EHSVHRYGQSTGEFLQVGGIHVVYDLSRKPGDRVVKLDVLCTKCRVPSYDPLKMDEVYKVILP
NFLANGGDGFQMIKDELLRHDSGDQDINVVSTYISKMKVIYPAVEGRIKF**GGS***HHHHHH*

Theoretical molecular weight is 63.446 kDa with and 59.366 kDa without secretion signal.
Legend: underline: secretion signal (cleaved after bolt A); italic: His-Tag; bolt: Connecting amino acids/thrombin cleavage site (LVPRGS); grey background: CD73

Chapter 3

Development and Application of a Fluorescence-based Assay for Nucleotide Pyrophosphatase/phosphodiesterases (NPPs)

Salahuddin Mirza[a], Nader Boshta, Maria Karpouchtsi, Ahmed Temirak, Victoria Johanna Vaaßen, Tobias Claff, Sangyong Lee and Christa E. Müller*[,a]

[a] *Pharma Center Bonn, Pharmaceutical Institute, Pharmaceutical Chemistry I, University of Bonn, An der Immenburg 4, D-53121 Bonn, Germany*

Running title: **Fluorescence-based NPP assay**

*Address correspondence to:

Prof. Dr. Christa Müller

Pharmazeutisches Institut, Pharmazeutische Chemie I

An der Immenburg 4, D-53121 Bonn, Germany

Phone: +49-228-73-2301

Fax: +49-228-73-2567

E-Mail: christa.mueller@uni-bonn.de

Summary

Nucleotide pyrophosphatase/phosphodiesterases (NPPs) are surface-located glycoproteins that hydrolyse extracellular nucleotides, yielding nucleoside monophosphates, mainly AMP, subsequently hydrolysed, e.g. by ecto-5'-nucleotidase (CD73) yielding adenosine. This hydrolysis transforms the pro-inflammatory into an anti-inflammatory tumour microenvironment. This study investigated the kinetic parameters for soluble human NPP3 vs. 23 nucleotide substrates. The primary substrates were nicotinamide adenine dinucleotide (NAD^+), adenosine diphosphate ribose (ADPR), nicotinic acid adenine dinucleotide ($NAAD^+$), diadenine tetraphosphate (Ap_4A). We developed and validated an efficient, robust, and sensitive high-throughput screening (HTS) assay by using the fluorescent substrates Ɛ-NAD^+, Ɛ -ADPR, and Ɛ-Ap_4Ɛ-A, which showed comparable kinetic parameters as their natural analogues NAD^+, ADPR, and Ap_4A. Assays were optimised for living cells utilising various cancer cell lines. The fluorescent assays developed in this study offer high sensitivity, robustness, and applicability. Our data suggests that NPP3 hydrolyses dinucleotides, e.g. NAD^+, NAAD, Ap_4A, and Ap_3A, better than triphosphates ATP, GTP, CTP, and UTP. Small-scale structure-activity relationship (SAR) studies were conducted for NPP3-selective *p*-aminobenzenesulfonamide derivatives. The core skeleton was replaced from phthalazine with isoquinoline and naphthalene. The new compound PZB08720015A bearing isoquinoline core showed comparatively better potency in inhibiting NPP3 activity with a K_i value of 0.322 ± 0.0014 µM under physiological pH conditions. We further identified a small molecule scaffold 4-((1*H*-indazol-3-yl)amino)benzenesulfonamide (NBO-MKA-29) that showed better solubility and comparable potency to PZB08720015A under both physiological and alkaline pH.

NPPs are metalloenzymes that need two Zn^{2+} ions for optimum activity. Sulfonamide moiety is, therefore, essential for binding with Zn^{2+} ions located in the active site of NPP3. Under alkaline reaction conditions, sulfonamide functionality shows better inhibition of the enzyme activity. However, changing reaction conditions to physiological pH led to a significant reduction of inhibitory potency. The newly synthesised compounds were tested in parallel at a pH of 7.4 and 9.0. For the most potent inhibitors, selectivity studies were performed on ectonucleotidases CD38, -39, -73, and NPP1 that showed this scaffold is

relatively selective for NPP3; however, some inhibitory activity was observed for NPP1, particularly NBO-NKA-29, In conclusion, we studied a comprehensive range of substrates hydrolysed by human NPP3 and developed HTS assays using multiple fluorescent substrates ε-NAD^+, ε-ADPR, εAp_4ε-A. These assays are suitable for monitoring NPPs' activity on living cancer cell lines. Our SAR studies resulted in the identification of potent and selective NPP3 inhibitors under physiological reaction conditions.

Keywords: Ecto-nucleotidases / NPPs/ enzyme kinetics/ HTS fluorescence assay / ε-NAD^+ / ε-ADPR/ ε-Ap_4ε-A/ Capillary electrophoresis/ indazol derivatives/ *p*-aminobenzene-sulfonamide derivatives

1.0 Introduction

1.1. Extracellular nucleotides trigger immune responses

Extracellular nucleotides act as modulators of immune responses that trigger numerous signalling mechanisms. Adenosine 5'-tri- and di-phosphate (ATP/ADP), nicotinamide adenine dinucleotide (NAD^+), adenosine diphosphate ribose (ADPR), and diadenosine polyphosphates (Ap_3A, Ap_4A) display pro-inflammatory functions (Zimmermann, 2020). The extracellular concentration of these nucleotides increases in inflamed tissues either through the activation of membrane-bound channels, e.g. connexin-43/pannexin, via vesicular transport or due to cellular necrosis. Increased nucleotide concentrations in the extracellular fluid provide a pro-inflammatory environment by activating purinergic receptors, P2X and P2Y. However, cancer cells express different surface-located ectoenzymes called ectonucleotidases, which sequentially hydrolyse these nucleotides to anti-inflammatory adenosine, activating P1 receptors and abolishing immune cell recruitment. Adenosine promotes cancer growth and metastasis (Dosch et al., 2018; Holger et al., 2012; Idzko, 2015; Song et al., 2011).

1.2. Ectonucleotidases

Expressed on the surface of many immune and cancer cells, ectonucleotidases control nucleotide- and nucleoside-(adenosine)-based activation of purinergic receptors. Ectonucleotidases are attached to the plasma membrane either through transmembrane spanning domains (two for NTPDases or one for NPPs and CD38) or by GPI-anchor (CD73, CD157 and APs) with their active sites in the extracellular environment. These enzymes cooperatively hydrolyse extracellular nucleotides (e.g. ATP/NAD^+) and generate the respective nucleosides (e.g. adenosine) as well as inorganic phosphates and pyrophosphates (P_i/PP_i). The five prominent ectonucleotidase families are ecto-nucleoside triphosphate diphosphohydrolases (E-NTPDases, EC 3.6.1.5), NAD^+ glycohydrolases (CD38/CD157, EC 3.2.2.5), ecto-nucleotide pyrophosphatase/ phosphodiesterases (E-NPPs, EC 3.6.1.9, EC 3.1.4.1), alkaline phosphatases (APs, EC 3.1.3.1) and ecto-5'-nucleotidases (eN, EC 3.1.3.5). Substrate-specificity and tissue distribution usually overlap, and multiple enzymes are expressed simultaneously in close locations. These enzymes work in tandem to convert nucleotides to their respective

nucleosides. E.NTPDases usually prefer hydrolysing tri- and di-phosphates of adenosine and uridine, yielding the respective monophosphates. Adenosine monophosphate is the dominant product, hydrolysed by CD73 to adenosine. APs are further divided into four subtypes capable of hydrolysing ATP to adenosine. CD38, on the other hand, prefers NAD^+ and hydrolyses it mainly to ADPR. cADPR is the main product of CD157-based reactions. cADPR is internalised to show its second messenger function in intracellular Ca^{2+} release. CD38 can also hydrolyse nicotinamide mononucleotide (NMN), a product of NPP-based NAD^+, to ribose-5'-phosphate (Liu et al., 2008).

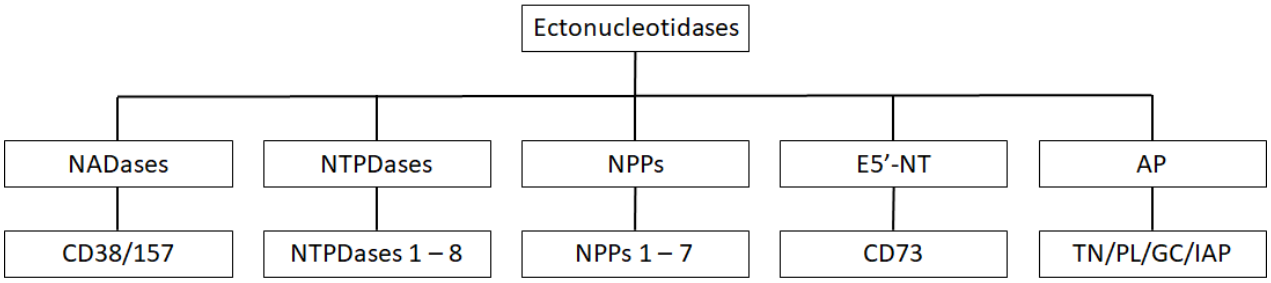

Figure 3.1: Classification of ectonucleotidases

1.3. Ecto-nucleotide pyrophosphatase/phosphodiesterases (NPPs)

NPPs are ectoenzymes subdivided into seven subtypes (NPP1 – 7) based on their discovery order (Borza et al., 2022). This enzyme's family members exhibit varying preferences for substrates despite having a similar catalytic site, the phosphodiesterase (PDE) domain, and a consistent arrangement of amino acids around two zinc ions. However, the active site of NPP5 contains three Zn^{2+} ions instead of characteristic two Zn^{2+}. NPP1–3 are multidomain enzymes in which the PDE domain is linked with a C-terminal inactive nuclease domain (NUC) to stabilise the enzymatic activity. The N-terminus contains Somatomedin B-like domains (SMB1, SMB2). On the other hand, NPP4–7 only possesses the PDE domain. NPP1, 3, 4, 5, and 7 are mainly transmembrane proteins. However, NPP2 is a secreted protein, while NPP6 is GPI-anchored. Only NPP1, -3, -4, and -5 are nucleotide hydrolysers and will be discussed here. The other NPPs subfamilies, although involved in different pathological conditions; however, due to different substrate preference and more intracellular localisation, they are not included in this dissertation.

a. Preferable substrates of NPPs

NPPs belong to a superfamily of alkaline phosphatases that show great diversity in substrate hydrolysis. NPP1, -3, -4 and -5 are mainly nucleotide hydrolysing enzymes, whereas NPP2, -6, and -7 prefer phospholipids. NPP1 hydrolyses extracellular ATP and diadenosine polyphosphate (Ap_4A) to AMP and pyrophosphate (*PPi*), a potent inhibitor of vascular calcification and bone mineralisation (Hessle et al., 2002; Bellosta et al., 2011). Besides this, it can hydrolyse cyclic nucleotides like c-AMP and 2',3'-cGAMP, which illustrates its role in the STING mechanism. The autotaxin NPP2 generates bioactive lysophosphatidic acid (LPA) from lysophosphatidylcholine or sphingomyelin as substrates and promotes cancer progression (Federico et al., 2016; Knowlden & Georas, 2014; Yang et al., 2002). NPP3 shares a similar substrate preference as NPP1 by potently hydrolysing nicotinamide adenine dinucleotide NAD^+, adenosine diphosphate ribose (ADPR), ATP, and Ap_nA. However, it has not yet been reported whether NPP3 can hydrolyse cyclic nucleotides like cAMP and 2',3'-cGAMP. NPP4 effectively hydrolyses Ap_3A and Ap_4A and was reported to influence platelet aggregation at the site of vascular injury (Albright et al., 2012). The broad expression of NPP5 in rat brains and its preference for NAD^+ suggests that NPP5 may be involved in neurodegenerative diseases (Cortelazzo et al., 2016; Gorelik, Randriamihaja, et al., 2017). Both NPP6 and NPP7 are alkaline sphingomyelinases that preferably hydrolyse dietary sphingomyelin in the presence of bile salts, nucleoside phosphates, and phospholipids (Gorelik, Liu, et al., 2017). Two nucleotide-hydrolysing pathways are reported: canonical (CD39/73) and non-canonical (CD38/NPPs/CD73). The former path prefers tri- and diphosphates of adenosine and uridine for hydrolysis, and the latter prefers substrates like NAD^+, ADPR, AP_nA, and ATP to produce immunosuppressive adenosine finally (Horenstein et al., 2013; Morandi et al., 2018). Unsurprisingly, certain tumour cell lines may possess both pathways to ensure a consistently high adenosine level (Antonioli et al., 2013, 2019; Haskó et al., 2008). Once produced, adenosine can either be transported into the cells via nucleoside transporters or converted to inosine by adenosine deaminases. However, more importantly, it activates adenosine receptors (A_1, A_{2A}, A_{2B}, and A_3) coupled with downstream signalling pathways, leading to intense immunosuppression in many disease conditions. Therefore inhibitors of these enzymes are important for these pathologies.

b. Tissue distribution and biological functions of NPPs

NPPs, particularly NPP1 and -3, show wide tissue distribution, which reflects their biological importance. They are expressed, e.g. on osteoblasts, epithelial surfaces, e.g. of the airways, liver, kidney, and intestinal epithelia (Borza et al., 2022; Zimmermann et al., 2012). NPP1 influences bone and soft-tissue mineralisation through the production of *PPi*. Moreover, NPP1 is a negative regulator of the cGAS-STING pathway of the innate immune system because of the hydrolysis of 2′,3′-cGAMP. Thus, recent studies link NPP1 to reduced immune cell infiltration and cancer (Onyedibe et al., 2019). The enzyme is reported to modulate glucose homeostasis and the advancement of diabetes (Dong et al., 2005). It is also widely reported in different cancer cell lines, such as the glioblastoma cell lines U87 (Stella et al., 2010). NPP2 is structurally related to NPP1; however, it has different substrate specificity, and its catalytic activity is observed in various biological fluids, including serum and cerebrospinal fluid. Lysophosphatidic acid (LPA) is produced to stimulate cell proliferation and migration. It is further associated with neurodegenerative diseases, neuropathic pain, cerebral ischemia, brain or spinal cord injury, as well as oncogenesis and cancer progression (Birgbauer, 2021; Federico et al., 2016; Yung et al., 2015).

NPP3 is overexpressed on activated basophil and mast cells (BP/MC) and often acts as an indicator for the activation of these cells. Where it hydrolyses nucleotides in the extracellular space (Tsai et al., 2015). Reports suggest high enzyme expression on the epithelial lining of the small intestine and renal tubules. Here, they are assumed to hydrolyse dietary nucleotides, causing immunomodulation (Colonna et al., 2004; Furuta et al., 2017; Stefan et al., 2005, 2006). NPP3 is involved in the hydrolysis of sugar donors such as UDP-glucose, UDP-galactose, and UDP-N-acetylglucosamine to monophosphate (UMP), a potent inhibitor of glycosyltransferases with low inhibitory potency (K_i) suggesting the enzyme's influence on cellular glycosylation (Korekane et al., 2013). Some report its overexpression in bile duct carcinoma and Walker 256 mammary cancer cells, in solid tumours and colorectal cancers (Buffon et al., 2010; Gõmez-Villafuertes, 2014; Yano et al., 2004). Despite these reports, the pathological role of NPP3 is less investigated, particularly concerning tumours.

NPP4 is another member of this family that was poorly investigated. The enzyme is predominantly expressed in endothelial cells lining the interior surface of blood vessels that perform vascular function. Moreover, the expression on platelets suggests a hemostatic and thrombotic role. Upon hydrolysis of AP_3A, the formed ADP activates P2Y purinergic receptors, promoting calcium-mediated platelet aggregation (Albright et al., 2012, 2014). The subtype NPP5 is among the least characterised NPP family members. It shows high expression in the epididymis and has a possible role in NAD-based neurotransmission in the brain (Gorelik, Randriamihaja, et al., 2017). NPP6, functioning as a lysophospholipase C and being choline-specific, was revealed to regulate choline metabolism, e.g. in fatty liver disease. Finally, NPP7 is involved in lipid metabolism, too, as it possesses alkaline sphingomyelinase activity. It is highly expressed in the intestine, where it digests dietary sphingomyelin, as well as on hepatocytes, and has been associated with hepatobiliary diseases along with colon tumorigenesis (Borza et al., 2022). Table 3.1 summarises the different NPP subtypes and their expression and pathophysiological functions.

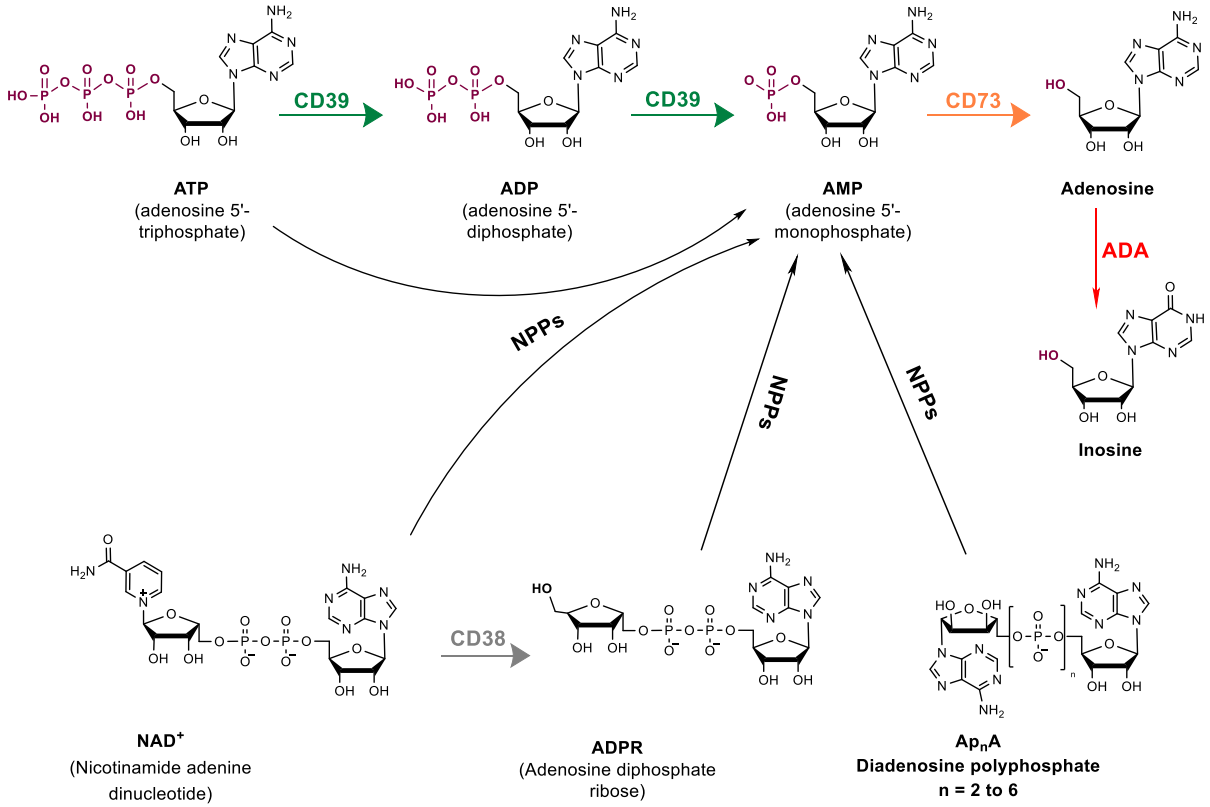

Figure 3.2: Hydrolysis of diverse substrates by ectonucleotidases. CD39 hydrolyses ATP to ADP and then AMP. APs cleave off one phosphate group after the other of ATP, yielding adenosine. The alternate

pathway comprising CD38 and NPPs utilises NAD^+, ADPR, ATP, and Ap_nA to produce AMP. AMP is converted to adenosine by CD73.

Table 3.1: Human NPPs, their cellular distribution, and pathophysiology

Subtype	Gene	Cellular dist.	Substrates	Pathological function
NPP1 (CD203a, PC-1)	*ENPP1*	fibroblasts, hepatocytes, osteoblasts, epithelial surfaces of lung, liver, kidney, and intestine B-cells and T-cells	ATP, Ap_nA, 2',3'-cGAMP, ADPR, cAMP, NAD^+	Bone and soft-tissue mineralisation, inflammation, tumorigenesis
NPP2 (Autotaxin, PD-1α)	*ENPP2*	Extracellular fluids, brain	Lysophosphotidyl-choline, nucleotides	Lipid metabolism, chemotaxis, neurodegenerative diseases
NPP3 (CD203c, PD-1β)	*ENPP3*	Basophil, mast cells epithelial surfaces of the lung, liver, kidney, and intestine, hepatocytes, osteoblasts	ADPR, NAD^+, Ap_nA, UTP, CTP, ATP, UDP-glucose	Inflammation, allergic response, tumorigenesis
NPP4	*ENPP4*	Brain, vascular endothelium	Ap_nA, NAD^+,	Thrombotic disorders
NPP5	*ENPP5*	Epididymis	NAD^+, ADPR	Neurotransmission
NPP6	*ENPP6*	Brain, kidney	Glycerophosphocholine	Lipid metabolism, choline metabolism disorders
NPP7	*ENPP7*	Intestine, liver	Sphingomyelin	Lipid metabolism, tumorigenesis

1.4. Small molecule inhibitors of NPP

This section will mainly focus on nucleotide-hydrolyzing NPPs such as NPP1, -3, -4 and -5. Most currently reported inhibitors target NPP1 or NPP3; only a single NPP4 inhibitor is reported.

i. NPP1 inhibitors

NPP1 is the best-investigated enzyme of this family, and several efforts have been made to discover potent and selective inhibitors. Different scaffolds belonging to nucleotidic and non-nucleotidic structures were investigated for this purpose. These efforts were fruitful, and high potency with the competitive mode of inhibition has already been achieved. Our research group has previously published a comprehensive review paper on NPP1 inhibitors, summarising both nucleotide and non-nucleotide scaffolds (Lee & Müller, 2017). Therefore, our focus will only be on the compounds published in recent years.

a. Nucleotidic scaffolds

Nucleotidic scaffolds were investigated to design competitive inhibitors by altering the substrate structures; therefore, more or less the same binding interactions are involved. Initial attempts were made by probing the β-γ-substituted ATP analogue (ARL67156). The compound appeared to be a weak competitive inhibitor of NPP1 activity with K_i of 12 µM using the artificial substrate *p*-NPh-5'-TMP under mild alkaline reaction conditions (pH 8.5). A direct comparison of ATP and ARL-67156's ability to inhibit the hydrolysis of *p*-NPh-5'-TMP revealed that 100 µM of ATP inhibits enzyme activity slightly better than the same concentration of ARL-67156 (Lévesque et al., 2007). This means that the inhibitor was not so active towards NPP1. Search for potent nucleotidic scaffolds for NPP1 continued, and different research groups (mainly Prof. Bilha Fischer) have further evaluated several non-hydrolysable nucleotide analogues belonging to adenosine and uridine base skeletons. Highly potent molecules were reported, which achieved K_i as low as 20 nM (Lecka, 2013; Nadel et al., 2014). Nucleotidic scaffolds mainly operate in a competitive mode of inhibition (MOI), although some molecules showed mixed inhibition models, which were primarily non-competitive. Moreover, despite showing excellent selectivity for the target enzymes, these compounds are subject to metabolism by different enzymes, including nucleases, kinases, phosphatases, and esterases. This leads to the breakdown of molecules into smaller fragments, which may lose their inhibitory potential and become inactive towards the target enzyme. This metabolic instability can lead to rapid clearance of the inhibitors from the systemic circulation, requiring frequent and higher dosages to maintain therapeutic efficacy and an increased risk of adverse effects. Other ectonucleotidases such as NTPDases, APs, and CD73 can sometimes attack ATP-, ADP-, or AMP-based scaffolds. This instability can significantly affect the pharmacokinetics profile and efficacy of these inhibitors as therapeutic agents; therefore, structural modifications could be made to protect vulnerable sites of the enzyme attack. Structural alterations on the nucleotidic scaffolds have already shown promising results, such as in the case of the CD73 enzyme. Efforts with human CD39 are already in progress. NPPs should be investigated for complete SAR studies concerning nucleotidic scaffolds. However, despite these measures, comprehensive in-vivo metabolic studies are essential for understanding the metabolic fate of nucleotidic inhibitors. The characteristics of potent nucleotidic scaffolds are depicted in Table 3.2

Table 3.2: Characteristics of nucleotidic inhibitors of NPP1

Inhibitor	Substrate	Enzyme	pH Rx	K_i µM	MOI**	Ref
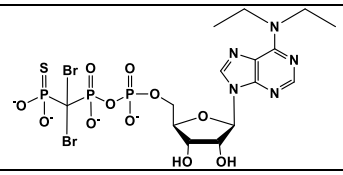	*p*-NPh-5'-TMP	MB-CL*	8.5	12 ± 3	Competitive	(Levesque et al., 2007)
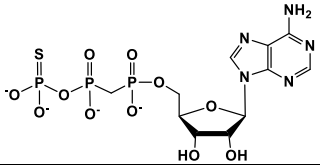	*p*-NPh-5'-TMP	MB-CL*	8.5	0.021 ± 0.001	Competitive	(Nadel et al., 2014)
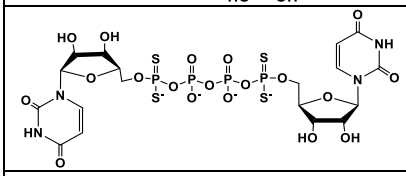	*p*-NPh-5'-TMP	MB-CL*	8.5	0.027 ± 0.009	ND#	(Zelikman et al., 2018)
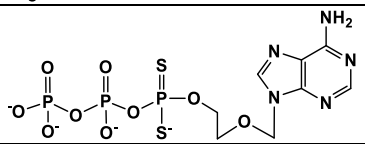	*p*-NPh-5'-TMP ATP	Rec. soluble NPP1	9.2 9.2	0.645± 0.051 2.49 ± 0.07	Mixed inhibition mode	(Nassir, Mirza, et al., 2019)
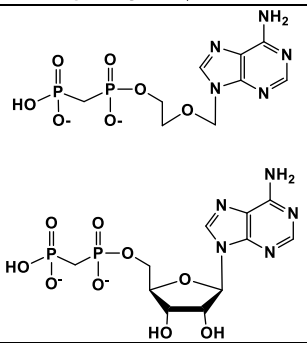	*p*-NPh-5'-TMP ATP	Rec. soluble NPP1	9.2 9.2	16.3 ± 2.5 9.60 ± 2.84	Non-competitive	(Nassir, Arad, et al., 2019)
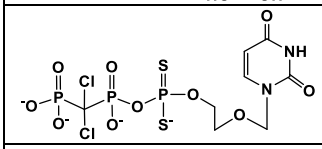	*p*-NPh-5'-TMP	MB-CL*	8.5	0.73 ± 0.15	ND#	(Nassir, Pelletier, et al., 2019)
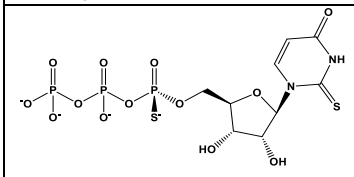	*p*-NPh-5'-TMP ATP	Rec. soluble NPP1	7.4	0.226 ± 0.091 0.109 ± 0.002	Competitive	(Zhang et al., 2024)

*Membrane bound-cell lysate #Not defined **Mechanism of inhibition

b. Non-nucleotidic scaffolds

Besides nucleotidic scaffolds, several non-nucleotidic inhibitors were previously reported, which showed tremendous potential as small molecule inhibitors for the target enzyme. Different research groups have achieved inhibitors with potency as low as the low

nanomolar range. Non-nucleotidic inhibitors are often preferred over nucleotide-based inhibitors due to their improved selectivity, reduced off-target effects, and better pharmacokinetics; however, compound solubility in the reaction buffers is sometimes not optimum, which could lead to inconsistent inhibitory activity. This characteristic could impact their bioavailability and, ultimately, their efficacy. Different approaches have been adapted to improve the solubility of the compounds and protection from gastric enzymes, e.g., synthesis as a Pro-drug or structural modifications such as incorporating more polar functional groups, halogen, or amino groups. Some potent non-nucleotidic NPP1 inhibitors are depicted in Table 3.3.

Table 3.3: Characteristics of non-nucleotidic NPP1 inhibitors

Inhibitor	Substrate	Enzyme	pH Rx	IC_{50} µM	MOI**	Ref
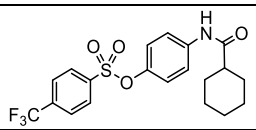	*p*-NPh-5'-TMP	MB-CL*	9.5	0.387 ± 0.007	ND#	(Semreen et al., 2019)
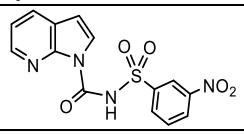	*p*-NPh-5'-TMP	MB-CL*	9.5	0.80 ± 0.04	Uncompetitive	(Ullah et al., 2021)
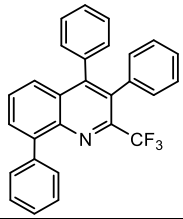	*p*-NPh-5'-TMP	MB-CL*	9.5	0.18±0.09	ND#	(Kuhrt et al., 2017)
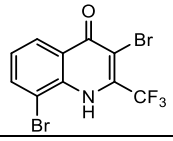	*p*-NPh-5'-TMP	MB-CL*	9.5	0.631±0.031	ND#	(Kuhrt et al., 2017)
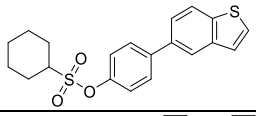	*p*-NPh-5'-TMP	MB-CL*	9.5	0.12 ± 0.02	Competitive	(Anbar et al., 2020)
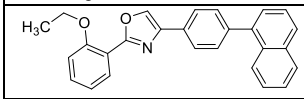	*p*-NPh-5'-TMP	MB-CL*	9.5	0.15 ± 0.01	ND#	(Ahmad et al., 2020)
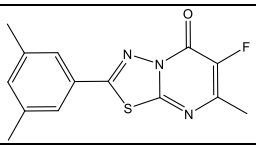	*p*-NPh-5'-TMP	MB-CL*	9.5	0.31± 0.01	competitive	(Jafari et al., 2016)
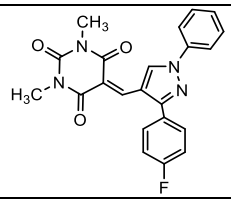	*p*-NPh-5'-TMP	MB-CL*	9.5	0.61 ± 0.05	competitive	(Andleeb et al., 2019)

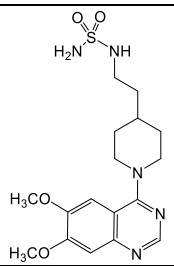	*p*-NPh-5'-TMP	MB-CL*	8.5	0.059±0.005 (K_i)	Non-competitive	(Shayhidin, 2015)
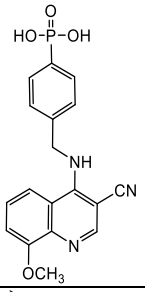	cGAMP	Mouse NPP1	7.4	< 0.002 (K_i)	competitive	(Carozza et al., 2020)
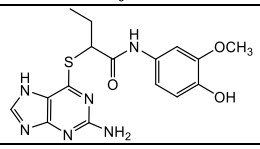	*p*-NPh-5'-TMP cGAMP	Human NPP1	9.2 9.5	0.041 (K_i) 0.002 (K_i)	ND#	(Gangar et al., 2022)
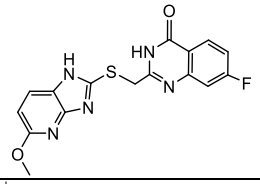	*p*-NPh-5'-TMP	Rec. NPP1	9.0	0.188	ND#	(Wang et al., 2022)
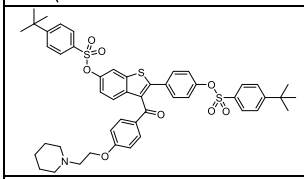	*p*-NPh-5'-TMP	MB-CL*	9.5	0.29 ±0.02	ND#	(El-gamal et al., 2019)
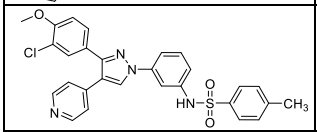	*p*-NPh-5'-TMP	MB-CL*	9.5	0.18 ± 0.01	ND#	(Ullah et al., 2020)
Sulfopolysaccharides Delesseria Sanguinea	*p*-NPh-5'-TMP	Rec. *h.*NPP1	9.0	0.0000517 (K_i)	Non-competitive	(Lopez et al., 2021)

*Membrane bound-cell lysate #Not defined **Mechanism of inhibition

ii. NPP3 inhibitors

Despite sharing up to 50 % identical sequence, standard structural features, and preferable substrates for hydrolysis, both NPP1 and -3 are different regarding nucleotidic inhibitors. ATP-based scaffolds are reported as potent inhibitors of NPP1, though not so impressive against NPP3, and only minor inhibition is observed at higher concentrations (Lévesque et al., 2007; Zimmermann et al., 2012). Our experience showed that monophosphates are a good starting point for studying NPP3 inhibition by nucleotidic scaffolds. No nucleotidic NPP3 inhibitors have been reported yet; therefore, for NPP3,

only the non-nucleotidic scaffolds are summarised in Table 3.4. Some of the scaffolds reported by Prof. Iqbal's group were also active towards NPP1 and NPP2. However, only those compounds that showed significantly better inhibitory potency towards NPP3 were selected.

Table 3.4: Non-nucleotidic NPP3 inhibitors

Inhibitor	Substrate	Enzyme	pH Rx	IC_{50} µM	MOI**	Ref
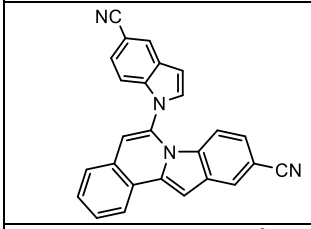	*p*-NPh-5'-TMP	MB-CL*	9.5	0.48 ± 0.01	Competitive	(Ausekle et al., 2016)
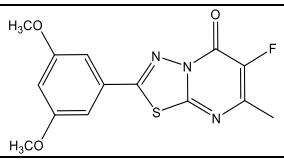	*p*-NPh-5'-TMP	MB-CL*	9.5	0.92 ± 0.02	Competitive	(Jafari et al., 2016)
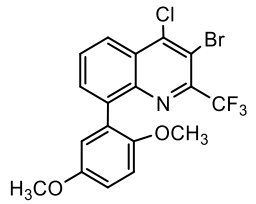	*p*-NPh-5'-TMP	MB-CL*	9.5	0.36±0.04	ND#	(Kuhrt et al., 2017)
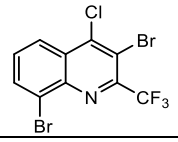	*p*-NPh-5'-TMP	MB-CL*	9.5	0.391±0.021	ND#	(Kuhrt et al., 2017)
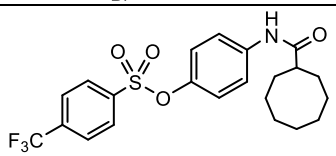	*p*-NPh-5'-TMP	MB-CL*	9.5	0.214 ± 0.012	ND#	(Semreen et al., 2019)
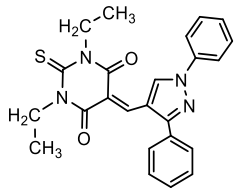	*p*-NPh-5'-TMP	MB-CL*	9.5	0.57 ± 0.01	Competitive	(Andleeb et al., 2019)
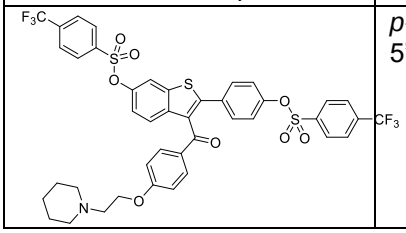	*p*-NPh-5'-TMP	MB-CL*	9.5	0.23 ±0.01	ND#	(El-gamal et al., 2019)

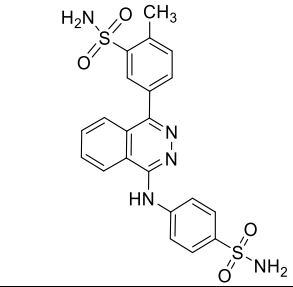	ATP	Rec.NPP3	9.2	0.053 ± 0.03 (K_i)	Competitive	(Lee et al., 2021)
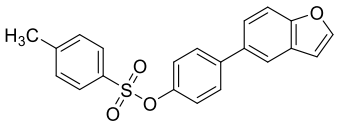	*p*-NPh-5'-TMP	MB-CL*	9.5	0.12 ± 0.01	Competitive	(Anbar et al., 2020)
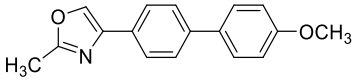	*p*-NPh-5'-TMP	MB-CL*	9.5	0.17 ± 0.01	ND*	(Ahmad et al., 2020)
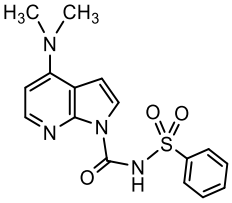	*p*-NPh-5'-TMP	MB-CL*	9.5	0.55 ± 0.01	Competitive	(Ullah et al., 2021)
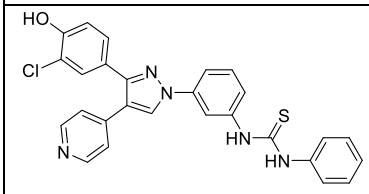	*p*-NPh-5'-TMP	MB-CL*	9.5	0.21 ± 0.01	N.D#	(Ullah et al., 2020)

*Membrane bound-cell lysate #Not defined **Mechanism of inhibition

iii. NPP4 inhibitors

NPP4 is poorly investigated for inhibitor analysis. The only reported compound is a polyoxometalate. During the selectivity testing of some AMP derivatives, we observed a few inhibitors that could hinder substrate hydrolysis by NPP4. The compound BCY-247 inhibited enzyme activity by >60% at 50 µM concentration under neutral pH conditions and in the presence of Zn^{2+} as a cofactor. Further assay details can be found in Chapter 6 of this dissertation.

Table 3.5: Reported NPP4 inhibitor

Inhibitor	**Substrate**	**Enzyme**	**pH Rx**	***IC*$_{50}$ µM**	**MOI****	**Ref**
$Na_6[H_2W_{12}O_{40}].21H_2O$	Ap_4A	Rec. h. NPP4	8.0	0.298 ± 0.052	Competitive	(Lopez et al., 2020)

**Mechanism of inhibition

IV. NPP5 inhibitors

NPP5 is currently the least investigated enzyme; the only information is about its substrate preference. The enzyme hydrolyses NAD^+, which could have a role in CNS pathology. Currently, no data comprising inhibition analysis of this enzyme is available. Our lab initiated an extensive HTS campaign against soluble NPP5 expressed and purified from an insect cell expression system. Moderately potent inhibitors were discovered; however, these results will not be part of this dissertation.

1.5 Assays for monitoring NPP reactions

p-Nitrophenyl 5'-thymidine monophosphate (*p*-Nph-5'-TMP) is often used as a synthetic substrate of NPPs, which allows colourimetric detection of its hydrolysis product *p*-nitrophenolate having intense yellow colour with λ_{max} at 405 nm (Laketa et al., 2010; Sakura et al., 1998). The assay is currently used as a standard for high-throughput screening (HTS) of inhibitor libraries against NPPs; however, the readout could be an issue when working with coloured compounds, e.g., plant pigments. Moreover, the substrate may allosterically modulate NPP1, and therefore, a significant difference in the potency of inhibitors was observed for using the natural substrate ATP as compared to the artificial substrate *p*-NPh-5'-TMP (Lee et al., 2017). The malachite green assay is another HTS assay utilising the natural substrate ATP (Baykov et al., 1988). The malachite green assay shares the same disadvantages as the *p*-NPh-5'-TMP assay, i.e., it is unsuitable for coloured compounds owing to the coloured molybdate. This malachite green dye is used to detect free phosphate liberated from ATP hydrolysis. NPP1 quickly hydrolyses ATP; however, slow hydrolysis is observed for other class members. To improve sensitivity and to overcome shortcomings of the malachite green assay for ATP hydrolysis, we recently developed a highly sensitive assay utilising ε-ATP assay. Although this assay is not affected by coloured compounds, it has another drawback: Low substrate hydrolysis is observed by NPP4 and 5, and therefore, this assay is mainly helpful for NPP1 and, to some extent, NPP3. Our research group previously published an HTS assay utilising Ap_4A as a substrate, where luminescence detects the formed ATP after hydrolysis (Lopez et al., 2020). However, this assay is not suitable for NPP1 and -3 since both enzymes further hydrolyse ATP to AMP. Moreover, while working with cancer cell lines where many enzymes work in tandem, NPP-specific substrates such as NAD^+, Ap_4A, and

ADPR may better predict the involvement of NPPs. With natural substrate, NPP-based reactions can be monitored using capillary electrophoresis or HPLC system coupled with a UV-detector. However, this assay is time-consuming and unsuitable for screening large compound libraries (Nassir, Mirza, et al., 2019). Isothermal titration calorimetry (ITC) is used by different research groups (Döhler et al., 2018). Like CE, the ITC assay can be used for most NPP substrates. However, the assay can also be time-consuming, and data reliability is sometimes poor. Kinetic parameters can be found in Table 3.6. All these assays were conducted under alkaline reaction conditions with pH values of 8.5 to 9.5, as we observed a high product turnover in this range.

Table 3.6: Kinetics parameters for NPPs applying different assay systems

Assays	Substrate	Detection mechanism	Subtype	K_m µM	Ref
Calorimetric	*p*-NPh-5'-TMP	*p*-nitrophenolate at λ405 nm	NPP1, 3	*NPP1* 222±44 20±4 *NPP3* 432±56 15±6	(Namasivayam et al., 2016) (Raza et al., 2011) (Lee et al., 2021)
	ATP ATP ADP GTP UTP CTP	Inorganic phosphate via MG# dye at 625 nm	NPP1 NPP3	ND* *NPP3* 61.5±6.5 74.7±6.8 123±6 120±10 120±26	(Lim et al., 2018) (Repen et al., 2012) (Gorelik, Randriamihaja, et al., 2017)
Luminescence	Ap_4A	ATP detection via firefly luciferase from *Photinus pyralis*	NPP4	*NPP4* 417 ± 25	(Lopez et al., 2020)
CE	ATP	UV detection of nucleotides at 254 nm	Suitable for all NPP isoenzymes	*NPP1* 6.27±1.5 *NPP3* 7.47±3.1	(Iqbal et al., 2008)
	p-NPh-5'-TMP			*NPP1* 281±25 *NPP3* 131±6	(Lee et al., 2012)
	UTP			*NPP1* 56.6 ± 9.9 *NPP1* 20.5 ± 3.1	(Namasivayam et al., 2016)
	Ap_4A			*NPP4* 220 ± 49	(Lopez et al., 2020)
Isothermal titration calorimetry	ATP GTP UTP CTP Ap_3A Ap_4A NAD^+	Measurement of heat evolved as a result of bond breakage	Suitable for all NPP isoenzymes	*NPP3* 44 ± 2 46.3 ± 0.5 44 ± 3 64 ± 17 31 ± 2 22.2 ± 0.1 163 ± 10	(Döhler et al., 2018)

ND* not determined # Malachite green

1.6. Aim of research

This research project aims to develop a sensitive HTS assay that could be used for different subtypes of NPPs. Previously, we have created an HTS assay for cancer cell lines overexpressing ATP, ADP, and AMP hydrolysing ectonucleotidases, such as CD39, NPP1, and CD73. A fluorescent modification of the adenine ring was made by introducing 1,N^6-etheno- bridge to the nucleotides ε-ATP, ε-ADP, and ε-AMP (Jackson et al., 2020). The main advantage of the ε-ATP assay is its HTS application using a 96-well plate format, robustness, and high sensitivity. The fluorescent analogue of nicotinamide adenine dinucleotide ε-NAD^+ is exclusively investigated for the reactions of NAD^+-consuming enzymes, including PARPs, CD38, and sirtuins (Blacher et al., 2015). The substrate possesses an intense intramolecular quenching effect because of ε-adenine and the nicotinamide group in the intact NAD^+ structure, leading to very low fluorescence intensity; however, quenching is disrupted by the enzymatic hydrolysis of the molecule, leading to approximately 10-fold increased fluorescence intensity of the product (Barrio et al., 1972). It was previously observed that apart from CD38, NPPs can hydrolyse NAD^+ very efficiently, thereby diminishing the internal quenching through the production of AMP. However, assay validation, enzyme kinetics, and inhibitor testing have not been performed. Therefore, we planned to investigate the fluorescent substrates of NPPs, including ε-NAD^+, ε-Ap_4-εA, and ε-ADPR, to study the possibility of using them as HTS substrates. Full-scale assay validation was performed by using ICH guidelines and standards. A small library of potential inhibitors was screened. The structures of substrates used in this study are presented in Figure 3.3. Furthermore, we screened a library of small-molecule inhibitors towards NPP3 using these newly developed assays. The compounds mainly belonged to the benzenesulfonamide scaffold that previously showed high potency (K_i 53.7 nM) and selectivity towards NPP3 under alkaline reaction conditions (Lee et al., 2021).

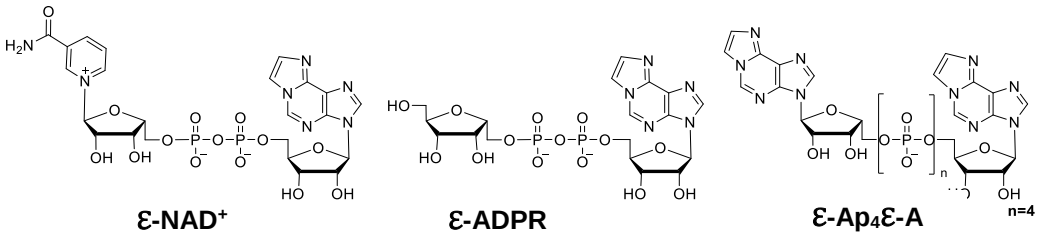

Figure 3.3: Structure of fluorescent nucleotides investigated in this study

2.0 Materials and Methods

a. *Substrates and chemicals*

Adenosine, adenosine 5'-mono, di- and tri-phosphate (AMP, ADP, ATP), adenosine diphosphate ribose (ADPR), Cytidine mono- and tri-phosphate (CMP, CTP), 2,3-Cyclic adenosine monophosphate (cAMP), Di-adenosine tri- and tetra-phosphate (Ap_3A, Ap_4A), guanidine mono-, di- and tri-phosphate (GMP, GDP, GTP), nicotinamide adenine dinucleotide (NAD^+) and its phosphate (NADP), nicotinic acid adenine dinucleotide (NAAD) and its phosphate analogue (NAADP), *p*-nitrophenyl 5'-thymidine monophosphate (*p*-Nph-5'-TMP) and *p*-nitrophenol (PNP), uridine 5'-di- and tri-phosphate (UDP, UTP), UDP-glucose (UDP-glu), UDP-galactose (UDP-GLC) were purchased from Sigma (Steinheim, Germany). Adenosine diphosphate ribose phosphate (ADPRP), 2,3 and 3,3 - cyclic guanine adenine monophosphate (2,3-cGAMP and 3,3-cGAMP), etheno-bridged NAD^+, ADPR, Ap_4A, AMP and adenosine (ε-NAD^+ and ε-ADPR, εAp_4-εA, ε-AMP, and ε-adenosine) were purchased from Biolog Life Sciences Institute, Bremen, Germany. Dimethyl sulfoxide (DMSO), disodium hydrogen phosphate (Na_2HPO_4), and sodium acetate (NaOAc) were obtained from Carl Roth (Karlsruhe, Germany). Chlorides of calcium, magnesium, and zinc ($CaCl_2$, $MgCl_2$, and $ZnCl_2$), Tris-HCl, 2-(cyclohexylamino) ethanesulfonic acid (CHES), lanthanum chloride heptahydrate ($LaCl_3$) Sigma–Aldrich (Steinheim, Germany). Proteins were expressed in-house using an insect cell expression system. cDNA of human NPP1 (NM_006208) NPP3, (NM_005021, CAT#: RC224818), and NPP5 (NM_021572) were purchased from Origene Technologies, USA. Restriction enzymes, T4 DNA ligase, and Q5 HF-DNA polymerase were purchased from New England BioLab GmbH. Corning® flat-bottom 96-well half-area microplates, black polystyrene, were purchased from Sigma–Aldrich (Steinheim, Germany). Cellfectin™ II Reagent (Thermo Fisher Scientific, MA, USA), baculovirus genomic ProEasy™ vector DNA (Cat. #A10S, AB vector, CA, USA). Insect-XPRESS™ media (#: BE12-730Q, Lonza, Switzerland) and HisPur™ Ni^{2+}-NTA spin columns (#: 88226, Thermo Fisher Scientific, MA, USA) were used as protein expression and purification tools—EDTA-free protease inhibitor cocktail tablets (Roche Diagnostic GmbH, Germany). Amicon® Ultra-15 concentrator with 10 kDa cut-off was purchased from Merck Millipore, MA, USA.

a. Instrumentation

Fluorescence was measured using a FlexStation® 3 Multi-Mode Microplate Reader (Medical Devices LLC. USA) for data collection using Softmax Pro 3.0 software. Nucleotides were precipitated in a 96-well plate using a SpeedVac plate centrifuge (LaboGene ApS, Denmark). Natural substrates were tested using a p/ACE™ MDQ plus capillary electrophoresis system (AB Sciex LLC, Framingham, USA). Data collection and peak area analysis were performed by the P/ACE MDQ software 32 KARAT obtained from Beckman Coulter (Fullerton, CA, USA). Mithras LB 940 (Berthold Technology, France).

2.1 Protein expression and purification

Proteins were recombinantly expressed as a soluble and membrane-bound variant in *Spodoptera frugiperda* (*sf9)* insect cells using ProEasy™ linearised baculovirus genomic DNA. Details of cloning tools used for both types of proteins are given in Table 3.7. As previously reported, soluble and membrane-bound enzymes were expressed (Lee et al., 2021). Briefly, for soluble enzymes only, each enzyme's transmembrane domain (TM) sequence is trimmed, and the gene of interest (GOI) was subcloned in the *p*-ACGP67-B expression vector between restriction sites. 10 % Cellfectin™, 1 µg of plasmid DNA containing GOI, and 2.5 µL of ProEasy™ DNA in 100 µL of culture media were incubated for 20 min at room temperature. The resulting DNA-cellfectin emulsion was used to infect semi-confluent *sf9* adherent cells culture for 96 h at 27 ^{o}C to amplify virus titer and protein expression. Medium-containing soluble enzymes were concentrated up to approximately 70 – 80 % with Amicon® Ultra 15 mL centrifugal filter with variable cut-off limits (10 – 50 kDa, 4500 x G, 30 min). Subsequently, His-tagged protein was purified by HisPur™ Ni^{2+}-NTA spin columns by increasing the imidazole concentration from 10 mM to 250 mM (*Manufacturer specs)*. The eluted enzyme was filtered and concentrated for buffer exchange in mM, 1 $MgCl_2$, 2 $CaCl_2$, 10 CHES, and pH 9.2 to eliminate imidazole. Protein concentration was determined by the Lowry method based on the oxidation of aromatic amino acids (tryptophan and tyrosine) with the folin-ciocalteu reagent (Randall & Lewis, 1951).

For the Membrane-bound enzyme, a full-length sequence of enzymes is sub-cloned in modified pfastbac1 expression vector [modifications; *(BamHI-HA-Tag (MKTIIALSYIFCLVFA)-FLAG tag (DYKDDDDA)-AscI-GOI-9- fold HIS-Tag-terminator-*

hind-III] (Claff et al., 2019). The engineered plasmid was amplified in DH5α cells subsequently 500 ng purified pFastBac1-plasmid (2-3 µl) is transformed into DH10αBac and applied to an agar plate containing (10 µg/mL Tetracycline, 7 µg/mL Gentamicin, 50 µg/mL Kanamycin, 40 µg/mL IPTG, 100 µg/mL X-Gal). Plates were incubated for 48 hours at 37 °C. White colony containing recombinant bacmid was amplified in 5 ml fresh medium containing 10 µg/mL Tetracycline, 7 µg/mL Gentamicin, and 50 µg/mL Kanamycin at 250 rpm for overnight incubation at 37 °C (~ 18 hours). Bacmid was purified by QIAprep Spin Miniprep Kit using the manufacturer's specifications and transfected in *Sf 9* insect cells (2 x 10^6 cells ml^{-1} in 2.5 ml cell suspension) with 3 µL X-tremeGENE HP emulsion in 100 µl. Protein was allowed to express for 48 hours after one-time virus amplification. The pellets were collected by centrifuging medium for 10 min at 4500 x g washed and re-suspended in buffer containing 10 mM HEPES, 10 mM $MgCl_2$, 20 mM KCl, and 30% (v/v) glycerol pH 7.5, homogenised in 25 ml low osmotic buffer (10 mM HEPES pH 7.5, 10 mM $MgCl_2$, 20 mM KCl) + protease inhibitor and centrifuged for 30 min at 48000 x g. The second wash used a high osmotic buffer (10 mM HEPES pH 7.5, 10 mM MgCl2, 20 mM KCl, 1 M NaCl). Finally, after centrifugation, the pellets were resuspended in buffer containing 10 mM HEPES, pH 7.4, 2 mM $CaCl_2$ 1 mM $MgCl_2$, 10% (v/v) glycerol.

Table 3.7: Tools for the expression of soluble and membrane-bound enzymes

Enzyme	A.A.*	Exp. Vec.!	R. S. **	Primers
Soluble				
NPP1	98-925	*p*ACGP67B	BamHI/NotI	*f'-5'- GATC-*GGATCCGCCACGAAAGAAGTTAAAAG TTGCAAA GG -3' *r'-*5'- GATC-GCGGCCGC**TTA**GTCTTCTTGGCTAAAG GTTG-3'
NPP3	31-875	*p*ACGP67B	BamHI/NotI	*f'-5'-GATC-*GGATCC-GCCACCATGTCACTTGGAT TAGGCCTGG-3' *r'-*3'-*GATC-*GCGGCCGC**TTA**GTGGTGGTGGTGG TGATGGTGGTGGTGAATAGTGGTTTCAAATGTTGG-5'
NPP5	25-430	*p*ACGP67A	XbaI/NotI	*f'-5'-GATC-*TCTAGA**A-**CACCACCACCATCACCACCACCACCACCCAGACCAGCAAA AGGTTC-3' *r'-*3'-*GATC-*GCGGCCGC**TTA**TGACCCCTCTTGGTCATATTC-5'
Membrane-bound				
NPP3		*pfastbac mod.*	AscI/HindIII	*f'-*5'-*GATC-* G-GGCGCGCC-ATGGAATCTACGTTGACTTTA GCAA CGG-3 *r'-*3'-*GATC-*AAGCTT**TTA**GTGGTGGTGGTGGTGATGGTGGTGGT GAATAGTGGTTTCAAATGTTGGTAAATATGTC-5'

*Amino acids,! Expression vector, ** Restriction site, Primers: Irrelevant base pairs are shown in *italics,* underlined sequence represents restriction sites, and bold letters are the stop codon

2.1.1 Cell culture and membrane preparation

Cell lines were cultured in Dulbecco's modified Eagle's medium (DMEM; GibcoBRL, Gaithersburg, MD., USA) supplemented with 10% fetal bovine serum (FBS; GibcoBRL), 1% Pen-strep at 37 °C in humidified 95% air and 10% CO_2. For U87 cell lines, 1% glutamine was added to the culture medium and incubated with 5% CO_2. Human TNBCs and astrocytoma cell lines were harvested using trypsin reagent after rinsing with 1 x PBS; however, U87 cell lines were readily dissociated by gently stroking the flask. Cells were regularly split to 0.3 million cells/ml every 4th day. Confluent cells were processed for buffer exchange using centrifugation at 1000 x g for 5 min and transferred to 15 ml Dounce. Cell membranes were disrupted with 25 ml of low osmotic buffer (10 mM HEPES, 10 mM $MgCl_2$, 20 mM KCl pH 7.5) with a protease inhibitor cocktail. Cell pellets were homogenised with repeated plunging on ice and centrifuged for 30 min at 48000 g. The pellets were washed with 25 mL of high osmotic buffer (10 mM HEPES, pH 7.5, 10 mM $MgCl_2$, 20 mM KCl, 1 M NaCl). Washed pellets are resuspended in 3 mL resuspension buffer (10 mM HEPES, pH 7.5, 10 mM $MgCl_2$, 20 mM KCl, 30% glycerol) and plunged 40 times in a 2 mL Dounce homogeniser on ice, then flash-frozen in liquid nitrogen and stored at -80 °C until further use.

2.1.2 Coomassie blue protein gel

10 % bis-Tris SDS-page gel was produced using a standard protocol. 500 ng of purified protein was dissolved in 4x NuPAGE LDS sample buffer. The sample was incubated with the loading dye for 30 min at RT. MOPS running buffer was prepared in VE water and filled in an electrophoresis chamber. 4 µL of pre-stained protein ladder and 30 µL of protein sample were loaded. Electrophoresis started at 50 V until the samples reached resolving gel and later proceeded with 120V.

2.2 Assays for measuring enzyme kinetics vs. different substrates

NPP3 can hydrolyse several extracellular nucleotides with high product turnover (Döhler et al., 2018; Gorelik et al., 2018). We further characterised the enzymes vs nucleotide substrates by emphasising di-nucleotides. Different assays were developed and optimised for NPPs, including HTS assay using fluorescent analogues ε-NAD^+, ε-ADPR, and ε-Ap_4ε-A, assays with a natural substrate using CE. The Enzymatic reactions were performed in reaction buffer, CHES buffer (10 mM CHES, pH 9.2, 2 mM $CaCl_2$, and 1 mM

$MgCl_2$). For *p*-NPh-5'-TMP assay only, Tris HCl buffer (50 mM Tris-HCl, pH 9.2, 2 mM $CaCl_2$, 0.2 mM $ZnCl_2$). The final concentration of DMSO was not allowed to exceed more than 2 % v/v.

a. Ɛ-NAD^+/Ɛ-Ap_4Ɛ-A as substrate

Disruption of internal quenching in Ɛ-NAD^+ between nicotinamide and Ɛ-adenine group that allows investigation of the product formation. The assay was optimised for Ɛ-NAD^+ and NPPs using the previously published methodology for measuring CD38 activity (Blacher et al., 2015; Schultz, 2018). Briefly, NPPs attack the α – β, phosphodiester bond of the molecule, leading to an approximately 92 % increase in fluorescence intensity. Six different concentrations of the soluble NPP3 (40 – 800 ng) and crude soluble NPP1 (0.08 – 4 µg) were incubated with 20 µM Ɛ-NAD^+ for 30 min at 37 ^oC in 96 wells plate. Estimation of fluorescence intensity was performed at λexcitation/emission (λex/em of 270/420 nm) in a fluorescence plate over a continuous plate reader FlexStation® 3 Multi-Mode Microplate Reader (Medical Devices LLC. USA) using *Softmax Pro* 3.0 software for data collection. The Ɛ-Ap_4Ɛ-A follows the exact mechanism as the Ɛ-NAD^+ assay; however, to minimise costs, the test was performed at five µM substrate concentration with a final volume of 50 µL.

b. Ɛ-ADPR as substrate

Ɛ-ADPR molecule is devoid of the quenching effect found in Ɛ-NAD^+ or Ɛ-Ap_4Ɛ-A and therefore, after hydrolysis by NPPs to Ɛ-AMP, it is not possible to differentiate fluorescence intensity of the substrate and product. For this purpose, both molecules must be separated to investigate product formation. Previously, we developed an HTS screening assay for cancer cell lines using Ɛ-ATP/ADP/AMP, where nucleotides were precipitated entirely from the reaction mixture, leaving only the product Ɛ-adenosine in the supernatant. The precipitation buffer [14.2 mM Na_2HPO_4 and 71.7 mM of $LaCl_3$/ NaOAc at pH 3.2] was added to the reaction samples, followed by centrifugation at 1200 rpm in a 96-well plate. With this assay, we could indirectly estimate the Ɛ-AMP formation in the enzymatic reaction based on the reduction of the RFU of the substrate Ɛ-ADPR. Though the substrate contains two phosphate groups in the molecule, the terminal group is not free and attached to a ribose molecule, possibly hindering the precipitation reaction. The schematic presentation of our assay mechanism is described in Figure 3.4.

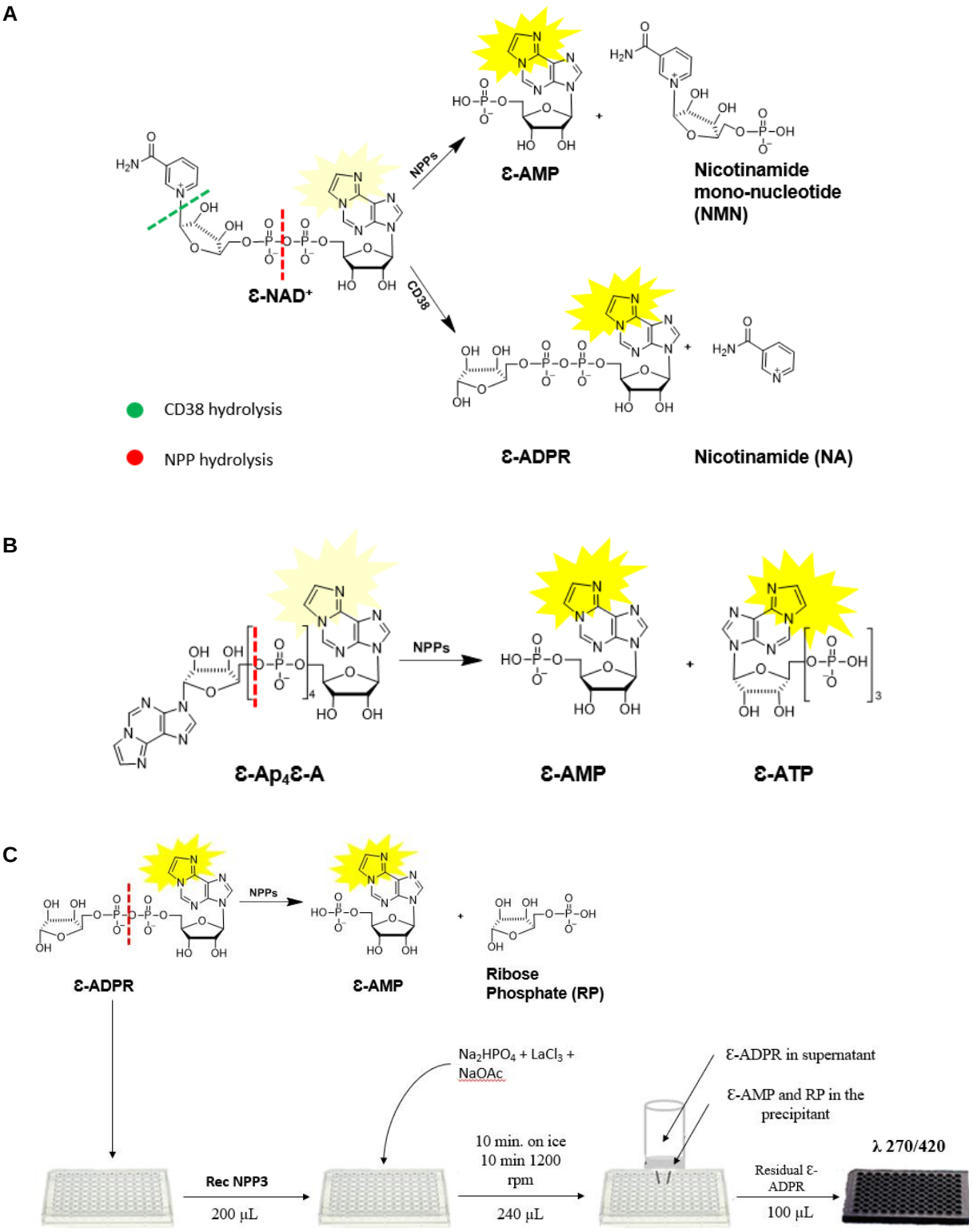

Figure 3.4: **Schematic presentation of proposed assay mechanism** involving A) ε-NAD+ B) ε-Ap4ε-A, C) ε-ADPR. Assays A and B are based on the disruption of the quenching effect after hydrolysis of an α,β-phosphodiester bond by NPPs, resulting in higher fluorescence intensity. The assay C is based on the precipitation of the products ε-AMP and RP containing terminal phosphate. Samples were treated with precipitation buffers, P.B I and II (NaH_2PO_4/$LaCl_3$-NaOAc, in mM, 14.2/71.7, pH 3.2), completely

precipitating ε-AMP and ribose phosphate. ε-ADPR is only marginally precipitated. The residual substrate's fluorescence intensity (λ270/420 nm) is recorded from the supernatant.

c. *p*-NPh-5'-TMP assay

Artificial substrate *p*- nitrophenyl-5'-thymidine-monophosphate (*p*-Nph-5'-TMP) based colourimetric assay was performed as previously reported (Cimpean et al., 2004). Briefly, NPP3 was treated with 400 µM of *p*-Nph-5'-TMP in 50 mM Tris reaction buffer for 30 min at 37 °C. The reaction was terminated by adding 20 µL of 0.1M NaOH, and the absorbance of *p*-nitrophenolate was measured at 405 nm using a Mithras LB 940 continuous plate reader and MikroWin software for data acquisition.

d. CE assay using a diode array (DAD) detector

Capillary electrophoresis assay (CE) is used to characterise enzyme vs. natural substrates under the same reaction conditions, 10 mM CHES buffer, and CE running conditions (50 mM phosphate buffer, separation voltage of -15 kV) with 30 cm capillary length as previously reported (Lee et al., 2017; Nassir, Mirza, et al., 2019) Briefly, reaction samples were electro-kinetically loaded (-6 kV, 30 sec) into Polyacrylamide-coated capillary [30 cm (20 cm effective length) × 50 µm (id), × 360 µm (od) and allowed to migrate through solution based on their ionic mobility and application of electric field (-15 kV, 0.1 psi pressure). Analysis was carried out using the P/ACE MDQ CE system (Beckman Instruments, Fullerton, CA, USA) equipped with either DAD (λabs 254 nm).

2.3 Assays linearity and method validation

Linear coefficient R^2 was determined for twelve concentration points analysis (0.05 to 10 µM) of ε- AMP. Simulation of reaction mix was made [a + b = 10 where a is the substrate (ε-NAD^+, ε-ADPR, ε-Ap_4ε-A) and b is ε-AMP]. A separate blank for each substrate concentration was taken as a control. Blank substrate values were deducted from the investigation sample. Sample precipitation and fluorescence detection are described in the assay mechanism. Linear regression was calculated for the concentration vs relative fluorescence unit (RFU of substrate retained in the supernatant) to calculate R^2 using GraphPad Prism 7.0 software through equation y = ax + b, where a = slope and b = y-intercept. Three independent tests were performed with triplicate measurements. Robustness and accuracy were measured for three concentrations in µM: 2.5, 1, 0.5, as described above. A total of 3 – 6 independent tests in triplicate were performed for relative

standard deviation and % accuracy. Z'-factor test was performed for 48 enzyme reactions in 3 independent tests of sixteen interventions (positive samples) with forty-eight control samples (without enzyme). In the positive enzyme samples, 160 ng of NPP3 was reacted with 20 µM of ε-NAD^+, 80 ng with 20 µM ε-ADPR, and 10 ng of NPP1 with 5 µM of ε-Ap_4ε-A. Samples were incubated for 30 min at 37 ^oC except for NPP1, which was incubated for 5 min only showing high product turnover. Z'- factor is calculated using an equation (Zhang et al., 1999).

$$\frac{1 - 3 * (\sigma p + \sigma n)}{(\mu \rho - \mu n)}$$

Where σ is the standard deviation of positive (σp) and negative (σn) enzyme samples, and µ is the mean value of 48 observations in positive and negative tests.

2.4 Kinetics testing of natural and fluorescent substrates

Michaelis-Menten kinetic constant K_m was measured for the natural substrates of NPP3 and their fluorescent substitutes. Twelve – to fifteen concentrations point analysis was made for natural substrates (20 – 1000 µM), fluorescent HTS substrates (1 to 250 µM), and *p*-NPh-5'-TMP (10-2000 µM). The assays' conditions and the reaction buffers were the same as previously described. To conduct the ε-ADPR assay, we processed blank dilutions (without enzyme) to represent each concentration point of the substrate using the same precipitation conditions as the enzyme samples. We measured the reduction in fluorescence units after the enzyme reaction by subtracting it from the control sample of each dilution. Three independent tests with duplicate observations were carried out. The rate of reaction V (y-axis) at a fixed enzyme concentration (pmol/min/mg protein) was plotted against the molar substrate concentration [S] on the X-axis by using non-linear regression to determine the Michaelis-Menten constant K_m with GraphPad Prism software 7.0. The turnover number (Kcat) of a substrate molecule to the product in one second per active site of the enzyme was measured using the equation: k_{cat} = vmax / [E] (vmax, maximal velocity (µM/s); [E], enzyme concentration (µM). Kcat was then divided by the determined K_m to obtain a specificity constant K_{cat}/K_m, which was then used to compare the substrate's preference by the enzyme.

2.5 Exploration of the benzenesulfonamide scaffold

Optimising different HTS assays for multiple NPPs helped us further explore a potent and selective benzenesulfonamide scaffold. Although the lead compound is highly selective for NPP3 regarding other ectonucleotidases, it showed an equal inhibitory potency towards carbonic anhydrases CA-II (K_i 74.7 nM) and CA-IX (K_i 20.3 nM). For this purpose, different modifications were proposed to the lead structure (Comp II). The outcomes of the previously published SAR studies are mentioned in Figure 3.5.

i. Modification of benzenesulfonamide scaffold

Based on these modifications, sixteen derivatives were synthesised by a master's student, Maria Karpouchtsi, under the supervision of Dr. Nader Boshta and Dr. Ahmed Temirak. Modifications were made by replacing the phthalazine core with various bioisosteres.

ii. Modification of reaction buffer, ionic contents, and pH

NPP show optimum activity under alkaline conditions, which are suitable for working with the artificial substrate *p*-NPh-5'-TMP. However, we investigated the newly synthesised compounds under alkaline and neutral pH conditions using either artificial substrate *p*-NPh-5'-TMP and Ɛ-NAD$^+$ or natural substrate NAD$^+$. The optimised reaction buffer was 10 mM HEPES (pH 7.4), 0.5 mM $CaCl_2$, and 0.01 mM $ZnCl_2$. The test was performed in a single parallel setting using similar reaction conditions, such as buffer and enzyme samples, to compare the results directly.

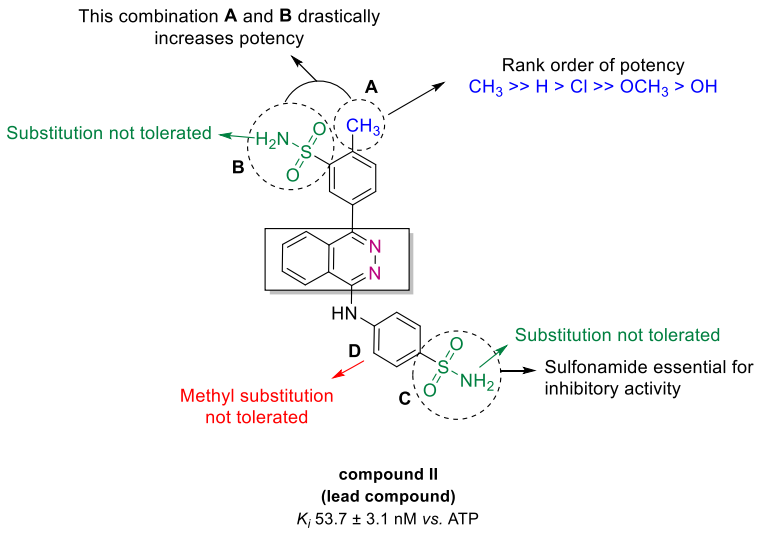

Figure 3.5: SAR outcome of *p*-aminobenzenesulfonamide scaffold reported in (Lee et al., 2021).

2.6 Testing of selected inhibitors vs. different substrates and assays

Our research group previously published NPP3 inhibitors of the benzenesulfonamide scaffold (Figure 3.5) with an inhibitory potency K_i of 53.7 nM vs ATP (Lee et al., 2021). The scaffold is further optimised by replacing the phthalazine core yielding PZB08720015A. The new compound is analysed vs different substrates *p*-NPh-5'-TMP, ATP, NAD^+, ADPR, and Ap_4A to compare IC_{50} values. For this purpose, 12 – 15 concentrations (0.005 – 100 µM) were tested. The assay conditions and detection method for each substrate were the same as described in the assay mechanism section. A total of three independent tests were performed with duplicate observations. IC_{50} values of the inhibitors were determined by nonlinear fitting of the experimental data using GraphPad Prism 7.0. Three independent experiments with triplicate observations were performed. K_i values were calculated from IC_{50} values using the Cheng-Prusoff equation (Cheng & Prusoff, 1973).

2.7 Mechanism of enzyme inhibition

The inhibition mode was measured for derivative NBO-MKA-29 at 0.5, 0, and 2-fold IC_{50} values for the tested compound vs five concentrations of substrates (50 - 500 µM), Ɛ-$NAD^{+,}$ and NAD^+. Reaction conditions for each assay are described in section 2.2 of this chapter. Two independent tests were performed with duplicate observations. The inhibition type was determined graphically from the Hanes-Woolf and Lineweaver-Burk plots.

2.8 Selectivity testing of potent inhibitors towards other ectonucleotidases

The test was performed using soluble enzymes expressed in-house using a baculovirus expression system in insect cells. The protein expression and purification steps were the same as described above in NPP3 expression and purification (*Details of CD39 and CD38 expression will be described in their respective chapters*). To be consistent with the reaction conditions of NPP3, the selectivity test was performed using a similar reaction buffer for NPP1, 4, and 5 (10 mM HEPES, pH 7.4, 0.5 mM $CaCl_2$, and 0.01 mM $ZnCl_2$) and for CD38, 10 mM HEPES pH 7.4 is used. For CD73 and CD39, HEPES 10 mM (Ph 7.4), 2 mM $CaCl_2$, and 1 mM $MgCl_2$ buffer were used. CE assay was performed with the natural substrate NAD^+ 100 µM for NPPS for 45 min. The CD38 reaction was carried out

for 15 minutes. CD39-based reactions were carried out with 100 µM ATP and soluble CD39 for 40 min. CD73 reactions were carried out by incubating the soluble enzyme with 10 µM ε-AMP (reaction details can be found in chapter 2 of this dissertation). Two independent tests were performed with triplicate observations.

2.9 Statistical analysis

Data analysis was performed using GraphPad Prism 7.0 for K_m calculation and IC_{50} determination. K_i is determined numerically by using the Cheng-Prusoff equation. A one-way ANOVA test is used to calculate the significant difference among parameters.

3.0 Results and Discussion

3.1 Protein Expression and Purification

Enzymes were expressed in *sf9* insect cells as soluble enzymes [truncation of the transmembrane domain (amino acids AA 1-33) in *p*ACGP67-B] or membrane-bound using a modified *pfastbac* expression plasmid. The modification was made by introducing an N-terminal HA tag and a FLAG tag for expression control. It is observed that the HA-tag, besides its role in affinity purification, improves the placement of the proteins into the membrane. Enzymes could be stably solubilised from membranes using mild detergents, dodecyl maltosides (DDM), and cholesteryl hemisuccinate (CHS) in buffer (50 mM HEPES, 800 mM NaCl, 1% DDM, 0.2% CHS). The functional analysis of the protein vs. vs. *p*-NPh-5'-TMP showed high product turnover that reflects the enzyme was successfully expressed in the membrane, further confirmed with western blot analysis using anti-His-tag antibodies and functional analysis. The soluble enzyme was purified with a Ni-NTA^{TM} column and eluted with an increasing concentration of imidazole, 10 to 250 mM (see manufacturer's specifications). The details of the expression are depicted in Figure 3.6; however, the purification of proteins needs further optimisation.

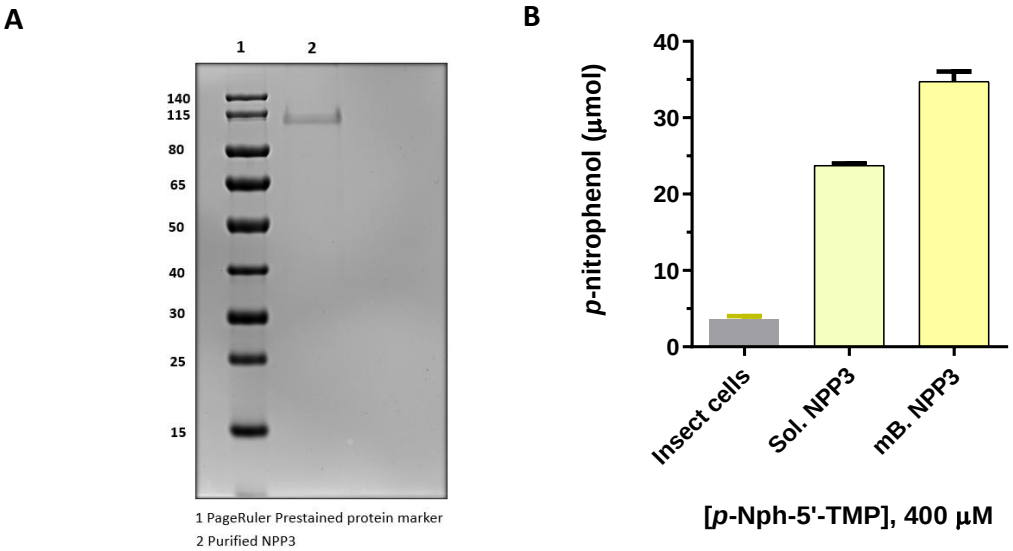

Figure 3.6: **Enzyme expression** A) Coomassie blue gel showing purified soluble NPP3. B) Hydrolysis of the standard substrate of NPPs, *p*-NPh-5'-TMP. Both soluble and membrane-bound enzymes potently hydrolysed the substrate.

3.2 Development and optimisation of enzyme assays

3.2.1 Fluorescence-based assays

a. Ɛ-NAD⁺ and Ɛ-Ap₄Ɛ-A as substrates

The fluorescent analogue of NAD⁺, 1, N^6-etheno-nicotinamide adenine dinucleotide Ɛ-NAD⁺ was previously reported for measuring enzyme kinetics and inhibition studies of NADases CD38/157 (Blacher et al., 2015). However, the use of Ɛ-NAD⁺ or Ɛ-Ap₄Ɛ-A as an NPP substrate is minimal. Both Ɛ-NAD⁺ and Ɛ-Ap₄Ɛ-A showed a similar internal quenching that led to a lowering of fluorescence intensity of both compounds (Barrio et al., 1972; Gasmi et al., 1998). Once NPPs hydrolyse the α-β phosphodiester bond of both substrates, the quenching effect is disrupted, resulting in an increase in fluorescence that reflects Ɛ-AMP formation. The difference in fluorescence of substrates and product is highly significant, which allows the use of these substrates for monitoring NPP activity in a variety of in-vitro and in-vivo cellular settings such as tumour cell culture and live cell assays if NPPs are expressed (Figure 3.7). The assay is straightforward and allows direct estimation of the product without requiring sophisticated equipment. The assay is highly efficient, and we can detect product formation quite quickly, which means a low amount of enzyme is needed to reach 20% substrate conversion. The assay is suitable for coloured compounds, such as plant pigments.

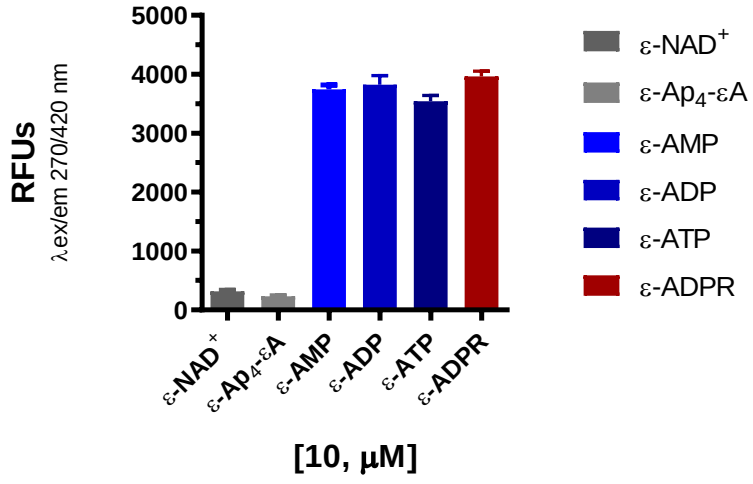

Figure 3.7: Comparison of relative fluorescence units (RFU) of 10 µM of Ɛ-NAD⁺, Ɛ-Ap₄Ɛ-A, and Ɛ-AMP. A significant difference in the RFUs of substrates was observed compared to the product, which reflects the loss of internal quenching and results in > 92 % higher RFUs observed for the same concentration. Two independent tests with triplicate observations were presented as mean ± SEM.

b. Ɛ-ADPR as a substrate

Indirect estimation of the NPP reactions is possible using Ɛ-ADPR with selective precipitation of the product Ɛ-ADPR using $NaH_2PO_4/LaCl_3$-NaOAc co-precipitation buffer followed by plate centrifugation at 1200 rpm for 10 min (See chapter 2 for further details). The supernatant exclusively contained the remaining Ɛ-ADPR. This assay is based on estimating the substrate's fluorescence reduction due to the enzymatic reaction. However, the reduction was calculated using a negative control of similar substrate concentration treated equally as the reaction samples, without adding enzyme. The fluorescence value of the enzyme sample is subtracted from the control to indirectly estimate the RFUs of Ɛ-AMP formed in the reaction sample using the equation

$$[Product\ formed = RFU\ of\ blank\ substrate\ (P.P) - RFU\ after\ enzyme\ reaction\ (P.P)]$$

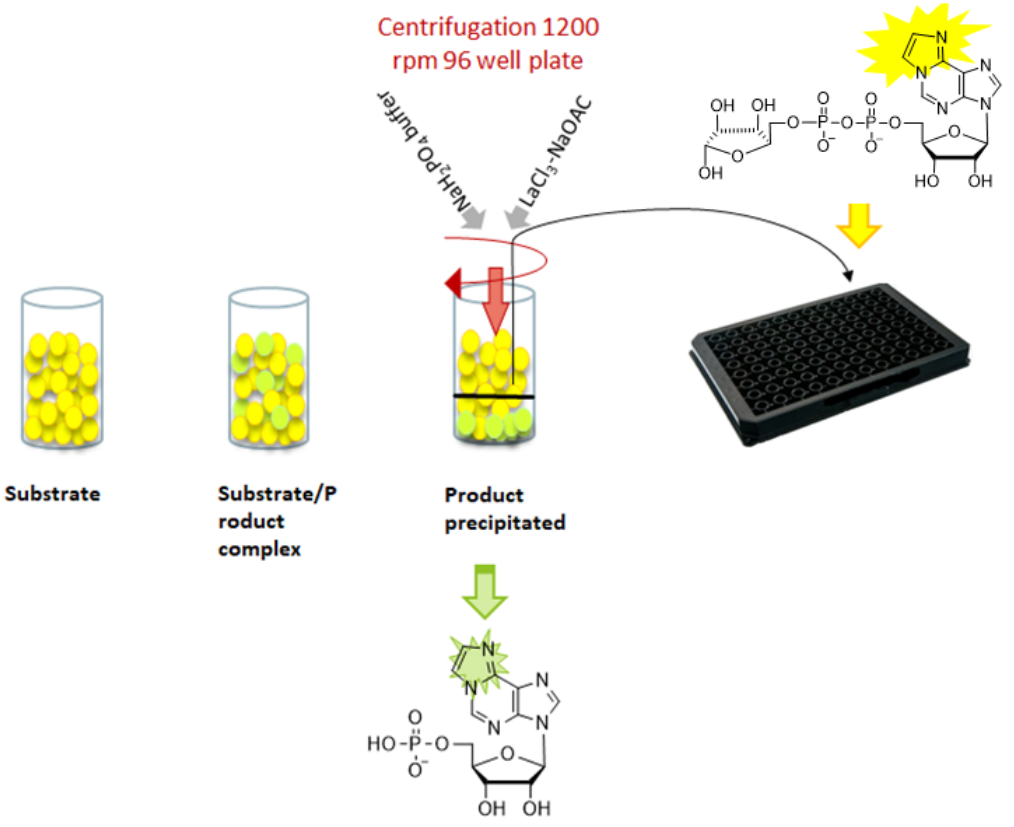

Figure 3.8: Schematic flow chart of Ɛ-ADPR assay mechanism. NPPs potently hydrolyse Ɛ-ADPR to Ɛ-AMP and ribose phosphate, which could be precipitated. Following the reactions of NPP1 and -3 with Ɛ-ADPR, high product conversion was observed; however, slow product turnover was observed for NPP4 and -5.

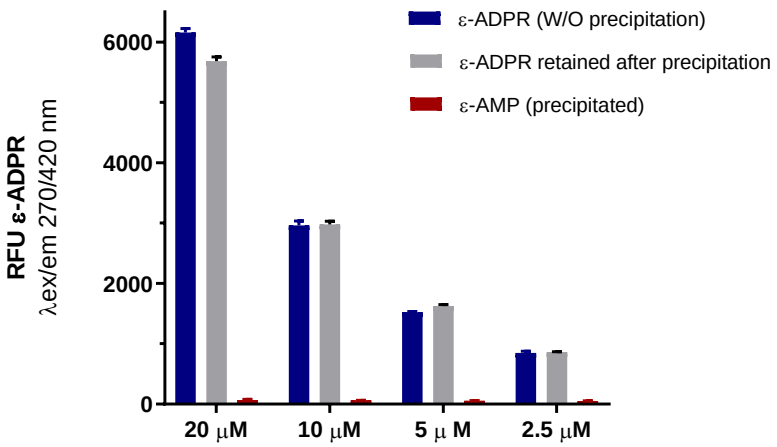

Figure 3.9: The effect of precipitation buffer on Ɛ-ADPR and Ɛ-AMP. Four concentrations (20, 10, 5, and 2.5 µM) were tested. Ɛ-ADPR is retained in the supernatant (more than 96 %) for all tested concentrations; however, for higher concentrations up to 150 µM, substrate retention is reduced to 85 -90 % (data not shown). Ɛ-AMP is wholly removed from the reaction mixture (more than 99 %). RFU values were measured at λex/em of 270/420 nm. The reduction of RFUs in the substrate sample owing to an enzyme reaction is calculated by subtracting the value from the blank sample (no enzyme) and considering the formed product.

3.3 Assay validation

Validation steps were adopted from previously reported guidelines for bioanalytical method development (Taverniers et al., 2004). The outcome of the validation steps is summarised in Table 3.8. Linear correlation was observed for the tested substrates, e.g. a correlation coefficient (R^2) of 0.9975 was observed for Ɛ-NAD^+, 0.9994 for Ɛ-ADPR, and 0.9992 for Ɛ-Ap_4Ɛ-A. The limit of detection (LOD) and limit of quantification (LOQ) for 10 – 12 concentrations of a simulation mixture [Ɛ-NAD^+/Ɛ-AMP, Ɛ-ADPR/Ɛ-AMP (0.01 – 10 µM), and Ɛ-Ap_4Ɛ-A/Ɛ-ATP/Ɛ-AMP (0.001 – 5 µM)] was measured up to a low nanomolar range representing the linearity and sensitivity of the assay. Lower LOD values allow it to work at lower substrate concentrations. On the one hand, it is economical since fewer enzymes and substrates are used. On the other hand, it allows them to work close to the Km values of these enzymes and helps better predict competitive inhibitors' Ki values. The accuracy and precision values aligned with the ICH acceptable range of 80 – 110 % and 8 – 22 %, respectively. The assay is well suited for high-throughput screening of compound libraries with a Z'-factor lying well within the acceptable range (0.5 – 1.0).

Table 3.8: Method validation according to ICH guidelines

	ε-NAD$^+$ [a]	**ε-ADPR [b]**	**εAp$_4$εA [c]**	**a. r.* [d]**
Equation	Y = 462.9*X - 94.34	Y = 506.9*X + 21.45	Y = 940.8*X + 32.16	
Linearity (n=3) R^2	0.9975	0.9994	0.9992	
Limit of detection LOD (nM)	75.2 ± 3.6	80.3 ±4.1	19.1 ± 0.8	
Limit of quantification LOQ (nM)	220 ± 6	240 ± 9	58.2 ± 2.1	
Accuracy (%), n=3 nM				
2500	98	99	99	90 – 107
1000	110	98	99	80 – 110
500	105	94	91	80 – 110
Precision (RSD %)* n= 3 nM				
2500	2.8	6.3	1.2	8
1000	3.8	7.2	2.6	16
500	22.9	10.0	15.2	22.6
Estimated detection time (min)	~ 2	~ 25	~2	
Z'-factor, n=48	0.71	0.75	0.63	0.5 - 1

[a] ε-NAD$^+$ assay (loss of quenching effect as a result of substrate hydrolysis)
[b] ε-ADPR assay (Precipitation of product ε-AMP and reduction in substrate's fluorescence intensity was monitored)
[c] ε-Ap$_4$-εA assay (loss of quenching effect as a result of substrate hydrolysis)
[d] Literature value (Taverniers et al., 2004) * acceptable range

The precipitation buffer (Na_2PO_4/$LaCl_3$-NaOAc) can remove ε-ATP/ADP/AMP from the reaction mixture up to the concentration of 250 mM (for further details, see Chapter 2). On the other hand, ε-ADPR is explicitly retained by more than 96 % up to the concentration of 20 µM. However, approximately 85 – 90 % retention is observed for 50 – 250 µM concentrations. The nicotinamide analogue of ε-ADPR (ε-NAD$^+$) also showed similar behaviour regarding precipitation, although both molecules contained a backbone of two phosphate groups. Despite precipitating ADP very efficiently, the precipitation of ε-ADPR is only marginal. One possible justification could be that the precipitation mixture (NaH_2PO_4/$LaCl_3$-NaOAc) bound well with the terminal free phosphate of the nucleotides, which is not available in the case of ADPR and NAD$^+$. The glucose moiety attached to the ADP backbone possibly altered its physical nature by neutralising the effect of the accessible OH on the terminal phosphate, thus hindering its precipitation by the buffer. Moreover, ε-ADPR assay is only suitable for recombinant NPPs or in settings where CD73 or AP are absent. Both these enzymes can further hydrolyse AMP to adenosine, making

it difficult to estimate the concentration of actual residual substrate left in the supernatant. Figure 3.10 further elaborates on the details of the calibration curve and Z-factor tests.

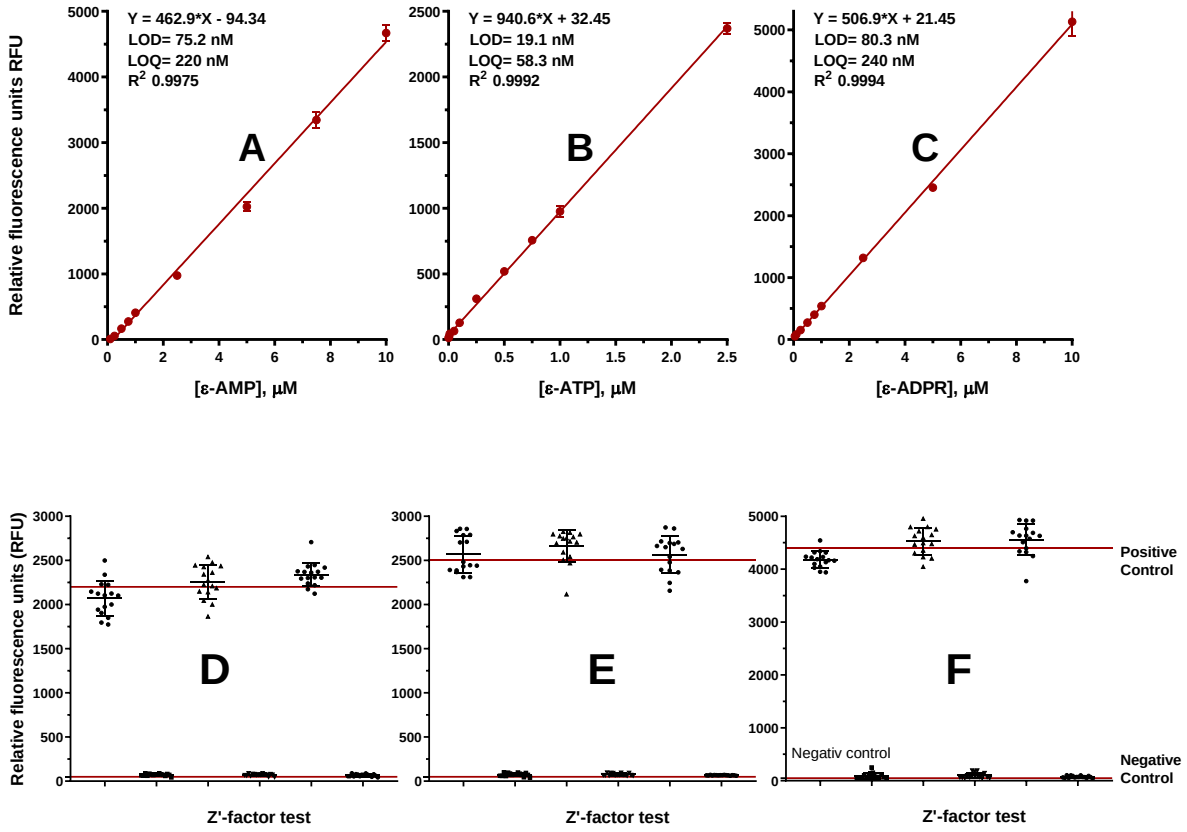

Figure 3.10: ***Assay validation steps.*** Linearity test portrays the correlation coefficient for A) ε-NAD^+ *(R^2=0.9975)*, B) $εAp_4εA$ *(R^2=0.9992),* and C) ε-ADPR *(R^2=0.9994)*. Z'-factor test (n =48, positive and negative samples) showed assay suitability for HTS D) ε-NAD^+ (Z'-factor 0.71), E) $εAp_4εA$ (Z'-factor 0.75), F) ε-ADPR (Z'-factor 0.63). A total of two independent tests were performed, each with triplicate observations. Data are presented as mean ± SEM.

3.3 Substrate screening for soluble NPPs

Our research on soluble human NPPs, primarily NPP3, and their interaction with twenty-three natural and artificial nucleotidic substrates, each with distinct nucleotide bases (adenine, guanine, cytosine, and uracil), was conducted using a rigorous methodology. Gorleik et al.'s study on kinetic parameters for soluble human enzymes vs ATP, ADP, GTP, UTP, and CTP showed a moderate hydrolysis of the substrates and a preference for uracil and cytosine bases. Similarly, the research group of Prof. Nobert Straeter's investigation on rat soluble enzymes against a substrate range covering triphosphates and dinucleotide polyphosphates, showed that the enzymes could better hydrolyse dinucleotides. Our data aligns with these findings for most of the substrates. However, we

observed a moderate hydrolysis of triphosphates, e.g. ATP and GTP, compared to the rat ortholog. This suggests that the enzymes prefer the following substrates: ADPR, NAD^+, NAAD, Ap_3A, and Ap_4A, showing high product turnover. The phosphate analogues of ADPR (ADPRP), NAD^+ (NADP), and NAAD (NAADP) showed less product turnover as compared to their dephosphorylated precursors, which indicates that a phosphate group on the ribose hinders enzyme reactions. Appreciable hydrolysis of uridine and cytidine triphosphate, UTP, and CTP was observed amongst the triphosphates. The diphosphates of adenosine, guanosine, cytidine, and uridine are less hydrolysed by the enzyme. Like NPP1, NPP3 could potently hydrolyse *p*-NPh-5'-TMP. The assay conditions were optimised to have a uniform setting to evaluate the substrate and its hydrolysis products. As a part of the substrate screening campaign, we first analysed substrate conversion to the product at a specific enzyme concentration of 150 ng/well. The assays' parameters (incubation time, reaction termination, and product estimation by CE) were kept constant for each substrate. We observed an extended migration time for ADPR, UDP-g, and NAD^+ than for ADP and UDP, which could be due to the extra ribose group's impact on the nucleotide diphosphates' overall negative charge.

3.3 Kinetic profiles of NPPs using different assays

The hydrolytic profile of NPPs was measured vs. natural and artificial substrates with a focus on human NPP3. The human enzyme variant was previously reported to hydrolyse ATP, GTP, CTP, and UTP; however, our substrate screening tests noticed potent di-nucleotide hydrolysis. Therefore, we performed a kinetic study of the substrates to find their K_m and V_{max} values under similar reaction and analytical conditions for direct comparison as previously described for NPP1 (Namasivayam et al., 2016). ADPR, NAD^+, and dinucleotide polyphosphates (Ap_3A and Ap_4A) and NAAD were well hydrolysed by NPP3 with a high product turnover. Noticeable reduction in hydrolysis was observed for phosphate derivatives of these substrates, i.e. ADPRP, NADP, and NAADP. These results highlight possible new dimensions towards the catalytic role of NPP3 other than hydrolysing ATP efflux from activated basophils and mast cells. Potent hydrolysis of the dinucleotide polyphosphates Ap_3A and Ap_4A needs further investigation of NPP3-based modulation of platelet functions as well as immuno-pathological conditions linked with its role in the non-canonical pathway (CD38/NPPs/CD73) active on leukocytes (Ferrero et

al., 2019). These enzymes' cascade provides an efficient and alternative production pathway for adenosine independent of the CD39/CD73 tandem pair. Potent hydrolysis of UDP-glucose is observed, strengthening the claim of its role in the cellular glycosylation process (Korekane et al., 2013). Based on enzyme kinetics and substrate hydrolysis, it is evident that NPPs are likely capable of regulating diverse physiological and immune mechanisms, thereby opening up new dimensions in NPPs' research and their therapeutic potential.

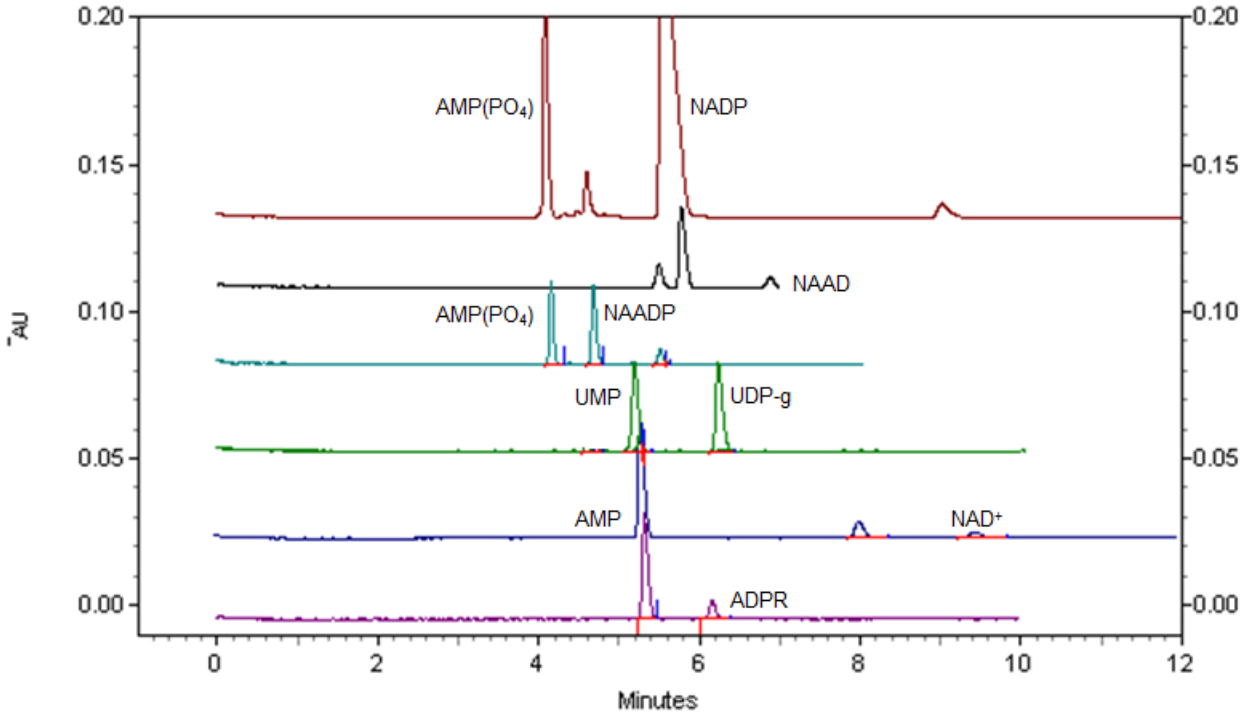

Figure 3.11: **Electropherogram representing migration time (MT)** of substrates (NAD^+, NADP, NAAD, NAADP, ADPR, UDP-glucose) and their hydrolysis products. The operation conditions were designed to investigate anions through electro-kinetic injection under -6kv voltage. Compounds containing more negative charge due to the phosphate group should appear first, e.g. tri- then -di and finally monophosphate-containing compounds. However, in this case, variation was observed in MT. NAD^+ and NAAD, despite having two phosphates, their flow through the capillary was delayed, and their MT significantly increased compared to AMP. Phosphorylated analogues of NAD^+ and NAAD, NADP and NAADP, respectively, appeared quickly in 5 min due to extra phosphate on the northern ribose. The positive charge of nicotinamide and nicotinic acid moieties may have a role in this delayed migration.

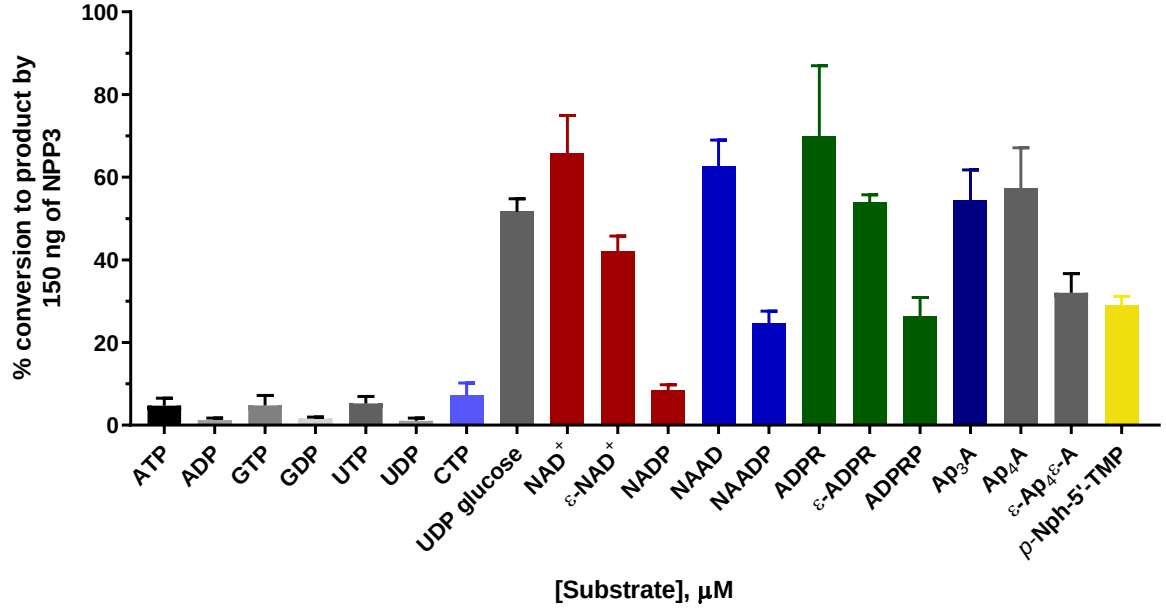

Figure 3.12: Hydrolysis of substrates by purified human NPP3. Three independent tests were performed in duplicate, and the data are presented as mean ± SEM.

Table 3.9: Kinetic parameter of NPP3 vs. diverse substrates

	Human soluble NPP3[a,b]			**Rat sol NPP3[c]**
Substrate	(K_m ± SEM) µM	(K_{cat} ±*SEM*) s^{-1}	(K_{cat}/K_m) $10^3.M^{-1}.\ s^{-1}$	(K_{cat}/K_m) $10^3.M^{-1}.\ s^{-1}$
NAD^+	41.8 ± 0.2	4.65 ± 0.21	**112**	**107[b]**
ε-NAD^+	40.3 ± 1.2	1.09 ± 0.01	**27.2**	N. D. [d]
NAAD	60.9 ± 4.7	3.91 ±0.44	**64.2**	N. D. [d]
ADPR	29.1 ± 6.9	8.23 ± 0.84	**283**	N. D. [d]
ε-ADPR	7.75 ± 0.44	1.04 ± 0.02	**134**	N. D. [d]
Ap_3A	27.5 ± 3.9	2.82 ± 0.11	**102**	**565 [b]**
Ap_4A	54.4 ± 10.2	3.74 ± 0.2	**68.7**	**810 [b]**
ε-Ap_4ε-A	25.7 ± 2.5	0.76 ± 0.05	**29.7**	N. D. [d]
p-NPh-5'-TMP	380 ± 8	5.95 ± 0.01	**15.6**	N. D. [d]

[a] All values represent mean ± SEM of three independent tests, each with duplicate observations determined by CE assay.

[b] Tests were performed under alkaline reaction conditions. K_{cat} will vary when physiological pH and better-purified protein are employed

[c] Literature value from rat soluble NPP3 (Döhler et al., 2018) .

[d] not determined

The kinetic data for natural substrate ADPR, NAD^+, Ap_4A, and their fluorescence analogues ε-ADPR, ε-NAD^+, and ε-Ap_4ε-A demonstrated specificity constant values in a similar range. However, the enzymes hydrolyse natural substrates comparatively better.

The same enzyme source and protein batch were used. The protein showed consistent product turnover throughout the experiment. However, an acceptable product turnover for Ɛ-NAD^+, Ɛ-Ap_4Ɛ-A, and Ɛ-ADPR emphasised the utility of the fluorescence HTS assays as a good alternative to *p*-NPh-5'-TMP and malachite green assays. It will be useful for screening large compound libraries, particularly in the search for competitive inhibitors to use a similar substrate concentration as the K_m value (Freundlieb et al., 2014). The comparison of the kinetic parameters of the enzyme for both substrates with their fluorescence analogues is given in Table 3.9. Ɛ-NAD^+ bound well with the enzyme, showing a higher affinity for the enzyme with favourable K_{cat} values. The determined K_m for the soluble enzyme is observed as **40.1 ± 1.8** µM, turnover number K_{cat} of 1.09 ± 0.01 $s^{-1,}$ and specificity constant (K_{cat}/K_m) of **27.2** x 10^3 $M^{-1}s^{-1}$ reflecting a better conversion of the substrate to the product as compared to *p*-NPh-5'-TMP. Ɛ-ADPR is potently hydrolysed by the enzyme with a favourable kinetics profile. The determined K_m value is observed to be **7.75 ± 0.43** µM, the substrate turnover number (K_{cat}) is 1.04 ± 0.02 $s^{-1,}$ and the specificity constant ratio is **134 x 10^3** $M^{-1}s^{-1}$. However, at higher substrate concentrations, i.e. 250 µM and above, incomplete substrate retention is observed in the supernatant following treatment with precipitation buffer. Possibly, at higher substrate concentrations, part of the substrate may be non-specifically precipitated by precipitation buffer; therefore, conducting a K_m determination to a maximum concentration of 150 – 200 µM is recommended. The enzyme could also potently hydrolyse ƐAp_4ƐA with a K_m of **25.7 ± 2.5** µM, K_{cat} 0.76 ± 0.05 s^{-1}, and specificity constant of **29.7** x 10^3 $M^{-1}s^{-1}$. Data further reflect the correlation of potent hydrolysis of NaAD, which mainly has an intracellular role as an intermediate in NAD^+ biosynthesis; however, the presence of an extracellular NaAD can't be denied considering numerous cellular transport processes taking place alongside cellular necrosis of inflamed and cancerous cells. Further investigation of its role in inflammation, immunomodulation and inter- and intracellular communication will be fascinating. In general, we observed potent hydrolysis of NAD^+ and similar substrates. Comparable product turnover was observed for natural substrates and their fluorescence analogues.

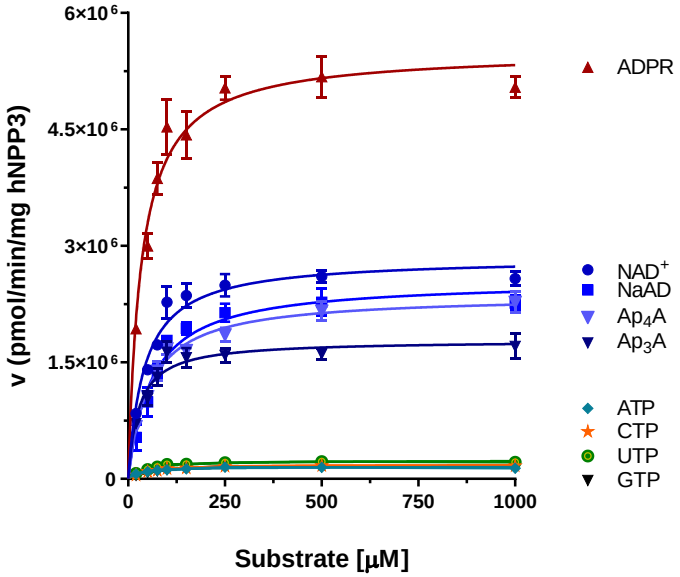

Figure 3.13: Michaelis-Menten constant for variable nucleotidic substrates vs human NPP3.

We investigated whether the membrane-bound NPP3 showed a different behaviour towards these substrates. The tests were performed under analogous conditions as used for the soluble enzymes, and they showed pretty similar K_m values of 41.1 ± 5.5 µM towards Ɛ-NAD$^+$. K_{cat} values were impossible to compare since protein concentration was not measured for membrane-bound enzymes. The substrate is accommodated equally in the binding pocket of the membrane-bound and the soluble variant of the enzyme, which makes it suitable for working with cell lines overexpressing NPPs. For the cell lines with concomitant expression of CD73 and NPPs, the Ɛ-ADPR assay is not applicable since CD73 further hydrolyses Ɛ-AMP to Ɛ-adenosine, which doesn't precipitate using our precipitation buffer. Therefore, the substrate can't be separated from the product. However, for these cell lines, both Ɛ-NAD$^+$ and Ɛ-Ap$_4$Ɛ-A suit well, and a high product conversion was observed mainly for NPP1 and NPP3. A comparison of kinetics and specificity constant data showed that the fluorescent substrates are well hydrolysed by NPPs. The determined K_m *is* in a similar range to the natural substrates, making these newly developed assays highly efficient and sensitive alternatives to the time-consuming CE or HPLC assays. The assays are more suitable than calourimetric *p*-NPh-5'-TMP and malachite green assays and are applicable in standard lab settings.

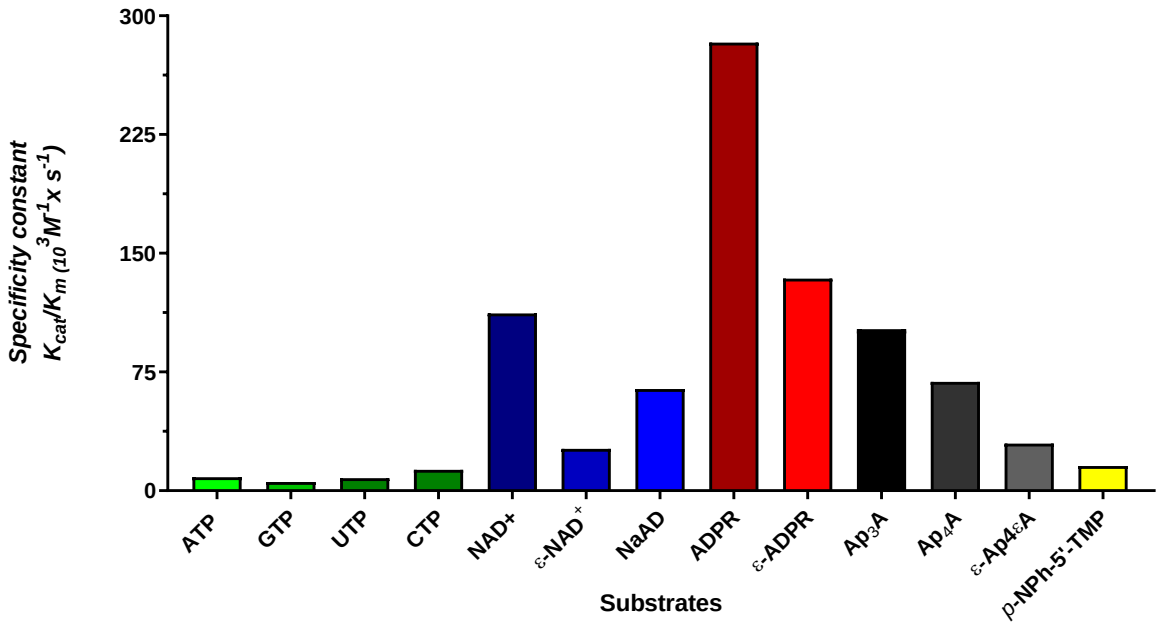

Figure 3.14: Comparison of specificity constant ratio with diverse substrates for NPP3.

We further evaluated the applicability of these assays towards monitoring cancer cell lines, including U87, TNBC, and astrocytoma cells, using ε-NAD^+ as substrate. Cell lines cultured in a suitable medium were harvested and washed multiple times with PBS and resuspended in the CHES/HEPES reaction buffer (pH 9.2/7.4) to a variable final cell count (300,000 – 15,000 cells/vial). The reaction started with adding the substrate ε-NAD^+ (20 µM) and incubated for 30 min at 37 °C. The increase in fluorescence units showed the formation of the product owing to NPP activity. U87 and TNBC showed a marked increase in fluorescence units for each detection point; however, slow product turnover is observed in astrocytoma cell lines. The buffer pH impacts the overall hydrolysis of the substrates, and less product turnover was observed at a pH of 7.4 compared to a pH of 9.2. However, the tumour microenvironment is linked to a marked difference in intra/extracellular pH due to the extracellular environment's hypoxia-induced acidosis and intracellular alkalosis (Kim et al., 2010; Persi et al., 2018). Therefore, a sensitive assay that gives high product turnover at neutral to slightly acidic pH would be advantageous in analysing these enzymes and cell lines close to natural conditions. We further analysed the maximum velocity for TNBC and astrocytoma cell lines by applying eight different ε-NAD^+ concentrations (5 – 250 µM) with 100,000 live cells/well of TNBC and 300,000 cells of

astrocytoma cell line using HEPES reaction buffer with neutral pH conditions (reaction conditions were the same as described previously). High product turnover was observed for TNBC, which suggests a higher NPP1 expression as compared to astrocytoma cells (Figure 3.15)

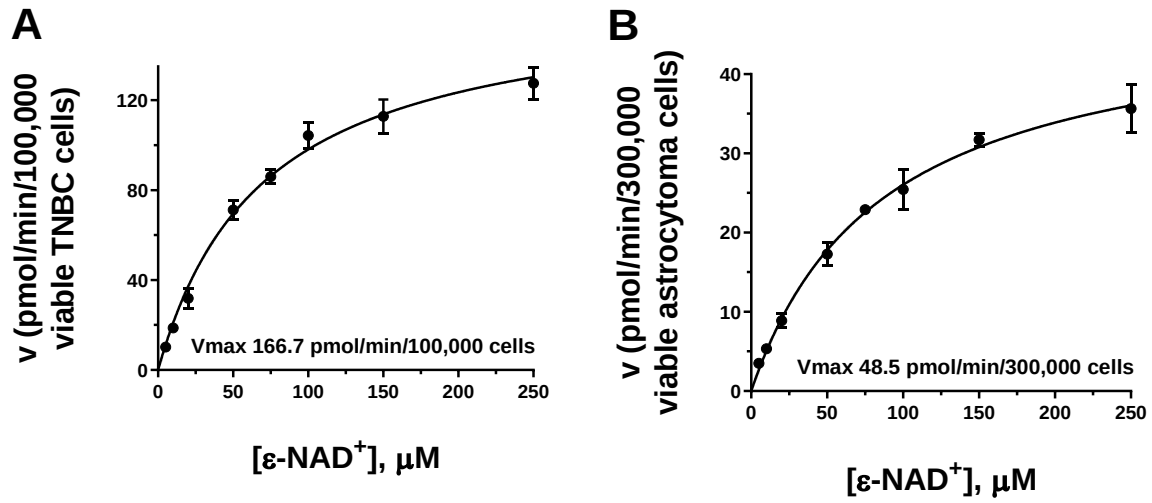

Figure 3.15: **Hydrolysis of ε-NAD⁺** (5 – 250 μM) using either (A) 100,000 live and viable cells of triple-negative breast cancer cells or (B) 300,000 live and viable astrocytoma cells. Three independent tests were performed using duplicate observations.

Potent hydrolysis of ε-NAD⁺ further increased our interest in testing if this is due to NPPs or CD38 since most ectonucleotidases are expressed in close localities and work in tandem. Therefore, we treated U87 and TNBC cell lines with ε-NAD⁺ in the presence of the acyclic ATP derivative adenine-(methoxy)ethoxy-Pα,α-dithio-triphosphate previously published as a potent inhibitor for recombinant NPP1. Tests were performed under described assay conditions using CHES reaction buffer and alkaline pH conditions. The enzymatic activity was inhibited with IC_{50} values in a similar range as 1.80 μM for recombinant NPP1, 0.368 μM for U87, and 0.317 μM for TNBC, both tested against ε-NAD⁺ (Figure 3.16). The same compound was previously published by our group, where IC_{50} of 2.49 ± 0.07 μM was recorded using ATP as a substrate (Nassir, Mirza, et al., 2019). This result further emphasises the utility of ε-NAD⁺ assay for NPP1 as the comparable inhibition was observed for natural substrate ATP and ε-NAD⁺ (2.49 vs 1.80 μM)

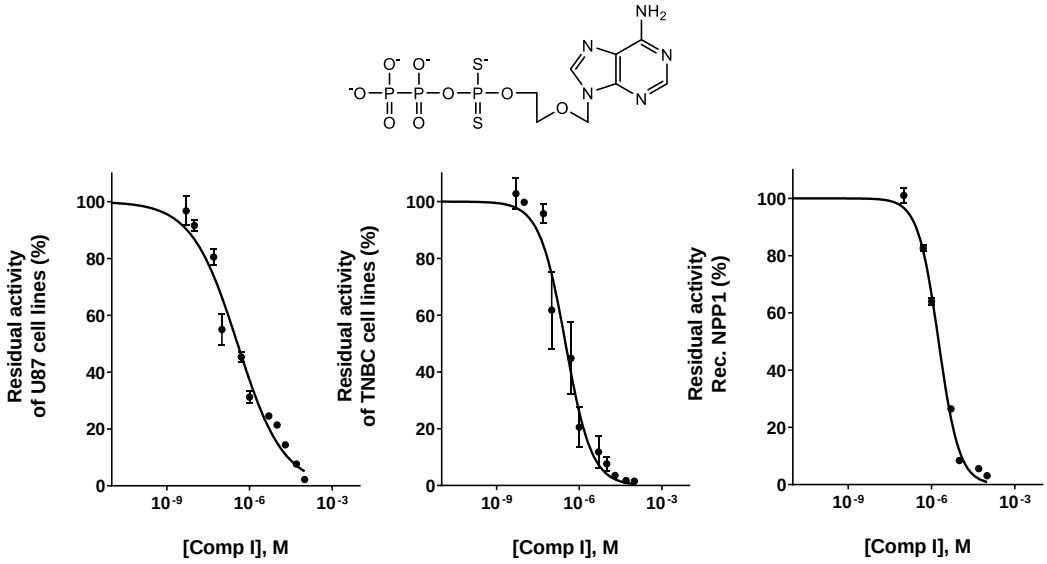

Figure 3.16 Concentration-dependent inhibition by compound I to hinder substrate hydrolysis in recombinant NPP1 U87, TNBC cell lines. The IC_{50} value was recorded at 1.80 ± 0.02 µM, for U87 0.368 ± 0.060 µM, and for TNBC 0.371 ± 0.087 µM.

3.3 Structure-activity relationship (SAR) studies of newly synthesised *p*-aminobenzenesulfonamide derivatives

As part of a new SAR campaign, we synthesised thirteen new compounds, mainly modifying the core skeleton. The novel *p*-aminobenzenesulfonamide derivatives were screened at 50 µM final concentration using three assays with *p*-NPh-5'-TMP, Ɛ-$NAD^{+,}$ and NAD^+ as substrate. Compounds were tested under physiological and alkaline pH using a similar reaction buffer [HEPES10 mM (pH 7.4) $CaCl_2$ 0.5 mM and $ZnCl_2$ 0.01 mM), CHES 10 mM (9.2) $CaCl_2$ 2 mM, $MgCl_2$ 1 mM] vs. *p*-Nph-5'-TMP, Ɛ-$NAD^{+,}$ and NAD^+. (See "Material and method section"). Furthermore, the CE assay is essential for confirmatory testing of IC_{50} values of the most potent inhibitors.

Screening results vs *p*-Nph-5'-TMP showed potent inhibition of the enzyme activity under alkaline buffer conditions, and a significantly reduced inhibition was noticed at physiological pH conditions. Under alkaline reaction conditions, the most potent inhibition of (91 %) was observed for NBO-MKA-29, (85 %) for PZB08720015A, and (82 %) for PZB08721014A. Compound NBO-MKA-10 and PZB08721017A showed equal inhibition of 76 % and 72 %, respectively. The inhibition (%) reduced significantly when testing was performed under physiological pH conditions (Table 3.11). This phenomenon was

previously reported for sulphonamide functionalities at pH 7.4 and 9.0 (Carozza et al., 2020). The amino group of sulphonamides is deprotonated under alkaline pH conditions; therefore, the compounds are negatively charged and can bind well with Zn^{2+} of the active site. However, the amino group is not deprotonated under neutral to acidic pH, exhibiting a lower affinity for Zn^{2+}. Why do most research groups use alkaline pH conditions when working with NPPs? Because the enzyme shows optimum activity under alkaline conditions and better product turnover is observed compared to neutral pH conditions. Nonetheless, an effective cancer immunotherapeutic must be potent at a physiological pH of 7.4 or even lower because of the acidic tumour microenvironment (Lin et al., 2019). The screening was additionally performed towards the natural substrate NAD^+ and its fluorescent analogue ε-NAD^+. Similar behaviour was observed with higher enzymatic activity under alkaline conditions than at neutral. When tested with NAD^+/ε-NAD^+, we observed that scaffolds like NBO-MKA-29, -10, PZB08720015A, and PZB08721017A retained some of their inhibitory potency at pH 7.4 though less as compared to pH 9.2; however, we didn't observe a total loss of activity. Scaffolds like PZB08721014A, PZB08721020A, PZB08721020A, PZB08720017A, and, to some extent, PZB08720015A showed fluorescence signals in the 300 – 410 nm; therefore, these compounds were tested using the natural substrate NAD^+. Five intermediate products such as NBO-MKA-05, -08, -10, -15, and -29, were also included where compounds -10 and -29 showed potent inhibition of the enzyme activity, and this inhibition was in a similar range under pH 7.4 and 9.2. We applied a third assay utilising natural substrate NAD^+ through CE assay to confirm our findings with ε-NAD^+. A relatively consistent replication of the results was observed for physiological and alkaline reaction conditions. The results of the screening campaign are summarised in Table 3.11.

A significant difference in the IC_{50} values was noted primarily due to the pH of the reaction buffer. This difference was more relevant for PZB08720015A, where an approximately 65-fold difference was observed (vs *p*-NPh-5'-TMP). Although PZB08720015A showed comparatively lower inhibition than NBO-MKA-29 at 50 µM, the IC_{50} values showed different outcomes. One possible justification is the solubility of both compounds. The latter compound was better soluble in 10% DMSO until the higher concentration of 500 µM; however, the former compound was not completely soluble at 50 µM because of two sulfonamide moieties. The solubility of PZB08720015A improved considerably in the

lower concentration. That could be why higher inhibition was observed at five µM compared to 50 µM for PZB08720015A (see Table 3.12, Figure 3.17). However, both the compounds, i.e. PZB08720015A and NBO-MKA-29, are good starting points for further lead optimisation.

Table 3.10 Percentage inhibition of human NPP3 using different substrates under neutral and alkaline pH

Compound	**% inhibition**					
	***p*-NPh-5'-TMP 400 µM**		***ε*-NAD$^+$ 40 µM**		**NAD$^+$ 100 µM**	
pH	Neutral	Alkaline	Neutral	Alkaline	Neutral	Alkaline
PZB08721015A	28 ± 2	17 ± 2	37 ± 1	18 ± 3	32 ± 8	18 ± 1
PZB08721013A	12 ± 1	25 ± 1	49 ± 1	57 ± 2	7 ± 3	32 ± 1
PZB08721014A	44 ± 11	82 ± 2	NA*	NA*	49 ± 1	81 ± 1
PZB08721016A	22 ± 1	29 ± 4	37 ± 1	39 ± 5	27 ± 15	28 ± 5
PZB08721017A	27 ± 3	72 ± 1	NA*	NA*	61 ± 4	91 ± 1
PZB08721018A	-2 ± 1	17 ± 1	NA*	NA*	3 ± 12	17 ± 5
PZB08721020A	-2 ± 1	-4 ± 2	NA*	NA*	-4 ± 5	1 ± 3
PZB08720015A	62 ± 3	85 ± 1	NA*	NA*	71 ± 14	86 ± 6
NBO-MKA-05	2 ± 1	-4 ± 1	21 ± 2	-9 ± 6	1 ± 9	-4 ± 0
NBO-MKA-08	2 ± 1	-2 ± 1	22 ± 2	-1 ± 9	8 ± 15	3 ± 3
NBO-MKA-10	55 ± 2	76 ± 1	63 ± 1	47 ± 3	61 ± 2	84 ± 1
NBO-MKA-15	3 ± 2	-1 ± 1	23 ± 3	12 ± 2	9 ± 16	1 ± 2
NBO-MKA-29	77 ± 1	91 ± 1	77 ± 1	60 ± 1	76 ± 5	93 ± 1

*Assay is not suitable for screening fluorescent compounds.

We further wanted to evaluate IC_{50} values for selected compounds using that natural substrate NAD$^+$ and a CE assay. Tests were performed at physiological pH. The results with the natural substrate correlated well with those using the artificial substrate *p*-NPh-5'-TMP. Compound PZB08721017A showed comparable inhibition potency as compound PZB08720015A, 1.97 vs 1.13 µM (See Figure 3.18)

Table 3.11 Differences in the IC_{50} values dependent on pH

	IC_{50}, nM (Mean ± SD) *p*-NPh-5'-TMP 400 µM	
	Neutral	Alkaline
PZB08720015A	3265 ± 422	52.1 ± 4.6
NBO-MKA-29	5991 ± 527	997 ± 89

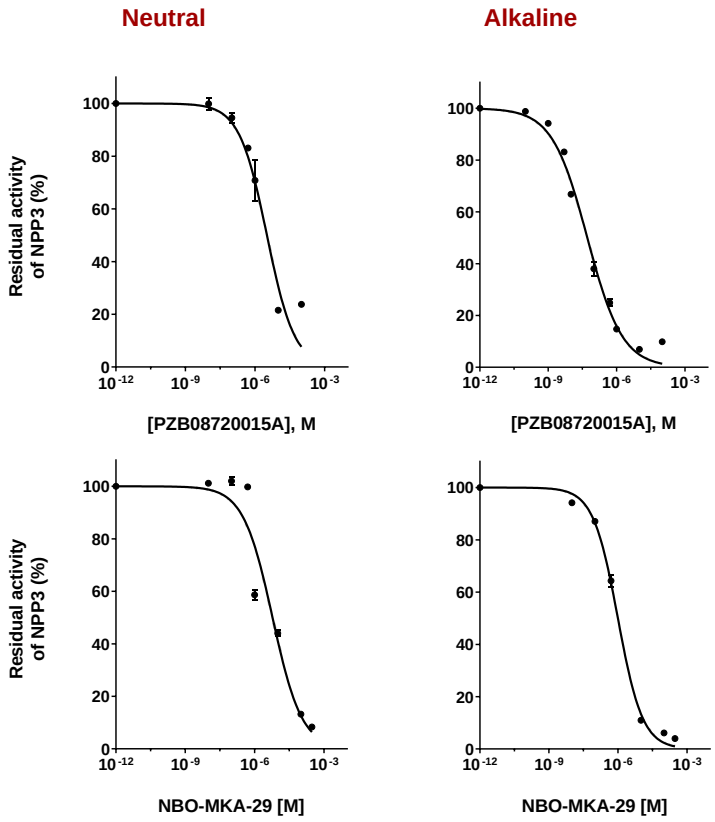

Figure 3.17 Concentration-dependent inhibition curve for the two most potent inhibitors at pH 7.4 and 9.2 using *p*-NPh-5'-TMP 400 µM as substrate. Three independent tests were performed with triplicate observations. Data are presented as mean ± SEM.

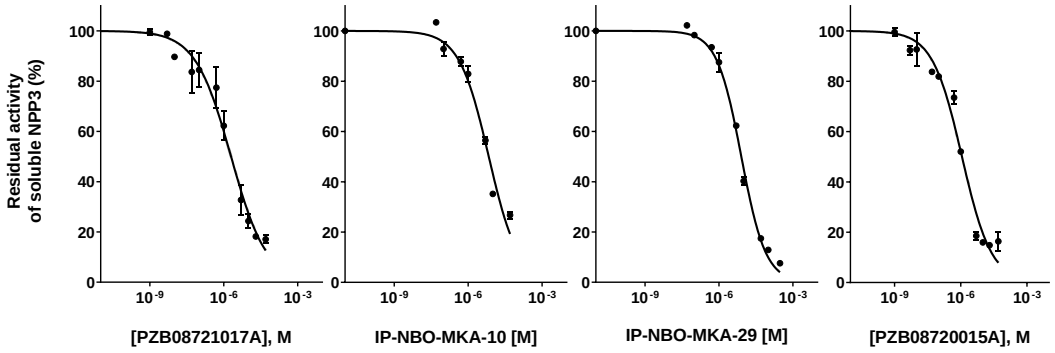

Parameters	PZB08721017A	10	29	PZB08720015A
IC_{50} µM	1.97 ± 0.06	8.08 ± 1.03	6.83 ± 0.91	1.13 ± 0.05
K_i µM	0.562 ± 0.017	2.30 ± 0.29	1.95 ± 0.26	0.322 ± 0.014

Figure 3.18: **IC_{50} curve for selected compounds vs NAD^+ as a substrate under physiological pH**. Three independent tests were performed in duplicate observations. Data are presented as mean ± SD. The K_m for soluble NPP3 vs. NAD^+ is 41.8 ± 0.2 µM.

3.7 Selectivity testing vs. multiple ectonucleotidases

The subsequent selectivity testing was performed for selected novel NPP3 inhibitors against other NPP family members, including NPP1, NPP4, and NPP5. NPP3 was included for comparison. NAD^+ 100 µM was used as a substrate. Other ectonucleotidases such as CD38 (NADase), CD39 (NTPDase1), and CD73 (ecto-5'-nucleotidase) using the following substrates: NAD^+, 100 µM for CD38, ATP, 100 µM for CD39, and ε-AMP, 20 µM for CD73 respectively. A CE assay *vs.* the natural substrate NAD^+ at pH 7.4 was performed, and the reaction conditions were comparable. As seen in Figure 3.19, the selected inhibitors mostly did not reach 50 % inhibition at 50 µM concentration. A noticeable inhibition was observed for NBO-MKA-29 and -10 for NPP1, with approximately 50 % inhibition at the tested concentration. The other noticeable inhibition was for PZB08721017A vs. NPP4, where close to 30 % inhibition was observed. Selectivity data reflects that these novel compounds are selective for inhibiting NPP3 and only marginally impact the other human enzymes. Selectivity tests with previously published comp II showed that the compound was equally potent towards CA-II and IX aa of NPP3; therefore, it is recommended to further test these derivatives against these enzymes, along with alkaline phosphatases (AP).

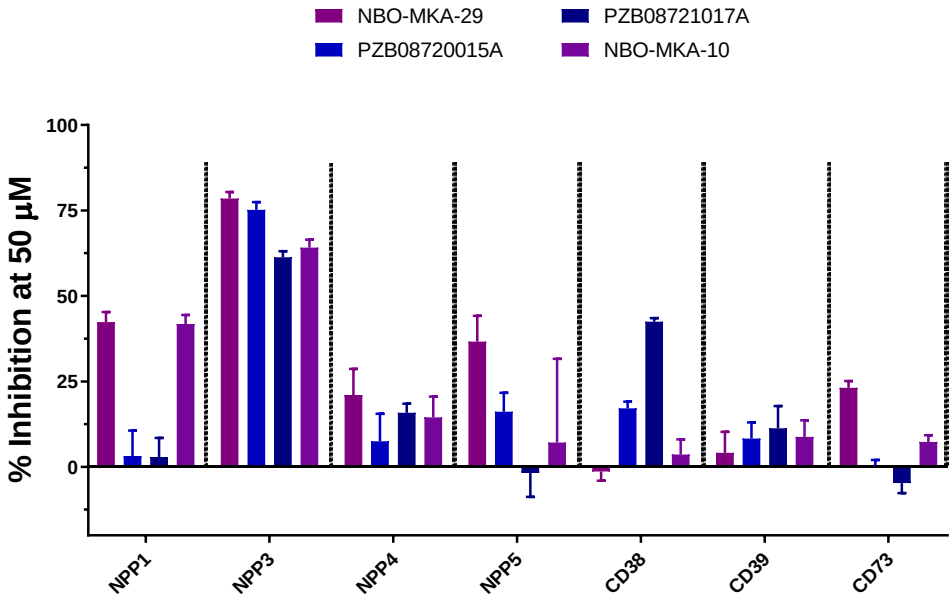

Figure 3.19: Selectivity testing vs multiple ectonucleotidases.

3.7 Mechanism of inhibition

The amino-benzenesulfonamides had demonstrated a competitive mechanism of inhibition towards NPP3 (S. Lee et al. 2021). Since PZB08720015A shares structural similarity to compound II, in this study, our prime focus is testing the mechanism of inhibition for the NBO-MKA-29 featuring a new scaffold. The compound has a significantly different core structure and a smaller size.The inhibition type testing was performed with both natural and fluorescence substrates NAD^+ and Ɛ-NAD^+ using varying concentrations (0, ~0.5-fold, ~1-fold, and ~2-fold of IC_{50} values) of the inhibitor. The data analysed by the Haanes-Woolf plot revealed a competitive mechanism of inhibition showing parallel lines in the Hanes-Woolf plot (Figure 3.20).

3.8 IC_{50} curve for NPP3 inhibitors using multiple assays/substrates

Finally, the most potent inhibitor from the current series PZB08720015A was further analysed using various substrates *p*-NPh-5'-TMP, ATP, NAD^+, ADPR, and Ap_4A under similar reaction conditions (CHES buffer pH 9.2, inhibitor solution, incubation). The inhibitory constant (K_i) values are identical with natural and artificial substrates (Figure 3.21). Moreover, we couldn't observe any significant difference in the IC_{50} values when tested against artificial and natural substrates, e.g., *p*-NPh-5'-TMP and ATP.

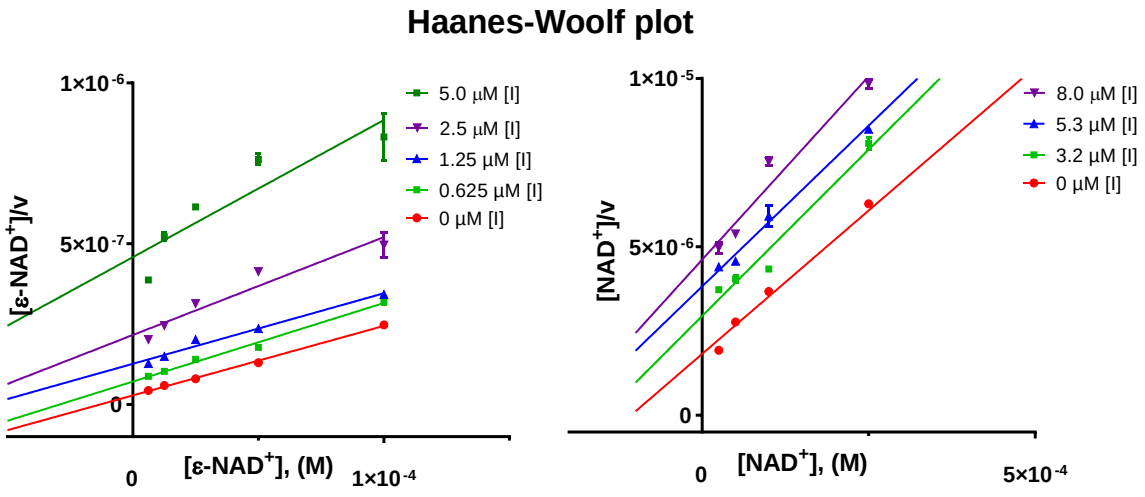

Figure 3.20: Mechanism of inhibition for NBO-MKA-29 vs. NAD^+ and Ɛ-NAD^+. Parallel lines reflect a competitive mechanism of inhibition.

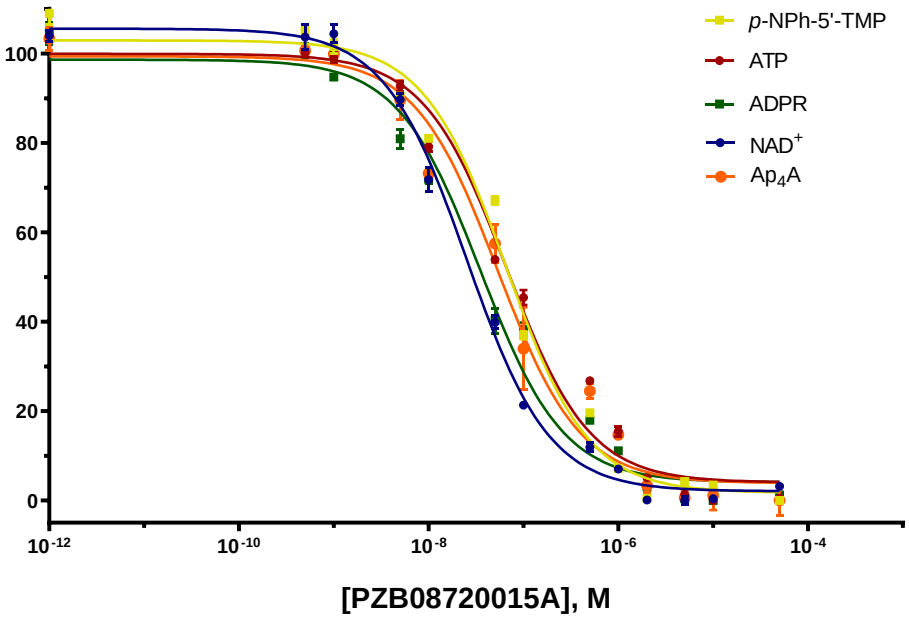

Figure 3.21: Concentration-dependent inhibition curve of PZB08720015A at human NPP3. Three independent tests were performed with duplicate observations. Data are presented as mean ± SEM.

Table 3.12: Comparison of K_i values of competitive inhibitors of NPP3 vs multiple substrates

Substrates	IC_{50} nM[a] (n 3, Mean ± SEM)	K_i nM[b] (n 3, Mean ± SEM)
	PZB08720015A	
ATP	105 ± 1	55.5 ± 0.5
p-NPh-5'-TMP	51.3 ± 8	25.0 ± 3.9
NAD^+	60.5 ± 1	17.8 ± 0.3
ADPR	119 ± 10	27.2 ± 2.2
Ap_4A	141 ± 18	50.3 ± 6.4

[a] IC_{50} is determined by nonlinear regression of data obtained from concentration-dependent inhibition of the enzyme.[b] K_i value is numerically calculated from IC_{50} values using the Cheng-Prusuff equation.

4.0. Conclusion and future objectives

In conclusion, we expressed soluble and membrane-bound NPP3. The membrane-bound enzyme required treatment with a solubilisation buffer containing mild detergents followed by affinity purification. It was observed that the enzyme retained its hydrolytic activity and substrate preference. Subsequently, the semi-purified soluble NPP3 was tested for hydrolysis of 23 potential nucleotidic substrates belonging to diverse scaffolds. Substrate

screening for NPP3 showed the enzyme's preference towards ADPR, Ap_3A, Ap_4A, NAD^+, and NAAD with a higher product turnover than the artificial substrate *p*-NPh-5'-TMP. Amongst the triphosphates, uracil and cytosine bases were preferred over adenine and guanine. Potent hydrolysis of ADPR and NAD^+ emphasises NPPs' role in the non-canonical pathway of adenosine production, predominantly active on leukocytes and lymphocytes (Ferrero et al., 2019). Hydrolysis of NAD^+ and overexpression in brain tissues requires further investigation for a neuro-degenerative role of the enzyme. Moreover, hydrolysis of Ap_3A and Ap_4A is interesting for further investigation into whether the enzyme has some vascular functions, particularly concerning overexpression on immune cells. Similarly, enhanced UDP-glucose and other sugars hydrolysis represents its role in cellular glycosylation profile and possibly in diabetes since the high expression of the enzymes is observed in the liver and pancreas (Nazawa et al., 1995).

A highly efficient and sensitive HTS fluorescence assay with ε-ADPR was developed based on selective and complete removal of the product from the reaction mixture, allowing specific determination of reduction in RFU values of the substrate at λ270/420 nm. The decrease in fluorescence intensity allows indirect estimation of the product ε-AMP being formed. ε-NAD^+ and ε-Ap_4ε-A assay is developed based on disruption of the quenching effect due to substrate hydrolysis by NPPs. The assays were validated using standard HTS assay development protocols (Taverniers et al., 2004). The sensitivity was measured by determining the limit of detection (LOD) and the limit of quantification (LOQ) values, indicating low nanomolar detection levels with a linear coefficient R^2 above 0.9994. Assay suitability for HTS was confirmed by conducting a Z'-factor test, and values appeared in line with recommended values (0.5 – 1.00). A comparison between natural substrates and their fluorescence analogues showed a similar kinetic profile; however, the product turnover was comparatively higher for the natural substrate than their ε-substituted compounds. The developed assays are better suited than the HTS *p*-NPh-5'-TMP assay in terms of sensitivity and broader applicability, particularly for testing coloured compounds. It offers robustness and greater efficiency over CE and HPLC assays concerning the time required for analysis, as 3 to 5 min are required for analysing each plate compared to 14 to 15 hours in CE and even more with HPLC assay.

NPPs have been proposed as promising drug targets in immuno-oncology. Therefore, potent and selective inhibitors are required to investigate their pathophysiological role in immune modulation and their potential role in cancer targeting further. This study found that the selective NPP3 inhibitor PZB08720015A showed higher inhibition with an IC_{50} value of 60.5 ± 1 nM vs NAD^+ (100 µM) under alkaline reaction conditions. A reduction of 20-fold was observed for neutral pH conditions yielding an IC_{50} value of 1131 ± 50 nM. This difference in IC_{50} values was even higher, i.e. 65-fold with the artificial substrate *p*-NPh-5'-TMP. Small-molecule derivative NBO-MKA-29 is a good starting point for further exploration. This discovery is of particular interest because the compound showed better solubility and good potency and offers the possibility for further structural modifications. Moreover, in contrast to other reported NPP3 antagonists, our compounds displayed high selectivity against other ectonucleotidases. So far, only a limited number of novel NPP3 inhibitors have been synthesised, and the most promising compounds should be used as starting points for future optimisation. Further exploration of a variety of core scaffolds and the introduction of different residues should be undertaken.

References

Ahmad, H., Ullah, S., Rahman, F., Saeed, A., Pelletier, J., Sévigny, J., Hassan, A., & Iqbal, J. (2020). Synthesis of biphenyl oxazole derivatives via Suzuki coupling and biological evaluations as nucleotide pyrophosphatase/phosphodiesterase-1 and -3 inhibitors. *Eur. J. Med. Chem.*, *208*, 1–9. https://doi.org/10.1016/j.ejmech.2020.112759

Albright, R. A., Chang, W. C., Robert, D., Ornstein, D. L., Cao, W., Liu, L., Redick, M. E., Young, J. I., De La Cruz, E. M., & Braddock, D. T. (2012). NPP4 is a procoagulant enzyme on the surface of vascular endothelium. *Blood*, *120*, 4432–4440. https://doi.org/10.1182/blood-2012-04-425215

Albright, R. A., Ornstein, D. L., Cao, W., Chang, W. C., Robert, D., Tehan, M., Hoyer, D., Liu, L., Stabach, P., Yang, G., De La Cruz, E. M., & Braddock, D. T. (2014). Molecular basis of Purinergic Signal Metabolism by Ectonucleotide Pyrophosphatase/Phosphodiesterases 4 and 1 and implications in Stroke. *J. Biol. Chem.*, *289*, 3294–3306. https://doi.org/10.1074/jbc.M113.505867

Anbar, H. S., El-Gamal, R., Ullah, S., Zaraei, S. O., Al-Rashida, M., Zaib, S., Pelletier, J., Sévigny, J., Iqbal, J., & El-Gamal, M. I. (2020). Evaluation of sulfonate and sulfamate derivatives possessing benzofuran or benzothiophene nucleus as inhibitors of nucleotide pyrophosphatases/phosphodiesterases and anticancer agents. *Bioorg. Chem.*, *104*, 1–11. https://doi.org/10.1016/j.bioorg.2020.104305

Andleeb, H., Hameed, S., Ejaz, S. A., Khan, I., Zaib, S., Lecka, J., Sévigny, J., & Iqbal, J. (2019). Probing the high potency of pyrazolyl pyrimidinetriones and thioxopyrimidinediones as selective and efficient non-nucleotide inhibitors of recombinant human ectonucleotidases. *Bioorg. Chem.*, *88*, 1–47. https://doi.org/10.1016/j.bioorg.2019.03.067

Antonioli, L., Blandizzi, C., Pacher, P., & Haskó, G. (2013). Immunity , inflammation and cancer : a leading role for adenosine. *Nat. Rev. Cancer*, *13*, 842–857.

Antonioli, L., Blandizzi, C., Pacher, P., & Haskó, G. (2019). The purinergic system as a pharmacological target for the treatment of immune-mediated inflammatory diseases. *Pharmacol. Rev.*, *71*, 345–382. https://doi.org/10.1124/pr.117.014878

Ausekle, E., Ejaz, S. A., Khan, S. U., Ehlers, P., Villinger, A., Lecka, J., Sévigny, J., Iqbal, J., & Langer, P. (2016). New one-pot synthesis of N-fused isoquinoline derivatives by palladium-catalyzed C-H arylation: potent inhibitors of nucleotide pyrophosphatase-1 and -3. *Org. Biomol. Chem.*, *14*, 11402–11414. https://doi.org/10.1039/c6ob02236g

Barrio, J. R., Secrist, J. A., & Leonard, N. J. et al. (1972). A Fluorescent Analog of Nicotinamide Adenine Dinucleotide. *Proc. Nat. Acad. Sci. USA*, *69*, 2039–2042.

Baykov, A. A., Evtushenko, O. A., & Avaeva, S. M. (1988). A malachite green procedure for orthophosphate determination and its use in alkaline phosphatase-based enzyme immunoassay. *Anal. Biochem.*, *171*, 266–270.

Birgbauer, E. (2021). Lysophosphatidic Acid Signalling in Nervous System Development and Function. *NeuroMol. Med.*, *23*, 68–85. https://doi.org/10.1007/s12017-020-08630-2

Blacher, E., Baruch, B. Ben, Levy, A., Geva, N., Green, K. D., Garneau-Tsodikova, S., Fridman, M., & Stein, R. (2015). Inhibition of glioma progression by a newly discovered CD38 inhibitor. *Int. J. Cancer*, *136*, 1422–1433. https://doi.org/10.1002/ijc.29095

Borza, R., Salgado-Polo, F., Moolenaar, W. H., & Perrakis, A. (2022). Structure and function of the ecto-nucleotide pyrophosphatase/ phosphodiesterase (ENPP) family: Tidying up diversity. *J. Biol. Chem.*, *298*, 1–12. https://doi.org/10.1016/j.jbc.2021.101526

Buffon, A., Casali, E. A., Cardoso, V. V., Zerbini, L. F., Robson, S. C., Sarkis, J. J. F., & Wink, M. R. (2010). Differential expression of nucleotide pyrophosphatase/phosphodiesterases by Walker 256

mammary cancer cells in solid tumors and malignant ascites. *Life Sciences*, *86*, 435–440. https://doi.org/10.1016/j.lfs.2010.01.015

Carozza, J. A., Brown, J. A., Bo, V., Mardjuki, R. E., & Smith, M. (2020a). Structure-Aided Development of Small-Molecule Inhibitors of ENPP1 , the Extracellular Phosphodiesterase of the Immunotransmitter cGAMP Article Structure-Aided Development of Small-Molecule Inhibitors of ENPP1 , the Extracellular Phosphodiesterase. *Cell Chem. Biol.*, *27*, 1–12. https://doi.org/10.1016/j.chembiol.2020.07.007

Carozza, J. A., Brown, J. A., Bo, V., Mardjuki, R. E., & Smith, M. (2020b). Structure Aided Development of Small-Molecule Inhibitors of ENPP1 , the Extracellular Phosphodiesterase of the Immunotransmitter cGAMP Development of Small-Molecule Inhibitors of ENPP1 , the Extracellular Phosphodiesterase of the Immunotr. *Cell Chem. Biol.*, *27*, 1347–1358. https://doi.org/10.1016/j.chembiol.2020.07.007

Cimpean, A., Stefan, C., Gijsbers, R., Stalmans, W., & Bollen, M. (2004). Substrate-specifying determinants of the nucleotide pyrophosphatases/ phosphodiesterases NPP1 and NPP2. *Biochem. J.*, *381*, 71–77.

Claff, T., Yu, J., Blais, V., Patel, N., Martin, C., Wu, L., Han, G. W., Holleran, B. J., Poorten, O. Van Der, White, K. L., Hanson, M. A., Sarret, P., Gendron, L., Cherezov, V., Katritch, V., Ballet, S., Liu, Z., Müller, C. E., & Stevens, R. C. (2019). Elucidating the active opioid receptor crystal structure with peptide and small-molecule agonists. *Sci. Adv.*, *5*, 1–12.

Colonna, M., Trinchieri, G., & Liu, Y. J. (2004). Plasmacytoid dendritic cells in immunity. *Nature Immunology*, *5*, 1219–1226. https://doi.org/10.1038/ni1141

Cortelazzo, A., De Felice, C., Guerranti, R., Signorini, C., Leoncini, S., Pecorelli, A., Scalabrì, F., Madonna, M., Filosa, S., Della Giovampaola, C., Capone, A., Durand, T., Mirasole, C., Zolla, L., Valacchi, G., Ciccoli, L., Guy, J., D'Esposito, M., & Hayek, J. (2016). Abnormal N-glycosylation pattern for brain nucleotide pyrophosphatase-5 (NPP-5) in Mecp2-mutant murine models of Rett syndrome. *zz*Crystal structure and substrate binding mode of ectonucleotide phosphodiesterase/pyrophosphatase-3 (NPP3). *Scientific Reports*, *8*, 10874. https://doi.org/10.1038/s41598-018-28814-y

Dong, H., Maddux, B. A., Altomonte, J., Meseck, M., Accili, D., Terkeltaub, R., Johnson, K., Youngren, J. F., & Goldfine, I. D. (2005). Increased hepatic levels of the insulin receptor inhibitor, PC-1/NPP1, induce insulin resistance and glucose intolerance. *Diabetes*, *54*, 367–372. https://doi.org/10.2337/diabetes.54.2.367

Dosch, Michel, Joël Gerber, F. J. and G. B. (2018). Mechanisms of ATP Release by Inflammatory Cells. *Int. J. Mol. Sci*, *19*, 1–16.

El-gamal, M. I., Ullah, S., Zaraei, S., Jalil, S., Zaib, S., Zaher, D. M., Omar, H. A., Anbar, H. S., Pelletier, J., & Sévigny, J. (2019). Synthesis, biological evaluation, and docking studies of new raloxifene sulfonate or sulfamate derivatives as inhibitors of nucleotide pyrophosphatase/phosphodiesterase. *Eur. J. Med. Chem.*, *181*, 1–30. https://doi.org/10.1016/j.ejmech.2019.07.063

Federico, L., Jeong, K. J., Vellano, C. P., & Mills, G. B. (2016). Autotaxin, a lysophospholipase D with pleomorphic effects in oncogenesis and cancer progression. *J. Lipid Res.*, *57*, 25–35. https://doi.org/10.1194/jlr.R060020

Ferrero, E., Faini, A. C., & Malavasi, F. (2019). A phylogenetic view of the leukocyte ectonucleotidases. In *Immunol. Lett.* (Vol. 205, pp. 51–58). Elsevier B.V. https://doi.org/10.1016/j.imlet.2018.06.008

Freundlieb, M., Zimmermann, H., & Müller, C. E. (2014). A new, sensitive ecto-5-nucleotidase assay for compound screening. *Anal. Biochem.*, *446*, 53–58.

Furuta, Y., Tsai, S., Kinoshita, M., & Fujimoto, K. (2017). E-NPP3 controls plasmacytoid dendritic cell numbers in the small intestine. *PloS One*, 1–19. https://doi.org/10.1371/journal.pone.0172509

Gangar, M., Goyal, S., Raykar, D., Khurana, P., Martis, A. M., Goswami, A., Ghoshal, I., Patel, K. V., Nagare, Y., Raikar, S., Mukherjee, A., Cyriac, R., Paquin, J. F., & Kulkarni, A. (2022). Design, synthesis and biological evaluation studies of novel small molecule ENPP1 inhibitors for cancer immunotherapy. *Bioorganic Chemistry*, *119*, 1–17. https://doi.org/10.1016/j.bioorg.2021.105549

Gasmi, L., Cartwright, J. L., & Mclennan, A. G. (1998). The hydrolytic activity of bovine adrenal medullary plasma membranes towards diadenosine polyphosphates is due to alkaline. *Biochim. Biophys. Acta, Mol. Cell Res.*, *1405*, 121–127.

Gõmez-Villafuertes, R. et. al. (2014). Ectonucleotide pyrophosphatase/phosphodiesterase activity in Neuro2A neuroblastoma cells: changes in expression associated with neuronal differentiation. *J. Neurochem.*, *131*, 290–302. https://doi.org/10.1111/jnc.12794

Gorelik, A., Liu, F., Illes, K., & Nagar, B. (2017). Crystal structure of the human alkaline sphingomyelinase provides insights into substrate recognition. *J. Biol. Chem.*, *292*, 7087–7094. https://doi.org/10.1074/jbc.M116.769273

Gorelik, A., Randriamihaja, A., Illes, K., & Nagar, B. (2017a). A key tyrosine substitution restricts nucleotide hydrolysis by the ectoenzyme NPP5. *FEBS Journal*, *284*, 3718–3726. https://doi.org/10.1111/febs.14266

Gorelik, A., Randriamihaja, A., Illes, K., & Nagar, B. (2017b). A key tyrosine substitution restricts nucleotide hydrolysis by the ectoenzyme NPP5. *FEBS Journal*, *284*, 3718–3726. https://doi.org/10.1111/febs.14266

Gorelik, A., Randriamihaja, A., Illes, K., & Nagar, B. (2018). Structural basis for nucleotide recognition by the ectoenzyme CD203c. *FEBS J.*, *285*, 2481–2494. https://doi.org/10.1111/febs.14489

Haskó, G., Linden, J., Cronstein, B., & Pacher, P. (2008). Adenosine receptors : therapeutic aspects for inflammatory and immune diseases. *Nature Reviews Drug Discovery*, *7*, 759–770. https://doi.org/10.1038/nrd2638

Hessle, L., Johnson, K. A., Anderson, H. C., Narisawa, S., Sali, A., Goding, J. W., Terkeltaub, R., & Millá, J. L. (2002). Tissue-nonspecific alkaline phosphatase and plasma cell membrane glycoprotein-1 are central antagonistic regulators of bone mineralization. *Proc Natl Acad Sci U S A* , *99*. https://doi.org/10.1073/pnas.142063399

Holger K. Eltzschig, M. V. S., & and Simon C. Robson. (2012). Purinergic Signaling during Inflammation. *N Engl j Med*, *367*, 2322–2333. https://doi.org/10.1056/NEJMra1205750

Horenstein, A. L., Chillemi, A., Zaccarello, G., Bruzzone, S., Quarona, V., Zito, A., Serra, S., & Malavasi, F. (2013). A CD38/CD203A/CD73 ectoenzymatic pathway independent of CD39 drives a novel adenosinergic loop in human T lymphocytes. *OncoImmunology*, *2*, 1–15. https://doi.org/10.4161/onci.26246

Iqbal, J., Lévesque, S. A., Sévigny, J., & Müller, C. E. (2008). A highly sensitive CE-UV method with dynamic coating of silica-fused capillaries for monitoring of nucleotide pyrophosphatase/ phosphodiesterase reactions. *Electrophoresis*, *29*, 3685–3693. https://doi.org/10.1002/elps.200800013

Jackson, E. K., Gillespie, D. G., Cheng, D., Mi, Z., & Menshikova, E. V. (2020). Characterization of the N6-etheno-bridge method to assess extracellular metabolism of adenine nucleotides: detection of a possible role for purine nucleoside phosphorylase in adenosine metabolism. *Purinergic Signalling*, *16*, 187–211. https://doi.org/https://doi.org/10.1007/s11302-020-09699-x

Jafari, B., Yelibayeva, N., Ospanov, M., Ejaz, S. A., Afzal, S., Khan, S. U., Abilov, Z. A., Turmukhanova, M. Z., Kalugin, S. N., Safarov, S., Lecka, J., Sévigny, J., Rahman, Q., Ehlers, P., Iqbal, J., & Langer, P. (2016). Synthesis of 2-arylated thiadiazolopyrimidones by Suzuki-Miyaura cross-coupling: a new class of

nucleotide pyrophosphatase (NPPs) inhibitors. *RSC Advances*, *6*, 1–39. https://doi.org/10.1039/c6ra22750c

JI-HU-Zhang, Thomas D.Y. Chung, kevin R. O. (1999). A simple statistical parameter for use in evaluation and validation of high throughput screening assays. *J. Biomol. Screening*, *4*, 67–72.

Kim, G. E. W., Ivan, M., Chiche, J., Brahimi-horn, M. C., & Pouysségur, J. (2010). Tumour hypoxia induces a metabolic shift causing acidosis : a common feature in cancer. *J. Cell. Mol.Med*, *14*, 771–794. https://doi.org/10.1111/j.1582-4934.2009.00994.x

Knowlden, S., & Georas, S. N. (2014). The Autotaxin–LPA Axis Emerges as a Novel Regulator of Lymphocyte Homing and Inflammation. *J. Immunol.*, *192*, 851–857. https://doi.org/10.4049/jimmunol.1302831

Korekane, H., Park, J. Y., Matsumoto, A., Nakajima, K., Takamatsu, S., Ohtsubo, K., Miyamoto, Y., Hanashima, S., Kanekiyo, K., Kitazume, S., Yamaguchi, Y., Matsuo, I., & Taniguchi, N. (2013). Identification of ectonucleotide pyrophosphatase/phosphodiesterase 3 (ENPP3) as a regulator of N-acetylglucosaminyltransferase GnT-IX (GnT-Vb). *J. Biol. Chem.*, *288*, 27912–27926. https://doi.org/10.1074/jbc.M113.474304

Kuhrt, D., Ejaz, S. A., Afzal, S., Khan, S. U., Lecka, J., Sévigny, J., Ehlers, P., Spannenberg, A., Iqbal, J., & Langer, P. (2017). Chemoselective synthesis and biological evaluation of arylated 2-(Trifluoromethyl) quinolines as nucleotide pyrophosphatase (NPPs) inhibitors. *Eur. J. Med. Chem.*, *138*, 816–829. https://doi.org/10.1016/j.ejmech.2017.07.017

Laketa, D., Bjelobaba, I., Savic, J., Lavrnja, I., Stojiljkovic, M., Rakic, L., & Nedeljkovic, N. (2010). Biochemical characterization of soluble nucleotide pyrophosphatase/phosphodiesterase activity in rat serum. *Mol. Cell. Biochem.*, *339*, 99–106. https://doi.org/10.1007/s11010-009-0373-1

Lecka, J. et al. (2013). Nonhydrolyzable ATP analogues as NPP1 inhibitors. *J.Med.Chem*, *56*, 8308–8320.

Lee, S., Namasivayam, V., Boshta, N. M., Perotti, A., Mirza, S., Bua, S., Supuran, C. T., & Müller, C. E. (2021a). Discovery of potent nucleotide pyrophosphatase/phosphodiesterase3 (NPP3) inhibitors with ancillary carbonic anhydrase inhibition for cancer (immuno)therapy. *RSC Med. Chem.*, *12*, 1187–1206. https://doi.org/10.1039/d1md00117e

Lee, S., Namasivayam, V., Boshta, N. M., Perotti, A., Mirza, S., Bua, S., Supuran, C. T., & Müller, C. E. (2021b). Discovery of potent nucleotide pyrophosphatase/phosphodiesterase3 (NPP3) inhibitors with ancillary carbonic anhydrase inhibition for cancer (immuno)therapy. *RSC Med. Chem.*, *12*, 1187–1206. https://doi.org/10.1039/d1md00117e

Lee, S. Y., Lévesque, S. A., Sévigny, J., & Müller, C. E. (2012). A highly sensitive capillary electrophoresis method using p-nitrophenyl 5'-thymidine monophosphate as a substrate for the monitoring of nucleotide pyrophosphatase/phosphodiesterase activities. *JJ. Chromatogr. B: Anal. Technol. Biomed. Life Sci.*, *911*, 162–169. https://doi.org/10.1016/j.jchromb.2012.10.044

Lee, S. Y., & Müller, C. E. (2017). Nucleotide pyrophosphatase/phosphodiesterase 1 (NPP1) and its inhibitors. *MedChemComm*, *8*, 823–840. https://doi.org/10.1039/c7md00015d

Lee, S. Y., Sarkar, S., Bhattarai, S., Namasivayam, V., De Jonghe, S., Stephan, H., Herdewijn, P., El-Tayeb, A., & Müller, C. E. (2017). Substrate-dependence of competitive nucleotide pyrophosphatase/phosphodiesterase1 (NPP1) inhibitors. *Front. Pharmacol.*, *8*, 1–7. https://doi.org/10.3389/fphar.2017.00054

Levesque et al. (2007). Specificity of the ecto-ATPase inhibitor ARL 67156 on human and mouse.pdf. *Br. J. Pharmacol.*, *152*, 141–150. https://doi.org/10.1038/sj.bjp.0707361

Lévesque, S. A., Lavoie, É. G., Lecka, J., Bigonnesse, F., & Sévigny, J. (2007). Specificity of the ecto-ATPase inhibitor ARL 67156 on human and mouse ectonucleotidases. *Br. J. Pharmacol.*, *152*, 141–150. https://doi.org/10.1038/sj.bjp.0707361

Lim, H. M., Heo, W., Han, J. W., Lee, M. G., & Kim, J. Y. (2018). NPP1 is responsible for potent extracellular ATP hydrolysis as NTPDase1 in primary cultured murine microglia. *Purinergic Signalling*, *14*, 157–166. https://doi.org/10.1007/s11302-018-9601-z

Lin, B., Chen, H., Liang, D., Lin, W., Qi, X., Liu, H., & Deng, X. (2019). Acidic pH and High-H 2 O 2 Dual Tumor Microenvironment-Responsive Nanocatalytic Graphene Oxide for Cancer Selective Therapy and Recognition. *ACS Appl. Mater. Interfaces*, *11*, 11157–11166. https://doi.org/10.1021/acsami.8b22487

Lopez, V., Lee, S.-Y., Stephan, H., & Müller, C. (2020a). Recombinant expression of ecto-nucleotide pyrophosphatase/phosphodiesterase4 (NPP4) and development of a luminescence-based assay to identify inhibitors. *Analyt. Biochem.*, *603*, 113774. https://doi.org/10.1016/j.ab.2020.113774

Lopez, V., Lee, S. Y., Stephan, H., & Müller, C. E. (2020b). Recombinant expression of ecto-nucleotide pyrophosphatase/phosphodiesterase 4 (NPP4) and development of a luminescence-based assay to identify inhibitors. *Anal. Biochem.*, *603*, 1–37. https://doi.org/10.1016/j.ab.2020.113774

Lopez, V., Schäkel, L., Schuh, H. J. M., Schmidt, M. S., Mirza, S., Renn, C., Pelletier, J., Lee, S. Y., Sévigny, J., Alban, S., Bendas, G., & Müller, C. E. (2021). Sulfated Polysaccharides from Macroalgae Are Potent Dual Inhibitors of Human ATP-Hydrolyzing Ectonucleotidases NPP1 and CD39. *Mar. Drugs*, *19*, 1–13. https://doi.org/10.3390/md19020051

Marco Idzko1, Davide Ferrari2, and H. K. E. (2015). Nucleotide signalling during inflammation. *Nature*, *509*, 310–317.

Morandi, F., Horenstein, A. L., Costa, F., Giuliani, N., Pistoia, V., & Malavasi, F. (2018). CD38 : A Target for Immunotherapeutic Approaches in Multiple Myeloma. *Front. Pharmacol.*, *9*, 1–9. https://doi.org/10.3389/fimmu.2018.02722

Nadel, Y., Lecka, J., Gilad, Y., Ben-David, G., Förster, D., Reiser, G., Kenigsberg, S., Camden, J., Weisman, G. A., Senderowitz, H., Sévigny, J., & Fischer, B. (2014a). Highly potent and selective ectonucleotide pyrophosphatase/ phosphodiesterase i inhibitors based on an adenosine 5′-(α or γ)-Thio-(α,β- or β,γ)-methylenetriphosphate scaffold. *J.Med.Chem*, *57*, 4677–4691. https://doi.org/10.1021/jm500196c

Nadel, Y., Lecka, J., Gilad, Y., Ben-David, G., Förster, D., Reiser, G., Kenigsberg, S., Camden, J., Weisman, G. A., Senderowitz, H., Sévigny, J., & Fischer, B. (2014b). Highly potent and selective ectonucleotide pyrophosphatase/ phosphodiesterase i inhibitors based on an adenosine 5′-(α or γ)-Thio-(α,β- or β,γ)-methylenetriphosphate scaffold. *J.Med.Chem*, *57*, 4677–4691. https://doi.org/10.1021/jm500196c

Namasivayam, V., Lee, S., & Christa, E. M. (2016a). The promiscuous ectonucleotidase NPP1: Molecular insights into substrate binding and hydrolysis. *Biochim. Biophys. Acta, Gen. Subj.*, *3*, 603–614. https://doi.org/10.1016/j.bbagen.2016.12.019

Namasivayam, V., Lee, S., & Christa, E. M. (2016b). The promiscuous ectonucleotidase NPP1: Molecular insights into substrate binding and hydrolysis. *Biochim. Biophys. Acta, Gen. Subj.*, *3*, 603–614. https://doi.org/10.1016/j.bbagen.2016.12.019

Nassir, M., Arad, U., Lee, S. Y., Journo, S., Mirza, S., Renn, C., Zimmermann, H., Pelletier, J., Sévigny, J., Müller, C. E., & Fischer, B. (2019). Identification of adenine-N9-(methoxy)ethyl-β-bisphosphonate as NPP1 inhibitor attenuates NPPase activity in human osteoarthritic chondrocytes. *Purinergic Signalling*, *15*, 247–263. https://doi.org/10.1007/s11302-019-09649-2

Nassir, M., Mirza, S., Arad, U., Lee, S., Rafehi, M., Yaw Attah, I., Renn, C., Zimmermann, H., Pelletier, J., Sévigny, J., Müller, C. E., & Fischer, B. (2019a). Adenine-(methoxy)-ethoxy-Pα,α-dithio-triphosphate inhibits pathologic calcium pyrophosphate deposition in osteoarthritic human chondrocytes. *Org. Biomol. Chem.*, *17*, 9913–9923.

Nassir, M., Mirza, S., Arad, U., Lee, S., Rafehi, M., Yaw Attah, I., Renn, C., Zimmermann, H., Pelletier, J., Sévigny, J., Müller, C. E., & Fischer, B. (2019b). Adenine-(methoxy)-ethoxy-Pα,α-dithio-triphosphate inhibits pathologic calcium pyrophosphate deposition in osteoarthritic human chondrocytes. *Org. Biomol. Chem.*, *17*(46), 9913–9923. https://doi.org/10.1039/c9ob02199j

Nassir, M., Pelletier, J., Arad, U., Arguin, G., Khazanov, N., Gendron, F. P., Sévigny, J., Senderowitz, H., & Fischer, B. (2019). Structure-activity relationship study of NPP1 inhibitors based on uracil-N1-(methoxy)ethyl-β-phosphate scaffold. *Eur. J. Med. Chem.*, *184*, 1–13. https://doi.org/10.1016/j.ejmech.2019.111754

Nazawa, J. O. J. I. I., Akamura, H. A. N., & Ano, K. I. S. (1995). Molecular Cloning and Chromosomal Assignment of the Human Brain-Type Phosphodiesterase I / Nucleotide Pyrophosphatase Gene (PDNP2). *Genomics*, *30*, 380–384.

Onyedibe, K. I., Wang, M., & Sintim, H. O. (2019). ENPP1, an old enzyme with new functions, and small molecule inhibitors-A sting in the tale of ENPP1. *Molecules*, *24*, 1–18. https://doi.org/10.3390/molecules24224192

Persi, E., Duran-Frigola, M., Damaghi, M., Roush, W. R., Aloy, P., Cleveland, J. L., Gillies, R. J., & Ruppin, E. (2018). Systems analysis of intracellular pH vulnerabilities for cancer therapy. *Nat. Commun.*, *9*, 1–11. https://doi.org/10.1038/s41467-018-05261-x

Qun Liu, Richard Graeff, Irina A. Kriksunov, Connie M. C. Lam, Hon Cheung Lee, and Q. H. (2008). Conformational Closure of the Catalytic Site of Human CD38 Induced by Calcium. *Biochem. J.*, *47*, 13966–13973. https://doi.org/https://doi.org/10.1021/bi801642q

Randall, R. J., & Lewis, A. (1951). protein measurment with the Folin phenol reagent. *J. Biol. Chem.*, *193*, 265–275.

Raza, R., Akhtar, T., Hameed, S., Lecka, J., Iqbal, J., & Sévigny, J. (2011). Identification of potent and selective human ecto-nucleotide pyrophosphatase/phosphodiesterase-3 (hNPP3) inhibitors. *Open Enzyme Inhib. J.*, *4*, 17–22. https://doi.org/10.2174/1874940201104010017

Repen, B., Schneider, E., & Alexiev, U. (2012). Optimization of a malachite green assay for detection of ATP hydrolysis by solubilized membrane proteins. *Analytical Biochemistry*, *426*(2), 103–105. https://doi.org/10.1016/j.ab.2012.04.016

Sakura, H., Nagashima, S., Nakashima, A., & Maeda, M. (1998). Characterization of Fetal Serum as a Platelet Aggregation Inhibitor in Fetal Circulation. *Thromb. Res.*, *91*, 83–89.

Schultz, M. (2018). Assays for NAD+ -Dependent Reactions and NAD+ Metabolites. *Methods Mol Biol.*, *1813*, 77–90. https://doi.org/10.1007/978-1-4939-8588-3

Semreen, M. H., El-Gamal, M. I., Ullah, S., Jalil, S., Zaib, S., Anbar, H. S., Lecka, J., Sévigny, J., & Iqbal, J. (2019). Synthesis, biological evaluation, and molecular docking study of sulfonate derivatives as nucleotide pyrophosphatase/phosphodiesterase (NPP) inhibitors. *Bioorg. Med. Chem.*, *27*, 2741–2752. https://doi.org/10.1016/j.bmc.2019.04.031

Shayhidin, E. E. et al. (2015). Quinazoline-4-piperidine sulfamides are specific inhibitors of human NPP1 and.pdf. *Br. J. Pharmacol.*, *172*, 4189–4199. https://doi.org/10.1111/bph.13204

Song, E. K., Rah, S. Y., Lee, Y. R., Yoo, C. H., Kim, Y. R., Yeom, J. H., Park, K. H., Kim, J. S., Kim, U. H., & Han, M. K. (2011). Connexin-43 hemichannels mediate cyclic ADP-ribose generation and its Ca 2+-

mobilizing activity by NAD +/cyclic ADP-ribose transport. *J. Bio. Chem*, *286*, 44480–44490. https://doi.org/10.1074/jbc.M111.307645

Stefan, C., Jansen, S., & Bollen, M. (2005). NPP-type ectophosphodiesterases: Unity in diversity. *Trends Biochem. Sci.*, *30*, 542–550. https://doi.org/10.1016/j.tibs.2005.08.005

Stefan, C., Jansen, S., & Bollen, M. (2006). Modulation of purinergic signaling by NPP-type ectophosphodiesterases. *Purinergic Signalling*, *2*, 361–370. https://doi.org/10.1007/s11302-005-5303-4

Stella, J., Bavaresco, L., Braganhol, E., Rockenbach, L., Farias, P. F., Wink, M. R., Azambuja, A. A., Barrios, C. H., Morrone, F. B., & Oliveira Battastini, A. M. (2010). Differential ectonucleotidase expression in human bladder cancer cell lines. *Urol. Oncol.: Semin. Orig. Invest.*, *28*, 260–267. https://doi.org/10.1016/j.urolonc.2009.01.035

Taverniers, I., De Loose, M., & Van Bockstaele, E. (2004). Trends in quality in the analytical laboratory. II. Analytical method validation and quality assurance. *TrAC, Trends Anal. Chem.*, *23*, 535–552.

Tsai, S. H., Kinoshita, M., Kusu, T., Kayama, H., Okumura, R., Ikeda, K., Shimada, Y., Takeda, A., Yoshikawa, S., Obata-Ninomiya, K., Kurashima, Y., Sato, S., Umemoto, E., Kiyono, H., Karasuyama, H., & Takeda, K. (2015). The Ectoenzyme E-NPP3 Negatively Regulates ATP-Dependent Chronic Allergic Responses by Basophils and Mast Cells. *Immunity*, *42*, 279–293. https://doi.org/10.1016/j.immuni.2015.01.015

Ullah, S., El-Gamal, M. I., El-Gamal, R., Pelletier, J., Sévigny, J., Shehata, M. K., Anbar, H. S., & Iqbal, J. (2021). Synthesis, biological evaluation, and docking studies of novel pyrrolo[2,3-b]pyridine derivatives as both ectonucleotide pyrophosphatase/phosphodiesterase inhibitors and antiproliferative agents. *Eur. J. Med. Chem.*, *217*, 1–13. https://doi.org/10.1016/j.ejmech.2021.113339

Ullah, S., El-Gamal, M. I., Zaib, S., Anbar, H. S., Zaraei, S. O., Sbenati, R. M., Pelletier, J., Sévigny, J., Oh, C. H., & Iqbal, J. (2020). Synthesis, biological evaluation, and docking studies of new pyrazole-based thiourea and sulfonamide derivatives as inhibitors of nucleotide pyrophosphatase/phosphodiesterase. *Bioorg. Chem.*, *99*, 1–31. https://doi.org/10.1016/j.bioorg.2020.103783

Villa-Bellosta, R., Wang, X., Millán, J. L., Dubyak, G. R., & Charles O'neill, W. (2011). Extracellular pyrophosphate metabolism and calcification in vascular smooth muscle. *Am J Physiol Heart Circ Physiol*, *301*, 61–68. https://doi.org/10.1152/ajpheart.01020.2010.-Extracellular

Wang, X., Lu, X., Yan, D., Zhou, Y., & Tan, X. (2022). Development of Novel Ecto-Nucleotide Pyrophosphatase / Phosphodiesterase 1 (ENPP1) Inhibitors for Tumor Immunotherapy. *Int. J. Mol. Sci*, *23*, 1–15. https://doi.org/https:// doi.org/10.3390/ijms23137104

Yang, S. Y., Lee, J., Park, C. G., Kim, S., Hong, S., Chung, H. C., Min, S. K., Han, J. W., Lee, H. W., & Lee, H. Y. (2002). Expression of autotaxin (NPP-2) is closely linked to invasiveness of breast cancer cells. *Clin. Exp. Metastasis*, *19*, 603–608. https://doi.org/10.1023/a:1020950420196

Yano, Y., Hayashi, Y., Sano, K., Nagano, H., Nakaji, M., Seo, Y., Ninomiya, T., Yoon, S., Yokozaki, H., & Kasuga, M. (2004). Expression and localization of ecto-nucleotide pyrophosphatase/ phosphodiesterase I-1 (E-NPP1/PC-1) and -3 (E-NPP3/CD203c/PD-Iβ/B10/ gp130RB13-6) in inflammatory and neoplastic bile duct diseases. *Cancer Letters*, *207*, 139–147. https://doi.org/10.1016/j.canlet.2003.11.002

Yung-Chi, C., & Prusoff, W. H. (1973). Relationship between the inhibition constant (KI) and the concentration of inhibitor which causes 50 per cent inhibition (I50) of an enzymatic reaction. *Biochem. Pharmacol.*, *22*, 3099–3108.

Yung, Y. C., Stoddard, N. C., Mirendil, H., & Chun, J. (2015). Lysophosphatidic Acid Signaling in the Nervous System. *Neuron*, *85*, 669–682. https://doi.org/10.1016/j.neuron.2015.01.009

Zelikman, V., Pelletier, J., Simhaev, L., Sela, A., Gendron, F. P., Arguin, G., Senderowitz, H., Sévigny, J., & Fischer, B. (2018). Highly Selective and Potent Ectonucleotide Pyrophosphatase-1 (NPP1) Inhibitors Based on Uridine 5′-P α,α -Dithiophosphate Analogues. *J.Med.Chem*, *61*, 3939–3951. https://doi.org/10.1021/acs.jmedchem.7b01906

Zhang, H. J., Ociepa, M., Nassir, M., Zheng, B., Lewicki, S. A., Salmaso, V., Baburi, H., Nagel, J., Mirza, S., Bueschbell, B., Al-Hroub, H., Perzanowska, O., Lin, Z., Schmidt, M. A., Eastgate, M. D., Jacobson, K. A., Müller, C. E., Kowalska, J., Jemielity, J., & Baran, P. S. (2024). Stereocontrolled access to thioisosteres of nucleoside di- and triphosphates. *Nat. Chem.*, *16*, 249–258. https://doi.org/10.1038/s41557-023-01347-2

Zimmermann, H. (2020). History of ectonucleotidases and their role in purinergic signaling. *Biochem. Pharmacol.*, 114322. https://doi.org/10.1016/j.bcp.2020.114322

Zimmermann, H., Zebisch, mathias, & Sträter, N. (2012). Cellular function and molecular structure. *Purinergic Signalling*, *8*, 437–502. https://doi.org/DOI 10.1007/s11302-012-9309-4

Soluble NPP3 sequence

ATGCTACTAGTAAATCAGTCACACCAAGGCTTCAATAAGGAACACACAAGCAAGATGGTAAGCGCTATTGTTTTATATGTGCTTTTG
GCGGCGGCGGCGCATTCTGCCTTTGCGGCGGATCTT**GGATCC**GCCACCATGTCACTTGGATTAGGCCTGGGGCTTGGACTCAGGAAA
CTGGAAAAGCAAGGCAGCTGCAGGAAGAAGTGCTTTGATGCATCATTTAGAGGACTGGAGAACTGCCGGTGTGATGTGGCATGTAAA
GACCGAGGTGATTGCTGCTGGGATTTTGAAGACACCTGTGTGGAATCAACTCGAATATGGATGTGCAATAAATTTCGTTGTGGAGAG
ACCAGATTAGAGGCCAGCCTTTGCTCTTGTTCAGATGACTGTTTGCAGAGGAAAGATTGCTGTGCTGACTATAAGAGTGTTTGCCAA
GGAGAAACCTCATGGCTGGAAGAAAACTGTGACACAGCCCAGCAGTCTCAGTGCCCAGAAGGGTTTGACCTGCCACCAGTTATCTTG
TTTTCTATGGATGGATTTAGAGCTGAATATTTATACACATGGGATACTTTAATGCCAAATATCAATAAACTGAAAACATGTGGAATT
CATTCAAAATACATGAGAGCTATGTATCCTACCAAAACCTTCCCAAATCATTACACCATTGTCACGGGCTTGTATCCAGAGTCACAT
GGCATCATTGACAATAATATGTATGATGTAAATCTCAACAAGAATTTTTCACTTTCTTCAAAGGAACAAAATAATCCAGCCTGGTGG
CATGGGCAACCAATGTGGCTGACAGCAATGTATCAAGGTTTAAAAGCCGCTACCTACTTTTGGCCCGGATCAGAAGTGGCTATAAAT
GGCTCCTTTCCTTCCATATACATGCCTTACAACGGAAGTGTCCCATTTGAAGAGAGGATTTCTACACTGTTAAAATGGCTGGACCTG
CCCAAAGCTGAAAGACCCAGGTTTTATACCATGTATTTTGAAGAACCTGATTCCTCTGGACATGCAGGTGGACCAGTCAGTGCCAGA
GTAATTAAAGCCTTACAGGTAGTAGATCATGCTTTTGGGATGTTGATGGAAGGCCTGAAGCAGCGGAATTTGCACAACTGTGTCAAT
ATCATCCTTCTGGCTGACCATGGAATGGACCAGACTTATTGTAACAAGATGGAATACATGACTGATTATTTTCCCAGAATAAACTTC
TTCTACATGTACGAAGGGCCTGCCCCCCGCATCCGAGCTCATAATATACCTCATGACTTTTTTAGTTTTAATTCTGAGGAAATTGTT
AGAAACCTCAGTTGCCGAAAACCTGATCAGCATTTCAAGCCCTATTTGACTCCTGATTTGCCAAAGCGACTGCACTATGCCAAGAAC
GTCAGAATCGACAAAGTTCATCTCTTTGTGGATCAACAGTGGCTGGCTGTTAGGAGTAAATCAAATACAAATTGTGGAGGAGGCAAC
CATGGTTATAACAATGAGTTTAGGAGCATGGAGGCTATCTTTCTGGCACATGGACCCAGTTTTAAAGAGAAGACTGAAGTTGAACCA
TTTGAAAATATTGAAGTCTATAACCTAATGTGTGATCTTCTACGCATTCAACCAGCACCAAACAATGGAACCCATGGTAGTTTAAAC
CATCTTCTGAAGGTGCCTTTTTTATGAGCCATCCCATGCAGAGGAGGTGTCAAAGTTTTCTGTTTGTGGCTTTGCTAATCCATTGCCC
ACAGAGTCTCTTGACTGTTTCTGCCCTCACCTACAAAATAGTACTCAGCTGGAACAAGTGAATCAGATGCTAAATCTCACCCAAGAA
GAAATAACAGCAACAGTGAAAGTAAATTTGCCATTTGGGAGGCCTAGGGTACTGCAGAAGAACGTGGACCACTGTCTCCTTTACCAC
AGGGAATATGTCAGTGGATTTGGAAAAGCTATGAGGATGCCCATGTGGAGTTCATACACAGTCCCCCAGTTGGGAGACACATCGCCT
CTGCCTCCCACTGTCCCAGACTGTCTGCGGGCTGATGTCAGGGTTCCTCCTTCTGAGAGCCAAAAATGTTCCTTCTATTTAGCAGAC
AAGAATATCACCCACGGCTTCCTCTATCCTCCTGCCAGCAATAGAACATCAGATAGCCAATATGATGCTTTAATTACTAGCAATTTG
GTACCTATGTATGAAGAATTCAGAAAAATGTGGGACTACTTCCACAGTGTTCTTCTTATAAAACATGCCACAGAAAGAAATGGAGTA
AATGTGGTTAGTGGACCAATATTTGATTATAATTATGATGGCCATTTTGATGCTCCAGATGAAATTACCAAACATTTAGCCAACACT
GATGTTCCCATCCCAACACACTACTTTGTGGTGCTGACCAGTTGTAAAAACAAGAGCCACACACCGGAAAACTGCCCTGGGTGGCTG
GATGTCCTACCCTTTATCATCCCTCACCGACCTACCAACGTGGAGAGCTGTCCTGAAGGTAAACCAGAAGCTCTTTGGGTTGAAGAA
AGATTTACAGCTCACATTGCCCGGGTCCGTGATGTAGAACTTCTCACTGGGCTTGACTTCTATCAGGATAAAGTGCAGCCTGTCTCT
GAAATTTTGCAACTAAAGACATATTTACCAACATTTGAAACCACTATT**CACCACCACCATCACCACCACCACCAC**TAA**GCGGCCGC**

Soluble NPP1 sequence

ATGCTACTAGTAAATCAGTCACACCAAGGCTTCAATAAGGAACACACAAGCAAGATGGTAAGCGCTATTGTTTTATATGTGCTTTTG
GCGGCGGCGGCGCATTCTGCCTTTGCG*GCGGATCTT***GGATCC**GCCACGAAAGAAGTTAAAAGTTGCAAAGGTCGCTGTTTCGAGAGA
ACATTTGGGAACTGTCGCTGTGATGCTGCCTGTGTTGAGCTTGGAAACTGCTGTTTAGATTACCAGGAGACGTGCATAGAACCAGAA
CATATATGGACTTGCAACAAATTCAGGTGTGGTGAGAAAAGGTTGACCAGAAGCCTCTGTGCCTGTTCAGATGACTGCAAGGAC**C**AG
GGCGACTGCTGCATCAACTACAGTTCTGTGTGTCAAGGTGAGAAAAGTTGGGTAGAAGAACCATGTGAGAGCATTAATGAGCCACAG
TGCCCAGCAGGGTTTGAAACGCCTCCTACCCTCTTATTTTCTTTGGATGGATTCAGGGCAGAATATTTACACACTTGGGGTGGACTT
CTTCCTGTTATTAGCAAACTAAAAAAATGTGGAACATATACTAAAAACATGAGACCGGTATATCCAACAAAAACTTTCCCCAATCAC
TACAGCATTGTCACCGGATTGTATCCAGAATCTCATGGCATAATCGACAATAAAATGTATGATCCCAAAATGAATGCTTCCTTTTCA
CTTAAAAGTAAAGAGAAATTTAATCCTGAGTGGTACAAAGGAGAACCAATTTGGGTCACAGCTAAGTATCAAGGCCTCAAGTCTGGC
ACATTTTTCTGGCCAGGATCAGATGTGGAAATTAACGGAATTTTCCCAGACATCTATAAAATGTATAATGGTTCAGTACCATTTGAA
GAAAGGATTTTAGCTGTTCTTCAGTGGCTACAGCTTCCTAAAGATGAAAGACCACACTTTTACACTCTGTATTTAGAAGAACCAGAT
TCTTCAGGTCATTCATATGGACCAGTCAGCAGTGAAGTCATCAAAGCCTTGCAGAGGGTTGATGGTATGGTTGGTATGCTGATGGAT
GGTCTGAAAGAGCTGAACTTGCACAGATGCCTGAACCTCATCCTTATTTCAGATCATGGCATGGAACAAGGCAGTTGTAAGAAATAC
ATATATCTGAATAAATATTTGGGGGATGTTAAAAATATTAAAGTTATCTATGGACCTGCAGCTCGATTGAGACCCTCTGATGTCCCA
GATAAATACTATTCATTTAACTATGAAGGCATTGCCCGAAATCTTTCTTGCCGGGAACCAAACCAGCACTTCAAACCTTACCTGAAA
CATTTCTTACCTAAGCGTTTGCACTTTGCTAAGAGTGATAGAATTGAGCCCTTGACATTCTATTTGGACCCTCAGTGGCAACTTGCA
TTGAATCCCTCAGAAAGGAAATATTGTGGAAGTGGATTTCATGGCTCTGACAATGTATTTTCAAATATGCAAGCCCTCTTTGTTGGC
TATGGACCTGGATTCAAGCATGGCATTGAGGCTGACACCTTTGAAAACATTGAAGTCTATAACTTAATGTGTGATTTACTGAATTTG
ACACCGGCTCCTAATAACGGAACTCATGGAAGTCTTAACCACCTTCTAAAGAATCCTGTTTATACGCCAAAGCATCCCAAAGAAGTG
CACCCCCTGGTACAGTGCCCCTTCACAAGAAACCCCAGAGATAACCTTGGCTGCTCATGTAACCCTTCGATTTTGCCGATTGAGGAT
TTTCAAACACAGTTCAATCTGACTGTGGCAGAAGAGAAGATTATTAAGCATGAAACTTTACCCTATGGAAGACCTAGAGTTCTCCAG
AAGGAAAACACCATCTGTCTTCTTTCCCAGCACCAGTTTATGAGTGGATACAGCCAAGACATCTTAATGCCCCTTTGGACATCCTAT
ACCGTGGACAGAAATGACAGTTTCTCTACGGAAGACTTCTCCAACTGTCTGTACCAGGACTTTAGAATTCCTCTTAGTCCTGTCCAT
AAATGTTCATTTTATAAAAATAACACCAAAGTGAGTTACGGGTTCCTCTCCCCACCACAACTAAATAAAAATTCAAGTGGAATATAT
TCTGAAGCTTTGCTTACTACAAATATAGTGCCAATGTACCAGAGTTTTCAAGTTATATGGCGCTACTTTCATGACACCCTACTGCGA

AAGTATGCTGAAGAAAGAAATGGTGTCAATGTCGTCAGTGGTCCTGTGTTTGACTTTGATTATGATGGACGTTGTGATTCCTTAGAG
AATCTGAGGCAAAAAAGAAGAGTCATCCGTAACCAAGAAATTTTGATTCCAACTCACTTCTTTATTGTGCTAACAAGCTGTAAAGAT
ACATCTCAGACGCCTTTGCACTGTGAAAACCTAGACACCTTAGCTTTCATTTTGCCTCACAGGACTGATAACAGCGAGAGCTGTGTG
CATGGGAAGCATGACTCCTCATGGGTTGAAGAATTGTTAATGTTACACAGAGCACGGATCACAGATGTTGAGCACATCACTGGACTC
AGCTTCTATCAACAAAGAAAAGAGCCAGTTTCAGACATTTTAAAGTTGAAAACACATTTGCCAACCTTTAGCCAAGAAGAC**TAA**GCG
GCCGC

Soluble NPP5

TCTAGAA**CACCACCACCATCACCACCACCACCAC**CCAGACCAGCAAAAGGTTCTACTAGTTTCTTTTGATGGATTCCGTTGGGATTA
CTTATATAAAGTTCCAACGCCCCATTTTCATTATATTATGAAATATGGTGTTCACGTGAAGCAAGTTACTAATGTTTTTATTACAAA
AACCTACCCTAACCATTATACTTTGGTAACTGGCCTCTTTGCAGAGAATCATGGGATTGTTGCAAATGATATGTTTGATCCTATTCG
GAACAAATCTTTCTCCTTGGATCACATGAATATTTATGATTCCAAGTTTTGGGAAGAAGCGACACCAATATGGATCACAAACCAGAG
GGCAGGACATACTAGTGGTGCAGCCATGTGGCCCGGAACAGATGTAAAAATACATAAGCGCTTTCCTACTCATTACATGCCTTACAA
TGAGTCAGTTTCATTTGAAGATAGAGTTGCCAAAATTATTGAATGGTTTACGTCAAAAGAGCCCATAAATCTTGGTCTTCTCTATTG
GGAAGACCCTGATGACATGGGCCACCATTTGGGACCTGACAGTCCGCTCATGGGGCCTGTCATTTCAGATATTGACAAGAAGTTAGG
ATATCTCATACAAATgctgaaaaaggcaaagttgtggaacactctgaacctaatcatcacaagtgatcatggaatgacgcagtgctctgaggaaa
ggttaATAGAACTTGACCAGTACCTGGATAAAGACCACTATACCCTGATTGATCAATCTCCAGTAGCAGCCATCTTGCCAAAAGAAG
GTAAATTTGATGAAGTCTATGAAGCACTAACTCACGCTCATCCTAATCTTACTGTTTACAAAAAAGAAGACGTTCCAGAAAGGTGGC
ATTACAAATACAACAGTCGAATTCAACCAATCATAGCAGTGGCTGATGAAGGGTGGCACATTTTACAGAATAAGTCAGATGACTTTC
TGTTAGGCAACCACGGTTACGATAATGCGTTAGCAGATATGCATCCAATATTTTTAGCCCATGGTCCTGCCTTCAGAAAGAATTTCT
CAAAAGAAGCCATGAACTCCACAGATTTGTACCCACTACTATGCCACCTCCTCAATATCACCGCCATGCCACACAATGGATCATTCT
GGAATGTCCAGGATCTGCTCAATTCAGCAATGCCAAGGGTGGTCCCTTATACACAGAGTACTATACTCCTCCCTGGTAGTGTTAAAC
CAGCAGAATATGACCAAGAGGGGTCA**TAA**GCGGCCGC

Chapter 4

Development and characterisation of nucleotide pyrophosphatase/phosphodiesterase inhibitors with selectivity for NPP3

Salahuddin Mirza[a], Ali Meshal, Ahmed Temirak[a], Christa E. Müller*, [a]

[a] *Pharma Center Bonn, Pharmaceutical Institute, Pharmaceutical Chemistry I, University of Bonn, An der Immenburg 4, D-53121 Bonn, Germany*

Running title: NPP inhibitors

*Address correspondence to:
Prof. Dr. Christa Müller

Pharmazeutisches Institut, Pharmazeutische Chemie I

An der Immenburg 4, D-53121 Bonn, Germany

Phone: +49-228-73-2301

Fax: +49-228-73-2567

E-Mail: christa.mueller@uni-bonn.de

Summary

Ecto-nucleotidases are expressed on the surface of many immune and tumour cells. They catalyse the hydrolysis of extracellular nucleotides such as ATP, NAD^+, dinucleotide polyphosphates, ADPR, and AMP to generate immunosuppressive adenosine. NPP1 is involved in different signalling pathways critical for tumour cell progression and metastasis, while NPP3 appears involved in allergic reactions and cancer. In Chapter 3, we reported potent and selective NPP3 inhibitors PZB08720015A and (NBO-MKA-29) bearing a sulfonamide moiety. However, we observed a > 20-fold reduction in IC_{50} values (vs NAD^+ as substrate) when physiological reaction conditions (pH 7.4) were applied as compared to alkaline conditions (pH >9.0), at which NPPs have their maximum activity. To address this decrease in potency, we bioisosterically replaced the sulfonamide functionality. The synthesised new compounds were tested at human NPP3 to evaluate their potential to block the activity of NPP3. Some of the inhibitors exhibited ancillary inhibition of human NPP1. Compounds 7a and 7b are the most potent and selective NPP3 inhibitors reported among the newly synthesised compounds. Compound 7a is an NPP3 inhibitor showing an IC_{50} value of 186 nM (vs. *p*-NPh-5'-TMP) and 98.1 nM (vs. NAD^+) (20-fold improvement compared to the lead structure PZB08720015A. Compound 7b displayed an IC_{50} value of 25.3 nM (vs *p*-NPh-5'-TMP) and 5.17 nM (vs NAD^+), approximately a 142-fold improvement compared to PZB08720015A. In addition, derivative 14 was developed as a new NPP3 inhibitor with a new scaffold. This compound showed an IC_{50} value of 465 nM (vs *p*-NPh-5'-TMP) and 302 nM (vs NAD^+), showing >15-fold increased potency compared to the corresponding sulfonamide-substituted lead structure (NBO-MKA-29). The NPP3 inhibitors developed in this study are the most potent ones reported so far, showing high activity under physiological conditions. These compounds represent novel and unique tool compounds that will be valuable for target validation studies and may be further developed as drug candidates for cancer therapy.

In addition to NPP3, compounds were also tested against NPP1, and some compounds like 9a, 9b, 10a, 10b, 11a, and 11b have shown highly potent inhibition of human NPP1. The compound 11b, in particular, has shown the IC_{50} of 77.1 ± 13.7 nM vs *p*-NPh-5'-TMP and 269 ± 34 nM vs ATP as a substrate. Another exciting candidate in the current series was compound 10b, which showed IC_{50} of 142 ± 6 nM vs *p*-NPh-5'-TMP and 909 ± 55 nM

vs ATP. The mechanism of inhibition was tested for 10b, and a competitive mode of inhibition was recorded.

1.0. Introduction

1.1. History of purinergic signaling

Purinergic signalling (PS) is a complicated system of cell membrane receptors, extracellular nucleotides, enzymes, and transporters to modulate intracellular processes. Its involvement in cellular activities under normal and pathological conditions has gained great scientific interest. Geoffrey Burnstock is credited for introducing the term "purinergic signalling" after he discovered that the purine nucleotide ATP is involved in extracellular signalling (Burnstock, 1972). However, the scientific community generally considered ATP an intracellular molecule involved in energy generation and believed it unlikely to be involved in extracellular signalling at that time. This disapproval somehow halted research in PS for several years. Geoffrey then produced another piece of research showing that ATP was co-transmitted with noradrenaline (NA) from sympathetic nerves (Burnstock & Street, 1990). The co-transmission of ATP with the neurotransmitters NA, γ-amino butyric acid (GABA), acetylcholine (Ach), glutamate, and nitric oxide (NO) is now widely accepted for peripheral and central nervous systems (Burnstock, 2012). Research on purinergic signalling significantly advanced once various subtypes of purinergic receptors were cloned and characterised. During the following years, the role of purinergic signalling in disease mechanisms was extensively studied (for further information, see Chapter 1 of this thesis). This also includes the role of certain ectoenzymes expressed on the cell membranes of immune and cancer cells called ectonucleotidases. The study of potent and targeted inhibitors of ectonucleotidases was advanced by their cloning, recombinant production, and characterisation. The pathogenic function of these enzymes, mainly nucleotide pyrophosphatases/phosphodiesterases (NPPs), will be the main focus of this chapter. In the corresponding parts of this thesis, the pathological roles of other families, such as NTPDases and NADases, will be highlighted.

1.2 Pathological role of nucleotide pyrophosphatases/phosphodiesterases (NPPs)

As described in Chapter 3, NPP1, NPP3, NPP4, and NPP5 are mainly involved in nucleotide hydrolysis. Therefore, other members of this class (NPP2, -6, and -7) are beyond the scope of this thesis. As the pathological role has been described mainly for

NPP1 and -3, only these two enzymes will be discussed here. Small molecule inhibitors of selected NPPs are summarised in Chapter 3 and will not be repeated here.

a. NPP1

i. Tissue expression

NPP1 is expressed throughout the body with variable expression levels (Borza et al., 2022). The enzyme is highly expressed in skeletal muscle tissues, including bone and cartilage, where it plays an integral role in the regulation of bone mineralisation by controlling levels of inorganic diphosphate (pyrophosphate, *ePPi)*, a mineralisation inhibitor in the extracellular matrix. In kidneys, it is mainly expressed in the proximal tubules. The enzyme is also found in fatty tissues, astrocytes (glial cells), liver, vascular smooth muscle cells, and endothelial cells of blood vessels. It is essential to consider that NPP1 expression may vary based on developmental stage, physiological conditions, and specific cellular state. The enzyme then hydrolyse ATP, UTP, CTP, GTP, nucleoside polyphosphates Ap_nA (n=2-5), NAD^+, cyclic nucleotides (cAMP, 2',3'-cGAMP) and nucleotide sugars (Namasivayam et al., 2016). NPP1's wide tissue expression and ability to hydrolyse a broad spectrum of nucleotide substrates make it a valuable target in various pathological conditions.

ii. Bone mineralisation and soft tissue calcification

NPP1 is known to modulate bone mineralisation by hydrolysing ATP to AMP. This reaction produces pyrophosphate, increasing its concentration in the extracellular environment (*PPi*). This metabolite is then transported into the matrix vesicle (MV) facilitated by cell surface-located ankylosis protein, ANKH (Mackenzie et al., 2012). On the intracellular side, it acts as an inhibitor of hydroxyapatite (HA) crystal formation and negatively impacts bone mineralisation. However, high extracellular concentrations of *ePPi* are reduced by surface-located tissue nonspecific alkaline phosphatases (TNAP), yielding P_i and maintaining homeostasis of the two metabolites. P_i crosses the cell membrane via Na^+-dependent P_i co-transporter 1 (P_iT-1) and, with the help of intracellular Ca^{2+}, promotes HA crystal formation and facilitates bone mineralisation (Murshed, 2018). NPP1's role in osteoblastic differentiation makes it an essential player in anabolic bone activity (Nam et al., 2011). Overexpression of NPP1 leads to the accumulation of ePP_i and, consequently,

the overproduction of calcium pyrophosphate dehydrate (CPPD) crystals, as observed in the synovial fluids of osteoarthritic patients (Gibilisco et al., 1985). *ePP$_i$* prevents pathological calcification of soft tissues such as blood vessels and heart valves. Several publications revealed a critical role of NPP1 in normal bone development and mineralisation. Similarly, malfunctioning of this protein can lead to severe pathological outcomes. A mutant gene for NPP1 expression leads to pathological bone calcification and significant alteration in bone mineralisation, such as generalised arterial calcification in infants (GACI) and hypophosphatemia. Approximately 40 mutations have been reported in the NPP1 gene causing GACI (Roberts et al., 2019). Malfunctioning of the NPP1 gene is related to ectopic calcifications of soft tissue that can lead to severe and life-threatening pathologies of cardiovascular systems, kidneys, and tendons. Overexpression of NPP1 and its polymorphism is reported in calcific aortic valve disease (CAVD) and its main components, valvular interstitial cells (VICs) and hypophosphatasia (Côté et al., 2012; Salles, 2020). NPP1 maintains tissue homeostasis by regulating *ePP$_i$* levels to balance bone formation and resorption. It further prevents pathological calcification in soft tissues by inhibiting the deposition of calcium phosphate crystals. Dysregulation of NPP1 due to mutations can lead to abnormal tissue mineralisation and calcification.

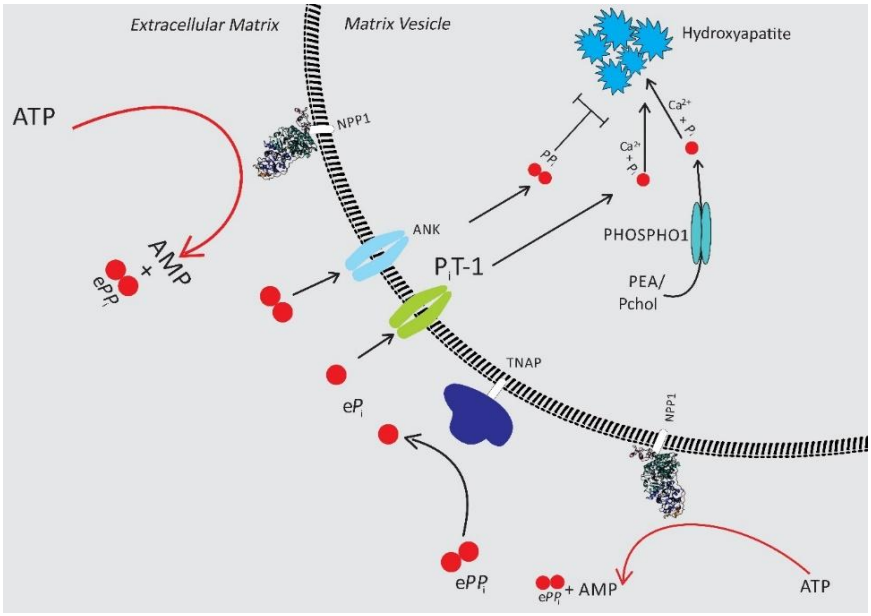

Figure 4.1: **Schematic presentation of bone mineralisation mechanism.** NPP1 and TNAP regulate this process. The figure is adopted from (Mackenzie et al., 2012)

Table 4.1: Physiological parameters that regulate bone mineralisation

Parameters	***Impact on mineralisation/mechanism***
NPP1	Inhibits/generates ePP_i
Ankylosis protein (ANK)	Inhibits/transports ePP_i
Tissue non-specific alkaline phosphatases (TNAP)	Facilitates/hydrolyses ePP_i to P_i
Na^+/phosphate co-transporter (P_it1/2)	Facilitates/P_i transport
Phosphoethanolamine/Phosphocholine Phosphatase 1 (PHOSPHO1)	Initiates/generates phosphate
Osteopontin (OPN)	Inhibits/binds hydroxyapatite (HA)
Matrix Gla protein (MGP)	Inhibits/binds hydroxyapatite (HA)

iii. Diabetes and cardiovascular ailments

Emerging evidence suggests that NPP1 expression is altered in diabetes, and its dysregulation may lead to pathology. The binding of insulin to its transmembrane glycoprotein receptor (IR) initiates intracellular signalling, also known as hormone signalling. IR consists of two α and two β subunits linked to protein with tyrosine kinase activity that phosphorylates tyrosine residues (auto-phosphorylation). Downstream signalling includes phosphorylation of insulin receptor substrate (IRS-1) and subsequent activation of phosphatidylinositol-3-kinase (PI_3K) and serine-threonine kinase-2 (Akt-2). The binding of insulin with IR modulates GLUT4 receptors on the plasma membrane. Opening of GLUT4 facilitates glucose uptake and glycogen synthesis. A large number of cellular mechanisms and energy generation processes take place as a result of intracellular glucose (Roberts et al., 2019). However, several negative modulators of insulin signalling have been described that produce *in vivo* human insulin resistance. One such inhibitory mechanism involves NPP1 through binding with the α-subunit of the IR to prevent β-subunit autophosphorylation and downstream signalling (Abate et al., 2006). Overexpression and overactivation of NPP1 are reported in type-II diabetes mellitus, particularly in the skeletal muscle, adipose tissues, and fibroblasts. Genetic analysis revealed a critical mutation (Lys121Gln) in the enzyme that was found to be higher in type-II diabetic patients and even of higher prevalence in type-II diabetes patients with coronary artery disease (CAD). The same mutation is also involved in atherosclerosis, myocardial infarction, and obesity (Bacci et al., 2005; Endler et al., 2002; Meyre et al., 2007). Overexpression of wild-type NPP1 is reported to inhibit insulin signalling in cultured HEK-

293 cells (Chin et al., 2009). NPP1$^{-/-}$mice showed insensitivity toward insulin and obesity in response to a chronic high-fed diet (Huesa et al., 2014). The extensive role of NPP1 in developing insulin resistance and inhibiting insulin signalling triggered the development of monoclonal antibodies against this enzyme as a new potential therapeutic strategy (Maddux & Goldfin, 2000).

The role of NPP1 in insulin signalling needs further exploration. Overexpression of NPP1 in fatty tissues and its upregulation in obesity has been associated with adipocyte dysfunction. These dysfunctional adipocytes then release pro-inflammatory cytokines and adipokines, such as tumour necrosis factor-alpha (TNF-α) and interleukin-6 (IL-6), which can impair insulin signalling (Chandalia & Abate, 2007; Longo et al., 2019). It is important to note that the specific role of NPP1 in insulin resistance is still evolving, and further research is needed to fully elucidate the underlying mechanisms. Insulin resistance is a complex condition influenced by various factors, and the contribution of NPP1 is likely to be interconnected with other molecular and cellular pathways involved in insulin signalling and metabolism.

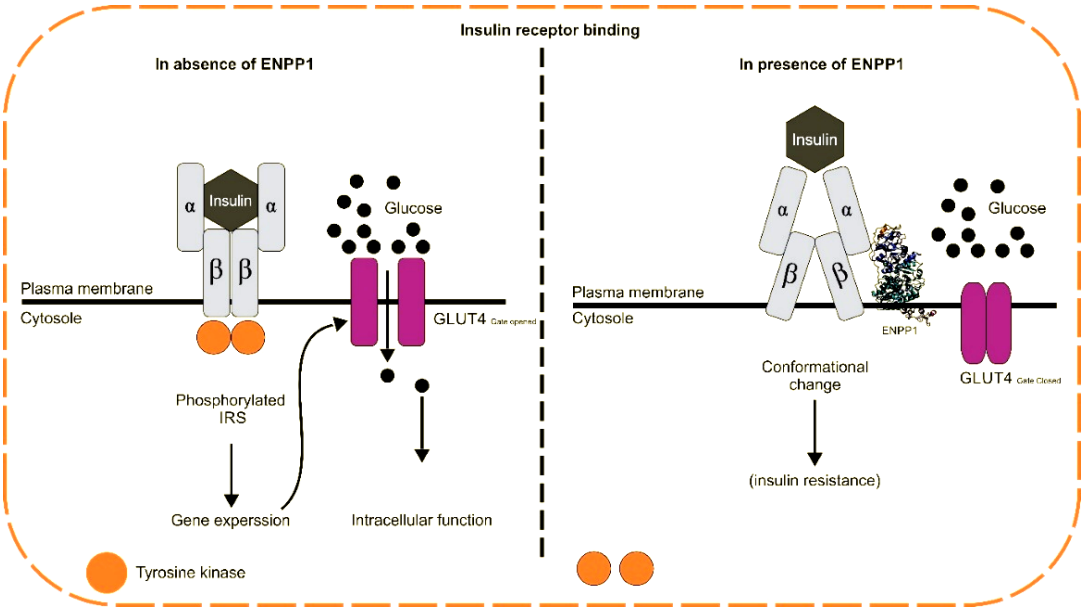

Figure 4.2: Schematic presentation of the molecular mechanism involved in insulin signalling in the absence or presence of NPP1 [modified from (Roberts et al., 2019)]

iv. Cancer

The pro-inflammatory nucleotides such as ATP, AP$_n$A, NAD$^+$, and ADPR are abundant in the tumour microenvironment (TME). These nucleotides cause an inflammatory

environment that might slow down the growth of tumours. For their defence, tumour cells overexpress ectonucleotidases such as CD39, NPP1, and CD73, which hydrolyse these nucleotides to AMP and adenosine. Anti-inflammatory and tumour-promoting adenosine then accumulate in the TME, which results in tumour progression and immune escape. There are reports of NPP1 overexpression in a variety of tumours, including human astrocytic brain tumours, glioblastoma U87 cell lines, neuroblastoma cells Neuro-2A and rat c6 glioma cells (Aerts et al., 2011; Gõmez-Villafuertes, 2014; Grobben et al., 2002; Lopez et al., 2021). The enzyme is widely expressed in the triple-negative breast cancer (TNBC) cell lines (MDA-MB-231), ovarian cancers, and astrocytoma cell lines (Chapters 2 and 3). The concomitant expression of CD73 in these cell lines, along with NPP1, allows the conversion of a large number of nucleotides to adenosine, thereby facilitating tumour cell proliferation and metastasis, as reported for Jurkat-T cell (Horenstein et al., 2013). Glioblastoma and TNBCs are considered difficult-to-treat cancers; however, simultaneous overexpression of NPP1 and CD73 on these tumours will allow targeted immunotherapy.

Apart from its expression as a membrane-bound enzyme, a soluble form of NPP1 has also been reported in the concentration range of low to high ng/ml circulating in blood plasma (Frittitta et al., 1999). This enzyme characteristic further extends its scope in immune escape and might be utilised for diagnosis. A recent study highlighting the expression of CD73 on secretory vesicles has increased interest in other ectonucleotidases that are also expressed on these vesicles (Schneider et al., 2021). Since the cell membranes of these secretary vesicles are consistent with those of tumour cells and originate from them, secretory vesicles hypothetically possess other ectonucleotidases such as NPP1 and CD39. These vesicles are much smaller and mobile, providing an additional defensive shield around tumour cells. This protective layer hydrolyses dispersed extracellular nucleotides to adenosine, further enforcing the immunosuppressant environment around tumour cells. In this way, enzymes expressed on the secretory vesicles perform a similar role as the soluble enzyme.

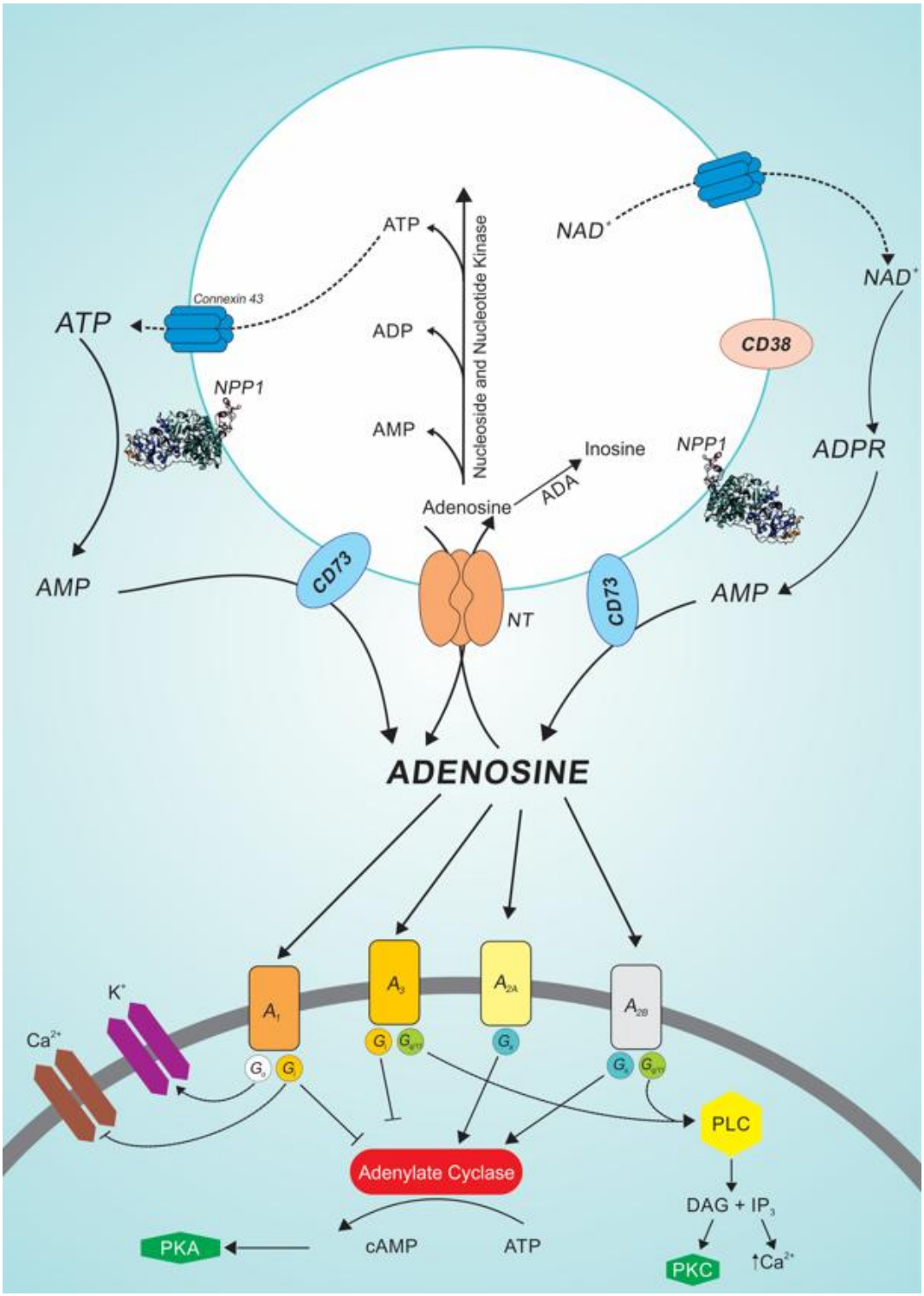

Figure 4.3: Schematic presentation of nucleotide hydrolysis by concerted action of NPP1 and CD73. Intracellular ATP and NAD^+ are transported via connexion-43 hemichannel to the extracellular side in case of hypoxia and inflammation. NPP1 potently hydrolyses both nucleotides to AMP, then hydrolysed to adenosine, leading to adenosine burden around tumour cells. Adenosine activates its receptors to produce intracellular signalling through activation of adenylate cyclase (converting ATP to cyclic AMP) and activation of the phospholipase C pathway (diacylglycerol and leading to protein kinase c activation and increase in intracellular calcium concentration).

V. STING signalling pathway

DNA typically resides in the nucleus and the mitochondria of eukaryotic cells. DNA damage or microbial infections cause DNA trafficking into the cytoplasm (cytoplasmic DNA), initiating a robust innate immune response. The cyclic GMP-AMP synthase (cGAS)–stimulator of interferon genes (STING) pathway is a critical signalling mechanism of the innate immune system, which is activated in the presence of cytoplasmic DNA. The pathway is increasingly documented to be involved in cancer (Chen et al., 2016; Vashi & Bakhoum, 2021). The entry of foreign DNA (viral, bacterial, or dead cells) into the cytoplasm activates the pathway. Reverse transcriptase enzymes convert retroviral RNA to DNA. CGAS utilises intracellular ATP and GTP upon sensing DNA to produce cyclic dinucleotides (CDNs), activating the STING protein. The release of CDNs also accompanies bacterial invasion. Being a transmembrane protein in the endoplasmic reticulum (ER), the cytosolic part of the protein acts as a dimer that contains the binding site for ligands (CDNs) such as 2',3'-cGAMP and 3',3'-cGAMP. A much higher affinity was observed for 2',3'-cGAMP to activate the STING proteins. Apart from natural agonists, efforts were made to test the synthetic agonist of STING (2',3'-cGsAsMP) by replacing oxygen of the phosphate group with sulphur, resulting in much-improved activity (Li et.al, 2015).

Upon activation, STING recruits and activates a protein complex known as TBK1 (Tank-Binding Kinase-1) that phosphorylates a transcription factor called IRF3 (Interferon Regulatory Factor-3), leading to its activation. Activated IRF3 translocate to the nucleus and promotes the expression of genes involved in the generation of pro-inflammatory cytokines such as interferon α and β (IFN-α/β), tumour necrosis factor (TNF), interleukin IL-1β, and IL-6. The cytokines contribute to the recruitment and activation of immune cells to eliminate the invading pathogens. It has been discovered that the cGAS-STING pathway plays numerous intricate roles in cancer. While its activation can boost the immune system's anti-tumor response, in some circumstances, it can also have the opposite effect, promoting tumour growth and immune evasion. Type I interferons and other immuno-stimulatory molecules are produced when the cGAS-STING pathway is activated, attracting and activating immune cells that can attack and destroy tumour cells

(Glickman et al., 2015). This activation may aid in regulating tumour growth and induce an anti-tumour immune response. In response, tumour cells can adopt strategies to avoid or reduce the cGAS-STING pathway, such as downregulating its expression, releasing substances that prevent STING from activating, or triggering the pathway's negative regulators. Due to this immune evasion, tumour cells can continue to spread and proliferate unchecked. In some circumstances, persistent activation of the cGAS-STING pathway in tumour cells or immune cells inside the tumour microenvironment might result in protracted inflammation. Prolonged inflammation can be harmful and aid in tumour angiogenesis, which is the development of new blood vessels to support tumour growth and the malfunctioning of immune cells. Regarding cancer immunotherapy, knowledge of the cGAS-STING pathway is essential. Many techniques are being developed to activate the route or circumvent its defences. These include employing STING agonists or combining immunotherapies with tactics that boost cGAS-STING signalling. These strategies are meant to increase the immune system's ability to fight cancer and make cancer therapies more effective (Decout et al., 2021; Y. Wang et al., 2020).

a. 2’,3’-cGAMP *hydrolysis*

Enzymes referred to as phosphodiesterases are responsible for the hydrolysis of 2',3'-cGAMP and control the activity of the cGAS-STING pathway. It has been established that NPP1 negatively controls the cGAS-STING signalling pathway by reducing cGAMP. The phosphodiester link between the 2'-OH and 3'-OH of 2',3'-cGAMP is hydrolysed by NPP1 (Figure 4.5), yielding AMP and GMP (Chen et al., 2016). Tumour cells may boost NPP1 expression to inhibit the immune system by reducing the cGAS-STING pathway. Over-activation of NPP1 regulates CDN concentrations, helping tumour cells escape immune identification and the immunological reactions that are supposed to fight them. It is important to remember that NPP1's role in the cGAS-STING pathway can vary depending on the cancer type and environment. CDNs have intracellular functions, and it is still a matter of scientific investigation to confirm whether intracellular or extracellular NPP1 hydrolyses these compounds. Several factors regulate the cGAS-STING pathway intricately. More research is needed to fully comprehend the relationship between NPP1 and the cGAS-STING pathway in cancer and to look into its potential therapeutic implications. The research on 2',3'-cGAMP hydrolysis is still underway, and other

enzymes or variables may have a role in controlling how much is degraded. A therapeutic option would be a small molecule inhibitor of NPP1. Synthetic agonists of the cGAS-STING pathway have attracted great interest; several are already under clinical investigation.

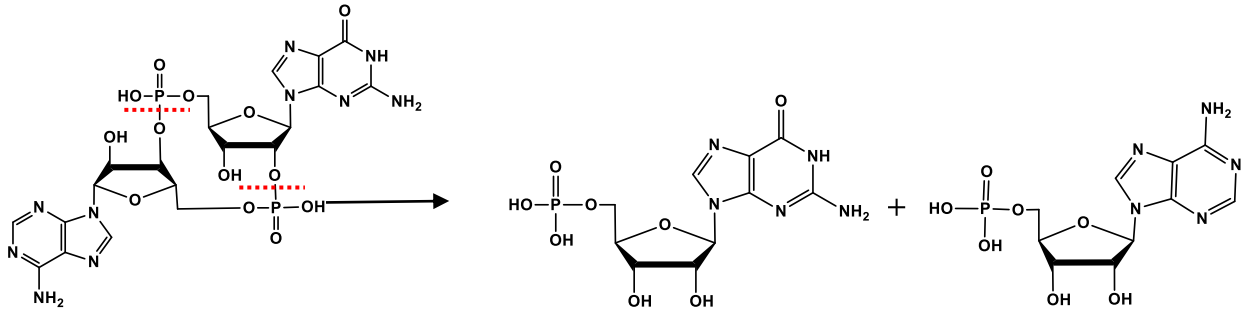

Figure 4.4: Hydrolysis of 2',3'-cGAMP by NPP1. The enzyme hydrolyses the compound at the 2'-OH and 3'-OH, producing AMP and GMP.

b. *cGAS-STING modulators*

The immune checkpoint inhibitors, chimeric antigen receptor T cells (CAR-T), have met with considerable clinical success as demonstrated by several programmed cell death receptor 1 (PD1/PD1 ligand (PD1-L)-directed antibodies or by anti-cytotoxic T lymphocyte-associated protein 4 (CTLA-4) antibodies that have received approval as cancer therapies (Ding et al., 2020). Due to limited tumour immunogenicity, most malignancies have modest clinical response rates toward these ICIs. Due to this, there is a need for more potent and selective inhibitors and activators of different pathways involved in metastasis. This section provides an updated analysis of advancements in small-molecule activators targeting the cGAS-STING signalling pathway as a potential immunostimulatory therapy. It is crucial to look at both activators and inhibitors of this signalling axis and their therapeutic potential to fully comprehend the interaction landscape.

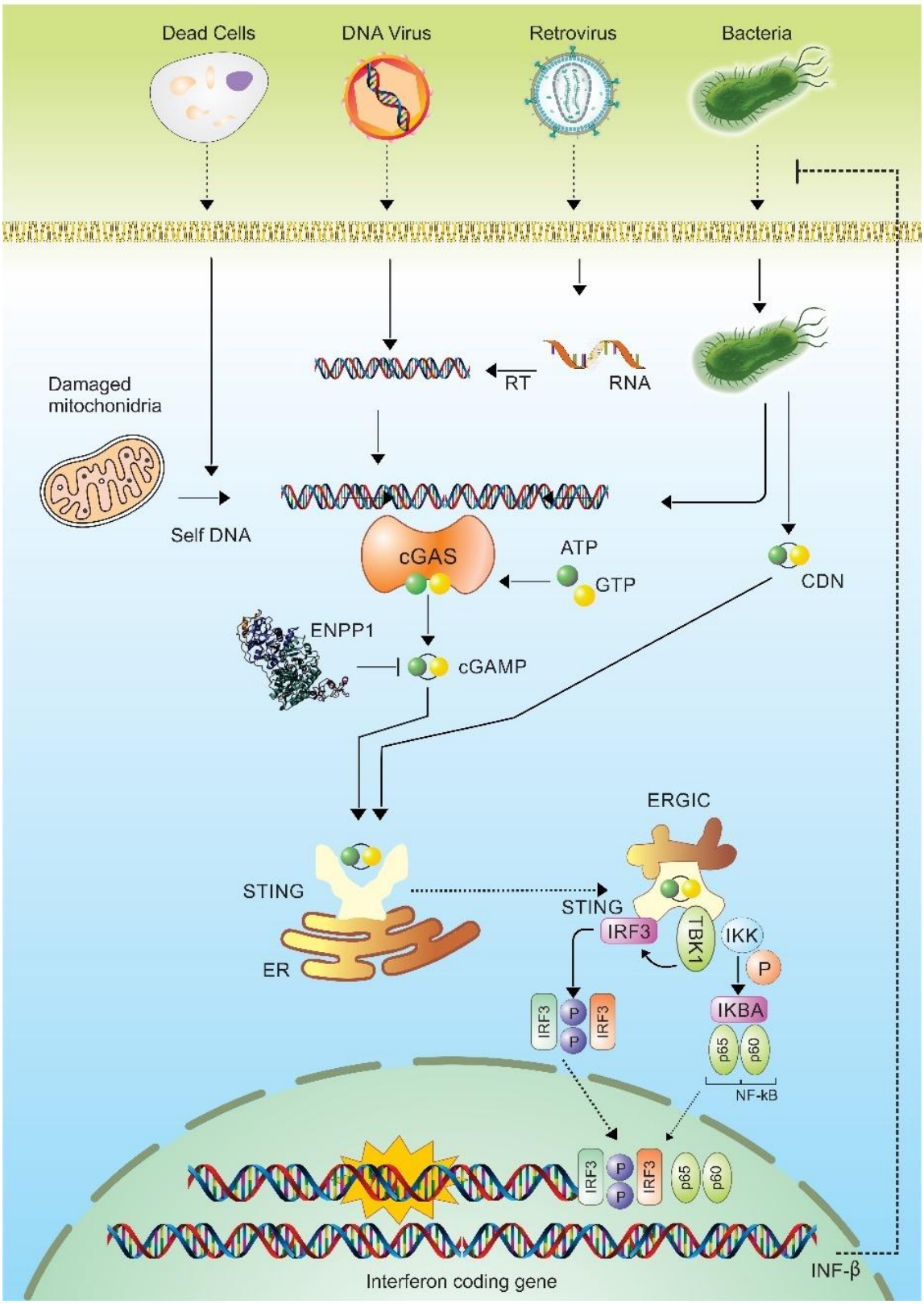

Figure 4.5: Schematic presentation of STING pathway [modified from (Chen et al., 2016)

i. STING agonists

Synthetic alternatives of 2',3'-cGAMP, which could initiate STING response and resist NPP1 hydrolysis, have gained interest from the scientific community. Agonist's binding to STING receptors and subsequent activation start intracellular signalling by releasing effector molecules such as type I interferons (including INF-α and -β) and other pro-inflammatory cytokines. The compounds belong to either nucleotidic or non-nucleotidic scaffolds. To act intracellularly, these agonists should have adequate lipophilicity to penetrate the cell membrane. Many compounds belonging to this concept are already under different phases of clinical investigations.

1. Nucleotidic human STING agonists

Different nucleotide analogues were synthesised, including those of 2',3'-cGAMP, 2',2'-cGAMP, 3',2'-cGAMP, and 3',3'-cGAMP (Zhang et al., 2013). The natural agonist 2',3'-cGAMP offered the highest binding affinity for the STING protein with a K_d value of 4 nM; however, strangely, all CDNs, including those with lower affinity, induce similar EC_{50} values to induce INF-β secretion (16 – 42 nM). The stimulation of alternate pathways may provide a reason for this erratic behaviour. Apart from the cGAMP scaffold, c-di-AMP and c-di-GMP were also investigated for initiating STING signalling. However, the response was lower as compared to 2',3'-cGAMP. Interesting outcomes from using natural CDNs motivated the research group to put more effort into producing synthetic analogues of natural CDNs. Dithio-substituted 2',3'-cGAMP (ADU-S100/ML RR-S2 CDA) showed an improved kinetic profile concerning stability toward NPP1 degradation, lipophilicity, and enhanced STING signalling (Glickman et al., 2015). The enhanced STING signalling triggers the release of interferon and other cytokines in the tumour environment, ultimately leading to tumour regression. The CDN scaffold was further improved by replacing the guanosine moiety with inosine, leading to cyclic adenosine-inosine monophosphate (cAIMP) derivatives offering a significant improvement over natural agonist 2',3'-cGAMP. The exciting feature of cAIMP derivatives is their resistance toward NPP1-based hydrolysis (Lioux et al., 2016). *In-vivo* investigations are yet to be performed for cAIMP derivatives, and their extraordinary kinetic profile certainly warrants *in-vivo* investigations. To further limit the hydrolysis by NPP1, the phosphate groups were replaced with triazole

and 2',5'-amide linkages; however, the resulting compound 2'^{AL},3'^{TL}-cGAMP failed to bind to the STING protein (Dialer et al., 2019). This outcome further emphasises the importance of negatively charged phosphate groups for binding within the active site of the STING protein. The structures and kinetics details of nucleotidic STING agonists are collected in Table 4.2.

Table 4.2: **Human STING agonists with a nucleotidic scaffold**

Agonist	Pharmacological parameters	Signaling pathway	Tumors	Administration	Ref
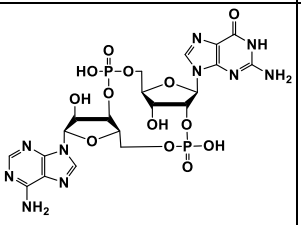 2',3'-cGAMP	K_d STING 4 nmol/L EC_{50}-INFβ 20 nmole/L 19.6 µM IRF 7.2 µM NF-*k*B 39.1 µM	Boost expression of STING and IRF3, secrete IFN-β	Murine colon 26 adenocarcinoma	I.V	(Zhang et al., 2013)
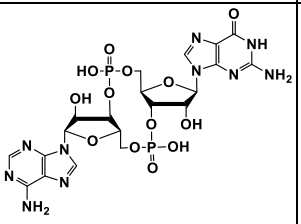 3',3'-cGAMP	K_d 1040 nmol/L EC_{50} 40 nmol/L	Secrete IFN-β	Malignant B-cell tumors chronic lymphatic leukaemia, multiple myeloma	I.V	(Gan et al., 2022)
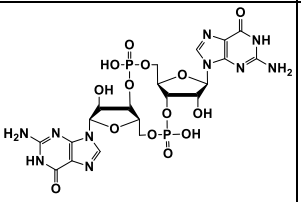 c-di-GMP	K_d 1200 nmol/L EC_{50} >500 nmol/L	Type 1 IFN	Mouse B16 melanoma Metastatic breast cancer 4T1	I.T	(Chandra et al., 2014) (Z. Wang et al., 2016)
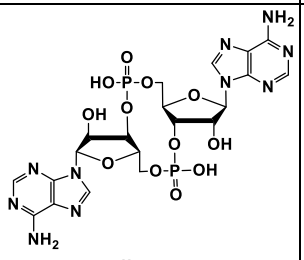 c-di-AMP	-	translocation of IRF-3 type-1 IFN	Breast cancer MDA-MB-231/MX-1 cells	In-vitro cell culture	(Vasiyani et al., 2021)
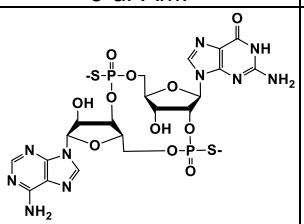 ML RR-S2 CDA	K_d 5 nM EC_{50} is 10-fold more potent than 2',3'-cGAMP Resist NPP1 hydrolysis	Activate all known human STING allelic variant	Balb-c mice with B16 melanoma, 4T1 colon or CT26 mammary carcinoma	I.T	(Glickman et al., 2015) (Li et.al, 2015)

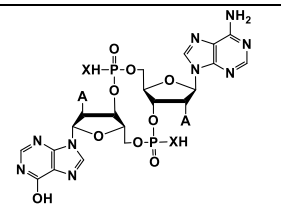 1 (X=O, A=OH) 2 (X=S, A=OH) 3 (X=O, A=F) 4 (X=S, A=F) cAIMP	EC_{50} IRF (0.3 – 5.1 µM) NF-*k*B (1.6 – 16 µM) IFN (0.4 – 10.6 µM)	IRF, NF-*k*B Type 1 IFN	In-vitro screening in murine macrophage cell lines Human monocytes	In-vivo testing is recommended	(Lioux et al., 2016)
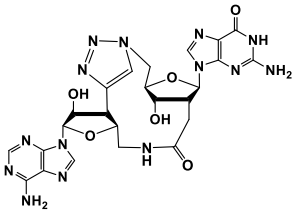 $2'^{AL},3'^{TL}$-cGAMP	Inactive in binding STING	-	-	-	(Dialer et al., 2019)

2. Non-nucleotidic small molecule human STING agonists

Apart from the nucleotidic scaffold, non-nucleotidic small molecules showed promising potential in activating the STING pathway. A large-scale screening campaign applying cell-based HTS assay yielded di-spiro-diketopiperazine derivatives that could successfully initiate STING response and associated downstream signalling mechanisms (Liu et al., 2017). Structure-activity relationship studies (SARs) of benzamide and its analogues are reported for the induction of interferon I and III release from human fibroblasts, peripheral blood mononuclear cells (PBMCs), and HEPG2 cells (Zhang et al., 2019). Another HTS campaign yielded a class of small molecule agonists of human STING response belonging to dimeric amido-benzimidazole (diABZIs) that led to the discovery of intravenously effective non-CDN agonist (Ramanjulu et al., 2018). diABZIs were further investigated by HITGEN China by replacing the benzimidazole part with the imidazopyridine group, which showed significant inhibition of tumour growth in balb-c mice bearing mammary carcinomas. Curade Pharm patented a series of bicyclic benzamides showing micromolar range activity in HEK293T cells (Banerjee, 2023). Merck Sharp & Dohme Corp put their efforts into benzothiophene derivatives, which showed high efficacy in activating the STING mechanism (Cemerski 2019). Non-nucleotidic agonists of the STING pathway are highly promising for cancer therapy, and further efforts are required to investigate their effects on these critical signalling pathways. Details on structures and pharmacological parameters of non-nucleotidic STING agonists are presented in Table 4.3.

Table 4.3: **Human STING agonists with non-nucleotidic scaffolds**

Agonist	Signaling pathway	Biological function	Admin.	Company	Ref
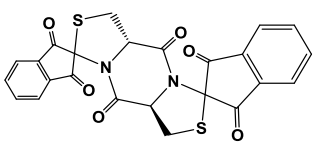	mRNA expression of Type I (INF-β) and III (IL-28A and IL-29)	INF-dominant cytokines in human skin fibroblasts and PBMCs Viral infection and cancers	In-vitro human hepatobla stoma (HepG2) cell culture	-	(Liu et al., 2017)
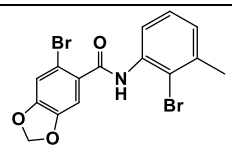	Type I and Type III interferon secretion	Primary human PBMCs and fibroblasts, myeloid DCs	HepG2/hS TING cell culture	-	(Zhang et al., 2019)
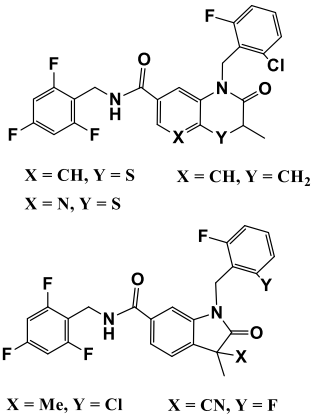	HEK293T-h STING INF-α/β, IL-6, CXCL-10 and TNF-α in hPBMCs	CT-26 tumor	i.t	Curade Pharm India	(Banerjee, 2023)
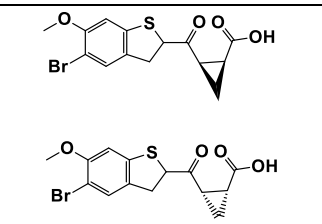	INF-β- secretion	MC38 mouse syngeneic tumour model, advance metastatic solid tumour and lymphomas	i.t	Merck Sharp & Dohme Corp	(Cemerski 2019)
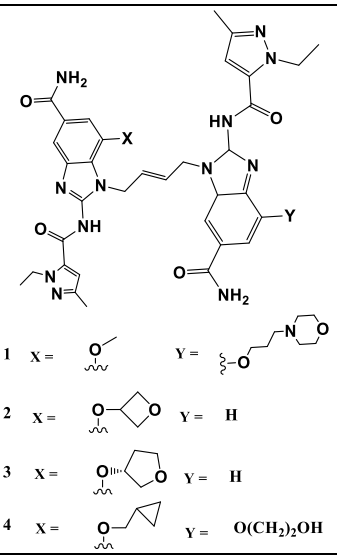	IFN-β secretion in PBMCs EC_{50} 1 =130 nmol/L CXCL-10 induction in PBMCs EC_{50} 2 =18 nmol/L 3 =33 nmol/L 4 =8.6 nmol/L	Subcutaneou s CT-26 mammary carcinoma	i.v	GlaxoSmith Kline (GSK) HITGEN China	(Ramanjul u et al., 2018) Immunom odulator." WO 20191 34705 (2019)

STING agonists can activate the immune system's innate and adaptive components. They facilitate dendritic cell (DC) maturation and activation. DCs are vital antigen-presenting cells that trigger immunological responses. As a result, cytotoxic T cells are primed, and tumour-specific immune responses are produced. Obstacles still exist in developing STING agonists for cancer treatment despite encouraging preclinical and early clinical results. Research is still being done to achieve optimal delivery, reduce off-target effects, and comprehend and avoid potential resistance mechanisms. It is crucial to remember that the development of STING agonists for clinical purposes is still in its early phases, and additional study is required to completely comprehend their safety and efficacy characteristics. Several STING agonists are presently being assessed in clinical trials for various cancer types, and efforts are being made to determine whether they could be used as a therapeutic approach for cancer immunotherapy. It is further essential to investigate non-hydrolysable analogues of 2',3'-cGAMP that could activate STING on one hand and block NPP1 on the other hand.

ii. STING antagonists

As STING agonists have gained massive interest in cancer immunotherapy, their antagonists have shown potential for inflammatory diseases. Certain difficult-to-treat autoimmune diseases, such as Aicardi–Goutière's syndrome, having characteristic overactivation of STING with resulting enhanced type I interferon and cytokines release, are a target for STING antagonists (Hong et al., 2021). Sometimes, mutations in the STING protein, such as STING-associated vasculopathy with onset in infancy (SAVI), underscore the need for the development of selective STING antagonists. So far, a limited number of compounds have been reported that could antagonise STING activity. The STING protein has a large binding pocket, but a significant molecular weight inhibitor likely has pharmacokinetic issues. The potency of the inhibitors was evaluated on their ability to displace the natural ligands 2',3'-cGAMP from its binding pocket in the STING protein.

Table 4.4: Kinetic parameters of STING antagonists

Antagonists	IC_{50} (nM)	Characteristics	Mechanism	Ref
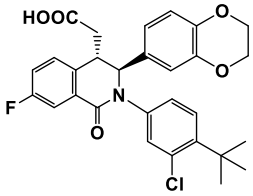	**68** (cGAMP displacement assay) **30,000 (**Inhibition of IFN-β production in cGAMP-stimulated THP1 cells)	A weak antagonist that binds to the cGAMP binding site. Featured with slow dissociation kinetics, oral bioavailability, and inhibition of cGAMP-dependent signalling *in vitro*.	The molecule displaces cGAMP, stabilises STING's "open" conformation, and prevents resulting signalling.	(Siu et al., 2019)
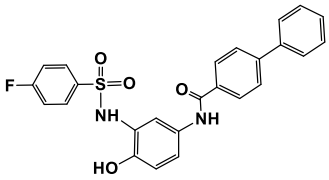	**76** Significant inhibition of INF-β, CXCL-10, and IL-6 mRNA induction	Selectively binds STING with higher affinity than 2′3′-cGAMP as it occupies the CDN-binding Pocket and is a well-tolerated and promising drug candidate for interferonopathies.	It prevents the release of INF and cytokines induced by 2′3′-cGAMP. STING is locked in an open inactive conformation.	(Hong et al., 2021b)
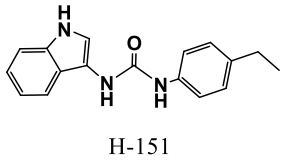 H-151 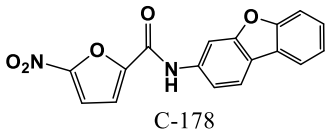 C-178	-	Potent and selective inhibitor for STING H-151 is human-specific C-178 prefers mouse STING	The compounds bind with the TM cysteine residue 91 and block STING activation Lead compounds for autoinflammatory diseases	(Haag et al., 2018)
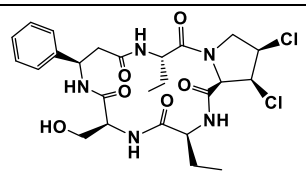	10.8 (μM) for human fibroblast	Specifically binds to STING	Blocks IRF3 recruitment on STING	(Li et al., 2018)

b. NPP3

i. Tissue distribution of NPP3

Similar in structure to NPP1, NPP3 has a similar substrate profile accepting such as NAD^+, ADPR, Ap_nA, and ATP. Cyclic nucleotides are less favoured by NPP3 according to our substrate screening campaign. NPP3 is widely expressed on the surface of immune cells such as basophils and mast cells, where it hydrolyses extracellular nucleotides. Enzyme expression is also observed in mast cells residing in the dermis and epidermis of the skin (Tsai et al., 2015). Tonsils, lymph nodes, and other lymphoid tissues, including the spleen, have been found to express NPP3. Within these tissues, it is located in particular immune

cell populations. Osteoblasts, the cells in charge of bone production, express NPP3. The enzyme has also been discovered in chondrocytes, which are cartilage's maintenance and synthesis cells (Picher, Graff, and Lee 2003). Vascular smooth muscle cells, which are found in blood vessels, have been shown to express NPP3 that is linked to cardiovascular conditions and vascular calcification processes. The renal tubular epithelial cells, among other kidney cell types, have been found to express NPP3 (Furuta et al., 2017). Other tissues, such as the brain, liver, small intestine, and reproductive systems, have also been found to express NPP3 (Stefan, Jansen, and Bollen 2006).

ii. Allergic reactions

Mast cells and basophils undergo degranulation, which involves the release of different mediators that have been stored in their cytoplasmic granules after exposure to an allergen. Subsequently, loads of ATP are released from activated basophils and mast cells to produce allergic inflammation by activating P2X7 receptors. NPP3 expression is upregulated on these immune cells, hydrolysing ATP to AMP and pyrophosphate, thereby neutralising ATP-based allergic reaction (Tsai et al., 2015). AMP is subsequently hydrolysed by surrounding CD73 to adenosine, which has various effects on allergic reactions functioning as an immunomodulatory molecule. It can suppress the release of pro-inflammatory mediators, block mast cell and basophil activation, and control immune cell activity. NPP3 upregulation was observed in chronic urticaria patients, characterised by itchiness. It has been demonstrated that NPP3 activity controls basophil and mast cell histamine release by hydrolysing ATP (Ye et al., 2014). NPP3 regulates the release of mediators from mast cells and basophils, modifies the release of histamine, and has anti-inflammatory effects via producing adenosine, all of which contribute to its crucial involvement in allergic reactions. The precise mechanisms and interactions contributing to NPP3-mediated modulation of allergic responses are still under investigation; nevertheless, NPP3 inhibitors constitute potential targets for therapeutic interventions in allergic diseases.

iii. Cancer

Adenosine is present at low concentrations in the extracellular fluids of normal tissues. However, its concentration rises quite sharply under pathological conditions, including

hypoxia, ischemia, inflammation, and cancer. This increase in adenosine concentration is achieved by activating nucleotide transporters, which pump it outside, or by activating connexion-43 hemichannels, which pump ATP and NAD^+ to the extracellular side. The nucleotides are pro-inflammatory molecules, whereas tumour cells overexpress ectonucleotidases, such as NPP3, that utilise these substrates to produce anti-inflammatory adenosine and avoid immune attack (Antonioli et al., 2013). Several reports suggest the emergence and spread of cancer linked to the enzyme. NPP3 transcripts were discovered in breast cancer cell lines (Walker 256 tumour), and several solid tumours showed high levels of the enzyme's expression. Although transcripts for other enzymes, including CD39, CD73, and NPP2, were also discovered, NPP3 was the most frequently expressed gene during tumour growth in vivo (Buffon et al., 2010). Tumor tissues of bile duct carcinoma patients showed increased expression of NPP3 protein (Yano et al., 2004). Immunohistochemistry of eutopic and ectopic endometrial tissues has demonstrated that NPP3 is overexpressed in the stroma of endometriosis, characterised by the presence of endometrial-like tissue outside the uterus, which leads to chronic inflammation. NPP3 has emerged as a histological marker of endometriosis (Trapero et al., 2019). In the endometriotic lesions, NPP3-mediated adenosine synthesis may alter the immune response and affect the inflammatory environment. Overexpression of NPP3 on activated basophils and mast cells highlights the need for further investigation since hyperresponsive basophils were observed in polycythemia vera patients (Marone et al., 2020). Moreover, the immunological environment of human lung adenocarcinoma and pancreatic cancer contained basophils. It is significant to highlight that NPP3's precise role and importance in cancer pathways have not yet been thoroughly elucidated. The function of NPP3 in tumour pathophysiology, particularly its interactions with immune cells, inflammation, angiogenesis, and pain pathways, requires further study. This will make comprehending the possible therapeutic effects of NPP3 targeting in treating tumours easier.

1.3 Bio-isosteric replacement in drug design

Replacing individual atoms, clusters of atoms, or entire scaffolds of a biologically active molecule with an analogous structure of similar volume, shape, biological, or physicochemical property is known as a bio-isosteric replacement (Bredael et al., 2022; Lassalas et al., 2016). Bio-isosteres are structurally related substances that can be

classified into classical and nonclassical ones. The functional groups used for classical isosteric replacement are similar in size and valence electron composition to their parent groups. Non-classical ones may differ significantly from the original moiety regarding steric and atom count. Interestingly, bio-isosteric replacement might alter physicochemical properties and other characteristics of novel products, resulting in the desired improvement compared to the original substance. It is impossible to predict with precision the efficacy of bio-isosteric replacements, which depends on the exact chemical environment of the binding site, for instance, whether the binding site can adapt to the surrogate structure and whether bio-isosteric replacements are likely to result in the necessary changes in the characteristics of new compounds.

Table 4.5: **Common bio-isosteres of different functional groups** (Bredael et al., 2022; Hevey, 2019)

Original group	Potential replacements
	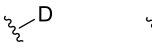
	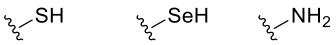
	
	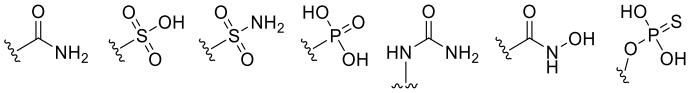

Several physicochemical factors, including acidity (pK_a), lipophilicity (log$D_{7.4}$), permeability coefficient (P_{app}), water solubility, and metabolic stability, can affect the results of bioisosteric replacement.

1.3.1 Phosphonic acids as phosphate and diphosphate bioisosteres

Phosphonic acid groups are frequently employed as bioisosteric substitutes for phosphates and diphosphates. The phosphonic acid moiety $P(O)(OH)_2$ is directly connected to the molecule by a stable P-C bond and is not hydrolysed by enzymes, unlike phosphates and diphosphates. This characteristic makes them a prospective candidate for local or systemic administration, e.g. in the treatment of cancer (Figure 4.6). Improvements in metabolic stability are brought about by the change that results from bio-isosteric replacement since P-C bonds are not cleaved by P-O-bond-cleaving enzymes (Carozza et al., 2020; Heidel & Dowd, 2019).

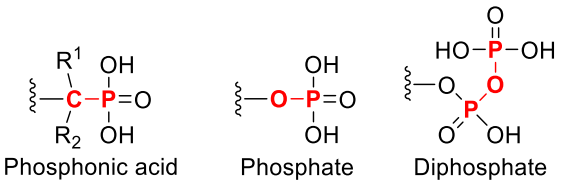

Figure 4.6: Structure of phosphonic acid, phosphate, and diphosphates.

1.3.2 Bioisosteric replacements of carboxylic acids

Sulfonamides and phosphonic acids can both function as bioisosteric substitutes for carboxylic acids. In general, phosphonic acids are more acidic, with anticipated pK_1 and pK_2 values of 1-2 and 6-7, than sulfonamides (pK_a of 10) (Franz, 2001). The pK_a values of phosphonic acids and sulfonamides can only be compared when bound to the same neighbouring group in the molecule because the neighbouring scaffold affects the value. The acidity of phosphonic acid makes organic molecules more soluble in water (Sevrain et al., 2017). Additionally, at a physiological pH of 7.4, the strong negative charge of phosphonic acids prevents them from penetrating cells, allowing them to continue working on targets in the extracellular environment. This is advantageous in the case of NPP3 inhibitors because the desired new inhibitors wouldn't need to penetrate the cell membrane. On the other hand, active transport mechanisms might be in place.

1.4 Research objectives

We previously demonstrated that the sulfonamide derivative PZB08720015A is an effective NPP3 inhibitor when measured at an alkaline pH of 9.2 (Chapter 3). NBO-MKA-29, a different sulfonamide derivative, also demonstrated the capacity to inhibit NPP3. Based on the inhibitors' ability to bind to the two Zn^{2+} ions in the active site, NPP3 is inhibited. It has recently been demonstrated that the sulfonamides PZB08720015A only weakly block enzymes at a physiological pH value of 7.4. This may be due to the sulfonamides' low acidity, which are expected not to be deprotonated at pH 7.4. In the current investigation, we substituted the sulfonamide group (pK_a of 10) in the lead structures PZB08720015A and NBO-MKA-29. It is projected that this bioisosteric substitution will increase the potency and aqueous solubility of our target molecules, in analogy to (Carozza et al., 2020). Ali Meshal and Dr. Ahmed Temirak, performed the

synthetic chemistry work. However, patent requirements restrict us from showing structures.

2.0 Material and method

b. Substrates and chemicals

Adenosine, adenosine 5'-mono, -di and -tri-phosphate (AMP, ADP, ATP), Nicotinamide adenine dinucleotide (NAD^+), *p*-nitrophenyl 5'-thymidine monophosphate (*p*-Nph-5'-TMP) and *p*-nitrophenol (PNP) were purchased from Sigma (Steinheim, Germany). Dimethyl sulfoxide (DMSO), disodium hydrogen phosphate (Na_2HPO_4), and sodium acetate (NaOAc) were obtained from Carl Roth (Karlsruhe, Germany). Calcium chloride, magnesium chloride, and zinc chloride ($CaCl_2$, $MgCl_2$, and $ZnCl_2$), Tris-HCl, 2-(cyclohexylamino) ethanesulfonic acid (CHES), and 4-(2-hydroxyethyl)piperazine-1-ethane sulfonic acid (HEPES) were purchased from Sigma–Aldrich (Steinheim, Germany). Corning® flat-bottom 96-well plates were purchased from Sigma–Aldrich (Steinheim, Germany). Recombinant human enzymes were expressed in-house (see Chapter 3 for protein expression).

c. Instrumentation

Tests with natural substrates (ATP and NAD^+) were performed using a p/ACETM MDQ plus capillary electrophoresis system (AB Sciex Germany GmbH, Landwehr str. 54, Darmstadt). Data collection and peak area analysis were performed using the P/ACE MDQ software 32 KARAT, Beckman Coulter (Fullerton, CA, USA). Mithras LB 940 (Berthold Technology, France) was used to measure the absorbance of *p*-nitrophenolate at 405 nm.

2.1 Assays for Biological Testing

e. p-NPh-5'-TMP assay

The assay was based on the colourimetric measurement of the enzymatic product p-nitrophenolate at 405 nm using a Mithras LB 940 continuous plate reader equipped with MikroWin software for data acquisition (Cimpean et al. 2004). *p*-Nph-5'-TMP is a common NPP substrate frequently used to assess NPP activity in tissue and cell culture. Most research groups employed alkaline reaction conditions for NPPs for artificial and natural substrates since a high product turnover is observed under alkaline conditions. Starting with the reaction buffer HEPES 10 mM, pH 7.4, 500 mM $CaCl_2$, and 10 mM $ZnCl_2$ with substrate 300 µM (NPP1) and 400 µM (NPP3), we screened the test compounds at a final

concentration of 50 µM. 896 ng of NPP1 and 985 ng of NPP3 were added to the reaction mixture to start the reaction. Samples were then allowed to incubate for 60 min at 37 °C before the reaction was stopped by adding 20 µL of 0.1M NaOH. Three separate experiments with duplicate measurements were conducted. The data are shown as mean ± SEM.

f. CE assay using a diode array (DAD) detector

A capillary electrophoresis assay (CE) characterises the enzymatic reaction utilising the natural substrates (ATP and NAD^+) in 10 mM HEPES reaction buffer of pH 7.4. The CE assay conditions were the same as previously reported, with minor modifications (Lee et al. 2017). Briefly, NPP1-based reactions were carried out using 100 µM ATP and 0.448 µg of enzyme in a flat bottom 96-well plate. For NPP3-based reactions, 100 µM NAD^+ was reacted with 0.422 µg of NPP3 in a 96-well plate. Samples were allowed to react for 45 minutes before denaturing at 90 °C for 10 minutes. After brief cooling on ice, the reaction samples were electrokinetically loaded (-6 kV, 30 s) into a *Polyacrylamide*-coated capillary [30 cm (20 cm effective length) × 50 µm (id), × 360 µm (od)] and allowed to migrate, using 50 mM phosphate as running buffer, based on their ionic mobility applying an electric field (-15 kV, 0.1 psi pressure). Analysis was conducted using the P/ACE MDQ CE system with a DAD detector (λabs 254 nm).

2.10 Inhibition screening and determination of IC_{50} values

Compounds were initially tested at a final concentration of 50 µM to investigate the inhibition of NPP1 and NPP3, respectively, using either artificial substrate (*p*-NPh-5'-TMP, 300 µM for NPP1, and 400 µM for NPP3) or the natural substrate (ATP, 100 µM vs NPP1, and 100 µM NAD^+ vs NPP3). The assay conditions, buffers, reaction time, and product estimation were the same as in section 2.1. The cut-off limit was set at 50%. The compounds that showed more than 50% inhibition were further tested for a full-scale IC_{50} curve (both for NPP1 and NPP3). IC_{50} values were determined against *p*-NPh-5'-TMP and versus the natural substrates ATP and NAD^+ using eight to ten concentration points. Two to three independent experiments were performed in duplicate observation. Data were analysed using GraphPad Prism 7.0.

2.11 Mechanism of enzyme inhibition

The inhibition mode was determined for compound **10b** since it potently inhibited both NPP1 and NPP3 with comparatively similar IC_{50} values against *p*-NPh-5'-TMP and natural substrate, either ATP (NPP1) or NAD^+ (NPP3). The other reason for selecting **10b** is that the compound showed a 5-fold increase in the IC_{50} values when tested against *p*-NPh-5'-TMP and ATP. A phenomenon previously observed and reported by our research group for competitive inhibitors of NPP1. However, no such effect was observed towards NPP3, and the compound showed similar inhibition towards artificial and natural substrates (for the final version of the paper, compound **11b** will also be included). Three to four inhibitor concentrations were selected (0.5- to 2-fold IC_{50} value) vs five substrate concentrations (50 - 500 µM). Reaction conditions for each assay are described in section 2.1. Two independent experiments were performed with duplicate observations. The inhibition type was determined graphically from the Hanes-Woolf plot and the Lineweaver-Burk plot by using GraphPad Prism 7.0.

2.12 Statistical analysis

Data analysis was performed using GraphPad Prism 7.0 for K_m calculation and IC_{50} determination. The K_i values were calculated by using the Cheng-Prusoff equation. A one-way ANOVA test was used to calculate significant differences among parameters.

3 Results and Discussion

The NPP family, in general, and NPP1 and -3, can hydrolyse various adenine nucleotides, including NAD^+, ATP, ADPR, and Ap_nA, to AMP. These substrates have higher extracellular concentrations under hypoxic and inflammatory conditions (Antonioli et al., 2013). Besides natural substrates, the enzymes can also potently hydrolyse the artificial substrate *p*-NPh-5'-TMP, yielding the yellow-coloured *p*-nitrophenolate used for calourimetric detection of product formation. The use of the synthetic substrate requires alkaline reaction conditions. Moreover, a significant difference in the IC_{50} values was observed for competitive inhibitors of NPP1 when tested against artificial as compared to natural substrates (Lee et al. 2017). We used artificial and natural substrates for direct comparison in the current project.

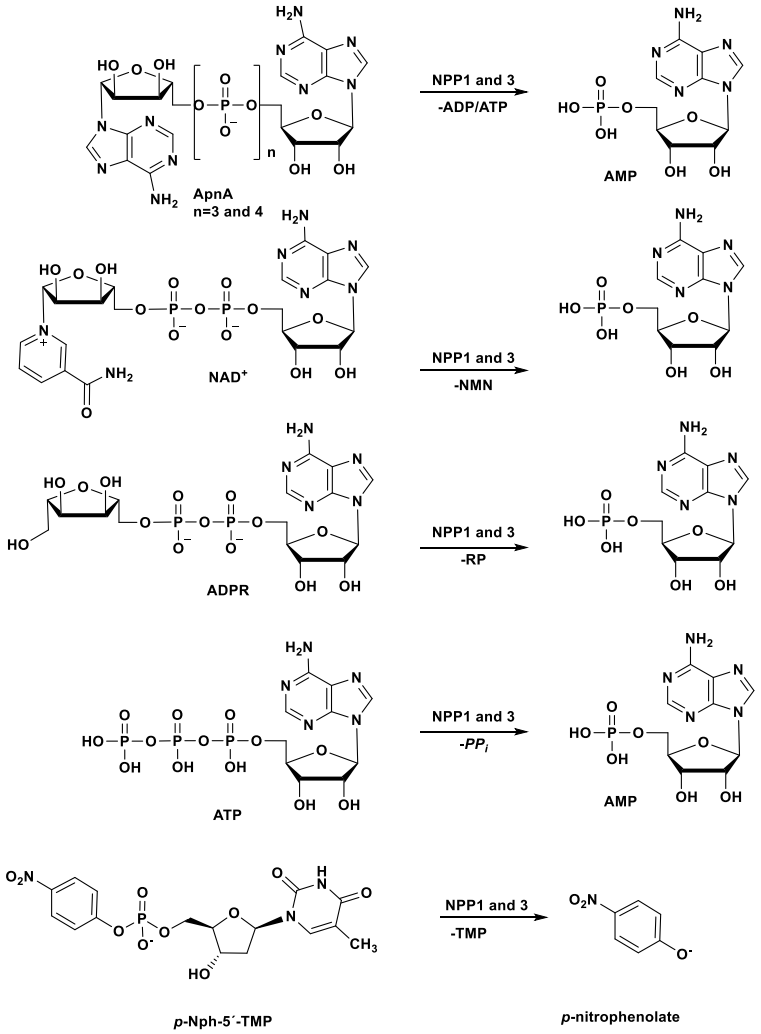

Figure 4.7: Schematic presentation of preferable substrates for NPP-1 and -3 alongside their reaction products and by-products.

3.1 Biological evaluation of new derivatives

Newly synthesised derivatives were tested for NPP1 and NPP3 inhibition using two orthogonal assay systems. At first, a colourimetric assay with *p*-NPh-5'-TMP as a substrate was used to screen compounds at 50 µM final concentration. To confirm the results, we performed tests using the natural substrate ATP (NPP1) and NAD^+ (NPP3) respectively. In our substrate screening campaign (Chapter 3), it was observed that NPP3 hydrolyses NAD^+ better than ATP. This study reports the most potent and selective NPP3 inhibitors (**7a** and **7b**) tested under physiological pH conditions. These structures were developed after modification of the lead structure **PZB08720015A** at the R^1 and R^2 positions and shifting the N atom between the X and Y positions of the core (Tables 4.10). The percentage of inhibition by compounds **4a-6a**, **4b-6b**, and **8a-b** was less than 50% at a high concentration of 50 µM. The half-maximal inhibitory concentration (IC_{50}) was measured for **7a-b**, **9a-11a**, and **9b-11b** exhibited more than 50% inhibition of enzymatic activity at 50 µM to analyse the potential improvement of potency and selectivity of the new NPP1 and NPP3 inhibitors and their structure-activity relationships.

3.1.1 Structure-activity relationship study

We found that diesters were completely ineffective in inhibiting both NPP1 and -3, and the inhibition was, in most cases, below 30% at a high concentration of 50 µM. The reason is that esters do not bind well to the Zn^+ ions in the active site. The inhibition data are collected in Table 4.9.

3.1.2 Structure-activity relationship study

The structures and IC_{50} values for **7a**-**7b**, **9a**-**11a**, and **9b**-**11b** are collected in Table 4.10. Investigating the structural modifications of lead structure **PZB08720015A** showed that the replacement of the sulfonamide in ring B led to the desired effective changes in the inhibition profile. Drastic improvements in the IC_{50} values against NPP3 were observed in the final derivatives **7a** and **7b**. The most potent and selective NPP3 inhibitor among the newly synthesised final compounds is **7b** with an IC_{50} of 25.3 nM vs (*p*-NPh-5'-TMP) and 5.18 nM vs (NAD^+). The compound showed a 142-fold improvement in the IC_{50} value compared to lead compound PZB08720015A (p-NPh-5'-TMP) and >200-fold improvement when using the natural substrate NAD^+. The final compound, 7a, is the

second most potent and selective NPP3 inhibitor with an IC_{50} value of 186 nM (*p*-NPh-5'-TMP) and 98.1 nM (NAD^+). Both compounds are selective for NPP3 as much higher IC_{50} values were observed at NPP1 (*p*-NPh-5'-TMP, ~ 40 µM, ATP > 50 µM).

The smaller derivatives **9a**-**11a** and **9b**-**11b** were also evaluated for their potential inhibitory effects against NPP1 and NPP3. The compounds inhibited both NPP1 and -3 equally. Compound **11b** inhibited NPP1 with an IC_{50} 77.1 ± 13.7 nM against *p*-NPh-5'-TMP. The IC_{50} values against ATP were recorded at 268 ± 34 nM under neutral reaction conditions, approximately 3-fold higher than *p*-NPh-5'-TMP. Moreover, compound **10b** showed roughly a 5-fold difference in IC_{50} values of artificial and natural substrates. We observed the same pattern in all treated compounds for *p*-NPh-5'-TMP and ATP towards NPP1. Similar behaviour for competitive inhibitors of NPP1 was previously reported, where significantly different IC_{50} values were recorded against artificial substrate *p*-NPh-5'-TMP and natural substrate ATP (Lee et al. 2017). Tests were performed in parallel, under similar conditions regarding enzyme source, ionic concentration of buffer, and reaction time. In contrast, under neutral reaction conditions, the IC_{50} values for NPP3 were comparatively similar against artificial and natural substrates. It is recommended to further confirm this outcome with a full-scale investigation of NPP1 using different natural substrates such as NAD^+, Ap_4A, and ADPR or their fluorescent analogues (etheno-bridged NAD^+, Ap_4A, and ADPR). The comparison of **9a** and **9b** with their isomers **11a** and **11b** showed significant differences in their inhibitory activities against NPP1. Compounds **11a** and **11b** are more potent at NPP1 than **9a** and **9b**. This notable improvement in IC_{50} values (5-8-fold) shows that changing the nitrogen atom's position in the heterocyclic scaffold from Y to X is crucial for the improved potency toward NPP1. Introducing an electron-withdrawing bromo substituent into the ring, as in **10a** and **10b**, led to a slight improvement in IC_{50} values at NPP1 and NPP3, compared to **9a** and **9b**. For bromo-containing compounds **10a** and **10b**, the combination of a bromo substituent and a methylene linker in **10b** resulted in good inhibitory potency at NPP1 (6-fold improvement) compared to **10a** but only minor improvement against NPP3. The compounds **10b** and **11a** did not only show significant inhibitory effects toward NPP1 but also exhibited ancillary NPP3 inhibition, thus acting as dual NPP1/NPP3 inhibitors. The

inhibition curves for NPP1 and -3 vs. *p*-NPh-5'-TMP are given in Figure 4.9 and 4.10, respectively.

Table 4.6: **Inhibition of NPP1 and -3 by novel diesters** 4a-6a, 4b-6b, and 8a-8b

Compounds	**Structure**	**% inhibition ± SEM at 50 µM**	
		NPP1 *p*-NPh-5'-TMP, 300 µM (K_m 222 µM)	**NPP3** *p*-NPh-5'-TMP, 400 µM (K_m 380 µM)
4a	*confidential*	2 ± 1	-2 ± 2
4b	*confidential*	24 ± 2	13 ± 1
5a	*confidential*	8 ± 6	1 ± 7
5b	*confidential*	20 ± 1	7 ± 1
6a	*confidential*	5 ± 3	23 ± 11
6b	*confidential*	-2 ± 2	-4 ± 1
8a	*confidential*	27 ± 3	17 ± 2
8b	*confidential*	21 ± 1	11 ± 1

Table 4.7: **Inhibition profile of novel compounds** 7a-7b, 9a-11a, and 9b-11b

Compounds	**Structure**	**IC_{50} ± SEM, nM**			
		NPP1		**NPP3**	
		p-NPh-5'-TMP, 300 µM (K_m 222 µM)	ATP, 100 µM (K_m 8.17 µM)	*p*-NPh-5'-TMP, 400 µM (K_m 380 µM)	NAD^+, 100 µM (K_m 42.8 µM)
7a	*confidential*	44832 ± 71	>50,000	186 ± 18	**98.1 ± 18.2**
7b	*confidential*	35671 ± 381	>50,000	25.3 ± 9.3	**5.18 ± 1.77**
PZB08720015A	*confidential*	not active	not active	3590 ± 103	1130 ± 50
9a	*confidential*	1076 ± 217	n.t*	999 ± 228	565 ± 40
9b	*confidential*	399 ± 47	1132 ± 42	684 ± 111	474 ± 122
10a	*confidential*	895 ± 216	n.t*	832 ± 414	537 ± 77
10b	*confidential*	**142 ± 6**	**909 ± 55**	294 ± 79	97.0 ± 2.0
11a	*confidential*	142 ± 3	n.t*	303 ± 101	n.t*
11b	*confidential*	**77.1 ± 13.7**	**269 ± 34**	305 ± 145	312 ± 11

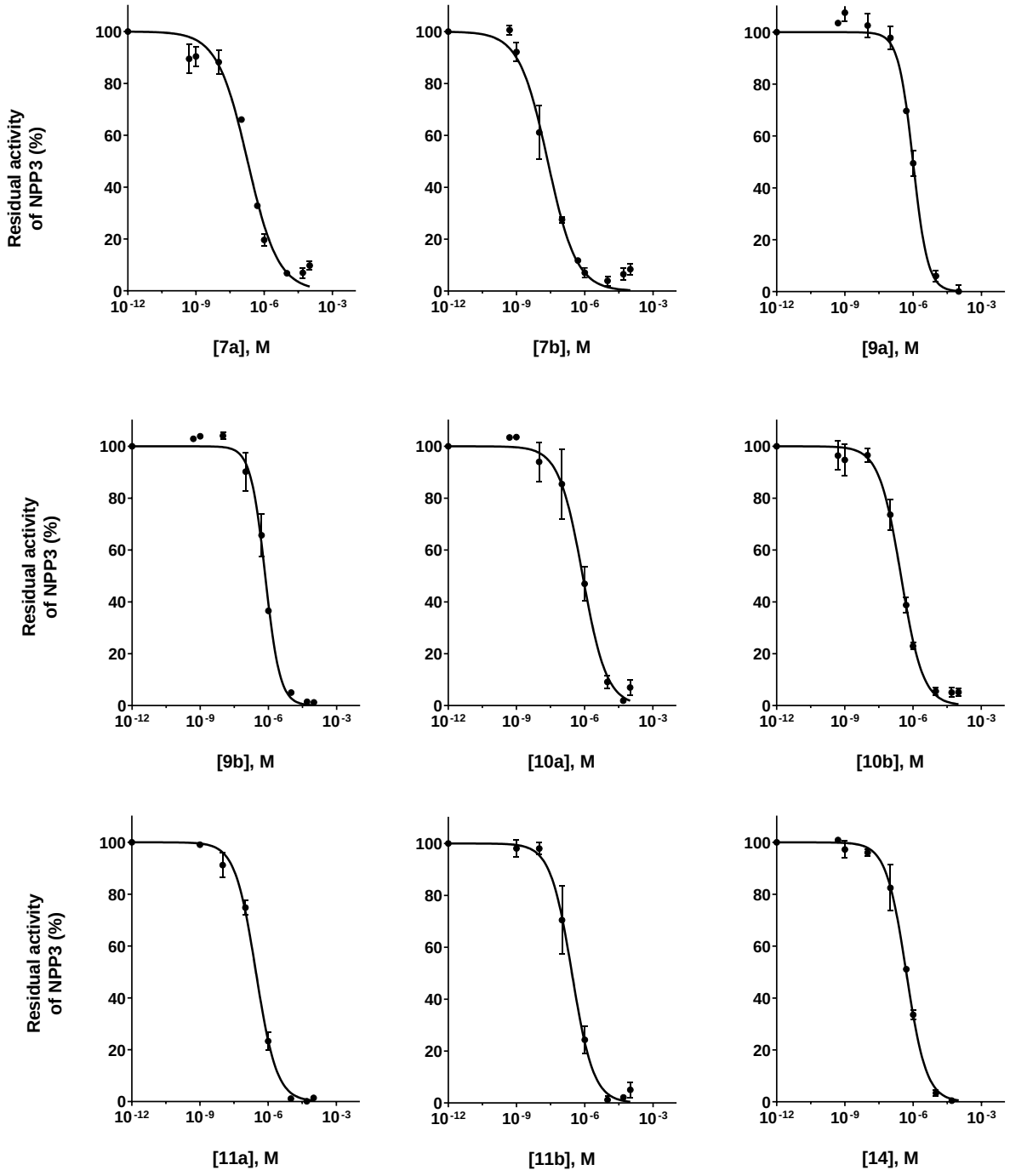

Figure 4.8: Concentration-inhibition curves for the current series of inhibitors at NPP3 using *p*-NPh-5'-TMP (400 µM) as a substrate at a physiological pH of 7.4. Three to four independent experiments were performed in duplicate observations. Data are presented as mean ± SEM. The K_m value of *p*-NPh-5'-TMP at soluble NPP3 was determined as 380 µM, which is used to calculate K_i values using the Cheng-Prusoff equation (Cheng & Prusoff, 1973).

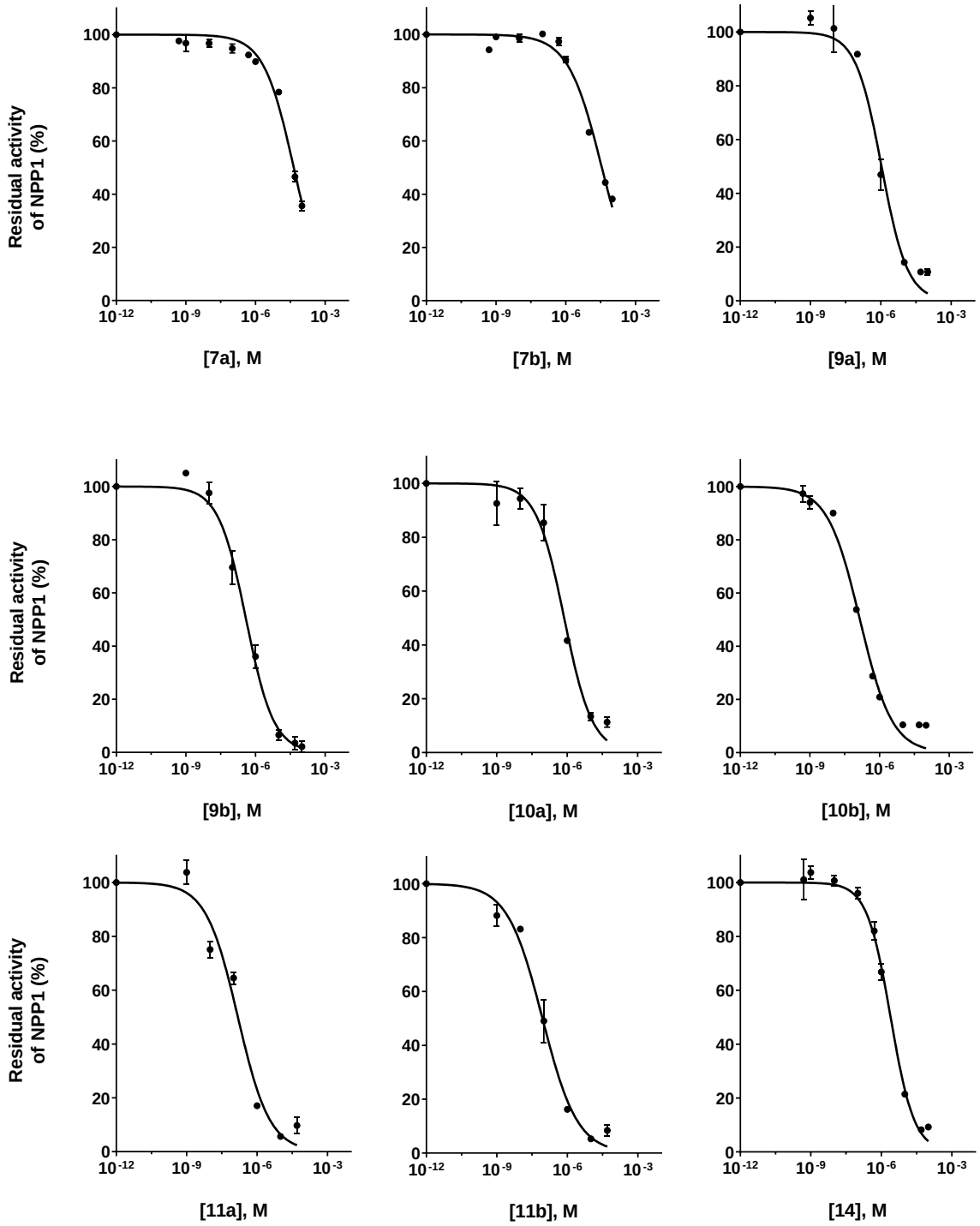

Figure 4.9: Concentration-inhibition curves for the current series at NPP1 using *p*-NPh-5'-TMP (300 µM) as a substrate at a physiological pH 7.4. Three to four independent tests were performed in duplicate observations. Data are presented as mean ± SEM. The K_m value of *p*-NPh-5'-TMP at soluble NPP1 was determined as 222µM, which is used to calculate K_i values using the Cheng-Prusoff equation (Cheng & Prusoff, 1973).

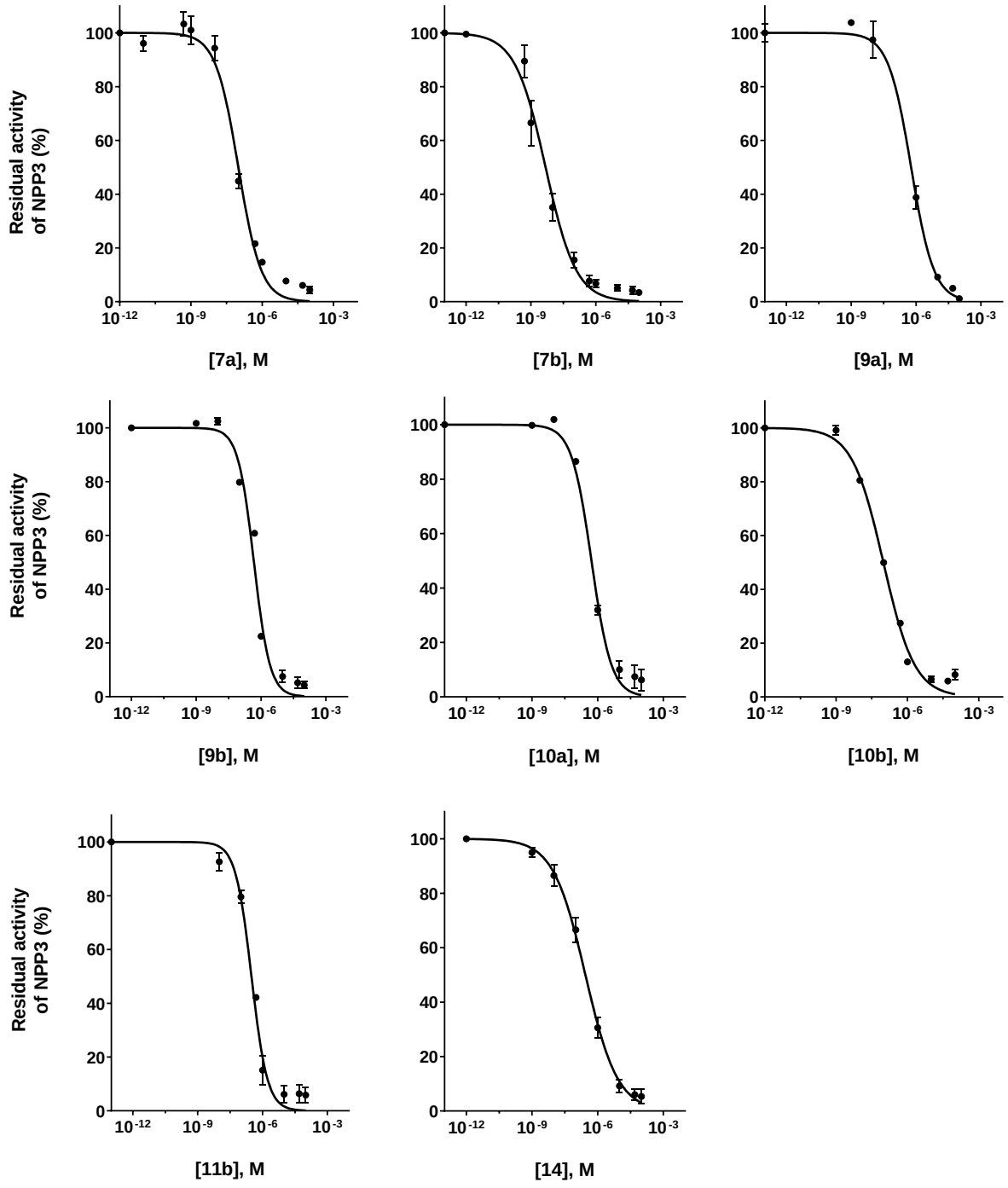

Figure 4.10: Concentration-inhibition curves for the current series of inhibitors at NPP3 using NAD^+ (100 µM) as a substrate at a pH of 7.4. Three to four independent tests were performed in duplicate observations. Data are presented as means ± SEM. The K_m value of NAD^+ at soluble NPP3 was determined as 42.8 µM, which is used to calculate K_i values using the Cheng-Prusoff equation (Cheng & Prusoff, 1973).

Replacing hydrogen (R) in the heterocyclic core with bromine improves the IC_{50} values. The shift of the nitrogen atom in the heterocyclic core plays an essential role in inhibition,

particularly at NPP1. Moving the nitrogen atom from position Y to X of the heterocyclic core drastically improves NPP1 inhibition. In addition, linking the metal-interacting moiety to the aromatic ring via a methylene linker shows enhanced NPP1 and -3 inhibition compared to the group directly connected to the aromatic ring. It can be concluded that the presence of a methylene bridge in the derivative is essential for blocking NPP1 activity with high potency.

The research conducted previously in our group shows that the replacement of the methyl substituent of methylbenzenesulfonamide residue (ring A) with other moieties such as ethyl, hydrogen, chloro, methoxy, or hydroxy groups decreases the inhibitory potency. This indicates the importance of the methyl group for high potency toward NPP3. In addition, substituting the sulfonamide functionality in ring A with other groups leads to a loss of potency. It can be concluded that the sulfonamide in ring A is essential for binding the active site of NPP3. Accordingly, combining a methyl group and sulfonamide in ring A increases the potency of NPP3 inhibitors. It is necessary to point out that an alkaline pH value is required for binding the sulfonamide group to the Zn^{2+} ion in the active site, and a significant decrease in potency is observed under neutral pH conditions. The heterocyclic cores show higher inhibitory activity than other aromatic systems. In the current study, replacing the sulfonamide in ring B improves the inhibitory potency towards NPP3. The methylene linker between the moiety and the aromatic ring further increases the inhibitory effects.

3.1.3 Mechanism of enzyme inhibition

Compound 10b, which showed equal potency at NPP1 and NPP3, was selected for studying the mechanism of inhibition (MOI). Three to four concentrations of **10b** were evaluated against five substrate concentrations using both artificial substrate *p*-NPh-5'-TMP and ATP for NPP1. NAD^+ is used as a natural substrate of NPP3 alongside *p*-NPh-5'-TMP. Data analysis showed a competitive inhibition mode of NPP1 and NPP3 by compound **10b**. Details are presented in Figure 4.14.

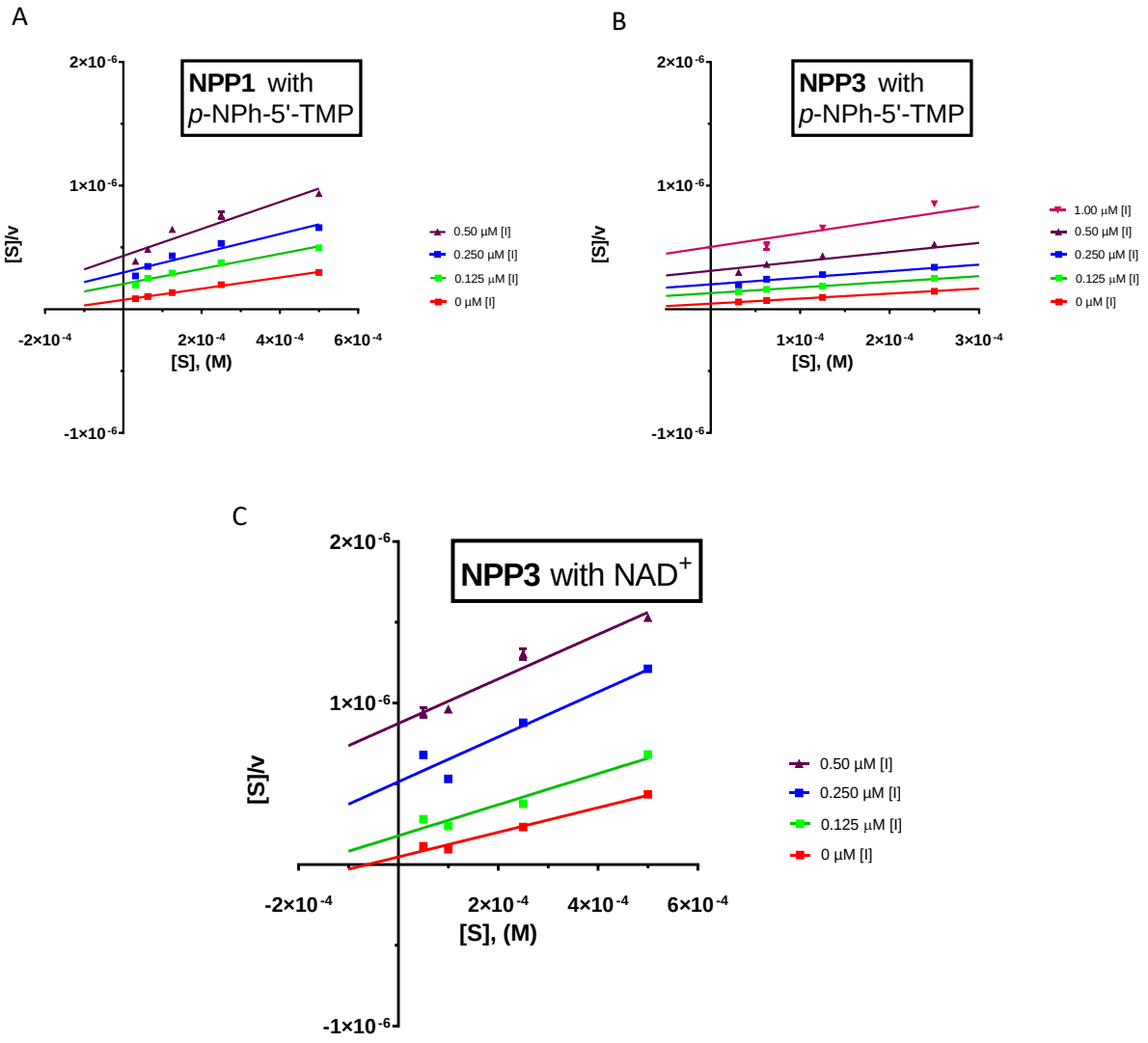

Figure 4.11: Mechanism of inhibition for compound 10b. **A.** NPP1 vs. *p*-NPh-5'-TMP. **B.** NPP3 vs. *p*-NPh-5'-TMP. **C.** NPP3 vs. NAD^+. Two independent experiments were performed in duplicate observations.

3.1.4 Evaluation of inhibition profile for inhibitor 14

Our research group previously synthesised derivative **NBO-MKA-29** (IC_{50} 5991 ± 527 nM vs *p*-NPh-5'-TMP and 6831 ± 91 nM vs NAD^+). The compound was moderately potent but exhibited good solubility in an aqueous solution. In this study, we replaced the sulfonamide function. The resulting compound **14** showed significantly improved NPP3 inhibition. The IC_{50} value was enhanced 15-fold compared to the lead structure **NBO-MKA-29** (Table 4.11). Compound **14** displayed moderate inhibition towards NPP1 (5 – 6-fold) lower than at NPP3.

From the current data, we can conclude that the new functionality is essential for interacting with the Zn^{2+} in the active site of the enzymes NPP1 and NPP3. Potent and selective inhibitors specific to each enzyme were discovered. In addition, the bicyclic indazole system can be considered as a new scaffold for novel selective NPP3 inhibitors.

Table 4.8: **Inhibition profile of indazole derivative**

Compounds	Structure	IC_{50} ± SEM at 50 nM			
		NPP1		NPP3	
		p-NPh-5'-TMP, 300 µM (K_m 222 µM)	ATP, 100 µM (K_m 8.17 µM)	*p*-NPh-5'-TMP, 400 µM (K_m 380 µM)	NAD^+, 100 µM (K_m 42.8 µM)
14	*confidential*	2243 ± 411	N.D*	465 ± 73	**302 ± 114**
NBO-MKA-29	*confidential*	50% inhibition at 50 µM		5991 ± 527	**6831 ± 91**

*****not determined

4.0 Conclusions

In the present work, 17 novel derivatives were synthesised by our group's colleagues and evaluated for their inhibitory activity at NPP3 as a primary objective. In addition, because NPP3 and NPP1 are the enzymes most closely related (51% of sequence identity), the potential of these compounds for NPP1 inhibition was also investigated. Moreover, the structure-activity relationships (SARs) at both enzymes were analysed.

The bio-isosteric replacement of the sulfonamide moiety of the previously synthesised and selective NPP3 inhibitor PZB08720015A resulted in remarkable outcomes. Biological testing showed that 7a and 7b, the novel analogues of PZB08720015A, resulted in a breakthrough in NPP3 inhibitors displaying inhibition constants in the low nanomolar range. Compound 7b blocked NPP3 activity (IC_{50} 5.17 nM) with 142-fold improved potency compared to the lead structure PZB08720015A. The new compounds 7a and 7b are the most potent and selective NPP3 inhibitors reported. Accordingly, compounds 7a and 7b have a promising potential as tool compounds for studying NPP3 and for further development as drug candidates for cancer immunotherapy.

Among the current series, some compounds also exhibited the ability to block NPP1 activity. For example, 11b was the most potent NPP1 inhibitor (IC_{50} 77.1 nM). Compound

11a was the second most potent NPP1 inhibitor. Compounds 10b and 11a showed moderate dual NPP1/NPP3 inhibition. The optimisation of compound NBO-MKA-29 resulted in the generation of compound 14, which led to an improved NPP3-inhibitory effect (15-fold improvement) and moderate NPP1 inhibition. Compound 14 represents a new NPP3 inhibitor scaffold. Future studies will involve extensive biological testing of the new inhibitors, e.g. on different cancer cell lines overexpressing NPPs, such as ovarian, HepG2, and triple-negative breast cancer cells.

5.0. Outlook

The current project results show that replacing one sulfonamide moiety with a bioisostere in the lead structure **PZB08720015A** delivered outstanding results regarding the potency and selectivity of new NPP3 inhibitors. Further structural optimisation might be fruitful. For example, replacing the sulfonamide moiety in the methyl benzenesulfonamide residue of **PZB08720015A** or both sulfonamide moieties is expected to yield new inhibitors that might block NPP3 activity even better. Another suggestion to generate new potent and selective inhibitors is the addition or modification of linkers such as methylene and ethylene, and even longer for attachment of the functional group. Besides potency and selectivity, further parameters must be studied and optimised, e.g. metabolic stability and toxicity. Since some of the newly obtained compounds showed the ability to block NPP1 activity, moving the nitrogen atom between the two positions in the scaffold combined with modification of the linkers might result in more potent NPP1 inhibitors or dual NPP1/NPP3 inhibitors, both of which are of considerable therapeutic interest.

Acknowledgement

During a two-month training course, the author thanks Mr Tahir (ColourGraphics D. I. Khan) for helping with figures using Corel Draw 16.

References:

Abate, Nicola, Manisha Chandalia, Rosa Di Paola, Daniel W Foster, Scott M Grundy, and Vincenzo Trischitta. 2006. “Mechanisms OfDisease: Ectonucleotide Pyrophosphatase Phosphodiesterase 1 as a ‘gatekeeper’ Ofil1sulin Receptors.” *Nat Clin Pract Endocrinol Metab* 2: 694–701. https://doi.org/10.1 0381ncpendmel0367.

Aerts, Indra, Jean Jacques Martin, Peter Paul De Deyn, Chris Van Ginniken, Xaveer Van Ostade, Mark Kockx, Guido Dua, and Herman Slegers. 2011. “The Expression of Ecto-Nucleotide Pyrophosphatase/Phosphodiesterase 1 (E-NPP1) Is Correlated with Astrocytic Tumor Grade.” *Clin Neurol Neurosurg* 113: 224–29. https://doi.org/10.1016/j.clineuro.2010.11.018.

Antonioli, Luca, Corrado Blandizzi, Pál Pacher, and György Haskó. 2013. “Immunity , Inflammation and Cancer : A Leading Role for Adenosine.” *Nat. Rev. Cancer* 13: 842–57.

Bacci, Simonetta, Ornella Ludovico, Sabrina Prudente, Yuan-yuan Zhang, Rosa Di Paola, Davide Mangiacotti, Anna Rauseo, et al. 2005. “The K121Q Polymorphism of the ENPP1/PC-1 Gene Is Associated With Insulin Resistance/Atherogenic Phenotypes, Including Earlier Onset of Type 2 Diabetes and Myocardial Infarction.” *Diabetes* 54: 3021–25. https://doi.org/10.2337/diabetes.54.10.3021.

Banerjee. 2023. Small molecule modulators of human STING, issued 2023.
Bastid, J, a Cottalorda-Regairaz, G Alberici, N Bonnefoy, J-F Eliaou, and a Bensussan. 2012. “ENTPD1/CD39 Is a Promising Therapeutic Target in Oncology.” *Oncogene* 32 (14): 1743–51. https://doi.org/10.1038/onc.2012.269.

Bergamin, Letícia Scussel, Elizandra Braganhol, Rafael Fernandes Zanin, Maria Isabel Albano Edelweiss, and Ana Maria Oliveira Battastini. 2012. “Ectonucleotidases in Tumor Cells and Tumor-Associated Immune Cells: An Overview.” *Journal of Biomedicine and Biotechnology* 2012: 10–12. https://doi.org/10.1155/2012/959848.

Borza, Razvan, Fernando Salgado-polo, Wouter H Moolenaar, and Anastassis Perrakis. 2022. “Structure and Function of the Ecto-Nucleotide Pyrophosphatase–Phosphodiesterase (ENPP) Family: Tidying up Diversity.” *J. Biol. Chem.* 24: 1–26. https://doi.org/10.1016/j.jbc.2021.101526.
Bredael, Kato, Silke Geurs, Dorien Clarisse, Karolien De Bosscher, and Matthias D’hooghe. 2022. “Carboxylic Acid Bioisosteres in Medicinal Chemistry: Synthesis and Properties.” *Journal of Chemistry* 2022: 1–21. https://doi.org/10.1155/2022/2164558.

Buffon, Andréia, Emerson A. Casali, Valesca V. Cardoso, Luiz F. Zerbini, Simon C. Robson, João J.F. Sarkis, and Márcia R. Wink. 2010. “Differential Expression of Nucleotide Pyrophosphatase/Phosphodiesterases by Walker 256 Mammary Cancer Cells in Solid Tumors and Malignant Ascites.” *Life Sciences* 86: 435–40. https://doi.org/10.1016/j.lfs.2010.01.015.

Bühring, Hans-jörg, and Anna Streble. 2004. “The Basophil-Specific Ectoenzyme E-NPP3 (CD203c) as a Marker for Cell.” *Int Arch Allergy Immunol* 133: 317–29. https://doi.org/10.1159/000077351.
Burnstock, G. 1972. “Purinergic Nerves.” *Pharmacol. Rev.* 24: 510–81.

Burnstock, G, and Gower Street. 1990. “Noradrenaline and ATP as Cotransmitters in Sympathetic Nerves.” *Neurchem. Int.* 17: 357–68. https://doi.org/10.1016/0197-0186(90)90158-p.

Carozza, Jacqueline A, Jenifer A Brown, Volker Bo, Rachel E Mardjuki, and Mark Smith. 2020. “Structure Aided Development of Small-Molecule Inhibitors of ENPP1 , the Extracellular Phosphodiesterase of the Immunotransmitter CGAMP Development of Small-Molecule Inhibitors of ENPP1 , the Extracellular Phosphodiesterase of the Immunotr.” *Cell Chem. Biol.* 27: 1347–58. https://doi.org/10.1016/j.chembiol.2020.07.007.

Cemerski. 2019. Benzothiophene STING agonists for cancer treatment, issued 2019.
Chandalia, Manisha, and Nicola Abate. 2007. “Metabolic Complications of Obesity: Inflated or Inflamed?”

J. Diabetes Its Complications 21: 128–36. https://doi.org/10.1016/j.jdiacomp.2006.10.004.

Chandra, Dinesh, Wilber Quispe-Tintaya, Arthee Jahangir, Denise Asafu-Adjei, Ilyssa Ramos, Herman O. Sintim, Jie Zhou, Yoshihiro Hayakawa, David K.R. Karaolis, and Claudia Gravekamp. 2014. "STING Ligand C-Di-GMP Improves Cancer Vaccination against Metastatic Breast Cancer." *Cancer Immunol. Res.* 2: 901–10. https://doi.org/10.1158/2326-6066.CIR-13-0123.

Chen, Qi, Lijun Sun, and Zhijian J. Chen. 2016. "Regulation and Function of the CGAS-STING Pathway of Cytosolic DNA Sensing." *Nat. Immunol.* 17: 1142–49. https://doi.org/10.1038/ni.3558.
Chin, Chen-ni, Qing Dallas-yang, Franklin Liu, Thu Ho, Kenneth Ellsworth, Paul Fischer, Tajneen Natasha, et al. 2009. "Evidence That Inhibition of Insulin Receptor Signaling Activity by PC-1 / ENPP1 Is Dependent on Its Enzyme Activity." *Eur. J. Pharmacol.* 606: 17–24. https://doi.org/10.1016/j.ejphar.2009.01.016.

Cimpean, Anisoara, Cristiana Stefan, Rik Gijsbers, Willy Stalmans, and Mathieu Bollen. 2004. "Substrate-Specifying Determinants of the Nucleotide Pyrophosphatases/ Phosphodiesterases NPP1 and NPP2." *Biochem. J.* 381: 71–77.

Colgan, Sean P., Holger K. Eltzschig, Tobias Eckle, and Linda F. Thompson. 2006. "Physiological Roles for Ecto-5'-Nucleotidase (CD73)." *Purinergic Signalling* 2 (2): 351–60.

Côté, Nancy, Diala El Husseini, Andrée Pépin, Sandra Guauque-Olarte, Valérie Ducharme, Pascale Bouchard-Cannon, Audrey Audet, et al. 2012. "ATP Acts as a Survival Signal and Prevents the Mineralization of Aortic Valve." *J. Mol. Cell. Cardiol.* 52: 1191–1202. https://doi.org/10.1016/j.yjmcc.2012.02.003.

Decout, Alexiane, Jason D. Katz, Shankar Venkatraman, and Andrea Ablasser. 2021. "The CGAS–STING Pathway as a Therapeutic Target in Inflammatory Diseases." *Nat. Rev. Immunol.* 21: 548–69. https://doi.org/10.1038/s41577-021-00524-z.

Dialer, Clemens Reto, Samuele Stazzoni, David Jan Drexler, Felix Moritz Müller, Simon Veth, Alexander Pichler, Hidenori Okamura, Gregor Witte, Karl Peter Hopfner, and Thomas Carell. 2019. "A Click-Chemistry Linked 2′3′-CGAMP Analogue." *Chem. - Eur. J.* 25: 2089–95. https://doi.org/10.1002/chem.201805409.

Ding, Chunyong, Zilan Song, Ancheng Shen, Tingting Chen, and Ao Zhang. 2020. "Small Molecules Targeting the Innate Immune CGAS–STING–TBK1 Signaling Pathway." *Acta Pharm. Sin. B* 10: 2272–98. https://doi.org/10.1016/j.apsb.2020.03.001.

Endler, Georg, Christine Mannhalter, Heike Sunder-plassmann Martin Schillinger, Alexandra Klimesch, Markus Exner, Sonja Kapiotis, Susanne Meier, et al. 2002. "The K121Q Polymorphism in the Plasma Cell Membrane Glycoprotein 1 Gene Predisposes to Early Myocardial Infarction." *J Mol Med (2002)* 80: 791–95. https://doi.org/10.1007/s00109-002-0385-8.

Franz, Robert G. 2001. "Comparisons of PKa and Log P Values of Some Carboxylic and Phosphonic Acids: Synthesis and Measurement." *AAPS PharmSci* 3: 1–13. https://doi.org/10.1208/ps030210.

Frittitta, Lucia, Stefania Camastra, Roberto Baratta, Benedetta V Costanzo, Monica D Adamo, Salvatore Graci, Daniela Spampinato, et al. 1999. "A Soluble PC-1 Circulates in Human Plasma: Relationship with Insulin Resistance and Associated Abnormalities." *J. Clin. Endocrinol. Metab.* 84: 3620–25.

Furuta, Yoki, Shih-han Tsai, Makoto Kinoshita, and Kosuke Fujimoto. 2017. "E-NPP3 Controls Plasmacytoid Dendritic Cell Numbers in the Small Intestine." *PloS One*, 1–19. https://doi.org/10.1371/journal.pone.0172509.

Gan, Yu, Xiaoying Li, Shuangze Han, Qi Liang, Xiaoqian Ma, Pengfei Rong, Wei Wang, and Wei Li. 2022. "The CGAS/STING Pathway: A Novel Target for Cancer Therapy." *Front. Immunol.* 12: 1–15.

https://doi.org/10.3389/fimmu.2021.795401.

Gessi, Stefania, Katia Varani, Stefania Merighi, Eleonora Fogli, Valeria Sacchetto, Annalisa Benini, Edward Leung, Stephen Mac-Lennan, and Pier Andrea Borea. 2007. “Adenosine and Lymphocyte Regulation.” *Purinergic Signalling* 3 (1–2): 109–16.

Ghiringhelli, Franois, Mélanie Bruchard, Fanny Chalmin, and Cédric Rébé. 2012. “Production of Adenosine by Ectonucleotidases: A Key Factor in Tumor Immunoescape.” *Journal of Biomedicine and Biotechnology* 2012. https://doi.org/10.1155/2012/473712.

Gibilisco, Paul A., H. Ralph Schumacher, Joseph L. Hollander, and Keith A. Soper. 1985. “Synovial Fluid Crystals in Osteoarthritis.” *Arthritis Rheum.* 28: 511–15. https://doi.org/10.1002/art.1780280507.

Glickman, Laura Hix, Leticia Corrales, David B. Kanne, Shailaja Kasibhatla, Jie Li, Anne Marie Culazzo Pferdekamper, Kelsey Sivick Gauthier, et al. 2015. “Direct Activation of STING in the Tumor Microenvironment Leads to Potent and Systemic Tumor Regression and Immunity.” *Cell Rep.* 11: 1018–30. https://doi.org/10.1158/1538-7445.am2016-sy39-02.

Gõmez-Villafuertes, Rosa et.al. 2014. “Ectonucleotide Pyrophosphatase/Phosphodiesterase Activity in Neuro02A Neuroblastoma Cells: Changes in Expression Associated with Neuronal Differentiation.” *J. Neurochem.* 131: 290–302. https://doi.org/10.1111/jnc.12794.

Grobben, Bert, Peter Paul De Deyn, and Herman Slegers. 2002. “Rat C6 Glioma as Experimental Model System for the Study of Glioblastoma Growth and Invasion.” *Cell Tisssue Res* 310: 257–70. https://doi.org/10.1007/s00441-002-0651-7.

Haag, Simone M., Muhammet F. Gulen, Luc Reymond, Antoine Gibelin, Laurence Abrami, Alexiane Decout, Michael Heymann, et al. 2018. “Targeting STING with Covalent Small-Molecule Inhibitors.” *Nature* 559: 269–73. https://doi.org/10.1038/s41586-018-0287-8.

Heidel, Kenneth M., and Cynthia S. Dowd. 2019. “Phosphonate Prodrugs: An Overview and Recent Advances.” *Future Med. Chem.* 11: 1625–43. https://doi.org/10.4155/fmc-2018-0591.
Hevey, Rachel. 2019. “Bioisosteres of Carbohydrate Functional Groups in Glycomimetic Design.” *Biomimetics* 4: 1–23. https://doi.org/10.3390/biomimetics4030053.

Hong, Ze, Jiahao Mei, Chenhui Li, Guohui Bai, Munire Maimaiti, Haiyang Hu, Wenying Yu, et al. 2021. “STING Inhibitors Target the Cyclic Dinucleotide Binding Pocket.” *Proc. Natl. Acad. Sci. U. S. A.* 118 (24). https://doi.org/10.1073/pnas.2105465118.

Horenstein, Alberto L., Antonella Chillemi, Gianluca Zaccarello, Santina Bruzzone, Valeria Quarona, Andrea Zito, Sara Serra, and Fabio Malavasi. 2013. “A CD38/CD203A/CD73 Ectoenzymatic Pathway Independent of CD39 Drives a Novel Adenosinergic Loop in Human T Lymphocytes.” *OncoImmunology* 2: 1–14. https://doi.org/10.4161/onci.26246.

Huesa, Carmen, Dongxing Zhu, James D Glover, Mathieu Ferron, Gerard Karsenty, Elspeth M Milne, José Luis Millan, et al. 2014. “Deficiency of the Bone Mineralization Inhibitor NPP1 Protects Mice against Obesity and Diabetes.” *Dis. Models Mech.* 7: 1341–50. https://doi.org/10.1242/dmm.017905.

Lassalas, Pierrik, Bryant Gay, Caroline Lasfargeas, Michael J. James, Van Tran, Krishna G. Vijayendran, Kurt R. Brunden, et al. 2016. “Structure Property Relationships of Carboxylic Acid Isosteres.” *J.Med.Chem* 59: 3183–3203. https://doi.org/10.1021/acs.jmedchem.5b01963.

Lee, Sang Yong, Soumya Sarkar, Sanjay Bhattarai, Vigneshwaran Namasivayam, Steven De Jonghe, Holger Stephan, Piet Herdewijn, Ali El-Tayeb, and Christa E. Müller. 2017a. “Substrate-Dependence of Competitive Nucleotide Pyrophosphatase/Phosphodiesterase1 (NPP1) Inhibitors.” *Frontiers in Pharmacology* 8: 1–15. https://doi.org/10.3389/fphar.2017.00054.

Li et.al. 2015. “Hydrolysis of 2′3′-CGAMP by ENPP1 and Design of Non- Hydrolyzable Analogs.” *Nat Chem Biol* 10: 1043–48. https://doi.org/10.1038/nchembio.1661.

Li, Senlin, Ze Hong, Zhe Wang, Fei Li, Jiahao Mei, Lulu Huang, Xiwen Lou, et al. 2018. “The Cyclopeptide Astin C Specifically Inhibits the Innate Immune CDN Sensor STING.” *Cell Rep.* 25: 3405-3421.e7. https://doi.org/10.1016/j.celrep.2018.11.097.

Lioux, Thierry, Marc Antoine Mauny, Alain Lamoureux, Nicolas Bascoul, Mathieu Hays, Fabienne Vernejoul, Anne Sophie Baudru, et al. 2016. “Design, Synthesis, and Biological Evaluation of Novel Cyclic Adenosine-Inosine Monophosphate (CAIMP) Analogs That Activate Stimulator of Interferon Genes (STING).” *J.Med.Chem* 59: 10253–67. https://doi.org/10.1021/acs.jmedchem.6b01300.

Liu, Bowei, Liudi Tang, Xiaohui Zhang, Julia Ma, Mohit Sehgal, Junjun Cheng, Xuexiang Zhang, et al. 2017. “A Cell-Based High Throughput Screening Assay for the Discovery of CGAS-STING Pathway Agonists.” *Antiviral Res.* 147: 37–46. https://doi.org/10.1016/j.antiviral.2017.10.001.

Longo, Michele, Federica Zatterale, Jamal Naderi, Luca Parrillo, Pietro Formisano, Gregory Alexander Raciti, Francesco Beguinot, and Claudia Miele. 2019. “Adipose Tissue Dysfunction as Determinant of Obesity-Associated Metabolic Complications.” *Int. J. Mol. Sci* 20: 1–23. https://doi.org/10.3390/ijms20092358.

Lopez, Vittoria, Laura Schäkel, H. J.Maximilian Schuh, Michael S. Schmidt, Salahuddin Mirza, Christian Renn, Julie Pelletier, et al. 2021. “Sulfated Polysaccharides from Macroalgae Are Potent Dual Inhibitors of Human ATP-Hydrolyzing Ectonucleotidases NPP1 and CD39.” *Mar. Drugs* 19: 1–13. https://doi.org/10.3390/md19020051.

Mackenzie, N. C.W., C. Huesa, F. Rutsch, and V. E. MacRae. 2012. “New Insights into NPP1 Function: Lessons from Clinical and Animal Studies.” *Bone* 51: 961–68. https://doi.org/10.1016/j.bone.2012.07.014.

Maddux, Betty A, and Ira D Goldfin. 2000. “Membrane Glycoprotein PC-1 Inhibition of Insulin Receptor Function Occurs Via Direct Interaction With the Receptor -Subunit.” *Diabetes* 49: 13–19. https://doi.org/10.2337/diabetes.49.1.13.

Marone, Giancarlo, John T. Schroeder, Fabrizio Mattei, Stefania Loffredo, Adriana Rosa Gambardella, Remo Poto, Amato de Paulis, Giovanna Schiavoni, and Gilda Varricchi. 2020. “Is There a Role for Basophils in Cancer?” *Front. Cell Dev. Biol* 11: 1–16. https://doi.org/10.3389/fimmu.2020.02103.

Meyre, David, Nabila Bouatia-naji, Agnès Tounian, Chantal Samson, Vincent Vatin, Maya Ghoussaini, Christophe Wachter, et al. 2007. “Variants of ENPP1 Are Associated with Childhood and Adult Obesity and Increase the Risk of Glucose Intolerance and Type 2 Diabetes.” *Nat Genet.* 37: 863–67. https://doi.org/10.1038/ng1604. Epub 2005 Jul 17.

Murshed, Monzur. 2018. “Mechanism of Bone Mineralization.” *Cold Spring Harbor Perspect. Med.* 8: 1–12. https://doi.org/10.1101/CSHPERSPECT.A031229.

Nam, Hwa Kyung, Jin Liu, Yan Li, Andrew Kragor, and Nan E. Hatch. 2011. “Ectonucleotide Pyrophosphatase/Phosphodiesterase-1 (ENPP1) Protein Regulates Osteoblast Differentiation.” *J. Biol. Chem.* 286: 39059–71. https://doi.org/10.1074/jbc.M111.221689.

Namasivayam, Vigneshwaran, Sang-yong Lee, and E M Christa. 2016. “The Promiscuous Ectonucleotidase NPP1: Molecular Insights into Substrate Binding and Hydrolysis.” *Biochim. Biophys. Acta, Gen. Subj.* 3: 603–14. https://doi.org/10.1016/j.bbagen.2016.12.019.

Picher, Maryse, Ronald D. Graff, and Greta M. Lee. 2003. “Extracellular Nucleotide Metabolism and Signaling in the Pathophysiology of Articular Cartilage.” *Arthritis Rheum.* 48: 2722–36. https://doi.org/10.1002/art.11289.

Ramanjulu, Joshi M., G. Scott Pesiridis, Jingsong Yang, Nestor Concha, Robert Singhaus, Shu Yun

Zhang, Jean Luc Tran, et al. 2018. “Design of Amidobenzimidazole STING Receptor Agonists with Systemic Activity.” *Nature* 564: 439–43. https://doi.org/10.1038/s41586-018-0705-y.
Roberts, Fiona, Dongxing Zhu, Colin Farquharson, and Vicky E Macrae. 2019. “ENPP1 in the Regulation of Mineralization and Beyond.” *Trends Biochem. Sci.* 44: 616–28. https://doi.org/10.1016/j.tibs.2019.01.010.

Salles, Jean Pierre. 2020. “Hypophosphatasia: Biological and Clinical Aspects, Avenues for Therapy.” *Clin. Biochem. Rev. (Ultimo, Aust.)* 41: 13–27. https://doi.org/10.33176/AACB-19-00031.
Sevrain, Charlotte M., Mathieu Berchel, Hélène Couthon, and Paul Alain Jaffrès. 2017. “Phosphonic Acid: Preparation and Applications.” *Beilstein J. Org. Chem.* 13: 2186–2213. https://doi.org/10.3762/bjoc.13.219.

Siu, Tony, Michael D. Altman, Gretchen A. Baltus, Matthew Childers, J. Michael Ellis, Hakan Gunaydin, Harold Hatch, et al. 2019. “Discovery of a Novel CGAMP Competitive Ligand of the Inactive Form of STING.” *ACS Med. Chem. Lett.* 10: 92–97. https://doi.org/10.1021/acsmedchemlett.8b00466.
Stagg, J, and M J Smyth. 2010. “Extracellular Adenosine Triphosphate and Adenosine in Cancer.” *Oncogene* 29 (39): 5346–58. http://dx.doi.org/10.1038/onc.2010.292.

Stefan, Cristiana, Silvia Jansen, and Mathieu Bollen. 2006. “Modulation of Purinergic Signaling by NPP-Type Ectophosphodiesterases.” *Purinergic Signalling* 2: 361–70. https://doi.org/10.1007/s11302-005-5303-4.

Trapero, Carla, August Vidal, Maria Eulàlia Fernández-Montolí, Buenaventura Coroleu, Francesc Tresserra, Pere Barri, Inmaculada Gómez De Aranda, et al. 2019. “Impaired Expression of Ectonucleotidases in Ectopic and Eutopic Endometrial Tissue Is in Favor of ATP Accumulation in the Tissue Microenvironment in Endometriosis.” *Int. J. Mol. Sci.* 20: 1–20. https://doi.org/10.3390/ijms20225532.

Tsai, Shih Han, Makoto Kinoshita, Takashi Kusu, Hisako Kayama, Ryu Okumura, Kayo Ikeda, Yosuke Shimada, et al. 2015. “The Ectoenzyme E-NPP3 Negatively Regulates ATP-Dependent Chronic Allergic Responses by Basophils and Mast Cells.” *Immunity* 42: 279–93. https://doi.org/10.1016/j.immuni.2015.01.015.

Vashi, Nimi, and Samuel F. Bakhoum. 2021. “The Evolution of STING Signaling and Its Involvement in Cancer.” *Trends Biochem. Sci.* 46: 446–60. https://doi.org/10.1016/j.tibs.2020.12.010.

Vasiyani, Hitesh, Anjali Shinde, Milton Roy, Minal Mane, Kritarth Singh, Jyoti Singh, Dhruv Gohel, et al. 2021. “The Analog of CGAMP, c-Di-AMP, Activates STING Mediated Cell Death Pathway in Estrogen-Receptor Negative Breast Cancer Cells.” *Apoptosis* 26: 293–306. https://doi.org/10.1007/s10495-021-01669-x.

Wang, Yang, Jingwen Luo, Aqu Alu, Xuejiao Han, Yuquan Wei, and Xiawei Wei. 2020. “CGAS-STING Pathway in Cancer Biotherapy.” *Mol. Cancer* 19: 1–16. https://doi.org/10.1186/s12943-020-01247-w.
Wang, Zili, Esteban Celis, Cancer Immunology, and Tolerance Program. 2016. “STING Activator C-Di-GMP Enhances the Anti-Tumor Effects of Peptide Vaccines in Melanoma-Bearing Mice.” *Cancer Immunol. Immunother.* 64: 1057–66. https://doi.org/10.1007/s00262-015-1713-5.STING.

Yano, Yoshihiko, Yoshitake Hayashi, Kimihiko Sano, Hidenobu Nagano, Miyuki Nakaji, Yasushi Seo, Toshiaki Ninomiya, Seitetsu Yoon, Hiroshi Yokozaki, and Masato Kasuga. 2004. “Expression and Localization of Ecto-Nucleotide Pyrophosphatase/ Phosphodiesterase I-1 (E-NPP1/PC-1) and -3 (E-NPP3/CD203c/PD-Iβ/B10/ Gp130RB13-6) in Inflammatory and Neoplastic Bile Duct Diseases.” *Cancer Letters* 207: 139–47. https://doi.org/10.1016/j.canlet.2003.11.002.

Ye, Young Min, Eun Mi Yang, Hye Soo Yoo, Yoo Seob Shin, Seung Hyun Kim, and Hae Sim Park. 2014. “Increased Level of Basophil CD203c Expression Predicts Severe Chronic Urticaria.” *J. Korean Med. Sci.* 29: 43–47. https://doi.org/10.3346/jkms.2014.29.1.43.

Yung-Chi, Cheng, and William H. Prusoff. 1973. “Relationship between the Inhibition Constant (KI) and the Concentration of Inhibitor Which Causes 50 per Cent Inhibition (I50) of an Enzymatic Reaction.” *Biochem. Pharmacol.* 22: 3099–3108.

Zhang, Xiaohui, Bowei Liu, Liudi Tang, Qing Su, Nicky Hwang, Mohit Sehgal, Junjun Cheng, et al. 2019. “Discovery and Mechanistic Study of a Novel Human-Stimulator-of-Interferon-Genes Agonist.” *ACS Infect. Dis.* 5: 1139–49. https://doi.org/10.1021/acsinfecdis.9b00010.

Zhang, Xu, Heping Shi, Jiaxi Wu, Xuewu Zhang, Lijun Sun, Chuo Chen, and Zhijian J. Chen. 2013. “Cyclic GMP-AMP Containing Mixed Phosphodiester Linkages Is an Endogenous High-Affinity Ligand for STING.” *Molecular Cell* 51: 226–35. https://doi.org/10.1016/j.molcel.2013.05.022.

Zimmermann, Herbert, Matthias Zebisch, and Norbert Sträter. 2012. “Cellular Function and Molecular Structure of Ecto-Nucleotidases.” *Purinergic Signal.* 8: 437–502.

Chapter 5

Small molecule inhibitors of CD38 with ancillary inhibition of CD39 and NPP1

Salahuddin Mirza, Zahid Shafique, Paul Stach, Ahmed Elgolkha, Christa E. Müller

Summary

The tumour microenvironment maintains intense immunosuppression in the extracellular environment. The concentration of damaged-associated molecular patterns (DAMP) such as NAD^+ and ATP increases during inflammation and cancer. This pro-inflammatory environment initiates immune cell recruitment and induces damage control mechanisms. However, Tumours exploit this condition by overexpressing ectonucleotidases such as CD38, CD39, NPP1, and CD73. These enzymes constitute canonical and non-canonical pathways of adenosine production. Reports suggest these ectoenzymes are present in the TME and work in tandem. This leads to intense immunosuppression induced by adenosine through its receptors, mainly A_2A and A_2B, contributing to the limited immune surveillance in cancer. This chapter delves into monitoring CD38 activity assays involving NAD^+, nicotinamide-mono-nucleotide NMN, and NaADP. Fluorescence monitoring involves Ɛ-NAD^+ and nicotinamide guanine dinucleotide (NGD^+). We review the reported co-crystal structures of soluble CD38 with different substrates and inhibitors. Glu^{226} in the binding pocket is mainly involved in the hydrolysis of the glycosidic bond between the nicotinamide and the ribose moiety. Other significant interactions include multiple hydrogen bonds with the diphosphate moiety involving Ser^{126}, Arg^{127}, Thr^{221}, and Phe^{222}. Glu^{146}, Asp^{155}, and Trp^{189}. These amino acids bind to the nicotinamide or nicotinic acid moiety. We briefly discuss the different small molecule inhibitors of human CD38 based on nucleotidic and non-nucleotidic scaffolds. Based on these findings, we highlight the potential of the *4H*-chromene scaffold for CD38 inhibition, underscoring the promise of this approach in cancer immunotherapy.

Recombinant CD38 was expressed in the insect cells expression system and subsequently purified using affinity chromatography exploiting a 9-fold His-tag. Kinetic parameters for CD38 expressed in insect cells aligned with previously reported assays using Ɛ-NAD^+, the natural substrate NAD^+ and yeast expression system. 4*H*-Chromene

compounds were screened at 50 µM concentration. Compounds that showed >50 % inhibition were subjected to IC_{50} value determination. The currently most potent 4*H*-chromene derivative against CD38 was PZB22222054A with a K_i-value of 0.064 ± 0.035 μM (vs. NAD^+), showing a competitive inhibition mode. Additionally, it is observed that the most potent CD38 inhibitors also inhibited CD39. The most potent inhibitor of soluble CD39, PZB22222043A, reached a K_i value of 0.154 ± 0.017 μM, showing a competitive inhibition mode. PZB22222043A displayed excellent inhibitory potency towards CD38 with a K_i value of 0.200 ± 0.048 μM. The compound showed a decent inhibitory potency against NPP1, displaying >80 % inhibition of enzymatic activity at 50 µM. Therefore, we conclude that PZB22222043A is a multi-target inhibitor that might be a new approach to limit the downstream accumulation of adenosine, as it can potentially inhibit both the canonical and the non-canonical pathways. Information on the structure-activity relationships of *4H*-chromenes as inhibitors of CD38, CD39 and NPP1 will lead to further scaffold improvement.

1.0 Introduction

1.1 Nicotinamide adenine-dinucleotide (NAD^+)

NAD^+ acts as a cofactor in the cellular energy generation pathways, such as glycolysis, the tricarboxylic acid (TCA) cycle, and oxidative phosphorylation. The molecule is a vital nucleotide in the intracellular environment, which involves numerous signalling mechanisms (Navas et al., 2021).

1.1.1 Biosynthesis of NAD^+

NAD+ biosynthesis occurs through four main pathways, including *de novo* synthesis, Preiss-Handler pathway, salvage pathway, and nucleoside pathway (Yang et al., 2016). The *de novo* synthesis of NAD^+ processes amino acid tryptophan (Trp) to quinolinate, and subsequently to nicotinic acid mononucleotide (NaMN) by quinolinate phosphoribosyltransferase (QPRT). NaMN links the *de novo* synthesis of NAD^+ with the Preiss-Handler pathway, where NAD^+ is synthesised from nicotinic acid (NA). NA is first converted to NaMN by the enzyme nicotinate phosphoribosyltransferase (Npt), which is then adenylated into nicotinic acid adenine dinucleotide (NaAD) by nicotinamide mononucleotide adenylyltransferases (NMNAT). Finally, NAD^+ synthase converts NaAD to NAD^+. In the salvage pathway, a by-product of the NAD^+ hydrolysis reaction, nicotinamide, is recycled back into NAD^+ in a two-step reaction. First, nicotinamide phosphoribosyltransferase (NAMPT) facilitates the coupling of nicotinamide with phosphoribosyl pyrophosphate (PRPP) to form nicotinamide mononucleotide (NMN). NMN is also produced in the extracellular environment due to NAD+ hydrolysis by surface-located glycoproteins, NPPs and CD73. NMN is either internalised and adenylated by NMNAT enzyme family to NAD+ or hydrolysed by CD73 to nicotinamide riboside (NR), which after internalisation is converted to NMN by the intracellular enzymes' nicotinamide riboside kinases NRK1/2 (Ratajczak et al., 2016). NMN is further adenylated to NAD+ (Figure 5.1).

1.1.2 Transport of NAD+ to the extracellular environment

NAD+ is a significant nucleotide component in the extracellular environment, and the term extracellular NADome, or DAMP, is used in a broader sense (Audrito, 2021). Under normal physiological conditions, the intracellular NAD^+ concentration is in the millimolar range, with a nanomolar concentration on the extracellular side.

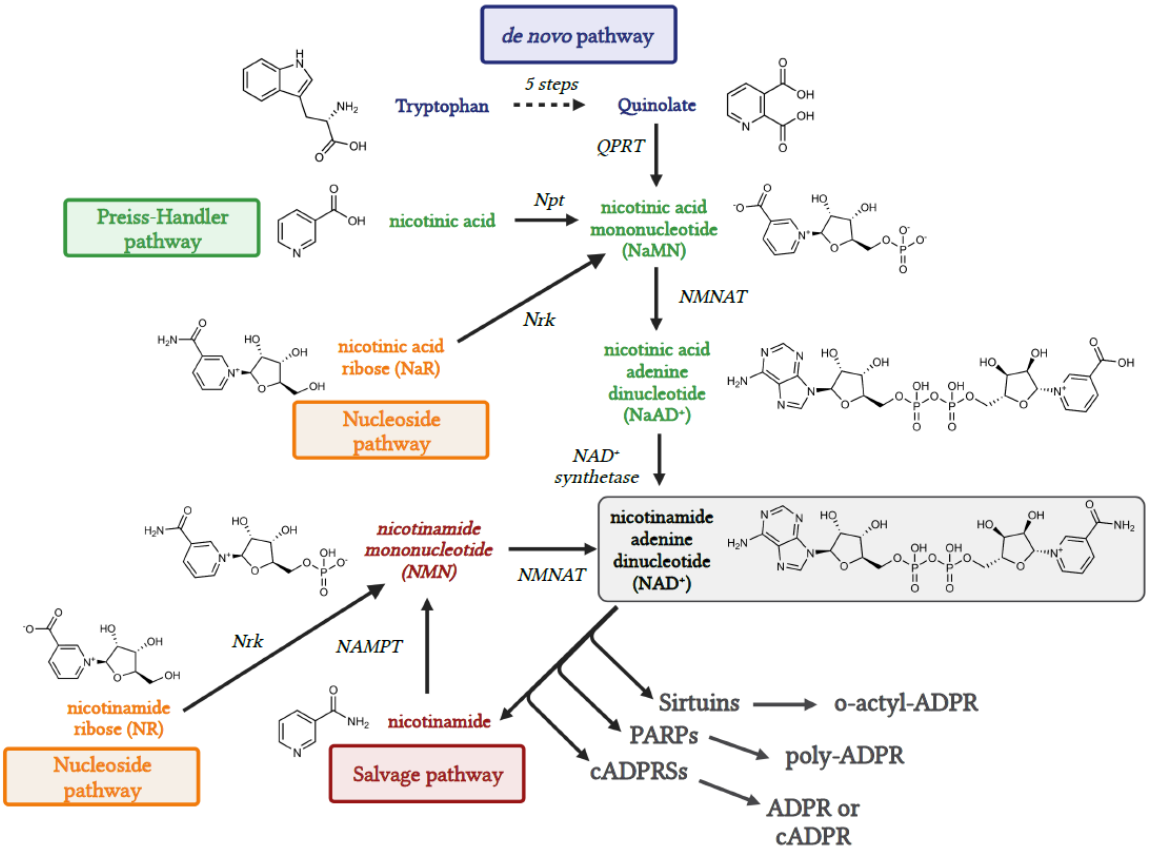

Figure 5.1: Intracellular NAD⁺ biosynthesis pathways (Stach et al., 2023)

QPRT = quinolinate phosphoribosyltransferase, Npt = nicotinate phosphoribosyltransferase, Nrk = nicotinamide riboside kinases, NMNAT = nicotinamide mononucleotide adenylyltransferases, NAMPT = nicotinamide phosphoribosyltransferase, PARPs = poly (ADP-ribose) polymerases, cADPRSs = cyclic ADP-ribose synthases.

On the intracellular side, a significant nucleotide abundance is observed in the mitochondria and cytosol. An acute inflammatory signal causes excessive NAD^+ release to the extracellular space through various mechanisms, including activating transport channels, connexin-43 hemichannels, pannexin-1, vesicular transport, and cellular necrosis. Little is known about the role of extracellular NAD^+ ($eNAD^+$) and how it modulates P2 purinergic receptor signalling compared to ATP. Previous research established a connection between $eNAD^+$ and P2 receptors, particularly $P2Y_1$ and $P2Y_{11}$ (Klein et al., 2009; Alefishat et al., 2015; Moreschi et al., 2006). The substrate modulates the vascular tone by interacting with purine receptors in the blood vessels. eNAD+ further influences T-reg cell function through the ADP ribosyltransferases (ART)-P2X7 receptor pathway (Hubert et al., 2010). Extracellular enzymes include NADases (CD38/CD157)

and nucleotide pyrophosphatase/ phosphodiesterases (NPP1, -3,-4, and -5). NADases hydrolyse the substrate into nicotinamide and ADPR (CD38) or cyclic-ADPR (CD157), both being crucial second messenger molecules involved in intracellular calcium mobilisation. Transmembrane transport is controlled by connexin-43 hemichannels that transport ADPR inward in exchange for more NAD^+ in the extracellular environment (Song et al., 2011). Moreover, non-selective transient receptor potential melastatin 2 (TRPM2) expressed on the plasma membrane is further involved in ADPR trafficking (Rah et al., 2015). However, NPPs, mainly NPP1 and -3, hydrolyse ADPR to nucleotide riboside (NR) and AMP. NR is internalised; however, AMP is further hydrolysed by CD73 to adenosine. Recently, it has been reported that CD73 also hydrolyses both NAD+ and the hydrolysis product nicotinamide mononucleotide (NMN) to nucleotide ribose. NMN is further produced due to NPP-based hydrolysis of NAD+ alongside AMP (Jablonska et al., 2021).

Table 5.1 Extracellular NADome in purinergic signalling

Substrates/ligands	Purinergic receptors/ Hydrolyzing enzymes	Functions
NAD^+	P2X/P2Y	Purinergic signalling
NAD^+/NADP/NMN/ NAAD/NAADP	CD38	Products: ADPR, cADPR, ADPRP, NMN, NAM Intracellular Ca^{2+} mobilisation, T-cell functions
NAD^+/ADPR/ cADPR	NPPs (1 – 5)	Products: NMN and AMP NMN internalisation, NAD^+ biosynthesis
NAD^+/NMN/AMP	CD73	Products: ADO, NR Immunosuppression
NAD^+	CD157	c-ADPR, a second messenger in Ca^{2+} mobilisation

1.1.3 NAD^+ glycohydrolases

Nicotinamide adenine-dinucleotide (NAD^+) glycohydrolase (CD38) possesses a unique topology belonging to either type II or type III glycoproteins (Zhao et al., 2012).

a. The enzyme's type II orientation with an extracellular catalytic domain allows it to hydrolyse extracellular substrates. It is involved in purinergic signalling by hydrolysing NAD^+ to ADPR. Moreover, in conjunction with NPPs and CD73, the enzyme suppresses immune functions by creating an immunosuppressive environment around the inflamed tissues by producing adenosine.
b. Type III oriented enzyme can hydrolyse intracellular substrates like nicotinamide adenine-dinucleotide phosphate (NADP) and nicotinic acid adenine dinucleotide phosphate (NaADP). CD38 functions both as an enzyme or regulates transmigration by interacting with its cognate receptor CD31, causing endothelial adhesion to initiate the inflammatory process (Quintero et al. 2020). The enzymatic functions involve a pH-based reaction on a substrate. Under alkaline/neutral pH, the enzyme processes NAD^+ to either adenosine diphosphate ribose (ADPR) or to cyclic ADPR (cADPR), which is hydrolysed back to ADPR by CD38. Under acidic pH, it facilitates the conversion of NaADP to ADPRP. The enzyme can also promote the formation of NAADP from NADP and nicotinic acid. Both cADPR and NaADP are second messengers involved in the release of Ca^{2+} from intracellular stores with a potential role in angiogenesis and other processes (Dwivedi et al., 2021). This diversity in the enzyme function makes CD38 an essential factor in cellular signalling, and any alteration of these mechanisms can lead to pathological conditions, e.g. ageing, cancer, and metabolic diseases (Hogan et al., 2019).

1.1.4 Tissue expression and pathological outcome

CD38 is widely expressed in immune cells, such as lymphocytes, monocytes, neutrophils, macrophages, dendritic cells, and natural killer (NK) cells. Higher expression is reported on non-lymphoid tissues such as the brain, β-cells of the pancreas, heart, and kidneys (Quarona et al. 2013; Amici et al. 2018). In the brain, it is located on neuronal and glial cells, which has a potential role in neurodegenerative diseases, e.g., Alzheimer's and Parkinson's (Guerreiro Serge 2020). CD38 inhibition significantly influences glioma progression in mice's experimentally induced brain tumour (Blacher et al., 2015). Age-related depletion of NAD+ is linked to the hydrolase function of CD38, thereby limiting adequate NAD+ supply for skeletal muscle development and functioning (Mattson et al., 2018; Schultz et al., 2016; Goody et al., 2018). Extracellular hydrolysis of NAD+ and nicotinamide mononucleotide (NMN) was observed in the aortic valves of patients with

calcific aortic valve disease (CAVD) predominantly due to overexpression of CD38 in the heart (Jablonska et al. 2021). Moreover, the enzyme is further involved in cardiac dysfunction due to NADPH depletion (Zhang et al., 2020; Reyes et al., 2015). These findings made CD38 a vital target for cardiovascular diseases (Zuo et al. 2021). Moreover, CD38-based Ca2+ signalling modulates hepatic gluconeogenesis with a possible role in type II diabetes (Rah et al., 2014). Boosting NAD+ levels through CD38 inhibition is reported to be beneficial in rheumatoid arthritis, systemic sclerosis, and systemic lupus erythematosus (Cole et al., 2018; Peclat et al., 2020). These reports suggest the role of CD38 activity in different pathological conditions in addition to cancer.

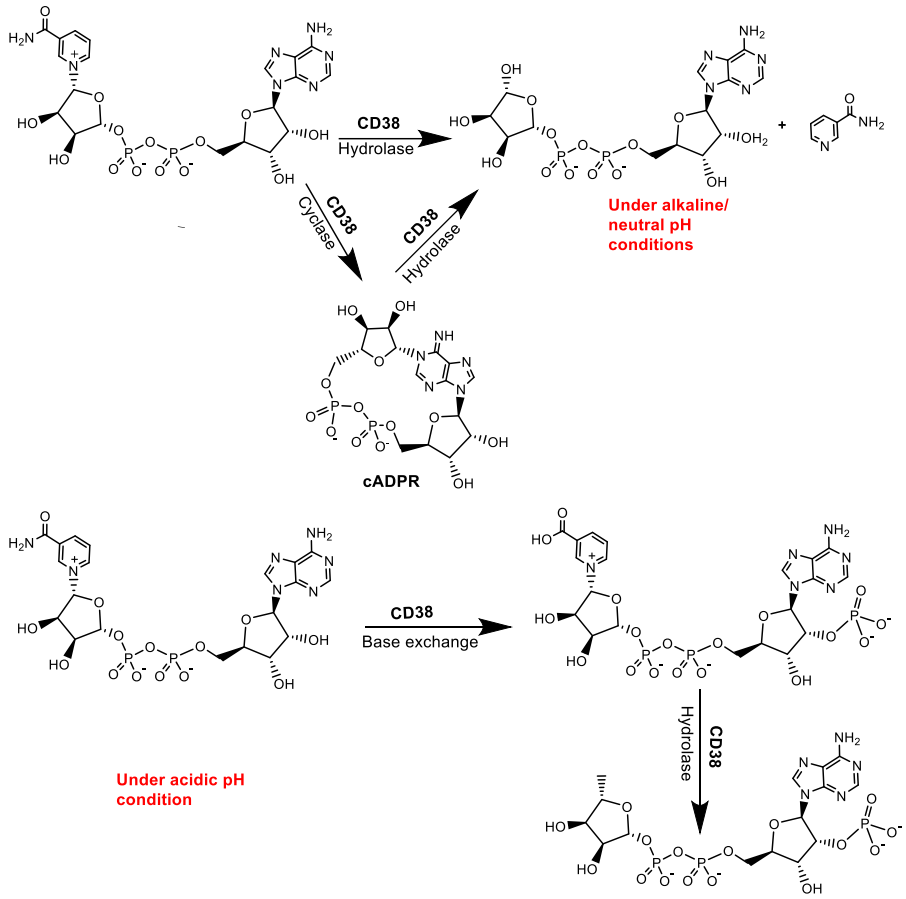

Figure 5.2: CD38 enzymatic functions: pH-based hydrolysis of NAD^+, NADP, and NaADP substrates.

1.1.5 CD38 in tumour microenvironment

The TME is a network comprising the cancer cells, surrounding stromal cells (immune cells, fibroblasts), and extracellular matrix components containing nucleotides, secreted cytokines, integrins, and factors. These elements communicate with each other and play a critical role in the survival of a growing tumour mass (Anderson et al., 2020; Alphonso

et al., 2009; Weber et al., 2012). CD38 play an essential role in different aspects of the tumour microenvironment due to its role in non-canonical adenosinergic pathways comprising CD38/NPP1/CD73, which is largely active in multiple myeloma and solid tumours (Jiao et al., 2020; Bonello et al., 2018; Shallis et al., 2017), nasopharyngeal carcinoma, lymphatic leukaemia, prostate cancer, and lung adenocarcinoma (Ge et al. 2019; Oh 2021; Gao et al. 2021). In multiple myeloma patients, it is observed that tumours treated with PD-1/PD-L1 blockade can upregulate the expression of CD38 over time and thus gain resistance to the treatment. For this reason, the co-inhibition of CD38 is emerging as a potential therapeutic strategy for PD-L1/PD-1 blockade (Verkleij et al., 2020; Chen et al., 2018). Consequently, CD38 antibodies have been identified as a promising tool for treating multiple myeloma. Several CD38 antibodies are in different phases of clinical testing, where daratumumab is approved for testing multiple myeloma (Donk et al., 2018). Gao et al. found that CD38 was highly expressed on the surface of A549 (adenocarcinomic human alveolar basal epithelial cells) and LLC (Lewis lung carcinoma) cells. A positive correlation was observed between CD38 activity and lung adenocarcinoma progression (Gao et al. 2021). In glioblastoma multiforme (GBM), tumour-associated microglia/macrophages (TMMs) constitute a significant part of the TME and play an essential role in tumour progression. Upregulation of CD38 on TMMs is recorded (Blacher et al., 2015). In summary, CD38 is an intricate enzyme whose functions and immunomodulatory properties make it an exciting target for tumour management through antibodies and small-molecule inhibitors.

1.2 Analytical assays for monitoring CD38 activity

Different assays have previously been reported and optimised to predict the hydrolase and cyclase activities of the enzyme. The hydrolase activity is assessed by using etheno-NAD^+ Ɛ-NAD^+) as a substrate which is hydrolysed to Ɛ-ADPR that is subsequently monitored using a fluorescence plate reader at a wavelength range of λex/em 270-300/410-420 nm (Barrio et al., 1972). The substrate Ɛ-NAD^+ possesses low fluorescence intensity because of the internal quenching effect of the nicotinamide unit, which suppresses the fluorescence signals produced by the etheno group. CD38 hydrolyses the β-glycosidic bond between the nicotinamide and the ribose unit to diminish this quenching effect, enhancing the product's fluorescence intensity of Ɛ-ADPR (Benton et al., 2021).

The NAD^+ hydrolysis can be further measured using HPLC, where the product ADPR is precisely estimated (Zhang et al., 2019). HPLC is used chiefly for NAD^+-related substrates such as NMN and NaADP. The cyclase function of the enzyme is measured by using nicotinamide guanine dinucleotide (NGD^+), which gets cyclised to cGDPR and gives a fluorescence maximum at λex/em 300/410 nm (Oliveira et al., 2018). Both substrates (Ɛ-NAD^+ and NGD^+) could further be applied in a continuous microplate reader using a 96-well plate, making them suitable substrates to analyse the hydrolase (Ɛ-NAD^+) and cyclase (NGD^+) functionality of the enzyme. It is important to note that inhibitor screening based on hydrolase and cyclase assays revealed that some inhibitors are significantly more selective to one enzyme function than the other (Benton et al., 2021). CD38 has a more dominant hydrolase function than CD157, which has a more dominant cyclase enzyme similar to *Aplysia* ADP ribosyl cyclase as presented in Figure 5.3 (Graeff et al., 2001) is presented in Figure 5.3. The kinetic parameters for different substrates towards soluble CD38 enzyme are summarised in Table 5.2.

Spectrophotometric detection measures the 2-phosphate derivative of NAD^+, i.e. NADP (Veskoukis et al., 2018). Total cellular NADP is isolated in tissue lysate which is mixed with cycling buffer (100 mM Tris–HCl at a pH of 8, 0.5 mM thiazolyl blue tetrazolium bromide (298-93-1) (MTT), 2 mM phenazine ethosulfate, 5 mM ethylenediaminetetraacetic acid tetrasodium salt (Na_4EDTA) and 1.3 µU/ml glucose 6-phosphate dehydrogenase (G6-PD), incubated in dark at 37 °C for 5 min. 10 mM glucose 6-phosphate was added, and a change in absorbance was monitored at 570 nm, representing formazan formation. Similarly, NAD^+ and NADH in the tissue lysate were processed to formazan; however, a different cycling buffer was used. Cellular NaADP concentration was measured using anion-exchange HPLC (Churamani et al., 2004). We optimised the capillary electrophoresis method to monitor the hydrolysis of NAD^+, NADP, NaAD, and NaADP in a mixture of the samples. Chapter 3 of this dissertation provides further details. The CE assay was performed for NPP3 only; however, other enzymes like CD38 and NPP1 can also be tested using the established protocols. Investigating the comparative analysis of NPPs and CD38 for hydrolysis of NAD+, NADP, NaAD, and NaADP will be interesting. Moreover, NMN is another exciting candidate for comparative analysis of CD73 and CD38.

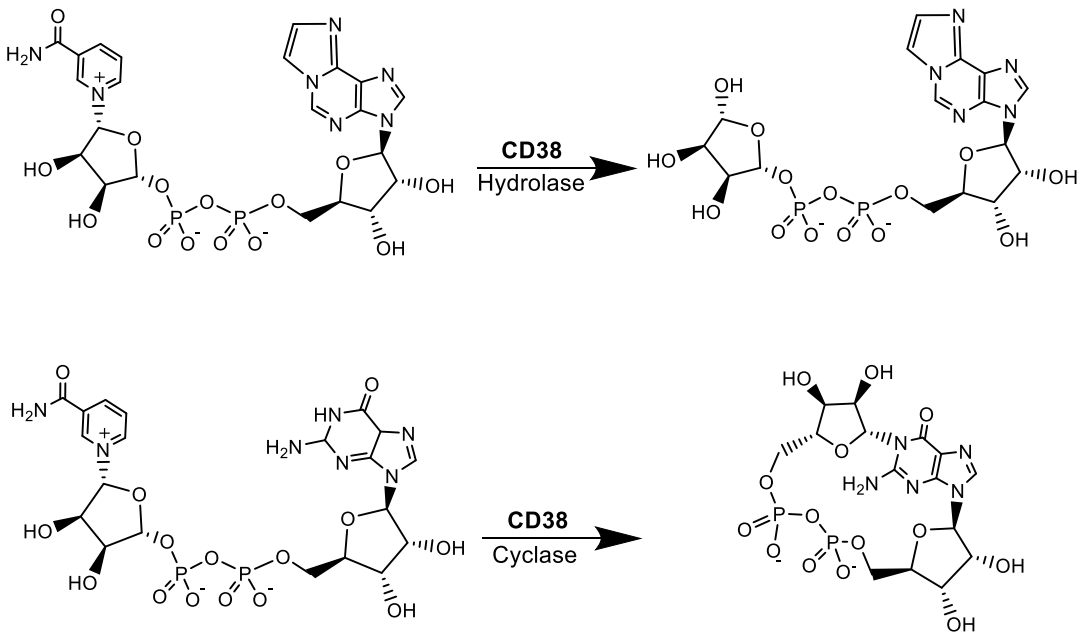

Figure 5.3: Schematic presentation of hydrolase assay with NAD^+ and cyclase assay with NGD^+

Table 5.2: Enzyme kinetics of CD38 towards multiple substrates

Substrate	Enzyme source	Assay	K_m (µM)	V_{max} or K_{cat} s^{-1}	Ref.
ε-NAD^+	Ba/F3 cell lines in DMEM, 10 % FCS, 1 % P/S, 400 mM glutamine, 37 °C, 5 % CO_2	Fluorescence detection[b]	30.9 ± 7.2	405 ± 40[a]	(Blacher et al., 2015)
ε-NAD^+	Soluble enzyme expressed in insect cell expression system and subsequently purified using His-tag	"	15.1 ± 1.9	249 ± 25[a]	**Optimised for this study**
NAD^+	Soluble enzyme expressed in *Pichia pastoris* with expression vector PHIL-SI	HPLC	14.8 ± 0.6 16 ± 1	98.0 ± 29.0 96 ± 5	(Graeffs et al., 1994) (Sauve et al., 1998)
NAD^+	Soluble enzyme expressed in insect cell expression system and subsequently purified using His-tag	CE[c]	48.5 ± 4.6	200 ± 12[a]	**Optimised for this study**
NHD^+	Soluble enzyme expressed in *Pichia pastoris* with expression vector PHIL-SI	HPLC	23 ± 4	7.11 ± 2.22	(Graeffs et al., 1994)
NGD^+	"	HPLC	2.2 ± 0.1	16.7 ± 2.0	((Graeffs et al., 1994)
NMN	"	HPLC	149 ± 15	512 ± 32	((Sauve et al., 1998)
NAADP	"	HPLC	104 ± 10	3,555±155[d]	(Graeff et al., 2006)

aVmax units (µmol/min/mgprotein), b. Removal of the quenching effect increases the fluorescence of the product ε-ADPR, c Capillary electrophoresis, and d Vmax (nmol/min/mg protein).

1.3 Crystal structures of human CD38

Following the first crystal structure of the ectodomain of human CD38 by (Liu et al., 2005). The protein data bank (PDB) now reveals several crystal structures for CD38 in complexes with different ligands and inhibitors, as summarised in Table 5.3. The human enzyme significantly differed from CD157 and *Aplysia* ADP-ribosyl cyclase at both C- and N-terminus. The N-terminus of human CD38 is more elongated than other orthologs and has more positively charged amino acids. Moreover, it also showed structural variations at the C-terminus. It has an additional disulfide bond between Cys119-Cys201 and five conserved disulfide bonds **(**Cys-Cys 67 – 82, 99 – 180, 160 – 173, 254 – 275, and 287 – 296). The soluble variant of CD38 appeared as a monomer, reflecting the transmembrane domain's possible role in dimerisation. Silencing potential glycosylation sites is essential for crystallisation; these sites do not participate in dimerisation in CD38 and CD157. The active site offers interactions where Glu^{226} is necessary for the enzyme's catalytic activity. Mutation of glutamic acid to glutamine (E226Q) leads to the cessation of NADase activity. The other mutations, e.g. E226D and E226G, still possess some residual hydrolase activity. The enzyme predominantly possesses hydrolase activity; however, mutation of Glu146Ala (E146A) leads to an increased cyclase activity (Zhang et al., 2011).

An inactive mutant (E226Q) was used for determining the crystal structures with substrates (NAD^+, cADPR, NGD^+, NaADP, and NMN) to capture them in the binding pocket without hydrolysis (Liu et al., 2006; Liu et al., 2008). The nicotinamide group in the case of NAD^+, NGD^+, and nicotinic acid in NaADP is located in the binding pocket interacting with residues Glu^{146} and Asp^{155} through H-bond and π-π interactions between the pyridine ring and Trp^{189}. The ribose attached to nicotinamide is further stabilised through H-bond formation via Glu^{226}, though it is 7.9 Å away from catalytic residue Glu^{226} (NAD^+ and cADPR). However, five water molecules form a stable H-bond between the residue and the ribose unit. Ser^{193} stabilises the intermediate state and has a regulatory role in the catalysis. Its mutation to alanine led to a significant reduction in enzyme activity. Diphosphates form four H-bonds with Ser^{126}, Arg^{127}, Thr^{221}, and Phe^{222} residues. The adenine ring of NAD^+ is observed away from the active site and is not stabilised as compared to the guanine ring stabilised by Thr^{221}. This leads to a better affinity towards

the active site, and guanine-based scaffolds could be a better option for designing inhibitors (Liu et al., 2007). Structural rearrangements were observed in Glu^{146} –Asp^{147} following interactions of cADPR and cGDPR with the active site after interaction of NAD^+ and NGD^+, respectively, with the wild-type enzyme. cGDPR accommodates better in the active site than cADPR and its northern ribose is 3.96 Å away from Glu^{226}, directly interacting with the residue's carboxyl group. The 2-phosphate of the southern ribose (adenine ring) in the case of NaADP and ADPRP does not interact with the active site. Therefore, NaADP is hydrolysed equally by enzymes like NAD^+ and NADP (Zhang et al., 2013).

Crystallisation studies of CD38 with covalent and non-covalent inhibitors give an essential insight into the active site interactions, which could serve as a foundation for developing potent and selective inhibitors. Conformational changes were observed in the presence of Ca^{2+}, where Trp^{125} moved 5A˚ towards $Trp^{189,}$ leading to the closure of the active site and enzyme inhibition (Liu et al., 2008). Potent inhibitors based on an NMN scaffold, arabinosyl-2-fluoro-2'-deoxynicotinamide mononucleotide (Ara-2'F-NMN), were modified at the free phosphate group to limit hydrolysis by alkaline phosphatases (Table 5.3), however, the substitution of the free phosphate led to a reduction in potency by at least 2- to 3- fold. The nicotinamide group is cleaved because of the electron-withdrawing effect of fluorine at position 2, and the anomeric carbon forms a covalent bond with the carbonyl group of Glu^{226}. The phosphate group was positioned well with Ser^{126}, $Arg^{127,}$ and Phe^{222} through H-bonding (Ting et al., 2012). The quest for non-covalent competitive inhibitors was resolved by using NAD^+, cADPR, and cIDPR scaffolds, where a significant improvement in IC_{50} value was observed, and 8-amino-*N*9-butyl-cIDPR exhibited an IC_{50} of 3.3 μM. The crystal structure showed the catalytic residue Glu^{226} to form hydrogen bonds with the northern ribose; however, the southern ribose can be replaced by an alkyl chain to improve its potency further. Besides small molecule inhibitors for treating CD38-based pathologies, efforts are underway to develop antibodies, and the FDA has approved daratumumab, elotuzumab, and isatuximab for treating multiple myeloma. The crystal structure of CD38 with both antibodies revealed the involvement of a different epitope with no similarity in the amino acid sequence of the two antibodies (Lee et al., 2021; Deckert et al., 2014).

Table 5.3: Reported crystal structures of human CD38

PDB ID	Mutation	Substrate	Active site amino acids	Interactions	Interacting Functional groups	Resolution (Å)	Ref.
1YH3	Wild type (WT)	cADPR	Trp125, 189 Lys129, Glu226, 146	Hydrophobic H- bond	N-atom of adenine 1'-OH of N. ribose	1.91	(Liu et al. 2005)
203Q 203R 203S 203T 203U	E226Q E226D E226G E226Q E226Q	cADPR cGDPR NGD$^+$	Trp189 Glu146, Asp155 Glu226	Hydrophobic H-bond	Adenine/ Guanine N. ribose	1.98 1.75 1.50 1.68 2.10	(Liu et al. 2007)
4F45 4F46	E226Q WT	NAADP ADPRP	Trp189 Glu146, Asp155 Glu226 Thr221, Ser126, Arg127 Thr221, Trp176 *Additional* Glu226	Hydrophobic H-bond - - - - H-bond	Nic. Acid – indole Carboxyl 3'-OH of N. ribose* di-phosphate chain adenine pointed outward 1'-OH, N. ribose*	2.10 1.70	(Zhang et al. 2013)
2165 2166 2167	E226Q WT -	NAD^+ GDPRI ADPR	Glu146,Asp155 Trp189 Glu226 Ser126,Arg127,Thr221 Ser193	H-bond π-π H-bond - -	Nicotinamide Pyridine-indole OH-N. ribose di-phosphate chain C-1 of N. ribose	1.90 1.76 1.76	(Liu et al. 2006)
3DZJ 2HCT 3DZH 3DZK 3DZI	E226Q WT - -	NMN GTP NMN/GTP R5PI/GTP	NA/N.ribose/phosphate: identical to NAD^+ Glu146, Asp155, Thr221 Glu226	 H-bond -	 Guanine 2'-3'-OH of R5P	1.90 1.73 1.81 1.73	(Liu et al. 2008) (Graeff et al. 2006)
		Inhibitors					
3DZF 3DZG	WT	Ara-F-R5P Ara-F-R5P-Nic	Glu226	Covalent H-bonding	Additional electrostatic interactions due to fluorine Phosphates	2.0 1.64	(Liu et al. 2008)
2PGJ	WT	N1-cIDPR	Glu226 Trp125, Ser126, Arg127, Thr221,Phe222, Glu146, Trp189	H-bond	2'-3'-N. ribose	1.70	(Liu et al. 2007)

2PGL	E226Q	-	Ser193			1.76	
3F6Y	WT	Ca^{2+}	Trp125,189	hydrophobic	Active site closure	1.45	(Liu et al. 2008)
3ROK 3ROQ 3ROM 3ROP	WT	CZ-27 CZ-46 CZ-48 CZ-50b	Glu226 Phe222, Arg127, Ser126	Covalent H-bond	Nicotinamide Phosphate	1.65 1.91 2.05 1.95	(Kwong et al. 2012)
4TMF	WT	8-NH_2-*N*9-butyl-cIDPR	Glu226 His133	H-bond	2'-3'-N. ribose	2.05	(Swarbrick et al. 2014)
4XJT 4XJS	WT	8-Quinoline carboxamide 4-NH2-8-Quinoline carboxamide	Glu146, Asp155 Trp189 Thr221	H-bond π-π stacking H-bond	Carboxamide nitrogen Quinoline group 4-benzyl amine	2.60 2.80	(Becherer et al. 2015)
6EDR	WT	S-NAD^+	Ser193, Glu146 and 226	H-bond	N. ribose	2.40	(Dai et al. 2018)

1.4 Small molecule inhibitors of CD38

Small molecule inhibitors of CD38 are reported in the literature (see Table 5.4). These inhibitors could block enzymatic activity in nano – to micromolar concentrations. The inhibitors are classified based on their scaffolds as nucleotidic or non-nucleotidic. A breakthrough in CD38-based multiple myeloma management was achieved by anti-CD38 antibodies, which have shown great potential. The first one received FDA approval for disease management. However, small-molecule inhibitors are increasingly getting attention as a combination therapy alongside anti-CD38 antibodies due to the emergence of resistance to antibody treatment. This Chapter will focus on the small molecule inhibitors of CD38.

a. Nucleotidic scaffolds

Nucleotidic scaffolds represent substrate analogues of NAD^+, NMN, NGD^+, or the product ADPR, resulting in highly potent inhibitors (Wang et al., 2014). Replacement of the 2-OH group of the northern ribose by fluorine in 2'-deoxy-2'-fluoroarabinosyl derivatives showed IC_{50} values in the low nanomolar range. The 2'-fluoro group is involved in additional electrostatic interactions with Glu^{226} that lead to covalent binding. Moreover, these molecules are targets for diphosphatases, possibly leading to significantly decreased potency under physiological conditions. To protect the free phosphate groups from phosphatase reaction, attempts were made to modify them through different substitutions; however, all such efforts led to a decrease in potency. Small molecules comprising

nicotinamide mononucleotide derivatives showed moderate inhibitory potency towards CD38. Attempts were made to protect the free phosphate group from physiological phosphatases, and a moderate potency was achieved. Thus, searching for potent and selective nucleotidic CD38 inhibitors is still an ongoing research and requires further investigation.

b. Non-nucleotidic scaffolds

The discovery of flavonoids from natural sources such as apigenin and luteolin as moderately potent inhibitors of CD38 led to an intense research interest in investigating different heterocyclic compounds. GSK extensively investigates quinoline derivatives and potency in the low nanomolar range has been achieved (Table 5.4). These compounds mainly exhibited a non-competitive mode of inhibition. However, the luteolin derivative, luteolidine, achieved competitive inhibition with moderate inhibition, showing IC_{50} values in the micromolar range. Flavonoids are usually non-selective and further modulate different targets, including enzymes and receptors. Therefore, searching for an ideal non-nucleotidic small molecule inhibitor of CD38 is still an appealing area of research. The suitable candidate must be potent and stable enough to withstand physiological conditions.

Table 5.4: Small molecule inhibitors of human CD38

Scaffolds	**Structures**	**IC_{50} or K_i nM**	**Mode of inhibition**	**Reference**
Nucleotidic				
Dinucleotide based derivatives				
Ara-F-NAD$^+$ Ara-F-NGD Ara-F-NHD	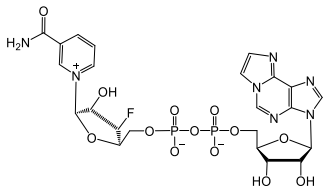	61.1 89.3 109	Covalent bonding due to fluorine at the C2 position of northern ribose with Glu^{226}	(Wang et al., 2014)
4'-thioribose NAD$^+$ (S-NAD$^+$)	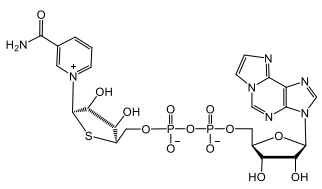	*28500*	Competitive	(Dai et al., 2018)

Nicotinamide				
Ara-F-NMN CZ-17	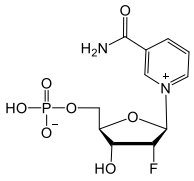	297 > 500	Covalent binding	(Wang et al., 2014) (Kwong et al., 2012)
CZ-48	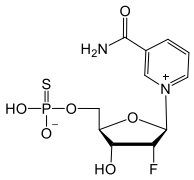	2000	Competitive	
Compound 4	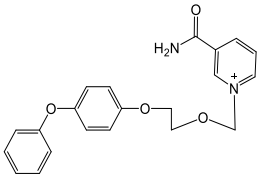	3.85 x 10^6	"	(Dong et al., 2011)
Non-nucleotidic				
Flavonoids				
Luteolidine	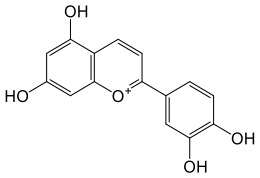	6000	Competitive	(Kellenberger et al., 2011)
Apigenin	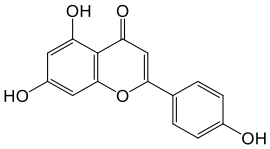	10310	NT*	(Escande et al., 2013)
Quercetin	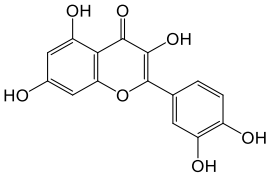	13801	NT*	
Tannic acid	$C_{76}H_{52}O_{46}$	33.8 nM	Competitive	(Blacher et al., 2015)
Anthraquinone				
Rhein K-Rhein	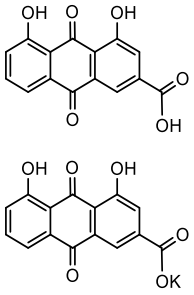	1240 840	Non-competitive	(Blacher et al., 2015)

Quinoline				
Quinoline carboxamide	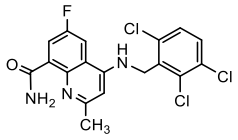	76.1	Mixed mode of inhibition	(Becherer et al., 2015)
Di-amino Quinazoline	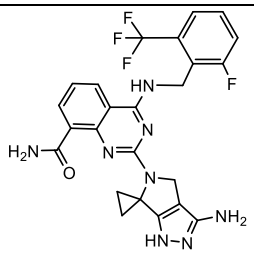	4.00	NT*	(Deaton et al., 2018)
Thiazoloquinolinone	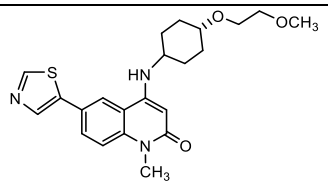	7.31	Non-competitive	(Haffner et al., 2015)
Miscellaneous scaffolds				
23	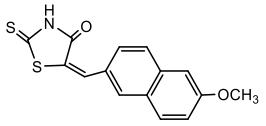	9300# 4650$	NT*	(Benton et al., 2021)
S125-8b	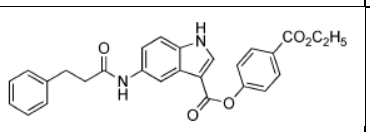	4700	Competitive	(Zhou et al., 2012)
LX-102	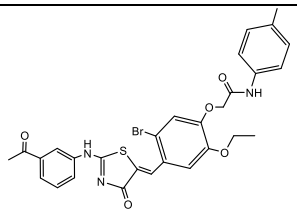	14910	Allosteric	(Yang et al., 2019)

*Not tested, # IC_{50} in hydrolase assay using ε-NAD^+, $ IC_{50} in cyclase assay using NGD^+

1.5 Research objective

This research project focuses on discovering and examining small-molecule inhibitors that can effectively compete with CD38. To achieve this goal, we have produced recombinant CD38 in insect cells. Our approach involves building upon previous studies on competitive *4H*-chromene and refining this chemical structure to enhance its ability to inhibit CD38. The resulting compounds will be evaluated for their selectivity towards other ecto-nucleotidases such as CD39, NPP1, NPP3, and CD73.

2.0 Materials and Methods

d. Substrates and chemicals

Adenosine, adenosine 5'-mono, di- and tri-phosphate (AMP, ADP, ATP), adenosine diphosphate ribose (ADPR), Nicotinamide adenine dinucleotide (NAD^+) and its phosphate analogue (NADP), Nicotinic acid adenine dinucleotide (NaAD) and its phosphate analogue (NaADP), *p*-nitrophenyl 5'-thymidine monophosphate (*p*-Nph-5'-TMP), and 4-(2-hydroxyethyl)-1-piperazine ethanesulfonic acid (HEPES) were purchased from Sigma (Steinheim, Germany. Fluorescence substrates Ɛ-NAD^+ and Ɛ-AMP were purchased from Biolog Life Sciences. cDNA of human CD38 (NM_001775) was purchased from Origene Technologies, USA. Restriction enzymes, T4 DNA ligase, and Q5 HF-DNA polymerase were purchased from New England BioLab GmbH. Corning® flat-bottom 96-well half-area microplates, black polystyrene, were purchased from Sigma–Aldrich (Steinheim, Germany). Cellfectin™ II Reagent (Thermo Fisher Scientific, MA, USA), baculovirus genomic ProEasy™ vector DNA (Cat. #A10S, AB vector, CA, USA), Insect-XPRESS™ media (#: BE12-730Q, Lonza, Switzerland) and HisPur™ Ni^{2+}-NTA spin columns (#: 88226, Thermo Fisher Scientific, MA, USA) were used as protein expression and purification tools. Amicon® Ultra-15 concentrator with 10 kDa cut-off was purchased from Merck Millipore, MA, USA.

e. Instrumentation

Fluorescence units were measured using a FlexStation® 3 Multi-Mode Microplate Reader (Medical Devices LLC, USA) and Softmax Pro 3.0 software for data collection. Tests with natural substrates were performed using a p/ACETM MDQ plus capillary electrophoresis system (AB Sciex LLC, Framingham, USA). Data collection and peak area analysis were conducted by the P/ACE MDQ software 32 KARAT obtained from Beckman Coulter (Fullerton, CA, USA).

2.1 Protein expression and purification

Proteins were recombinantly expressed as soluble enzymes, excluding the transmembrane domain in *Spodoptera frugiperda* (*sf9)* insect cells using ProEasy™ linearised baculovirus genomic DNA. Details of cloning tools used for both types of proteins are given in Table 5.5. Protein was expressed as previously reported (Lee et al.,

2017). Briefly, for soluble enzymes, the sequence for the transmembrane domain (TM) of each enzyme is trimmed, and the gene of interest (GOI) was subcloned in the *p*-ACGP67-A expression vector between restriction sites. 10 % Cellfectin^{TM}, 1 µg of plasmid DNA containing GOI, and 2.5 µL of ProEasy^{TM} DNA in 100 µL of culture media were incubated for 20 min at room temperature. The resulting DNA emulsion was used to infect semi-confluent *sf9* adherent cells culture for 96 h at 27 ^{o}C to amplify virus titer and protein expression. Medium-containing soluble enzymes were concentrated up to approximately 70 – 80 % with Amicon® Ultra 15 mL centrifugal filter with variable cut-off limits (10 kDa, 4500 x G, 30 min). Subsequently, His-tagged protein was purified by HisPur^{TM} Ni^{2+}-NTA spin columns by increasing the imidazole concentration from 10 mM to 250 mM (*Manufacturer's specs)*. The eluted enzyme was filtered and concentrated with 10 mM HEPES pH 7.2 buffer to remove imidazole. Protein concentration was determined by the Lowry method (Randall et al. 1951). The enzyme was stored at -80 ℃ in a buffer containing 10 mM HEPES, 10 % glycerol, and 50 mM NaCl.

2.1.1 Western blot for expression analysis

The proteins were loaded onto 10 % bis-Tris SDS-page gel produced using a standard protocol. 100 ng of purified protein was dissolved in 4x NuPAGE LDS sample buffer. The sample was incubated with the loading dye for 30 min at RT. MOPS running buffer was prepared in VE water and filled in an electrophoresis chamber. 4 µL of pre-stained protein ladder and 30 µL of protein sample were loaded. Electrophoresis was initially started at 50 V until the samples reached the resolving gel, and later, we proceeded with 120V. The protein gel was either treated with Coomassie blue dye or transferred to nitrocellulose membranes for western blot analysis. Anti-His tag primary antibodies were allowed to interact overnight with the membranes in a cold room with temperature control (4 ℃). NPP3 and -5 have been used as positive control samples.

2.2 Biological assays

a. ε-NAD^+ assay for CD38

The assay is based on the disruption of internal quenching in ε-NAD^+ between nicotinamide and ε-adenine group, allowing investigation of the product formed during the reaction. The assay was optimised based on a previously published methodology for measuring CD38 activity (Schultz, 2018). Briefly, CD38 attacks the glycosidic bond

between the ribose unit and the nicotinamide group of the molecule. It disrupts the internal quenching effect due to the nicotinamide moiety and the adenine ring, leading to an approximately 92% increase in fluorescence intensity. Further details of assay validation and calibration are given in chapter 3 of this dissertation. Six different concentrations of the soluble CD38 (1 – 250 ng) were incubated with 20 µM Ɛ-NAD^+ for 30 min at 37 ^oC in 96-well plates to get suitable enzyme concentration for 20% hydrolysis the substrate. Fluorescence intensity was estimated at λexcitation/emission (λex/em 300/410 nm) in a fluorescence plate using a continuous plate reader FlexStation® 3 Multi-Mode Microplate Reader (Medical Devices LLC. USA).

Table 5.5: Cloning tools for the expression of soluble and membrane-bound enzymes

Enzymes	A.A.*	Vector	R. S. **	Primers
Soluble				
CD38	(43-300)	*p-ACGP67-A*	XbaI/NotI	*f'-5'-GATC-*TCTAGA-**A-**GTCCCGAGGTGGCGC-3' *r'-*5'-*GATC-*GCGGCCGC**TTA**GTGGTGGTGGTGGTGA TGGTGGTGGTGGATCTCAGATGTGCAAGATGAA-3'

*Amino acids, Expression vector, ** Restriction site, Expression vector, Primers: Irrelevant base pairs are shown in *italics,* underlined sequence represents restriction sites, and bold letters are the stop codon

b. p-NPh-5'-TMP assay for NPPs

The artificial substrate *p*-nitrophenyl-5'-thymidine monophosphate-(*p*-Nph-5'-TMP) based colourimetric assay was performed as previously reported (Cimpean et al., 2004). Briefly, 985 ng of soluble NPP3 was treated with 400 µM of *p*-Nph-5'-TMP in 10 mM HEPES, pH 7.4, $CaCl_2$ 0.5 mM, and $ZnCl_2$ 0.01 mM for 30 min at 37 °C. The reaction was terminated by adding 20 µL of 0.1M NaOH, and the absorbance of *p*-nitrophenolate was measured at 405 nm using Mithras LB 940 continuous plate reader and MikroWin software for data acquisition.

c. Ɛ-AMP assay for CD73

During this research project, I developed a highly sensitive and robust fluorescence assay for CD73 that applies to cancer cell lines that overexpress CD39, NPP1, and CD73. Briefly, a suitable enzyme concentration (capable of hydrolysing 20% of Ɛ-AMP to the product Ɛ-adenosine) was mixed with 50 µM of inhibitors and 20 µM of substrate. The mixture was allowed to react for 30 min at 37℃. Samples were subjected to intense

precipitation conditions capable of removing free phosphates and terminal phosphate-containing reactants from the reaction mix, leaving only Ɛ-adenosine in the solution, which was then transferred to a black 96-well plate. The details of the assay procedure and precipitation buffer can be found in Chapter 2 of this dissertation. Fluorescence measurement was the same as previously described in Ɛ-NAD^+ assay conditions.

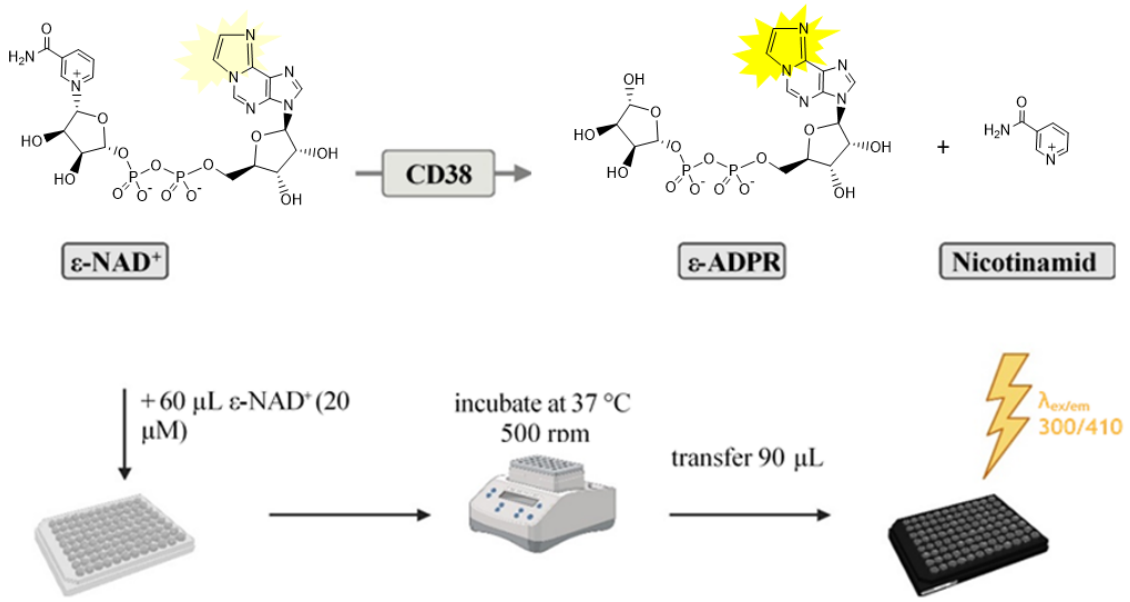

Figure 5.4: Schematic presentation of the assay procedure involving Ɛ-NAD^+. The assay is based on the disruption of the quenching effect after hydrolysis of a β-glycosidic bond by CD38, resulting in increased fluorescence intensity (Stach et al., 2023).

d. CE assay using a diode array (DAD) detector

Capillary electrophoresis assay (CE) characterises CD38, CD39, and NPP1 vs. natural substrates: NAD^+ 100 µM for CD38, ATP 100 µM for CD39 and NPP1. The reaction buffers were specific for each enzyme; for CD38 (10 mM HEPES pH 7.2), CD39 (10 mM HEPES, 2 mM $CaCl_2$, 1 mM $MgCl_2$ pH 7.4), and NPP1 (10 mM HEPES, 500 µM $CaCl_2$, 10 µM $ZnCl_2$ pH 7.4). CE running conditions (50 mM phosphate buffer, 0.002% polybrene with separation voltage of -15 kV) using 30 cm capillary length as previously reported (Lee et al., 2017). Briefly, reaction samples were electro-kinetically loaded (-6 kV, 30 sec) into a fused silica-coated capillary [30 cm (20 cm effective length) × 50 µm (id), × 360 µm (od) and allowed to migrate through solution based on their ionic mobility and application of electric field (-15 kV, 0.1 psi pressure). Analysis was carried out using the P/ACE MDQ

CE system (Beckman Instruments, Fullerton, CA, USA) equipped with either DAD (λabs 254 nm).

The percentage inhibition was calculated by using the Equation 5.1:

$$\%\, inhibition = B - T/B * 100 \qquad 5.1$$

B= Blank sample without inhibitor

T= Test sample with inhibitors

2.3 Michaelis-Menten (K_m) constant

The Km value for human soluble CD38 was measured towards both Ɛ-NAD+ and the natural substrate NAD+. Ten concentration point analyses were performed (1 to 500 µM for Ɛ-NAD+) and 5 to 500 µM for NAD+. The subsequent steps of the reaction methodology and product monitoring were the same as described in the assay mechanism part. For Ɛ-NAD+, the background fluorescence values were subtracted from the out of the enzyme reaction. Moreover, in the natural substrate NAD^+, background values of ADPR were also subtracted.

2.4 Screening of compound libraries

Stock solutions for ε-NAD^+ at 20 µM were prepared in the buffer in the needed volume. The inhibitors were synthesised by Dr Zahid Shafiq (ZS-compounds), Dr Ahmed Elgokha (AE-compounds), and Dr Lukas Wendt (LW-compounds). The compounds were dissolved in 100 % DMSO to reach a concentration of 100 mM. For the compounds ZS-44 (PZB22222033A), ZS-45 (PZB22222034A), ZS-52 (PZB22222036A), ZS-ML26 (PZB22222039A), ZS-ML27 (PZB22222040A), ZS-ML28 (PZB22222041A), ZS-ML29 (PZB22222042A), ZS-ML30 (PZB22222043A), ZS-ML32, ZS-ML33, ZS-ML39 (PZB22222045A), ZS-ML40 (PZB22222046A), ZS-62 (PZB22222050A), ZS-68 (PZB22222052A), ZS-74 (PZB22222053A), ZS-77 (PZB22222054A), ZS-78 (PZB22222055A), ZS-14, ZS-87 (PZB22222057A), ZS-98 (PZB22222060A), ZS-99 (PZB22222061A), ZS-100 (PZB22222062A), ZS-101 (PZB22222063A), and ZS-111 (PZB22222067A), 1 M NaOH-solution (approximately 2 – 8 µL) was added to dilute them properly. The abbreviation notifies the compounds not registered in the compound library and is denoted by the chemist's initials.

2.5 Determination of concentration inhibition (IC_{50} values)

After the initial screening of the compounds at 50 µM against CD38, CD39, NPP1, and CD73, inhibitors that showed >50 % inhibition were further subjected to IC_{50} value determination using 12 to 15 concentration points (500 – 0.001 µM). The subsequent reaction conditions and procedure remained the same as described before. For Ɛ-NAD^+, the background fluorescence signals were measured before the addition of the enzyme and were subtracted from test values. The residual activity of the enzyme was normalised and plotted against inhibitor concentration. The nonlinear regression was performed using GraphPad Prism.

2.6 Selectivity testing for the most potent inhibitors

a. Towards ectonucleotidases

Selectivity testing was initially planned to include NTPDases (2, 3, and 8), NPPs (3, 4, and 5), CD73, CD157, and alkaline phosphatases; however, due to time constraints, we could only include NPP3 and CD73. The remaining tests will be performed before the submission of the paper. The most potent inhibitors from the current study were treated with the respective enzymes at 50 µM concentration using previously described assay conditions for NPP3 and CD73. The % inhibition was calculated using equation 5.1

b. A_1 and A_{2A} adenosine receptors

Jonathan Schlegel transiently expressed human A_1 and A_{2A} adenosine receptors in FreeStyle™ CHO-S cells. Radioligand binding experiments were performed in an incubation buffer (50 mM Tris, pH 7.4). The binding of the compound was determined versus [^{3}H]CCPA (A_1AR, final conc. 1 nM) and [^{3}H]MSX-2 (A_2A, final conc. 1 nM)] respectively. The binding affinity was determined using liquid scintillation counting. Two concentrations of 1 and 10 µM were used during the test.

2.7 Determination of inhibition type

The most potent inhibitor amongst the current series PZB22222054A was further analysed for inhibition type determination using five different NAD^+ concentrations (500, 250, 125, 62.5, and 31.2 µM) and six inhibitor concentrations (1.5, 0.75, 0.375, 0.187,

0.093, and 0 μM). The reaction conditions were the same as described in the assay mechanism section. Similarly, PZB22222043A was tested for its inhibition mechanism towards soluble CD39.

3.0 Results and Discussion

3.1 Protein expression and purification

Soluble CD38 was recombinantly expressed using the insect cell expression system. The expression plasmid contains a secretion sequence before the gene of interest to traffick the protein to the medium from where it was collected. The protein collection from the medium was initially performed by concentrating it using an Amikon filter with a 10 kDa cut-off limit, followed by washing the crude protein with HEPES 10 mM pH 7.2. The washing step removed the residuals of the medium necessary for increased binding of the His-tagged proteins to the Ni beads. The crude proteins were then subjected to purification by using Ni-NTA affinity chromatography. After incubating the expressed protein with Ni beads for four hours on a rotating wheel, the desired protein is eluted by increasing concentrations of imidazole from 10 to 250 mM. Subsequently, the solution containing purified protein and imidazole was further subjected to buffer exchange with 10 mM HEPES, 10 % glycerol, pH 7.2, aliquoted, and stored at -80 ℃ for further use.

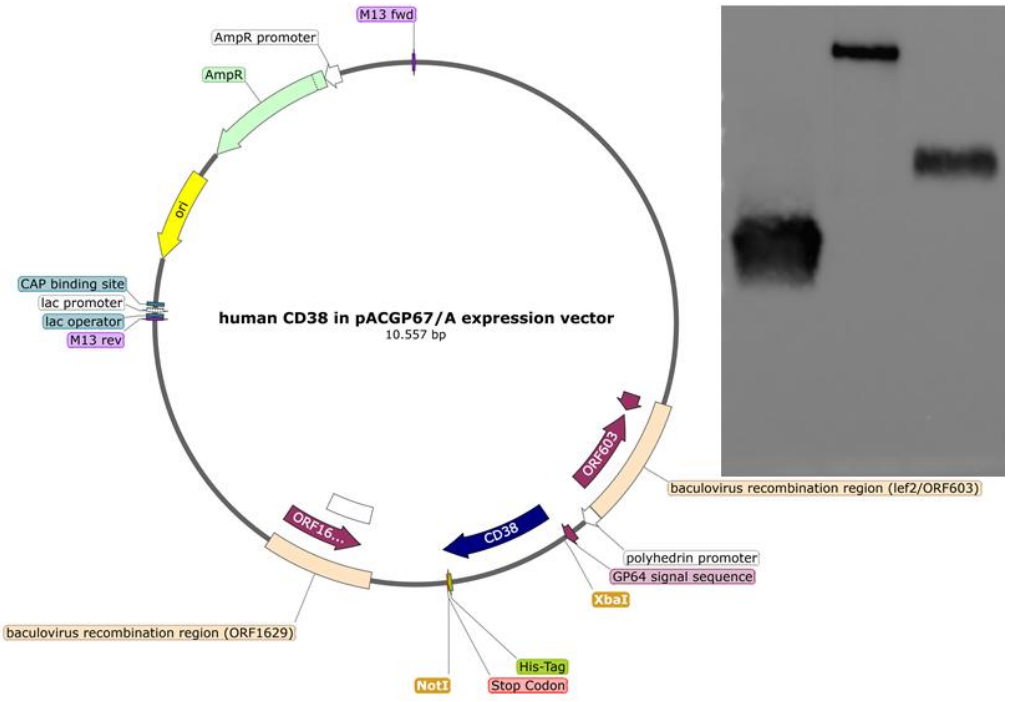

Figure 5.5: CD38 sequence in pACGP67-A expression vector. A His-tag sequence is found at the C-terminus and a GP64 secretion signal sequence at the N-terminus. Western blot confirmed the expression of the 9-fold histidine tag.

The Michaelis-Menten constant was measured for soluble CD38 using either the fluorescence assay with Ɛ-NAD^+ or the CE assay using natural substrate NAD^+. The determined K_m was recorded as 15.1 µM for Ɛ-NAD^+ and 48.5 µM using NAD^+ as substrates. Three independent tests were performed in triplicate observations. The curves are shown in Figure 5.6.

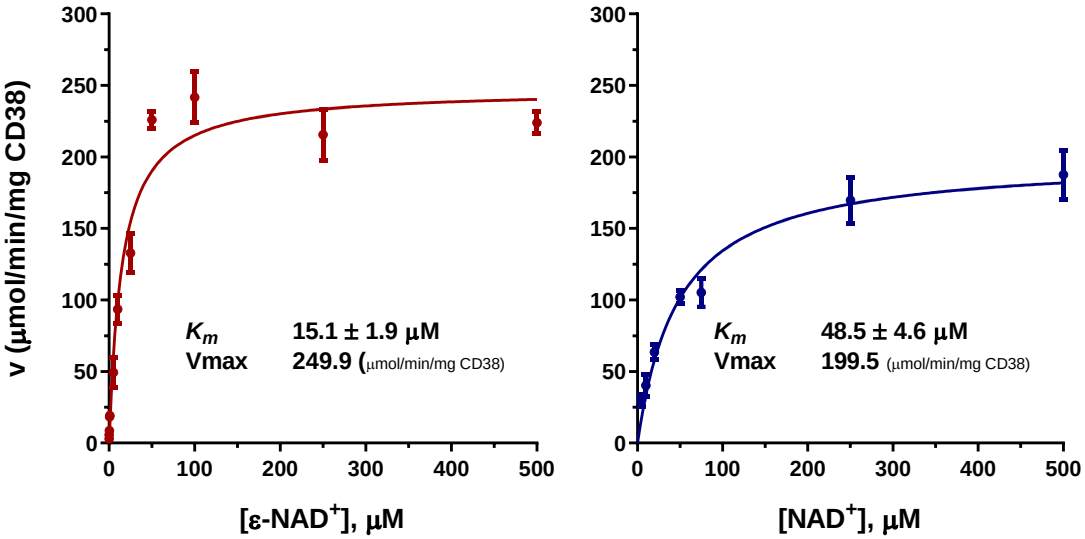

Figure 5.6: **Michaelis-Menten constant for CD38** using A) artificial substrate Ɛ-NAD^+ and B) natural substrate NAD^+.

3.2 Screening campaign

Table 5.5 summarises the outcome of the screening campaign towards CD38, CD39, NPP1, and CD73. The initial screening was performed at 50 µM inhibitor concentration using Ɛ-NAD^+ (20 µM) for CD38 and ATP (100 µM) for CD39 and NPP1. Ɛ-AMP (20 µM) was used for monitoring CD73 activity. The reaction procedure and analytical methods of different assays are described in section 2.2 of this Chapter. Interesting results were obtained for a few compounds where an increase in the soluble CD39 activity was observed, and %inhibition was recorded in up to (-)100%; however, we couldn't confirm these findings using membrane-bound CD39. Currently, we cannot fully justify this activation of the enzyme activity. Therefore, we didn't make these findings part of this thesis.

3.3 Concentration-dependent inhibition curve (IC_{50}) and K_i value determination

a. CD38

The IC_{50} values at CD38 were primarily measured using Ɛ-NAD^+ as a substrate. The cut-off percentage was set at 50%. The compounds with IC_{50} value < 2 µM were further analysed using the natural substrate NAD^+ in CE assays. K_i values were calculated from the IC_{50} values by using equation 5.2 (Cheng-Prusoff 1973).

$$Ki = IC50 \div (1 - \frac{S}{Km})\text{------} \qquad 5.2$$

Table 5.6: Inhibitory potency of compounds in the current study

Internal/ PZB I.D.	K_i in µM (% inhibition at 50 µM)			
	sCD38 (Ɛ-NAD^+ 20 µM)[a]	sCD39 (ATP 100 µM)[b]	NPP1 (ATP 100 µM)[c]	CD73 (Ɛ-AMP 10 µM)[d]
ZS-37F2	**9.16 ± 0.43** (77 ± 1)	(43)	(-12)	(-3)
34iv	**4.07 ± 0.50** (77 ± 1)	(38)	(10)	(-10)
PZB22222034A	(24 ± 12)	(31)	(15)	(0)
PZB22222035A	(24 ± 15)	(17)	(17)	(4)
PZB22222036A	(26 ± 13)	(31)	(19)	(1)
PZB22222033A	(28 ± 13)	(18)	(0)	(2)
PZB22222041A	**27.5 ± 1.9** 54 ± 21 %	(51)	(-16)	(25)
PZB22222044A	(47 ± 9)	-	-	-
PZB22222045A	**33.5 ± 5.0** (55 ± 3)	(71)	(16)	(-6)
PZB22222050A	(6 ± 1)	-	-	-
PZB22222052A	**16.6 ± 2.6** (60 ± 4)	(59)	(25)	(16)
PZB22222060A	(20 ± 4)	(30)	(43)	(15)
PZB22222061A	(14 ± 9)	(10)	(51)	(3)
PZB22222039A	**23.5 ± 2.5** (60 ± 4)	**5.54 ± 1.20** (80)	(-18)	(17)
PZB22222040A	**0.542 ± 0.073** (99 ± 1)	**0.653 ± 0.234** (95)	(78 ± 13)	(14)
PZB22222043A	**0.237 ±0.128** 99 ± 0 %	**0.154 ± 0.017** (97)	(83 ± 8)	(35)
PZB22222055A	**0.872 ± 0.092** (98 ± 0)	**0.597 ± 0.123** (98)	(81 ± 5)	(40)
PZB22222067A	**(0.535 ± 0.065)**	**1.31 ± 0.67**		

	(98 ± 0)	(99)	(80 ± 5)	(-5)
PZB22222057A	**4.15 ± 0.10** 93 ± 0 %	**7.60** (78)	(57)	(20)
PZB22222053A	**0.300 ± 0.035** (97 ± 2)	**2.32 ± 0.15** (81)	(63 ± 20)	(14)
PZB22222054A	**0.201 ± 0.022** 97 ± 1 %	**2.71 ± 0.62** (91)	(72 ± 14)	(17)
PZB22222059A	**2.72 ± 0.52** 93 ± 4 %	(38)	(42)	(44)
ZS-ML32	**8.75 ± 0.31** (84 ± 0)	**27.8 ± 2.6** (78)	(28)	(13)
ZS-ML33	**(4.64 ± 0.71)** (88 ± 4)	**1.54 ± 0.73** (98)	(72)	(21)
PZB22222042A	**5.15 ± 0.71** (88 ± 4)	**5.36 ± 0.94** (75)	(18)	(20)
PZB22222046A	**15.3 ± 2.1** (65 ± 10)	**6.55 ± 0.23** (70)	(33)	(19)
PZB22222037A	(40 ± 13)	(53)	(-6)	(-3)
ZS-ML23	(26 ± 9)	(4)	(50)	(2)
ZS-ML24	(28 ± 7)	(51)	(39)	(-15)
ZS-75	(43 ± 3)	(42)	(40)	(20)
ZS-76	(-2 ± 7)	(-19)	(47)	(13)
ZS-84	(28 ± 4)	(-5)	(39)	(16)
ZS-85	(7 ± 1)	(-4)	(49)	(4)
PZB22222056A	(-4 ± 1)	(3)	(50)	(8)
PZB22222064A	**12.0 ± 2.3** (67 ± 0)	**7.56 ± 3.15** (71)	(32)	(2)
PZB22222063A	**25.7 ± 5.0** (62 ± 6)	(46)	(18)	(-7)
PZB22222062A	(12 ± 7)	(21)	(50)	(3)
PZB16321014A	**2.50 ± 0.11** (89 ± 0)	(63)	(12)	(27)
PZB16321023A	**4.60 ± 0.24** (81 ± 1)	(6)	(-10)	(61)
PZB16321060A	**5.91 ± 0.81** (77 ± 1)	(-40)	(31)	(4)
PZB16321061A	**7.92 ± 0.19** (73 ± 0)	(8)	(19)	(3)
PZB16321062A	**20.2 ± 3.8** (67 ± 0)	(-5)	(8)	(17)
PZB16321013A	(26 ± 8)	(-41)	(-1)	(21)
PZB16321011A	(43 ± 4)	(-51)	(30)	(15)
PZB16321010A	**10.8 ± 1.7** (63 ± 5)	(-19)	(10)	(26)
PZB16321018A	(3 ± 5)	(-52)	(10)	(8)

PZB16321029A	(39 ± 4)	(-42)	(8)	(3)
PZB16321019A	(-1 ± 5)	(-32)	(26)	(-7)
PZB16321031A	**9.79 ± 1.39** 58 ± 2	(77)	(-7)	(4)
PZB16321020A	**13.3 ± 1.2** 58 ± 3	(20)	(-4)	(27)
PZB16321021A	(17 ± 5)	(-18)	(17)	(24)
PZB16321024A	(12 ± 8)	(-38)	(10)	(11)
PZB16321035A	**12.6 ± 0.7** 53 ± 4	(-2)	(15)	(3)
PZB16321036A	**15.5 ± 0.8** 57 ± 5	(-9)	(18)	(19)
PZB16321067A	(38 ± 3)	(-100)	(17)	(17)
PZB16321033A	**2.42 ± 0.10** (83 ± 3)	(-67)	(12)	(-27)
PZB16321026A	**4.60 ± 0.30** (73 ± 0)	(-39)	(9)	(15)
PZB16321027A	(40 ± 5)	(-64)	(9)	(34)
LW-345	**5.81 ± 0.69** (96 ± 0)	(49)	(60)	(86)
LW-236	**11.3 ± 0.7** 84 ± 1	(76)	(34)	(-3)
LW-268	**10.2 ± 2.0** 88 ± 3	(-63)	(15)	(8)
PZB16321003A	(42 ± 21)	(-6)	(47)	(0)
PZB16321004A	(22 ± 15)	(-2)	(49)	(6)
PZB16321005A	(44 ± 9)	(-51)	(-1)	(34)
PZB16321009A	(13 ± 12)	(-89)	(4)	(10)
PZB16321006A	(16 ± 12)	(-64)	(-1)	(-2)
PZB16321007A	(38 ± 5)	(5)	(-8)	(-11)
PZB16321008A	(17 ± 10)	(-17)	(-11)	(30)
PZB16321012A	(36 ± 4)	(-36)	(-4)	(50)
PZB16321015A	(24 ± 37)	(-54)	(-8)	(36)
PZB16321030A	(10 ± 6)	(-41)	(7)	(-6)
PZB16321032A	(4 ± 3)	(-28)	(5)	(24)
PZB16321022A	(51 ± 3)	(-8)	(1)	(27)
PZB16321025A	(34 ± 8)	(-16)	(5)	(33)
PZB16321027A	(40 ± 5)	(-64)	(9)	(34)
PZB16321034A	**6.42 ± 1.09**			

	(70 ± 4)	(59)	(34)	(41)
PZB16321037A	(38 ± 6)	(-64)	(5)	(14)
PZB16321052A	**10.2** ± **1.5** 72 ± 3	(-68)	(14)	(7)
PZB16321053A	29 ± 8	(-75)	(15)	(9)
PZB16321055A	**15.5** ± **4.5** 53 ± 6	(-75)	(-5)	(-2)
PZB16321056A	(53 ± 6)	(-80)	(7)	(-6)
PZB16321057A	(72 ± 3)	(-67)	(9)	(-6)
PZB16321058A	(27 ± 3)	(-7)	(2)	(20)
PZB16321059A	(70 ± 1)	(-62)	(8)	(26)
PZB16321068A	(13 ± 10)	(-81)	(16)	(-3)
PZB16321069A	(25 ± 1)	(-85)	(18)	(-7)
PZB16321070A	(28 ± 1)	(51)	(25)	(-19)

[a] Values were determined using the *ε*-NAD^+ Assay with 20 *μ*M *ε*-NAD^+ as the substrate, %inhibition was calculated in a single test as the mean ± SEM) of two observations, *K*i values were calculated as the mean value from the three experiments, testing was performed by Master student Paul Stach.
[b] Values were determined using CD39 CE-assay with 100 *μ*M ATP as the substrate, %inhibition was calculated in a single test with one observation by Salahuddin Mirza, and *K*i values were calculated as mean values from the two/three different experiments by Salahuddin Mirza and Paul Stach.
[c] precipitation assay with 10 *μ*M *ε*-AMP as the substrate, %inhibition was calculated in a single test with one observation by Salahuddin Mirza.
[d] NPP1 CE-assay with 100 *μ*M ATP, % inhibition was calculated in a single test by Salahuddin Mirza.

a. CD39

From our screening campaign towards soluble CD39 at 50 µM inhibitor concentration, it is observed that some compounds are exciting candidates for CD39 inhibition. Compounds like ZS-ML26 (PZB22222039A), 27 (PZB22222040A), 30 (PZB22222043A), 33, ZS-74 (PZB22222053A), 77 (PZB22222054A), 78 (PZB22222055A), and 111 (PZB22222067A) were further selected for the determination of full-scale IC_{50} values against soluble CD39. Three to four separate tests were performed in triplicate using 100 µM ATP as a substrate. Compound (PZB22222043A) is the most potent inhibitor from the current series towards soluble CD39. The IC_{50} value is determined at 0.380 ± 0.041 µM, making it a potent dual inhibitor of CD38 and CD39. Our previous experience with soluble and membrane-bound CD39 shows that soluble CD39 is more flexible in accommodating the competitive inhibitors than the membrane-bound variant (Details will be given in

Chapter 6 of this monograph). We further compared the IC_{50} values of (PZB22222043A) and (PZB22222040A) towards membrane-bound variants of CD39. The IC_{50} values are observed to be somehow higher for membrane-bound enzymes compared to the soluble variant (Figure 5.8).

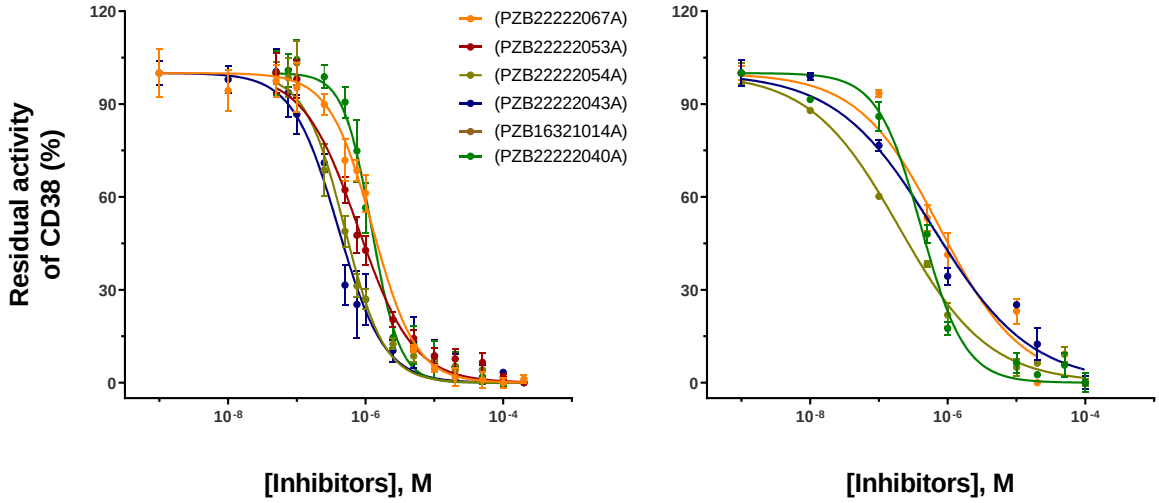

Figure 5.7: **Concentration-dependent inhibition of CD38.** A) vs. ε-NAD^+ B) vs. NAD^+.

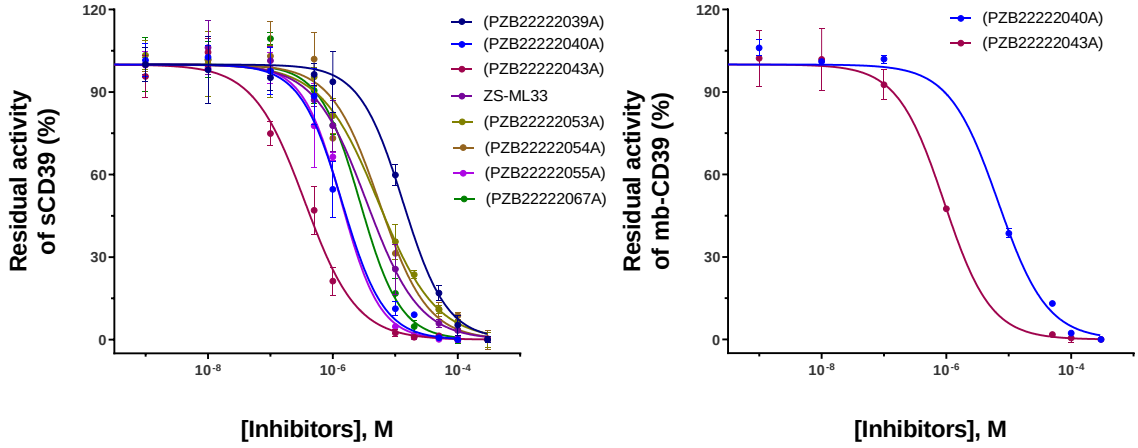

Figure 5.8: **Concentration-dependent inhibition of CD39**. A) soluble CD39, B) membrane-bound (mb) CD39. Two independent tests were performed in triplicate observations. Data are presented as mean ± SEM. For mb-CD39, a single test was performed in triplicate observation. The IC_{50} for (PZB22222040A) was recorded at 6.76 µM while 0.918 µM was calculated for (PZB22222043A).

3.4 Selectivity testing

a. Ectonucleotidases

IC_{50} testing revealed that the most potent CD38 inhibitors (PZB22222043A) and (PZB22222054A) showed a decent inhibition of CD39. However, from the screening campaign at 50 µM, we further observed promising results for NPP1 inhibition by some compounds (Table 5.5). (PZB22222043A) appears to be non-selective towards other NADases and ATPases such as NPPs, precisely NPP1, where >70% inhibition was observed at the tested inhibitor concentration. Additionally, selected most potent CD38/39 inhibitors from the current series (PZB22222040A), (PZB22222043A), ZS-ML 33(PZB22222053A), (PZB22222054A), (PZB22222055A) and (PZB22222067A) have inhibited NPP1 activity. The inhibition testing used orthogonal assays (CE and fluorescent). Furthermore, the 4*H*-chromene scaffold is less accepted by NPP3. (PZB22222043A) could inhibit NPP3 activity by approximately 50 % at 50 µM. The decent % inhibition against NPP3 highlights the broad range of inhibitory profiles for (PZB22222043A) in NADases and ATPases. Other enzymes utilise NAD^+ in their cellular operation, such as CD157 and CD73, which gave us the impression that the binding pocket of these enzymes might have similar acceptance for the 4*H*-chromene. However, screening towards CD73 revealed that most compounds could not inhibit CD73 activity at the tested concentration of 50 µM. Three compounds, LW-345, AE-L45, and AE-L54, have shown some activity. LW-345 could inhibit CD73 activity by nearly 86 % at 50 µM.

These findings showed that the current series is most active at CD38, CD39, and NPP1. These compounds are suitable candidates for testing on cancer cell lines that overexpress multiple enzymes that work in tandem, such as CD39, CD38, NPP1, and CD73. With this inhibitory profile, the 4H-chromene scaffolds are ideal for limiting adenosine production through multiple pathways like canonical (CD39-CD73) and non-canonical pathways (CD38-NPP1-CD73). A comparison of the inhibitory profile is given in Table 5.6. Inhibitory tests were performed towards CD157; however, we could not proceed further with the testing due to the enzyme shortage. Moreover, the assay system of CD157 needs further optimisation. It will be interesting to monitor the cyclase functionality by using NGD^+ as a substrate in the future.

Table 5.7: Selectivity tests for potent compounds from the current series. K_i values in μM or percentage inhibition (in %)

Comp.ID	sCD38 vs. 100 μM NAD^+ (K_m 48.5 μM)	sCD38 vs. 20 μM ε-NAD^+ (K_m 15.1 μM)	sCD39 vs. 100 μM ATP (K_m 67.9 μM)	sNPP1 vs. 100 μM ATP (K_m 8.17 μM)	sNPP3 vs. 100 μM NAD^+ (K_m 41.2 μM)	sCD73 vs. 10 μM ε-AMP (K_m 6.45 μM)
(PZB22222040A)	0.135 ± 0.001	0.542 ± 0.073	0.635 ± 0.234	<50 (78)	>50 (28)	>50 (14)
(PZB22222043A)	0.200 ± 0.038	0.273 ± 0.128	**0.154 ± 0.017**	<50 (83)	50 (60)	>50 (35)
(PZB22222053A)	**0.089 ± 0.021**	0.300 ± 0.035	2.32 ± 0.15	<50 (63)	>50 (49)	>50 (14)
(PZB22222054A)	**0.064 ± 0.035**	0.201 ± 0.022	2.71 ± 0.62	<50 (72)	>50 (23)	>50 (17)
(PZB22222055A)	0.312 ± 0.158	0.872 ± 0.092	0.579 ± 0.123	<50 (81)	>50 (49)	>50 (40)
(PZB22222067A)	0.251 ± 0.009	0.535 ± 0.065	1.31 ± 0.67	<50 (80)	>50 (40)	>50 (5)
LW-345	N.D*	1.32 ± 0.29	50 (49 %)	50 (60)	N.D*	<50 (86)

*not determined

b. Adenosine receptors

We further analysed the affinity of ten selected compounds (PZB22222040A), (PZB22222043A), ZS-ML-33, (PZB22222053A), (PZB22222054A), (PZB22222055A), (PZB22222067A), (PZB22222057A), (PZB22222059A), and PZB16321023A towards A_1 and A_2A receptors at two different concentrations of 1 and 10 µM. A single experiment was performed with duplicate observations (Figure 5.9). Our results showed that the tested compounds cannot inhibit radioligand binding by more than 50 %. Interestingly, some of the tested compounds showed a good affinity for A_2A receptors at 1 µM concentration; however, at higher concentrations of 10 µM, these compounds (PZB22222054A), (PZB22222059A), (PZB22222067A) did not show any improvement in the inhibitory activity. This issue can be further analysed using concentrations of the inhibitors. The current series of compounds are generally for NAD+ and ATP hydrolysing enzymes 38, 39, and NPP1 rather than blocking adenosine receptors.

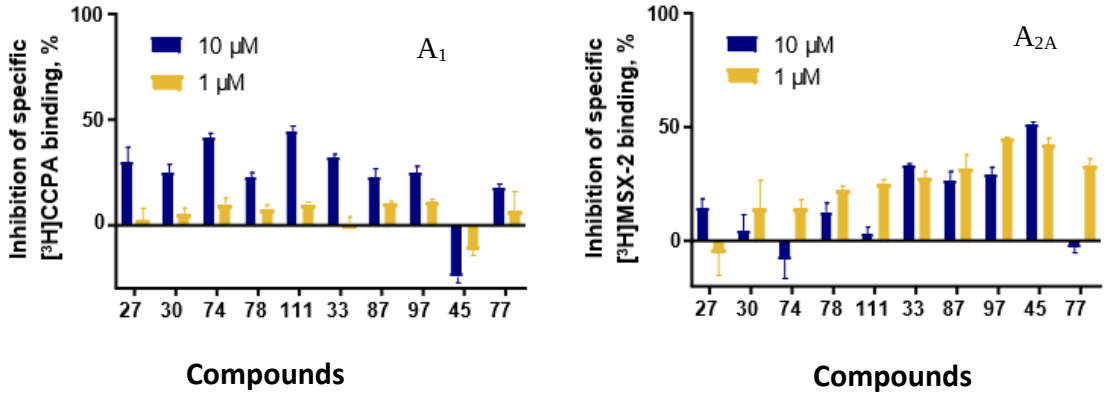

Figure 5.9: Tests for affinity of selected compounds towards A1 and A_2A receptors. X-axis = compound number, y-axis = (a): Inhibition of specific [3H]CCPA binding, (b): Inhibition of specific [3H]MSX-2 binding. Jonathan Schlegel performed testing.

3.5 Determination of inhibition type

The IC_{50} results showed potent dual inhibitors of CD38 and CD39, which further sparked our interest in gaining more insight into the binding mode. Since the current series of compounds share a standard 4*H*-chromene base structure, two representative compounds were selected, which showed high inhibitory potency towards CD38 and 39. The inhibition mechanism was determined for (PZB22222054A) against CD38 and (PZB22222043A) against CD39. A single test was performed in triplicate point analysis. Figures 5.10 and 5.11 represent the Lineweaver-Burk and Hans-Woolf plots in the presence of inhibitors accompanied by tables containing apparent V_{max} and K_m values. The Lineweaver-Burk plots at CD38 and CD39 showed that multiple lines coincide at the y-axis, which indicates a stable apparent V_{max} and an increase in the apparent K_m value. These findings suggest a competitive mode of inhibition for the compounds towards CD38 and CD39. Additionally, the Hanes-Wolf plot further confirms the competitive mode of inhibition, where different lines representing different inhibitor dilutions appeared parallel to each other while crossing the Y-axis. The K_m values for (PZB22222043A) towards CD39 showed an outlier value for the inhibitor concentration of 0.375 µM (K_m is reduced), which needs further repetition before publication. From the current test campaign, (PZB22222043A) was discovered as a potent multi-target inhibitor that showed K_i value in the nanomolar range towards CD38 and CD39. We further observed that this compound inhibited NPP1 by approximately 85 % inhibition and NPP3 by approximately 60 %. The inhibition type was determined for CD38 and CD39, where we observed a competitive

mode of inhibition towards both enzymes (only data for sCD38 and sCD39 are presented here). However, we will further investigate its inhibitory mechanism towards NPP1.

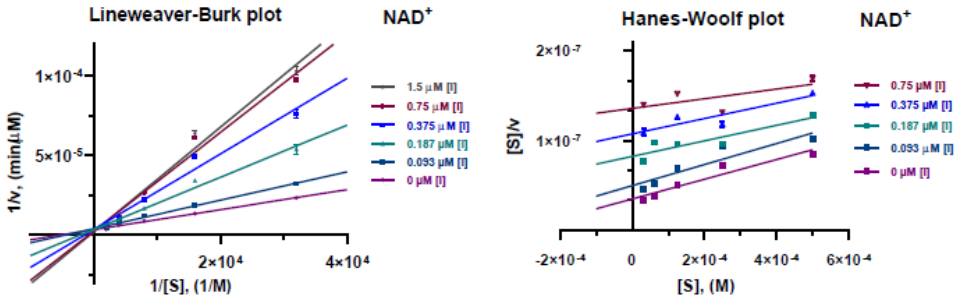

	[ZS-77], μM				
Best-fit values	0	0.093	0.187	0.375	0.750
V_{max} (μM/min/mg protein)	487,378	557,930	470,094	483,645	518,414
K_m (μM)	434	762	801	1,102	1,392

Figure 5.10: Lineweaver-Burk and Hanes-Woolf plot of (PZB22222054A) at different NAD^+ concentrations versus CD38 (Stach et al., 2023)

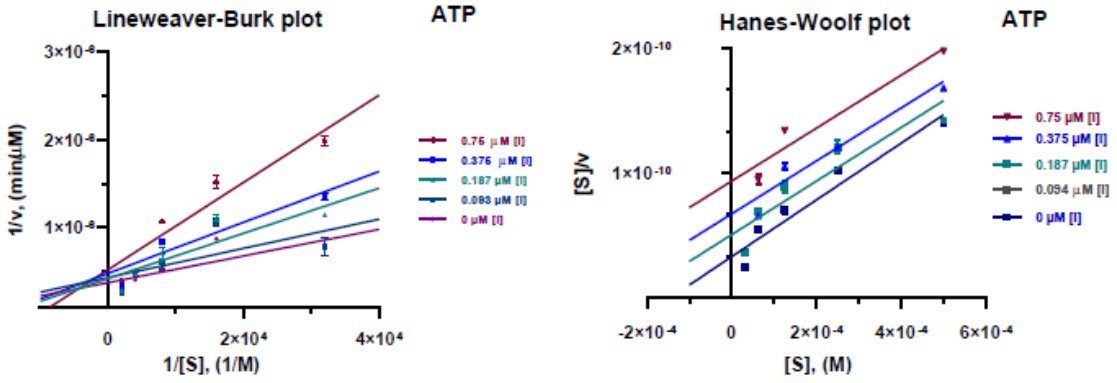

	[ZS-ML30], μM				
Best-fit values	0	0.093	0.187	0.375	0.750
V_{max} (μM/min/mg protein)	4,433,515	5,726,817	5,998,366	4,324,380	4,614,161
K_m (μM)	156	304	396	263	418

Figure 5.11 Lineweaver-Burk and Hanes-Woolf plot of (PZB22222043A) at different ATP concentrations versus CD39 (Stach et al., 2023)

3.6 Structure-activity relationship (SAR) for CD38

The 4*H*-chromene structure was modified at four different positions, that is, positions 2, 4, 6, and 8). Figure 5.12 represents the lead structure.

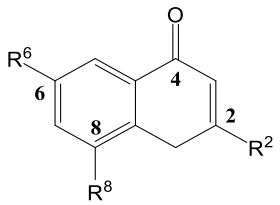

Figure 5.12: General structure of investigated 4*H*-chromene

a. Position 2

The most potent molecules have carboxylic acid ethyl esters at the 2-position. However, the chain length of the alkyl portion of this structure remained unchanged. Therefore, we could not test the potency, e.g. of a methyl- or propyl-ester structure. The potency decreases when the carboxylic acid replaces the ester. When comparing (PZB22222042A) (K_i vs ε-NAD^+ 5.15 ± 0.71 µM) and (PZB22222046A) (K_i vs ε-NAD^+ 15.3 ± 2.1 µM), for instance, the 2-position is the only distinction between the two compounds. The potency was reduced by 3-fold upon switching from the ethyl ester to the carboxylate. Due to the high hydrolase activity of esterases in the human body, the ester structure has a significant risk of metabolic instability, which is a drawback even though the ethyl ester has great inhibitory potency. This could lead to molecules with a relatively short half-life. One possible substitute for the 2-position would be a nitrile group. Compounds belonging to the AE-L series have nitrile groups in the 2-position. PZB16321014A and PZB16321033A, with K_i values of 2.50 ± 0.11 and 2.42 ± 0.10 µM (against Ɛ-NAD^+), were the most potent nitrile-substituted compounds. These compounds could not achieve potencies lower than 1 µM; however, they both had a nitro group in the 8-position. A nitro-group at the 8-position significantly decreases potency, as seen in (PZB22222053A) and PZB16321037A. The sole difference between these molecules is the 8-position substituents. With a K_i value of 0.300 ± 0.035 µM (Ɛ-NAD^+), (PZB22222053A) is one of the most potent inhibitors at 50 µM, PZB16321037A which has a nitro group in the 8-position does not even exhibit 50% inhibition. Because of the nitro group at position 8, the potency of these two molecules varies by approximately 100-fold. Therefore, the compounds PZB16321014A and, in particular, PZB16321033A would probably reach the lower nanomolar IC_{50} values if they had more perfect replacements in the 8- and 4-

position. This is also consistent with PZB16321033A and PZB16321026A. The 2-position substitution is the only difference between these molecules. The nitrile group stated earlier is present in PZB16321033A, and the ethyl ester group in PZB16321026A is the same as that of the most potent inhibitors (PZB22222043A) (PZB22222053A), (PZB22222054A), etc.). The K_i value of AE-L51 is 4.60 ± 0.30 μM (Ɛ-NAD^+). Therefore, switching from ethyl ester to nitrile could increase the potency by about two-fold. In addition, one of the compounds (PZB22222041A) has an additional intriguing substituent, tetrazole, in the 2-position. The compound's K_i value of 27.5 ± 1.9 μM (Ɛ-NAD^+) is higher. However, it cannot achieve potency due to unfavourable substitutes in the 2- and 8-position. One may deduce that the compound could attain substantially higher potency with better substituents in the 4- and 8-position if (PZB22222041A) and (PZB22222039A) were compared. (PZB22222039A) has a better substituent in the 4-position and the same substituents in the 6- and 8-position. This is particularly evident when the two compounds have similar potencies despite (PZB22222039A) having a significantly more favourable thioketone group in the 4-position. The tetrazole group may have greater potency than the ethyl ester group. Since (PZB22222041A) is the sole compound with this group, a precise estimation of the contribution of the tetrazole could not be obtained.

b. Position 4

All compounds with a K_i value below 2 μM share the thioketone structure in the 4-position. PZB16321033A, with a K_i value of 2.42 ± 0.10 μM, is the most potent compound with a ketone in the 4-position. Interestingly, the natural flavonoid and the CD38-inhibitor Luteolin (see Table 5.4) also share the same 4*H*-chromene structure with most of the compounds tested for this study. Luteolin also possesses an oxygen atom in the 4-position, and its IC_{50} value is 8.20 μM. Replacement of the thioketone with a ketone functionality at position 4 led to a significant decrease in the inhibitory potency.

c. Position 8

The ethyl malonate monoamide structure can be found in all six of the most effective compounds (PZB22222040A, PZB22222043A, PZB22222067A, PZB22222053A, PZB22222054A, PZB22222055) when looking at the 8-position. Potency is lost when ethyl malonate monoamide's chain length is changed to ethyl succinate monoamide. This can be seen by contrasting PZB22222042A with PZB22222043A (K_i value vs ε-NAD^+ 0.237± 0.128 μM). Here, the ethyl succinate monoamide structure of PZB22222042A causes a

20-fold reduction in efficacy, with a K_i value of 5.15 ± 0.71 μM (vs Ɛ-NAD^+). This suggests that the efficacy is significantly influenced by the structure of ethyl malonate monoamide, where the side chain comfortably fills the binding pocket or the involvement of the carbonyl group's location plays a significant role in hydrogen bonding. The ester group's metabolic instability causes this structure to have the same issue as the ethyl-formate structure in the 2-position, although offering the highest potency. The substitution at the 8-position needs to be changed to either a completely different substituent or bio-isosteres of the ester group to counteract the metabolic instability and, hopefully, improve the pharmacokinetic aspects of the molecules. Potency may be lost, but the pharmacokinetic benefits would probably exceed the pharmacodynamic drawbacks. The tested compounds previously partially revealed the position, 8 of the 4H-chromene base structure's SAR of an alternative side chain. ZS-ML33, for instance, has a malonamic acid residue at this location. Compared to Ɛ-NAD^+, this compound's K_i value was merely 4.64 ± 0.71 μM. Nonetheless, the compound may achieve a significantly lower K_i value if the 2-position of ZS-ML33 is substituted with a carboxylate group in conjunction with a nitrile group. It is once more evident how important the length of the carbon chain connecting the two carbonyl groups is when comparing ZS-ML33 to ZS-ML32, LW-236, and PZB16321031A. LW-236 and PZB16321031A, which have an oxamic acid residue, showed K_i values of 11.3 ± 0.7 and 9.79 ± 1.39 μM, respectively. In contrast, ZS-ML32 has a succinamic acid residue, and its K_i value (Ɛ-NAD^+) was 8.75 ± 0.31 μM. Hence, the malonate-structured molecule exhibited significantly greater potency than its succinate counterpart. Testing the oxalic acid equivalent of compounds with a carboxylic acid group in the 8-position was also possible, which produced considerably less efficacy. This demonstrates how the carbonyl oxygen's location within the malonate molecule affects efficacy. Sadly, a methyl malonate monoamide structure was not synthesised, although it could have provided more details for the SAR. None of the other substituents in the 8-position showed promising potency.

d. Position 6

Various substituents for the 6-position have shown good inhibitory potency. These substituents include halogens or six-membered aromatic rings. PZB22222054A exhibited the highest potency against both substrates, with K_i values of 0.201 ± 0.022 μM against Ɛ-NAD^+ and 0.064 ± 0.035 μM against NAD^+. The 6-position of PZB22222054A

constitutes a 2,4,5-trifluorobenzene moiety. The way the benzene was substituted differed depending on the inhibitor. PZB22222053A exhibited a K_i of 0.089 ± 0.018 μM against NAD^+ and 0.300 ± 0.035 μM against Ɛ-NAD^+. Its benzene ring was not substituted. Thus, the efficacy was diminished by the missing substitution. With a K_i of 2.72 ± 0.52 μM (vs Ɛ-NAD^+), the 2,4-dichlorobenzene compound PZB22222059A demonstrated a much lower potency when compared to the other two benzene-substituted compounds. A *para*-pyridine appears to be another tolerated aromatic residue for the 6-position. In this case, the previously described PZB16321033A demonstrated good potency even with a less-than-ideal substituent in the 4- and 8-position. Interestingly, when PZB16321033A and PZB16321023A were compared (IC_{50} = 4.60 ± 0.24 μM vs Ɛ-NAD^+), *para*-pyridine increased almost two-fold. Like PZB22222053A, PZB16321023A has the already well-tolerated unsubstituted benzene residue. As a result, the *para*-pyridine may be able to reach a potency range that is comparable to that of 2,4,5-trifluorobenzene. 6-halogen-substituted compounds also showed very high potency, as was previously reported. Br and Cl, in particular, achieved high inhibitory potency. K_i values for the bromo-substituted compound PZB22222043A against NAD^+ and Ɛ-NAD^+ were found to be 0.200 ± 0.038 μM and 0.237 ± 0.128 μM, respectively. Conversely, the chloro-substituted compound PZB22222040A showed a K_i of 0.542 ± 0.073 μM against Ɛ-NAD^+ and 0.152 ± 0.001 μM against NAD^+. The iodo-substituted PZB22222067A and the fluoro-substituted compounds PZB22222053A exhibited potency for both substrates and had K_i values between 0.300 and 1.00 μM. Compound PZB22222056A, which lacks a substitution in the 6-position, was inactive at 50 μM against CD38, demonstrating the significance of a substituent. PZB22222053A's potency could be significantly increased by adding a simple methyl group in the 6-position, achieving a K_i value of less than 5 μM versus Ɛ-NAD^+.

3.7 Structure-activity relationships (SAR) at CD39

Compounds most effective against CD38 also exhibited some degree of NTPDase enzyme inhibition. As a result, the SARs for CD39 and CD38 have some similarities. For instance, the most effective compounds have the 4-thioketone structure. On the other hand, the SARs for CD39 also show significant differences. For example, the 2-nitrile-substituted molecules were much less potent at CD39. This is particularly true for PZB16321033A, which demonstrated reasonable inhibition of CD38 and no inhibitory

effect. Instead, it appeared to activate CD39. PZB16321014A and PZB16321031A were the only two nitrile-substituted compounds with over 60% inhibition at 50 μM. Like CD38, the most effective molecules have the ethyl ester at the 2-position. The molecules with a carboxylate group in the 2-position were more effective at CD39 than CD38; their potency is comparable to that of the ethyl-ester-substituted derivatives. Two distinct observations demonstrate this. One aspect to consider is the enhanced effectiveness of ZS-ML33 against CD39, as evidenced by its K_i value of 1.54 ± 0.73 μM when using ATP as a substrate. Conversely, as demonstrated by the PZB22222042A and PZB22222046A, the potency difference between the ethyl ester compound PZB22222042A (K_i value vs ATP = 5.36 ± 0.94 μM) and the carboxylate PZB22222046A (K_i value vs ATP = 6.55 ± 0.23 μM) was significantly lower at CD38. Consequently, the carboxylate group in this location may offer CD39 a comparable efficacy with enhanced metabolic stability. The most potent molecules regarding the 8-position have an ethyl-malonic acid monoamide structure. The malonate structure is necessary for maximum potency. Furthermore, compared to CD38, the succinate structure seems to have somewhat lower potency. The comparison of the K_i values of PZB22222042A and PZB22222043A (0.154 ± 0.017 μM vs ATP) demonstrates a nearly 40-fold reduction in potency. However, ZS-ML33's malonamic acid group appears to have greater potency for CD39 than CD38. Additionally, there was a considerable decrease in the potency difference between PZB22222040A and ZS-ML33. Since the 4- and 6-position substituents of these two compounds are identical, the enhanced potency of the malonic acid group in the 8-position and the carboxylate group in the 2-position can explain ZS-ML33's higher potency. These two groups could be better substituents for compounds in the future since they would offer higher metabolic stability.

In the 6-position, the presence of a halogen atom is critical. The highest potency was obtained with bromine, and the only one that could achieve an IC_{50} value below 0.500 μM for CD39 was PZB22222043A. With K_i values for PZB22222055A and PZB22222040A of 0.597 ± 0.123 μM and 0.653 ± 0.234 μM, respectively, chloro and fluoro showed similar potency. At 1.31 ± 0.67 μM, the iodo-substituted compound PZB22222067A had the lowest potency among halogens. The compounds with an unsubstituted benzene ring (PZB22222053A) had the highest potency with a K_i value of 2.32 ± 0.15 μM, followed closely by the 2,4,5-trifluorobenzene compound (PZB22222054A) with a K_i value of 2.71

± 0.62 µM. The compounds with six-membered aromatic rings in this position showed significantly reduced potency compared to CD38. Conversely, at 50 µM, the 2,4-dichlorobenzene-substituted compound (PZB22222059A) did not even approach 50% inhibition. PZB22222057A, the methyl derivative, also exhibited diminished potency, displaying a K_i value of 7.60 µM.

3.8 Outlook

a. SARs

The issue of possible metabolic instability for most compounds has been mentioned. This primarily affects the ester groups in the 2- and 8-positions. The thioketone structure in the 4-position may also be affected. It has not yet been investigated whether the thioketone structure at the 4-position is susceptible to metabolic instability, particularly oxidative desulfurisation to carbonyl derivatives (Rice et al., 2014). The compound PZB16321033A has a carbonyl group in the 4-position; however, it showed decent inhibition of sCD38 with a K_i value of 2.50 µM. The compound contained a NO_2 group at position 8, and a more suitable substitution would possibly improve potency further. Several substitutes for the ester group at position 2 have already been identified in the SAR studies. Nitrile, carboxylate, and tetrazole substitution at this position need further investigation. An in-depth assessment is further required for the *para*-pyridine substitution at position 6. Malonic acid in ZS-ML33 is the only substitution that might increase metabolic stability and show acceptable potency. Bio-isosteres can improve pharmacokinetic properties, potency, selectivity, and toxicity. An excellent review was previously published that highlights bio-isosteric ester (and amide) replacements (Kumari et al., 2020). Sulfonamide, urea, carbamate, simple amide, or trifluoroethylamine are possible bio-isosteric replacements.

b. Biological and computational aspects

Molecular docking or X-ray crystallography could be performed to gain further insight into the interaction between the small molecule inhibitors and the target enzymes (CD38 and CD39). Additionally, the selectivity testing of the compound can be further expanded. This would mainly entail more ectonucleotidases and cancer cell lines. For ectonucleotidases, the additional extracellular NTPDase-2, -3, and -8), NPP-4 and -5), CD157, and alkaline phosphatases (TNAP) would present attractive targets and could give additional

information on the selectivity of the 4*H*-chromene derivatives. Cancer cell lines with overexpression of relevant ectonucleotidases could further be utilised. Furthermore, the metabolic stability of the compounds should be tested in liver homogenate.

4.0 Conclusions

This project aimed to investigate and conduct SAR studies of 4*H*-chromenes as potential inhibitors of CD38. Novel inhibitors for CD38 were identified and further characterised. Additionally, the *4H*-chromosomes were screened against other ectonucleotidases to study their selectivity. In the present screening campaign, more than 150 compounds were tested for their inhibition of CD38 using the synthetic substrate Ɛ-NAD^+, and subsequently, 49 compounds were selected for K_i value determination. Six compounds reached a K_i value below 1 μM. The six most potent compounds were also tested against the natural substrate NAD+ with a CE-UV assay to confirm these results. After both tests, the inhibition type for the most potent compound was determined to gain further insights into the binding mode to calculate the K_i values from the IC_{50} values. Thus, the currently most potent 4*H*-chromene derivative against CD38 was PZB16321054A with a K_i-value of 0.064 ± 0.035 μM (vs. NAD^+) and a competitive inhibition mode. Sixteen compounds were further tested for their K_i value towards CD39, and three compounds showed a K_i value below 1 μM for CD39, while three other compounds reached a decent potency against CD39 with K_i values still below 3 μM. The most potent compound, PZB16321043A, displayed a K_i value of 0.154 ± 0.017 μM and a competitive inhibition mode. Additionally, PZB16321043A showed excellent inhibitory potency against CD38 with a K_i of 0.200 ± 0.038 μM and decent inhibitory potency against NPP1 with a percentage inhibition >80 % at 50 µM. The most potent compounds showed dual inhibition for CD38 and CD39. PZB16321043A especially reached nanomolar potency at both enzymes. Currently, no dual inhibitors for CD38 and CD39 have been published. This dual inhibition of CD38 and CD39 might be a new approach to reduce the downstream accumulation of adenosine, as it can potentially inhibit both the canonical and the non-canonical pathways. Additionally, much information on the structure-activity relationships of 4*H*-chromenes as inhibitors for CD38 and CD39 was obtained, which provides the basis for future research.

References

Alefishat, E., S. P.H. Alexander, and V. Ralevic. 2015. “Effects of NAD at Purine Receptors in Isolated Blood Vessels.” *Purinergic Signalling* 11 (March):47–57. https://doi.org/10.1007/s11302-014-9428-1.

Alphonso, Aimee, and Suresh K. Alahari. 2009. “Stromal Cells and Integrins: Conforming to the Needs of the Tumor Microenvironment.” *Neoplasia* 11:1264–71. https://doi.org/10.1593/neo.91302.

Amici, Stephanie A., Nicholas A. Young, Janiret Narvaez-Miranda, Kyle A. Jablonski, Jesus Arcos, Lucia Rosas, Tracey L. Papenfuss, Jordi B. Torrelles, Wael N. Jarjour, and Mireia Guerau-de-Arellano. 2018. “CD38 Is Robustly Induced in Human Macrophages and Monocytes in Inflammatory Conditions.” *Front. Immunol.* 9:1–13. https://doi.org/10.3389/fimmu.2018.01593.

Anderson, Nicole M, and M Celeste Simon. 2020. “The Tumor Microenvironment.” *Curr. Biol.* 30:905–31. https://doi.org/10.1016/j.cub.2020.06.081.

Audrito, Valentina. 2021. “The Extracellular NADome Modulates Immune Responses.” *Front. Immunol.* Frontiers Media S.A. https://doi.org/10.3389/fimmu.2021.704779.

Barrio, Jorge R, John A Secrist, and Nelson J et al. Leonard. 1972. “A Fluorescent Analog of Nicotinamide Adenine Dinucleotide.” *Proc. Nat. Acad. Sci. USA* 69:2039–42.

Becherer, J. David, Eric E. Boros, Tiffany Y. Carpenter, David J. Cowan, David N. Deaton, Curt D. Haffner, Michael R. Jeune, et al. 2015. “Discovery of 4-Amino-8-Quinoline Carboxamides as Novel, Submicromolar Inhibitors of NAD-Hydrolyzing Enzyme CD38.” *J. Med. Chem.* 58 (September):7021–56. https://doi.org/10.1021/acs.jmedchem.5b00992.

Benton, Thomas, Mills, Catherine, Turner, Jonathan, Worster, Patrick. 2021. “Selective Targeting of CD38 Hydrolase and Cyclase Activity as an Approach to Immunostimulation.” *RSC Advance* 11:33260–70. https://doi.org/10.1039/d1ra06266b.

Blacher, Eran, Bar Ben Baruch, Ayelet Levy, Nurit Geva, Keith D. Green, Sylvie Garneau-Tsodikova, Micha Fridman, and Reuven Stein. 2015. “Inhibition of Glioma Progression by a Newly Discovered CD38 Inhibitor.” *Int. J. Cancer* 136:1422–33. https://doi.org/10.1002/ijc.29095.

Blacher, Eran, Ayelet Levy, Bar Baruch, Keith Green, and Reuven Stein. 2015. “Targeting CD38 in the Tumor Microenvironment; a Novel Approach to Treat Glioma.” *Cancer Cell Microenviron.* 2 (January):1–6. https://doi.org/10.14800/ccm.486.

Bonello, Francesca, Mattia D Agostino, Maria Moscvin, Chiara Cerrato, and Francesca Gay. 2018. “CD38 As an Immunotherapeutic Target in Multiple Myeloma.” *Expert Opin. Biol. Ther.* 18 (0): 1209–21. https://doi.org/10.1080/14712598.2018.1544240.

Chen, Limo, Lixia Diao, Yongbin Yang, Xiaohui Yi, B. Leticia Rodriguez, Yanli Li, Pamela A. Villalobos, et al. 2018. “CD38-Mediated Immunosuppression as a Mechanism of Tumor Cell Escape from PD-1/PD-L1 Blockade.” *Cancer Discov.* 8 (September):1156–75. https://doi.org/10.1158/2159-8290.CD-17-1033.

Churamani, Dev, Elizabeth A Carrey, George D Dickinson, and Sandip Patel. 2004. “Determination of Cellular Nicotinic Acid – Adenine Dinucleotide Phosphate (NAADP) Levels.” *Biochem. J.* 454:449–54.

Cimpean, Anisoara, Cristiana Stefan, Rik Gijsbers, Willy Stalmans, and Mathieu Bollen. 2004. “Substrate-Specifying Determinants of the Nucleotide Pyrophosphatases/ Phosphodiesterases NPP1 and NPP2.” *Biochem. J.* 381:71–77.

Cole, Suzanne, Alice Walsh, Xuefeng Yin, Mihir D. Wechalekar, Malcolm D. Smith, Susanna M. Proudman, Douglas J. Veale, et al. 2018. “Integrative Analysis Reveals CD38 as a Therapeutic Target for Plasma Cell-Rich Pre-Disease and Established Rheumatoid Arthritis and Systemic Lupus Erythematosus.” *Arthritis Res. Ther.* 20:1–14. https://doi.org/10.1186/s13075-018-1578-z.

Dai, Zhefu, Xiao Nan Zhang, Fariborz Nasertorabi, Qinqin Cheng, Hua Pei, Stan G. Louie, Raymond C. Stevens, and Yong Zhang. 2018. “Facile Chemoenzymatic Synthesis of a Novel Stable Mimic of NAD+.” *Chemical Science* 9:8337–42. https://doi.org/10.1039/c8sc03899f.

Deaton, David N., Curt D. Haffner, Brad R. Henke, Michael R. Jeune, Barry G. Shearer, Eugene L. Stewart, J. Darren Stuart, and John C. Ulrich. 2018. “2,4-Diamino-8-Quinazoline Carboxamides as Novel, Potent Inhibitors of the NAD Hydrolyzing Enzyme CD38: Exploration of the 2-Position Structure-Activity Relationships.” *Bioorg. Med. Chem.* 26 (May):2107–50. https://doi.org/10.1016/j.bmc.2018.03.021.

Deckert, Jutta, Marie Cécile Wetzel, Laura M. Bartle, Anna Skaletskaya, Victor S. Goldmacher, François Vallée, Qing Zhou-Liu, et al. 2014. “SAR650984, a Novel Humanized CD38-Targeting Antibody, Demonstrates Potent Antitumor Activity in Models of Multiple Myeloma and Other CD38+ Hematologic Malignancies.” *Clin. Cancer Res.* 20:4574–83. https://doi.org/10.1158/1078-0432.CCR-14-0695.

Dong, Min, Yuan Qi, Shuang Yong-Sun, Xiao-Ping Pu, and Hong Cheung Lee. 2011. “Design Synthesis and Biological Characterization of Novel CD38 Inhibitors.” *Org. Biomol. Chem.* 9:3246–57. https://doi.org/10.1039 / C0ob00768d.

Donk, Niels W.C.J. Van De, and Saad Z. Usmani. 2018. “CD38 Antibodies in Multiple Myeloma: Mechanisms of Action and Modes of Resistance.” *Front Immunol.* 9 (September):1–12. https://doi.org/10.3389/fimmu.2018.02134.

Dwivedi, Sanyog, Erika P Rendón, Rend´ Rendón-Huerta, Vianney Ortiz-Navarrete, and Luis F Montaño. 2021. “CD38 and Regulation of the Immune Response Cells in Cancer.” *J. Oncol.* 2021:1–11. https://doi.org/10.1155/2021/6630295.

Escande, Carlos, Veronica Nin, Nathan L. Price, Verena Capellini, Ana P. Gomes, Maria Thereza Barbosa, Luke O’Neil, Thomas A. White, David A. Sinclair, and Eduardo N. Chini. 2013. “Flavonoid Apigenin Is an Inhibitor of the NAD+ase CD38: Implications for Cellular NAD+ Metabolism, Protein Acetylation, and Treatment of Metabolic Syndrome.” *Diabetes* 62 (April):1084–93. https://doi.org/10.2337/db12-1139.

Gao, Long, Yuan Liu, Xiaohong Du, Sai Ma, Minmin Ge, Haijun Tang, Chenfeng Han, Xin Zhao, and Yanbin Liu. 2021. “The Intrinsic Role and Mechanism of Tumor Expressed-CD38 on Lung Adenocarcinoma Progression.” *Cell Death Dis.* 12:1–13. https://doi.org/10.1038/s41419-021-03968-2.

Ge, Yanshan, Yuehua Long, Songshu Xiao, L I N Liang, and Zhengxi He. 2019. “CD38 Affects the Biological Behavior and Energy Metabolism of Nasopharyngeal Carcinoma Cells.” *Int. J. Oncol.* 54:585–99. https://doi.org/10.3892/ijo.2018.4651.

Goody, Michelle F., and Clarissa A. Henry. 2018. “A Need for NAD+ in Muscle Development, Homeostasis, and Aging.” *Skeletal Muscle* 8 (March):1–14. https://doi.org/10.1186/s13395-018-0154-1.

Graeff, Richard, Qun Liu, Irina A. Kriksunov, Quan Hao, and Cheung Lee Hon. 2006. “Acidic Residues at the Active Sites of CD38 and ADP-Ribosylt Cyclase Determine Nicotinic Acid Adenine Dinucleotide Phosphate (NAADP) Synthesis and Hydrolysis Activities.” *J. Bio. Chem.* 281 (September):28951–57. https://doi.org/10.1074/jbc.M604370200.

Graeff, Richard, Cyrus Munshi, Robert Aarhus, Malcolm Johns, and Hon Cheung Lee. 2001. “A Single Residue at the Active Site of CD38 Determines Its NAD Cyclizing and Hydrolyzing Activities.” *J. Bio. Chem.* 276 (April):12169–73. https://doi.org/10.1074/jbc.M011299200.

Graeffs, Richard M, F Timothy, Kathryn Fryxells, and Dale Branton. 1994. “Enzymatic Synthesis and Characterizations of Cyclic GDP-Ribose.” *J. Biol. Chem.* 269:30260–67. https://doi.org/10.1016/S0021-9258(18)43806-9.

Guerreiro Serge, Privat Anne-Laure, Bressac Laurence, and Toulorge Damien. 2020. “CD38 in Neurodegeneration and Neuroinflammation.” *Cells* 9:1–10. https://doi.org/10.3390/cells9020471.

Haffner, Curt D., J. David Becherer, Eric E. Boros, Rodolfo Cadilla, Tiffany Carpenter, David Cowan, David N. Deaton, et al. 2015. “Discovery, Synthesis, and Biological Evaluation of Thiazoloquin(Az)Olin(on)Es as Potent CD38 Inhibitors.” *J. Med. Chem.* 58 (April):3548–71. https://doi.org/10.1021/jm502009h.

Hogan, Kelly A., Claudia C.S. Chini, and Eduardo N. Chini. 2019. “The Multi-Faceted Ecto-Enzyme CD38: Roles in Immunomodulation, Cancer, Aging, and Metabolic Diseases.” *Front. Immunol.* 10:1–12. https://doi.org/10.3389/fimmu.2019.01187.

Hongmin Zhang, Richard Graeff, Hon Cheung Lee, and Quan Hao. 2011. “Dynamic Conformations of the CD38-Mediated NAD Cyclization Captured in a Single Crystal.” *J Mol Biol.* 405:1070–78. https://doi.org/10.1016/j.jmb.2010.11.044.Dynamic.

Hubert, Sandra, Björn Rissiek, Katjana Klages, Jochen Huehn, Tim Sparwasser, Friedrich Haag, Friedrich Koch-Nolte, Olivier Boyer, Michel Seman, and Sahil Adriouch. 2010. “Extracellular NAD+ Shapes the Foxp3+ Regulatory T Cell Compartment through the ART2-P2X7 Pathway.” *J. Exp. Med.* 207 (November):2561–68. https://doi.org/10.1084/jem.20091154.

Jablonska, Patrycja, Barbara Kutryb-Zajac, Paulina Mierzejewska, Agnieszka Jasztal, Barbara Bocian, Romuald Lango, Jan Rogowski, Stefan Chlopicki, Ryszard T. Smolenski, and Ewa M. Slominska. 2021. “The New Insight into Extracellular NAD+ Degradation-the Contribution of CD38 and CD73 in Calcific Aortic Valve Disease.” *J. Cell. Mol. Med.* 25 (July):5884–98. https://doi.org/10.1111/jcmm.15912.

Jiao, Ying, Ming Yi, Linping Xu, Qian Chu, Yongxiang Yan, Suxia Luo, and Kongming Wu. 2020. “CD38: Targeted Therapy in Multiple Myeloma and Therapeutic Potential for Solid Cancers.” *Expert Opin. Invest. Drugs* 29 (0): 1295–1308. https://doi.org/10.1080/13543784.2020.1814253.

Kellenberger, Esther, Isabelle Kuhn, Francis Schuber, and Hélène Muller-Steffner. 2011. “Flavonoids as Inhibitors of Human CD38.” *Bioorg. Med. Chem. Lett.* 21 (July):3939–42. https://doi.org/10.1016/j.bmcl.2011.05.022.

Klein, Carina, Anja Grahnert, Aliaa Abdelrahman, Christa E. Müller, and Sunna Hauschildt. 2009. “Extracellular NAD+ Induces a Rise in [Ca2+]i in Activated Human Monocytes via Engagement of P2Y1 and P2Y11 Receptors.” *Cell Calcium* 46:263–72. https://doi.org/10.1016/j.ceca.2009.08.004.

Kumari, Shikha, Angelica V. Carmona, Amit K. Tiwari, and Paul C. Trippier. 2020. “Amide Bond Bioisosteres: Strategies, Synthesis, and Successes.” *J. Med. Chem.* 63 (November):12290–358. https://doi.org/10.1021/acs.jmedchem.0c00530.

Kwong, Anna Ka Yee, Zhe Chen, Hong Min Zhang, Fung Ping Leung, Connie Mo Ching Lam, Kai Yiu Ting, Liangren Zhang, Quan Hao, Li He Zhang, and Hon Cheung Lee. 2012. “Catalysis-Based Inhibitors of the Calcium Signaling Function of CD38.” *Biochemistry* 51 (January):555–64. https://doi.org/10.1021/bi201509f.

Lee, Hyun Tae, Yujin Kim, Ui Beom Park, Tae Jun Jeong, Sang Hyung Lee, and Yong Seok Heo. 2021. “Crystal Structure of CD38 in Complex with Daratumumab, a First-in-Class Anti-CD38 Antibody Drug for Treating Multiple Myeloma.” *Biochem. Biophys. Res. Commun.* 536:26–31. https://doi.org/10.1016/j.bbrc.2020.12.048.

Lee, Sang Yong, Soumya Sarkar, Sanjay Bhattarai, Vigneshwaran Namasivayam, Steven De Jonghe, Holger Stephan, Piet Herdewijn, Ali El-Tayeb, and Christa E. Müller. 2017. “Substrate-Dependence of Competitive Nucleotide Pyrophosphatase/Phosphodiesterase1 (NPP1) Inhibitors.” *Frontiers in Pharmacology* 8:1–15. https://doi.org/10.3389/fphar.2017.00054.

Lee Sang-Yong, Vigneshwaran Namasivayam et. al. 2017. “Substrate-Dependence of Competitive Nucleotide Pyrophosphatase/Phosphodiesterase1 (NPP1) Inhibitors.” *Front. Pharmacol.* 1:1–15. https://doi.org/10.3389/fphar.2017.00054.

Liu, Qun, Irina A. Kriksunov, Richard Graeff, Cheung Lee Hon, and Quan Hao. 2007. “Structural Basis for Formation and Hydrolysis of the Calcium Messenger Cyclic ADP-Ribose by Human CD38.” *J. Biol. Chem.* 282:5853–61. https://doi.org/10.1074/jbc.M609093200.

Liu, Qun, Irina A. Kriksunov, Richard Graeff, Cyrus Munshi, Cheung Lee Hon, and Quan Hao. 2005. “Crystal Structure of Human CD38 Extracellular Domain.” *Structure* 13:1331–39. https://doi.org/10.1016/j.str.2005.05.012.

Liu, Qun, Irina A Kriksunov, Richard Graeff, Cyrus Munshi, Hon Cheung Lee, and Quan Hao. 2006. “Structural Basis for the Mechanistic Understanding of Human CD38-Controlled Multiple Catalysis *.” *J. Biol. Chem.* 281:32861–69. https://doi.org/10.1074/jbc.M606365200.

Liu, Qun, Irina A. Kriksunov, Christelle Moreau, Richard Graeff, Barry V.L. Potter, Cheung Lee Hon, and Quan Hao. 2007. “Catalysis-Associated Conformational Changes Revealed by Human CD38 Complexed with a Non-Hydrolyzable Substrate Analog.” *J. Bio. Chem.* 282 (August):24825–32. https://doi.org/10.1074/jbc.M701653200.

Mattson, Mark P., Deborah L. Croteau, Xiuli Dan, Tyler G. Demarest, Mustafa N. Okur, Vilhelm A. Bohr, Nima B. Fakouri, and Mansi Babbar. 2018. “NAD + Metabolism in Aging and Cancer.” *Annu.Rev.Cancer Biol.* 3:105–30. https://doi.org/10.1146/annurev-cancerbio-030518-055905.

Moreschi, Iliana, Santina Bruzzone, Robert A. Nicholas, Floriana Fruscione, Laura Sturla, Federica Benvenuto, Cesare Usai, et al. 2006. “Extracellular NAD+ Is an Agonist of the Human P2Y11 Purinergic Receptor in Human Granulocytes.” *J. Bio. Chem.* 281 (October):31419–29. https://doi.org/10.1074/jbc.M606625200.

Navas, Lola E., and Amancio Carnero. 2021. “NAD+ Metabolism, Stemness, the Immune Response, and Cancer.” *Signal Transduction Targeted Ther.* Springer Nature. https://doi.org/10.1038/s41392-020-00354-w.

Oh, David Y. 2021. “CD38 as a Novel Immunosuppressive Target in Prostate Cancer.” *Eur. Urol.* 79:747–49. https://doi.org/10.1016/j.eururo.2021.02.022.

Oliveira, Guilherme C De, Karina S Kanamori, and Maria Auxiliadora-martins. 2018. “Measuring CD38 Hydrolase and Cyclase Activities: 1,N6-Ethenonicotinamide Adenine Dinucleotide (ε-NAD) and Nicotinamide Guanine Dinucleotide (NGD) Fluorescence-Based Methods.” *Bio-Protoc.* 8:1–10. https://doi.org/10.21769/BioProtoc.2938.

Peclat, Thais Ribeiro, Bo Shi, John Varga, and Eduardo Nunes Chini. 2020. “The NADase Enzyme CD38: An Emerging Pharmacological Target for Systemic Sclerosis, Systemic Lupus Erythematosus and Rheumatoid Arthritis.” *Curr. Opin. Rheumatol.* 32 (6): 488–96. https://doi.org/10.1097/BOR.0000000000000737.

Piedra-Quintero, Zayda L., Zachary Wilson, Porfirio Nava, and Mireia Guerau-de-Arellano. 2020. “CD38: An Immunomodulatory Molecule in Inflammation and Autoimmunity.” *Front. Immunol.* 11:3–6. https://doi.org/10.3389/fimmu.2020.597959.

Quarona, Valeria, Gianluca Zaccarello, Antonella Chillemi, Enrico Brunetti, Vijay Kumar Singh, Enza Ferrero, Ada Funaro, Alberto L. Horenstein, and Fabio Malavasi. 2013. “CD38 and CD157: A Long Journey from Activation Markers to Multifunctional Molecules.” *Cytometry, Part B* 84:207–17. https://doi.org/10.1002/cyto.b.21092.

Qun Liu, Irina A. Kriksunov, Hong Jiang, Richard Graeff, Hening Lin, Hon Cheung Lee and Quan Hao. 2008. “Covalent and Noncovalent Intermediates of an NAD Utilizing Enzyme, Human CD38.” *Chem. Biol* 15:1068–78. https://doi.org/10.1016/j.chembiol.2008.08.007.

Qun Liu, Richard Graeff, Irina A. Kriksunov, Connie M. C. Lam, Hon Cheung Lee, and Quan Hao. 2008. “Conformational Closure of the Catalytic Site of Human CD38 Induced by Calcium.” *Biochem. J.* 47:13966–73. https://doi.org/https://doi.org/10.1021/bi801642q.

Rah, So-young, and Uh-hyun Kim. 2014. “CD38-Mediated Ca 2 + Signaling Contributes to Glucagon-Induced Hepatic Gluconeogenesis.” *Nature* 5:1–9. https://doi.org/10.1038/srep10741.

Rah, So Young, Jae Yong Kwak, Yun Jo Chung, and Uh Hyun Kim. 2015. “ADP-Ribose/TRPM2-Mediated Ca 2+ Signaling Is Essential for Cytolytic Degranulation and Antitumor Activity of Natural Killer Cells.” *Sci. Rep.* 5 (March):1–10. https://doi.org/10.1038/srep09482.

Randall, Rose J, and A Lewis. 1951. “Protein Measurment with the Folin Phenol Reagent.” *J. Biol. Chem.* 193:265–75.

Ratajczak, Joanna, Magali Joffraud, Samuel A.J. Trammell, Rosa Ras, Nuria Canela, Marie Boutant, Sameer S. Kulkarni, et al. 2016. “NRK1 Controls Nicotinamide Mononucleotide and Nicotinamide Riboside Metabolism in Mammalian Cells.” *Nat. Commun.* 7 (October):1–11. https://doi.org/10.1038/ncomms13103.

Reyes, Levy, Boslett James, Varadharaj Saradhadevi, Pascali, Francesco, Hemann, Craig et.al. 2015. “Depletion of NADPH Due to CD38 Activation Triggers Endothelial Dysfunction in Postischemic Heart.” *PNAS* 112:11648–53.

Rice, Joseph E, Amsterdam • Boston, • Heidelberg, • London, Paris • San, Diego San, Francisco • Singapore, and Sydney • Tokyo. 2014. *Organic Chemistry Concepts and Applications for Medicinal Chemistry*. https://doi.org/https://doi.org/10.1016/C2013-0-18544-3.

Sauve, Anthony A, Cyrus Munshi, Hon Cheung Lee, and Vern L Schramm. 1998. “The Reaction Mechanism for CD38. A Single Intermediate Is Responsible for Cyclization, Hydrolysis, and Base-Exchange Chemistries †.” *Biochemistry* 37:13239–49. https://doi.org/10.1021/bi981248s.

Schultz, Michael. 2018. “Assays for NAD+ -Dependent Reactions and NAD+ Metabolites.” *Methods Mol Biol.* 1813:77–90. https://doi.org/10.1007/978-1-4939-8588-3.

Schultz, Michael B., and David A. Sinclair. 2016. “Why NAD+ Declines during Aging: It’s Destroyed.” *Cell Metab.* 23 (June):965–66. https://doi.org/10.1016/j.cmet.2016.05.022.

Shallis, Rory M, Christopher M Terry, and Seah H Lim. 2017. “The Multi-Faceted Potential of CD38 Antibody Targeting in Multiple Myeloma.” *Cancer Immunol. Immunother.* 66 (0): 697–703. https://doi.org/10.1007/s00262-017-1990-2.

Song, Eun Kyung, So Young Rah, Young Rae Lee, Chae Hwa Yoo, Yu Ri Kim, Ji Hyun Yeom, Kwang Hyun Park, Jong Suk Kim, Uh Hyun Kim, and Myung Kwan Han. 2011. “Connexin-43 Hemichannels Mediate Cyclic ADP-Ribose Generation and Its Ca 2+-Mobilizing Activity by NAD +/Cyclic ADP-Ribose Transport.” *J. Bio. Chem* 286 (December):44480–90. https://doi.org/10.1074/jbc.M111.307645.

Stach, Paul, Christa E Müller Zweitgutachterin, and PD Anke Schiedel. 2023. “Small Molecule Inhibitors of CD38 with Ancillary CD39 Inhibition.”

Swarbrick, Joanna M., Richard Graeff, Hongmin Zhang, Mark P. Thomas, Quan Hao, and Barry V.L. Potter. 2014. “Cyclic Adenosine 5′-Diphosphate Ribose Analogs without a Southern Ribose Inhibit ADP-Ribosyl Cyclase-Hydrolase CD38.” *J. Med. Chem.* 57 (October):8517–29. https://doi.org/10.1021/jm501037u.

Ting, Kai Yiu, Liangren Zhang, Quan Hao, Li-he Zhang, and Hon Cheung Lee. 2012. “Catalysis-Based Inhibitors of the Calcium Signaling Function of CD38.” *Biochem. J.* 51:555–64.

T.Z.Benton et al. 2021. “Selective Targeting of CD38 Hydrolase and Cyclase Activity as an Approach to Immunostimulation.” *RSC Adv.* 11:33260–70.

Verkleij, Christie, Amy Jhatakia, Marloes Broekmans, and Niels Donk. 2020. “Preclinical Rationale for Targeting the PD-1_PD-L1 Axis in Combination with a CD38 Antibody in Multiple Myeloma and Other CD38-Positive Malignancies.” *Cancers (Basel)* 12:1–19. https://doi.org/10.3390/cancers12123713.

Veskoukis, Aristidis S, Nikos V Margaritelis, Antonios Kyparos, Michalis G Nikolaidis, Aristidis S Veskoukis, Nikos V Margaritelis, Antonios Kyparos, Aristidis S Veskoukis, and Nikos V Margaritelis. 2018. “Spectrophotometric Assays for Measuring Redox Biomarkers in Blood and Tissues : The NADPH Network Spectrophotometric Assays for Measuring Redox Biomarkers in Blood and Tissues :” *Redox Rep.* 23:47–56. https://doi.org/10.1080/13510002.2017.1392695.

Wang, Shengjun, Zhu, Wenjie, Wang, Xuan, Li, Gianguo Zhang, Lihe. 2014. “Design, Synthesis, and SAR Studies of NAD Analogues as Potent Inhibitors Towards CD38 NADase.” *Molecule* 19:15754–67. https://doi.org/10.3390/molecules191015754.

Weber, Cynthia E., and Paul C. Kuo. 2012. “The Tumor Microenvironment.” *Surg Oncol.* 21 (September):172–77. https://doi.org/10.1016/j.suronc.2011.09.001.

Yang, Lixin, Ting Li, Songlu Li, Yang Wu, Xiaomeng Shi, Hongwei Jin, Zhenming Liu, et al. 2019. “Rational Design and Identification of Small-Molecule Allosteric Inhibitors of CD38.” *ChemBioChem* 20 (October):2485–93. https://doi.org/10.1002/cbic.201900169.

Yang, Yue, and Anthony A. Sauve. 2016. “NAD+ Metabolism: Bioenergetics, Signaling and Manipulation for Therapy.” *Biochim. Biophys. Acta, Proteins Proteomics* 1864 (December):1787–1800. https://doi.org/10.1016/j.bbapap.2016.06.014.

Yung-Chi, Cheng, and William H. Prusoff. 1973. “Relationship between the Inhibition Constant (KI) and the Concentration of Inhibitor Which Causes 50 per Cent Inhibition (I50) of an Enzymatic Reaction.” *Biochem. Pharmacol.* 22:3099–3108.

Zhang, Liangren, Zhenming Liu, Zhao Yongjuan, and Han Jin. 2019. “Rational Design and Identification of Small-Molecule Allosteric Inhibitors Of.” *Chembiochem* 20:2485–93. https://doi.org/10.1002/cbic.201900169.

Zhang, Xingyue, Lingfei Li, Qiong Zhang, Qinglin Wei, Jiezhi Lin, Jiezhi Jia, Junhui Zhang, et al. 2020. “CD38 Causes Autophagic Flux Inhibition and Cardiac Dysfunction Through a Transcriptional Inhibition Pathway Under Hypoxia/Ischemia Conditions.” *Front. Cell Dev. Biol* 8:1–19. https://doi.org/10.3389/fcell.2020.00191.

Zhao, Yong Juan, Connie Mo, Ching Lam, and Hon Cheung Lee. 2012. “The Membrane-Bound Enzyme CD38 Exists in Two Opposing Orientations.” *Sci. Signal.* 5:1–10. https://doi.org/10.1126/scisignal.2002700.

Zhou, Yi, Kai Yiu Ting, Connie Mo Ching Lam, Anna Ka Yee Kwong, Jie Xia, Hongwei Jin, Zhenming Liu, Liangren Zhang, Hon CheungLee, and Lihe Zhang. 2012. “Design, Synthesis and Biological Evaluation of Noncovalent Inhibitors of Human CD38 NADase.” *ChemMedChem* 7 (February):223–28. https://doi.org/10.1002/cmdc.201100487.

Zuo, Wanyun, Na Liu, Yunhong Zeng, Yaozhong Liu, Biao Li, Keke Wu, Yunbin Xiao, and Qiming Liu. 2021. “CD38 : A Potential Therapeutic Target in Cardiovascular Disease.” *Cardiovasc. Drugs Ther.* 35:815–28.

CD38 gene sequence in the *p*ACGP67-A expression vector

ATGCTACTAGTAAATCAGTCACACCAAGGCTTCAATAAGGAACACACAAGCAAGATGGTAAGCGCTATTGTTTTATAT
GTGCTTTTGGCGGCGGCGGCGCATTCTGCCTTTGCGGCGGATCCCGGGTACCTTCTAGAAGTCCCGAGGTGGCGCCAG
CAGTGGAGCGGTCCGGGCACCACCAAGCGCTTTCCCGAGACCGTCCTGGCGCGATGCGTCAAGTACACTGAAATTCAT
CCTGAGATGAGACATGTAGACTGCCAAAGTGTATGGGATGCTTTCAAGGGTGCATTTATTTCAAAACATCCTTGCAAC
ATTACTGAAGAAGACTATCAGCCACTAATGAAGTTGGGAACTCAGACCGTACCTTGCAACAAGATTCTTCTTTGGAGC
AGAATAAAAGATCTGGCCCATCAGTTCACACAGGTCCAGCGGGACATGTTCACCCTGGAGGACACGCTGCTAGGCTAC
CTTGCTGATGACCTCACATGGTGTGGTGAATTCAACACTTCCAAAATAAACTATCAATCTTGCCCAGACTGGAGAAAG
GACTGCAGCAACAACCCTGTTTCAGTATTCTGGAAAACGGTTTCCCGCAGGTTTGCAGAAGCTGCCTGTGATGTGGTC
CATGTGATGCTCAATGGATCCCGCAGTAAAATCTTTGACAAAAACAGCACTTTTGGGAGTGTGGAAGTCCATAATTTG
CAACCAGAGAAGGTTCAGACACTAGAGGCCTGGGTGATACATGGTGGAAGAGAAGATTCCAGAGACTTATGCCAGGAT
CCCACCATAAAAGAGCTGGAATCGATTATAAGCAAAAGGAATATTCAATTTTCCTGCAAGAATATCTACAGACCTGAC
AAGTTTCTTCAGTGTGTGAAAAATCCTGAGGATTCATCTTGCACATCTGAGATC**CACCACCACCATCACCACCACCAC**
CACTAA**GCGGCCGC**TGCAGA

Secretion signal sequence- **Blue bold**

Restriction site XbaI and NOTI-**Red**

His-tag sequence- **Green bold**

Stop codon-**TAA**

Chapter 6

Expression of human, mouse, and *Plasmodium falciparum* ectonucleoside triphosphate diphosphohydrolases (NTPDases) and their inhibition

Salahuddin Mirza, Chunyang Bi, Laura Schäkel, Tobias Claff, Victoria Johanna Vaaβen, Sangyong Lee, Christa E. Müller

Summary

In this chapter, we present the recombinant expression of CD39 as soluble and membrane-bound proteins belonging to different species, namely human, mouse, and *Plasmodium Falciparum* NTPDase (*pf. apyrase)*. The enzymes were purified by affinity chromatography and characterised by their ability to hydrolyse nucleotides. These experiments were performed using capillary electrophoresis. The human and mouse enzymes (soluble and membrane-bound) were enzymatically active and hydrolysed nucleotides, ATP and ADP, to AMP. The parasitic enzyme was only weakly active, although some ATP and ADP hydrolysis were recorded compared to the control. Small molecule inhibitors with a nucleotidic scaffold were tested against soluble human CD39. The IC_{50} and K_i values were determined for the most potent compounds with ATP 150 µM. Compounds inhibited soluble CD39 with the following K_i (in µM): BCY110 (**0.058** ± 0.03), BCY231 (**0.232 ±** 0.011), BCY 247 (**0.469 ±** 0.031), BCY108 (**8.60 ±** 1.19), CS052 (**2.29 ±** 0.36), CS094**/**BCY308 (**5.93 ±** 3.31), CS347-2 (**0.851 ±** 0.291), CS209-1 (**0.576 ±** 0.106), CS207-1 (**0.733 ±** 0.386), and BCY131 (**1.95 ±** 0.29). The most potent inhibitors, BCY110, -231, and -247, were further tested against human and mouse membrane-bound CD39, where a comparable inhibition of both variants was observed. Moreover, all three inhibitors were equally active in inhibiting the soluble and membrane-bound human CD39, showing K_i values in the same range. A comparative analysis was performed on human and mouse membrane-bound CD39, and it was found that these inhibitors showed comparable potency towards both orthologs. We further tested the selectivity of the current series of inhibitors towards other ectonucleotidases, including NPP1, -3, -4, -5, and -CD38. Data shows that most of these compounds were not active in modulating these enzyme's activities, although some, e.g., BCY110, inhibited NPP3 activity by

approximately 50% at 50 µM inhibitors concentration. A similar inhibition of NPP4 was also recorded by BCY-247 (60% at 50 µM).

1.0 Introduction

1.1 Purinergic signalling

Purinergic signalling comprises transmembrane purine receptors, ectoenzymes, and extracellular nucleotides (Zimmermann, 2020).

1.1.1 Purinergic receptors

Chapter 1 of this dissertation provided many details on purinergic receptors, including their agonists and antagonists. Briefly, two main categories of purinergic receptors include P1 receptors for adenosine and P2 receptors for ATP/ADP. The four distinct subtypes of P1 receptors (A_1, A_{2A}, A_{2B}, and A_3) have been cloned and characterised. These are all members of the family of G protein-coupled receptors that resemble rhodopsin. P2X and P2Y receptors are two significant subtypes of P2 receptors. P2X receptors constitute a trimeric ion pore and are ATP-gated ion channel receptors. There are seven subunits (P2X1–7) that can combine to generate homo- or heterotrimers. Eight subtypes of G protein-coupled P2Y receptors are known ($P2Y_{1,2,4,6,11–14}$).

1.1.2 Adenosine triphosphate (ATP)

Intracellularly, ATP acts as energy currency. Cells phosphorylate ADP to ATP and store the energy produced by glycolysis and the citric acid cycle. This energy is utilised for numerous cellular functions, such as transport, movement, and anabolic reactions, by hydrolysing phosphodiester bonds to produce adenosine diphosphate (ADP) and phosphate.

a. Extracellular ATP

The intracellular (i) concentration of ATP under normal steady-state conditions is in the mM range (approximately 3 – 10 mM), while the extracellular (e) concentration is in the low nM range (Trautmann, 2009). This generates a colossal concentration gradient of approximately 10^6-fold that the cell membrane has to maintain. Maintenance of an adequate balance of iATP/eATP is critical for normal cellular functioning. However, under inflammatory and cancerous conditions, iATP outbursts are observed in the extracellular environment (Idzko et al., 2015). Cell membranes contain nucleotide transporters, such as connexin-43, pannexin-1, and ABC transporters, that systematically transport iATP to

the extracellular milieu. However, besides this, a large amount of iATP is released due to cellular necrosis and vesicular transport. These vesicles originate from the cell membrane; therefore, the outer membrane of secretory vesicles is consistent with the cellular membranes. This systematic and non-systematic ATP release can cause a many-fold increase in the nucleotide's concentration in the extracellular environment (Dosch et al., 2018). Extracellular ATP is a significant signalling nucleotide, alongside NAD^+, involved in purinergic signalling under inflammatory and cancerous conditions. Enhanced ATP concentrations induce pro-inflammatory signals that lead to immune cell recruitment. This characteristic of eATP as an extracellular messenger makes it an essential damage-associated molecular pattern (DAMP). The nucleotide can effectively interact with different P2 purinergic receptors and induce innate immune system response.

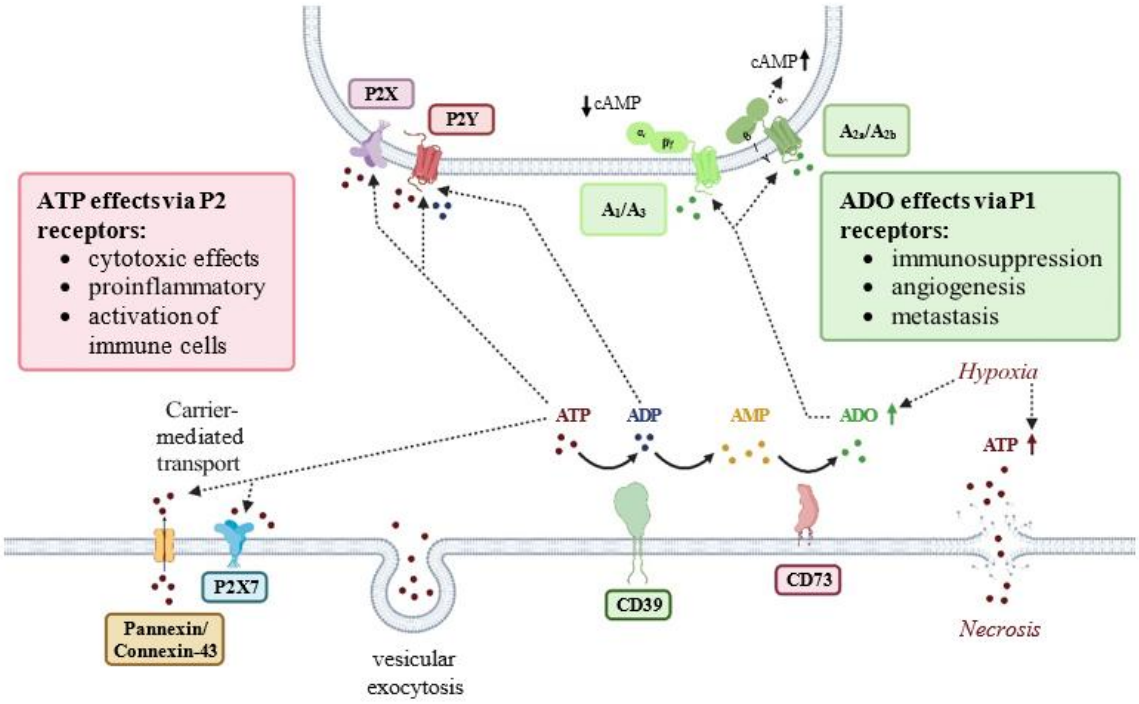

Figure 6.1: Extracellular ATP and its targets. The figure was produced using biorender software (Stach et al., 2023)

Transmembrane P2X receptor subtypes have variable affinity for ATP ranging from nanomolar to micromolar levels, with P2X7 having the lowest affinity for ATP above 100 µM (Allard et al., 2020). Expressed on the surface of several immune cells, including dendritic cells, macrophages, Treg cells, and T-cells, P2X7 receptor activation is significant. Low affinity for ATP means receptors are only active under inflammatory

conditions with higher extracellular ATP concentrations. ATP further interacts with different sub-types of P2Y receptors to initiate either calcium mobilisation from intracellular Ca^{2+} stores or reduced cAMP accumulation. However, the overexpression of surface-located ectonucleotidases like CD39 and NPP1 potently hydrolyse ATP to AMP and, with the help of CD73 to adenosine, making ATP unavailable for purinergic receptors to initiate pro-inflammatory responses. In contrast to ATP, adenosine exerts anti-inflammatory effects via adenosine receptors. Details of extracellular signalling based on ATP are presented in Figure 6.1.

1.1.3 Ectonucleotidases

These ectoenzymes are expressed on the cellular membranes with their catalytic domain pointing to the extracellular environment where they hydrolyse extracellular nucleotides. Ectonucleotidases thus control the activation of membrane-bound P2 purine and pyrimidine receptors. Nucleotides are hydrolysed to their respective nucleotides/nucleosides and affect physiological processes. In previous chapters, it is discussed in detail the five families of ectonucleotidases: ecto-nucleoside triphosphate diphosphohydrolases (E-NTPDases, e.g. CD39), NAD^+ glycohydrolases (NADases, CD38), ecto-nucleotide pyrophosphatases/ phosphodiesterases (E-NPPs, e.g. NPP1), alkaline phosphatases (APs, e.g. TNAP [tissue nonspecific alkaline phosphatase]) and ecto-5'-nucleotidase (eN, e.g. CD73) (Robson et al., 2006). The NTPDases are nucleotide-specific ectonucleotidases that hydrolyse nucleoside triphosphates and -diphosphates to produce nucleoside monophosphates (Zimmermann et al., 2012). Among eight subtypes of NTPDases, only NTPDase1, -2, -3, and -8 are localised on the cell surface. NTPDase4, -5, -6, and -7 are intracellularly localised and will be described briefly. Ecto-5'-nucleotidase hydrolyses nucleoside monophosphates (e.g. AMP) and produces nucleoside (e.g. adenosine). The details of each enzyme family, including CD73, CD38, and NPPs, are given in their respective chapters. This chapter will focus on NTPDases with particular emphasis on CD39. The general characteristics of the NTPDases family are summarised in Table 6.1.

Table 6.1. Nomenclature, tissue distribution, and substrate specificity of NTPDases[a]

NTPDases	Other names	Gene name	Substrate preference	Cellular location	Distribution in tissues
1	CD39, ATPDase, ecto-apyrase	*ENTPD1*	ATP ≈ ADP	Cell Surface	Lymphocytes, Endothelial Cells
2	CD39L1, ecto-ATPase	*ENTPD2*	ATP >> ADP	Cell Surface	Brain, Muscle, Hepatoma, Lung Carcinoma
3	CD39L3, HB6	*ENTPD3*	ATP > ADP	Cell Surface	Liver, Stomach, Oviduct
4	Golgi-UDPase	*ENTPD4*	NTP, NDP, little ATP, ADP	Golgi, Lysosome	Not yet known
5	CD39L4, ER-UDPase,	*ENTPD5*	UDP, GDP, CDP, ADP, little ATP	ER	Macrophages, liver, kidney, prostate
6	CD39L2	*ENTPD6*	GDP, IDP, UDP, CDP	Golgi	Heart
7	LALP1	*ENTPD7*	UTP, GTP, CTP, little ATP	lumen of cytoplasmic organelles	Under-investigated
8	Liver canalicular Ecto-ATPases	*ENTPD8*	ATP > ADP	Cell Surface	Liver in rats, mice, and chicken

LALP1 Lysosomal apyrase-like protein1

[a]Adapted from (Kukulski et al., 2011; Robson et al., 2006)

1.2 NTPDases

NTPDases1, -2, -3, and -8 are attached to the membrane through two transmembrane-spanning domains, with their catalytic domain pointing towards the extracellular environment. These nucleotide-specific enzymes can hydrolyse tri- and di-phosphates of adenine, uridine, and other nucleobases with variable kinetic profiles, as in Table 6.2.

Table 6.2. Substrate preferences of human and mouse ecto-NTPDases

Name	Substrates	Preferable substrate (K_m µM)	
		Human[a]	**Mouse[b]**
NTPDase1	NTP, NDP	ATP (17) ~ ADP (22) >UTP>UDP (135)	ATP (12) = ADP (13)
NTPDase2	NTP	ATP (70) >>UTP (393)	ATP (37) > UTP (49)
NTPDase3	NTP, NDP	ADP (31) > UTP ~ UDP > ATP (75)	UTP (10) ~ ATP (11) > ADP (19)
NTPDase8	NTP, NDP	ATP (81) > ADP > UDP > UTP (480)	ATP (13) > ADP (41)

[a] K_m of hNTPdases1-3 from (Kukulski et al., 2005), hNTPDase8 from (Fausther et al., 2007). [b]K_m of mNTPDase1-2 from (Kukulski et al., 2005), mNTPDase3 from (Lavoie et al., 2004), mNTPDase8 from (Bigonnesse et al., 2004)

1.2.1 NTPDase orthologs

NTPDase1 orthologs have been identified in eukaryotes and prokaryotes based on five apyrase-conserved regions (ACRs). In this section, we shall describe important NTPDase orthologues of selected species.

a. *Legionella pneumophila* (*L. pneumophila*)

Fiona et al. first reported that recombinant bacterial *L. pneumophila* NTPDase can hydrolyse ATP/ADP, and NTPDase selective inhibitor ARL67156 could inhibit this hydrolysis (Sansom et al., 2007). Enzyme potently hydrolysed ATP and GTP with similar product turnover; however, a higher turnover was recorded for GDP than ADP (Sansom et al., 2008). Newton et al. further reviewed the cellular mechanism underlying the spread of *L. pneumophila* infections, including hospital-acquired pneumonia (Newton et al., 2010). Efforts were previously made to investigate inhibitors for *L. pneumophila* NTPDases. Our research group has identified a moderately potent sulfoanthraquinone derivative with an IC_{50} value of 4.24 µM (Fiene et al., 2016).

b. *Leishmania infantum (L. infantum)*

The catalytic domain of the recombinant *L. infantum* NTPDase (rLi-NTPDase) was previously expressed and purified from the *E. coli* expression system (Souza et al., 2013). The enzyme can hydrolyse ATP and ADP in the presence of divalent cations such as magnesium, calcium, manganese, and zinc (Vieira et al., 2018). Interaction of *L. infantum* with macrophages activates purinergic signalling mechanisms that lead to the pathogenesis of *Leishmania* disease (Figueiredo et al., 2016). Substrate hydrolysis studies with rLi-NTPDase1 and -2 showed that the enzyme can hydrolyse nucleoside diphosphates (ADP, GDP, UDP) with better product turnover as compared to their triphosphate counterparts (Bastos et al., 2017). The existence of an antigenic domain in the catalytically active Leishmania NTPDase has been previously reported that could be the target of inhibitory antibodies (Maia et al., 2019). Small molecule inhibitors are poorly investigated, and very little has been reported.

c. *Plasmodium falciparum* (*P. falciparum*)

Involvement of purinergic signalling was reported in the *P. falciparum* parasite. The expression of a GFP-tagged short NTPDase sequence (first ~ 500 bp) in vivo in the

parasite was significantly inhibited by suramin (Pereira et al., 2017). ATPase activity was observed for non-purified membrane preparations using ATP as a substrate in a reaction buffer (in mM; 116 NaCl, 5.4 KCl, 0.8 $MgSO_4$, 5.5 D-glucose, 50 MOPS, 2 $CaCl_2$ pH 7.4). The GFP tag indicated the protein was localised at the parasitophorous or food vacuole. Despite its documented role in purinergic signalling in malarial parasites, the protein is still not recombinantly expressed and characterised.

d. Mouse

NTPDase1 activity was found in the peritoneal cavity of the mouse and is dependent on divalent cations Ca^{2+} and Mg^{2+} at physiological pH (Dias et al., 2017). The enzyme hydrolyses ATP and ADP with a similar kinetic profile (K_m= ~510 µM and ~660 µM). However, the enzyme isolated from the mouse spleen showed higher product turnover with a K_m of 23.3 µM and K_{cat} of 142 s^{-1}, representing a favourable specificity constant (Lee et al., 2018). Tucuma oil (*Astrocaryum vulgare*) treatment was reported to have the potential to inhibit purinergic signalling in diabetic mice (Baldissera et al., 2017).

e. Rat

Upregulation of the enzyme was observed in rat platelets and lymphocytes after regular high-energy intake, where the NTPDase activity was linked with hypertension (Kaizer et al., 2017; Cardoso et al., 2015). The uridine-based signal transduction pathway is reported in rat brains where α-terpene-dependent memory defects are due to changes in ATPase activity (Baldissera et al., 2016; Cansev et al., 2015). Moreover, secretary vesicles containing NTPDase and CD73 in abundance were reported, which further increased the scope of this enzyme in the extracellular environment (González et al., 2015). Kinetic parameters were tested towards ATP and ADP with a determined K_m of 135 µM for ATP and 214 µM for ADP; however, a K_m of 18.5 µM was also reported for ADP (Lee et al., 2018). The enzymatic activity in the lymphocytes was suppressed by treatment with quercetin in hyperlipidaemic rats and rat models of rheumatoid arthritis (Braun et al., 2018; Saccol et al., 2019).

f. Schistosoma mansoni (*S. mansoni*)

Parasitic *S. mansoni* ATPDase1 and -2 containing conserved ACR1-5 region were recombinantly expressed (hydrophilic domain only) in the bacterial expression system (DeMarco et al., 2003). The enzyme is localised on the cell surface, as demonstrated by

using confocal microscopy (Garcia et al., 2007). The enzyme can hydrolyse nucleotides (ATP, ADP) with a comparable kinetic profile (Maia et al., 2011; Silva, 2016). Thiosulphuric acid derivatives were reported to moderately inhibit the enzyme activity with a K_i of 0.1 to 1 mM. The enzymes are valuable therapeutic targets for schistosomiasis; therefore, potent and selective inhibitors are needed to study their role in causing the disease (Penido et al., 2007).

g. Toxoplasma gondii (T. gondii)

NTPDases1 was recovered from lymphocytes after experimentally induced toxoplasmosis in a mouse model (Tonin et al., 2013). Enzymatic activity of isolated lymphocytes from tachyzoites of parasites showed ATP hydrolysis ≥ ADPase activity along with potent hydrolysis of AMP to adenosine (Tonin et al., 2015). Expression of P1 and P2Y receptors on the lymphocytes emphasised the involvement of purinergic signalling in toxoplasmosis. Although *T. gondii* NTPDase isoforms -1 and -3 share 97 % sequence identity, NTPDase3 showed much higher hydrolysis of ATP >>>ADP; however, NTPDase1 hydrolyse both substrates similarly (Krug et al., 2012).

h. Trichomonas vaginalis (T. vaginalis)

Ectonucleotidase (NTPDase/CD73) activity was first reported from the in vitro cultured samples of the isolated parasites and later from the clinical isolates (Tasca et al., 2005; Frasson et al., 2012; Frasson et al., 2012). The parasite expressed 5 NTPDase types, amongst which NTPDase2 and -4 mainly showed ATP and ADP hydrolysis. The guanosine concentration was increased in *T. vaginalis,* showing potent hydrolysis of GTP, GDP, and GMP with K_m values (in µM) of 1.12, 1.11, and 6.38, respectively (Menezes et al., 2016; Menezes et al., 2016). It was further reviewed that the parasite utilises purinergic signalling pathways to bypass the host immune defence and cause trichomonosis (Menezes et al., 2016). Plant alkaloids licorine, candimine (potent) and dehydroepiandrosterone sulfate, 17-β-estradiol (moderate) have inhibitory effects on the ectonucleotidase activity (Rückert et al., 2010; Giordani et al., 2010). The compounds further showed cytotoxic effects.

i. *Trypanosoma brucei brucei* (*T. brucei brucei*)

Ecto-ATPase activity was observed in *T. brucei brucei* cultured cells with a K_m value of 600 µM. The enzyme could also hydrolyse GTP, UTP, CTP, ITP, and diphosphates, e.g.

ADP (Leite et al., 2009). NTPDase activity was further observed in lymphocytes of infected mice with *T. evansi* and in the adipose tissues (Trindade et al., 2016; Oliveira et al., 2012). The parasite can evade host defence mechanisms, and the enzyme is crucial for the spread of trypanosomiasis (Caljon et al., 2018).

j. *Trypanosoma cruzi* (*T. cruzi*)

Parasitic *T. cruzi* NTPDase (TcNTPDase 1) is capable of hydrolysing di phosphates (GDP, UDP) better than GTP=UTP >> ADP>ATP (Moura et al., 2014). The purinergic pathways are reported to be overexpressed in platelets of infected mice, leading to thrombocytopenia (Carmo et al., 2017). NTP hydrolysis is considered to be an essential factor for parasite involvement in the aetiology of Chagas disease as ectonucleotidase activity is altered in the lymphocytes of patient samples suffering from Chagas disease (Santos et al., 2009; Souza et al., 2012; Fietto et al., 2004).

1.2.2 Human NTPDase 1 (CD39)

CD39 is a membrane-bound enzyme composed of 510 amino acids with a MW of approximately 58 kDa. The protein is localised in the cellular membranes through two transmembrane domains, with a small cytoplasmic domain of both N- and C-terminal sequences. The sizeable catalytic domain protrudes into the extracellular environment, showing its hydrolytic potential (Robson et al. 2006). The catalytic domain has five apyrase-conserved regions (ACRs) that are critical in substrate binding and hydrolysis. The catalytic activity occurs in millimolar concentrations of Ca^{2+} and Mg^{2+}(Zimmermann et al., 2012). Different research groups work with either the membrane-bound or the soluble form. The soluble form is produced by cutting off the sequences of the transmembrane domains. Soluble CD39 is a monomer emphasising the TM domain's involvement in dimer and tetramer formation. The enzyme shows a similar preference for both ATP and ADP.

1.2.3 Catalytic Mechanism of CD39

CD39 hydrolyses ATP in two steps: first, it is hydrolysed to ADP, and in the second step, ADP is dephosphorylated to AMP. The ADP from the first step remains attached to the active site, and only a brief accumulation of ADP occurs. This two-step hydrolysis yields two molecules of P_i contrary to NPP1, which liberates a single molecule of PP_i; however,

during UTP hydrolysis, a significant amount of UDP accumulates (Kukulski et al., 2005; Robson et al., 2006). Although CD39 hydrolyses both di- and triphosphates of purine and pyrimidine nucleotides equally well, the pyrimidine nucleotides UTP and UDP have reduced affinity for CD39 than ATP and ADP, possibly due to their smaller size, which makes them unable to adapt the same binding mode as purine does (Zebisch et al., 2012). The catalytic mechanism is schematically described in Figure 6.3.

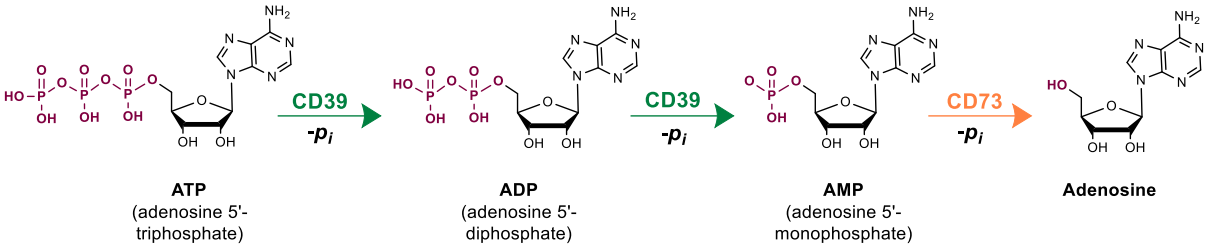

Figure 6.3: ATP hydrolysis via ADP and AMP to adenosine by CD39 and CD73

1.3 Tissue expression of CD39 and pathology

CD39 is expressed on the surface of immune cells such as leukocytes, neutrophils, monocytes, and β-lymphocytes (Pulte et al., 2007). The enzyme is further reported in the vasculature in vascular endothelial (VETCs) and vascular smooth muscle cells (VSMCs).

1.3.1 *Vascular diseases*

The role of ATP in maintaining cardiovascular tone in association with purinergic receptors is well documented. Overexpression of CD39 in vasculature was observed in pathological conditions. A significantly increased ATPase activity was observed in patients' samples suffering from cardiovascular diseases (Kittel et al., 2005). Altered nucleotide hydrolysis in the stenotic valve induces valve calcification (Zajac et al., 2020). Moreover, CD39 knock-out mice showed a decrease in coronary output, emphasising the regulatory role of CD39 in endothelium-dependent arterial diseases (Favre et al., 2023). In tissue injury, platelets are activated to release their stored nucleotides ATP and ADP into the extracellular milieu. CD39, which is widely expressed in the vasculature and on the platelet surface, hydrolyses these nucleotides to AMP, and subsequently, CD73 produces adenosine, thereby limiting thrombotic events (Morello et al., 2021). There are further reports related to CD39 and CD73 as tandem partners in connection with arterial thrombosis, where it is observed that CD39 on hematopoietic-derived cells, mainly

monocytes, protect against thrombosis (Covarrubias et al., 2016). Moreover, the NADases such as CD38 expressed on endothelial or immune cells integrate with CD39 to control vascular thrombosis, inflammation, and abnormal immune reactivity (Deaglio et al., 2011). The regulatory role of CD39 in diabetes mellitus has been reviewed by (Zeng et al., 2020).

1.3.2 Cancer immunotherapy

CD39 is upregulated in several solid tumours like pancreatic cancer, ovarian cancer, follicular lymphoma, head and neck cancer, and chronic lymphocytic leukaemia (Cai et al., 2015; Bastid et al., 2015). Its primary expression in immune cells is observed at the cell surface of regulatory T cells (Tregs), where it converts pro-inflammatory ATP and ADP into AMP. Subsequently, CD73 converts AMP to adenosine (Bastid et al., 2015). Adenosine is a potent immunosuppressor and binds to its receptors (adenosine receptors) at the surface of CD4, CD8 T cells, and NK cells to inhibit effector cell response, which facilitates tumour progression (Antonioli et al., 2013). Adenosine also binds to A_{2A} or A_{2B} receptors on macrophages and dendritic cells (DC), inhibits phagocytosis and antigen presentation, and increases secretion of pro-tumourigenic factors, such as VEGF, TGF-β, and lL-6 (Kumar, 2013). Tregs suppress the immune system response to malignancies; therefore, the progression of the tumour occurs. Immunotherapies that target Tregs non-specifically showed significant results in some cancer patients, including complete responses in advanced-stage disease. However, immunotherapies include serious adverse effects as they affect both regulatory and effector T cells, compromising their net effect; the overall efficacy of these therapies is modest (Bastid et al., 2012). Those limitations prompt another strategy, such as blocking the CD39 function. Blockade of CD39 can increase the concentration of ATP, but at the same time, it also decreases the concentration of adenosine by reducing the concentration of its precursor AMP. Both can lead to an enhancement of the immune response in the body. Hence, interfering with the CD39–adenosine pathway represents a novel immunotherapeutic strategy for inhibiting tumour cell-mediated immunosuppression, and this goal can be achieved by inhibitors of CD39, which may have the potential for the treatment of cancer and immunodeficiency disorders (Bastid et al., 2012). Table 6.3 summarises CD39 expression in different cancers.

Table 6.3: CD39 expression and functions in different cancers

Cancer	CD39 activity	References
Lung	The enzyme is widely expressed in MDSC and TILs and leads to immune evasion in lung cancer patients	(Li et al., 2017; Chen et al., 2020)
Stomach	Upregulation of CD39 is associated with the poor prognosis of gastric cancer	(Shi et al., 2018; Cai et al., 2015)
Hepatocellular carcinoma	Increased tumour relapse was observed due to overexpression of CD39 in hepatocellular carcinoma	(Wang et al., 2021)
Colorectal	Overexpression of CD39 on Treg creates immunosuppression via purinergic signalling in colon adenocarcinomas	(Roliano et al., 2022)
Ovarian	Overexpression of CD39 on solid ovarian tumour led to increased ATP hydrolysis that was significantly reduced by metformin	(Li et al., 2018; Barrio et al., 2016)
Breast	Overexpression of CD39 is reported in patients with luminal breast cancer	(Ni et al., 2021)
Melanoma	Increased CD39 expression is positively associated with immunosuppression, inflammation, and tumor-promoting activity	(Mallardo et al., 2023)
Head and neck	Significantly higher expression of CD39 in metastatic lymph nodes linked with inferior survival rate in HNSCC	(Mandapathil et al., 2018)
Leukaemia/ Lymphoma	Adult T-cell leukaemia/lymphoma cells highly express CD39 to help them escape immune surveillance	(Nagate et al., 2021)

1.3.3 Microbial diseases

NTPDase orthologs were previously reported in numerous prokaryotic and eukaryotic species, as detailed in section 1.2.1 of this chapter. The roles of purinergic signalling and NTPDases in spreading different diseases caused by these organisms are also summarised there. Here in this section, we will briefly discuss some critical pathologies. *Legionella pneumophila* is the primary causative agent of Legionnaires' disease, a severe form of acute pneumonia (Sansom et al., 2007). In a recent genome sequence study, three strains of *L. pneumophila* have been reported to carry putative proteins that share sequence similarity with eukaryotic proteins. Among those putative products, two uncharacterised genes annotated as *lpg1905* and *lpg0971* in the genome sequence of *L. pneumophila* strain Philadelphia share sequence similarity with the human NTPDase1 and other eukaryotic ecto-NTPDases (Larsson et al., 1999). The product of lpg1905 exhibited the same enzymatic activity as human CD39, and L. pneumophila may manipulate host pathways regulated by CD39 during human infection. Thus, inhibition of CD39 might help treat Legionnaires' disease.

1.4 Assays for monitoring NTPDase activity

In chapter 3 of this thesis, we already described some assays that are currently in practice for monitoring the ATPase activity of NPPs. The same assay protocol is also applicable for monitoring NTPDase activity; however, in the case of NPPs, PP_i is released due to ATP hydrolysis. NTPDases hydrolyse the terminal phosphodiester bond of ATP to ADP and subsequently to AMP, producing a single molecule of P_i after each hydrolysis step. Therefore, we will re-discuss monitoring assays focusing on NTPDases. The malachite green assay is the most widely used one for analysing NTPDase activity that detects liberated P_i in the samples that form a colour complex with malachite green, and the phosphomolybdate complex can be measured at 625 nm. Thus, the liberated P_i can be quantified calorimetrically (Baykov et al., 1988). The assay is suitable for high-throughput screening but involves a high signal/noise (S/N) ratio and needs a high substrate concentration. To work with the substrate concentration in a similar range as the K_m of the enzymes, our research group has previously discovered a fluorescence polarisation immunoassay using Alexa 633 tracer antibodies that can distinguish between ATP and AMP (Fiene et al., 2015). The assay is highly sensitive and allows it to work at low substrate concentrations around the K_m values of enzymes; however, the expensive material and sophisticated handling make this assay less applicable in general lab settings. Soluble and membrane-bound CD39 activity was previously monitored using an AMP-glow assay (Goueli et al., 2019). CD39 initially hydrolyses ATP to AMP. In the second step, the remaining ATP is depleted from the reaction mix by adenylate cyclase (AC), which converts it to cAMP. AMP, at the same time, is converted to ADP by AMP-phosphotransferase. In the last step, ADP is converted to ATP by adenylate kinase, which is then quantified by interacting with D-luciferin in the presence of firefly luciferase. FPIA and AMP-glow assays are suitable for inhibitor testing at low substrate concentrations; however, the published reports have not included kinetic parameters. Moreover, FPIA assay involves a highly costly antibody solution. A phosphate sensor assay can further monitor ATPase activity where *E. coli* phosphate binding protein (PBP) binds specifically to monophosphate. The fluorophore, *N*-[2-(l-maleimidyl)ethyl]-7-(diethylamino)coumarin-3-carboxamide (MDCC), was attached to the single cysteine of PBP. The labelled protein shows an increase in fluorescence intensity when complexed with P_i, corresponding to the enzyme activity (Brune et al., 1994). Apart from these HTS assays, NTPDase activity

can also be measured using HPLC or capillary electrophoresis that specifically detect the hydrolysis product AMP through UV absorption at 254 nm. Moreover, our group previously published a highly sensitive fluorescence-based assay using N^6-fluorescein-labeled- ATP and CE with fluorescence detection (Lee et al., 2018). The assay is currently the most sensitive for monitoring NTPDase activity with an LOD in the picomolar range. Some groups also work with isothermal titration calorimetry (ITC), where the heat evolution is measured to represent the breakage of the bond (Zebisch et al., 2012). ITC assay is diversified, like CE and HPLC, and multiple substrates can be analysed. However, the assay, like CE and HPLC, is again time-consuming. Moreover, heat is a universal signal, and in the samples where multiple enzymes are expressed, the specific contribution of different enzymes is challenging to measure accurately. The details of different assays reported for monitoring NTPDase activity are detailed in Table 6.4.

Table 6.4: Kinetic parameters of reported assays for NTPDases

Assay	Substrate	Detection mechanism	Subtype	K_m (µM)/ Vmax (nmol/min/mg protein)	Ref.
Calourimetric	ATP	Inorganic phosphate via MG# dye at 625 nm	NTPDase1 NTPDase2 NTPDase3	17 ± 1/0.92 ± 0.02* 70 ± 2/2.3 ± 0.03* 75 ± 10/0.79 ± 0.03*	(Kukulski et al., 2005)
Luminescence AMP-glow	ATP	ATP detection via Firefly luciferase from *Photinus pyralis*	NTPDase1	N.D#	(Goueli et al., 2019)
CE	ATP	UV detection of nucleotides at 254 nm	NTPDase 1 NTPDase 2 NTPDase 3	76.0 ± 12/230 ± 2 11.4 ± 5.1/ 82.5 ± 5.5 203 ± 8/210 ± 2 311 ± 4/100 ± 1	(Iqbal et al., 2005) (Lee et al., 2018)
FFCE	fluorescein-labeled-ATP	LIF@ detector using 488 nm for excitation and 520 nm for emission	NTPDase 1 mNTPDase 1 rNTPDase 1	19.6 ± 3.7/ 119 ± 12 23.3 ± 2.6/ 142 ± 22 18.5 ± 4.4/ 104 ± 12	(Lee et al., 2018)
HPLC	ATP ADP	-Do-	LicNTPDase2	4.8 mmol/L 0.4 mmol/L	(Magalhães et al., 2016)
Isothermal titration calorimetry	ADP UTP UDP GTP GDP ITP IDP	Measures heat evolved as a result of bond breakage	rNTPDase 1	4.70 ± 0.3/77.3 ± 4.2$ 10.0 ± 1.4/103 ± 4$ 11.3 ± 0.5/80.9 ± 2.1$ 9.00 ± 1.1/80.9 ± 2.2$ 11.4 ± 1.2/83.2 ± 8.0$ 10.8 ± 0.4/105 ± 2$ 10.5 ± 1.7/79.9 ± 4.6$	(Zebisch et al., 2012)

*U/mg protein, $ Kcat s^{-1}, #Not determined @ LIF laser-induced fluorescence detector

1.5 Reported crystal structures of NTPDases

Overall, 48 crystal structures have been reported for NTPDases so far. The bacterium *Legionella pneumophila* (LpNTPDases) has the most significant crystal structures (18 total) of these reported crystal structures. *Rattus norvegicus* (*Rn*NTPDases) has 13 crystal structures and *toxoplasma gondii* (TgNTPDases) has 8 crystal structures. Human NTPDases are challenging targets for crystallisation studies, and till now, only one crystal structure is known for NTPDase4. Apart from this, not so much success has been achieved for human isoenzymes.

a. Legionella pneumophila

The enzyme is expressed on the surface of the bacterial cells and plays a vital role in infection and virulence of *L. pneumophila*. Reports suggest that parasitic NTPDase can regulate ATP and adenosine levels in the host cell, thereby modulating the host's immune response by increasing intracellular cAMP and triggering inflammation (Paes-Vieira et al., 2021). *Lp*1NTPDases are structurally related to mammalian NTPDases. The apyrase-conserved regions (ACR 1 – 5) are well resolved in the previously reported crystal structures of *Lp*1NTPDase ectodomain co-crystallized with the non-hydrolysable ATP analogue adenylyl imidodiphosphate (AMPPNP) and the inhibitor ARL67154 (Vivian et al. 2010). Moreover, *Lp*1NTPDase co-crystal structures with polyoxometalates (decavandate, hepta/octa-molybdate, POM1) are also reported (Zebisch et al., 2014). The details of reported crystal structures are summarised in Table 6.5.

Table 6.5: Reported crystal structures of NTPDases

PDB-id	Enzyme	Mutation	Substrate/ inhibitor	Active site A.A	Interactions	The functional group in the compounds	Res (Å)	Ref.
3AAP 3AAQ 3AAR	*L.p*1-NTPDase	Wt	Open/Apo ARL67154 AMPPNP	G299, N302, L303, Y346, Y350 and L353 Y346 ACR1=S52, T53, R56 ACR4=G189	Hydrophobic H-bond H-bond	Adenine Ribose Phosphates	1.60 2.00 1.65	(Vivian et al., 2010)
4BR4 4BR7 4BR9 4BRA 4BRC 4BRD 4BRE		 Q193E	Open/Apo AMPNP Apo Mg^{2+}-AMPPNP Mg^{2+}-AMPNP Mg^{2+}-AMPPNP				1.45 1.80 1.40 1.60 1.30 1.50 1.60	(Zebisch et al., 2014) (Zebisch et al., 2013)

4BRF			Mg^{2+}-AMP-VO_4^{3-}				1.60	
4BRQ			Mg^{2+}-AMP-MoO_4^{2-}				1.45	
4BRG			Mg^{2+}-AMP-Pi-Pi				1.45	
4BRH			Mg^{2+}-GMPPNP				1.69	
4BRI			Mg^{2+}-TMP-VO_4^{3-}				1.75	
4BRK		N302Y	Mg^{2+}-UMPPNP				1.50	
4BRL			Mg^{2+}-UMPPNP				1.60	
4BRM			Mg^{2+}-GMP-VO_4^{3-}				2.02	
4BRN			Apo, S-SAD				1.69	
4BRO			Mg^{2+}-AMP				1.99	
4BRP			Apo				2.50	
4BVP			Apo				1.49	
4BVO			Heptamolybdate POM1				1.70	
3ZX0	*Rn*NTPDase1	Wt	Heptamolybdate	Nucleoside binding site-K257, F364, Y409, and Y413	hydrophobic H-bond with 2-OH	Adenine ring	2.50	(Zebisch et al., 2012)
3ZX2			Decavandate				1.81	
3ZX3			Native				1.70	
3CJ1	*Rn*NTPDase2					Adenine ring 3-OH of ribose β, γ-PO_4	1.70	(Zebisch et al., 2008)
3CJ7			Apo	Y350, R394, R245, A347	Hydrophobic pocket H-bond		1.80	
3CJ9			AMP				1.80	
3CJA			Ca^{2+}-AMP-PO_4	R245, D246			2.10	
			Ca^{2+}-AMPPNP	S48, S49, H50, G204, A205, S206	H-bond			
4BQZ	*Rn*NTPDase2						2.05	(Zebisch et al., 2013)
4BR0			Mg^{2+}-GMPPNP				2.05	
4BR2			Ca^{2+}-AMPNP				2.00	
4BR5			Ca^{2+}-UMPPNP				1.75	
4CD1			Zn^{2+}-AMPPNP				2.00	
4CD3			PSB-071 PSB-071				2.19	(Zebisch et al., 2014)
4JEP	*Tg*NTPDase1	Wt	Intermediate tetramer conformation	R492/E493	Hydrophobic	Adenine	3.10	(Krug et al., 2013)
4A5B		C258S/C268S	Apo				2.48	
4KH4		-Do-	Mg^{2+}-AMPPNP				3.00	
4KH5		-Do-	Mg^{2+}-AMPNP				3.00	
4KH6		C258S/C268S/E493G	Mg^{2+}-AMPNP				2.40	(Krug et al., 2012)
4A57	*Tg*NTPDase3	Wt	Apo	G492/493 S/74/73/282, thr188, Ala189	Hydrophobic H-bond	Adenine Phosphate	2.00	
4A5A		C258S/C268S	Mg^{2+}-AMPPNP				2.85	
4A59		Wt	AMP				2.20	
6WG5	hNTPDase4	Wt	Apo	Asn331 and Lys492	H-bond	Ribose	2.60	(Gorelik et al., 2020)

b. Rat NTPDases

The research group of Nobert Sträter previously resolved the crystal structures of rat NTPDase1 and -2 with a high resolution of 1.7 – 2.19 Å. The wild-type sequence of the

ectodomain is mainly used to cut off the transmembrane region. The structures were produced in the presence of different inhibitors, as summarised in Table 6.5. The structures of *Rn*NTPDase1 and -2 are successfully resolved with the non-hydrolysable analogues AMPPNP, UMPPNP, GMPPNP, AMPNP, AMP-PO_4 alongside Ca^{2+}, Mg^{2+}, and Zn^{2+}. Polyoxometalates, heptamolybdate, decavandate (*Rn*NTPDase1), and PSB-071 (*Rn*NTPDase2) were successfully co-crystalized (Table 6.6 for references). These crystal structures revealed valuable information about the overall architecture of the active site, including the amino acid arrangements. Moreover, a comparative analysis was performed for rat and Legionella NTPDase crystal structures, highlighting the evolutionary relationship and functional differences among these enzymes.

c. Toxoplasma gondii

A protozoan parasite, *T. gondii*, possesses NTPDases that are reported to be relevant for its pathogenesis and survival within the host. *Tx*NTPDases are structurally similar to their mammalian variants; however, they exhibit salient features that can be exploited to develop selective inhibitors to target toxoplasmosis. So far, eight crystal structures have been reported for *Tx*NTPDases, of which five are of NTPDase1, and three correspond to NTPDase3 (Table 6.5). Crystal resolution was improved from 3.10 to 2.48 Å when C258S and C268S mutations were inserted in NTPDase1 and -3. Additionally, the E493G mutation yielded 2.40 Å crystals of NTPDase1 in the presence of Mg^{2+}-AMPPNP and Mg^{2+}-AMPNP.

d. Human NTPDase

Human variants of NTPDases are challenging targets for crystallisation, and currently, only the long isoform of NTPDase4 (LALP70) has been successfully crystallised (Gorelik et al., 2020). Mainly expressed in the Golgi bodies, the protein plays a glycosylation role. The recombinant enzyme was expressed in *Sf9* insect cells using the *p*fastbac expression system. The construct starts with melittin as a signal peptide MKFLVNVALVFMVVYISYIYA, a hexa-histidine tag DRHHHHHHKL and the gene of interest (UniProt: Q9Y227, residues 58–559, long isoform containing the VSFASSQQ segment). The enzyme hydrolyses UTP, UDP, CTP, and CDP more efficiently than ATP and ADP.

1.6 Small molecule inhibitors of CD39

Inhibitors targeting CD39 have gained attention for their potential therapeutic applications in various diseases, including cancer, immune diseases, and thrombosis. Several small-molecule inhibitors, including nucleotidic and non-nucleotidic scaffolds, have been identified and developed to modulate CD39 activity.

a. Nucleotidic scaffold

Nucleotidic substrates of CD39, such as ATP and ADP, and the product AMP were modified to design competitive inhibitors. The first reported nucleotidic CD39 inhibitor is ARL67156, where the 6-amino group is substituted by ethyl groups (diethylamino). It further contains a dibromo methylene bridge between the β and γ-phosphate to block the hydrolysis of the terminal phosphate. In subsequent efforts, position 8 of the adenine ring was substituted with the 8-butylthio group to yield moderately potent competitive CD39 inhibitors. Extensive SAR studies were conducted by our research group, and we have synthesised numerous nucleotide-based inhibitors of CD39. The biological activity of these inhibitors was initially tested against membrane-bound CD39 either transiently expressed in COS-7 cells or isolated from the human umbilical cord. Moreover, metabolic stability testing was performed for these inhibitors, where many showed susceptibilities toward liver microsomal enzymes (Schäkel et al., 2020). In general, the advantages of nucleotidic inhibitors include straightforward drug development due to their structural similarity with the substrate. However, despite this, they also possess some disadvantages, e.g. due to negative charge, the intestine does not effectively absorb them and, therefore, has low bioavailability upon oral administration. Furthermore, they may have low chemical and metabolic stability because of liver metabolic enzymes and phosphatases that could hydrolyse them, leading to low in-vivo activity. Besides, these inhibitors might also have intrinsic activities on P2 receptors.

b. Non-nucleotidic scaffolds

The search for small molecule inhibitors bearing non-nucleotidic scaffolds resulted in numerous inhibitors. The research group of Professor Iqbal has published a few scaffolds that achieved low nanomolar IC_{50} values. Most of these compounds non-competitively inhibited CD39 activity apart from the tryptamine scaffold that competitively inhibited

enzyme activity with an IC_{50} value of 210 nM. The highest potency was observed with a thiadiazoleamide derivative with an IC_{50} of 50 nM. Despite achieving excellent potency, these scaffolds were not further optimised to attain selectivity, solubility, and pharmacokinetic profile (Table 6.6). A significant difference in the IC_{50} values was observed in two published reports involving thienopyridine glycinates (100 nM) and 2-substituted thienotetrahydropyridine (84,700 nM) using a similar protein source (expressed in CHO mammalian cells) and the assay system. This thesis further reports the discovery of 4*H*-chromene scaffold as CD39 inhibitors where a K_i value of 150 nM (soluble CD39) was achieved that showed a competitive mode of inhibition (Chapter 5). In summary, a lack of selective and competitive CD39 inhibitors of pharmacological relevance is urgently required for the functional study of CD39 in physiological and pathophysiological conditions. To add further here, the HTS assay described in Chapter 1 involving Ɛ-ATP, Ɛ-ADP, and Ɛ-AMP can be a tool for analysing CD39/73 activity in live cells of different cell lines.

Table 6.6 summarises the reported nucleotidic and non-nucleotidic scaffolds with their structure and kinetic parameters.

Table 6.6: Reported small molecule inhibitors of human CD39

Scaffold	Structure	IC_{50} or K_i (nM)	Mechanism of inhibition	Ref.
Nucleotidic scaffold				
ARL-67156	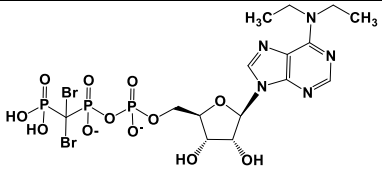	*11,000 ± 3000*	Competitive	(Lévesque et al., 2007; Schäkel et al., 2020)
PSB-172102	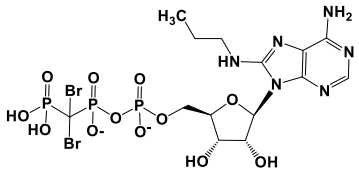	*973 ± 239* *1130 ± 230*		
8-BuS-ATP 8-BuS-ADP 8-BuS-AMP	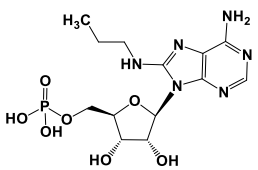	*800 ± 200* *900 ± 200* *800 ± 100*	Competitive	(Lecka et al., 2013)

Non-nucleotidic scaffolds				
Thienopyrimidine glycinates	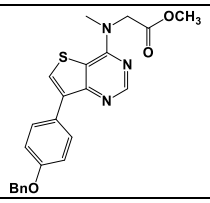	110 ± 10	N.D*	(Begum et al., 2022)
2-Substituted Thienotetrahydropyridine	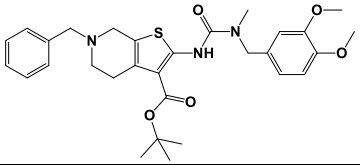	84,800 ± 15,800! 45,200 ± 4,100!!	Non-competitive	(Schäkel et al., 2021)
Thiadiazoleamide	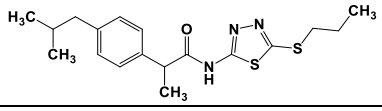	50 ± 8	Non-competitive	(Abbas et al., 2022)
Oxoindoline-phenylhydrazine carboxamide	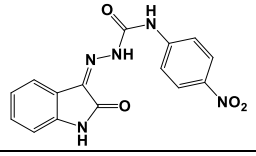	120 ± 3	Un-competitive	(Afzal et al., 2021)
Oxoindoline hydrazine carboxamide	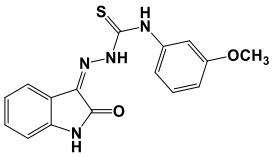	150 ± 9	Non-competitive	(Afzal et al., 2020)
Quinoline	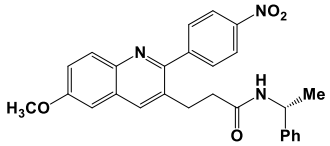	200 ± 20	Non-competitive/ mixed inhibition model	(Murtaza et al., 2021)
	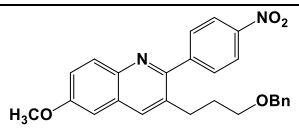	230 ± 10	Un-competitive	(Hayat et al., 2019)
Sulfamoyl-benzamide	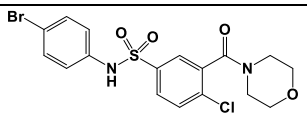	2,880 ± 130	N.D*	(Zaigham et al., 2023)
Tryptamine derivative	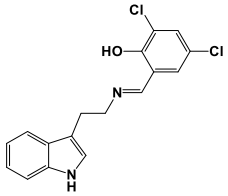	210 ± 1	Competitive	(Kanwal et al., 2019)
Imidazothiazole	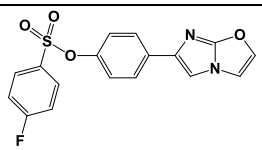	360 ± 20	N.D*	(Shehata et al., 2023)
Anthraquinone	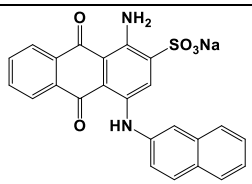	*K_i 328 ±110*	Competitive	(Baqi et al., 2009)

Ceritinib	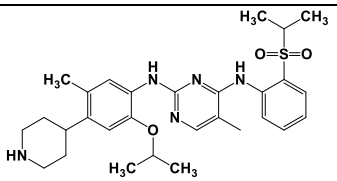	11,300 ± 800	Non-competitive	(Schäkel et al., 2022)
Ticlopidine	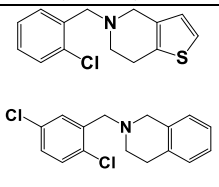	81,700 ± 5,000 14,000 39,000 ± 4,500	Non-competitive	(Schäkel et al., 2021) (Lecka et al., 2014) (Bi et al., 2023)
PSB-POM142	$K_{10}[CO_4(H_2O)_2(PW_9O_{34})_2].22H_2O$	3.88 ± 1.40	Non-competitive	(Lee et al., 2015)
Polysaccharides from sea algae Fucoidan	*Saccharina latissimi*	0.408 ± 0.001	Non-competitive/ mixed inhibition	(Lopez et al., 2021)

1.7 Research objectives

This study aimed to express and purify soluble and membrane-bound forms of NTPDase belonging to different species, including humans, mice, and Plasmodium falciparum, using the *Sf9* insect cell expression system. The recombinant proteins were planned to be characterised and used in inhibition assays to evaluate species differences. The purified proteins are further planned to be crystallised in the future. Some potential nucleotidic inhibitors were tested for IC_{50} value determination using recombinantly expressed soluble CD39.

2 Material and Methods

f. Substrates and chemicals

Adenosine, adenosine 5'-mono-, di- and tri-phosphate (AMP, ADP, ATP), nicotinamide adenine dinucleotide (NAD^+), and *p*-nitrophenyl 5'-thymidine monophosphate (*p*-Nph-5'-TMP) were purchased from Sigma (Steinheim, Germany). Dimethyl sulfoxide (DMSO), disodium hydrogen phosphate (Na_2HPO_4), and sodium acetate (NaOAc) were obtained from Carl Roth (Karlsruhe, Germany). Chlorides of Calcium, magnesium, and zinc ($CaCl_2$, $MgCl_2$, and $ZnCl_2$), Tris HCl, 2-(Cyclohexylamino)ethanesulfonic acid (CHES), 4-(2-hydroxyethyl)piperazine-1-ethane sulfonic acid (HEPES), and lanthanum chloride heptahydrate ($LaCl_3$) were supplied by Sigma–Aldrich (Steinheim, Germany). cDNAs of human CD39 (NM_001776), and mouse CD39 (NM_009848) were purchased from Origene Technologies, USA. Codon-optimized cDNA of *P. falciparum* NTPDases was synthesised by Biocat GmbH, Heidelberg, Germany. Restriction enzymes, T4 DNA ligase, and Q5 HF-DNA polymerase were purchased from New England BioLab GmbH. Corning® flat-bottom 96-well half-area microplates, black polystyrene, were purchased from Sigma–Aldrich (Steinheim, Germany). Cellfectin™ II Reagent (Thermo Fisher Scientific, MA, USA) and baculovirus genomic ProEasy™ vector DNA (Cat. #A10S, AB vector, CA, USA) were used. Insect-XPRESS™ media (#: BE12-730Q, Lonza, Switzerland) and HisPur™ Ni^{2+}-NTA spin columns (#: 88226, Thermo Fisher Scientific, MA, USA) were used as protein expression and purification tools. EDTA-free Protease inhibitor cocktail tablets (Roach Diagnostic GmbH, Germany) were employed. Amicon® Ultra-15 concentrator with 10 kDa cut-off was purchased from Merck Millipore, MA, USA.

g. Instrumentation

Fluorescence units were measured using a FlexStation® 3 Multi-Mode Microplate Reader (Medical Devices LLC. USA) using *Softmax Pro* 3.0 software for data collection. Nucleotides were precipitated in a 96-well plate using a SpeedVac plate centrifuge (LaboGene ApS, Denmark). Natural substrates were tested using p/ACE™ MDQ plus capillary electrophoresis system (AB Sciex LLC, Framingham, USA). Data collection and peak area analysis were conducted by the P/ACE MDQ software 32 KARAT obtained from Beckman Coulter (Fullerton, CA, USA). Mithras LB 940 (Berthold Technology, France) was utilised to measure absorbance in the range of 400 nm.

2.1 Protein expression and purification

Proteins were recombinantly expressed as a soluble and membrane-bound variant in *Spodoptera frugiperda* (*sf9)* insect cells using ProEasy™ linearised baculovirus genomic DNA. Details of cloning tools used for both types of proteins are given in Table 3.7. Soluble and membrane-bound enzymes were expressed, as previously reported for NPP3, -5, and CD38 (Chapter 3 and 5). The transmembrane domain (TM) was cut off for soluble enzymes, and the gene of interest (GOI) was subcloned in the *p*-ACGP67-B expression vector between restriction sites. 10% Cellfectin™, 1 µg of plasmid DNA containing GOI, and 2.5 µL of ProEasy™ DNA in 100 µL of culture media were incubated for 20 min at room temperature. The resulting DNA-collection emulsion was used to infect semi-confluent *sf9* adherent cells for 96 h at 27 ^{o}C to amplify virus titer and protein expression. Medium-containing soluble enzymes were concentrated up to approximately 70 – 80% with Amicon® Ultra 15 mL centrifugal filter with variable cut-off limits (10 – 50 kDa, 4500 x G, 30 min). Subsequently, His-tagged protein was purified by HisPur™ Ni^{2+}-NTA spin columns by increasing the imidazole concentration from 10 mM to 250 mM (*Manufacturer's specification)*. To eliminate imidazole, the eluted enzyme was filtered and concentrated for buffer exchange (in mM, 1 $MgCl_2$, 2 $CaCl_2$, 10 HEPES, and pH 7.4). Protein concentration was determined by the Lowry method based on the oxidation of aromatic amino acids (tryptophan and tyrosine) with the folin-ciocalteu reagent (Randall and Lewis 1951).

An in-house optimised protocol was used for the membrane-bound enzyme. A full-length sequence of enzymes is sub-cloned into a modified *pfastbac1* expression vector [modifications; *(BamHI-HA-Tag (MKTIIALSYIFCLVFA)-FLAG tag (DYKDDDDA)-AscI-GOI-10- fold HIS-Tag-Hind-III)*. The engineered plasmid was amplified in DH5α cells, and subsequently 500 ng purified *pFastBac1*-plasmid (2-3 µl) were transformed into DH10αBac and applied to an agar plate containing 10 µg/mL Tetracycline, 7 µg/mL Gentamicin, 50 µg/mL Kanamycin, 40 µg/mL IPTG, 100 µg/mL X-Gal. Plates were incubated for 48 hours at 37 °C. The white colony containing recombinant bacmid was amplified in 5 ml fresh medium containing 10 µg/mL tetracycline, 7 µg/mL gentamicin, and 50 µg/mL kanamycin at 250 rpm with overnight incubation at 37 °C (~ 18 hours). Bacmid was purified by QIAprep Spin Miniprep Kit using the manufacturer's specifications and transfected in *Sf9* insect cells (2 x 10^6 cells ml^{-1} in 2.5 ml cell suspension) with 3 µL X-

tremeGENE HP emulsion in 100 µl volume. Protein was allowed to express for 48 hours after one-time virus amplification. The pellets were collected by centrifuging medium for 10 min at 4500 x g, washed and re-suspended in buffer containing 10 mM HEPES, 10 mM $MgCl_2$, 20 mM KCl, and 30% (v/v) glycerol pH 7.5, homogenised in 25 ml low osmotic buffer (10 mM HEPES pH 7.5, 10 mM $MgCl_2$, 20 mM KCl) + protease inhibitor and centrifuged for 30 min at 48000 x g. The second wash used a high osmotic buffer (10 mM HEPES pH 7.5, 10 mM MgCl2, 20 mM KCl, 1 M NaCl). Finally, after centrifugation, the pellets were resuspended in buffer containing 10 mM HEPES, pH 7.4, 2 mM $CaCl_2$ 1 mM $MgCl_2$, 10% (v/v) glycerol. Subsequently, the proteins were recovered from the membranes by treating samples with mild solubilisation buffer containing 50 mM HEPES, pH 7.4, 800 mM NaCl, 1% DDM, and 0.2% CHS for 3 hours at 4 ^{o}C. The samples were centrifuged at 48,000 x g for 30 min to separate membranes from proteins. The membrane proteins, which now appeared as soluble fractions, were purified using affinity chromatography. For purification, TALON IMAC Co-resin beads (Clontech) were added to the supernatant and incubated overnight at 4 ^{o}C. The proteins were then recovered from beads by washing them with increasing imidazole concentrations.

Table 6.7: Cloning tools for the expression of soluble and membrane-bound enzymes

Enzymes	Amino acids	Exp. Vector	Restriction sites	Primers
Soluble				
Human	38-478	*p*ACGP67B	BamHI/XbaI	*f'*-5'-*GATC* GGATCC CCACC**ATG**G ACCCAGAACAAAGC ATTGCCA-3' *r'*-5'-*GATC* TCTAGA **TTA** ATGGTGGTGGTGATGATG GACATAGGTGGAGTGGGAGA-3'
Membrane-bound				
Human	1-510	*pfastbac mod.*	AscI/HindIII	*f'*-5'- GGTAC-G-GGCGCGCCATGGAAGATACAAAGGAGT CTAACGTG-3' *r'-5'*- TACC-AAGCTT-**TTA**GTGGTGGTGGTGATGATGGT GATGATGGTGTACCATATCTTTCCAGAAATATGAAGGC-3'
Mouse	1-510	*pfastbac mod.*	AscI/HindIII	*f'*-5'- GGTAC-G-GGCGCGCC ATGGAAGATATAAAGGAT TCTAAGGTG -3' *r'-5'*- *TTAC*-AAGCTT-**TTA**GTGGTGGTGGTGATGATGGT GATGATGGTGTACTGCCTCTTTCCAGAAATATGAAGG -3'
P. falciparum	1-2622			*f'*-5'- *GATC*-GGCGCGCCATGGAGAACCTGATCGGCAC -3'

	r'-5'- *GATC*-AAGCTT-**TTA-**GTGGTGGTGGTGGTGATG GTGGTGGTGCAGGAACCTGTACTTCTTGTTC-3'

Irrelevant base pairs are shown in *italics, the* underlined sequence represents restriction sites, and bold letters are the stop codon.

2.2 Cell culture and membrane preparation

The different cancer cell lines were cultured in Dulbecco's modified Eagle's medium (DMEM; GibcoBRL, Gaithersburg, MD., USA) supplemented with 10% fetal bovine serum (FBS; GibcoBRL), 1% Pen-strep at 37 °C in humidified 95% air and 10% CO_2. For U87 cell lines, 1% glutamine was added to the culture medium and incubated with 5% CO_2. Cells were split to 0.3 million cells/ml every 4th day. Human TNBCs and astrocytoma cell lines were harvested by adding trypsin to the adherent cells and incubated for 5 min, subsequently rinsed with 1 x PBS to collect whole cells. U87 cell lines were detached by gently stroking the flask. Whole cells were collected by centrifugation at 1000 x g for 5 min. The pellets were then transferred to a 15 ml Dounce vial. Cell membranes were disrupted with 25 ml of low osmotic buffer (10 mM HEPES, 10 mM $MgCl_2$, 20 mM KCl pH 7.5) with a protease inhibitor cocktail. Cell pellets were homogenised with repeated plunging on ice followed by centrifugation (48000 g and 30 min). The pellets were further homogenised with 25 mL of high osmotic buffer (10 mM HEPES, pH 7.5, 10 mM $MgCl_2$, 20 mM KCl, 500 mM NaCl) in a Dounce vial and subsequent centrifugation (48,000 x g, 30 min). Pellets were then resuspended in 3 mL resuspension buffer (10 mM HEPES, pH 7.5, 10 mM $MgCl_2$, 20 mM KCl, 30% glycerol) and homogenised on ice, flash-frozen in liquid nitrogen and stored at -80 °C.

2.3 Coomassie blue protein gel

10% bis-Tris SDS-page gel was produced using a standard protocol. The protein solution was dissolved in 4x NuPAGE LDS sample buffer and 200 mM DDT. The samples were incubated for 30 min at RT. MOPS running buffer was prepared in VE water and filled into an electrophoresis chamber. 4 µL of pre-stained protein ladder and 30 µL of protein sample were loaded. Electrophoresis was initially started at 50 V until the samples reached resolving gel and later proceeded with 120 V. The gel was then treated with Coomassie-blue dye and washed with destaining methanol, acetic acid, and water solution. Gel pictures were collected using a trans-blot.

2.4 CE assay using a diode array (DAD) detector

Capillary electrophoresis assay (CE) was used to analyse the ATPase activity of the NTPDases. Moreover, CE assay was also used for selectivity testing versus different ectonucleotidases like NPP1, -3, -4, -5, and -CD38 by using NAD^+ as a substrate. CE running conditions include 50 mM phosphate buffer, pH 6.5, separation voltage of -15 kV and 30 cm capillary length, as previously reported (Lee et al. 2017). Briefly, CD39, either soluble or membrane-bound, was treated with 150 µM ATP at 37 ºC for 30 min in the presence of reaction buffer; 10 mM HEPES, 2 mM $CaCl_2$, 1 mM $MgCl_2$, pH 7.4. Reactions were terminated by boiling the samples for 10 min at 95 ^oC. After briefly cooling the plate on ice, samples were loaded into CE for evaluation. Reaction samples were electro-kinetically loaded (-6 kV, 30 s) into a *Polyacrylamide*-coated capillary [30 cm (20 cm effective length) × 50 µm (id), × 360 µm (od)] and allowed to migrate based on their ionic mobility by application of an electric field (-15 kV, 0.1 psi pressure). Analysis was carried out using the P/ACE MDQ CE system (Beckman Instruments, Fullerton, CA, USA) equipped with either DAD (λabs 254 nm). The 32-Karat®5.0 (Beckman Instruments, Fullerton, CA, USA) software was used for data collection. GraphPad Prism 7.0 was used to analyse the data.

a. Determination of IC_{50} and K_i values

Full-scale inhibition analysis was performed using 12-15 different inhibitor concentrations (0.0005 – 300 µM) to determine the IC_{50} and K_i values calculated by the Cheng-Prusoff equation. (Cheng and Prusoff 1973). The IC_{50} values were determined by nonlinear concentration-inhibition curve fitting using the GraphPad Prism 7.0 software (GraphPad Software, San Diego, CA, USA).

For competitive inhibitors, the following equation was employed:

$$K_i = \frac{IC_{50}}{1+\frac{[S]}{K_m}}$$

2.5 Selectivity testing of potent inhibitors versus other ectonucleotidases

The selectivity tests were performed at different ectonucleotidases expressed in-house using a baculovirus expression system. To be consistent with the reaction conditions for all NPPs, the selectivity test was performed using a similar reaction buffer for NPP1, -3. -

4, and -5 (10 mM HEPES, pH 7.4, 0.5 mM $CaCl_2$, and 0.01 mM $ZnCl_2$) and for CD38 (10 mM HEPES pH 7.4). For CD73, HEPES 10 mM (pH 7.4), 2 mM $CaCl_2$, and 1 mM $MgCl_2$ buffer were used. CE assays were performed with the natural substrate NAD^+ (100 µM) with the following enzymes (per well): crude enzyme, 900 ng of NPP1, 985 ng of NPP3, semi-purified enzymes 120 ng of NPP4, 280 ng of NPP5, and 4 ng of CD38. The reaction time was 45 min except for the CD38 reaction, which was carried out for 15 minutes. CD73 reactions were carried out by incubating 150 ng of the soluble enzyme with 10 µM ε-AMP (reaction details can be found in Chapter 2 of this dissertation). Three independent tests were performed with duplicate observations.

2.6 Small-molecule inhibitors of CD39 used in the current studies

During this study, various scaffolds were analysed for their inhibitory effect on CD39, including non-nucleotidic compounds, namely ticlopidine, ceritinib, and thienotetrahydropyrimidine derivatives. Moreover, extensive work has been performed on nucleotide derivatives based on the AMP scaffold. The compounds were initially screened at 50 µM concentration, followed by full-scale IC_{50} curve determination of the potent inhibitors. The most promising compounds, BCY-110, 247, and 231, were further analysed for species differences in human and mouse enzymes in a parallel reaction setting. The structures of the investigated molecules are given in Table 6.8.

3 RESULTS AND DISCUSSION

3.1 Recombinant expression of NTPDases

CD39 was expressed in *sf9* insect cells either as soluble human enzymes [truncation of the transmembrane domain (amino acids AA 38-478) in *p*ACGP67-B] or as membrane-bound full-length sequence (human, mouse, and *p. falciparum*) using a modified *pfastbac* expression plasmid (Fig 6.6). The modifications were made by introducing the N-terminal HA tag for efficient protein trafficking to the membrane. A FLAG tag for expression control followed the HA-tag sequence. A 10-fold His-tag sequence was used at the C-terminus for affinity purification. It was observed that the HA-tag, besides its role in affinity purification, helps better translocate recombinant proteins into the membrane. The soluble enzyme was successfully expressed and reached a reasonable purity. A western blot analysis using anti-His-tag antibodies and functional analysis with ATP as a substrate further supplemented the characterisation. The soluble enzyme was purified with a Ni-NTA column and eluted with an increasing concentration of imidazole 10 to 250 mM. Moreover, membrane-bound enzymes were solubilised from the membranes using mild detergents, dodecyl maltosides (DDM), and cholesteryl hemisuccinate (CHS), in buffer (50 mM HEPES, 800 mM NaCl, 1% DDM, 0.2% CHS). The proteins appeared as a stable band on Coomassie blue gel and showed ATPase activity in the functional assay using CE.

a. Soluble and membrane-bound CD39 expression

Human soluble CD39 containing a 6-fold His-tag was successfully expressed in the insect cell expression system using a *p*ACGP67-B expression vector. The crude enzyme retained high enzymatic activity after protein purification using affinity chromatography. Expression was confirmed using anti-His-tag antibodies and is presented in Figure 6.7. Coomassie blue staining showed adequate protein purity that was sufficient to conduct inhibition testing. The membrane-bound variant containing the full-length sequence was also well expressed using the *pfastbac* expression system. The FACS data showed an intracellular HA tag, which means the proteins are well placed in the membrane. Moreover, the whole cells containing the human and mouse CD39 showed high NTPDase activity, which further reflects the presence of an extracellular catalytic domain. The

inhibitor BCY-110 significantly reduced the enzymatic activity at 50 µM concentration (Figure 6.11).

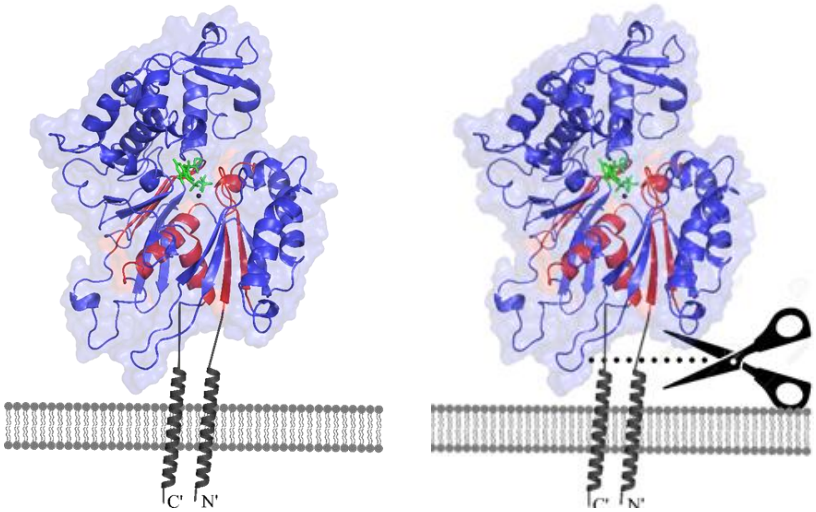

Figure 6.5: Schematic presentation of a membrane-bound and soluble variant of NTPDase1. The transmembrane domains are cut-off for soluble enzyme expression.

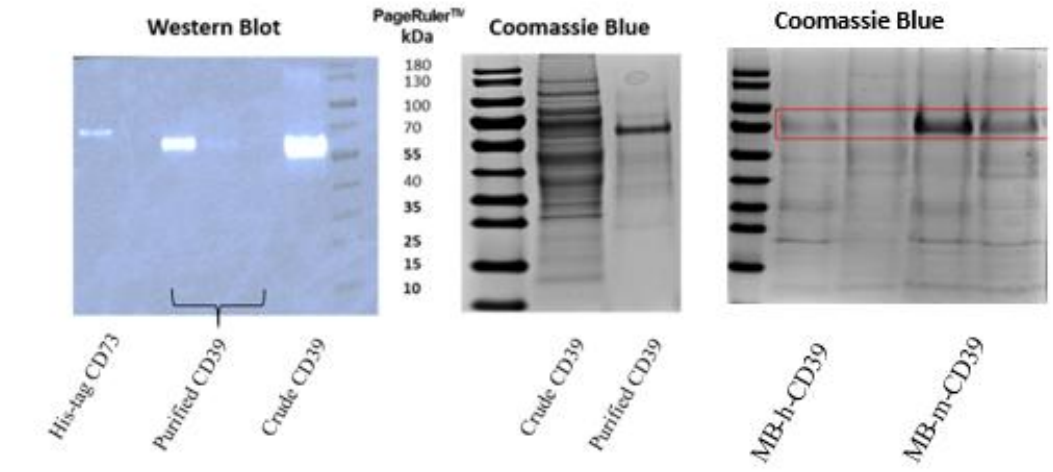

*

Figure 6.6: Purification of His-tag protein with Ni-NTA affinity chromatography. The western-blot sample used 70 kDa His-tag protein as positive control (CD73). The Coomassie gel showed the purity achieved for soluble human CD39 and membrane-bound human and mouse CD39.

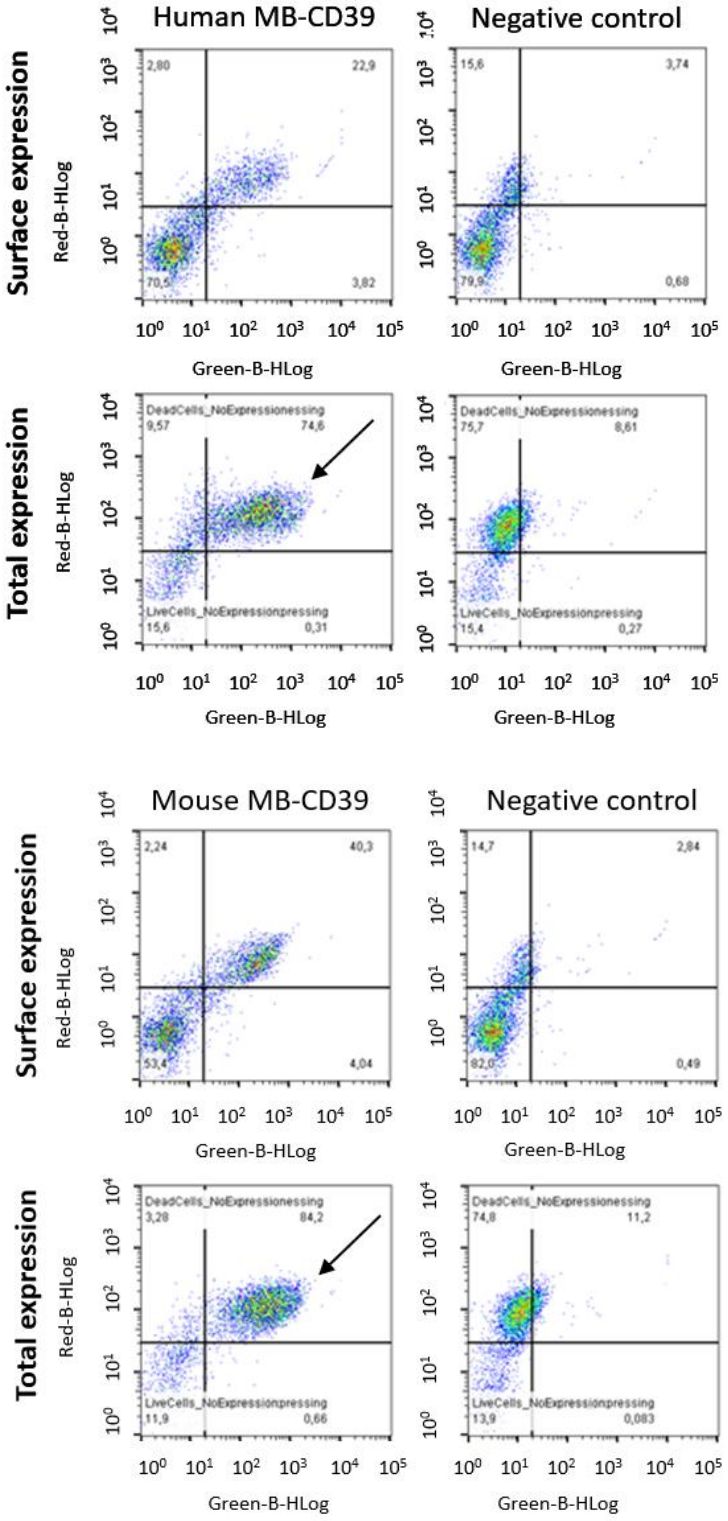

Figure 6.7: FACS data representing membrane-bound human and mouse CD39 expression. Negative controls are soluble CD39 that doesn't have a FLAG tag. Data indicates that the N-terminus is expressed intracellularly as the dead cells incubated with Triton to make the cell membranes permeable for antibodies, showing most of the fluorescence signals.

The *P. falciparum* NTPDase was also successfully expressed; however, deficient ATPase activity was observed compared to the other enzymes (human and mouse CD39). The anti-FLAG-FITC antibody treatment shows an intracellular N-terminus with a clear rightward shift in the sample expressing *P. falciparum* NTPDase. However, despite healthy expression, the enzyme did not show strong hydrolysis of ATP, although at least 2-fold higher ATPase activity was observed compared to control samples treated with BCY-110 at 50 µM. The cDNA sequence we used for expressing *P. falciparum* NTPDase was a codon-optimized sequence for expression in mammalian cells expression and was synthetically generated, as the original sequence is way too adenine-rich. The possible explanation for the low activity in the P. falciparum sample is that the mosquitoes used a different folding mechanism than humans, usually triggered by *pfHSP70.* Since this folding machinery is not present in the mammalian system, improper folding could be the reason for protein inactivity. To address this problem, we planned to co-express *P. falciparum* NTPDase with *pfHSP70* by using a modified *pfastbac* dual plasmid with different promotor sequences for both proteins. Therefore, it will be interesting to see how the protein behaves when co-expressed with plasmodium heat shock proteins. For this purpose, *pfHSP-70* cDNA has already been acquired through collaboration.

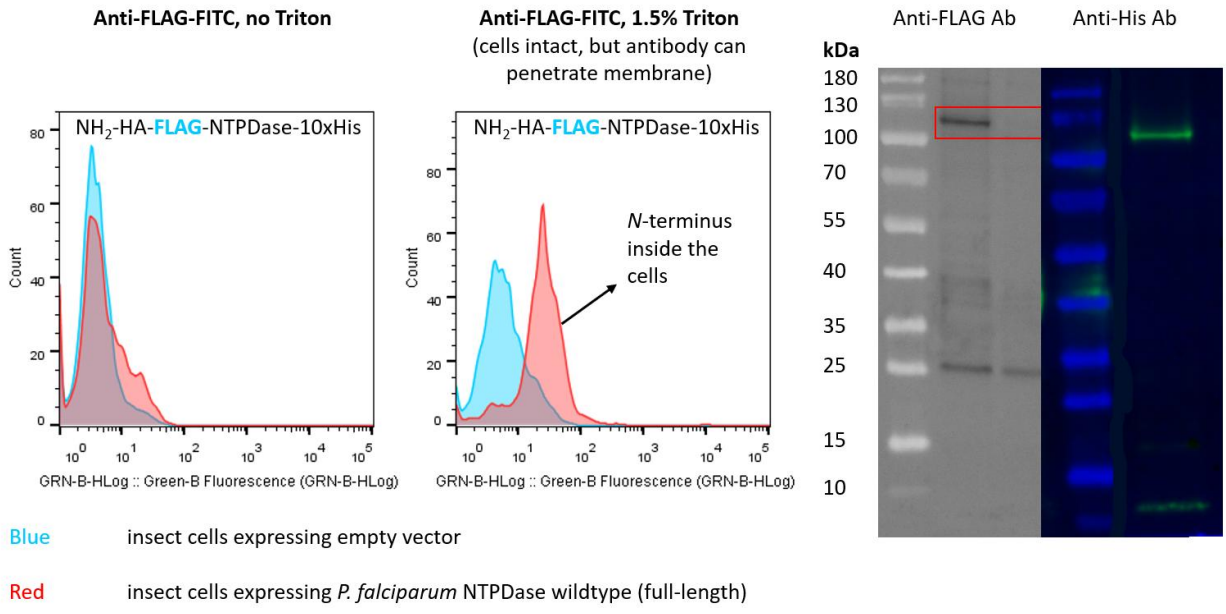

Figure 6.8: Confirmatory tests for the expression of *p. falciparum* NTPDase. The stable protein band in the range of 105 kDa showed the parasitic enzyme.

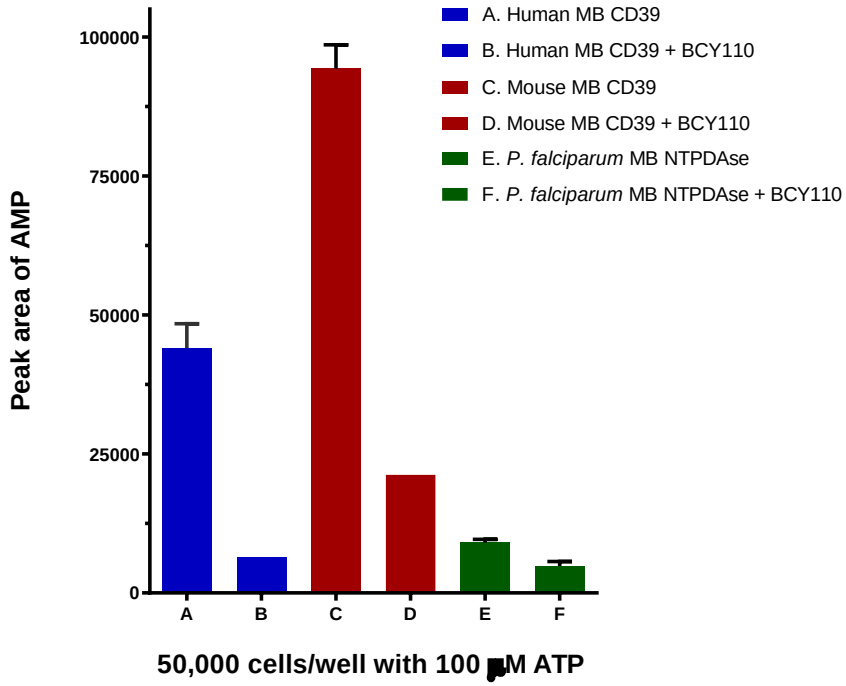

Figure 6.9: ATP hydrolysis by human, mouse, and *P. falciparum* NTPDases. 50 µM of the CD39 inhibitor BCY-110 significantly inhibited ATP hydrolysis.

3.2 Michaelis-Menten constant for soluble CD39

Eight different concentrations of ATP (5 – 1000 µM) were treated with 60 ng of semi-purified enzyme for 30 min at 37 ^{o}C, followed by boiling samples at 95 ^{o}C for 10 min. Reaction buffer and CE operation conditions were reported in the material and method section. The K_m value was determined to be 67.9 ± 4.2 µM and the Vmax value was 3.28 ± 0.5 µmol/min/mg protein. The reaction showed a product turnover of 2.94 s^{-1} and a ratio of k_{cat}/K_m of 43331 M^{-1}. s^{-1}. The determined K_m value is within a similar range as previously reported (17 ± 1 µM) for membrane-bound CD39 expressed in COS7 cells (Kukulski et al., 2005). The membrane-bound variants were also subjected to K_m value determination. The mb-human CD39 showed a K_m of 93.9 µM for ATP, while the mouse mb-CD39 has a value of 100 µM towards ATP. As previously discussed, the turnover number can't be compared since the protein was not super pure; however, all the testing was performed using the same batch of protein with the same protein concentration, which means that data helps compare the affinity amongst the substrate ATP/ADP. The spectrum of substrate preference can further be extended towards UTP, GTP, CTP and a few other

substrates; however, this can be done by future students if they are interested in knowing why the mb-bound CD39 expressed in insect cells showed higher K_m for ATP as compared to the one expressed in mammalian expression system.

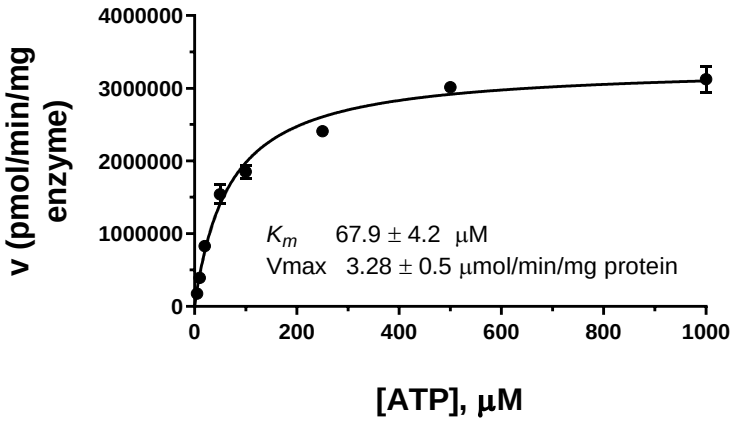

Figure 6.10: Determination of K_m value for soluble, purified human CD39. Three independent tests were performed in triplicate observations. Data are shown as mean ± SEM.

3.3 Concentration-dependent inhibition of human soluble CD39

Selected nucleotide and non-nucleotidic derivatives were tested under previously described assay conditions vs 150 µM ATP as a substrate. 10 mM stock solutions of inhibitors were diluted with 10% DMSO to obtain 12 – 15 concentrations. The kinetic tests performed by Laura Schäkel demonstrate that the inhibitors competitively inhibit CD39 activity. Table 6.9 comprises the comparison of K_i values calculated from IC_{50} values, thereby using the Cheng-Prusoff equation (Cheng and Prusoff 1973). Tests were performed as 2 – 3 independent observations in triplicate. Data are presented as means ± SEM. Our data showed that AMP derivatives BCY-110, -247, and -231 are the most potent inhibitors of human CD39, showing K_i values in the nanomolar range. These compounds are readily soluble in aqueous solutions and 10% DMSO. Notably, the compound BCY-110 showed an IC_{50} of 0.058 µM towards soluble CD39 and 0.440 µM towards mb-variant expressed in COS-7 cells. This difference is approximately 7-fold. However, since soluble enzymes are expressed in insect cells, we can't directly compare the outcomes of proteins belonging to different expression systems.

Table 6.8: Characterisation of newly developed CD39 inhibitors

Code	CD39 K_i ± SEM *[µM]*	Soluble human CD39 K_i ± SEM *[µM]*
Bcy-231	**0.768** ± 0.052 [a]	**0.232 ±** 0.011
Bcy-247	**0.735** ± 0.056 [a]	**0.469 ±** 0.031
8-BuS-AMP (CS207-1)	**1.10** ± 0.62 [a] **0.847** ± 0.194 [a]	**0.733 ±** 0.386
CS-052	**0.660** ± 0.072 [a] **4.89** ± 1.23 [a]	**2.29 ±** 0.36
CS-094 (BCY308)	**1.40** ± 0.12 [a] **7.08** ± 0.68 [a]	**5.93 ±** 3.31
Bcy-110	**0.440 ± 0.060** [a]	**0.058 ± 0.030**
Bcy-108	**1.54** ± 0.36 [a]	**8.60 ±** 1.19
CS-347-2	**4.56** ± 0.30 [a] **1.20** ± 0.09 [a]	**0.851 ±** 0.291
CS-209-1	**1.83** ± 0.33 [a]	**0.576 ±** 0.106
Bcy-131	**2.32** ± 0.54 [a]	**1.95 ±** 0.29
Ceritinib	**10.9** [a]	Not Active
Ticlopidine	**87.7** ± 0.50 [a]	**31.1 ±** 0.9
Gü1306	**115** ± 33 [a]	**45.1 ±** 5.8

[a]Tests were performed by former coworkers Laura Schäkel and Sangyong Lee.

3.3.1 Concentration-dependent inhibition of human and mouse membrane-bound CD39

The most potent AMP derivatives, BCY110, BCY247, and BCY231, were further tested under optimised assay conditions vs 150 µM ATP as a substrate. 10 mM stock solution of inhibitor was diluted with 10% DMSO to obtain 14-15 different concentrations (300-0.0005 µM). Table 6.10 compares the K_i values calculated from IC_{50} values using the Cheng-Prusoff equation. The results demonstrated that the compounds generally showed similar inhibition of human and mouse membrane-bound enzymes. However, a difference of 3 – 4-fold is observed in soluble and membrane-bound variants. One possible explanation for this enhanced potency could be the flexibility of the active site interactions offered by the soluble enzyme compared to the membrane-bound enzyme. This hypothesis needs

further clarification, for example, through X-ray crystallographic studies. Our colleagues are extending this work for crystallographic evidence of human CD39. The research outcome will help design small molecule inhibitors based on active site interactions that could achieve the required potency and selectivity.

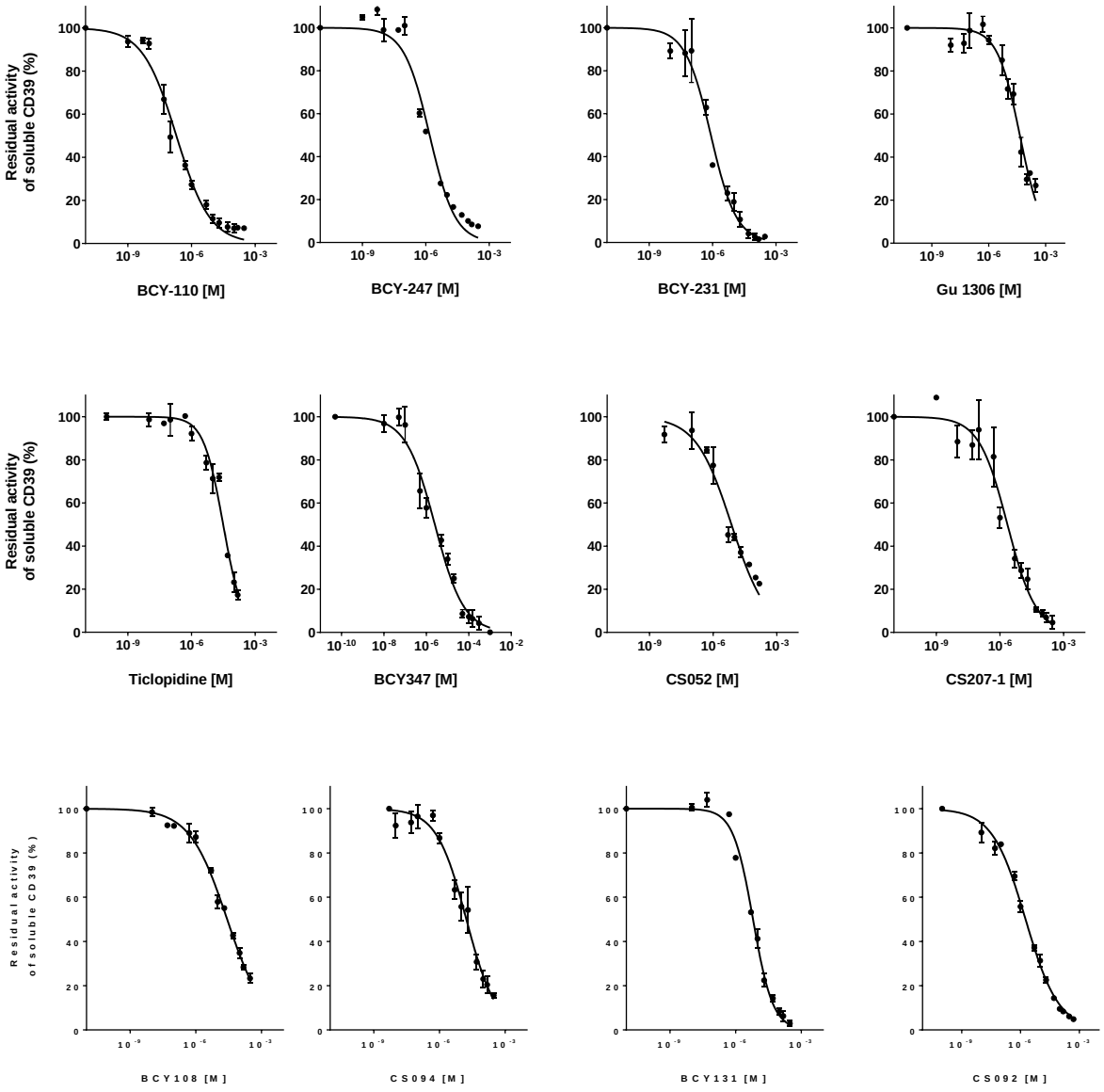

Figure 6.11: Concentration-dependent inhibition of human soluble CD39 by nucleotidic and non-nucleotidic inhibitors. Data is collected as 2 – 3 independent tests with triplicate observations and presented as mean ± SEM.

Table 6.10: Characterisation of CD39 inhibitors on soluble and membrane-bound human and mouse CD39.

Code	Mb-h-CD39 (COS-7) K_i ± SEM *[µM]*	Mb-hCD39 (Insect cell) K_i ± SEM *[µM]* [a]	Sol. h-CD39 K_i ± SEM *[µM]*	Mb-mCD39 (Insect cell) K_i ± SEM *[µM]* [b]
Bcy-110	**0.440** ± 0.060 [c]	**0.315 ±** 0.016	**0.058 ±** 0.030	**1.18 ±** 0.12
Bcy-231	**0.768** ± 0.052 [c]	**1.03 ± 0.13**	**0.232 ±** 0.011	**0.42 ± 0.16**
Bcy-247	**0.735** ± 0.056 [c]	**1.29 ± 0.27**	**0.469 ±** 0.031	**1.32 ± 0.13**

[a] K_m values at human mb-CD39 for ATP is 93.9 µM. [b] K_m value for mouse mb-CD39 is 100 µM [c] Test against human mb-CD39 expressed in COS-7 cells was performed by Laura Schäkel.

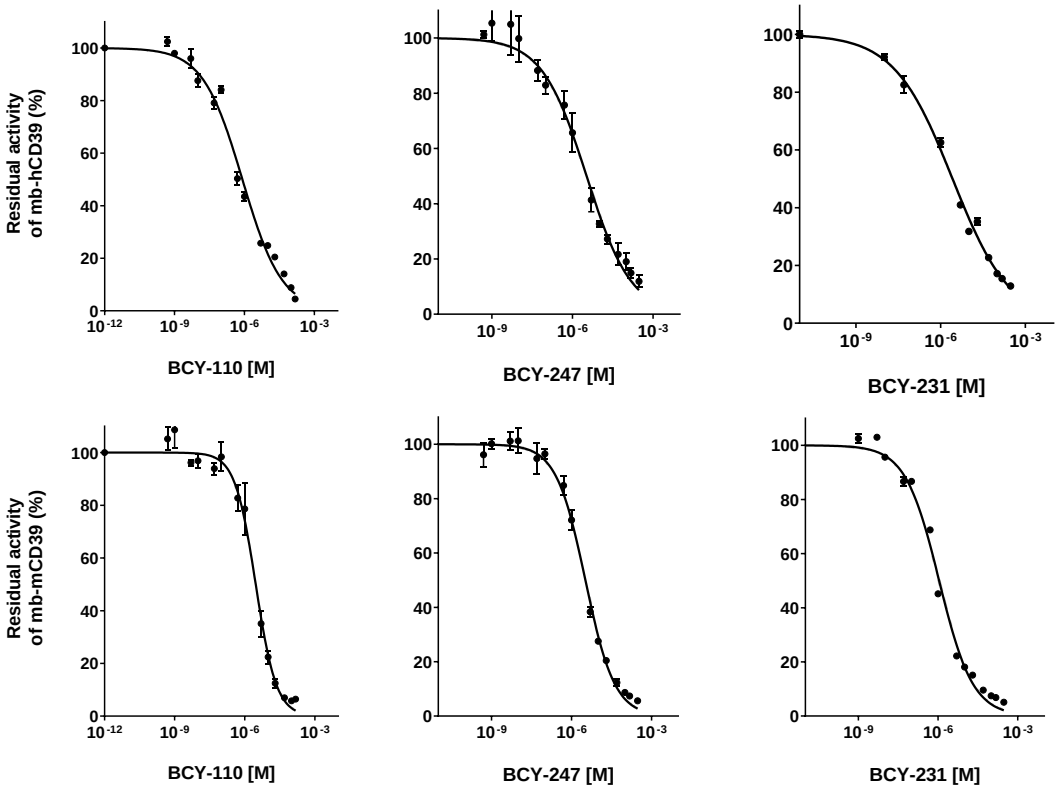

Figure 6.13: IC_{50} curves for the most potent inhibitors from the current series against membrane-bound human and mouse CD39. Two to three independent tests were performed in triplicate.

3.4 Selectivity testing towards multiple ectonucleotidases

Selectivity testing was performed towards other ectonucleotidases such as NPP1, -3, -4, -5, and CD38 under neutral pH conditions. The material and method section describe the reaction procedure, buffer composition, enzyme concentration, and incubation time. The

compounds in the current series were highly selective for CD39, and their presence mostly unaffected other ectonucleotidases. A notable effect was observed for BCY110 towards NPP3, where approximately 50% inhibition was observed at 50 µM. Moreover, the compound 247 showed nearly 60% inhibition of NPP4 at the same concentration. Apart from this, most of the potent CD39 inhibitors selectively target CD39. It is also observed that the same AMP derivatives, when tested under alkaline reaction conditions (pH 9.2) and without Zn^{2+} ions, did not show similar inhibition towards NPP3. This exciting observation needs further exploration.

Table 6.11: Selectivity testing of CD39 inhibitors at ectonucleotidases.

***K_i* ± SEM [µM]** *(inhibition % at 50 µM)* [a]								
Compd.	**NTPDase2**	**NTPDase3**	**NTPDase8**	**CD38**	**NPP1**	**NPP3**	**NPP4**	**NPP5**
Bcy-231	**82.9** ± 17.7	**54.8** ± 9.2	(0)	*(-2 ± 7)*	*(-2 ± 2)*	*(36 ± 6)*	*(14 ± 8)*	*(-5 ± 18)*
Bcy-247	**24.3** ±5.9	**4.74** ±0.45	(8)	*(2 ± 3)*	*(8 ± 3)*	*(33 ± 8)*	*(60 ± 4)*	*(13 ± 12)*
Bcy-112	(15)	(22)	(11)	*(4 ± 8)*	*(24 ± 7)*	*(46 ± 2)*	*(36 ± 3)*	*(42 ± 4)*
Bcy-347-2	n.d.	n.d.	n.d.	*(20 ± 12)*	*(3 ± 21)*	*(40 ± 6)*	*(41 ± 4)*	*(22 ± 5)*
Bcy-308 CS-094	**1.97** ±0.06	(35)	(-11)	(3 ± 13)	(9 ± 10)	(21 ± 4)	(18 ± 3)	(11 ± 13)
Bcy-110	**2.64** ± 0.28	**29.1** ± 2.30	(38)	(1 ± 7)	(22 ± 4)	(50 ± 3)	(20 ± 13)	(20 ± 12)
CS-210-1	n.d.	n.d.	n.d.	(2 ± 7)	(2 ± 3)	(5 ± 6)	(0 ± 21)	(15 ± 21)
CS-209-1	n.d.	n.d.	n.d.	(10 ± 4)	(11 ± 17)	(34 ± 8)	(4 ± 4)	(15 ± 8)

[a]Capillary electrophoresis assay was employed for inhibition testing using NAD^+ 100 µM for NPPs (1, -3, -4, and -5) or CD38. Initial inhibitor screening was performed at 50 µM. *compound peak appears at the same migration time as product peak (ADPR). The background was subtracted from the reaction values to determine the inhibitory impact on CD38 reactions. All testing towards NPPs was performed using reaction buffer with physiological pH conditions: HEPES 10 mM (pH 7.4), $CaCl_2$ 0.5 mM, $ZnCl_2$ 0.01 mM. Testing against NTPDase 2, -3, and -8 was carried out by Laura Schäkel. A total of three independent tests were performed in duplicate. Data are presented as mean ± SEM.

4.0 Conclusions

We recombinantly expressed different CD39 enzymes from human, mouse and *Plasmodium falciparum* origin using an insect cell expression system. Soluble and membrane-bound enzymes were expressed, purified and analysed for their nucleotide (ATP and ADP) hydrolysing abilities—human and mouse enzymes, both as soluble and

membrane-bound enzymes, efficiently hydrolysed ATP and ADP. However, low ATP hydrolysis was observed for the parasitic enzymes. The *P. falciparum* NTPDase project needs further optimisation in expression and enzyme reaction conditions. One such optimisation could be the co-expression of the enzyme with *pfHSP70.*

We further tested different small molecule inhibitors of human CD39 belonging to both nucleotidic and non-nucleotidic scaffolds. Based on the lead structure 8-BuS-AMP, different derivatives were synthesised by Chunyang Bi. For SAR analysis, positions 2-, 6-, and 8- of the adenine core were mainly explored. The inhibitory potency was successfully increased, and compounds BCY-110, -231, -247, and CS-209-1 were identified as the most potent CD39 inhibitors. The combination of 8-butylthio and N^6-4-phenylbutyl on the AMP scaffold (Bcy-110) increased the inhibitory potency by approximately 10-fold as compared to 8-BuS-AMP (against soluble enzyme) and by 2-fold at the membrane-bound enzyme (mammalian and insect cells expression system). More combinations of beneficial 8- and N^6-substituents on AMP should be investigated. From the selectivity studies, Bcy-231, -247, -148, -308, -110, -237, -88, -71, -221, -108, CS-209-1, and 347-2 were identified as novel dual CD39/CD73 inhibitors. Furthermore, CS-052/Bcy-148 was the first selective CD39 inhibitor described so far, and it is recommended as a pharmacological tool compound for CD39 *in vitro* study. Bcy-110 (and Bcy-247) are the most potent CD39 inhibitors and the best candidate for further drug development. It is also metabolically stable due to protective 8-substituent as 8-BuS-AMP. The potent CD39 inhibitors probably have the potential for the immunotherapy of cancer.

References

Abbas, Sadia, Saira Afzal, Humaira Nadeem, Dilawar Hussain, Peter Langer, Jean Sévigny, Zaman Ashraf, and Jamshed Iqbal. 2022. “Synthesis, Characterization and Biological Evaluation of Thiadiazole Amide Derivatives as Nucleoside Triphosphate Diphosphohydrolases (NTPDases) Inhibitors.” *Bioorg. Chem.* 118 (January):1–11. https://doi.org/10.1016/j.bioorg.2021.105456.

Afzal, Saira, Mariya al-Rashida, Abdul Hameed, Julie Pelletier, Jean Sévigny, and Jamshed Iqbal. 2020. “Functionalized Oxoindolin Hydrazine Carbothioamide Derivatives as Highly Potent Inhibitors of Nucleoside Triphosphate Diphosphohydrolases.” *Front. Pharmacol.* 11 (November):1–18. https://doi.org/10.3389/fphar.2020.585876.

Allard, David, Bertrand Allard, and John Stagg. 2020. “On the Mechanism of Anti-CD39 Immune Checkpoint Therapy.” *J Immunother Cancer* 8 (February):1–11. https://doi.org/10.1136/jitc-2019-000186.

Antonioli, Luca, P??l Pacher, E. Sylvester Vizi, and Gy??rgy Hask?? 2013. “CD39 and CD73 in Immunity and Inflammation.” *Trends in Molecular Medicine* 19 (6): 355–67. https://doi.org/10.1016/j.molmed.2013.03.005.

Baldissera, Matheus D., Carine F. Souza, Pedro H. Doleski, Thirssa H. Grando, Michele R. Sagrillo, Aleksandro S. da Silva, Daniela B.R. Leal, and Silvia G. Monteiro. 2017. “Treatment with Tucumã Oil (Astrocaryum Vulgare) for Diabetic Mice Prevents Changes in Seric Enzymes of the Purinergic System: Improvement of Immune System.” *Biomed. Pharmacother.* 94 (October):374–79. https://doi.org/10.1016/j.biopha.2017.07.113.

Baldissera, Matheus D., Carine F. Souza, Thirssa H. Grando, Michele R. Sagrillo, Gerson F. De Brum, Kátia Nascimento, Diulle S. Peres, et al. 2016. “Memory Deficit, Toxic Effects and Activity of Na+, K+-ATPase and NTPDase in Brain of Wistar Rats Submitted to Orally Treatment with Alpha-Terpinene.” *Environ. Toxicol. Pharmacol.* 46 (September):1–8. https://doi.org/10.1016/j.etap.2016.06.024.

Baqi, Younis, Stefanie Weyler, Jamshed Iqbal, Herbert Zimmermann, and Christa E. Müller. 2009. “Structure-Activity Relationships of Anthraquinone Derivatives Derived from Bromaminic Acid as Inhibitors of Ectonucleoside Triphosphate Diphosphohydrolases (E-NTPDases).” *Purinergic Signalling* 5:91–106. https://doi.org/10.1007/s11302-008-9103-5.

Bastid, J, a Cottalorda-Regairaz, G Alberici, N Bonnefoy, J-F Eliaou, and a Bensussan. 2012. “ENTPD1/CD39 Is a Promising Therapeutic Target in Oncology.” *Oncogene* 32 (14): 1743–51. https://doi.org/10.1038/onc.2012.269.

Bastid, Jeremy, Anne Regairaz, Nathalie Bonnefoy, Cécile Déjou, Jérôme Giustiniani, Caroline Laheurte, Stéphanie Cochaud, et al. 2015. “Inhibition of CD39 Enzymatic Function at the Surface of Tumor Cells Alleviates Their Immunosuppressive Activity.” *Cancer Immunology Research* 3 (3): 254–65. https://doi.org/10.1158/2326-6066.CIR-14-0018.

Bastos, M. S., A. Tremblay, J. M. Agripino, I. L.A. Rabelo, L. P. Barreto, J. Pelletier, J. Lecka, et al. 2017. “The Expression of NTPDase1 and -2 of Leishmania Infantum Chagasi in Bacterial and Mammalian Cells: Comparative Expression, Refolding and Nucleotidase Characterization.” *Protein Expression Purif.* 131 (March):60–69. https://doi.org/10.1016/j.pep.2016.11.004.

Baykov, A A, A Evtushenko, and S M AVAEVA A N Belozersky. 1988. “A Malachite Green Procedure for Orthophosphate Determination and Its Use in Alkaline Phosphatase-Based Enzyme Immunoassay.” *Anal. Biochem.* 171:266–70. https://doi.org/10.1016/0003-2697(88)90484-8.

Begum, Zahra, Saif Ullah, Muhammad Akram, Muhammad Uzair, Farman Ullah, Ahsanullah, Julie Pelletier, Jean Sévigny, Jamshed Iqbal, and Abbas Hassan. 2022. “Identification of Thienopyrimidine Glycinates as Selective Inhibitors for H-NTPDases.” *Bioorg. Chem.* 129 (December):1–7. https://doi.org/10.1016/j.bioorg.2022.106196.

Bi, Chunyang, Laura Schäkel, Salahuddin Mirza, Katharina Sylvester, Julie Pelletier, Sang Yong Lee, Thanigaimalai Pillaiyar, Jean Sévigny, and Christa E. Müller. 2023. “Synthesis and Structure–Activity Relationships of Ticlopidine Derivatives and Analogs as Inhibitors of Ectonucleotidase CD39.” *Bioorg. Chem.* 135 (June):1–17. https://doi.org/10.1016/j.bioorg.2023.106460.

Bigonnesse, François, Sébastien A. Lévesque, Filip Kukulski, Joanna Lecka, Simon C. Robson, Maria J.G. Fernandes, and Jean Sévigny. 2004. “Cloning and Characterization of Mouse Nucleoside Triphosphate Diphosphohydrolase-8.” *Biochemistry* 43 (May):5511–19. https://doi.org/10.1021/bi0362222.

Borges-Pereira, Lucas, Kamila Anna Meissner, Carsten Wrenger, and Célia R.S. Garcia. 2017. “Plasmodium Falciparum GFP-E-NTPDase Expression at the Intraerythrocytic Stages and Its Inhibition Blocks the Development of the Human Malaria Parasite.” *Purinergic Signalling* 13 (September):267–77. https://doi.org/10.1007/s11302-017-9557-4.

Braun, Josiane B.S., Jader B. Ruchel, Alessandra G. Manzoni, Fátima H. Abdalla, Emerson A. Casalli, Lívia G. Castilhos, Daniela F. Passos, and Daniela B.R. Leal. 2018. “Pretreatment with Quercetin Prevents Changes in Lymphocytes E-NTPDase/E-ADA Activities and Cytokines Secretion in Hyperlipidemic Rats.” *Mol. Cell. Biochem.* 444 (July):63–75. https://doi.org/10.1007/s11010-017-3231-6.

Brune, Martin, Jackie L Hunter, John E T Corrie, and Martin R Webb’. 1994. “Direct, Real-Time Measurement of Rapid Inorganic Phosphate Release Using a Novel Fluorescent Probe and Its Application to Actomyosin Subfragment 1 ATPase?” *Biochemistry* 33:8262–8827. https://doi.org/https://doi.org/10.1021/bi00193a013.

Cai, Xiao-Yan, Xue-Fei Wang, Jun Li, Jiang-Nan Dong, Jiang-Qi Liu, Neng-Ping Li, Bei Yun, and Rong-Long Xia. 2015a. “Overexpression of CD39 and High Tumoral CD39(+)/CD8(+) Ratio Are Associated with Adverse Prognosis in Resectable Gastric Cancer.” *International Journal of Clinical and Experimental Pathology* 8 (11): 14757–64.

Caljon, Guy, Dorien Mabille, Benoît Stijlemans, Carl De Trez, Massimiliano Mazzone, Fabienne Tacchini-Cottier, Marie Malissen, et al. 2018. “Neutrophils Enhance Early Trypanosoma Brucei Infection Onset.” *Scientific Reports* 8 (December):1–11. https://doi.org/10.1038/s41598-018-29527-y.

Cansev, Mehmet, Fulya Orhan, Esra O. Yaylagul, Esra Isik, Mesut Turkyilmaz, Sami Aydin, Abdullah Gumus, et al. 2015. “Evidence for the Existence of Pyrimidinergic Transmission in Rat Brain.” *Neuropharmacology* 91:77–86. https://doi.org/10.1016/j.neuropharm.2014.12.019.

Cardoso, Andréia Machado, Fátima Husein Abdalla, Margarete Dulce Bagatini, Caroline Curry Martins, Daniela Zanini, Roberta Schmatz, Jeandre Augusto Jaques, Daniela Bitencourt Rosa Leal, Vera Maria Morsch, and Maria Rosa Chitolina Schetinger. 2015. “Swimming Training Prevents Alterations in Ecto-NTPDase and Adenosine Deaminase Activities in Lymphocytes from Nω-Nitro-L-Argininemethyl Ester Hydrochloride Induced Hypertension Rats.” *J. Hypertens.* 33 (April):763–72. https://doi.org/10.1097/HJH.0000000000000468.

Carmo, Guilherme M. do, Pedro H. Doleski, Mariângela F. de Sá, Thirssa H. Grando, Nathieli B. Bottari, Daniela B.R. Leal, Lucas T. Gressler, et al. 2017. “Purinergic Ecto-Enzymes Participate in the Thromboregulation in Acute in Mice Infection by Trypanosoma Cruzi.” *Mol. Cell. Biochem.* 432 (August):1–6. https://doi.org/10.1007/s11010-017-2992-2.

Chen, Shanhao, Shengyu Wu, Liping Zhang, Wei Zhang, Yu Liu, Bin Chen, Sha Zhao, et al. 2020. “CD39: The Potential Target in Small Cell Lung Cancer.” *Transl. Lung Cancer Res.* 9 (4): 1483–95. https://doi.org/10.21037/tlcr-20-798.

Covarrubias, Roman, Elena Chepurko, Adam Reynolds, Zachary M. Huttinger, Ryan Huttinger, Katherine Stanfill, Debra G. Wheeler, et al. 2016. “Role of the CD39/CD73 Purinergic Pathway in Modulating Arterial Thrombosis in Mice.” *Arterioscler., Thromb., Vasc. Biol.* 36 (September):1809–20. https://doi.org/10.1161/ATVBAHA.116.307374.

Deaglio, Silvia, and Simon C. Robson. 2011. “Ectonucleotidases as Regulators of Purinergic Signaling in Thrombosis, Inflammation, and Immunity.” *Adv. Pharmacol.* 61:301–32. https://doi.org/10.1016/B978-0-12-385526-8.00010-2.

DeMarco, Ricardo, Andre T. Kowaltowski, Renato A. Mortara, and Sergio Verjovski-Almeida. 2003. “Molecular Characterization and Immunolocalization of Schistosoma Mansoni ATP-Diphosphohydrolase.” *Biochemical and Biophysical Research Communications* 307 (4): 831–38. https://doi.org/10.1016/S0006-291X(03)01268-3.

Dias, Dhébora Albuquerque, Bruna de Barros Penteado, Lucas Derbocio dos Santos, Pedro Mendes dos Santos, Carla Cardozo Pinto Arruda, Maria Rosa Chitolina Schetinger, Daniela Bitencourt Rosa Leal, and Jeandre Augusto dos Santos Jaques. 2017. “Characterization of Ectonucleoside Triphosphate Diphosphohydrolase (E-NTPDase; EC 3.6.1.5) Activity in Mouse Peritoneal Cavity Cells.” *Cell Biochem. Funct.* 35 (October):358–63. https://doi.org/10.1002/cbf.3281.

Dosch, Michel, Joël Gerber, Fadi Jebbawi and Guido Beldi. 2018. “Mechanisms of ATP Release by Inflammatory Cells.” *Int. J. Mol. Sci* 19:1–16.

Fausther, Michel, Joanna Lecka, Filip Kukulski, Sébastien A Lévesque, Julie Pelletier, Herbert Zimmermann, Jonathan A Dranoff, and Jean Sévigny. 2007. “Cloning, Purification, and Identification of the Liver Canalicular Ecto-ATPase as NTPDase8.” *Am J Physiol Gastrointest Liver Physiol* 292:785–95. https://doi.org/10.1152/ajpgi.00293.2006.-Extra.

Favre, Julie, Charlotte Roy, Anne Laure Guihot, Annick Drouin, Manon Laprise, Marc Antoine Gillis, Simon C. Robson, et al. 2023. “NTPDase1/CD39 Ectonucleotidase Is Necessary for Normal Arterial Diameter Adaptation to Flow.” *Int. J. Mol. Sci.* 24 (October). https://doi.org/10.3390/ijms242015038.

Fiene Amelie, Baqi Younis, Lecka Joanna, Sévigny Jean, and Müller Christa E. 2015. “Amelie-2012-FPIA Assay CD39.” *Analyst* 140:140–48. https://doi.org/10.1039/c4an01694g.

Fiene, Amelie, Younis Baqi, Enas M. Malik, Patrice Newton, Wenjin Li, Sang Yong Lee, Elizabeth L. Hartland, and Christa E. Müller. 2016. “Inhibitors for the Bacterial Ectonucleotidase Lp1NTPDase from Legionella Pneumophila.” *Bioorg. Med. Chem.* 24:4363–71. https://doi.org/10.1016/j.bmc.2016.07.027.

Fietto, Juliana L.R., Ricardo DeMarco, Ivan P. Nascimento, Ieso M. Castro, Técia M.U. Carvalho, Wanderley De Souza, Maria T. Bahia, Maria J.M. Alves, and Sergio Verjovski-Almeida. 2004. “Characterization and Immunolocalization of an NTP Diphosphohydrolase of Trypanosoma Cruzi.” *Biochem. Biophys. Res. Commun.* 316 (April):454–60. https://doi.org/10.1016/j.bbrc.2004.02.071.

Figueiredo, Amanda Braga de, Miriam Conceicao Souza-Testasicca, and Luis Carlos Crocco Afonso. 2016. “Purinergic Signaling and Infection by Leishmania: A New Approach to Evasion of the Immune Response [Figure Presented].” *Biomed. J.* 39 (August):244–50. https://doi.org/10.1016/j.bj.2016.08.004.

Frasson, Amanda Piccoli, Geraldo Attilio De Carli, Carla Denise Bonan, and Tiana Tasca. 2012. “Involvement of Purinergic Signaling on Nitric Oxide Production by Neutrophils Stimulated with Trichomonas Vaginalis.” *Purinergic Signalling* 8 (1): 1–9. https://doi.org/10.1007/s11302-011-9254-7.

Frasson Amanda Piccoli, Charão Mariele Feiffer, Rosemberg Denis Broock, de Souza Ana Paula de Souza, and Tasca Tiana. 2012. “Analysis of NTPDase in Trichomonas Vaginalis.” *Mem Inst Oswaldo Cruz* 107:170–77. https://doi.org/10.1590/s0074-02762012000200004.

Giordani, Raquel B., Marina Weizenmann, Denis Broock Rosemberg, Geraldo Attilio De Carli, Mauricio Reis Bogo, José Angelo S. Zuanazzi, and Tiana Tasca. 2010. “Trichomonas Vaginalis Nucleoside Triphosphate Diphosphohydrolase and Ecto-5′-Nucleotidase Activities Are Inhibited by Lycorine and Candimine.” *Parasitol. Int.* 59 (June):226–31. https://doi.org/10.1016/j.parint.2010.02.004.

González, Débora A., Patricia Egido, Noelia B. Balcarcel, Claude Hattab, Martín M. Barbieri van Haaster, Julie Pelletier, Jean Sévigny, and Mariano A. Ostuni. 2015. “Rat Submandibular Glands Secrete

Nanovesicles with NTPDase and 5′-Nucleotidase Activities.” *Purinergic Signalling* 11 (February):107–16. https://doi.org/10.1007/s11302-014-9437-0.

Gorelik, Alexei, Jonathan M. Labriola, Katalin Illes, and Bhushan Nagar. 2020. “Crystal Structure of the Nucleotide-Metabolizing Enzyme NTPDase4.” *Protein Sci.* 29 (October):2054–61. https://doi.org/10.1002/pro.3926.

Gorelik, Alexei, Antsa Randriamihaja, Katalin Illes, and Bhushan Nagar. 2018. “Structural Basis for Nucleotide Recognition by the Ectoenzyme CD203c.” *FEBS Journal* 285:2481–94. https://doi.org/10.1111/febs.14489.

Goueli, Said A., and Kevin Hsiao. 2019. “Monitoring and Characterizing Soluble and Membrane-Bound Ectonucleotidases CD73 and CD39.” *PLoS ONE* 14 (October):1–19. https://doi.org/10.1371/journal.pone.0220094.

Hayat, Komal, Saira Afzal, Altaf Saeed, Amna Murtaza, Shafiq Ur Rahman, Khalid Mohammed Khan, Aamer Saeed, et al. 2019. “Investigation of New Quinoline Derivatives as Promising Inhibitors of NTPDases: Synthesis, SAR Analysis and Molecular Docking Studies.” *Bioorg. Chem.* 87 (June):218–26. https://doi.org/10.1016/j.bioorg.2019.03.019.

Iqbal, Jamshed, Petra Vollmayer, Norbert Braun, Herbert Zimmermann, and Christa E. Müller. 2005. “A Capillary Electrophoresis Method for the Characterization of Ecto-Nucleoside Triphosphate Diphosphohydrolases (NTPDases) and the Analysis of Inhibitors by in-Capillary Enzymatic Microreaction.” *Purinergic Signalling* 1 (December):349–58. https://doi.org/10.1007/s11302-005-8076-x.

Kaizer, Rosilene Rodrigues, Eduarda Costa, Cínthia Melazzo de Andrade, Roberta Schmatz, Jessié Martins Gutierres, Danieli Brolo Martins, Vera Maria Morsch, and Maria Rosa Chitolina Schetinger. 2017. “Effect of Long-Term Exposure to Aluminum and High-Fat Diet on NTPDase and 5′-Nucleotidase Activities in Lymphocytes and Platelets of Rats.” *Environ. Qual. Manag.* 27 (September):67–73. https://doi.org/10.1002/tqem.21507.

Kanwal, Khalid Mohammed Khan, Uzma Salar, Saira Afzal, Abdul Wadood, Muhammad Taha, Shahnaz Perveen, et al. 2019. “Schiff Bases of Tryptamine as Potent Inhibitors of Nucleoside Triphosphate Diphosphohydrolases (NTPDases): Structure-Activity Relationship.” *Bioorg. Chem.* 82 (February):253–66. https://doi.org/10.1016/j.bioorg.2018.10.046.

Kittel, Ágnes, Anna L. Kiss, Nándor Müllner, Ida Matkó, and Beáta Sperlágh. 2005. “Expression of NTPDase1 and Caveolins in Human Cardiovascular Disease.” *Histochem. Cell Biol.* 124 (August):51–59. https://doi.org/10.1007/s00418-005-0018-8.

Krug, Ulrike, Robert Totzauer, Matthias Zebisch, and Norbert Sträter. 2013. “The ATP/ADP Substrate Specificity Switch between Toxoplasma Gondii NTPDase1 and NTPDase3 Is Caused by an Altered Mode of Binding of the Substrate Base.” *ChemBioChem* 14 (November):2292–2300. https://doi.org/10.1002/cbic.201300441.

Krug, Ulrike, Matthias Zebisch, Michel Krauss, and Norbert Sträter. 2012a. “Structural Insight into Activation Mechanism of Toxoplasma Gondii Nucleoside Triphosphate Diphosphohydrolases by Disulfide Reduction.” *J. Bio. Chem.* 287 (January):3051–66. https://doi.org/10.1074/jbc.M111.294348.

Kukulski, Filip, S??bastien A. L??vesque, and Jean S??vigny. 2011. *Impact of Ectoenzymes on P2 and P1 Receptor Signaling*. *Advances in Pharmacology*. Vol. 61. https://doi.org/10.1016/B978-0-12-385526-8.00009-6.

Kukulski, F, Sa Lévesque, G Lavoie, J Lecka, F Bigonnesse, Af Knowles, SC Robson, TL Kirley, and J Sévigny. 2005. “Comparative Hydrolysis of P2 Receptor Agonists by NTPDases 1, 2, 3, and 8.” *Purinergic Signaling* 1:193–204. https://doi.org/10.1007/s11302-005-6217-x.

Kumar, V. 2013. “Adenosine as an Endogenous Immunoregulator in Cancer Pathogenesis: Where to Go?” *Purinergic Signalling* 9 (2): 145–65. https://doi.org/10.1007/s11302-012-9349-9.

Kutryb-Zajac, Barbara, Patrycja Jablonska, Marcin Serocki, Alicja Bulinska, Paulina Mierzejewska, Daniela Friebe, Christina Alter, et al. 2020. “Nucleotide Ecto-Enzyme Metabolic Pattern and Spatial Distribution in Calcific Aortic Valve Disease; Its Relation to Pathological Changes and Clinical Presentation.” *Clin Res Cardiol.* 109 (February):137–60. https://doi.org/10.1007/s00392-019-01495-x.

Larsson, Anders, Bo Nilsson, and Mats Eriksson. 1999. “Thrombocytopenia and Platelet Microvesicle.” *Journal of Immunological Methods* 96:391–97.

Lavoie, Élise G., Filip Kukulski, Sébastien A. Lévesque, Joanna Lecka, and Jean Sévigny. 2004. “Cloning and Characterization of Mouse Nucleoside Triphosphate Diphosphohydrolase-3.” *Biochem. Pharmacol.* 67 (May):1917–26. https://doi.org/10.1016/j.bcp.2004.02.012.

Lecka, Joanna, Michel Fausther, Beat Künzli, and Jean Sévigny. 2014. “Ticlopidine in Its Prodrug Form Is a Selective Inhibitor of Human Ntpdase1.” *Mediators of Inflammation* 2014:1–9. https://doi.org/10.1155/2014/547480.

Lecka, Joanna, Irina Gillerman, Michel Fausther, Mabrouka Salem, Mercedes N. Munkonda, Jean Philippe Brosseau, Christine Cadot, et al. 2013. “8-BuS-ATP Derivatives as Specific NTPDase1 Inhibitors.” *Br. J. Pharmacol.* 169 (May):179–96. https://doi.org/10.1111/bph.12135.

Lee, Sang Yong, Amelie Fiene, Wenjin Li, Theodor Hanck, Konstantin A. Brylev, Vladimir E. Fedorov, Joanna Lecka, et al. 2015. “Polyoxometalates - Potent and Selective Ecto-Nucleotidase Inhibitors.” *Biochem. Pharmacol.* 93 (January):171–81. https://doi.org/10.1016/j.bcp.2014.11.002.

Lee, Sang Yong, Xihuan Luo, Vigneshwaran Namasivayam, Jennifer Geiss, Salahuddin Mirza, Julie Pelletier, Holger Stephan, Jean Sévigny, and Christa E. Müller. 2018. “Development of a Selective and Highly Sensitive Fluorescence Assay for Nucleoside Triphosphate Diphosphohydrolase1 (NTPDase1, CD39).” *Analyst* 143 (November):5417–30. https://doi.org/10.1039/c8an01108g.

Lee, Sang Yong, Soumya Sarkar, Sanjay Bhattarai, Vigneshwaran Namasivayam, Steven De Jonghe, Holger Stephan, Piet Herdewijn, Ali El-Tayeb, and Christa E. Müller. 2017. “Substrate-Dependence of Competitive Nucleotide Pyrophosphatase/Phosphodiesterase1 (NPP1) Inhibitors.” *Frontiers in Pharmacology* 8:1–15. https://doi.org/10.3389/fphar.2017.00054.

Leite, Milane S., Rachel Thomaz, José Henrique M. Oliveira, Pedro L. Oliveira, and José Roberto Meyer-Fernandes. 2009. “Trypanosoma Brucei Brucei: Effects of Ferrous Iron and Heme on Ecto-Nucleoside Triphosphate Diphosphohydrolase Activity.” *Exp. Parasitol.* 121:137–43. https://doi.org/10.1016/j.exppara.2008.10.018.

Levano-Garcia, Julio, Renato A. Mortara, Sergio Verjovski-Almeida, and Ricardo DeMarco. 2007. “Characterization of Schistosoma Mansoni ATPDase2 Gene, a Novel Apyrase Family Member.” *Biochemical and Biophysical Research Communications* 352 (2): 384–89. https://doi.org/10.1016/j.bbrc.2006.11.023.

Lévesque, S. A., É G. Lavoie, J. Lecka, F. Bigonnesse, and J. Sévigny. 2007. “Specificity of the Ecto-ATPase Inhibitor ARL 67156 on Human and Mouse Ectonucleotidases.” *Br. J. Pharmacol.* 152 (September):141–50. https://doi.org/10.1038/sj.bjp.0707361.

Li, Jieyao, Liping Wang, Xinfeng Chen, Lifeng Li, Yu Li, Yu Ping, Lan Huang, et al. 2017. “CD39/CD73 Upregulation on Myeloid-Derived Suppressor Cells via TGF-β-MTOR-HIF-1 Signaling in Patients with Non-Small Cell Lung Cancer.” *OncoImmunology* 6 (June):1–14. https://doi.org/10.1080/2162402X.2017.1320011.

Li, Lifeng, Liping Wang, Jieyao Li, Zhirui Fan, Li Yang, Zhen Zhang, Chaoqi Zhang, et al. 2018. “Metformin-Induced Reduction of CD39 and CD73 Blocks Myeloid-Derived Suppressor Cell Activity in

Patients with Ovarian Cancer." *Cancer Res.* 78 (April):1779–91. https://doi.org/10.1158/0008-5472.CAN-17-2460.

Lopez, Vittoria, Laura Schäkel, H J Maximilian Schuh, Michael S Schmidt, Salahuddin Mirza, Christian Renn, Julie Pelletier, et al. 2021. "Sulfated Polysaccharides from Macroalgae Are Potent Dual Inhibitors of Human ATP-Hydrolyzing Ectonucleotidases NPP1 and CD39 Polysaccharides from Macroalgae Are Potent Dual Inhibitors of Human ATP-Hydrolyzing Ectonucleotidases." *Mar. Drugs* 19:1–13. https://doi.org/https://doi.org/10.3390/md19020051.

Luiz Oliveira Penido, Marcus, Dayse Moura Resende, Marco Aurélio Vianello, Fábio Humberto da Silveira Bordin, Alexandre Arthur Jacinto, Walkyria Dutra Dias, Maria Ângela Montesano, David Lee Nelson, Paulo Marcos Zech Coelho, and Eveline Gomes Vasconcelos. 2007. "A New Series of Schistosomicide Drugs, the Alkylaminoalkanethiosulfuric Acids, Partially Inhibit the Activity of Schistosoma Mansoni ATP Diphosphohydrolase." *European Journal of Pharmacology* 570 (1–3): 10–17. https://doi.org/10.1016/j.ejphar.2007.05.028.

Magalhães, Luana, Arthur Henrique Cavalcante de Oliveira, Raphael de Souza Vasconcellos, Christiane Mariotini-Moura, Rafaela de Cássia Firmino, Juliana Lopes Rangel Fietto, and Carmen Lúcia Cardoso. 2016. "Label-Free Assay Based on Immobilized Capillary Enzyme Reactor of Leishmania Infantum Nucleoside Triphosphate Diphosphohydrolase (LicNTPDase-2-ICER-LC/UV)." *J. Chromatogr. B: Anal. Technol. Biomed. Life Sci.* 1008 (January):98–107. https://doi.org/10.1016/j.jchromb.2015.11.028.

Maia, Ana Carolina Ribeiro Gomes, Michelle Lima Detoni, Gabriane Nascimento Porcino, Thais Vieira Soares, Michelia Antônia do Nascimento Gusmão, Melissa Regina Fessel, Marcos José Marques, et al. 2011. "Occurrence of a Conserved Domain in ATP Diphosphohydrolases from Pathogenic Organisms Associated to Antigenicity in Human Parasitic Diseases." *Dev. Comp. Immunol.* 35 (October):1059–67. https://doi.org/10.1016/j.dci.2011.03.026.

Maia, Ana Carolina Ribeiro Gomes, Gabriane Nascimento Porcino, Priscila Faria-Pinto, Túlio Vieira Mendes, Luciana Maria Ribeiro Antinarelli, Elaine Soares Coimbra, Alexandre Barbosa Reis, et al. 2019. "Leishmania Infantum Nucleoside Triphosphate Diphosphohydrolase 1 (NTPDase 1) B-Domain: Antibody Antiproliferative Effect on the Promastigotes and IgG Subclass Responses in Canine Visceral Leishmaniasis." *Vet. Parasitol.* 271 (July):38–44. https://doi.org/10.1016/j.vetpar.2019.06.004.

Mallardo, Domenico, Mario Fordellone, Andrew White, Margaret Ottaviano, Francesca Sparano, Michael Bailey, Arianna Bianca Facchini, et al. 2023. "CD39 and LDHA Affects the Prognostic Role of NLR in Metastatic Melanoma Patients Treated with Immunotherapy." *J. Transl. Med.* 21 (December):1–13. https://doi.org/10.1186/s12967-023-04419-6.

Mandapathil, Magis, Mehtap Boduc, Marion Roessler, Christian Güldner, Ute Walliczek-Dworschak, and Robert Mandic. 2018. "Ectonucleotidase CD39 Expression in Regional Metastases in Head and Neck Cancer." *Acta Oto-Laryngol.* 138 (April):428–32. https://doi.org/10.1080/00016489.2017.1405278.

Marco Idzko1, Davide Ferrari2, and Holger K. Eltzschig. 2015. "Nucleotide Signalling during Inflammation." *Nature* 509:310–17.

Mariotini-Moura, Christiane, Matheus Silva e. Bastos, Felipe Freitas de Castro, Mellina Lanna Trindade, Raphael de Souza Vasconcellos, Myrian Augusta Araújo Neves-do-Valle, Bernardo Pereira Moreira, et al. 2014. "Trypanosoma Cruzi Nucleoside Triphosphate Diphosphohydrolase 1 (TcNTPDase-1) Biochemical Characterization, Immunolocalization and Possible Role in Host Cell Adhesion." *Acta Tropica* 130 (February):140–47. https://doi.org/10.1016/j.actatropica.2013.11.008.

Menezes, Camila Braz, Juliano Durgante, Rafael Rodrigues De Oliveira, Victor Hugo Jacks Mendes Dos Santos, Luiz Frederico Rodrigues, Solange Cristina Garcia, Odelta Dos Santos, and Tiana Tasca. 2016. "Trichomonas Vaginalis NTPDase and Ecto-5′-Nucleotidase Hydrolyze Guanine Nucleotides and Increase Extracellular Guanosine Levels under Serum Restriction." *Mol. Biochem. Parasitol.* 207 (May):10–18. https://doi.org/10.1016/j.molbiopara.2016.04.003.

Menezes, Camila Braz, and Tiana Tasca. 2016. “Trichomoniasis Immunity and the Involvement of the Purinergic Signaling.” *Biomed. J.* 39 (August):234–43. https://doi.org/10.1016/j.bj.2016.06.007.

Montalbán del Barrio, Itsaso, Cornelia Penski, Laura Schlahsa, Roland G. Stein, Joachim Diessner, Achim Wöckel, Johannes Dietl, et al. 2016. “Adenosine-Generating Ovarian Cancer Cells Attract Myeloid Cells Which Differentiate into Adenosine-Generating Tumor Associated Macrophages - a Self-Amplifying, CD39- and CD73-Dependent Mechanism for Tumor Immune Escape.” *JITC* 4 (1): 1–16. https://doi.org/10.1186/s40425-016-0154-9.

Morello, Silvana, Elisabetta Caiazzo, Roberta Turiello, and Carla Cicala. 2021. “Thrombo-Inflammation: A Focus on Ntpdase1/Cd39.” *Cells* 10 (September):1–13. https://doi.org/10.3390/cells10092223.

Murtaza, Amna, Saira Afzal, Gohar Zaman, Aamer Saeed, Julie Pelletier, Jean Sévigny, Jamshed Iqbal, and Abbas Hassan. 2021. “Divergent Synthesis and Elaboration of Structure Activity Relationship for Quinoline Derivatives as Highly Selective NTPDase Inhibitor.” *Bioorg. Chem.* 115 (October):1–9. https://doi.org/10.1016/j.bioorg.2021.105240.

Nagate, Yasuhiro, Sachiko Ezoe, Jiro Fujita, Daisuke Okuzaki, Daisuke Motooka, Tomohiko Ishibashi, Michiko Ichii, et al. 2021. “Ectonucleotidase CD39 Is Highly Expressed on ATLL Cells and Is Responsible for Their Immunosuppressive Function.” *Leukemia* 35 (January):107–18. https://doi.org/10.1038/s41375-020-0788-y.

Newton, Hayley J., Desmond K.Y. Ang, Ian R. Van Driel, and Elizabeth L. Hartland. 2010. “Molecular Pathogenesis of Infections Caused by Legionella Pneumophila.” *Clin. Microbiol. Rev.* 23 (April):274–98. https://doi.org/10.1128/CMR.00052-09.

Ni, Xiaojian, Wenze Wan, Jingjing Ma, Xinyou Liu, Bohao Zheng, Zhixian He, Weige Yang, and Lihong Huang. 2021. “A Novel Prognostic Biomarker of Luminal Breast Cancer: High CD39 Expression Is Related to Poor Survival.” *Front. Genet.* 12 (June):1–11. https://doi.org/10.3389/fgene.2021.682503.

Oliveira, Camila B., Aleksandro S. Da Silva, Viviane C.G. Souza, Marcio M. Costa, Jeandre A.S. Jaques, Daniela B.R. Leal, Sonia T.A. Lopes, and Silvia G. Monteiro. 2012. “NTPDase Activity in Lymphocytes of Rats Infected by Trypanosoma Evansi.” *Parasitology* 139 (February):232–36. https://doi.org/10.1017/S0031182011001879.

Paes-Vieira, Lisvane, André Luiz Gomes-Vieira, and José Roberto Meyer-Fernandes. 2018. “NTPDase Activities: Possible Roles on Leishmania Spp Infectivity and Virulence.” *Cell Biol. Int.* 42 (June):670–82. https://doi.org/10.1002/cbin.10944.

Pulte, E. Dianne, M. Johan Broekman, Kim E. Olson, Joan H.F. Drosopoulos, Jorge R. Kizer, Naziba Islam, and Aaron J. Marcus. 2007. “CD39/NTPDase-1 Activity and Expression in Normal Leukocytes.” *Thromb. Res.* 121:309–17. https://doi.org/10.1016/j.thromres.2007.04.008.

Randall, Rose J, and A Lewis. 1951. “Protein Measurment with the Folin Phenol Reagent.” *J. Biol. Chem.* 193:265–75.

Robson, Simon C., Jean Sévigny, and Herbert Zimmermann. 2006. “The E-NTPDase Family of Ectonucleotidases: Structure Function Relationships and Pathophysiological Significance.” *Purinergic Signalling* 2 (May):409–30. https://doi.org/10.1007/s11302-006-9003-5.

Robson, Simon C., Jean Sevigny, and Herbert Zimmermann. 2006. “The E-NTPDase Family of Ectonucleotidases: Structure Function Relationships and Pathophysiological Significance.” *Purinergic Signalling* 2 (2): 409–30. https://doi.org/10.1007/s11302-006-9003-5.

Roliano, Gabriela Gonçalves, Juliana Hofstätter Azambuja, Veronica Toniazzo Brunetto, Hannah Elizabeth Butterfield, Antonio Nochi Kalil, and Elizandra Braganhol. 2022. “Colorectal Cancer and Purinergic Signalling: An Overview.” *Cancers* 14 (October):1–29. https://doi.org/10.3390/cancers14194887.

Rückert, Caroline, Cristiane dos Santos Stuepp, Barbara Gottardi, Jessica Rosa, Julia Cisilotto, Fernanda Pires Borges, Denis Broock Rosemberg, et al. 2010. “Trichomonas Vaginalis: Dehydroepiandrosterone Sulfate and 17β-Estradiol Alter NTPDase Activity and Gene Expression.” *Exp. Parasitol.* 125 (July):187–95. https://doi.org/10.1016/j.exppara.2010.01.029.

Saccol, Renata da Silva Pereira, Karine Lanes da Silveira, Stephen Adeniyi Adefegha, Alessandra Guedes Manzoni, Leonardo Lanes da Silveira, Ana Paula Visintainer Coelho, Livia Gelain Castilhos, et al. 2019. “Effect of Quercetin on E-NTPDase/E-ADA Activities and Cytokine Secretion of Complete Freund Adjuvant–Induced Arthritic Rats.” *Cell Biochem. Funct.* 37 (October):474–85. https://doi.org/10.1002/cbf.3413.

Sansom, Fiona M., Hayley J. Newton, Sandra Crikis, Nicholas P. Cianciotto, Peter J. Cowan, Anthony J.F. d’Apice, and Elizabeth L. Hartland. 2007. “A Bacterial Ecto-Triphosphate Diphosphohydrolase Similar to Human CD39 Is Essential for Intracellular Multiplication of Legionella Pneumophila.” *Cell. Microbiol.* 9 (August):1922–35. https://doi.org/10.1111/j.1462-5822.2007.00924.x.

Sansom, Fiona M., Patrice Riedmaier, Hayley J. Newton, Michelle A. Dunstone, Christa E. Müller, Holger Stephan, Emma Byres, et al. 2008. “Enzymatic Properties of an Ecto-Nucleoside Triphosphate Diphosphohydrolase from Legionella Pneumophila: Substrate Specificity and Requirement for Virulence.” *J. Biol. Chem.* 283 (May):12909–18. https://doi.org/10.1074/jbc.M801006200.

Santos, Ramon F., Marcela A.S. Pôssa, Matheus S. Bastos, Paulo M.M. Guedes, Márcia R. Almeida, Ricardo DeMarco, Sergio Verjovski-Almeida, Maria T. Bahia, and Juliana L.R. Fietto. 2009. “Influence of Ecto-Nucleoside Triphosphate Diphosphohydrolase Activity on Trypanosoma Cruzi Infectivity and Virulence.” *PLoS Neglected Trop. Dis.* 3:1–11. https://doi.org/10.1371/journal.pntd.0000387.

Schäkel, Laura, Salahuddin Mirza, Markus Pietsch, Sang-yong Lee, and Christa E Müller. 2021. “2-Substituted Thienotetrahydropyridine Derivatives_ Allosteric Ectonucleotidase Inhibitors _ Enhanced Reader.” *Arch. Pharm.* 354:1–18. https://doi.org/https://doi.org/10.1002/ardp.202100300.

Schäkel, Laura, Salahuddin Mirza, Riekje Winzer, Vittoria Lopez, Riham Idris, Haneen Al-Hroub, Julie Pelletier, Jean Sévigny, Eva Tolosa, and Christa E. Müller. 2022. “Protein Kinase Inhibitor Ceritinib Blocks Ectonucleotidase CD39 - a Promising Target for Cancer Immunotherapy.” *J Immunother Cancer* 10 (August):1–14. https://doi.org/10.1136/jitc-2022-004660.

Schäkel, Laura, Constanze C. Schmies, Riham M. Idris, Xihuan Luo, Sang Yong Lee, Vittoria Lopez, Salahuddin Mirza, et al. 2020. “Nucleotide Analog ARL67156 as a Lead Structure for the Development of CD39 and Dual CD39/CD73 Ectonucleotidase Inhibitors.” *Front. Pharmacol.* 11 (September):1–23. https://doi.org/10.3389/fphar.2020.01294.

Shehata, Mahmoud K., Muhammad Uzair, Seyed–Omar –O Zaraei, Afnan I. Shahin, Syed J.A. Shah, Saif Ullah, Jamshed Iqbal, and Mohammed I. El–Gamal. 2023. “Synthesis, Biological Evaluation, and Molecular Modeling Studies of a New Series of Imidazothiazole or Imidazooxazole Derivatives as Inhibitors of Ectonucleoside Triphosphate Diphosphohydrolases (NTPDases).” *Med. Chem. Res.* 32 (February):314–25. https://doi.org/10.1007/s00044-022-03000-y.

Shi, Linsen, Lin Yang, Zhaoyin Wu, Wei Xu, Jun Song, and Wenxian Guan. 2018. “Adenosine Signaling: Next Checkpoint for Gastric Cancer Immunotherapy?” *Int. Immunopharmacol.* 63 (October):58–65. https://doi.org/10.1016/j.intimp.2018.07.023.

Silva, Claudia Lucia Martins. 2016. “Purinergic Signaling in Schistosomal Infection.” *Biomed. J.* 39 (October):316–25. https://doi.org/10.1016/j.bj.2016.06.006.

Souza, Ronny Francisco De, Yaro Luciolo dos Santos, Raphael de Souza Vasconcellos, Lucas Borges-Pereira, Ivo Santana Caldas, Márcia Rogéria de Almeida, Maria Terezinha Bahia, and Juliana Lopes Rangel Fietto. 2013. “Recombinant Leishmania (Leishmania) Infantum Ecto-Nucleoside Triphosphate

Diphosphohydrolase NTPDase-2 as a New Antigen in Canine Visceral Leishmaniasis Diagnosis." *Acta Trop.* 125 (January):60–66. https://doi.org/10.1016/j.actatropica.2012.09.011.

Souza, Viviane do Carmo Gonçalves, Karine Bizzi Schlemmer, Cristiano Bicca Noal, Jeandre Augusto dos Santos Jaques, Carine Eloise Prestes Zimmermann, Cláudio Alberto Martins Leal, Juliana Fleck, et al. 2012. "E-NTPDase and E-ADA Activities Are Altered in Lymphocytes of Patients with Indeterminate Form of Chagas' Disease." *Parasitol. Int.* 61 (December):690–96. https://doi.org/10.1016/j.parint.2012.07.008.

Stach, Paul, Christa E Müller Zweitgutachterin, and PD Anke Schiedel. 2023. "Small Molecule Inhibitors of CD38 with Ancillary CD39 Inhibition."

Tasca, T., C. D. Bonan, G. A. De Carli, J. J.F. Sarkis, and J. F. Alderete. 2005. "Heterogeneity in Extracellular Nucleotide Hydrolysis among Clinical Isolates of Trichomonas Vaginalis." *Parasitology* 131 (1): 71–78. https://doi.org/10.1017/S0031182005007377.

Tonin, Alexandre A., Aleksandro S. Da Silva, Jader B. Ruchel, João F.P. Rezer, Giovana Camillo, Luciana Faccio, Raqueli T. França, et al. 2013. "E-NTPDase and E-ADA Activities in Lymphocytes Associated with the Immune Response of Rats Experimentally Infected with Toxoplasma Gondii." *Exp. Parasitol.* 135 (October):325–30. https://doi.org/10.1016/j.exppara.2013.07.014.

Tonin, Alexandre A., Aleksandro S. Da Silva, Daniele Zanini, Luana P. Pelinson, Maria Rosa C. Schetinger, Giovana Camillo, Fernanda S.F. Vogel, Mario de La Rue, Jeandre A. Jaques, and Sonia T.A. Lopes. 2015. "Biochemical Detection of Enzymes NTPDase in Tachyzoites of Toxoplasma Gondii and Possible Functional Correlations." *Comp. Clin. Pathol.* 24 (March):393–97. https://doi.org/10.1007/s00580-014-1911-0.

Trautmann, Alain. 2009. "Extracellular ATP in the Immune System: More than Just a 'Danger Signal.'" *Sci. Signaling* 2 (February):1–3. https://doi.org/10.1126/scisignal.256pe6.

Trindade, Sandra, Filipa Rijo-Ferreira, Tânia Carvalho, Daniel Pinto-Neves, Fabien Guegan, Francisco Aresta-Branco, Fabio Bento, et al. 2016. "Trypanosoma Brucei Parasites Occupy and Functionally Adapt to the Adipose Tissue in Mice." *Cell Host Microbe* 19 (June):837–48. https://doi.org/10.1016/j.chom.2016.05.002.

Vivian, Julian P., Patrice Riedmaier, Honghua Ge, Jérôme Le Nours, Fiona M. Sansom, Matthew C.J. Wilce, Emma Byres, et al. 2010. "Crystal Structure of a Legionella Pneumophila Ecto -Triphosphate Diphosphohydrolase, A Structural and Functional Homolog of the Eukaryotic NTPDases." *Structure* 18 (February):228–38. https://doi.org/10.1016/j.str.2009.11.014.

Wang, Sheng, Songsen Gao, Dexi Zhou, Xueyi Qian, Jiajie Luan, and Xiongwen Lv. 2021. "The Role of the CD39–CD73–Adenosine Pathway in Liver Disease." *J. Cell. Physiol.* 236 (February):851–62. https://doi.org/10.1002/jcp.29932.

Yung-Chi, Cheng, and William H. Prusoff. 1973. "Relationship between the Inhibition Constant (KI) and the Concentration of Inhibitor Which Causes 50 per Cent Inhibition (I50) of an Enzymatic Reaction." *Biochem. Pharmacol.* 22:3099–3108.

Zaigham, Zahid Hussain, Saif Ullah, Julie Pelletier, Jean Sévigny, Jamshed Iqbal, and Abbas Hassan. 2023. "Synthesis and Biological Evaluation of Sulfamoyl Benzamide Derivatives as Selective Inhibitors for H-NTPDases." *RSC Advances* 13 (July):20909–15. https://doi.org/10.1039/d3ra03874b.

Zebisch, Matthias, Younis Baqi, Petra Schäfer, Christa E. Müller, and Norbert Sträter. 2014. "Crystal Structure of NTPDase2 in Complex with the Sulfoanthraquinone Inhibitor PSB-071." *J. Struct. Biol.* 185:336–41. https://doi.org/10.1016/j.jsb.2014.01.005.

Zebisch, Matthias, Michel Krauss, Petra Schäfer, Peter Lauble, and Norbert Sträter. 2013. “Crystallographic Snapshots along the Reaction Pathway of Nucleoside Triphosphate Diphosphohydrolases.” *Structure* 21 (August):1460–75. https://doi.org/10.1016/j.str.2013.05.016.

Zebisch, Matthias, Michel Krauss, Petra Schäfer, and Norbert Sträter. 2012a. “Crystallographic Evidence for a Domain Motion in Rat Nucleoside Triphosphate Diphosphohydrolase (NTPDase) 1.” *J. Mol. Bio.* 415 (January):288–306. https://doi.org/10.1016/j.jmb.2011.10.050.

Zebisch, Matthias, and Norbert Strä. 2008. “Structural Insight into Signal Conversion and Inactivation by NTPDase2 in Purinergic Signaling.” *Proc Natl Acad Sci U S A* 105:6882–87. https://doi.org/https://doi.org/10.1073/pnas.0802535105.

Zeng, Jianrui, Zhaochen Ning, Yuzhong Wang, and Huabao Xiong. 2020. “Implications of CD39 in Immune-Related Diseases.” *Int. Immunopharmacol.* 89 (December):1–10. https://doi.org/10.1016/j.intimp.2020.107055.

Zimmermann, Herbert. 2020. “History of Ectonucleotidases and Their Role in Purinergic Signaling.” *Biochem. Pharmacol.*, 114322. https://doi.org/10.1016/j.bcp.2020.114322.

Zimmermann, Herbert, Matthias Zebisch, and Norbert Sträter. 2012a. “Cellular Function and Molecular Structure of Ecto-Nucleotidases.” *Purinergic Signalling* 8 (3): 437–502. https://doi.org/10.1007/s11302-012-9309-4.

HA-Tag, Flag-tag, His-tag, Restriction sites

Synthesised codon-optimized sequence of *P. falciparum* NTPDase in pfastbac expression system

ATGAAGACCATCATCGCTCTGTCCTACATCTTCTGCCTCGTGTTCGCCGACTACAAGGACGATGACGATAAG**GGGCGC**
GCCATGGAGAACCTGATCGGCACCCCTCTGATCGAGAAGAAGAAGAAGGAGTCCCACATCAGCATCCGGAAGGACAAG
AAGCTGAATGACATCGAGGGCGAGAAGAAGGAGAAGAAGATCAAGGAGCGGCTGTTCCTGTGCCTGATCTGCCTGCTG
GTCATTATCTGGCTGATCTATTTTTGCTATAAGAACCACATCTTCCTGAGCTATCTGCAGAATGAGAAGGAGTACGGC
ATCATCATCGATGCCGGCAGCAACGGCACCCGGATTCATCTGTTTGAGTGGAAGAAGCGGGAGTACGAGCTGAGCAAT
AAGAAGGAGGAGAATAACCTGATCGAGCTGAAGGAGATCTTCAACGCCAAGGTGAAGAAGAGCATCAGCACCATCAGC
TACAACGAGATCAAGGACATCCTGATCTATCTGATCAATAAGGTCATTGACCACCTGATCGAGAAAAAGATCTATGTG
TACAATAAGCAGAAGTGGAAGTCCTACCCTTTTTACTTTCAGGCTACCGGCGGCATGCGGAACCTGAAGCAGGAGGAC
AGGAATCTGAGGATGAAGTACATCAAGAACATCCTGTCCAACGATAATTATAATCCTTTCTATTTCCTGAACGAGTAC
GCCAGGATCTTGTCCGGCGAGGAGGAGGGCATCTATGGCTGGCTGGCTGTGAACAACCTGCTGAACTCCATCTTTAGC
AAGCCCAACAACACCTATGGCGCCATCGATCTGGGCGGCTCCTCCACACAGATCACCTTTTATCCCATGGACCACAAT
ATCCTGGAGAACTATAATAGCATCCTGCTGAACAACATCCTGATCAGGCTGTATAGCCACTCCTTCATCGGCTACGGC
TGGATCGACTCCCTGTTCCGGGTGAACATCTACCTGTGTCTGGAGATCATCAAGAAGCTGTCCACCCGGAACATCAAG
AACATCTATCAGCTGGAGAATTACTATGACGATTACATCAACGATTACTTCTATAATAACCTGCCCAACTACAACTGG
TTCTTTTATTCCACCAAGAAGATCATCAACAACAACAAGGAGAACTATAACCACCACAACTATGAGAACATCAATTAT
GACGTGAATAAGCGGAATTACCCCTATAATAATTTCCAGCAGAAGTACATCCACACCAACCCCAAGAAGGGCAACTAC
ACCAAGGGCAATATCAATAATTCCAACAAGTCCTACAAGAACCTGAGCAACATCCTGCTGCAGGAGATCGTGAAGTAT
ATCCAGCACAGCCAGAATGACTATCCTTACTCCTCCCTGACCGACATCTACGACTACACCTACAACATCTATGATGAG
AAGCCCTACGACATTGAGAACTTCATCAAGACCATCAAGAACTTCAACCGGCACTCCAAGGAGGACACCATCATGCTG
GTGCAGAACCCTTGCCTGCCCTACCCCTATGAGATGAAGATCACCTTTCCCACCTACAATCTGGTGACCTCCCAGTTT
GTGATCCTGAAGAAGAACTCCCGGAATGAGATCGGCAACATCAACGACATCAAGAATGACGGCAACAACTACACCCAG
AACGATGACAATAACTACACCCAGAATGACGGCAATTATTACAGGCAGAATGTGGGCAATTACTATCGGCACAACCAC
AACATCAACGATGTGTATGAGCTGAATTCCTCCGAGTCCTACGATAACTTTATCTCCAATTTCGTGCTGAAGCTGAAG
ATCATCAATAATAATATGAGCCTGATGGATAACATCTATGAGGACTTCAAGAATAAGGGCTACCTGAATAACGTGCTG
AAGAAGGTGAATGACAATAAGATCAGCAATACCCTGAAGAATGAGATCATCAAACGGCTGTTCGAGAAGATCATCAAC
GAGAAGATCAAGAAGCTCTATATCAATATCACCGTGAGGATCGTGGGCAGCAACGACTTCAAGAAGTGTCTGGAGAAT
ACCAAGAAGCTGTTTTACGAGCAGCCCTGCTTCCTGAGCTCCTGTTCCTTTAATGGCATCTATCAGCCTAATCTGGAG
AACAATAAGTTCGTGCTGCACGGCCAGTTCAAGAAGGTCATTACCTATCTGGGCTTCAAGAAGTACGTGGATCTGAAC
CAGATGAAGATCTACATCCAGAAGCTGTGCAATATGAATCTGTATGAGCTGACCTATAACATGTCCAATAAGATCATG
CACAACCAGATCCCTACCTTTTGTTGGAAGTCCATCTGGTCCTACAGCCTGCTGTTCTATGGCTTTAAGTTCAAGGAG
ACAACCAAGCTGCTGATCATCAACGACAACACCAATATCAGCTATGATTCCAGCTCCACCAGCCAGGCCTCCAAGCAG
TTCTACAAGCGGGTGGAGAATAAGGAGCAGAATAACTACCTGCACGACAAGACCAACTATAATAACGAGTATAATCTG
AACAACAAGATCGATAATATCTCCTGGACCCACGGCTCCATGATCTATCAGATCAACATCTTTCAGGAGAGGTTTAAC
AGCCGGAAGTACAAGCTGTATTCCGAGGTGTTTTTCGTGCTGTTTCTGATCATCTTTATCATCCTGATCATCCTGGGC
GGCTATATCTTTAAGTTTAAGGAGATCCTGAACAAGAAGTACAGGTTCCTG**CACCACCACCATCACCACCACCACCAC**
TAAAAGCTT

Human membrane-bound CD39 in *pFastbac* expression system

ATGAAGACCATCATCGCTCTGTCCTACATCTTCTGCCTCGTGTTCGCCGACTACAAGGACGATGACGATGCT**GGGCGC**
GCCATGGAAGATACAAAGGAGTCTAACGTGAAGACATTTTGCTCCAAGAATATCCTAGCCATCCTTGGCTTCTCCTCT
ATCATAGCTGTGATAGCTTTGCTTGCTGTGGGGTTGACCCAGAACAAAGCATTGCCAGAAAACGTTAAGTATGGGATT
GTGCTGGATGCGGGTTCTTCTCACACAAGTTTATACATCTATAAGTGGCCAGCAGAAAAGGAGAATGACACAGGCGTG
GTGCATCAAGTAGAAGAATGCAGGGTTAAAGGTCCTGGAATCTCAAAATTTGTTCAGAAAGTAAATGAAATAGGCATT
TACCTGACTGATTGCATGGAAAGAGCTAGGGAAGTGATTCCAAGGTCCCAGCACCAAGAGACACCCGTTTACCTGGGA
GCCACGGCAGGCATGCGGTTGCTCAGGATGGAAAGTGAAGAGTTGGCAGACAGGGTTCTGGATGTGGTGGAGAGGAGC
CTCAGCAACTACCCCTTTGACTTCCAGGGTGCCAGGATCATTACTGGCCAAGAGGAAGGTGCCTATGGCTGGATTACT
ATCAACTATCTGCTGGGCAAATTCAGTCAGAAAACAAGGTGGTTCAGCATAGTCCCATATGAAACCAATAATCAGGAA
ACCTTTGGAGCTTTGGACCTTGGGGGAGCCTCTACACAAGTCACTTTTGTACCCCAAAACCAGACTATCGAGTCCCCA
GATAATGCTCTGCAATTTCGCCTCTATGGCAAGGACTACAATGTCTACACACATAGCTTCTTGTGCTATGGGAAGGAT

CAGGCACTCTGGCAGAAACTGGCCAAGGACATTCAGGTTGCAAGTAATGAAATTCTCAGGGACCCATGCTTTCATCCT
GGATATAAGAAGGTAGTGAACGTAAGTGACCTTTACAAGACCCCCTGCACCAAGAGATTTGAGATGACTCTTCCATTC
CAGCAGTTTGAAATCCAGGGTATTGGAAACTATCAACAATGCCATCAAAGCATCCTGGAGCTCTTCAACACCAGTTAC
TGCCCTTACTCCCAGTGTGCCTTCAATGGGATTTTCTTGCCACCACTCCAGGGGGATTTTGGGGCATTTTCAGCTTTT
TACTTTGTGATGAAGTTTTTAAACTTGACATCAGAGAAAGTCTCTCAGGAAAAGGTGACTGAGATGATGAAAAAGTTC
TGTGCTCAGCCTTGGGAGGAGATAAAAACATCTTACGCTGGAGTAAAGGAGAAGTACCTGAGTGAATACTGCTTTTCT
GGTACCTACATTCTCTCCCTCCTTCTGCAAGGCTATCATTTCACAGCTGATTCCTGGGAGCACATCCATTTCATTGGC
AAGATCCAGGGCAGCGACGCCGGCTGGACTTTGGGCTACATGCTGAACCTGACCAACATGATCCCAGCTGAGCAACCA
TTGTCCACACCTCTCTCCCACTCCACCTATGTCTTCCTCATGGTTCTATTCTCCCTGGTCCTTTTCACAGTGGCCATC
ATAGGCTTGCTTATCTTTCACAAGCCTTCATATTTCTGGAAAGATATGGTA**CACCATCATCACCATCATCACCACCAC**
CACTAA**AAGCTT**GTCGAGAAGATACCCG

Human CD39 (Soluble), *p*ACGP67B expression vector

GGATCCCCACC**ATGG**ACCCAGAACAAAGCATTGCCAGAAAACGTTAAGTATGGGATTGTGCTGGATGCGGGTTCTTCT
CACACAAGTTTATACATCTATAAGTGGCCAGCAGAAAAGGAGAATGACACAGGCGTGGTGCATCAAGTAGAAGAATGC
AGGGTTAAAGGTCCTGGAATCTCAAAATTTGTTCAGAAAGTAAATGAAATAGGCATTTACCTGACTGATTGCATGGAA
AGAGCTAGGGAAGTGATTCCAAGGTCCCAGCACCAAGAGACACCCGTTTACCTGGGAGCCACGGCAGGCATGCGGTTG
CTCAGGATGGAAAGTGAAGAGTTGGCAGACAGGGTTCTGGATGTGGTGGAGAGGAGCCTCAGCAACTACCCCTTTGAC
TTCCAGGGTGCCAGGATCATTACTGGCCAAGAGGAAGGTGCCTATGGCTGGATTACTATCAACTATCTGCTGGGCAAA
TTCAGTCAGAAAACAAGGTGGTTCAGCATAGTCCCATATGAAACCAATAATCAGGAAACCTTTGGAGCTTTGGACCTT
GGGGGAGCCTCTACACAAGTCACTTTTGTACCCCAAAACCAGACTATCGAGTCCCCAGATAATGCTCTGCAATTTCGC
CTCTATGGCAAGGACTACAATGTCTACACACATAGCTTCTTGTGCTATGGGAAGGATCAGGCACTCTGGCAGAAACTG
GCCAAGGACATTCAGGTTGCAAGTAATGAAATTCTCAGGGACCCATGCTTTCATCCTGGATATAAGAAGGTAGTGAAC
GTAAGTGACCTTTACAAGACCCCCTGCACCAAGAGATTTGAGATGACTCTTCCATTCCAGCAGTTTGAAATCCAGGGT
ATTGGAAACTATCAACAATGCCATCAAAGCATCCTGGAGCTCTTCAACACCAGTTACTGCCCTTACTCCCAGTGTGCC
TTCAATGGGATTTTCTTGCCACCACTCCAGGGGGATTTTGGGGCATTTTCAGCTTTTTACTTTGTGATGAAGTTTTTA
AACTTGACATCAGAGAAAGTCTCTCAGGAAAAGGTGACTGAGATGATGAAAAAGTTCTGTGCTCAGCCTTGGGAGGAG
ATAAAAACATCTTACGCTGGAGTAAAGGAGAAGTACCTGAGTGAATACTGCTTTTCTGGTACCTACATTCTCTCCCTC
CTTCTGCAAGGCTATCATTTCACAGCTGATTCCTGGGAGCACATCCATTTCATTGGCAAGATCCAGGGCAGCGACGCC
GGCTGGACTTTGGGCTACATGCTGAACCTGACCAACATGATCCCAGCTGAGCAACCATTGTCCACACCTCTCTCCCAC
TCCACCTATGTC**CATCATCACCACCACCAT**TAATCTAGA

Mouse membrane-bound CD39, pFastbac expression vector

GGCCGGGGACTGAAGAC**CATCATCGCTCTGTCCTACATCTTCTGCCTCGTGTTCGCC**GACTACAAGGACGATGACGAT
GCTG**GGCGCGCC**ATGGAAGATATAAAGGATTCTAAGGTGAAGAGATTTTGCTCCAAAAATATTCTGATCATCCTTGGT
TTCACCTCTATCTTGGCTGTGATAGCTTTGATTGCTGTGGGACTGACCCAGAACAAACCTTTGCCAGAAAATGTTAAG
TATGGGATTGTGTTGGATGCGGGGTCGTCTCACACCAACCTGTACATCTACAAGTGGCCAGCCGAGAAGGAGAATGAC
ACAGGGGTGGTGCAGCAGTTAGAGGAATGCCAAGTGAAAGGTCCTGGAATCTCAAAATATGCTCAGAAAACAGATGAA
ATCGGTGCATACCTGGCCGAATGCATGGAACTGTCCACCGAACTGATACCAACATCCAAGCATCACCAGACTCCTGTC
TACCTGGGAGCCACAGCAGGCATGCGCTTGCTTAGAATGGAAAGTGAACAATCGGCAGACGAGGTCCTGGCTGCAGTG
TCAACGAGCCTTAAGGGCTACCCCTTTGACTTCCAGGGTGCCAAGATCATCACGGGACAAGAGGAAGGTGCCTATGGG
TGGATTACTATTAACTATCTGCTGGGCAGATTCACTCAGGAACAGAGTTGGCTAAGCCTCATCTCAGACAGTCAGAAA
CAGGAAACCTTTGGCGCTTTGGATCTCGGCGGAGCCTCCACACAAATCACCTTCGTGCCCCAAAACAGCACTATAGAG
TCCCCAGAAAACTCTCTGCAATTCCGTCTCTATGGCGAGGACTATACTGTGTACACACACAGCTTCCTGTGCTATGGG
AAGGATCAGGCTCTCTGGCAGAAACTGGCCAAGGACATTCAGGTTTCAAGTGGTGGCGTCCTTAAGGACCCGTGCTTT
AACCCAGGATACGAGAAGGTTGTGAATGTAAGTGAGCTCTATGGCACTCCCTGCACCGAAAGATTCGAAAAGAAGCTA
CCGTTTGATCAGTTTCGAATCCAGGGCACTGGAGACTACGAACAGTGCCACCAGAGCATCCTTGAGCTCTTCAACAAC
AGCCACTGCCCTTACTCCCAGTGTGCCTTCAATGGCGTCTTCCTGCCACCTCTCCATGGGAGTTTTGGGGCGTTTTCT
GCTTTCTACTTTGTGATGGATTTTTTTAAGAAGGTAGCGAAAAACAGTGTCATCTCTCAGGAGAAAATGACCGAGATA
ACAAAAAATTTTTGCTCAAAATCTTGGGAAGAGACAAAGACATCTTATCCTTCAGTAAAGGAGAAGTACCTGAGTGAG
TACTGCTTCTCGGGTGCCTACATCCTCTCTCTCCTGCAAGGCTATAACTTCACAGACAGCTCCTGGGAACAGATTCAT

TTTATGGGCAAGATCAAAGACAGCAACGCGGGGTGGACTTTGGGCTACATGCTGAACTTGACCAACATGATCCCAGCT
GAACAGCCGTTGTCCCCGCCTCTCCCTCACTCCACCTACATTGGCCTCATGGTTCTCTTCTCCCTGCTCTTGGTTGCT
GTGGCCATCACAGGCCTGTTCATCTATAGCAAGCCTTCATATTTCTGGAAAGAGGCAGTA**CACCATCATCACCATCAT**
CACCACCACCACTAA**AAGCTT**TCGAGAAGCTAGCCT

CACCATCATCACCATCACCACCACCACTAA

Apyrase conserved regions in NTPDase orthologs

> *Plasmodium falciparum* NTPDase1

MENLIGTPLIEKKKKESHISIRKDKKLNDIEGEKKEKKIKERLFLCLICLLVIIWLIYFCYKNHIFLSYLQNEKEYGIIIDAGSNGT
RIHLFEWKKREYELSNKKEENNLIELKEIFNAKVKKSISTISYNEIKDILIYLINKVIDHLIEKKIYVYNKQKWKSYPFYFQATGGM
RNLKQEDRNLRMKYIKNILSNDNYNPFYFLNEYARILSGEEEGIYGWLAVNNLLNSIFSKPNNTYGAIDLGGSSTQITFYPMDHNIL
ENYNSILLNNILIRLYSHSFIGYGWIDSLFRVNIYLCLEIIKKLSTRNIKNIYQLENYYDDYINDYFYNNLPNYNWFFYSTKKIINN
NKENYNHHNYENINYDVNKRNYPYNNFQQKYIHTNPKKGNYTKGNINNSNKSYKNLSNILLQEIVKYIQHSQNDYPYSSLTDIYDYT
YNIYDEKPYDIENFIKTIKNFNRHSKEDTIMLVQNPCLPYPYEMKITFPTYNLVTSQFVILKKNSRNEIGNINDIKNDGNNYTQNDD
NNYTQNDGNYYRQNVGNYYRHNHNINDVYELNSSESYDNFISNFVLKLKIINNNMSLMDNIYEDFKNKGYLNNVLKKVNDNKISNTL
KNEIIKRLFEKIINEKIKKLYINITVRIVGSNDFKKCLENTKKLFYEQPCFLSSCSFNGIYQPNLENNKFVLHGQFKKVITYLGFKK
YVDLNQMKIYIQKLCNMNLYELTYNMSNKIMHNQIPTFCWKSIWSYSLLFYGFKFKETTKLLIINDNTNISYDSSSTSQASKQFYKR
VENKEQNNYLHDKTNYNNEYNLNNKIDNISWTHGSMIYQINIFQERFNSRKYKLYSEVFFVLFLIIFIILIILGGYIFKFKEILNKK
YRFL

>Mouse NTPDase1

MAAGRGLARFTDLEELDEVITERKTKRHKLRSYQDSKVKRFCSKNILIILGFTSILAVIALIAVGLTQNKPLPENVKYGIVLDAGSS
HTNLYIYKWPAEKENDTGVVQQLEECQVKGPGISKYAQKTDEIGAYLAECMELSTELIPTSKHHQTPVYLGATAGMRLLRMESEQSA
DEVLAAVSTSLKSYPFDFQGAKIITGQEEGAYGWITINYLLGRFTQEQSWLSLISDSQKQETFGALDLGGASTQITFVPQNSTIESP
ENSLQFRLYGEDYTVYTHSFLCYGKDQALWQKLAKDIQVSSGGVLKDPCFNPGYEKVVNVSELYGTPCTKRFEKKLPFDQFRIQGTG
DYEQCHQSILELFNNSHCPYSQCAFNGVFLPPLHGSFGAFSAFYFVMDFFKKVAKNSVISQEKMTEITKNFCSKSWEETKTSYPSVK
EKYLSEYCFSGAYILSLLQGYNFTDSSWEQIHFMGKIKDSNAGWTLGYMLNLTNMIPAEQPLSPPLPHSTYIGLMVLFSLLLVAVAI
TGLFIYSKPSYFWKEAV

> Rat NTPDase1

MEDIKDSKVKRFCSKNILIILGFSSVLAVIALIAVGLTQNKPLPENVKYGIVLDAGSSHTNLYIYKWPAEKENDTGVVQQLEECQVK
GPGISKYAQKTDEIAAYLAECMKMSTERIPASKQHQTPVYLGATAGMRLLRMESKQSADEVLAAVSRSLKSYPFDFQGAKIITGQEE
GAYGWITINYLLGRFTQEQSWLNFISDSQKQATFGALDLGGASTQITFVPLNSTLEAPETSLQFRLYGTDYTVYTHSFLCYGKDQAL
WQKLAQDIQVSSGGILKDPCFYPGYKKVVNVSELYGTPCTKRFEKKLPFNQFQVQGTGDYEQCHQSILKLFNNSHCPYSQCAFNGVF
LPPLQGSFGAFSAFYFVMDFFKKMANDSVSSQEKMTEITKNFCSKPWEEVKASYPTVKEKYLSEYCFSGTYILSLLLQGYNFTGTSW
DQIHFMGKIKDSNAGWTLGYMLNLTNMIPAEQPLSPPLPHSTYISLMVLFSLVLVAMVITGLFIFSKPSYFWKEAV

> Human NTPDase1

MEDTKESNVKTFCSKNILAILGFSSIIAVIALLAVGLTQNKALPENVKYGIVLDAGSSHTSLYIYKWPAEKENDTGVVHQVEECRVK
GPGISKFVQKVNEIGIYLTDCMERAREVIPRSQHQETPVYLGATAGMRLLRMESEELADRVLDVVERSLSNYPFDFQGARIITGQEE
GAYGWITINYLLGKFSQKTRWFSIVPYETNNQETFGALDLGGASTQVTFVPQNQTIESPDNALQFRLYGKDYNVYTHSFLCYGKDQA
LWQKLAKDIQVASNEILRDPCFHPGYKKVVNVSDLYKTPCTKRFEMTLPFQQFEIQGIGNYQQCHQSILELFNTSYCPYSQCAFNGI
FLPPLQGDFGAFSAFYFVMKFLNLTSEKVSQEKVTEMMKKFCAQPWEEIKTSYAGVKEKYLSEYCFSGTYILSLLLQGYHFTADSWE
HIHFIGKIQGSDAGWTLGYMLNLTNMIPAEQPLSTPLSHSTYVFLMVLFSLVLFTVAIIGLLIFHKPSYFWKDMV

>Human NTPDase2

MAGKVRSLLPPLLLAAAGLAGLLLLCVPTRDVREPPALKYGIVLDAGSSHTSMFIYKWPADKENDTGIVGQHSSCDVPGGGISSYAD
NPSGASQSLVGCLEQALQDVPKERHAGTPLYLGATAGMRLLNLTNPEASTSVLMAVTHTLTQYPFDFRGARILSGQEEGVFGWVTAN
YLLENFIKYGWVGRWFRPRKGTLGAMDLGGASTQITFETTSPAEDRASEVQLHLYGQHYRVYTHSFLCYGRDQVLQRLLASALQTHG
FHPCWPRGFSTQVLLGDVYQSPCTMAQRPQNFNSSARVSLSGSSDPHLCRDLVSGLFSFSSCPFSRCSFNGVFQPPVAGNFVAFSAF
FYTVDFLRTSMGLPVATLQQLEAAAVNVCNQTWAQQLLSRGYGFDERAFGGVIFQKKAADTAVGWALGYMLNLTNLIPADPPGLRKG
TDFSSWVVLLLLFASALLAALVLLLRQVHSAKLPSTI

>Human NTPDase3

MFTVLTRQPCEQAGLKALYRTPTIIALVVLLVSIVVLVSITVIQIHKQEVLPPGLKYGIVLDAGSSRTTVYVYQWPAEKENNTGVVS
QTFKCSVKGSGISSYGNNPQDVPRAFEECMQKVKGQVPSHLHGSTPIHLGATAGMRLLRLQNETAANEVLESIQSYFKSQPFDFRGA
QIISGQEEGVYGWITANYLMGNFLEKNLWHMWVHPHGVETTGALDLGGASTQISFVAGEKMDLNTSDIMQVSLYGYVYTLYTHSFQC
YGRNEAEKKFLAMLLQNSPTKNHLTNPCYPRDYSISFTMGHVFDSLCTVDQRPESYNPNDVITFEGTGDPSLCKEKVASIFDFKACH
DQETCSFDGVYQPKIKGPFVAFAGFYYTASALNLSGSFSLDTFNSSTWNFCSQNWSQLPLLLPKFDEVYARSYCFSANYIYHLFVNG
YKFTEETWPQIHFEKEVGNSSIAWSLGYMLSLTNQIPAESPLIRLPIEPPVFVGTLAFFTAAALLCLAFLAYLCSATRRKRHSEHAF
DHAVDSD

>Human NTPDase8

MGLSRKEQVFLALLGASGVSGLTALILLLVEATSVLLPTDIKFGIVFDAGSSHTSLFLYQWLANKENGTGVVSQALACQVEGPGISS
YTSNAAQAGESLQGCLEEALVLIPEAQHRKTPTFLGATAGMRLLSRKNSSQARDIFAAVTQVLGRSPVDFWGAELLAGQAEGAFGWI
TVNYGLGTLVKYSFTGEWIQPPEEMLVGALDMGGASTQITFVPGGPILDKSTQADFRLYGSDYSVYTHSYLCFGRDQMLSRLLVGLV
QSRPAALLRHPCYLSGYQTTLALGPLYESPCVHATPPLSLPQNLTVEGTGNPGACVSAIRELFNFSSCQGQEDCAFDGVYQPPLRGQ
FYAFSNFYYTFHFLNLTSRQPLSTVNATIWEFCQRPWKLVEASYPGQDRWLRDYCASGLYILTLLHEGYGFSEETWPSLEFRKQAGG
VDIGWTLGYMLNLTGMIPADAPAQWRAESYGVWVAKVVFMVLALVAVVGAALVQLFWLQD

P. falciparum	DAGSNGTRQATGGMRNLGEEEGIYGWLAVNDLGGSSTQSWTHGSMIY
Mouse NTPDase	DAGSSHTGATAGMRLLGQEEGAYGWITINDLGGASTQGWTLGYMLNL
Rat NTPDase	DAGSSHTGATAGMRLLRGQEEGAYGWITINDLGGASTQGWTLGYMLNL
Human NTPDas1	DAGSSHTGATAGMRLLGQEEGAYGWITINDLGGASTQGWTLGYMLNL
Human NTPDase2	DAGSSHTGATAGMRLLGQEEGVFGWVTANDLGGASTQGWALGYMLNL
Human NTPDase3	DAGSSRTGATAGMRLLGQEEGVYGWITANDLGGASTQAWSLGYMLSL
Human NTPDase8	DAGSSHTGATAGMRLLGQAEGAFGWITVNDMGGASTQGWTLGYMLNL

7.0 Summary

7.1 Modulatory role of purinergic signalling in cancer

The tumour microenvironment components work together for a common goal, i.e. to avoid defence mechanisms. This chapter briefly discussed cancer cell-specific signalling mechanisms. The role of purinergic signalling in tumour progression and metastasis is discussed, including the upregulation of purinergic receptors and ectonucleotidases associated with cancer. This process involves extracellular nucleotides such as ATP and NAD^+, creating a pro-inflammatory environment that attracts immune cells. However, the upregulation of ectonucleotidases in tumours can transform this environment into an anti-inflammatory one, allowing tumours to evade immune surveillance. The research investigates pathways for adenosine production and potential therapeutic modalities to target this escape route.

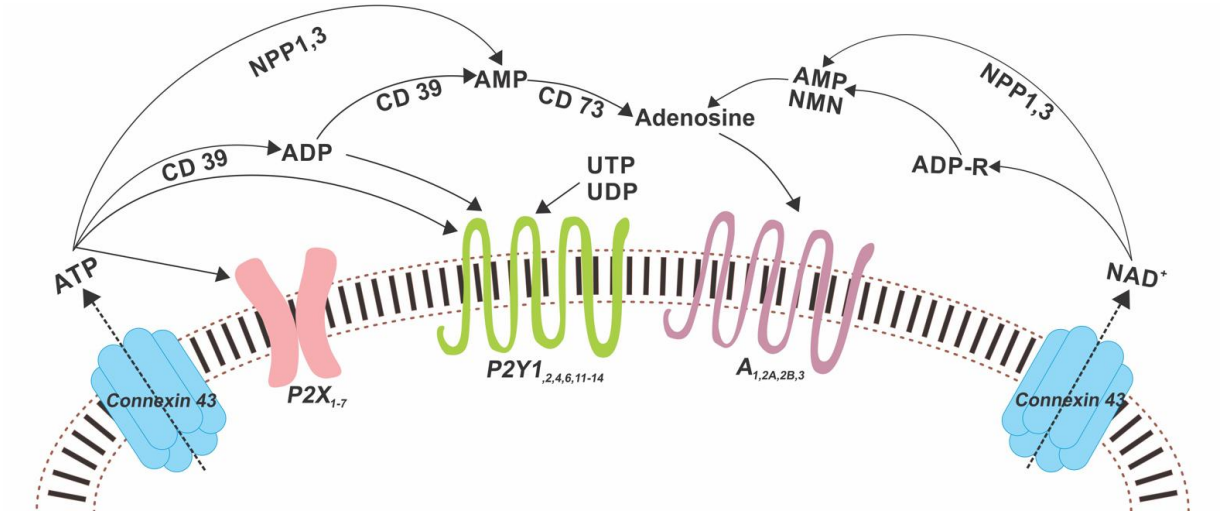

Overview of purinergic signalling

7.2 Sensitive fluorescence-based high-throughput assay for monitoring ectonucleotidase activity in cancer cell lines

Chapter 1 summarised the overexpression of ectonucleotidases in multiple cancer types linked with the high production of immunosuppressive adenosine surrounding tumour cells. This immunosuppressive environment helps tumours evade immune surveillance. To quantify adenosine production by cancer cell lines, such as U87, astrocytoma, and triple-negative cancer (TNBC), we developed a sensitive fluorescence HTS assay to

monitor ATPase, ADPase, and AMPase activity. The assay involves the hydrolysis of Ɛ-ATP, Ɛ-ADP, and Ɛ-AMP to Ɛ-adenosine in the cellular culture. The product is then specifically quantified using a precipitation buffer of 14.2 mM NaH_2PO_4 and 71.7 mM $LaCl_3$/NaOAc at pH 3.2. The precipitation buffer removes substrates from the reaction mix, allowing only product Ɛ-adenosine in the supernatant. We observed strong ATPase activity on these cell lines, possibly due to CD39 and NPP1. NPP1 activity is independently monitored using the NPP-specific substrate *p*-NPh-5'-TMP. The assay is a safer, more efficient, cost-effective, and robust alternative to radioassays with minimal equipment and lab requirements.

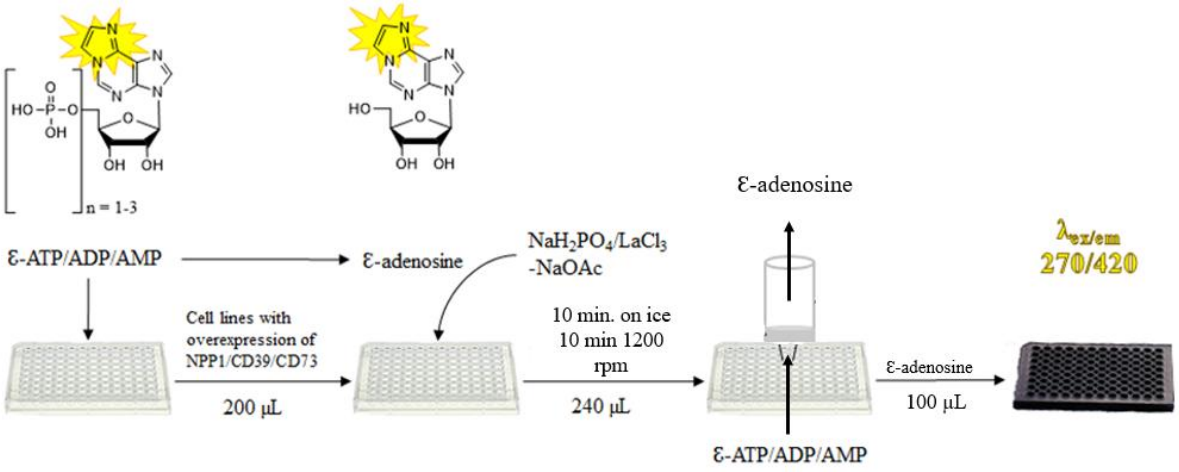

Assay procedure of fluorescence-based HTS assay for monitoring ectonucleotidase reactions.

7.3 Development and application of fluorescence-based assay for nucleotide pyrophosphatase/phosphodiesterases (NPPs)

In the extracellular environment, adenosine is produced by two pathways. The canonical pathway (CD39/CD73) using ATP, ADP, and AMP to produce adenosine is described in Chapter 2. The non-canonical pathway (CD38/NPP/CD73) is more diversified as it uses not only ATP/AMP but also hydrolyses NAD^+, ADPR, and Ap_nA. Therefore, the fluorescence assay described in section 7.2 applies to some extent, as not all NPPs can hydrolyse ATP. To go deep into this pathway, we developed another HTS fluorescence assay involving Ɛ-NAD^+, Ɛ-ADPR, and Ɛ-AP_4-ƐA. These assays were optimised for recombinant enzymes and applied to cancer cell lines. Ɛ-NAD^+ and Ɛ-AP_4-ƐA assays

were based on disruption of the quenching effect. In contrast, the Ɛ-ADPR assay is based on precipitation of the product Ɛ-AMP from the reaction sample, allowing quantification of Ɛ-ADPR. These newly developed assays are better suited than the *p*-NPh-5'-TMP assay in terms of sensitivity and applicability, particularly in testing coloured compounds.

NPPs, particularly NPP1 and NPP3, are essential in immuno-oncology and constitute potential targets for drug development. In this study, we have developed potent and selective NPP3 inhibitors. One of the compounds, PZB08720015A, exhibited promising inhibitory potency under alkaline reaction conditions of 17.8 ± 0.3 nM vs NAD^+ as a substrate; however, potency dropped considerably under neutral pH conditions resulting in an IC_{50} of 322 ± 14 nM. Moreover, NBO-MKA-29 showed good solubility and acceptable potency, making it a promising starting point for further exploration. These compounds displayed selectivity against other enzymes and are potent and selective NPP3 inhibitors.

A

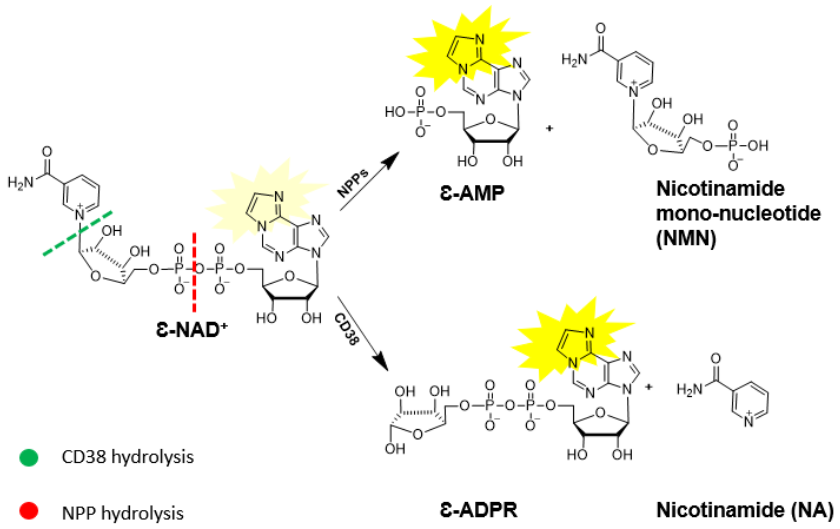

B

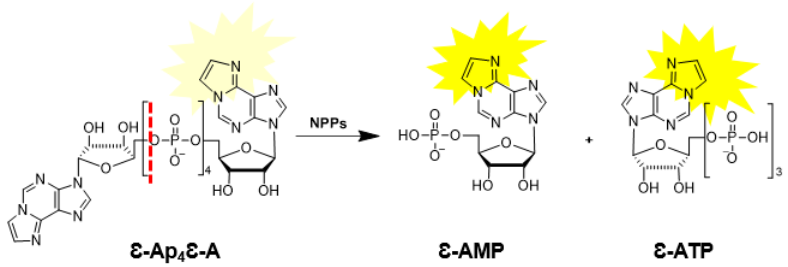

C

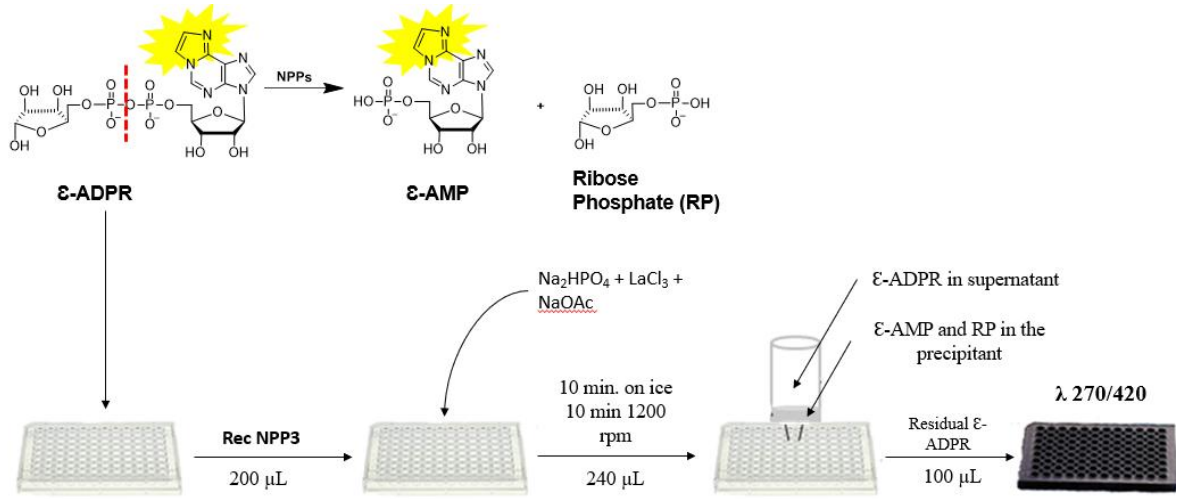

Schematic presentation of proposed assay mechanism involving A) ε-NAD⁺ B) ε-Ap₄ε-A, C) ε-ADPR.

7.4 Development and characterisation of nucleotide pyrophosphatase/ phosphodiesterase inhibitors with selectivity for NPP3

The sulfonamide group in PZB08720015A is essential for binding to the Zn^{2+} in the enzyme's active site. Under alkaline pH conditions, the sulfonamide group is negatively charged and potently interacts in the enzyme's active site. However, under neutral conditions, a significant reduction in potency was observed. We planned a bio-isosteric replacement of the sulfonamide to counter this challenge. Biological testing showed that derivatives 7a and 7b, novel analogues of PZB08720015A, resulted in a breakthrough in NPP3 inhibitors. Compound 7b selectively blocked NPP3 activity (IC_{50} 5.17 nM) with 142-fold improved potency compared to the lead structure PZB08720015A. Some intermediate compounds further exhibited the ability to block NPP1 activity in addition to NPP3. For example, 11b was the most potent NPP1 inhibitor (IC_{50} 77.1 nM). Compounds 10b and 11a showed dual NPP1/NPP3 inhibition. The optimisation of compound NBO-MKA-29 resulted in the generation of compound 14, which led to an improved NPP3-inhibitory effect (15-fold improvement).

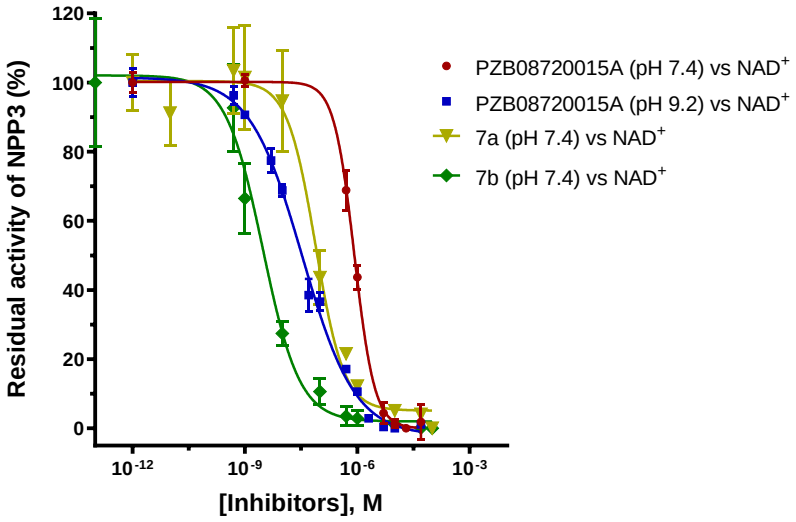

Concentration-dependent inhibition of NPP3

7.5 Small molecule inhibitors of CD38 with ancillary inhibition of CD39 and NPP1

We intended to pursue a multitarget approach towards CD38, CD39, and NPP1. Bioflavonoids, such as Quercetin, were previously reported to inhibit human CD38 with an IC_{50} value of 13.8 µM (Escande et al. 2013). During the in-house investigation, we found that Quercetin inhibits soluble hCD39 with a K_i of 0.495 ± 0.038 µM. Structure-activity relationship (SAR) studies of 4*H*-chromenes were subsequently performed. Novel inhibitors for CD38 were identified and further characterised. The most potent 4*H*-chromene derivative against CD38 was PZB22222054A with a K_i-value of 0.0641 ± 0.0351 μM (vs. NAD^+) and a competitive inhibition mode. The compound PZB22222043A displayed a K_i value of 0.154 ± 0.017 μM towards soluble CD39 and displayed a competitive inhibition mode. Additionally, PZB22222043A showed excellent inhibitory potency against CD38 with a K_i of 0.200 ± 0.038 μM and decent NPP1 approximately ~ 300 nM. Therefore, PZB22222043A is a multitarget inhibitor blocking both canonical and non-canonical pathways.

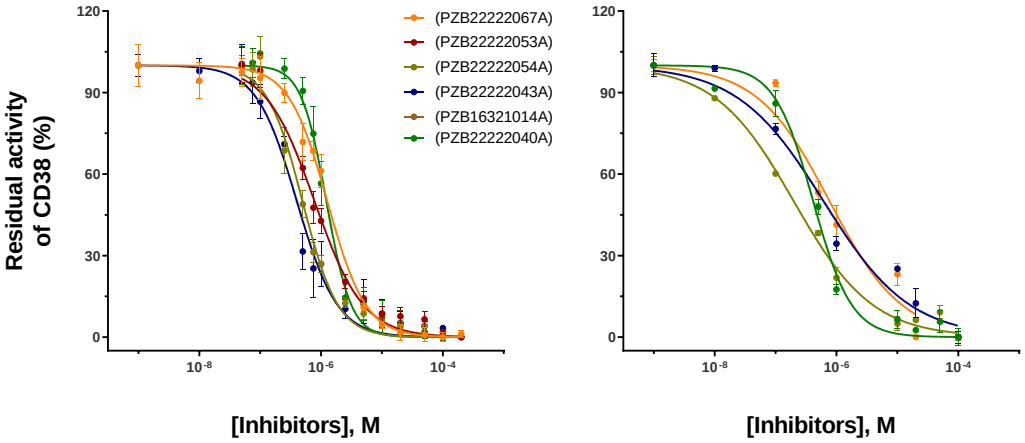

Concentration-dependent inhibition of CD38. A) vs. ε-NAD^+ B) vs. NAD^+.

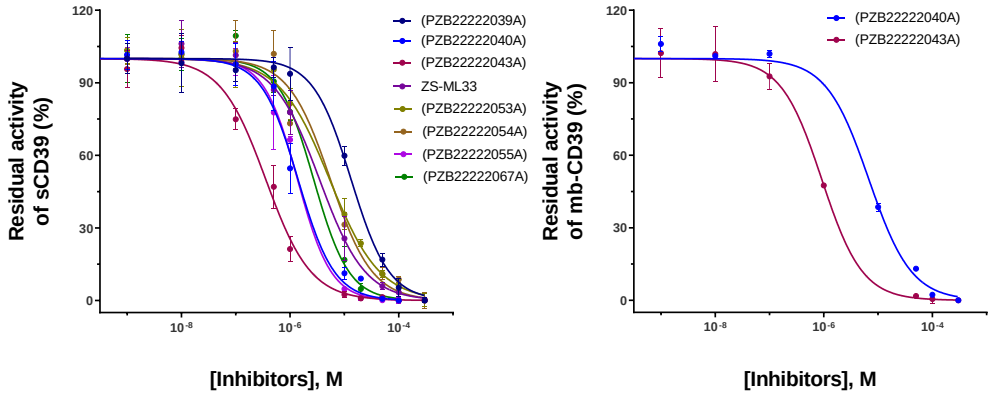

Concentration-dependent inhibition of CD39. A) soluble CD39, B) membrane-bound (mb) CD39.

7.6 Expression of human, mouse, and *Plasmodium falciparum* ectonucleoside triphosphate diphosphohydrolases (NTPDases) and their inhibition

In this project, we recombinantly expressed CD39 orthologs from human, mouse, and *Plasmodium falciparum* origin using an insect cell expression system. Soluble and membrane-bound enzymes were expressed. Human and mouse enzymes, both soluble and membrane-bound variants, efficiently hydrolysed ATP and ADP. However, low ATP hydrolysis was observed for the parasitic enzymes. The adequate purity of proteins was achieved, and they were suitable for inhibitor testing but needed to be sufficiently pure for crystallisation experiments. We mainly focused on investigating nucleotidic scaffolds for inhibition analysis, although some non-nucleotidic scaffolds were also examined and published during this research. SAR studies for AMP derivatives revealed BCY-110, -231,

-247, and CS-209-1 as the most potent CD39 inhibitors. Combining 8-butylthio and N^6-4-phenylbutyl on the AMP scaffold (BCY-110) increased the inhibitory potency by approximately 10-fold compared to 8-BuS-AMP. The compound inhibited soluble human CD39 with a K_i value of 58.1 nM. BCY-110 (and BCY-247) are the most potent CD39 inhibitors and the best candidate for further drug development. It is also metabolically stable due to protective 8-substituent as 8-BuS-AMP.

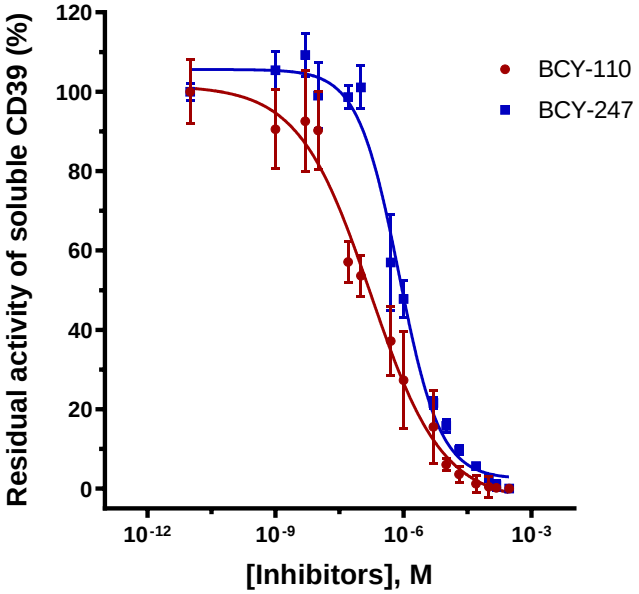

In summary, this thesis discusses primary cancers where an overexpression of ectonucleotidases is reported. Newly developed high-throughput screening assays investigated some representative tumour cell lines. The assays were optimised for monitoring ATPases, AMPases, NADases, ADPR, and Ap_4A-hydrolases. These newly developed assays were highly sensitive, measuring relative fluorescence units. A comprehensive review was performed for major ectonucleotidases (NPP1, NPP3, NPP4, CD38, CD39, CD73) regarding their substrate specificity, tissue expression, pathological outcome, monitoring assays, and small-molecule inhibitors with both nucleotidic and non-nucleotidic scaffolds. Our search for small-molecule inhibitors for these enzymes yielded positive results, including the most potent competitive inhibitors of NPP3 described so far that are active under physiological conditions (neutral pH). We also discovered competitive inhibitors of NPP1 with comparable K_i to the previously reported most active

scaffold. Multitarget inhibitors of CD38, CD39, and NPP1 are reported. And finally, CD39-selective nucleotide inhibitors were discussed.

The results of this thesis provide a basis for future research in the field of ectonucleotidases, and they may contribute to the development of novel anti-cancer drugs.

References

Duangiad, Peeradon, Bodee Nutho, Thawatchai Chaijarasphong, Noppawan Phumala Morales, Thunyarat Pongtharangkul, Itaru Hamachi, Akio Ojida, and Jirarut Wongkongkatep. 2024. “Naturally Occurring Quercetin and Myricetin as Potent Inhibitors for Human Ectonucleotide Pyrophosphatase/Phosphodiesterase 1.” *Scientific Reports* 14 (December). https://doi.org/10.1038/s41598-023-50590-7.

Escande, Carlos, Veronica Nin, Nathan L. Price, Verena Capellini, Ana P. Gomes, Maria Thereza Barbosa, Luke O’Neil, Thomas A. White, David A. Sinclair, and Eduardo N. Chini. 2013. “Flavonoid Apigenin Is an Inhibitor of the NAD+ase CD38: Implications for Cellular NAD+ Metabolism, Protein Acetylation, and Treatment of Metabolic Syndrome.” *Diabetes* 62 (April):1084–93. https://doi.org/10.2337/db12-1139.

Ferrero, Enza, Angelo C Faini, and Fabio Malavasi. 2018. “A Phylogenetic View of the Leukocyte Ectonucleotidases.” *Immunol. Lett.* 205:51–58. https://doi.org/10.1016/j.imlet.2018.06.008.

Ferrero, Enza, Angelo C. Faini, and Fabio Malavasi. 2019. “A Phylogenetic View of the Leukocyte Ectonucleotidases.” *Immunol. Lett.* Elsevier B.V. https://doi.org/10.1016/j.imlet.2018.06.008.

Marco Idzko1, Davide Ferrari2, and Holger K. Eltzschig. 2015. “Nucleotide Signalling during Inflammation.” *Nature* 509:310–17.

Roberts, Fiona, Dongxing Zhu, Colin Farquharson, and Vicky E Macrae. 2019. “ENPP1 in the Regulation of Mineralization and Beyond.” *Trends Biochem. Sci.* 44:616–28. https://doi.org/10.1016/j.tibs.2019.01.010.

Zimmermann, Herbert. 2020. “History of Ectonucleotidases and Their Role in Purinergic Signaling.” *Biochem. Pharmacol.*, 114322